Somatosensory Cortical input to the Striatum

Sankari Ramanathan

Thesis submitted for the degree of PhD.

University of Edinburgh

September 2003

Dedicated To

Shobu, Appa and Amma

Declaration

I hereby declare that the work contained within this thesis was all my own work except for the following:

Chapter 2

- Injections of the tracer into the barrel cortex, and perfusion of animals were done by Ann Wright.
- Figure 2.7 was prepared by Ann Wright.

Chapter 3

- Some of the results were part of my Masters thesis (Striatal Responses to Whisker Related Stimulus in Rats by Sankari Ramanathan - A thesis submitted as part requirement for the degree of Master of Science in Neuroscience University of Edinburgh, Scotland, August 1999). These include extracellular records from 59 striatal neurones, intracellular records from 3 cortical and 47 striatal neurones.

Chapter 5

- The 6-OHDA lesions were either done or supervised by Ann Wright.

Chapter 6

- Injection of tracers, perfusion of animals and preparation of the tissue for LM and EM was done by Jason Hanley.
- Figures 6.1C, D & 6.5 were prepared by Jason Hanley.
- Figure 6.6 was prepared by Paul Jays.

Sankari Ramanathan
September 2003

Publication

I hereby declare that the work contained within this thesis has not been previously published except for the following:

Chapter 3

- A.K. Wright, S. Ramanathan and G.W. Arbuthnott (2001). Identification of the source of the diffuse projection system from cortex to somatosensory neostriatum and an exploration of its physiological actions. *Neuroscience* **103** (1): 87-96

Chapter 4

- S. Ramanathan, A.K. Wright and G.W. Arbuthnott (2002). A physiological investigation of the two corticostriatal systems in rat somatosensory striatum. In: *The Basal Ganglia VII, Advances in behavioural biology Volume 52* (Nicholson, L. F. B and Faull, R. L. M. eds) pp 389-397. Kluwer Academic/Plenum Publishers.

Chapter 5

- S. Ramanathan, A. K. Wright, G. W. Arbuthnott (2002). Effects of dopamine on interaction of the two corticostriatal systems in rat somatsensory striatum. *Proceedings of the 9th International Conference on Neural Information Processing.*

Chapter 6

- S. Ramanathan, J. J. Hanley, J. M. Deniau and J. P. Bolam (2002). Synaptic convergence of motor and somatosensory cortical afferents onto GABAergic interneurons in the rat striatum. *Journal of Neuroscience* **22** (18): 8158-8169

Copies of the publications have been included in the appendix.

Sankari Ramanathan
September 2003

Acknowledgements

I would like to thank my supervisors Gordon and Cali for all the help, support, friendship and superb supervision over the past 4 years. Still can't believe that I can record from cells and do EM and I actually managed to write it all up. Thanks for believing in my abilities even when I had serious doubts. A big thanks also to Ann, who helped me every step of the way, and for being my mum away from home. Could not have done it without you, cause I can never find anything in the lab! Linda, thanks for all the help with the EM and for your friendship over all these years.

I would like to express my deepest gratitude to Paul Bolam, Mark Bevan, Pete Magill, Paul Jays and Caroline Francis at the MRC Anatomical Neurophramacology Unit in Oxford. Without the help of all of you, I would have never learnt the wonders of EM and have such pretty pictures in my thesis. It was a great year and thanks for teaching me so much and for saving my behind.

I would like to express my deepest gratitude to the Wellcome trust and the MRC for funding my PhD.

To all at the Department of Preclinical Vet sciences, especially Colin Warwick, Steve Mitchell, Graham Moodie, Andy Macrae and Simon Allen, thanks for the excellent technical advice. I would also like to thank Vince Molony and Gareth Leng, who were part of my thesis committee and helped me make sure that I submitted in time.

To all my friends that have made the last 5 (!) years in Edinburgh and Oxford, one of the most memorable periods of my life, thanks so much guys. I have to say I have been one of the lucky ones to share an office with some of the best

people, Benjy, Felix and Vickers, you guys! Rock on 361ers. Thanks for keeping me sane. Don't worry I'll be there to encourage you when you write up!! Also a big thanks to Simon (sorry for making you read the thesis), Karen, Noi, Giacomo, Tan, Fabio, Steph, Patrick, Praju, June and Elyana. I have to mention the patience of Sabrina (my fellow sufferer, what would I have done without you!), James, Cathy and Nigel, who put up with my insanity and managed to not call the guys in the white coats. Thanks so much for the support especially during the last month. I made it!

To my family, Appa, Amma, Shobu, Peri, Periappa, Anna, Jay, Kay, Hari, Monisha, Sanjay, Aakhash and Krishan, you guys are the best. I love you all. Without your support and love throughout all these years, I don't think I could have achieved so much. Thank you.

Abstract

The information from whiskers is processed in layer IV of the cortex by groups of neurones arranged in discrete functional units known as barrels. Each barrel processes input obtained from a single whisker. The barrel cortex can be differentiated into the cytochrome rich barrel centres and the septal cells surrounding the barrels. Previous work in the laboratory had established two cortical inputs to striatum from the barrel cortex. One of these arises from septal cells and is bilateral and composed of thin calibre fibres. The other route involves the barrel centres, is only unilaterally represented and is composed of topographically arranged, thick fibres. Based on these morphological differences, the postsynaptic targets of the two pathways with reference to the two output pathways of the striatum were examined. A method was also developed to examine the physiological consequences of stimulation of the two pathways upon the striatal output cells of the anaesthetised rat in both normal and dopamine-depleted animals. An anatomical study of the cortical input to the GABAergic interneurones was also undertaken as these cells strongly modulate the output of striatal neurones.

The pathways differ in their connectivity, with the bilateral pathway contacting the neurones of the striatopallidal pathway more often than the fibres of the topographic system. The stimulation of the two pathways can depolarise striatal cells and give rise to EPSPs, which can be differentiated based on their rise times. EPSPs in response to whisker pad stimulation have a rapid rise time, while the contralateral cortically derived EPSPs are slower to rise and the spike initiation latency more variable. Both pathways interacted at the level of a single striatal cell and gave rise to a summation of EPSPs at a time interval of 10ms, followed by a

period of inhibition, the extent of which was dependent on the order and source of the stimuli. This pattern of interaction was not seen in cortical neurones. In dopamine depleted animals both stimuli were also able to depolarise the spiny neurones to their firing threshold. However the EPSPs to whisker pad stimulation were significantly slower to rise compared to control animals and were similar to the rise times of EPSPs in response to contralateral cortical stimulation. The interaction of the two pathways was also affected by the loss of dopamine and the summation of EPSP amplitude observed when stimuli were delivered 10ms apart in control animals was no longer present. The anatomical study revealed that GABAergic interneurones receive convergent cortical input from both motor and sensory cortices and that their pattern of innervation is different from the cortical innervation of striatal output neurones.

The results of this thesis suggest that the two inputs from the barrel cortex differ in their physiological influence on striatal neurones, and that they might convey different aspects of somatosensory information to the striatum. The changes observed in dopamine-lesioned animals indicate that the topographic, ipsilateral pathway is selectively affected by the loss of dopamine suggesting that dopamine-depletion does not have a generalized action that is independent of presynaptic or postsynaptic origins. Rather its effects are specific to the neuronal subtype affected as well to the origin of the synapses. The complex pattern of innervation of striatal interneurones suggests that these cells play a very important role in striatal physiology and that their modulation by dopamine may serve as a possible explanation for the effects seen after lesion in this study.

Contents

Dedication ii

Declaration iii

Publications iv

Acknowledgements v

Abstract vii

Table of contents ix

List of Figures xvii

List of Tables xxii

List of Abbreviations xxiv

Chapter 1: General Introduction

1.1) Introduction 2

1.1.1) Striatum 2

1.1.2) Barrel cortex 3

1.1.3) Aim of the thesis 4

Chapter 2: Postsynaptic striatal targets of the two input pathways originating from the barrel cortex.

2.1) Introduction 9

2.1.1) Information pathways in the basal ganglia 9

2.1.2) Organisation of the striatum 14

2.1.3) Dopamine in the striatum 18

2.1.4) Segregation of the striatonigral and striatopallidal pathways 22

2.1.5) Corticostriatal input to the two striatal pathways 23

2.1.6) Aim 24

2.2) Experimental Procedures 25

2.2.1) Preparation of animals 25

2.2.2) Perfusion fixation 26

2.2.3) Preparation of tissue for electron microscopy 26

2.2.3.1) Localisation of anterograde tracer 26

2.2.3.2) Immunocytochemistry for D_1 group of dopamine receptor 28
2.2.3.3) Controls 28
2.2.4) Analysis of material 29
2.2.5) Statistical analysis of material 30
2.3) Results 32
2.3.1) Light microscopic observations 32
2.3.1.1) Appearance of the reaction products 32
2.3.1.2) Injection sites 32
2.3.1.3) Distribution of anterograde labelling 32
2.3.1.4) D_1 immunoreactive structures 35
2.3.1.5) Controls 37
2.3.1.6) Light microscopic analysis of contacts 37
2.3.2) Electron microscopic observations 37
2.3.2.1) Synaptic boutons from ipsilateral thick fibres (topographic pathway) 49
2.3.2.2) Synaptic boutons from ipsilateral thin fibres (diffuse pathway) 50
2.3.2.3) Synaptic boutons from contralateral thin fibres (diffuse pathway) 50
2.4) Discussion 55
2.4.1) Technical considerations 56
2.4.2) Cortical input to striatal neurones 58
2.4.3) Connectivity of the two input pathways to the two output pathways 60
2.4.4) Functional significance 61
2.5) Conclusions 63

Chapter 3: Response of cortical and striatal cells to electrical stimulation of whisker pad and contralateral cortical stimulation.

3.1) Introduction 66
3.1.1) Corticostriatal projections 66
3.1.2) Whiskers 72
3.1.3) Information relay 73
3.1.4) Barrels and septae 74
3.1.5) Projections from the barrel cortex to the striatum 76
3.1.6) Aim 82

3.2) Experimental Procedures 83
3.2.1) Extracellular recording 83
3.2.1.1) Anaesthesia 83
3.2.1.2) Surgical procedures 83
3.2.1.3) Whisker stimulus 84
3.2.1.4) Contralateral stimulating electrode 84
3.2.1.5) Extracellular recordings 85
3.2.1.6) Perfusion and histology 87
3.2.2) Intracellular recording 88
3.2.2.1) Anaesthesia 88
3.2.2.2) Surgical procedures 88
3.2.2.3) Stimulus protocol 88
3.2.2.4) Intracellular recordings 90
3.2.2.5) Perfusion and histology 91
3.2.3) Acquisition and analysis of data 92
3.2.3.1) Data acquisition - MacLab and Signal 92
3.2.3.2) Data analysis 93
3.2.3.3) Statistical analysis 93
3.2.4) Electroencephalogram 95
3.2.5) Cortical spreading depression 95
3.2.6) Acute and chronic callosal cuts 95
3.3) Results 97
3.3.1) Cortical cells 97
3.3.1.1) Extracellular electrophysiology 97
3.3.1.2) Intracellular electrophysiology 97
3.3.2) Striatal cells 106
3.3.2.1) Extracellular electrophysiology 106
3.3.2.2) Intracellular electrophysiology 111
3.3.2.3) Individual whisker deflection 122
3.3.3) Electroencephalogram 125
3.3.4) Cortical spreading depression 125
3.3.5) Acute and chronic callosal cuts 128

3.3.6) Morphology of cells 131
3.4) Discussion 135
3.4.1) Cortical cells 135
3.4.2) Striatal cells 145
3.5) Conclusions 158

Chapter 4: Interaction of the two corticostriatal systems in rat somatsensory cortex and striatum.

4.1) Introduction 160
4.1.1) Gating of inputs to the nucleus accumbens 160
4.1.2) Diffuse pathway from the barrel cortex is a gating pathway 162
4.1.3) Aim 163
4.2) Experimental Procedures 165
4.2.1) Anaesthesia 165
4.2.2) Surgical procedures 165
4.2.3) Stimulus protocol 166
4.2.4) Intracellular recordings and pairing protocols 166
4.2.5) Perfusion and histology 168
4.2.6) Acquisition and analysis of data 169
4.2.6.1) Data acquisition - MacLab and Signal 169
4.2.6.2) Data analysis 169
4.2.6.3) Statistical analysis 172
4.3) Results 174
4.3.1) Cortical cells 174
4.3.1.1) Protocol 1: Whisker pad – contralateral cortex interaction 178
4.3.1.2) Protocol 2: Contralateral cortex – whisker pad interaction 181
4.3.1.3) Protocol 3: Whisker pad – whisker pad interaction 183
4.3.1.4) Protocol 4: Contralateral cortex – contralateral cortex interaction 183
4.3.2) Striatal cells 186
4.3.2.1) Protocol 1: Whisker pad – contralateral cortex interaction 190
4.3.2.1.1) Averaged results from all (up, down and transition) states 190
4.3.2.1.2) Averaged results from up states 190

4.3.2.1.3) Averaged results from down states 193
4.3.2.2) Protocol 2: Contralateral cortex – whisker pad interaction 193
4.3.2.2.1) Averaged results from all (up, down and transition) states 193
4.3.2.2.2) Averaged results from up states 196
4.3.2.2.3) Averaged results from down states 196
4.3.2.3) Protocol 3: Whisker pad – whisker pad interaction 199
4.3.2.3.1) Averaged results from all (up, down and transition) states 199
4.3.2.3.2) Averaged results from up states 199
4.3.2.3.3) Averaged results from down states 202
4.3.2.4) Protocol 4: Contralateral cortex – contralateral cortex interaction 202
4.3.2.4.1) Averaged results from all (up, down and transition) states 202
4.3.2.4.2) Averaged results from up states 202
4.3.2.4.3) Averaged results from down states 206
4.4) Discussion 208
4.4.1) Cortical cells 208
4.4.2) Striatal cells 213
4.5) Conclusions 220

Chapter 5: Effects of dopamine on interaction of the two corticostriatal systems in rat somatsensory striatum.

5.1) Introduction 223
5.1.1) Dopamine in the striatum 223
5.1.2) Effects of dopamine on the electrophysiological characteristics of striatal neurones 224
5.1.3) Morphological changes as a result of the loss of dopamine 227
5.1.4) Aim 228
5.2) Experimental Procedures 229
5.2.1) Unilateral lesion of midbrain dopaminergic neurones with 6-hydroxydopamine 229
5.2.1.1) Anaesthesia and surgery 229
5.2.1.2) Testing for successful 6-OHDA lesions 230
5.2.2) Anaesthesia 230

5.2.3) Surgical procedures 230
5.2.4) Stimulus protocol 231
5.2.5) Intracellular recordings and pairing protocols 231
5.2.6) Perfusion and histology 233
5.2.6.1) Immunocytochemistry for D_1 group of dopamine receptor 233
5.2.7) Acquisition and analysis of data 234
5.2.7.1) Data acquisition - MacLab and Signal 234
5.2.7.2) Data analysis 235
5.2.7.3) Statistical analysis 235
5.3) Results 236
5.3.1) Histological verification of 6-OHDA lesions 236
5.3.2) Striatal intracellular electrophysiology 236
5.3.3) Response characteristics to two forms of stimulation 239
5.3.4) Pairing protocols in 6-OHDA treated animals 248
5.3.4.1) Protocol 1: Whisker pad – contralateral cortex interaction 248
5.3.4.2) Protocol 2: Contralateral cortex – whisker pad interaction 248
5.3.4.3) Protocol 3: Whisker pad – whisker pad interaction 251
5.3.4.4) Protocol 4: Contralateral cortex – contralateral cortex interaction 251
5.3.5) Pairing protocol in control vs. 6-OHDA animals 255
5.3.5.1) Protocol 1: Whisker pad – contralateral cortex interaction 256
5.3.5.2) Protocol 2: Contralateral cortex – whisker pad interaction 256
5.3.5.3) Protocol 3: Whisker pad – whisker pad interaction 256
5.3.5.4) Protocol 4: Contralateral cortex – contralateral cortex interaction 257
5.4) Discussion 259
5.4.1) Striatal neurones 259
5.5) Conclusions 266

Chapter 6: Synaptic convergence of motor and sensory cortical afferents onto GABAergic interneurones in the rat striatum.

6.1) Introduction 269
6.1.1) Information processing in the basal ganglia 269
6.1.2) Organisational principles of the corticostriatal projections 270

6.1.3) Cortical input to the striatum 273
6.1.4) GABAergic parvalbumin interneurones 273
6.1.5) Aim 275
6.2) Experimental Procedures 276
6.2.1) Preparation of animals 276
6.2.2) Perfusion fixation 277
6.2.3) Preparation of tissue for light microscopy 277
6.2.3.1) Localisation of anterograde tracers 277
6.2.3.2) Immunocytochemistry for parvalbumin 279
6.2.4) Preparation of tissue for electron microscopy 279
6.2.5) Analysis of material 280
6.3) Results 282
6.3.1) Light microscopic observations 282
6.3.1.1) Appearance of the reaction products 282
6.3.1.2) Injection sites 282
6.3.1.3) Distribution of anterograde labelling 284
6.3.1.4) Parvalbumin-positive GABAergic interneurones 287
6.3.1.5) Light microscopic analysis of convergence 289
6.3.2) Electron microscopic observations 292
6.4) Discussion 300
6.4.1) Parvalbumin immunoreactivity 300
6.4.2) Anterograde labelling 301
6.4.3) Anterograde labelling and parvalbumin immunoreactivity 301
6.4.4) Quantification of convergence 302
6.4.5) Pattern of cortical innervation of PV-positive interneurones 303
6.4.6) Functional significance 305
6.5) Conclusions 308

Chapter 7: General Discussion

7.1) Discussion 310
7.1.1) Main findings 310
7.1.2) Future work 317

7.2) Conclusions 319

References 321

Appendix

Appendix 1. Correlation between the size of the EPSPs in response to the initial stimulus and second stimulus, for each time interval for all 4 paring protocols in cortical neurones 366

Appendix 2. Correlation coefficient and the R-squared value from regression analysis of the membrane potential on the amplitude of the response to the second stimulus for each time interval for all 4 paring protocols in cortical neurones. 368

Appendix 3. Publications 370

List of Figures

Chapter 2: Postsynaptic striatal targets of the two input pathways originating from the barrel cortex.

2.1. Flow of information through the basal ganglia. 10

2.2. Updated model of the flow of information through the basal ganglia. 13

2.3. Inputs to a striatal neurone. 16

2.4. Segregation of the striatal output pathways. 17

2.5. Experimental set up. 27

2.6. Injection sites. 33

2.7. Anterograde labelling in the striatum. 34

2.8. D_1 immunoreactivity. 36

2.9. Location of fibres and summary of results. 38

2.10. Correlated light and electron microscopy of a thick fibre in the ipsilateral striatum contacting an D_1 immunopositive spine. 40

2.11. Correlated light and electron microscopy of a thick fibre in the ipsilateral striatum contacting an D_1 immunonegative spine. 42

2.12. Correlated light and electron microscopy of a thin fibre in the ipsilateral striatum contacting a D_1 immunopositive and a D_1 immunonegative spine. 44

2.13. Correlated light and electron microscopy of a thin fibre in the contralateral striatum contacting both D_1 immunonegative and immunopositive spines. 46

2.14. Correlated light and electron microscopy of a swelling arising from a thin fibre in the contralateral striatum that did not give rise to a bouton at the ultrastructural level. 51

2.15. Immunoreactive targets of the projection from the barrel cortex to the striatum. 52

2.16. Simple vs. complex synapses made by the projections from the barrel cortex to the striatum. 53

Chapter 3: Response of cortical and striatal cells to electrical stimulation of whisker pad and contralateral cortical stimulation.

3.1. Flow of information from the whisker pad to the striatum. 81

3.2. Experimental set-up. 86

3.3. Experimental set-up for deflection of individual whiskers. 89
3.4. Definition of measurements. 94
3.5. Distribution of cortical neurones from which records were obtained. 98
3.6. Extracellular traces of responding cortical neurones. 99
3.7. Spontaneous activity of cortical neurones. 101
3.8. Current injection into cortical neurones. 102
3.9. Intracellular traces of a responding cortical neurone. 104
3.10. Influence of membrane potential on the size of the EPSP and the size and duration of the IPSP in cortical neurones. 105
3.11. Whisker pad vs. contralateral cortical stimulation in cortical neurones. 107
3.12. Distribution of striatal neurones recorded extracellularly. 109
3.13. Extracellular traces of responding striatal neurones. 112
3.14. Spontaneous activity of striatal neurones. 113
3.15. Current injection into striatal neurones. 115
3.16. Distribution of striatal neurones recorded intracellularly. 116
3.17. Intracellular traces of responding striatal neurones. 119
3.18. Influence of the membrane potential on the size of the EPSP in striatal neurones. 120
3.19. Whisker pad vs. contralateral cortical stimulation in striatal neurones. 121
3.20. Response of striatal neurones to increasing whisker pad and contralateral cortical stimulation. 123
3.21. Individual whisker deflection. 124
3.22. Cortical EEG and spontaneous striatal activity. 126
3.23. Cortical shutdown. 127
3.24. Extent and histological verification of callosal cuts. 129
3.25. Response to both forms of stimulation in control vs. acute callosal cut animals. 130
3.26. Response to both forms of stimulation in control vs. chronic callosal cut animals. 132
3.27. Morphology of filled striatal neurones. 133

Chapter 4: Interaction of the two corticostriatal systems in rat somatsensory cortex and striatum.

4.1. Measurement of the duration of an EPSP. 170

4.2. Measurement of the response characteristics of EPSPs as a result of the second stimulus in the pairing protocol. 171

4.3. Distribution of cortical neurones from which records were obtained. 175

4.4. Influence of the state of the cell on the duration of the EPSP. 177

4.5. Response of cortical neurones to whisker pad-contralateral cortex pairing protocol. 179

4.6. Amplitude of the second EPSP is partly dependent on the size of the first EPSP. 180

4.7. Response of cortical neurones to contralateral cortex-whisker pad pairing protocol. 182

4.8. Response of cortical neurones to whisker pad-whisker pad pairing protocol. 184

4.9. Response of cortical neurones to contralateral cortex-contralateral cortex pairing protocol. 185

4.10. Distribution of striatal neurones from which records were obtained. 187

4.11. Response of striatal neurones to whisker pad-contralateral cortex pairing protocol. 191

4.12. Response of striatal neurones to whisker pad-contralateral cortex pairing protocol, when the whisker pad stimulus was delivered in the up state. 192

4.13. Response of striatal neurones to whisker pad-contralateral cortex pairing protocol, when the whisker pad stimulus was delivered in the down state. 194

4.14. Response of striatal neurones to contralateral cortex-whisker pad pairing protocol. 195

4.15. Response of striatal neurones to contralateral cortex-whisker pad pairing protocol, when the contralateral cortical stimulus was delivered in the up state. 197

4.16. Response of striatal neurones to contralateral cortex-whisker pad pairing protocol, when the contralateral cortical stimulus was delivered in the down state. 198

4.17. Response of striatal neurones to whisker pad-whisker pad pairing protocol. 200

4.18. Response of striatal neurones to whisker pad-whisker pad pairing protocol, when the whisker pad stimulus was delivered in the up state. 201

4.19. Response of striatal neurones to whisker pad-whisker pad pairing protocol, when the whisker pad stimulus was delivered in the down state. 203
4.20. Response of striatal neurones to contralateral cortex-contralateral cortex pairing protocol. 204
4.21. Response of striatal neurones to contralateral cortex-contralateral cortex pairing protocol, when the contralateral cortical stimulus was delivered in the up state. 205
4.22. Response of striatal neurones to contralateral cortex-contralateral cortex pairing protocol, when the contralateral cortical stimulus was delivered in the down state. 207

Chapter 5: Effects of dopamine on interaction of the two corticostriatal systems in rat somatsensory striatum.

5.1. Anatomical verification of unilateral nigral lesions. 237
5.2. Spontaneous activity of striatal neurones. 238
5.3. Current injection into striatal neurones. 240
5.4. Distribution of striatal neurones from which records were obtained. 241
5.5. Intracellular traces of responding striatal neurones. 243
5.6. Influence of the membrane potential on the size of the EPSP in striatal neurones. 244
5.7. Whisker pad vs. contralateral cortical stimulation in striatal neurones. 246
5.8. Response of striatal neurones to whisker pad-contralateral cortex pairing protocol. 249
5.9. Response of striatal neurones to contralateral cortex-whisker pad pairing protocol. 250
5.10. Response of striatal neurones to whisker pad-whisker pad pairing protocol. 252
5.11. Prolonged inhibition of striatal neurones to dual whisker pad stimuli. 253
5.12. Response of striatal neurones to contralateral cortex-contralateral cortex pairing protocol. 254

Chapter 6: Synaptic convergence of motor and sensory cortical afferents onto GABAergic interneurones in the rat striatum.

6.1. Injection sites. 283
6.2. Anterograde labelling in the thalamus. 285

6.3. Axonal arborisation of corticostriatal projections. 286
6.4. Pattern of anterograde labelling from S1 in caudal striatum. 288
6.5. Apposition of cortical terminals from M1 and S1 cortices onto PV interneurones. 290
6.6. Multiple contacts of corticostriatal axons onto PV-positive interneurones. 291
6.7. Synaptic contact of an anterogradely labelled corticostriatal terminal. 294
6.8. Synaptic convergence of motor and somatosensory cortical afferents onto a parvalbumin-positive, GABAergic interneurone in the striatum: correlated light and electron microscopy. 295
6.9. Synaptic convergence of motor and somatosensory cortical afferents onto a parvalbumin-immunolabelled, GABAergic interneurone in the striatum: correlated light and electron microscopy. 296
6.10. Multiple synaptic contact of a single motor cortical axon onto a parvalbumin-positive GABAergic interneurone in the striatum: correlated light and electron microscopy. 297
6.11. Other synaptic contacts of PV interneurones. 298

List of Tables

Chapter 3: Response of cortical and striatal cells to electrical stimulation of whisker pad and contralateral cortical stimulation.

3.1. Summary of electrophysiological characteristics of cortical cells to electrical whisker pad stimulation and contralateral cortical stimulation. 106

3.2. Mean latencies of extracellularly recorded striatal cells to electrical whisker pad stimulation and contralateral cortical stimulation. 110

3.3. Mean latencies of intracellularly recorded striatal cells to electrical whisker pad stimulation and contralateral cortical stimulation. 117

3.4. Summary of electrophysiological characteristics of striatal cells to electrical whisker pad and contralateral cortical stimulation. 118

Chapter 4: Interaction of the two corticostriatal systems in rat somatsensory cortex and striatum.

4.1. Summary of the pairing protocols. 168

4.2. Summary of electrophysiological characteristics of cortical cells to electrical stimulation of the whisker pad and contralateral cortical stimulation. 176

4.3. Summary of the results of the pairing protocols in cortical neurones. 186

4.4. Response characteristics of striatal neurones to whisker pad and contralateral cortical stimulation. 188

4.5. Comparison of the response characteristics of striatal neurones to whisker pad stimulation during up, down or averaged traces. 189

4.6. Comparison of the response characteristics of striatal neurones to contralateral cortical stimulation during up , down or averaged traces. 189

4.7. Summary of the results of the pairing protocols in striatal neurones. 206

Chapter 5: Effects of dopamine on interaction of the two corticostriatal systems in rat somatsensory striatum.

5.1. Comparison of electrophysiological properties of striatal neurones from control and lesioned animals. 242

5.2. Summary of electrophysiological characteristics of striatal cells to electrical whisker pad and contralateral cortical stimulation. 245

5.3. Comparison of the of electrophysiological characteristics of striatal cells in control and 6-OHDA lesioned animals to electrical whisker pad stimulation. 247
5.4. Comparison of the electrophysiological characteristics of striatal cells in control and 6-OHDA lesioned animals to contralateral cortical stimulation. 247
5.5. Summary of the results of the pairing protocols in striatal neurones. 255
5.6. Summary of the results of the pairing protocols in striatal neurones. 258

Chapter 6: Synaptic convergence of motor and sensory cortical afferents onto GABAergic interneurones in the rat striatum.

6.1. Summary of correlated light and electron microscopy results. 299

List of Abbreviations

6-OHDA	-	6-hydroxydopamine
AA	-	Arachidonic Acid
ABC	-	avidin-biotin-peroxidase complex
ACh	-	acetylcholine
AChE	-	acetylcholinesterase
aCSF	-	artificial cerebrospinal fluid
AI	-	agranular insular cortex
AMPA	-	α-amino-3-hydroxy-5-methyl-4-isoxazoleproprionic acid
ANOVA	-	analysis of varience
AP	-	anterior posterior
BDA	-	biotinylated dextran amine
BSA	-	bovine serum albumin
bv	-	blood vessel
C	-	capillary
Ca^{2+}	-	calcium
cAMP	-	adenosine- 3', 5'- cyclic monophosphate
cb	-	cell body
CC	-	corpus callosum
CPu	-	caudate putamen
CSF	-	cerebrospinal fluid
Ctx	-	cortex
D_1 (-)	-	D_1 immunonegative
D_1 (-) Sp	-	D_1 immunonegative spine
D_1 (+) Den	-	D_1 immunopositive dendrite
D_1 (+) Sp	-	D_1 immunopositive spine
DA	-	dopamine
DAB	-	diaminobenzidine
DG	-	[^{14}C]deoxyglucose
DOPAC	-	dihydroxyphenylacetic acid
DV	-	dorsoventral
dyp	-	dynorphin

EEGs	-	electroencephalograms
enk	-	enkephalin
EP	-	entopeduncular nucleus
EPSP	-	excitatory postsynaptic potential
FB	-	fibre bundle
Fr	-	frontal cortex
GABA	-	gamma-aminobutyric acid
GAD	-	glutamic acid decarboxylase
GP	-	globus pallidus
GPe	-	external segment of the gobus pallidus
GPi	-	internal segment of the globus pallidus
HBN	-	lateral habenular nucleus
HP	-	hippocampus
IC	-	internal capsule
IgG	-	immunoglobulin
IPSP	-	inhibitory postsynaptic potential
K^+	-	potassium
L	-	lateral
LTD	-	long term depression
LTP	-	long term potentiation
m	-	mitochondria
M1	-	primary motor cortex
mRNA	-	messenger ribonucleic acid
nDAB	-	nickel diaminobenzidine
NMDA	-	N-methyl-D-aspartate
NS	-	neostriatum
PAP	-	peroxidase-antiperoxidase
Par	-	parietal cortex
PB	-	phosphate buffer
PBS	-	phosphate buffered saline
PBS-TX	-	Triton-X in PBS
PHAL	-	*Phaseolus vulgaris* Leucoagglutinin

PI	-	phosphoinositide
PKA	-	protein kinase A
Po	-	posterior thalamic nucleus
PPN	-	pedunculopontine nucleus
PrV	-	principal trigeminal nucleus
PSD	-	postsynaptic density
PV	-	parvalbumin
RF	-	parvicellular reticular formation
RT	-	reticular thalamus
S.D	-	standard deviation
S1	-	primary sensory cortex
SC	-	superior colliculus
SII	-	secondary sensory cortex
SN	-	substantia nigra
SNpc	-	substantia nigra pars compacta
SNpr	-	substantia nigra pars reticulata
SP	-	substance P
SpV	-	spinal trigeminal nucleus
SpVc	-	spinal trigeminal nucleus subnucleus caudalis
SPVi	-	spinal trigeminal nucleus subnucleus interpolaris
SpVo	-	spinal trigeminal nucleus subnucleus oralis
STN	-	subthalamic nucleus
Str	-	striatum
STRN	-	striatonigral
STRP	-	striatopallidal
TH	-	tyrosine hydorxylase
VL	-	ventrolateral nucleus of thalamus
VM	-	ventromedial nucleus of thalamus
VPL	-	lateral aspect of ventroposterior nucleus of thalamus
VPM	-	venteroposterior nucleus of thalamus
VTA	-	ventral tegmental area

CHAPTER 1

GENERAL INTRODUCTION

1.1) Introduction

1.1.1) Striatum

The striatum is one of the nuclei of the basal ganglia, which is a group of sub-cortical structures involved in a variety of processes including motor, associative, cognitive and mnemonic functions. The striatum is considered the main input structure of the basal ganglia, and has been implicated in playing a role in learning and memory and is necessary for the formation of stimulus-response associations that are built up through reinforcements (Graybiel, 1995).

The striatum is made up of two main cell types, projection neurones and the interneurones. The projection neurones, or medium sized densely spiny neurones named according to their morphological characteristics, are the main cell type in the striatum (~95% of striatal cell population) and send their axons to other nuclei in the basal ganglia (Bolam and Bennett, 1995). These target structures include the globus pallidus (GP), the substantia nigra pars reticulata and the entopeduncular nucleus. The interneurones are by comparison much rarer (~3-5%, of striatal cell population) and four main classes of interneurones have been identified using cytochemical, physiological and morphological methods (Kawaguchi et al., 1995). These interneurones contact striatal projection neurones and other interneurones (Kawaguchi et al., 1995). Despite their low occurrence, these cells are able to strongly modulate the behaviour of the projection neurones.

The behaviour of striatal cells, which affects downstream basal ganglia nuclei is dependent on the inputs to this brain structure. The striatum receives projections from the cerebral cortex, the intralaminar nuclei of the thalamus, the dopaminergic neurones of the substantia nigra pars compacta, the serotonergic

neurones of the dorsal raphe nucleus and the basolateral nucleus of the amygdala (Smith et al., 1998). The entire cortical mantle sends a topographic projection to the striatum providing the main excitatory drive to the neurones. The cells that give rise to this corticostriatal projection are heterogeneous and differ in their cortical layer of origin as well as in the target of their collateral axons (Donoghue and Kitai, 1981; Royce, 1983; Tanaka, 1987; Wilson, 1987; McGeorge and Faull, 1989; Cowan and Wilson, 1994).

There is a large body of experimental data showing that the behaviour of striatal neurones is modulated by dopamine (Cepeda et al., 1993; Nicola et al., 2000; Onn et al., 2000). While the effects of dopamine on the electrophysiological properties and response of striatal neurones to corticostriatal stimulation has been extensively studied, there are few experiments that address the differential effects of dopamine on specific corticostriatal pathways.

1.1.2) Barrel cortex

Whiskers are the primary sensory receptors in rodents. The information from the whiskers is processed in layer IV of the cortex by groups of neurones arranged in discrete functional units known as barrels (Woolsey and Van der Loos, 1970). The areas of cortex above and below a barrel are known as barrel columns and each barrel processes input obtained from a single whisker. Areas known as septa separate the barrels. The number of barrels equates to the number of vibrissae on the contralateral side of the face and has a faithful one-to-one representation of the spatial organisation of the whiskers. This feature of the barrel cortex, has been exploited and numerous investigators have used this system to study regulation of cortical development, cortical integration of peripheral input and experience

dependent synaptic plasticity (Armstrong-James and Callahan, 1991; Armstrong-James et al., 1991; Schlaggar et al., 1993; Schlaggar and O'Leary, 1993; Micheva and Beaulieu, 1997; Finnerty et al., 1999; Glazewski et al., 1999; Wallace and Fox, 1999a, b; Medina et al., 2001; Mirabella et al., 2001; Fox, 2002).

Recent anatomical data indicates that the corticostriatal projection arising from this area of the cortex also has some unique properties (Alloway et al., 1998; Alloway et al., 1999; Wright et al., 1999). Two corticostriatal systems originate from the barrel cortex and they differ in their cells of origin, their morphology and terminal patterns in the striatum (Alloway et al., 1998; Alloway et al., 1999; Wright et al., 1999; Wright et al., 2001). The first pathway originates from the layer V cortical cells found beneath the barrels themselves (Wright et al., 1999). The axons of cells involved in this pathway, project their axons to the brainstem and thalamus, while also sending a collateral branch to the striatum (Wright et al., 1999). This pathway is made up of thick fibres and has a topographic representation in the ipsilateral somatosensory striatum and has been termed the topographic pathway (Alloway et al., 1998; Alloway et al., 1999; Wright et al., 1999). The other diffuse pathway arises from layer V cells found beneath the septa and sends a projection to both ipsilateral and contralateral striata (Wright et al., 1999; Wright et al., 2001). This pathway which arises as the collateral of a corticocortical projection has a diffuse pattern of innervation to the striatum and is composed of thin fibres (Wright et al., 1999). Both these corticostriatal pathways contact the medium sized densely spiny projection neurones of the striatum (Wright et al., 1999).

1.1.3) Aim of the thesis

The barrel cortex system is an ideal model for studying the influence of the different corticostriatal pathways on striatal cell behaviour. Moreover it can be used to study if and how, dopamine modulates the different pathways. The difference in morphology of the two systems allows identification of both fibre types at the light microscope level, while the difference in the origin of both pathways and projection to either one striata (topographic pathway) or both striata (diffuse pathways) allows stimulation of either pathway electrophysiologically. This thesis explores the connections of the corticostriatal pathways arising from the barrel cortex to cells in the striatum both anatomically and physiologically.

There are five main aims in this thesis and the experimental work carried out to address these issues is presented in chapters 2 to 6.

1. **To localise precisely, the postsynaptic targets of the topographic and diffuse pathways.**

   The experiments designed to tackle this are described in Chapter 2 and involve the labelling of cortical afferents from the barrel cortex by anterograde tracers. This was combined with the immunolabelling of striatal neurones, with D_1 receptor antibody to identify one set of striatal neurones that belong to the direct pathway.

2. **To compare and contrast the physiological responses of striatal and Layer V barrel cortical neurones to stimulation of the topographic and diffuse pathways.**

   The experiments are described in Chapter 3 and involve, the stimulation of the both pathways (topographic pathway by an electrical stimulus to the whisker pad and diffuse pathway by a contralateral cortical electrode).

3. **To study the physiological responses of striatal and Layer V barrel cortical neurones to asynchronously delivered pairs of stimuli to the topographic and diffuse pathways.**

   Chapter 4 investigated the possible roles of the two corticostriatal pathways. Pairs of stimuli were delivered and the responses of striatal and layer V cortical cells was recorded. The pairs of stimuli were delivered to investigate the effect of an initial stimulus on the response of striatal and layer V cortical cells to a second stimulus. The pairs of stimuli investigated, the effect of one pathway on another (stimulation of topographic pathway followed by stimulation of the diffuse pathway and vice versa) and the effect of a pathway on itself (dual stimulation of the topographic pathway or diffuse pathway).

4. **To understand the response of striatal neurones in Parkinson's disease, the physiological response of striatal neurones to stimulation of the topographic and diffuse pathways and asynchronously delivered pairs of stimuli to the topographic and diffuse pathways when the dopaminergic input to striatal neurones was destroyed.**

   In chapter 5, the role of dopamine in processing 'whisker' information in the striatum was studied by inducing the loss of dopamine by 6-OHDA treatment. The two corticostriatal systems arising from the barrel cortex were stimulated as before and the response of striatal neurones to these stimuli was compared with control animals.

5. **To localise precisely, the motor and somatosensory cortical input to GABAergic interneurones in the striatum with the specific aim of examining possibility of convergence.**

In chapter 6, cortical afferents from the primary motor cortex (M1) and primary somatosensory cortex (S1) were labelled by different anterograde tracers, and the convergence and pattern of innervation of these interneurones by individual cortical axons was investigated.

In chapter 7, the main findings of the thesis are summarised and future experiments are discussed.

CHAPTER 2

POSTSYNAPTIC STRIATAL TARGETS OF THE TWO INPUT PATHWAYS ORIGINATING FROM THE BARREL CORTEX

2.1) Introduction

2.1.1) Information pathways in the basal ganglia

Cortical information is transmitted to the basal ganglia via 2 main nuclei; the striatum and the subthalamic nucleus (STN). The striatum, which receives a massive topographic input from the entire cortical mantle (Goldman and Nauta, 1977; Selemon and Goldman-Rakic, 1985; McGeorge and Faull, 1989), is considered the main input nucleus of the basal ganglia. Cortical information relayed to the striatum is processed and transmitted to the output nuclei of the basal ganglia, the entopeduncular nucleus (EP) [or the internal segment of the globus pallidus (GPi) in primates] and the substantia nigra pars reticulata (SNpr).

The concept of the direct and indirect pathway as introduced by Albin (Albin et al., 1989) and expanded by numerous investigators (reviewed by Smith et al., 1998), has long been regarded as the basic circuitry of the basal ganglia. According to this basic model (Fig. 2.1), incoming cortical information is channelled via 2 pathways, a direct projection from the striatum to the output nuclei (EP/SNpr) and an indirect pathway which involves a projection from the striatum to the globus pallidus (external segment of the gobus pallidus, GPe, in primates), a projection from the GP to the STN and a projection from the STN to the output structures. Disinhibition has been proposed as the basic mechanism by which these basal ganglia circuits affect behaviour (Chevalier et al., 1985; Deniau and Chevalier, 1985). Targets of the basal ganglia comprising of the thalamus, superior colliculus, lateral habenula, mesopontine tegmentum and reticular formation, are tonically inhibited by the basal ganglia output nuclei (EP/SNpr). Cortical excitation of inhibitory striatal projection neurones to the EP and SNpr leads to increased inhibition of the output nuclei. This

Figure 2. 1. Flow of information through the basal ganglia.

The figure illustrates the flow of information through the basal ganglia as put forward by Albin (Albin, 1989). Excitatory inputs are marked by red lines, while inhibitory pathways are blue. Information is segregated into the direct and indirect pathways. The direct pathway, involves channelling cortical information directly from the striatum to the output nuclei via a subset of striatal projection neurones (striatonigral) expressing substance P (SP) and dynorphin (dyp) and D_1 dopamine receptors. The other pathway involves striatal information transmitted to the globus pallius (GP) and then onto the subthalamic nucleus (STN). This indirect pathway is mediated by a subset of projection neurones (striatopallidal), coexpressing enkephalin (enk) and D_2 dopamine receptors. A dopaminergic projection from the substantia nigra pars compacta (SNpc) modulates the striatal pathways differentially, via their different sets of dopamine receptors with dopamine (DA) exciting the direct pathway and inhibiting the indirect pathway. The output structures of the basal ganglia, inhibit the targets of the basal ganglia, which includes the thalamus, which sends a projection back to the cortex. Both output nuclei also project to the pedunculopontine nucleus (PPN), with the entopeduncular (EP) nucleus additionally projecting to the lateral habenular nucleus (HBN) and the substantia nigra pars reticulata (SNpr) projecting to the superior colliculus (SC), and parvicellular reticular formation (RF). Cortical information is also conveyed direct to the STN via a corticosubthalamic pathway. Modified from Fig. 1 in Smith et. al., 1998.

(GPe - external segment of the globus pallidus, GPi - internal segment of the globus pallidus)

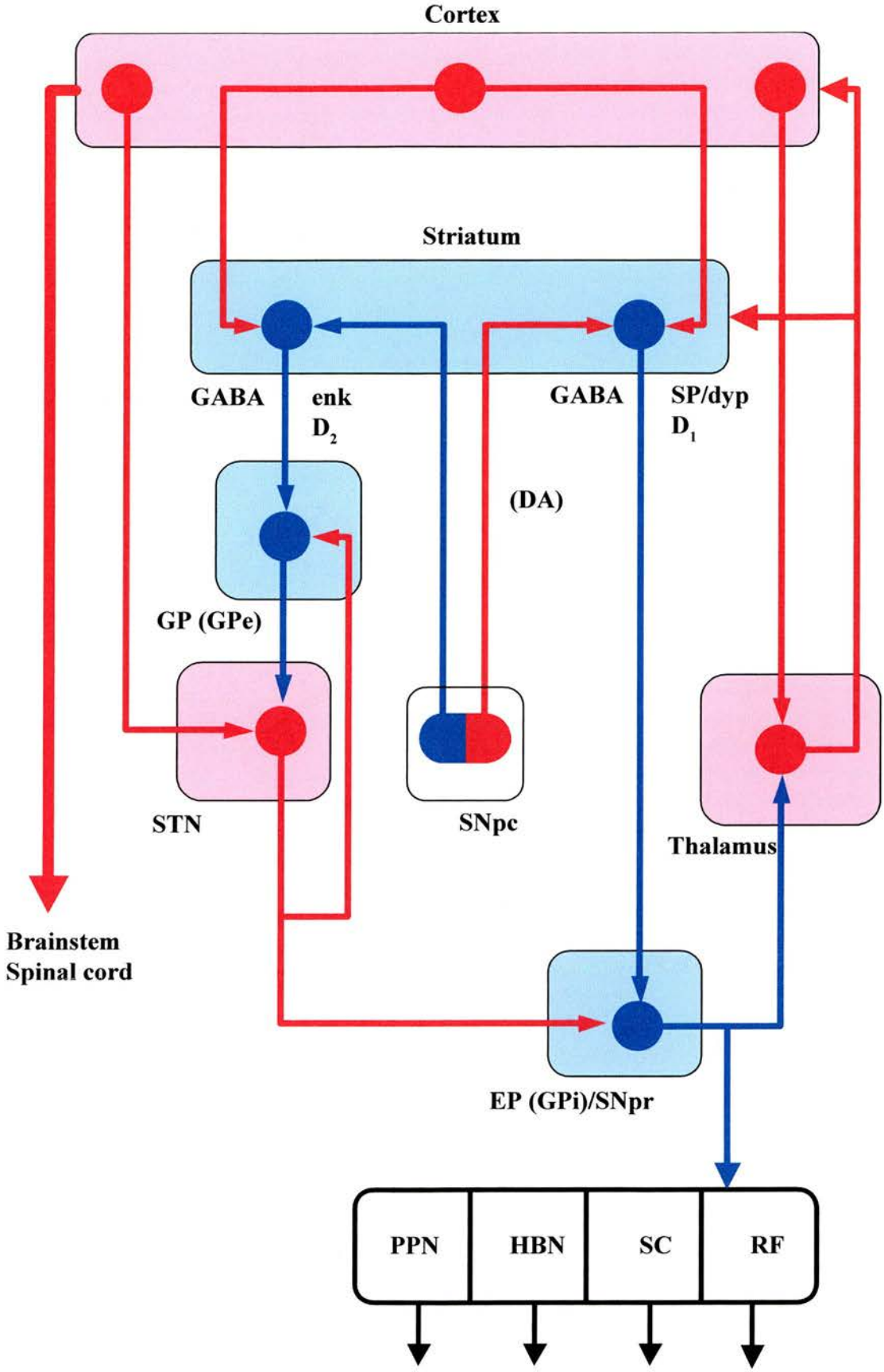
Cortex
Striatum
GABA
enk
D_2
GABA
SP/dyp
D_1
(DA)
GP (GPe)
STN
SNpc
Thalamus
Brainstem
Spinal cord
EP (GPi)/SNpr
PPN
HBN
SC
RF

results in reduced inhibition or disinhibition of the targets of the basal ganglia (Chevalier et al., 1985; Deniau and Chevalier, 1985), due to pauses in the tonic activity of output neurones (Hikosaka and Wurtz, 1983a, b). This increased activity of the direct pathway has been associated with the facilitation of movement (Alexander and Crutcher, 1990; DeLong, 1990). Activity in the indirect pathway opposes the end result of activation of the direct pathway. Increased activity in the indirect pathway (which by way of polysynaptic connections) affects the GP and the STN. The overall increased excitation of the STN, leads to an increased activity of the output nuclei thus inhibiting the targets of the basal ganglia (Alexander and Crutcher, 1990; DeLong, 1990). This increased inhibition has been linked with the cessation of movement as well as the suppression of nonselected movement (Alexander and Crutcher, 1990; DeLong, 1990). It's thought that the dopaminergic input from the substantia nigra pars compacta (SNpc) to the striatum, facilitates the flow of information via the direct pathway while having the opposite effect on the indirect pathway. The imbalance of information flow through these two pathways has been proposed to be the mechanism underlying movement disorders, with akinetic motor disorders such as Parkinson's disease favouring the indirect pathway and hyperkinetic motor disorders such as Huntington's chorea favouring the direct pathway (Bergman et al., 1990; DeLong, 1990).

Other pathways than those described above exist, leading to the renaming of the indirect pathway as an indirect network (reviewed by Smith et al., 1998). The GP and the STN are reciprocally connected (Rouzaire-dubois et al., 1980; Kita et al., 1983; Smith et al., 1990; Ryan and Clark, 1991; Maurice et al., 1998) as are the GP and the striatum (Shu and Peterson, 1988; Walker et al., 1989; Groenewegen et al.,

1993; Rajakumar et al., 1994a; Bevan et al., 1998). A projection also exists from the GP direct to the output structures of the basal ganglia (Haber et al., 1985; Smith and Bolam, 1990b; Haber et al., 1993; Bevan et al., 1996), which is formed by collaterals of the pallidosubthalamic projections (Kita and Kitai, 1994). These pathways by no means complete the circuitry of the basal ganglia but they illustrate the complexity of the functional organisation of the basal ganglia (Fig. 2.2).

In addition to the direct and indirect pathway, another input pathway exists. This third pathway transmits information from the cortex directly to the STN (Figs. 2.1, and 2.2). The STN, unlike the striatum receives a more restricted projection from the cortex which is mainly from the frontal lobe (Monakow et al., 1978), as well as somatotopically organised projections from the primary motor and supplementary premotor cortices (Kitai and Deniau, 1981; Nambu et al., 1996; Nambu et al., 1997). This glutamatergic corticosubthalamic projection (Monakow et al., 1978; Bevan and Bolam, 1995) is reflected in the short latency, excitatory responses in STN neurones following cortical stimulation (Kitai and Deniau, 1981; Ryan and Clark, 1991; Fujimoto and Kita, 1993; Maurice et al., 1998). This pathway called the hyperdirect pathway (Nambu et al., 2002), has been implicated in mediating the earliest excitatory response in the triphasic response of the EP and the SNpr following cortical stimulation (Kitai and Deniau, 1981; Ryan and Clark, 1991; Kita and Kitai, 1994; Maurice et al., 1999). This hyperdirect pathway conveys excitatory information from motor related cortical areas to the pallidum without involvement of the striatum and has a faster conduction time than both the direct and indirect pathways, thus playing an important role in information processing in the basal ganglia (Nambu et al., 2002). Thus context-dependent behaviour mediated by the

Figure 2. 2. Updated model of the flow of information through the basal ganglia.

The figure illustrates the new anatomical connections that have been revealed, after the basic circuitry was described by Albin (Albin, 1989) (see Fig. 1). As before red line indicate excitatory connections while blue lines highlight inhibitory connections. Interneurones (●) in the striatum play a major role in striatal function and strongly modulate the behaviour of the output cells. These interneurones get input from various cortical regions and can potentially inhibit large numbers of striatal neurones (see Chapter 6). They are also selectively innervated by the globus pallidua (GP). The figures also illustrates the connectivity of the GP directly to the output structures of the basal ganglia as well as a projection to the reticular thalamus (RT). Modified from Fig. 12 in Smith et. al., 1998.

(D_1 – D_1 dopamine receptors, D_2 – D_2 dopamine receptors, DA – dopamine, dyp - dynorphin, enk – enkephalin, EP – entopeduncular, GPe - external segment of the globus pallidus, GPi - internal segment of the globus pallidus, HBN - lateral habenular nucleus, PPN - pedunculopontine nucleus, SC - superior colliculus, SNpc - substantia nigra pars compacta, SNpr - substantia nigra pars reticulata, SP - substance P, STN - subthalamic nucleus, RF - parvicellular reticular formation)

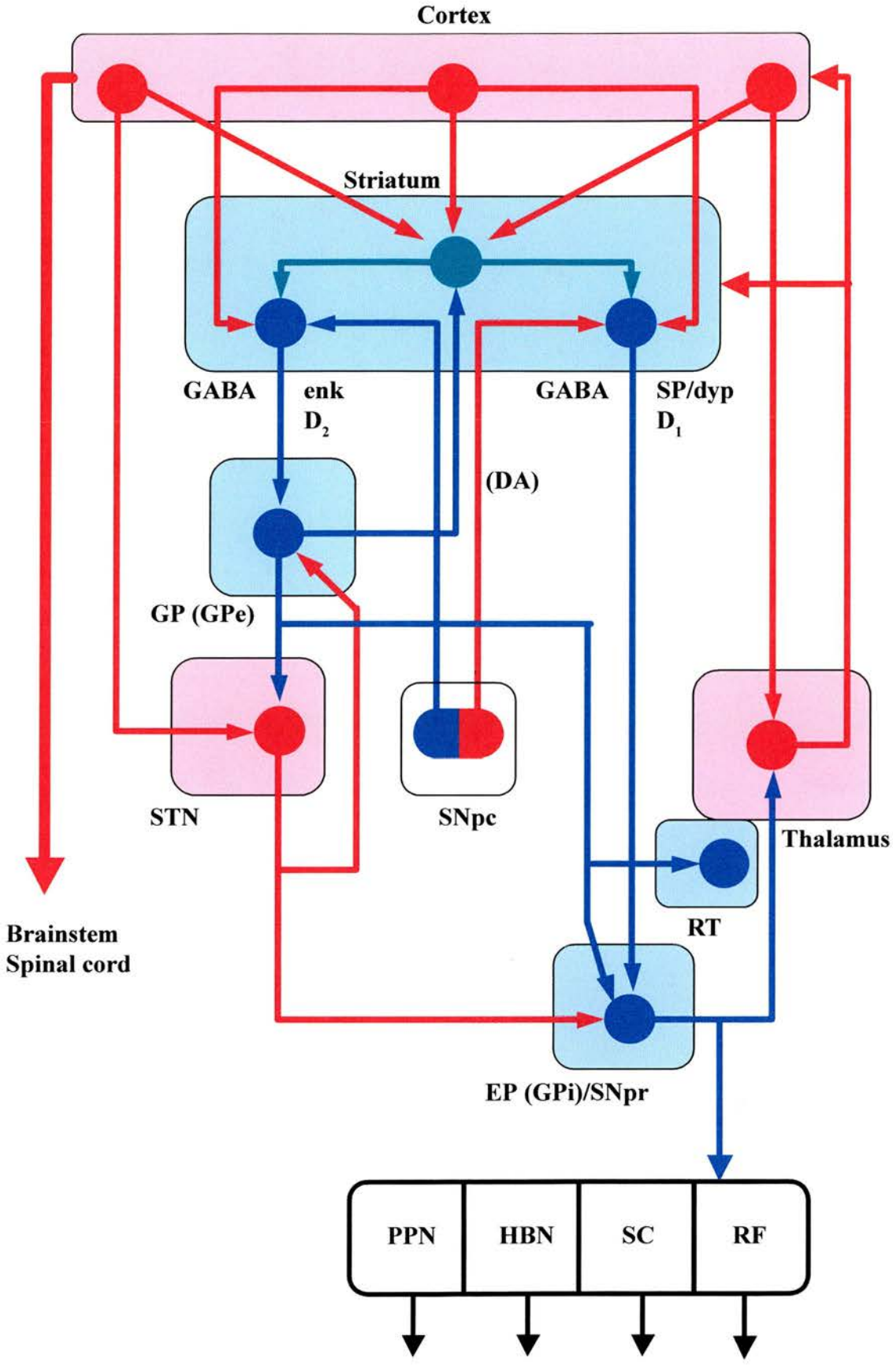
Cortex
Striatum
GABA
enk
D2
GABA
SP/dyp
D1
(DA)
GP (GPe)
STN
SNpc
Thalamus
RT
Brainstem
Spinal cord
EP (GPi)/SNpr
PPN
HBN
SC
RF

basal ganglia involves spatial and temporal coordination of information flowing through all 3 pathways. This chapter will focus mainly on the input pathways mediated through the striatum.

2.1.2) Organisation of the striatum

Cortical information that ultimately results in the generation of movement has to be channelled via the 2 striatal output systems. The majority of the striatal cell population (90-95%) is made up of medium sized densely spiny striatal neurones (referred to as striatal neurones from here on) (Bolam and Bennett, 1995). These neurones have a cell body of approximately 20-25 μm in diameter from which dendrites containing spines radiate out (Kemp and Powell, 1971; Wilson and Groves, 1980). These striatal neurones are the major targets of extrinsic afferents. Excitatory inputs from the cortex and the thalamus form asymmetric synapses mainly on the heads of the spines (Kemp and Powell, 1971; Frotscher et al., 1981; Somogyi et al., 1981a; Dube et al., 1988; Smith et al., 1994). The striatum also receives a massive dopaminergic input from the ventral tegmental area (VTA) substantia nigra (SN) and retrorubal area (Freund et al., 1984; Jimenez-Castellanos and Graybiel, 1987). These inputs form symmetrical synapses on the necks of spines and on interspine dendritic shafts (Smith et al., 1994) and play an important role in modulating the responsiveness of striatal neurones to cortical and thalamic inputs. Striatal neurones also receive projections from the amygdala (Fuller et al., 1987; Kita and Kitai, 1990; McDonald, 1991a, b) as well as serotonergic projections from the raphe (Soghomonian et al., 1989). Spiny neurones also give rise to extensive local axon collaterals that arborise close to their dendritic field and are synaptically connected with other spiny neurones (Wilson and Groves, 1980; Somogyi et al., 1981a). Striatal

interneurones, of which there are 3 immunohistochemically distinct groups, also modulate striatal neurones (Kawaguchi, 1993; Kawaguchi et al., 1995; Kawaguchi, 1997). These interneurones have been implicated in the feedforward control of cortical information to spiny striatal neurones (Pennartz et al., 1991; Jaeger et al., 1994; Plenz and Kitai, 1998). These striatal neurones are also the main output cells and they utilise gamma-aminobutyric acid (GABA) as their neurotransmitter, thus inhibiting their targets The topography of the inputs to a striatal cell is summarised in Fig. 2.3.

Striatal neurones can be differentiated into 2 groups based primarily on their targets (Fig. 2.4). Striatopallidal neurones project to the GP and are part of the indirect pathway, while striatonigral neurones project to the EP and SNpr and form the direct pathway. Many neurones extend axons to each of the target nuclei (Kawaguchi et al., 1990), thus the relative extent of arborisation in a particular target provides the basis for defining the two output nuclei (Gerfen, 1992). Striatopallidal neurones tend to have dense arborisations in the GP and minimal axonal collaterals in the EP and SNpr, while striatonigral neurones have the majority of their axon collaterals in the EP and SNpr with sparse arborisation in the GP (Kawaguchi et al., 1990; Parent et al., 1995; Wu et al., 2000). Quantitative studies have shown that the number of cells belonging to either group is approximately the same and the cells are present in equal numbers in the patch and matrix compartments (Loopuijt and van der Kooy, 1985; Gerfen, 1992). Both neuronal types are also synaptically connected with other neurones of the same type as well as with neurones belonging to the other group (Somogyi et al., 1982; Aronin et al., 1986; Bolam and Izzo, 1988; Yung et al., 1996).

Figure 2. 3. Inputs to a striatal neurone.

The figure is a schematic showing the topography of the various inputs to a spiny projection neurone. Inputs coming from the cortex and thalamus, which use glutamate as the neurotransmitter, make excitatory asymmetric connections onto the heads of spines (red). A dopaminergic projection arising from mid-brain dopamine (DA) neurones synapses onto the necks of spines and onto the dendritic shafts (blue). Structures containing substance P (SP) (light blue) and enkephalin (enk) (orange) and GABA (purple) arise from other spiny neurones and contact neurones in proximal parts of the dendrites well as the cell body. The GABAergic projection is also a contribution from parvalbumin positive GABAergic interneurones which form a basket like arborisation pattern on the cell body of striatal neurones (purple). Inputs from large cholinergic interneurones, which utilise acetylcholine (ACh), terminate in an intermediate position (green). All these inputs interact to influence the output of these projection neurones. Modified from Fig. 3 in Smith and Bolam (1990).

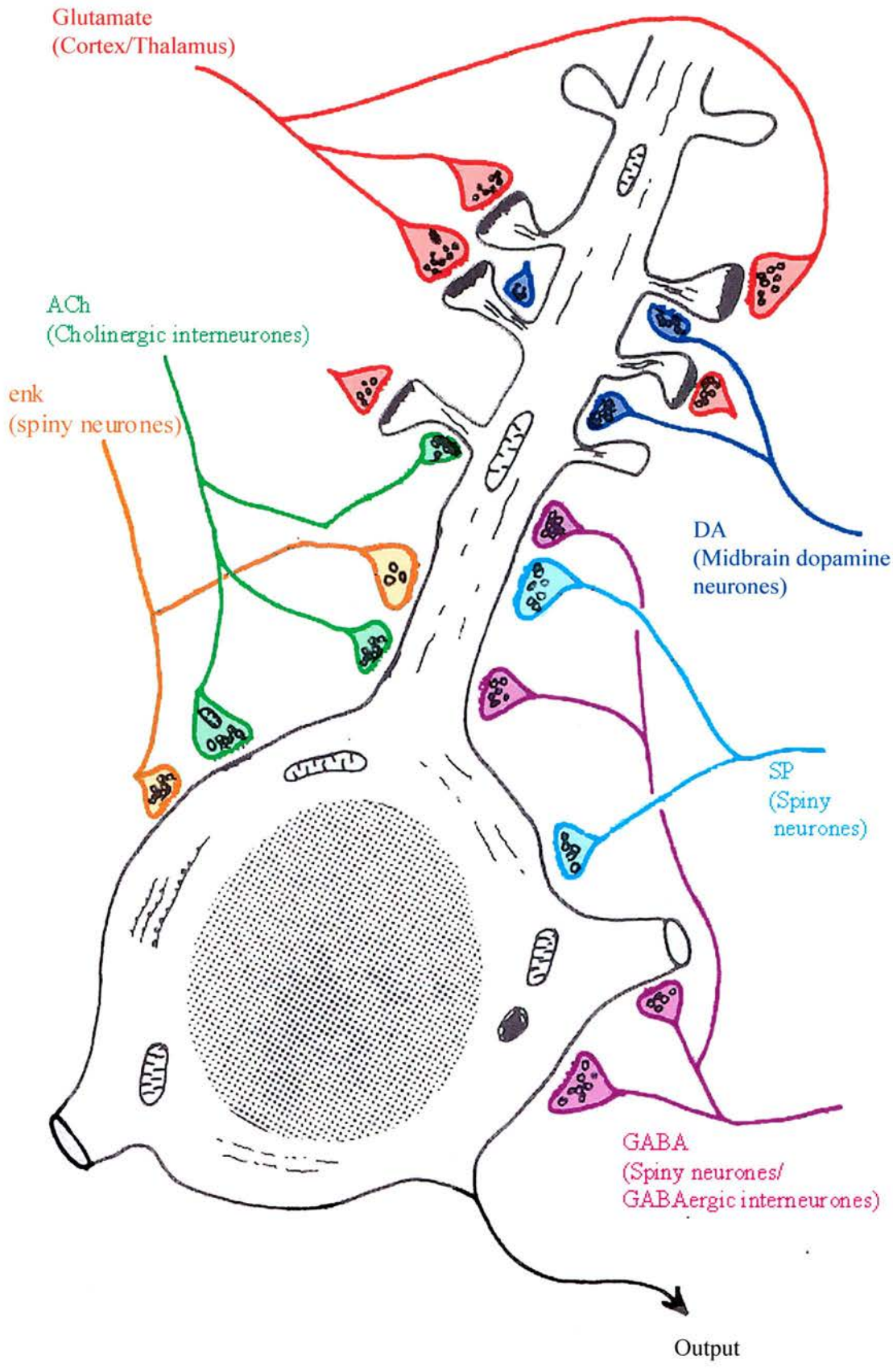
Glutamate
(Cortex/Thalamus)
ACh
(Cholinergic interneurones)
enk
(spiny neurones)
DA
(Midbrain dopamine
neurones)
SP
(Spiny
neurones)
GABA
(Spiny neurones/
GABAergic interneurones)
Output

Figure 2. 4. Segregation of the striatal output pathways.

The figures illustrate the segregation of the striatum into two outputs pathways, the direct (STRN-striatonigral) and indirect (STRP-striatopallidal) pathway.

A In the traditional view there are two groups of striatal neurones. The striatonigral neurones are part of the direct pathway and project exclusively to the entopeduncular (EP) and the substantia nigra pars reticulata (SNpr). These cells express both substance P (SP) and D_1 dopamine receptors. The second group consists of cells that send their axon collaterals to the globus pallidus (GP). These striatopallidal neurones contain enkephalin (enk) and have the D_2 dopamine receptors.

B Taking recent evidence into consideration, there is no clear segregation of striatal cells to the two output pathways. All striatal cells send axon collaterals to the GP, meaning that there are no neurones that project exclusively to the SNr and EP. Also approximately a quarter of striatal neurones express both SP and enk. Most cells also contain both subtypes of dopamine receptors though the mRNA is found in differing amounts and is reflected in the diagrams by the size of the lettering. Values are obtained from (Wu et al., 2000, Surmeier et al., 1996).

A

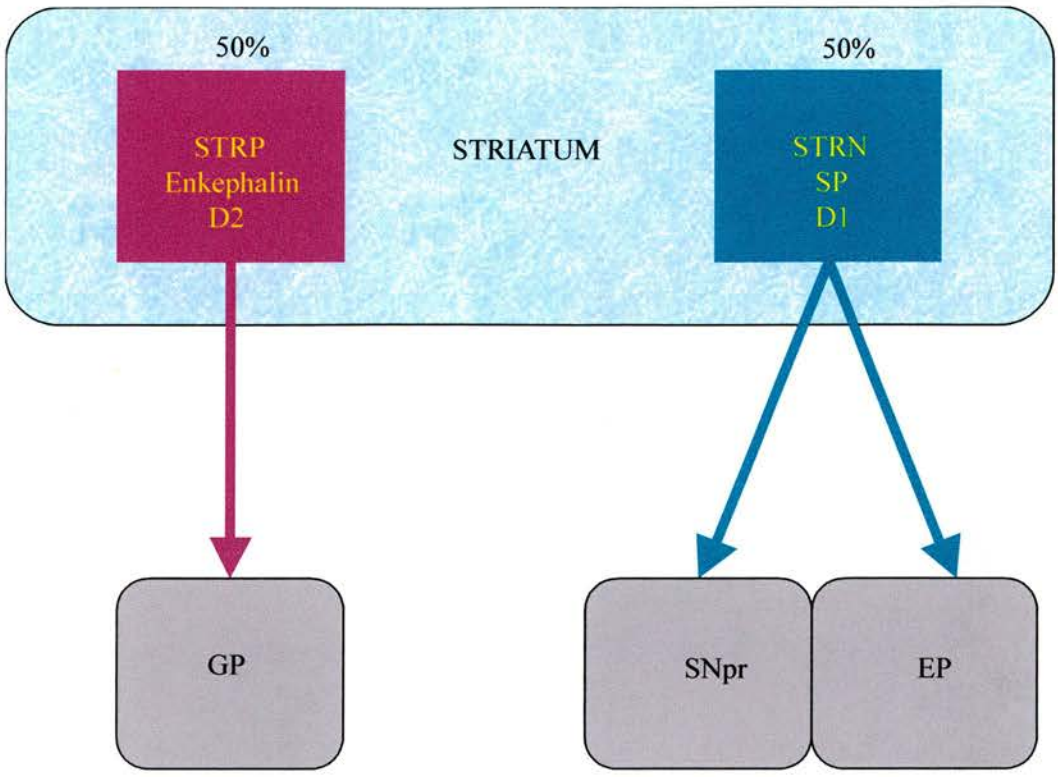
50%
50%
STRP
Enkephalin
D2
STRIATUM
STRN
SP
D1
GP
SNpr
EP

B

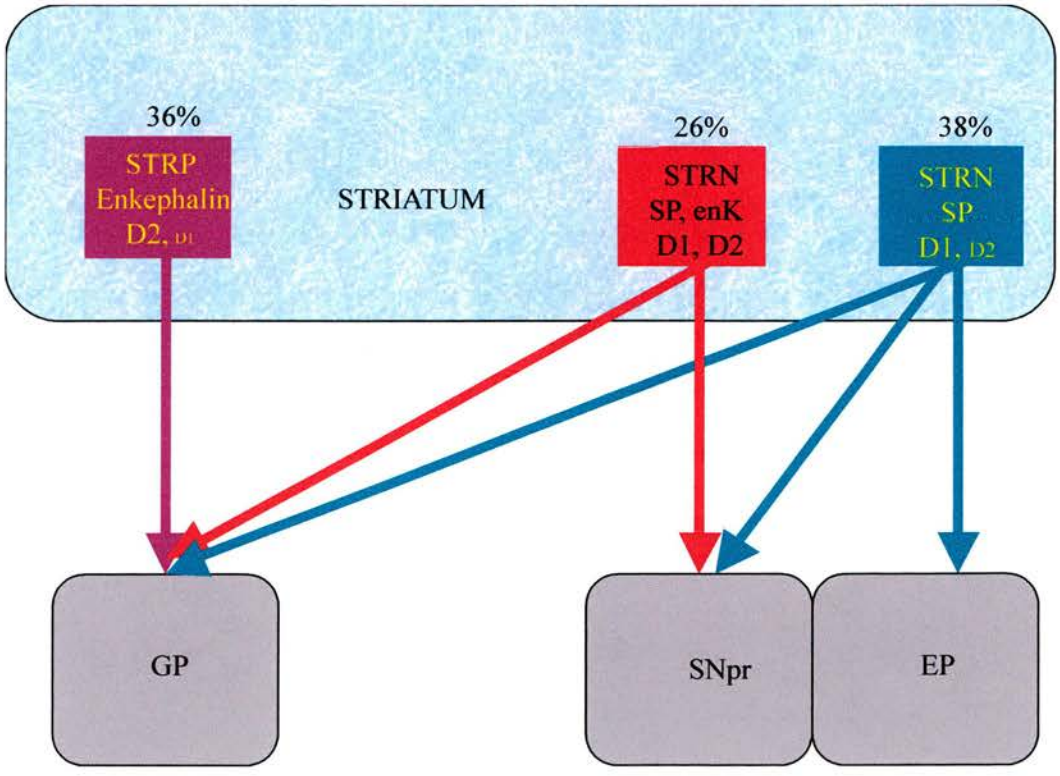
36%
26%
38%
STRP
Enkephalin
D2, D1
STRIATUM
STRN
SP, enK
D1, D2
STRN
SP
D1, D2
GP
SNpr
EP

These 2 classes of striatal neurones can also be differentiated on the basis of their neuropeptides (Fig. 2.4). All medium sized densely spiny neurones contain glutamic acid decarboxylase (GAD), the synthetic enzyme for GABA (Penny et al., 1986; Kita and Kitai, 1988). Enkephalin is another neuropeptide closely associated with striatal neurones. Enkephalin activates μ and δ opioid receptors (Steiner and Gerfen, 1999). The overall function of the striatal enkephalin system is still unclear as there have been contradictory studies showing this system to dampen as well as enhance activity of the nigrostriatal pathway (Heimer et al., 1991; Schad et al., 1995; Chatterjie et al., 1998; Gerfen et al., 1998; Steiner and Gerfen, 1998; Rawls and McGinty, 2000). Enkephalin containing neurones project mainly to the GP (Gerfen and Young, 1988; Gerfen, 1992; Gerfen and Wilson, 1996). Striatonigral neurones however, contain substance P (SP) and dynorphin (Gerfen and Young, 1988; Gerfen, 1992; Gerfen and Wilson, 1996). Substance P modulates ionic conductances, the mechanisms of which are dependent on the neuronal type (Bley and Tsien, 1990; Shen and North, 1992; Bertrand and Galligan, 1994). In the striatum, SP facilitates the release of acetylcholine and increases the firing of neurones (most likely interneurones) by affecting tetrodotoxin-insensitive cation channels (Aosaki and Kawaguchi, 1996). Striatopallidal and striatonigral neurones can also be differentiated based on their expression of dopamine receptors (Fig. 2.4).

2.1.3) Dopamine in the striatum

Dopamine plays a key role in basal ganglia function, where it is involved in both pre- and post- synaptic mechanisms. Dopamine has been implicated in pathologic conditions such as Parkinson's disease, Huntington's disease and schizophrenia. The striatum is innervated by dopamine synthesising neurones of the SNpc.

Dopaminergic neurones in the ventral tier of the SNpc preferentially project to patches, while dorsal tier dopamine neurones project to the matrix (Gerfen et al., 1987; Jimenez-Castellanos and Graybiel, 1987; Hanley and Bolam, 1997). These two groups of dopamine neurones while having very different neurochemistry (Gerfen et al., 1987; Lavoie and Parent, 1991) and anatomy (Tepper et al., 1987), have a similar pattern of innervations in the patch and matrix (Hanley and Bolam, 1997) suggesting that dopaminergic modulation of cortical information is similar in both compartments.

Dopamine acts on striatal neurones via dopamine receptors which have differing biochemical activities and distributions (Gingrich and Caron, 1993). Dopamine receptors belong to the family of 7 transmembrane domain G-protein coupled receptors. The C terminus contains sites that allow modifications such as phosphorylation and palmitoylation and is thought to be involved in agonist-dependent receptor desensitisation (Bates et al., 1991; Ng et al., 1994). Based on pharmacology, physiology and anatomy, 2 main subfamilies, D_1 and D_2 like dopamine receptors have been identified. Five distinct genes code for individual receptors and the D_1 subfamily comprises of D_1 and D_5 receptors and D_2, D_3 and D_4 receptors comprise the D_2 subfamily (Missale et al., 1998).

The effects of dopamine mediated through its receptors is via a modulation of both the adenosine- 3', 5'- cyclic monophosphate (cAMP) pathway and calcium (Ca^{2+}) signalling. The D_1 subfamily activates adenylate cyclase (Dearry et al., 1990; Monsma et al., 1990; Zhou et al., 1990; Sunahara et al., 1991; Jackson and Westlind-Danielsson, 1994) and the stimulation of this receptor results in the activation of protein kinase A (PKA), which results in phosphorylation of proteins involved in the

regulation of ion channels as well as desensitisation of other G coupled receptors, which modulate the response of cells to neurotransmitter release (Choi et al., 1993). Conversely, the D_2 subfamily has an inhibitory effect and in some cases no effect on adenylate cyclase (De Camilli et al., 1979; Onali et al., 1981; McDonald et al., 1984; Onali et al., 1985) with D_2 receptors inhibiting cAMP more efficiently than D_3 receptors (Missale et al., 1998). Dopamine receptors also modulate intracellular Ca^{2+} levels by various mechanisms. D_1 receptors affect the activity of Ca^{2+} channels. In striatal neurones D_1 agonists increase Ca^{2+} currents via L-type Ca^{2+} channels while reducing N and P type Ca^{2+} currents (Surmeier et al., 1995) via a direct or indirect action of PKA. There have been inconclusive findings on the role of D_1 receptors in the mobilisation of intracellular Ca^{2+} stores by activation of phosphoinositide (PI) hydrolysis (Missale et al., 1998). D_2 receptors modulate intracellular Ca^{2+} concentration stores by reducing the L-type Ca^{2+} currents in striatal cholinergic interneurones (Yan et al., 1997) while the effect on P1 hydrolysis is still unclear (Missale et al., 1998). The effects of dopamine receptors on potassium channels (K^+) has also been investigated. Activation of D_1 receptors inhibits a K^+ current in rat striatal neurones (Kitai and Surmeier, 1993) while increasing the K^+ current in chick retinal cells via a cAMP-independent mechanism (Laitinen, 1993). D_2 like receptors increase outward K^+ currents in striatal neurones (Kitai and Surmeier, 1993; Greif et al., 1995) resulting in membrane hyperpolarisation. Both subfamilies of dopamine receptors play a role in arachidonic acid (AA) synthesis. In striatal neurones D_1 receptors have been shown to inhibit Ca^{2+} evoked AA release, while D_2 receptors potentiate AA release (Schinelli et al., 1994). The two subfamilies of receptors have different and in some cases opposing signal transduction mechanisms. Thus the

response of a cell to dopamine will be determined by the receptors expressed by the cell. The effects of dopamine on the response of striatal neurones will be further discussed in Chapter 5.

Both subfamilies of dopamine receptors are highly expressed in the basal ganglia. Electron microscopic observations have shown that D_1 and D_5 receptors have both pre- and post- synaptic localisation, though the latter is more commonly observed (Hersch et al., 1995). D_1 and D_5 receptors are found at postsynaptic densities of dopamine terminals as well as presynaptically on axons forming asymmetrical synapses, while D_1 receptors are present postsynaptic to asymmetrical synapses (Levey et al., 1993; Bergson et al., 1995; Hersch et al., 1995; Yung et al., 1995; Yung et al., 1996). While there is strong immunostaining for D_1 receptors in the striatum, EP and the SNR (Gerfen et al., 1990; Le Moine et al., 1991; Gerfen, 1992; Hersch et al., 1995; Yung et al., 1995; Yung et al., 1996), no D_1 receptor mRNA has been detected in the latter 2 structures (Dearry et al., 1990; Fremeau et al., 1991), suggesting that the dopamine receptor immunoreactivity present is due to the projection from the striatum. D_1 receptors are preferentially localised on striatal neurones expressing SP (i.e. striatonigral neurones that are part of the direct pathway) (Gerfen et al., 1990; Le Moine et al., 1991). D_2 receptors have also been found in the striatum. These receptors are concentrated more in the spines and dendrites than the cell body and are often found presynaptic on symmetrical synapses (Levey et al., 1993; Hersch et al., 1995; Yung et al., 1995; Yung et al., 1996). D_2 receptors are preferentially expressed by striatal GABAergic neurones that contain enkephalin (i.e. striatopallidal neurones which are part of the indirect pathway) (Gerfen et al., 1990).

2.1.4) Segregation of the striatonigral and striatopallidal pathways

In the traditional view, the striatofugal pathway is clearly divided into 2 groups, with the striatonigral neurones, expressing D_1 receptors, SP and dynorphin and sending their axons to the output nuclei of the basal ganglia and the striatopallidal neurones expressing D_2 receptors and enkephalin and sending their axons to the globus pallidus (Fig. 2.4).

As mentioned earlier striatofugal cells do send axon collaterals to more than one target (Kawaguchi et al., 1989; Parent et al., 1995). Recent work by Wu and Parent shows that striatal neurones display a high degree of axonal collateralisation (Wu et al., 2000). Using juxtacellular labelling, the investigators discovered that approximately a quarter of striatofugal neurones send projections to the GP and SNpr (type II, in the study), while the remaining cells were equally divided into cells that projected to the GP alone (type I, in the study) and cells that projected to the GP, EP and SNpr (type III, in the study) (Wu et al., 2000). Based on their data, all striatofugal cells send fibres to the GP and there are no cells that exclusively project to the output nuclei of the basal ganglia. Supporting this are the recent immunohistochemical experiments which have demonstrated both dynorphin and SP immunoreactivity in boutons within the GP (Sadek et al., 2002), providing further evidence that the direct/indirect pathway organisation of the striatofugal system is not as clear-cut as originally proposed (Fig. 2.4).

There is also much controversy surrounding the distribution of dopamine receptors in the striatum. While anatomical and *in situ* hybridisation support a segregation of D_1 and D_2 receptors (Le Moine et al., 1991; Gerfen, 1992; Levey et al., 1993; Hersch et al., 1995; Yung et al., 1995), electrophysiological and molecular

biological data strongly suggest that the two receptors are colocalised (Uchimura et al., 1986; Surmeier et al., 1992b; Cepeda et al., 1993; Surmeier et al., 1993; Surmeier et al., 1996) (Fig. 2.4).

2.1.5) Corticostriatal input to the two striatal pathways

Cortical input to the striatum has been studied extensively, both physiologically and anatomically. While studies have looked at cortical projections giving rise to the patch and matrix distribution (Graybiel and Ragsdale, 1978; Ragsdale and Graybiel, 1981; Gerfen, 1984; Donoghue and Herkenham, 1986; Gerfen, 1989; Berendse et al., 1992), there have been few reports on the cortical projections connecting to the output pathways of the striatum. To date, one paper has directly addressed ipsilateral and contralateral motor cortical input to the 2 subtypes of striatal projection neurones (Hersch et al., 1995). They found that ipsilateral corticostriatal afferents synapsed more often with D_1 immunopositive than D_2 immunopositive spines, while contralateral corticostriatal afferents made no such distinction and tended to form more axodendritic synapses (Hersch et al., 1995). Most corticostriatal projections have a contralateral projection, which tends to be less extensive (Kunzle, 1975; Wilson, 1987; Canteras et al., 1988; McGeorge and Faull, 1989). While the function of this contralateral projection is still uncertain, anatomical and biochemical data suggests that contralateral cortical areas provide an important cholecystokinin input to the striatum (Herrera-Marschitz et al., 1992; Morino et al., 1992; Morino et al., 1994; You et al., 1994).

The barrel cortex is an ideal system to further study the connectivity of the ipsilateral and contralateral cortical projections to the two output pathways of the striatum. The barrel cortex gives rise to 2 pathways, one of which is strictly

ipsilateral while the other is bilateral (Wright et al., 1999). Both types of fibres have different morphologies and different patterns of innervation in the striatum (Alloway et al., 1998; Alloway et al., 1999; Wright et al., 1999). The ipsilateral pathway which originates from cells below the barrels, has thicker axons that are visible at magnifications of x 40 and below, while the bilateral pathway that arises from the cells below the septa, gives rise to fibres that are present bilaterally and have thin calibre axons that are visible only at magnifications higher than x 40 (Wright et al., 1999). For a detailed description of the inputs to these two cortical domains and their pattern of arborisation in the striatum, refer to Chapter 3.

2.1.6) Aim

While the initial experiments looking at the ultrastructure of both fibre types arising from the barrel cortex identified their targets as the spines of medium sized densely spiny striatal projection neurones (Wright et al., 1999), no attempt was made to identify the type of neurone (i.e. striatopallidal vs. striatonigral). The aim of this study was to determine the connectivity of the projections from the barrel cortex to the 2 output pathways of the striatum. To do this cortical afferents from the barrel cortex were labelled by anterograde tracers. A D_1 receptor antibody was used to identify a subset of striatal neurones that belong to the direct pathway as these cells have been shown to preferentially express D_1 receptors (Gerfen et al., 1990; Le Moine et al., 1991). The contacts made by both fibre types onto immunoreactive structures was studied.

2.2) Experimental Procedures

2.2.1) Preparation of animals

Eight adult male Sprague Dawley rats (200-350g, Harlan Olac, Bicester, UK) were used in the present study. They were maintained on a 12 hour light/12 hour dark cycle with free access to food and water. Procedures involving animals were carried out in strict accordance with the Animals (Scientific Procedures) Act, 1986. They were anaesthetised by halothane in O_2. Stable levels of anaesthesia were maintained throughout the surgical procedure to ensure the absence of a foot withdrawal reflex. Each rat was placed in a stereotaxic frame and the head was secured in the frame via ear and tooth bars. The scalp was cut from the anterior of the Bregma to the base of the skull and the overlaying tissue was pulled back and clamped. The skull surface was cleaned to reveal the Bregma and the midline. Rostrocaudal and mediolateral co-ordinates for the placement of the neuronal tracers were calculated using Bregma as a reference point and the stereotaxic co-ordinates were derived from the atlas of Paxinos and Watson (Paxinos and Watson, 1986). Access to the brain was made using a hand held dental drill and bit to create a burr hole. Drilling was stopped to leave a thin transparent layer of bone overlaying the brain. This was gently picked away to prevent accidental damage to the cortical surface and to ensure that no skull fragments entered the cortex. A hole was created in the dura to expose the cortical surface to facilitate the passage of the glass micropipette and to prevent the tip becoming blocked by adhering dura. The animals received unilateral deposits of Biotinylated dextran amine (BDA; 5% in 0.9% NaCl; Molecular Probes, U.S.A.) in the primary somatosensory cortex (S1). Electrodes were inserted 800 μm into the cortex which corresponded to the region of the cortex that contained the barrel field.

The anterograde tracers were delivered by iontophoresis via glass micropipettes. Positive cathodal current (5-10 μA), pulsed 7 s on and 7 s off was passed for 5-10 min. After careful withdrawal of the micropipette, the skin overlying the exposed cranium was drawn together and sutured. The animals were kept warm and after recovery from the anaesthetic they were returned to their home cages. A schematic diagram of the experimental set up is shown in Figure. 2.5.

2.2.2) Perfusion fixation

Following a survival time of 14 days, the rats were deeply anaesthetised with sodium pentobarbital (Sagatal, 200 mg/kg; Rhône Mérieux, Tallaght, Dublin). Saline containing heparin (2000 units/l) was perfused through the aorta at approximately 30 ml/min for 1 min followed by 300 ml of 0.1% glutaraldehyde and 3% paraformaldehyde in 0.1M phosphate buffer (PB, pH 7.4), at the same rate. Following fixation, the brain was removed from the skull and stored in phosphate buffered saline (PBS) at 4°C prior to further processing. Coronal sections including tracer injection sites, and transport sites in both striata were cut on a vibrating microtome at 70 μm. All sections were washed several times in PBS.

2.2.3) Preparation of tissue for electron microscopy

2.2.3.1) Localisation of anterograde tracer

All striatal sections were processed for electron microscopy. To increase the penetration of reagents, the sections were freeze-thawed in isopentane (BDH, UK) cooled in liquid nitrogen for up to 3 times. The sections were washed 12 times in PBS (10 min, each) before the tracer and D_1 receptors were revealed as described below. Injected and transported BDA was revealed by incubation overnight at room

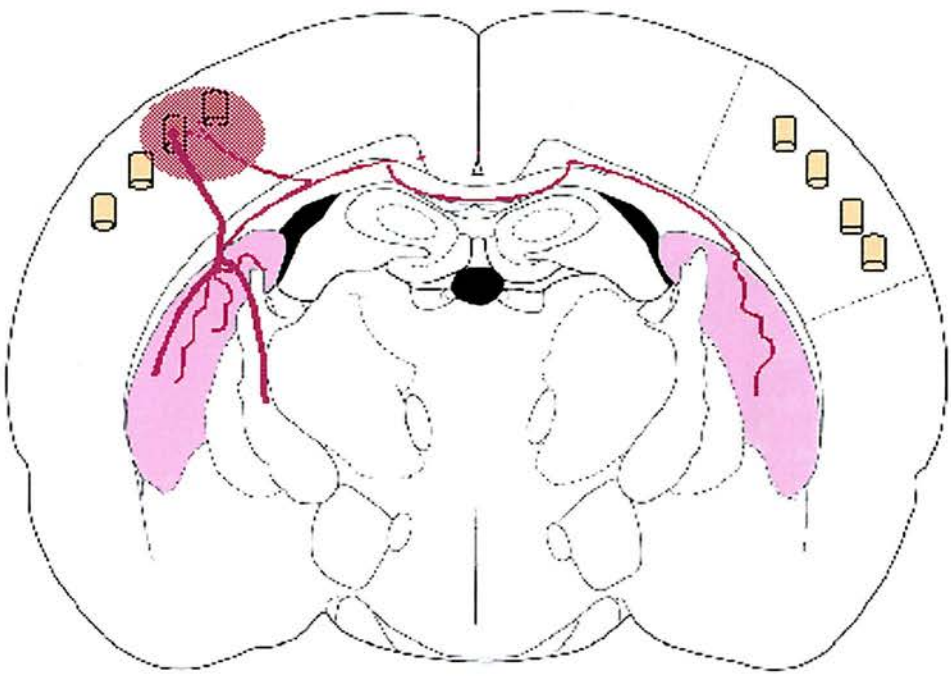

Figure 2. 5. Experimental set up.

Schematic representation (modified from Paxinos and Watson 1996) of the experimental protocol which highlights the different corticostriatal pathways arsing from the barrel cortex. Injections of BDA (⬭) into the barrel cortex fills both the barrel centres and septal cells. This gives rise to two types of anterogardely labelled corticostriatal fibres (brown lines) which are easily distinguished by their morphology. Fibres that arise from cells below the barrels give rise to thick (thick brown lines) calibre axons that are only found ipsilaterally and have a topographic projection in the striatum that follows the curvature of the corpus callosum. Fibres that arise from cells below the septa are thinner (thin brown lines) and are found bilaterally. This projection does not have a topographic projection in the striatum. The striatum is then reacted with the appropriate antibodies, which highlight D_1 dopamine receptors (⬭) , enabling the connectivity of the two input pathways to be studied with regard to the two output pathways of the striatum.

temperature in an avidin-biotin-peroxidase complex (ABC; 1:100 in PBS, Vector Labs, UK). Sections were washed and equilibrated in Tris buffer (0.05M, pH 7.6) for 5-10 min. This was followed by an incubation in a solution containing diaminobenzidine (DAB, 25 mg/100 ml Tris buffer; Sigma, Dorset, UK) and 0.006% hydrogen peroxide for 10-15 min. The reaction was terminated by rinsing several times in Tris buffer.

2.2.3.2) Immunocytochemistry for D_1 group of dopamine receptor

Striatal sections were then reacted with antibodies against D_1 receptors for 48 h at 4^0C with gentle agitation (1:1000 in PBS). Reaction with goat-antimouse IgG (1:200 in PBS, Jackson Immunoresearch, West Grove, PA, USA) for 2 h at room temperature was carried out followed by an ABC reaction (1:100 in PBS, Vector Labs, UK). Sections were washed and equilibrated in Tris buffer (0.05M, pH 7.6) for 5-10 min. The bound peroxidase was then revealed with DAB (25 mg/100 ml Tris buffer; Sigma, Dorset, UK) in the presence of nickel ions (nDAB).

The double-labelled sections of the striatum were placed flat at the bottom of a petri dish and post fixed in 1% osmium tetroxide (Oxkem, UK), 5% βD-Glucose (BDH Labs, Poole, UK) in 0.1M PB at pH 7.4 for 60-70 min, to maintain colour separation (Acsady et al., 1996). The sections were dehydrated through a graded series of dilutions of acetone (with 1% uranyl acetate in the 70% solution) and infiltrated with resin overnight (Durcupan, Fluka Chemicals, UK). They were then mounted in resin on greased glass microscope slides and polymerised in a 60°C oven for 48 h.

2.2.3.3) Controls

Brains from 4 out of the 8 animals, were used in control experiments. These animals had received unilateral deposits of BDA in the barrel cortex but were not used for EM, as it was later revealed that the injections were too small, due to the blockage of the electrode. This resulted in injection of the tracer in a single barrel without the involvement of the septa and thus there was no contralateral labelling (Wright et al., 2001). The brains from these animals were processed to reveal BDA as described above. Some of the striatal sections were then used as controls for D_1 receptor immunohistochemistry. These sections were processed as described above, but the D_1 antibody was omitted. The remainder of the sections were processed for D_1 immunohistochemistry as described above. All sections from the four animals were processed for light microscopy. The sections were well rinsed in PBS before being mounted on subbed slides. The slides were oven dried for 1 week. The sections were dehydrated in ethanol in the following concentrations (70%, 90%, 95%, 100%, 100%, 100%, 5 min each), cleared in xylene (10 min) and coverslipped with DPX (BDH Laboratory Supplies).

2.2.4) Analysis of material

All sections of the striatum that contained both the anterograde tracer and D_1 immunoreactivity revealed by distinct chromogens were examined at the light microscope level. Both striata containing fibres were examined and the type of fibre identified. Fibres of the ipsilateral (topographic) pathway (which will be referred to as thick fibres) could be seen at the light microscope level under the x40 objective lens and generally followed the curvature of the corpus callosum. The diameter of thick fibres was greater than 0.18 μm. Fibres of the bilateral (diffuse) pathway (which will be referred to as thin fibres) were only clearly visible at higher

magnifications (x100 objective lens) even though the varicosities were visible at lower magnifications and tended not to follow any orientation. The diameter of thin fibres was less than 0.14 μm (see below and results). Although there was some overlap in the classification, fibres that clearly fell into one of the groups were chosen for the study. In the ipsilateral striatum where both types of fibres were present, thin fibres which were chosen for the correlated light and electron microscopic study were picked from areas which contained both fibres types. Once the fibres were classified, the varicosities which were to be studied were identified and numbered and these were examined at different focal planes and confirmed to be in striatum where there was strong D_1 immunoreactivity. The position of the fibres in the striatum was drawn using a drawing tube and the fibres of interest were drawn and photographed at high magnification and examined by correlated light and electron microscopy. The coverslip overlying the tissue was removed using a razor blade. The area of interest was cut from the microscope slide and glued to the top of a blank cylinder of resin using cyanoacrylate glue. Serial ultrathin sections of 40-60 nm thickness were cut on a Reichert-Jung Ultracut E ultramicrotome (Leica) and collected on Pioloform-coated single slot copper grids. The ultrathin sections were then contrasted with lead citrate for 2-3 min and examined in either a Philips CM 10 or 12 electron microscope.

2.2.5) Statistical analysis of material

Once a bouton identified at the electron microscope level was correlated with the light micrographs, the number and type of contact (simple vs. complex) made by the bouton was recorded. A synapse was classified as complex if there was a discontinuity in the postsynaptic density. The immunoreactivity of the structure

making contact with the labelled bouton was then ascertained. Immunoreactivity was determined by the presence of electron dense reaction product in the structure. Figure 2.13F illustrates a spine that displays strong immunoreactivity and there is a dense accumulation of reaction product that is membrane bound and confined to the spine. In comparison Figure 2.11E illustrates an immunonegative spine that does not contain any reaction product. A structure was considered to be immunopositive when 75% of its serial sections showed some degree of immunoreactivity. If only one section from the entire series appeared to display immunoreactivity, the bouton was excluded from analysis. As a D_1 immunonegative structure could reflect the lack of penetration of immunohistochemical reagents, rather than lack of D_1 receptors, sections containing the profile of a labelled bouton were scanned to ensure that there was D_1 immunoreactivity in surrounding structures. All electron micrographs were also viewed by an observer who was kept blind to the type of fibre. If the classification of the dendritic spine as being immunoreactive or not was different from my classification, the spine was excluded from statistical analysis. In addition to the marked boutons, the diameter of the fibres was also measured. Three electron micrographs were taken along the length of a fibre (no synaptic vesicles present) and the average diameter of the fibre was calculated. Fishers exact test was used to compare the proportion of contacts onto immunopositive structures made by thick and thin fibres. The probability level for statistical significance was set at $p < 0.05$. The values obtained from the thin fibres from both striata were pooled unless otherwise stated.

2.3) Results

2.3.1) Light microscopic observations

2.3.1.1) Appearance of the reaction products

The anterogradely labelled and immunolabelled structures were visualised with different chromogens for the peroxidase reactions that were distinguishable at the light microscopic level. Structures visualised with DAB as the chromogen for the peroxidase reaction were characterised by the presence of the typical reddish-brown amorphous reaction product (Figs. 2.6, 2.7, 2.10A, 2.11A, 2.12A, 2.13A, 2.14A) and those visualised with nDAB contained the typical blue-black reaction product (Figs. 2.7D, 2.8, 2.10A, 2.11A, 2.12A, 2.13A, 2.14A).

2.3.1.2) Injection sites

The location of the injection sites was confirmed by visualisation of the tracer in the barrel cortex. The deposits of neuronal tracers spanned most of the cortical laminae without inclusion of the underlying corpus callosum (Fig. 2.6A-C). The labelled cells sent axons that entered the subcortical white matter (Fig. 2.6B, C) while some fibres were seen crossing the midline (Fig. 2.6D, E).

2.3.1.3) Distribution of anterograde labelling

Injection of the tracer in the barrel cortex led to intense labelling of axon terminals in the ipsilateral caudal dorsolateral striatum where both types of fibres were observed (Fig. 2.7A, B). The majority of corticostriatal axons were collected in the fascicles of axon bundles traversing the striatum on their way to the internal capsule. Branches of these thick fibres arose at right angles and they were found just below the corpus callosum and followed the curvature of the corpus callosum (Fig. 2.7A). The fibres

Figure 2. 6. Injection sites.

The light micrographs illustrate the extent of the BDA injection into the cortex and the resulting labelling of corticostriatal fibres.

A The BDA injection which has been visualised using DAB, thus giving a reddish brown reaction product is seen to span most of the cortical lamina, with no inclusion of the corpus callosum. Scale bar 200 μm.

B The photograph is the same as **A** but taken at a higher magnification. The blood vessel marked by (*) in **A** is visible in the picture. At this magnification it is clear that the injection did not include the corpus callosum. Fibres labelled by the tracer can be seen leaving the cortex and entering the white matter (arrow). Scale bar 100 μm.

C The light micrograph shows the injection site from another animal. Here a large number of thick calibre fibres (arrows) can be seen descending along the corpus callosum. The fibres can be seen entering the striatum, which is seen in the foreground and is above the plane of focus. Scale bar 100 μm.

D The light micrograph shows the contralateral corpus callosum at the same anterior-posterior location as **C**. At that magnification no fibres are clearly visible in the contralateral hemisphere. Scale bar 100 μm.

E Higher magnification of the photograph in **D** with (*) marking the same blood vessel in both pictures. The fibres (arrows) can be seen in the contralateral corpus callosum. These however are much less frequent and thinner that those present in the ipsilateral corpus callosum (compare with **C**). Scale bar 20 μm.

(CC - corpus callosum, Ctx - cortex, Str - striatum)

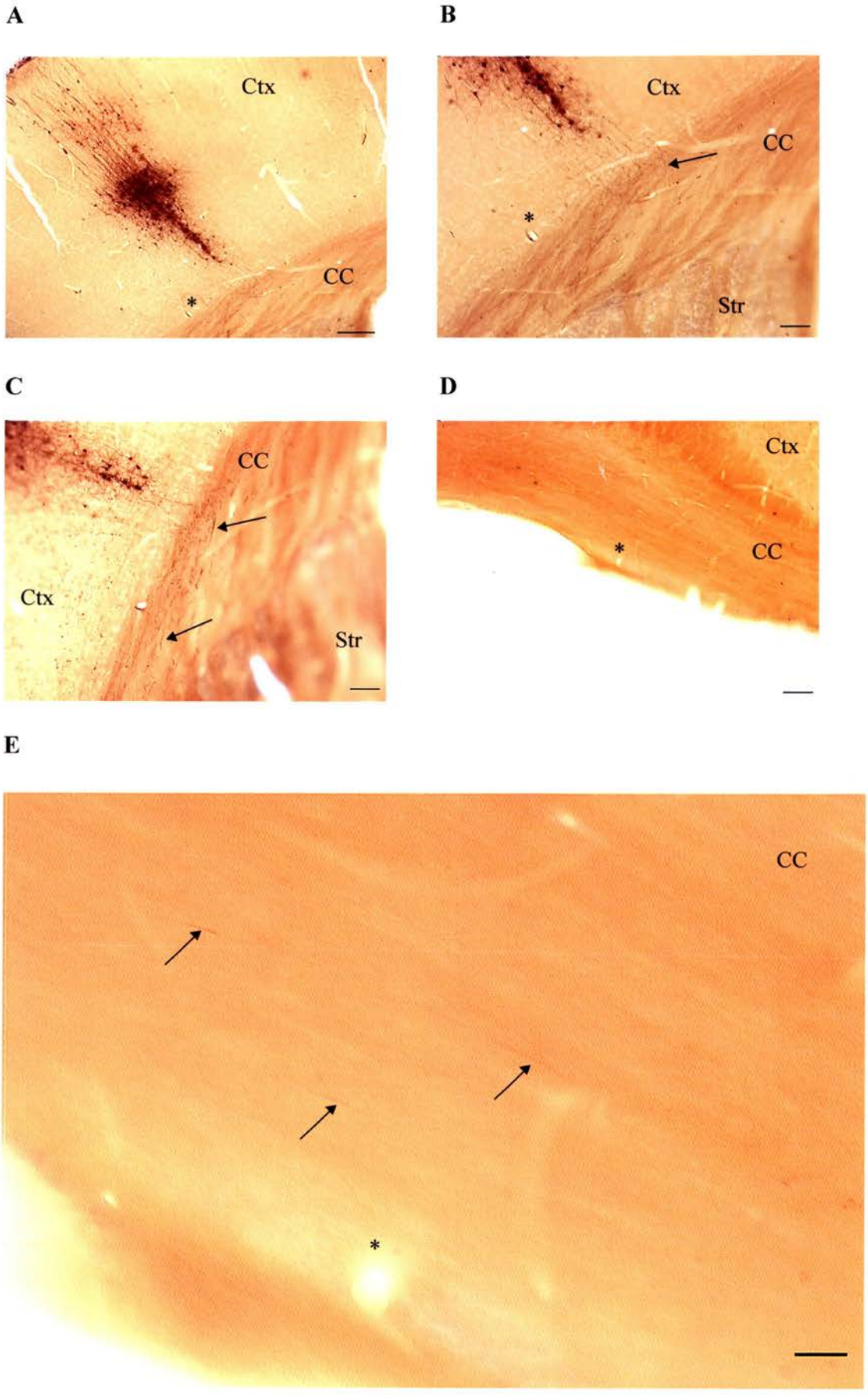
A
Ctx
CC
*
B
Ctx
CC
*
Str
C
CC
Ctx
Str
D
Ctx
*
CC
E
CC
*

Figure 2. 7. Anterograde labelling in the striatum.

A Photomicrograph illustrating anterograde labelling in the striatum. This photograph was taken at a magnification of x 20. At that magnification, labelled fibres can be seen entering the striatum via the fibres bundles (arrows). Thick calibre fibres are clearly visible and they are found beneath and run parallel to the corpus callosum. Note that the orientation of the blood vessel is parallel to the corpus callosum. The background purple staining is immunolabelling for D_1 receptor. Scale bar 100 μm.

B The same photomicrograph as **A** but at a higher magnification. The same blood vessel (*) and fibres bundle (FB*) that are visible and marked in **A** are also identified in the pictures as points of reference. At this higher magnification swellings (arrowheads) are clearly visible on the thick fibres. Varicosities (arrows) are also visible in the same plane of focus. In comparison with the thick fibres, the fibres associated with the varicosities are not clearly visible and fit the definition of thin fibres. However as the fibres seem to follow the curvature of the corpus callosum they are unsuitable for the correlated light and electron microscopy study. Scale bar 20 μm.

C The same photomicrograph as **B** but in a different plane of focus. Once again the blood vessel (*) and fibre bundle (FB*) are marked. Swellings (arrows) are visible at this magnification and the associated fibres fit the description of thin fibres. As this fibre has a more lateromedial orientation it represents a fibre that would be considered for ultrastructural study. Scale bar 20 μm.

D A photomicrograph of the contralateral striatum at the same level as **B**. However unlike the ipsilateral striatum, there are very few fibres observed. All the fibres observed are thin calibre fibres which meander throughout the striatum (arrows). Scale bar 20 μm.

E The same photomicrograph as **D** but at a higher magnification. The same fibre bundle (FB) that is visible and marked in **D** is also identified in the picture as a point of reference. The thin calibre fibre is clearly visible (arrows). Scale bar 20 μm.

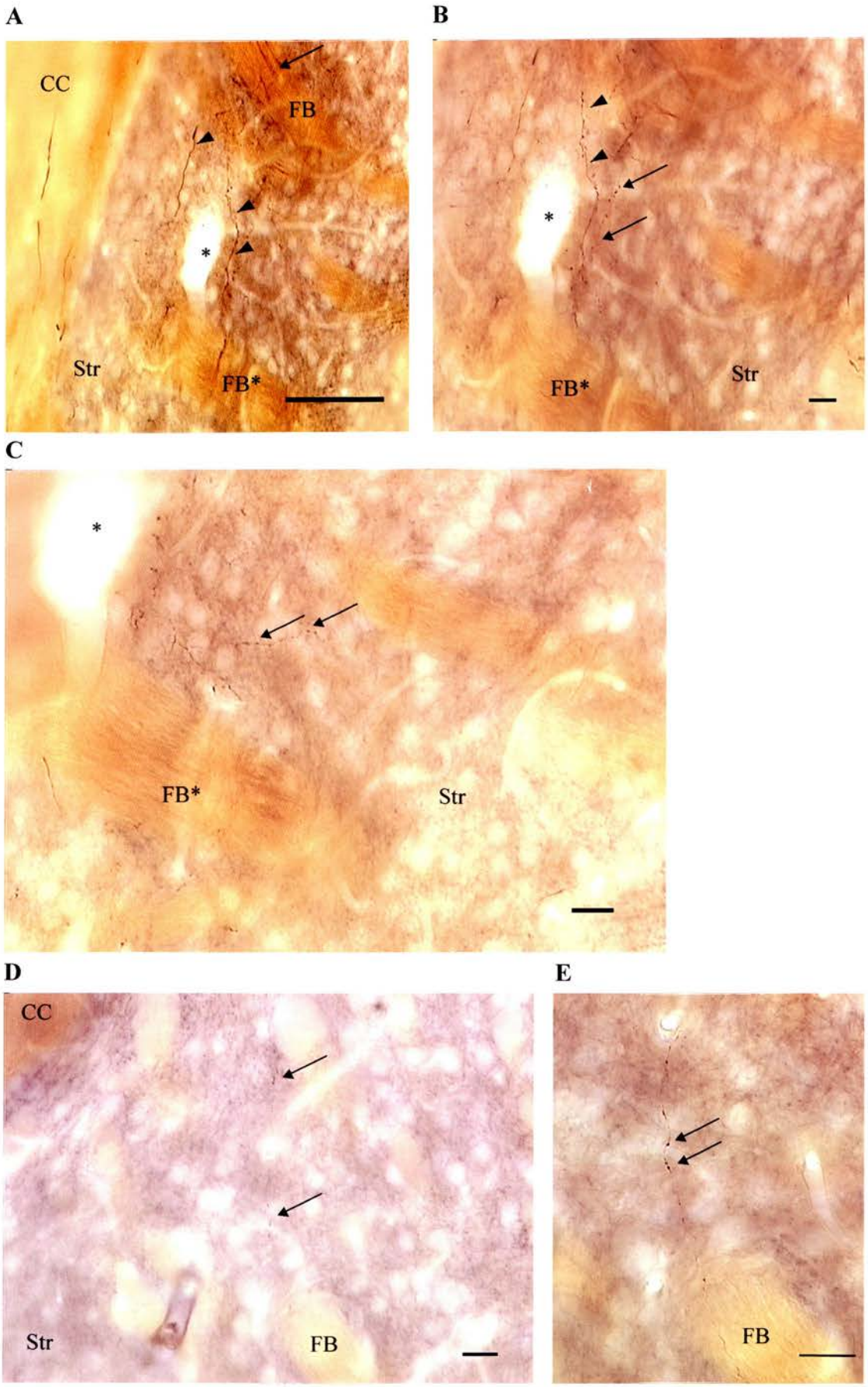
A
CC
FB
*
Str
FB*
B
*
FB*
Str
C
*
FB*
Str
D
CC
Str
FB
E
FB

formed numerous large 'boutons en passant' (Fig. 2.7A, B). Thinner fibres were also observed and these did not have any discernable topography in the striatum (Fig. 2.7B, C). The fibres entered the striatum at a more acute angle and they formed smaller varicosities. The projection patterns and morphology of the two-corticostriatal pathways agrees with previously published work (Alloway et al., 1998; Alloway et al., 1999; Wright et al., 1999). Labelling was also observed in the contralateral striatum (Fig. 2.7D). The fibres had small diameters, even though the varicosities were clearly visible (Fig. 2.7D). In many cases numerous varicosities were observed under a x 40 objective even though the fibres were not visible at that magnification (Fig. 2.7D). This morphology agrees with the diffuse projection in the contralateral striatum previously described (Wright et al., 1999). These fibres did not form any discernable topographic projection.

2.3.1.4) D_1 immunoreactive structures

Striatal sections incubated to reveal imuunoreactivity for D_1 receptors were densely stained by the peroxidase reaction product (Fig. 2.8A). The staining throughout the striatum was intense compared to other brain regions. There was dense fibre and punctate staining and the intensity of the staining and the thickness of the striatal sections made it difficult to identify individual immunoreactive structures (Fig. 2.8A, B). Myelinated fibres passing through the striatum and cell bodies were immunonegative (Fig. 2.8B). In addition to the striatum, the olfactory tubercle and nucleus accumbens (core and shell) were immunoreactive for D_1 receptor antibodies. However the immunoreactivity was uneven. The cortex was also slightly immunoreactive (Fig. 2.8A). Bundles of fibres passing through the globus pallidus were immunoreactive for D_1 receptors and the intensity of the staining, when

Figure 2. 8. D_1 immunoreactivity.

A Photomicrograph taken from a striatal section that was not prepared for electron microscopy. The section was only reacted with D_1 antibodies which was later reacted with nDAB in the peroxidase reaction giving, positively labelled structures a bluish appearance. There is strong immunolabelling in the striatum (Str) and the cortex (Ctx) also shows some weak immunoreactivity. Scale bar 200 μm.

B A high power photomicrograph of the striatum showing immunolabelled fibres. Due to the thickness of the sections details of the immunoreactive structures were not visible. Myelinated fibre bundles (FB) and cells (*) show no immunoreactivity for the antibody. Scale bar 20 μm.

C Strong immunolabelling is visible in the enterpeduncular nucleus (EP) and fibres passing through the internal capsule (IC) also show some immunoreactivity. Scale bar 100 μm.

D The section is from a brain that was processed for electron microscopy and the treatment of sections with osmium textroxide makes it harder to identify immunopositive structures even though glucose was added to ensure colour separation. While no immunopositive structures are visible in this photomicrograph, the striatum was immunopositive for D_1 receptors. The subthalamic nucleus (STN) which is visible in the section is not immunoreactive for D_1. Scale bar 200 μm.

E The section contains both the globus pallidus (GP) and the striatum and while the latter is strongly immunoreactive, the GP is largely immunonegative. Some immunoreactivity is observed in fibres of passage as they descend through the structure. Scale bar 200 μm.

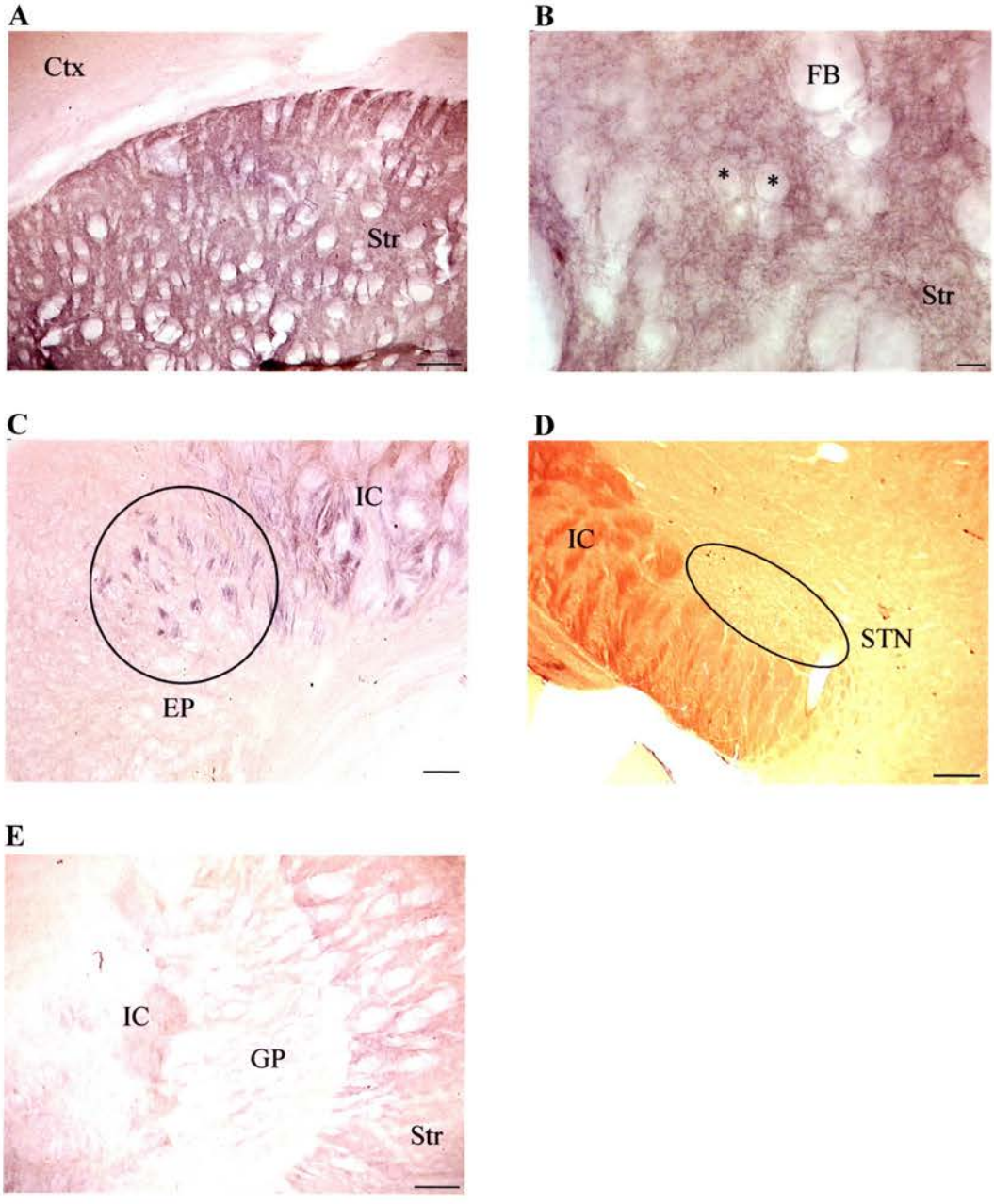
A
Ctx
Str
B
FB
*
*
Str
C
IC
EP
D
IC
STN
E
IC
GP
Str

observed, was similar to the immunopositive structures in the striatum (Fig. 2.8E). There was also some staining in the entopeduncular nucleus (Fig. 2.8C). whilst the subthalamic nucleus was unstained (Fig. 2.8D)

2.3.1.5) Controls.

The omission of the D_1 antibody did not result in the labelling of any structures in the basal ganglia.

2.3.1.6) Light microscopic analysis of contacts.

While staining of the striatal sections with D_1 antibodies led to intense labelling of structures in the striatum at the LM level it was difficult to identify corticostriatal boutons apposing D_1 immunoreactive spines. Thus analysis was only done at the EM level (Fig. 2.7).

2.3.2) Electron microscopic observations

To study the contacts made by the different types of fibres to structures in the striatum, labelled fibres were examined by electron microscopy. Correlated light and electron microscopy was carried out, as it allowed the study of contacts made by fibres identified to be thick and thin at the light microscope level. A total of 4 thick fibres (all ipsilateral) from 4 animals and 6 thin fibres (3 ipsilateral, 3 contralateral) from 3 animals were studied at the electron microscopic level. The location of the fibres in the striatum obtained from each animal is shown in Figure 2.9. Anterogradely labelled axon terminals were identified by the presence of reaction product as well as by their position in relation to landmarks such as blood vessels, fibres bundles, unstained neurones and glial cells (Figs. 2.10A, B, 2.11A, B, 2.12A,

Figure 2. 9. Location of fibres and summary of results.

The figures and the underlying tables summarise the results obtained for the 4 animals (**A-D**) on which the correlated light and electron microscopy was carried out. The approximate positions of the fibres are marked and the number of boutons studied and the ultrastructural features of the contacts, which are also colour coded are detailed for each animal. Thick fibres (blue fibres) which were chosen for the study were found in the dorsolateral striatum and all the fibres followed the curvature of the callosum. Thin fibres (red fibres) chosen for the study had a more lateral to medial orientation. As the thin fibres in the contralateral striatum (green fibres) were rare and due to the fact that they were the only fibre type present any fibres that were found in the depth of striatum that contained strong immunolabelling were chosen for the study regardless of their spatial orientation. Note that in two animals (**A** and **B**), none of the boutons originating from thin fibres on the ipsilateral striatum formed any synaptic contact with a D_1 immunopositive structure. Detailed study of the mediolateral position of the thin fibres and the number of contacts with D_1 immunonegative structures revealed no correlation.

(GP - globus pallidus, IC - internal capsule, Str - striatum)

A

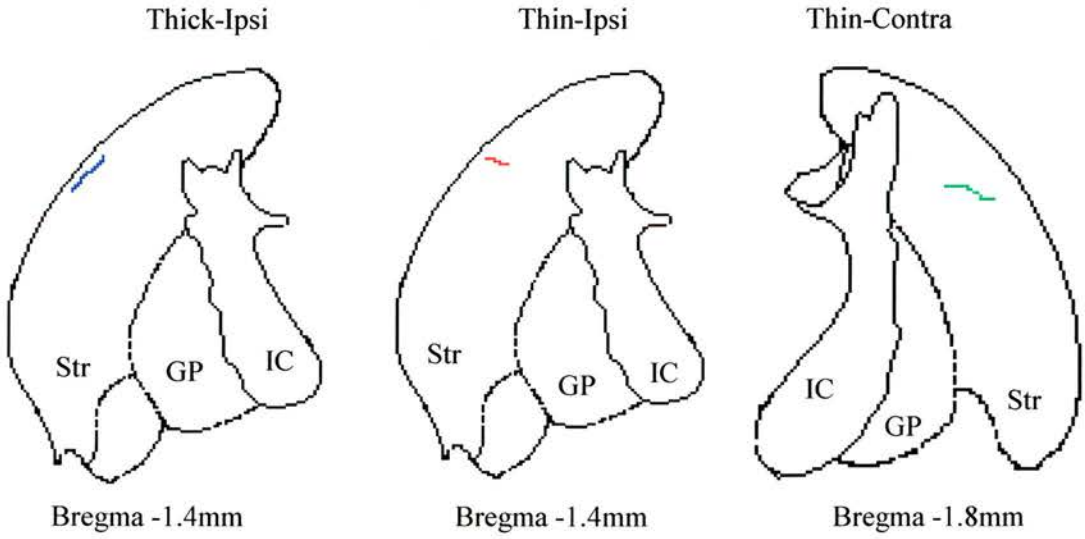

Type of fibre	No. of boutons	No. of synapses	D1 (+)	D1 (-)	Simple	Complex
Thick (Ipsilateral)	8	10	6	4	6	4
Thin (Ipsilateral)	9	9	0	9	9	0
Thin (Contralateral)	3	3	0	3	3	0

B

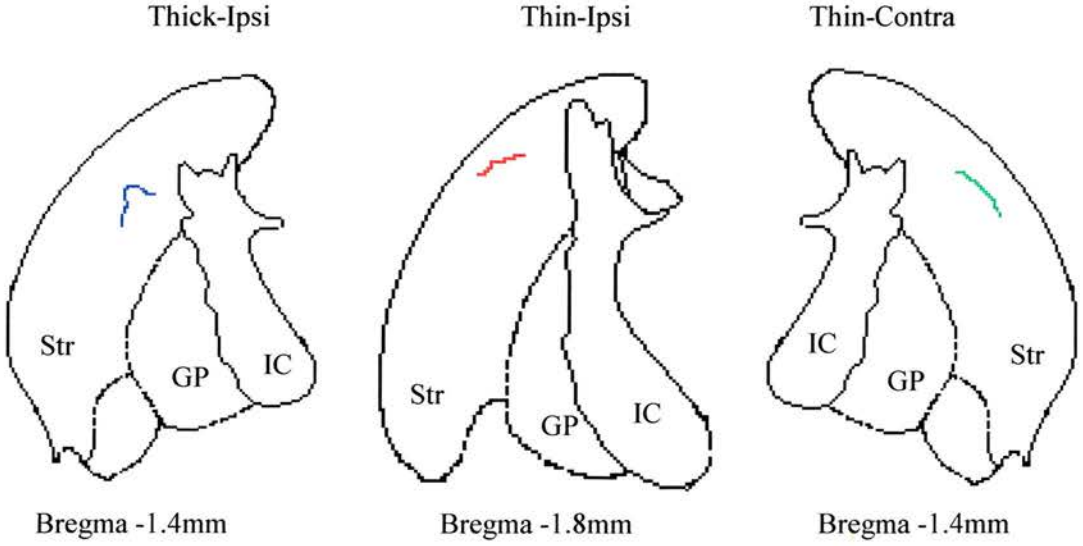

Type of fibre	No. of boutons	No. of synapses	D1 (+)	D1 (-)	Simple	Complex
Thick (Ipsilateral)	7	9	2	7	9	0
Thin (Ipsilateral)	12	14	0	14	11	3
Thin (Contralateral)	8	12	2	10	9	3

C

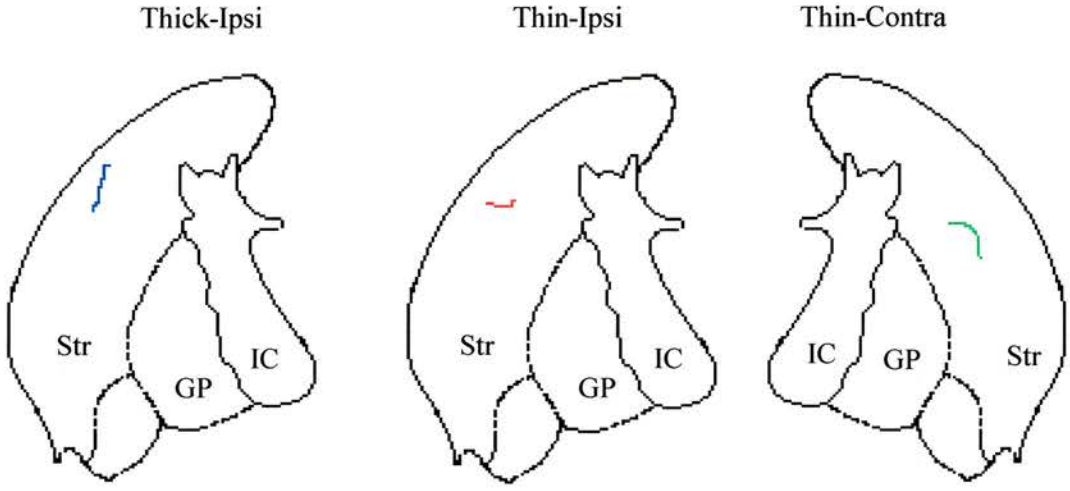

Bregma -1.4mm Bregma -1.4mm Bregma -1.4mm

Type of fibre	No. of boutons	No. of synapses	D1 (+)	D1 (-)	Simple	Complex
Thick (Ipsilateral)	8	15	7	8	5	10
Thin (Ipsilateral)	12	15	4	11	7	8
Thin (Contralateral)	6	7	2	5	6	1

D

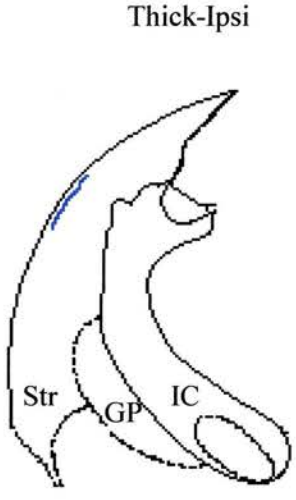

Bregma -2.12mm

Type of fibre	No. of boutons	No. of synapses	D1 (+)	D1 (-)	Simple	Complex
Thick (Ipsilateral)	13	16	11	5	8	8

Figure 2. 10. Correlated light and electron microscopy of a thick fibre in the ipsilateral striatum contacting an D_1 immunopositive spine.

A Light micrograph of thick fibres in the ipsilateral striatum. The fibres were revealed using DAB giving them a reddish brown colour. The fibres are present at a level of striatum that is strongly immunoreactive for D_1 receptor, as seen by the bluish fibre-like staining, as D_1 immunoreactivity was revealed using nDAB as the chromogen. Landmarks such as blood vessels (bv), cell bodies (cb) and fibre bundles (FB) are labelled for correlation. At the plane of focus 3 varicosities are visible and are marked B1 to B3. Scale bar 20 μm.

B Low power electron micrograph of the same fibre. The landmarks and varicosities marked in the light micrograph are visible. Scale bar 50 μm.

A

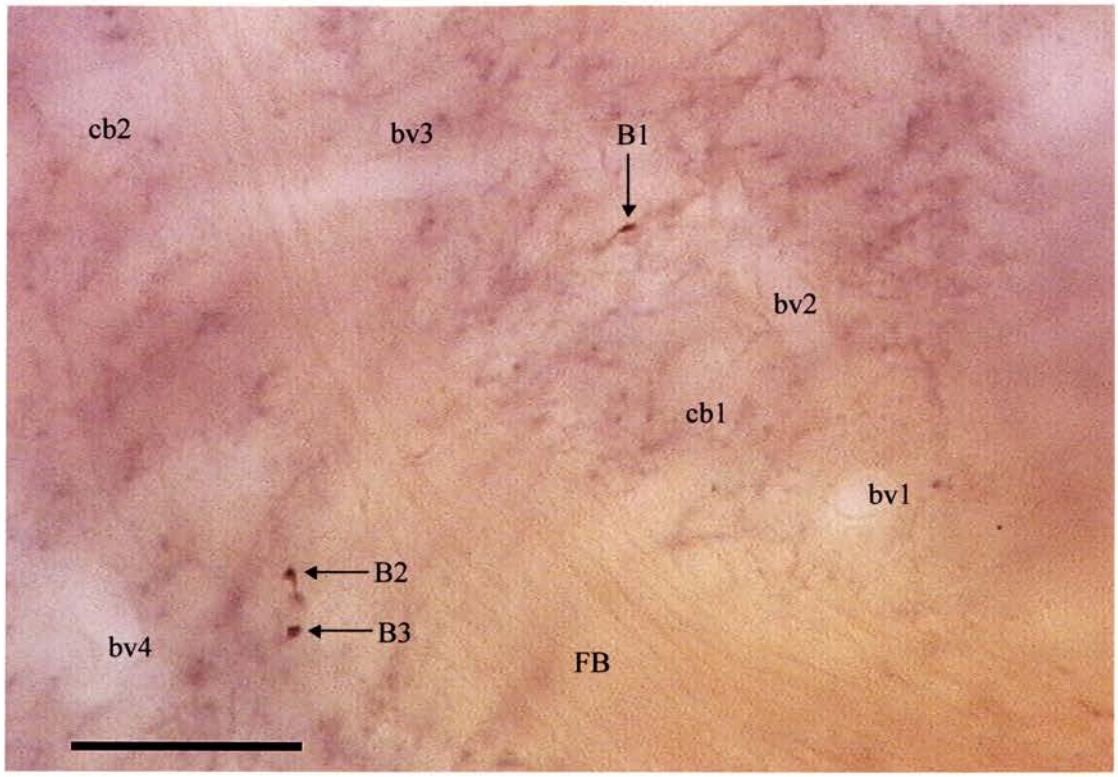
cb2
bv3
B1
bv2
cb1
bv1
B2
B3
bv4
FB

B

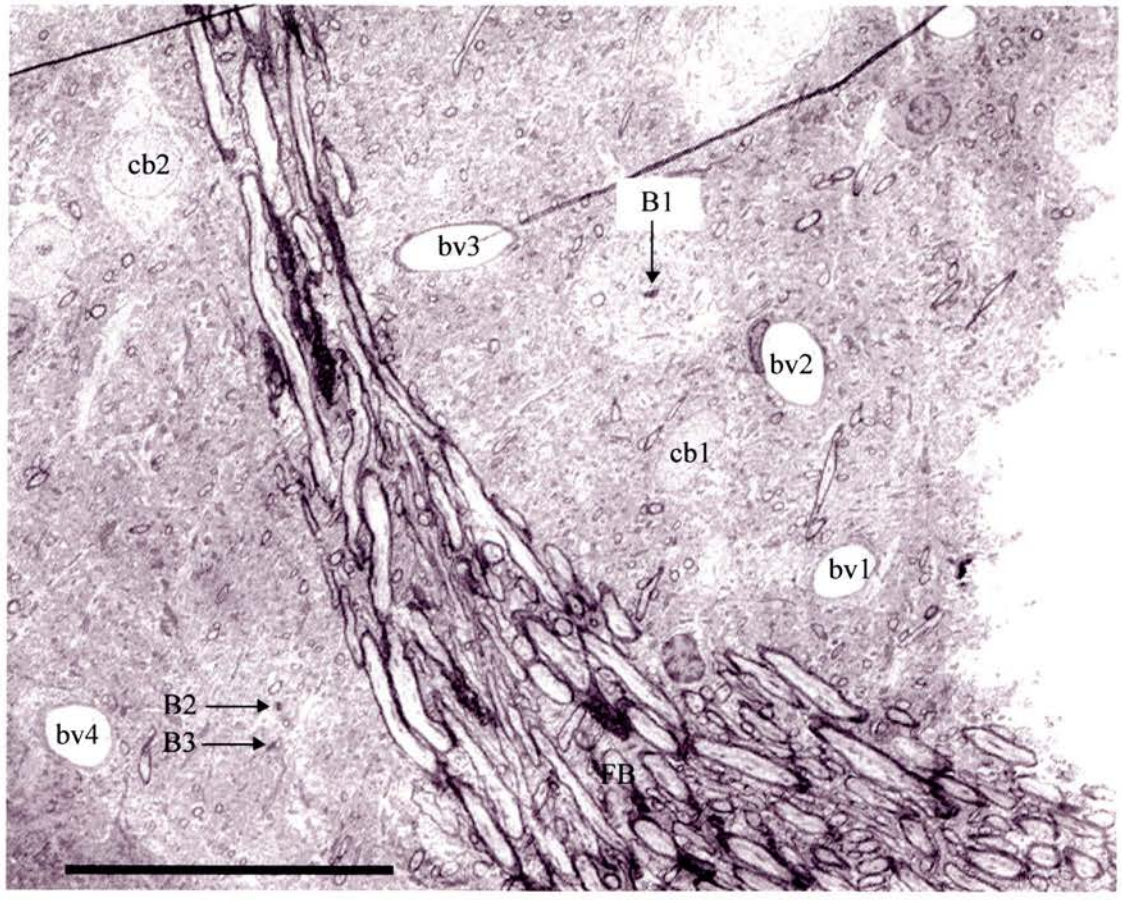
cb2
B1
bv3
bv2
cb1
bv1
B2
B3
bv4
FB

Figure 2. 10. Correlated light and electron microscopy of a thick fibre in the ipsilateral striatum contacting an D_1 immunopositive spine.

C High power electron micrograph of bouton B1. The bouton, which contains the BDA reaction product contains numerous synaptic vesicles as well as mitochondria (m). The bouton is in synaptic contact (arrowhead) with a D_1 immunopositive spine (D1(+)Sp). The spine is filled with an amorphous reaction product, which fills the whole extent of the spine. In comparison there are surrounding structures which show no such immunoreactivity (D1(-)). Scale bar 0.45 μm.

D Another section in the series of serial sections of bouton B1. In this, a clear perforation is seen in the synapse (arrowheads) and this perforation extends for 3 serial sections, thus classifying the synapse as a complex synapse. Scale bar 0.45 μm.

E A serial section of bouton B1, where it can be seen making a perforated asymmetric synapse with a D_1 immunopositive spine (arrowheads). In this section, a positively immunolabelled dendrite (D1(+)Den) can be clearly seen. In latter sections when the bouton no longer exists, the spine can be seen originating from this immunopositive dendrite. Scale bar 0.45 μm.

F In this section the perforation, no is no longer present and the bouton makes a asymmetric synapse (arrowheads) with the positively immunolabelled spine which contains a spine apparatus (*). Scale bar 0.45 μm.

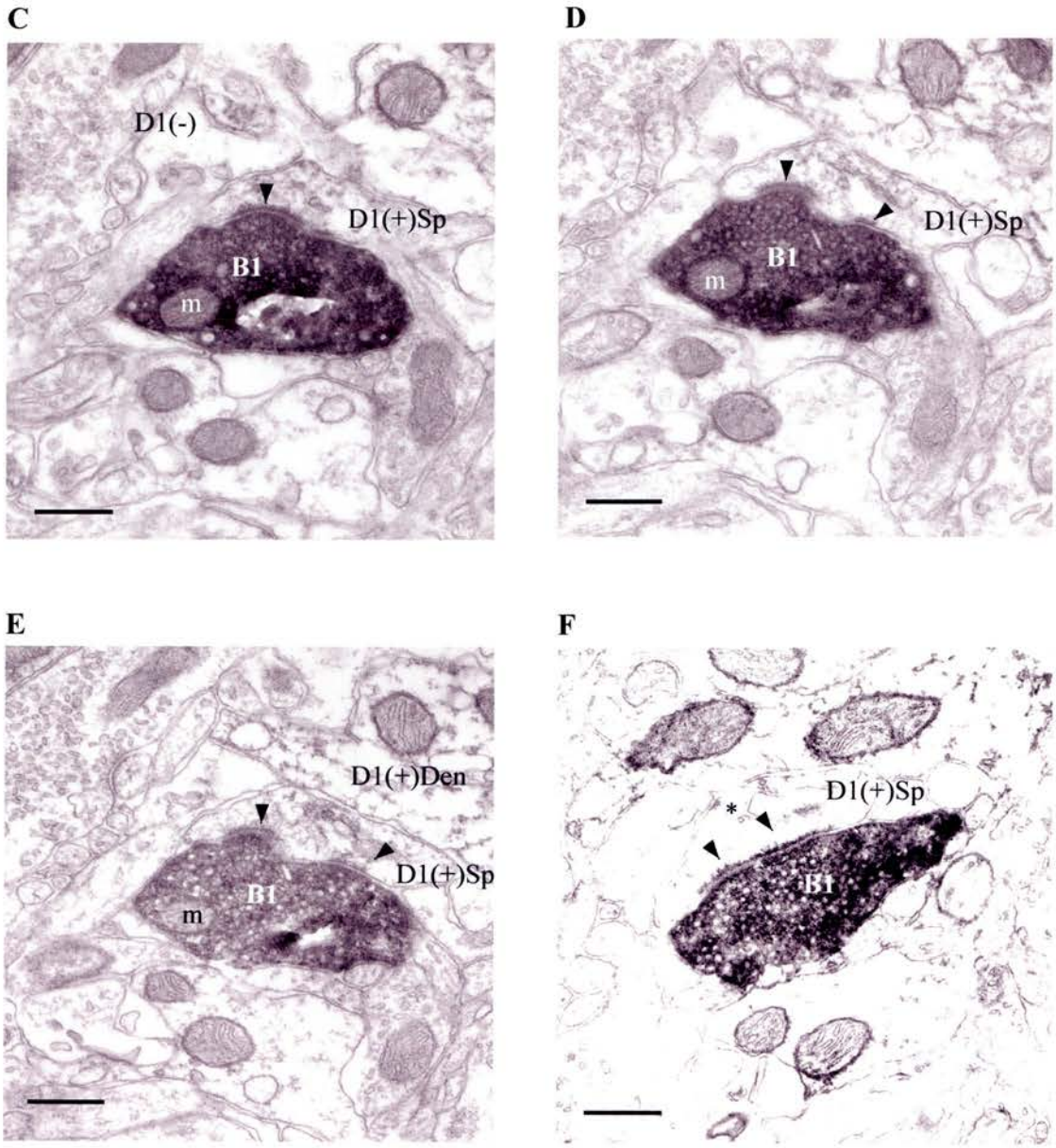
C
D1(-)
D1(+)Sp
B1
m
D
D1(+)Sp
B1
m
E
D1(+)Den
D1(+)Sp
B1
m
F
D1(+)Sp
*
B1

Figure 2. 11. Correlated light and electron microscopy of a thick fibre in the ipsilateral striatum contacting an D_1 immunonegative spine.

A Light micrograph of a thick fibre revealed with DAB in the ipsilateral striatum (same fibre as illustrated in Fig. 2.10). The fibre is present at a level of striatum that is strongly immunoreactivity for D_1 receptor antibody. Landmarks such as blood vessels (bv), glial cell bodies (cb) and fibre bundles (FB) are labelled for correlation. At the plane of focus 1 varicosity is visible and is marked as B1. Scale bar 20 μm.

B Low power electron micrograph of the same fibre. The landmarks and varicosity marked in the light micrograph are visible. Scale bar 50 μm.

A

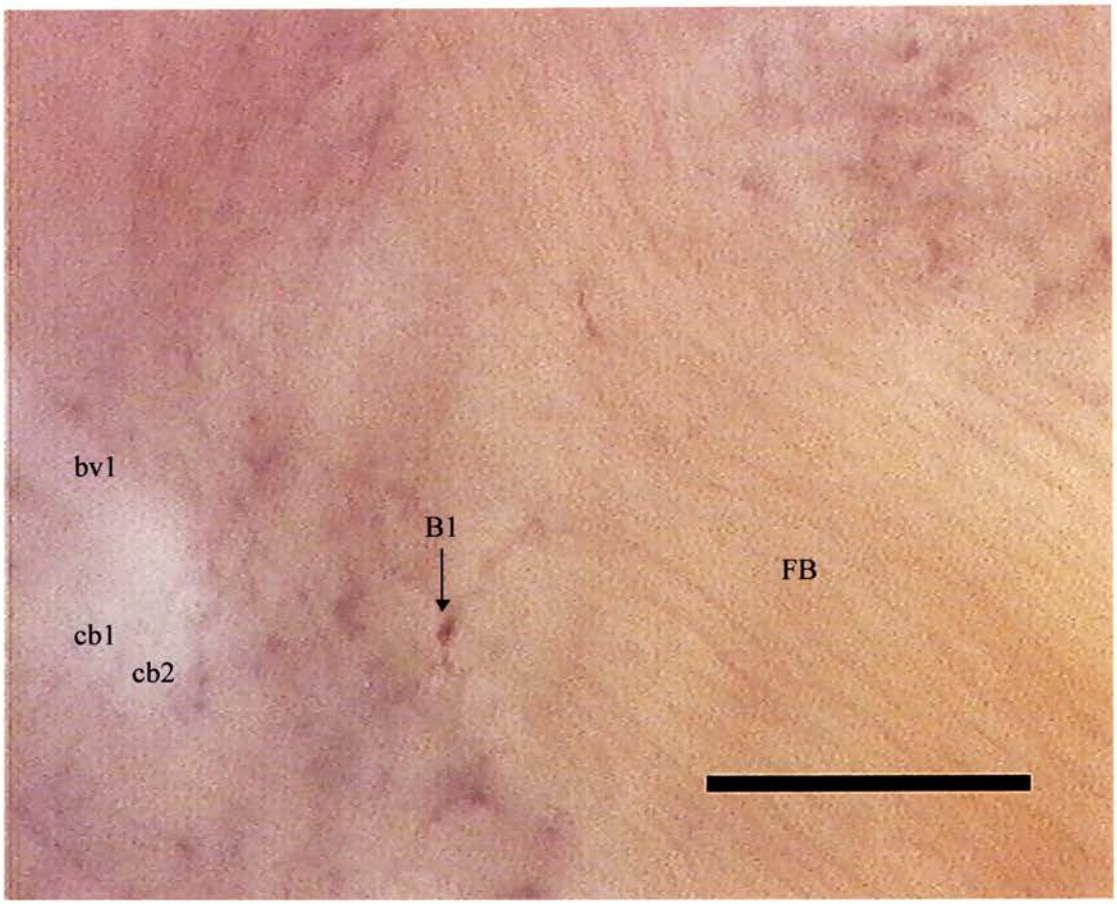

B

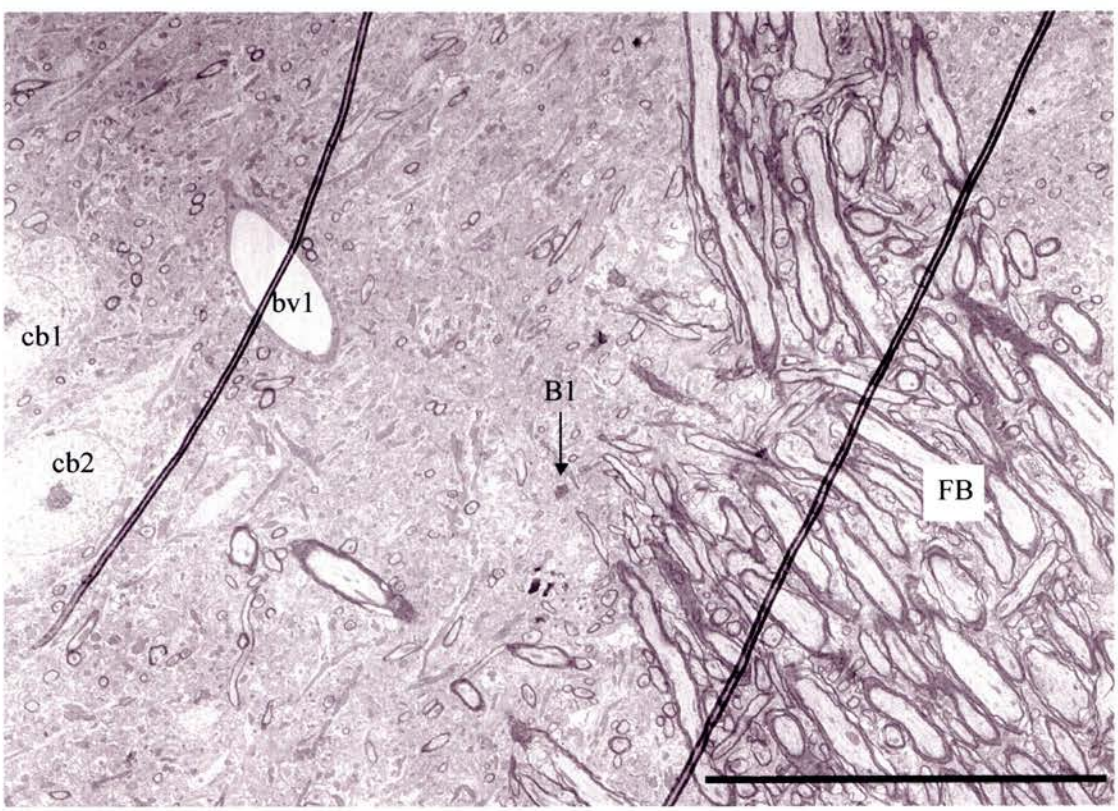

Figure 2. 11. Correlated light and electron microscopy of a thick fibre in the ipsilateral striatum contacting an D_1 immunonegative spine.

C High power electron micrograph of bouton B1. The bouton, which makes a simple asymmetric contact (arrowheads) with a D_1 immunonegative spine (D1(-)Sp) has features such as numerous synaptic vesicles as well as mitochondria (m) that are typical of cortical boutons. Scale bar 0.45 μm.

D The section is the same as the one in **C**. The section however was rotated using a goniometer at an angle of 45^0. The rotation revealed a clear postsynaptic density (arrowheads) as well as a synaptic cleft and synaptic material. Once again no reaction product is observed in the spine which contains a spine apparatus (*). Scale bar 0.45 μm.

E A serial section of bouton B1, where it is still making a simple asymmetric synapse with an immunonegative spine (arrowheads). In this section the neck of the spine (arrow) can be clearly seen. Although an attempt was made to trace the spine back to its parent dendrite to check for immunoreactivity, it was not possible to do so. Scale bar 0.45 μm.

F This is the last section in the series of serial sections, where synaptic contact is seen with the bouton and the spine (arrowhead). In this section we can see the emergence of a D_1 immunopositive spine (D1(+)) which in latter sections make a synaptic contact with a bouton that has the morphological characteristics of a cortical bouton. As this was the deepest section with respect to the other serial sections (with deeper sections having less immunoreactivity), it confirmed that penetration of reagents still occurred at that depth. Scale bar 0.45 μm.

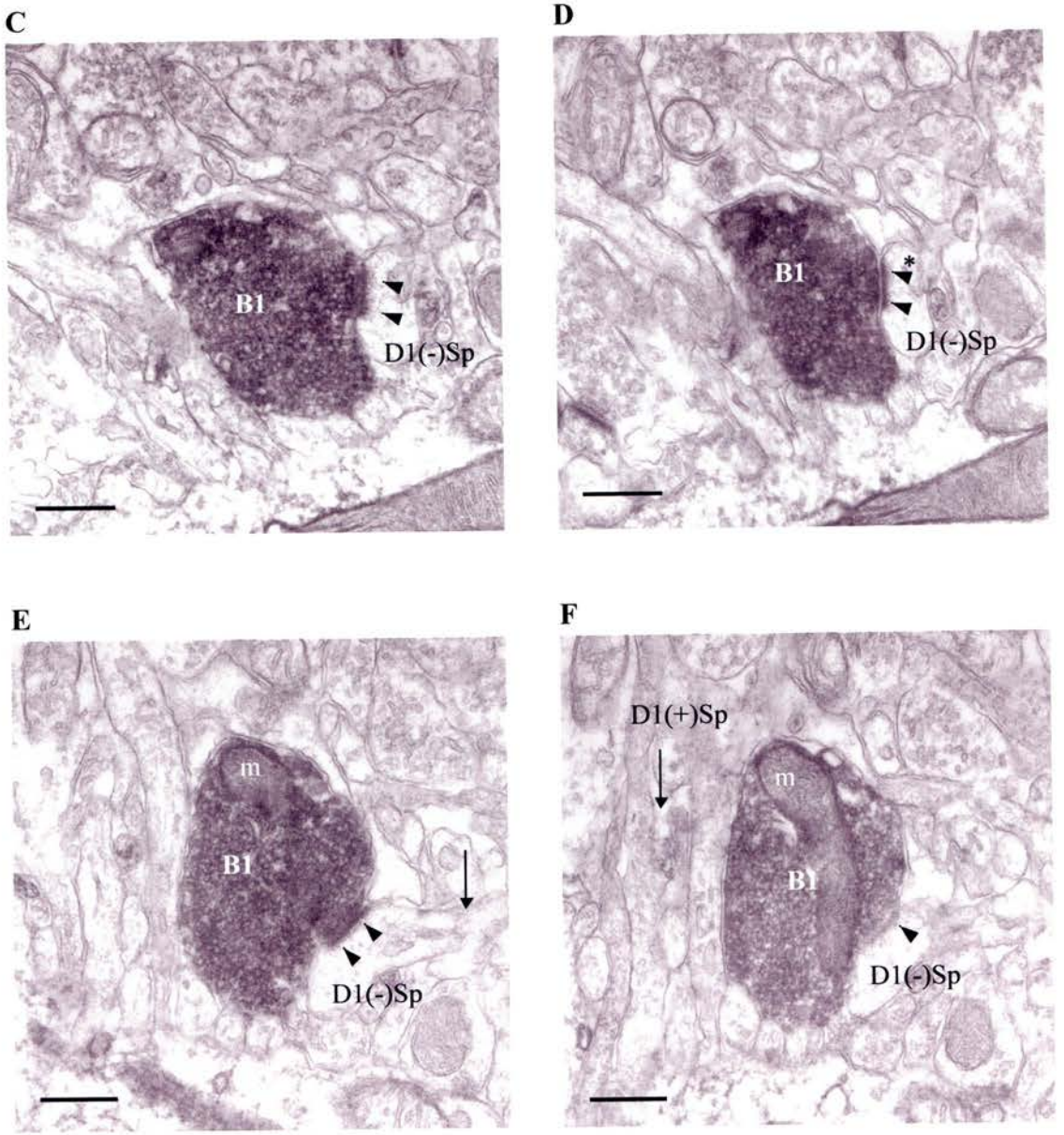
C
B1
D1(-)Sp
D
B1
*
D1(-)Sp
E
m
B1
D1(-)Sp
F
D1(+)Sp
m
B1
D1(-)Sp

Figure 2. 12. Correlated light and electron microscopy of a thin fibre in the ipsilateral striatum contacting a D_1 immunopositive and a D_1 immunonegative spine.

A Light micrograph of a thin fibre in the ipsilateral striatum, that was from an animal different to the one illustrated in Figs. 2.10 and 2.11. The fibre was revealed using DAB giving it a reddish brown colour. The fibre is present at a level of striatum that is strongly immunoreactivity for D_1 receptor as seen by the bluish fibre-like staining, as D_1 immunoreactivity was revealed using nDAB as the chromogen. Landmarks such as blood vessels (bv) and cell bodies (cb) are labelled for correlation. At the plane of focus 3 varicosities are visible and are marked B1 to B3. Scale bar 20 μm.
B Low power electron micrograph of the same fibre. The landmarks and varicosities marked in the light micrograph are visible. Scale bar 50 μm.

A

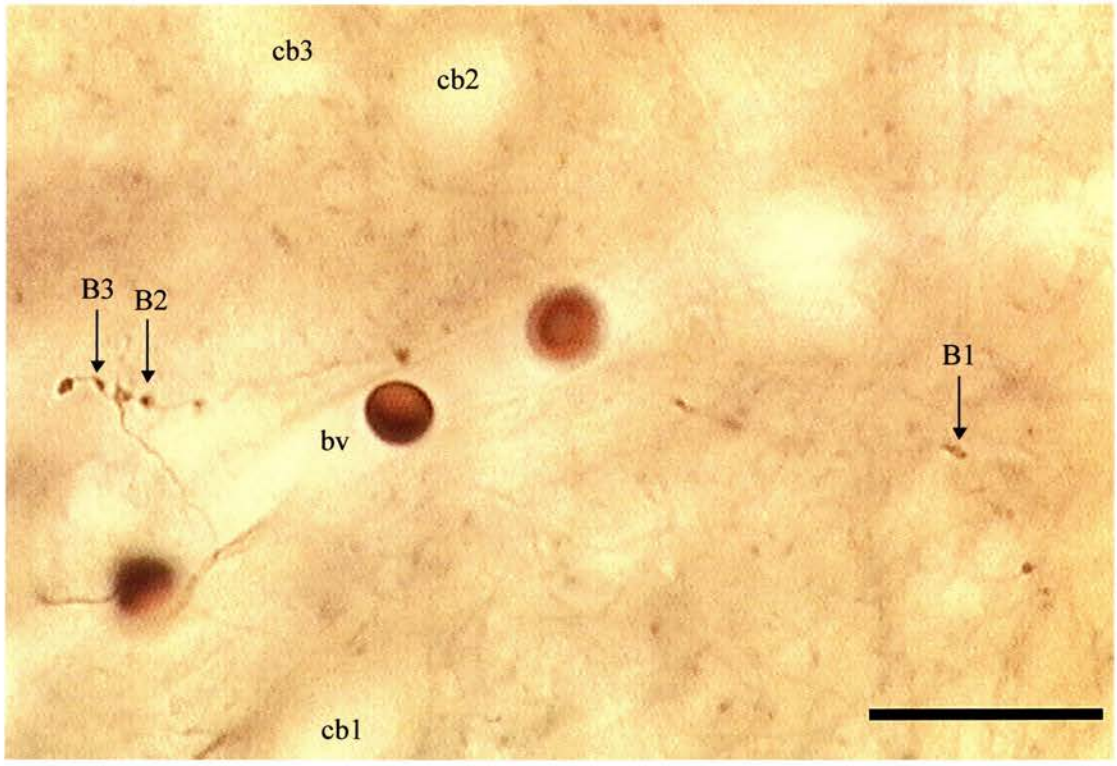

B

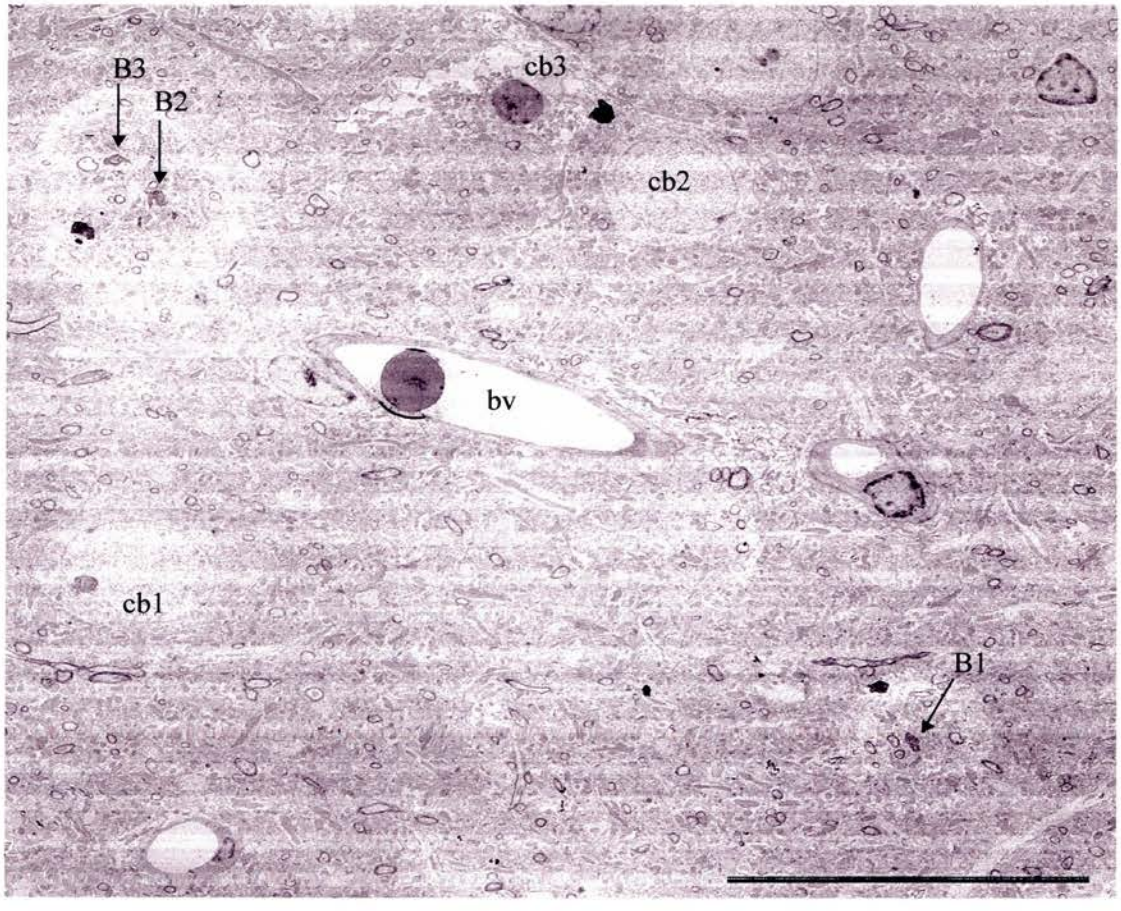

Figure 2. 12. Correlated light and electron microscopy of a thin fibre in the ipsilateral striatum contacting a D_1 immunopositive and a D_1 immunonegative spine.

C High power electron micrograph of bouton B1. The bouton, which contains the BDA reaction product contains numerous synaptic vesicles as well as numerous mitochondria (m). The bouton is in clear asymmetric synaptic contact (arrowhead) with a D_1 immunonegative spine (D1(-)Sp). Opposite to this synapse, the bouton can also be seen making contact with another emerging spine (Sp). At this level, it is difficult to decipher the immunoreactivity of the spine. Scale bar 0.45 μm.

D Another section in the series of serial sections of bouton B1. In this, 2 clear postsynaptic targets can be seen, with one spine immunonegative for the D_1 and the other immunopositive. Perforation of the postsynaptic densities is also seen in both synapses (arrowheads), thus classifying both synapses as complex. Scale bar 0.45 μm.

E A serial section of bouton B1, where it can be still be seen making 2 perorated asymmetric synapses with 2 postsynaptic targets (arrowheads). In this section the amorphous reaction product is obvious in the immunopositive spine and this reaction product is seen in all sections that contain the spine. On the other hand the spine which is classified as immunonegative appears to contain reaction product in this section, but the other serial sections of the labelled bouton do not contain reaction product and have a granular appearance and is likely to reflect background staining. Scale bar 0.45 μm.

F In this section the perforations, are no longer present, and are asymmetric synapses (arrowheads). This section shows a strong reactivity in the immunopositive spine that is membrane bound and more dense than the surrounding structures, while the immunonegative structures has a level of staining that is similar to the background. Scale bar 0.45 μm.

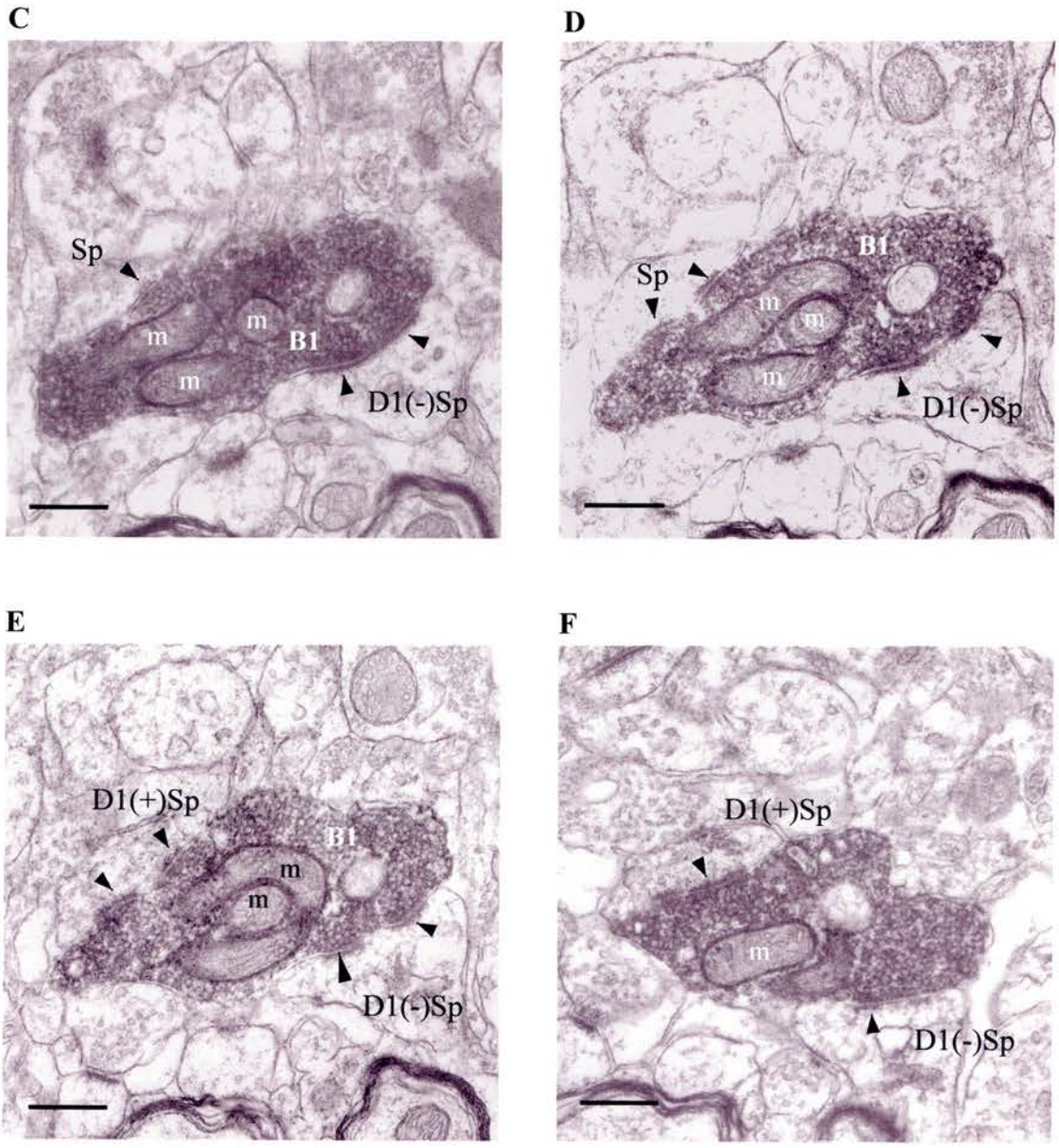
C
Sp
m
m
B1
m
D1(-)Sp
D
B1
Sp
m
m
m
D1(-)Sp
E
D1(+)Sp
B1
m
m
D1(-)Sp
F
D1(+)Sp
m
D1(-)Sp

Figure 2. 13. Correlated light and electron microscopy of a thin fibre in the contralateral striatum contacting both D_1 immunonegative and immunopositive spines.

A Light micrograph of a thin fibre revealed with DAB in the contralateral striatum and is obtained from a different animal as shown by Figs. 2.10, 2.11 and 2.12. The fibre is present at a level of striatum that is strongly immunoreactive for D_1 receptor antibody. Landmarks such as blood vessels (bv), cell bodies (cb) and fibre bundles (FB) are labelled for correlation. At the plane of focus 2 varicosities are visible and are marked as B1 and B2. Scale bar 20 μm.

B Low power electron micrograph of the same fibre. The landmarks and varicosity marked in the light micrograph are visible. Scale bar 50 μm.

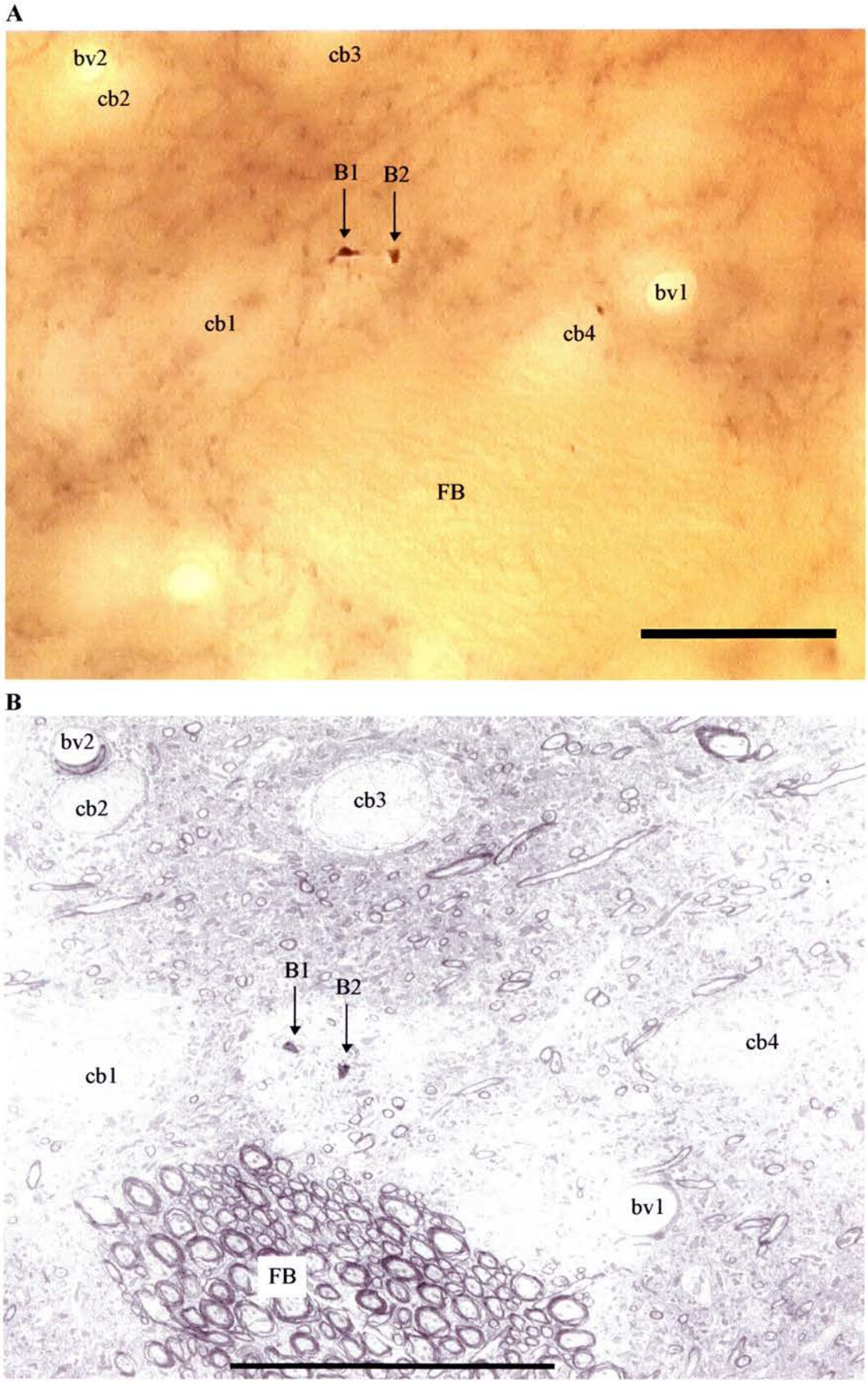
A
bv2
cb3
cb2
B1
B2
bv1
cb1
cb4
FB
B
bv2
cb2
cb3
B1
B2
cb4
cb1
bv1
FB

Figure 2. 13. Correlated light and electron microscopy of a thin fibre in the contralateral striatum contacting both D_1 immunonegative and immunopositive spines.

C High power electron micrograph of bouton B1. The bouton, which makes a simple asymmetric contact (arrowheads) with a D_1 immunopositive spine (D1(+)Sp) has features such as numerous synaptic vesicles as well as mitochondria (m) that are typical of cortical boutons. Scale bar 0.45 μm.

D This is the section following the one in **C**. Here it can be seen that the spine contains amorphous reaction product unlike the spine (D1(-)Sp) which is immunonegative and is making a synapse with what looks like a cortical bouton. Scale bar 0.45 μm.

E A serial section of bouton B1, where it is still making a simple asymmetric synapse with an immunopositive spine (arrowhead). In this section the dense reaction product within the spine is clearly visible. Scale bar 0.45 μm.

F Another serial section of bouton B1 where synaptic contact is seen between the bouton and the spine (arrowhead). In this section we can see the emergence of a D_1 immunonegative spine (D1(-)Sp) which is make a synaptic contact with a bouton that has the morphological characteristics of a cortical bouton. This bouton lasted 15 serial sections. Scale bar 0.45 μm.

G High power electron micrograph of bouton B2. The bouton, which contains the BDA reaction product contains numerous synaptic vesicles as well as mitochondria (m). The bouton is in synaptic contact (arrowhead) with a D_1 immunopositive spine (D1(+)Sp). The spine is filled with an amorphous reaction product, which fills the whole extent of the spine. In comparison there are surrounding structures which show no such immunoreactivity. Scale bar 0.45 μm.

H This is the section following the one in **G**. Once again we can see the bouton forming a simple asymmetric synapse with a immunopositive spine. However unlike the B1 the synapse lasted all of two sections (all serial sections were collected). Scale bar 0.45 μm.

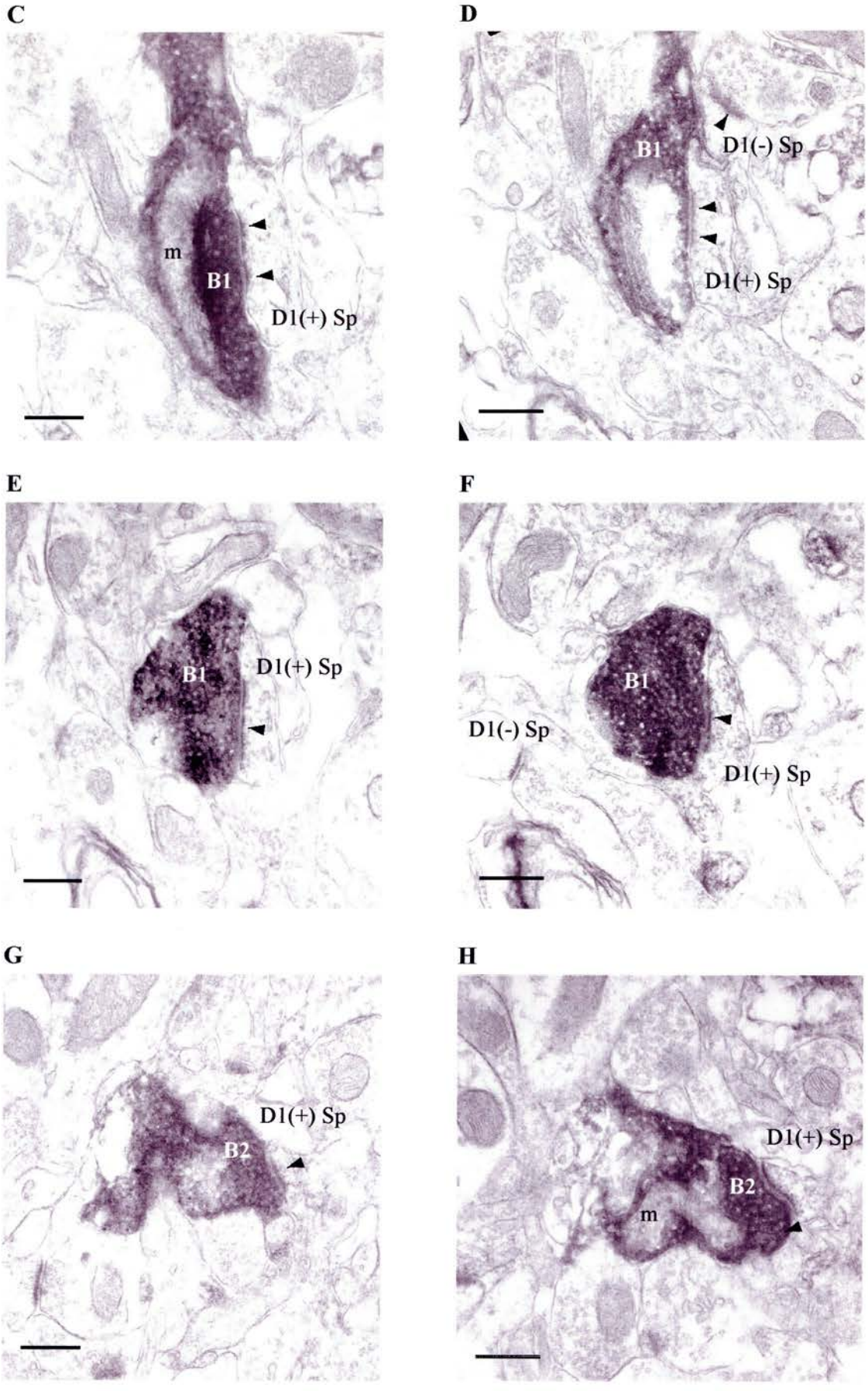
C
m
B1
D1(+) Sp
D
B1
D1(-) Sp
D1(+) Sp
E
B1
D1(+) Sp
F
B1
D1(-) Sp
D1(+) Sp
G
D1(+) Sp
B2
H
D1(+) Sp
B2
m

Figure 2. 13. Correlated light and electron microscopy of a thin fibre in the contralateral striatum contacting both D_1 immunonegative and immunopositive spines.

I This another serial section of bouton B2. The bouton is making a simple synapse with a very small spine (arrowhead), which due to the lack of reaction product is classified as a immunonegative spine. Scale bar 0.45 μm.

J This is the section following the one in **I**. This is the last section where bouton B2 was observed and as in **H** the synapse with the immunonegative spine extended to only two sections despite the fact that all serial sections were collected. Scale bar 0.45 μm.

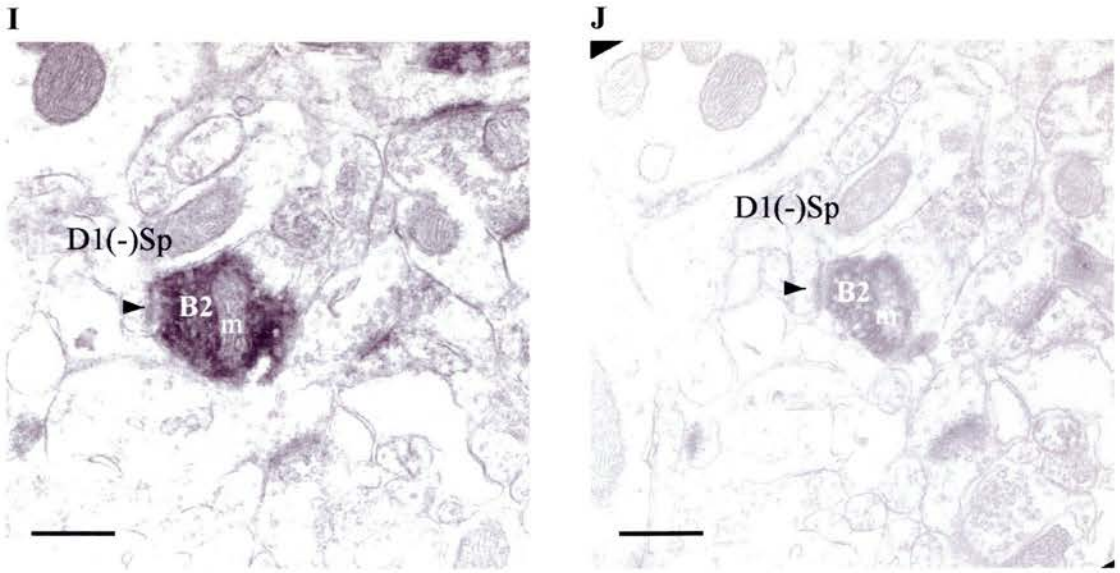
I
D1(-)Sp
B2
m
J
D1(-)Sp
B2
m

B, 2.13A, B, 2.14A, B). The average diameter of thick fibres was 0.19 ± 0.09 μm and all thick fibres analysed had a diameter greater than 0.18 μm. In contrast the average diameter of thin fibres (ipsilateral and contralateral) was 0.13 ± 0.04 μm and all thin fibres analysed had a diameter less than 0.14 μm. The boutons were packed with round vesicles and usually contained one or more mitochondria and they formed asymmetric synapses exclusively with dendritic spines (Figs. 2.10C-F, 2.11C-F, 2.12C-F, 2.13C-J). In the electron microscope D_1 immunoreactivity was identified by the presence of a electron dense precipitate associated with the internal plasma membrane (Figs. 2.10C-F, 2.11C-F, 2.12C-F, 2.13C-J). Immunopositivity was only observed in structures resembling dendrites or dendritic spines (Figs. 2.10C-F, 2.11C-F, 2.12C-F, 2.13C-J).

2.3.2.1) Synaptic boutons from ipsilateral thick fibres (topographic pathway)

All the boutons examined (n = 36) made asymmetric synaptic contact with dendritic spines. Just under one third (30.5%) of these boutons (n = 11) contacted more than one target (8 with 2 spines and 3 with 3 spines) giving rise to a total of 50 synapses. It is unclear from this study if the different targets arose from the same neurone. Approximately half of the synaptic contacts were discontinuous {classified as complex synapses (28 simple synapses vs. 22 complex synapses). Boutons of thick fibres contacted D_1 immunopositive and immunonegative structures with equal frequency [26 synaptic contacts with D_1 immunopositive structures (52%) vs. 24 synaptic contacts with D_1 immunonegative structures (48%)]. Out of the 22 complex synapses, 11 synapsed with D_1 immunopositive spines.

2.3.2.2) Synaptic boutons from ipsilateral thin fibres (diffuse pathway)

A total of 33 boutons from 3 fibres from 3 different animals were studied. In contrast to the thick fibres most of the boutons had a single postsynaptic target and only 15% had more than one target. All 5 boutons which made multiple synaptic contacts, had a maximum of 2 postsynaptic targets. Twenty seven of the 38 synaptic contacts were simple asymmetric synapses while the remaining 11 were complex synapses, 2 of which were onto D_1 immunopositive spines. Boutons of the ipsilateral diffuse system tended to contact more immunonegative spines (34 synapses onto D_1 immunonegative spines vs. 4 synapses onto D_1 immunopositive spines). In 2 animals all boutons arising from thin fibres avoided contacting D_1 immunopositive structures.

2.3.2.3) Synaptic boutons from contralateral thin fibres (diffuse pathway)

Three fibres from 3 animals gave rise to 17 boutons with 4 boutons making multiple synaptic contacts (3 boutons with 2 postsynaptic targets and 1 bouton with 3 postsynaptic targets). This proportion while being smaller than that of thick fibres is larger than thin fibres on the ipsilateral striatum (15% in thin ipsilateral fibres vs. 23% in thin contralateral fibres). Similar to the boutons arising from thin fibres on the ipsilateral striatum, the majority of synapses (81%) were on D_1 immunonegative spines. Eighteen of the 22 synapses were simple asymmetric synapses and 3 out of the 4 complex synapses were onto D_1 immunonegative structures. In two cases from 2 different animals, swellings observed at the light microscope level which were comparable in size to other varicosities proved not to be boutons (Fig. 2.14). These swellings were a result of the presence of mitochondria.

Although no quantitative analysis was done, boutons arising from the thick fibres tended to be larger, even though some very small boutons were observed in

Figure 2. 14. Correlated light and electron microscopy of a swelling arising from a thin fibre in the contralateral striatum that did not give rise to a bouton at the ultrastructural level.

A Light micrograph of a thin fibre revealed with DAB in the contralateral striatum and is the same fibre as illustrated by Figs. 2.13. The fibre is present at a level of striatum that is strongly immunoreactive for D_1 receptor antibody. Landmarks such as blood vessels (bv), cell bodies (cb) and fibre bundles (FB) are labelled for correlation. At the plane of focus 2 varicosities are visible and are marked as B1 and B2. Even though B1 is clearly smaller than B2, in another animal 2 swellings of the same size gave rise to boutons. Scale bar 20 μm.

B Low power electron micrograph of the same fibre. The landmarks and varicosity marked in the light micrograph are visible. Scale bar 50 μm.

C High power electron micrograph of 'bouton' B1. All 4 serial sections which contained this varicosity were collected and examined. The 'bouton', which contains numerous synaptic vesicles does not make any synaptic contact even though it is surrounded by structures that resemble spines. Scale bar 0.45 μm.

D This is the section following the one in **C**. This is the last section where, the 'bouton' exists as the following sections all show fibres (no serial sections were lost). The 'bouton was traced and was compared to the previous section to determine if the postsynaptic density was obscured as a result of the plane of sectioning. However no synapse could be found. Scale bar 0.45 μm.

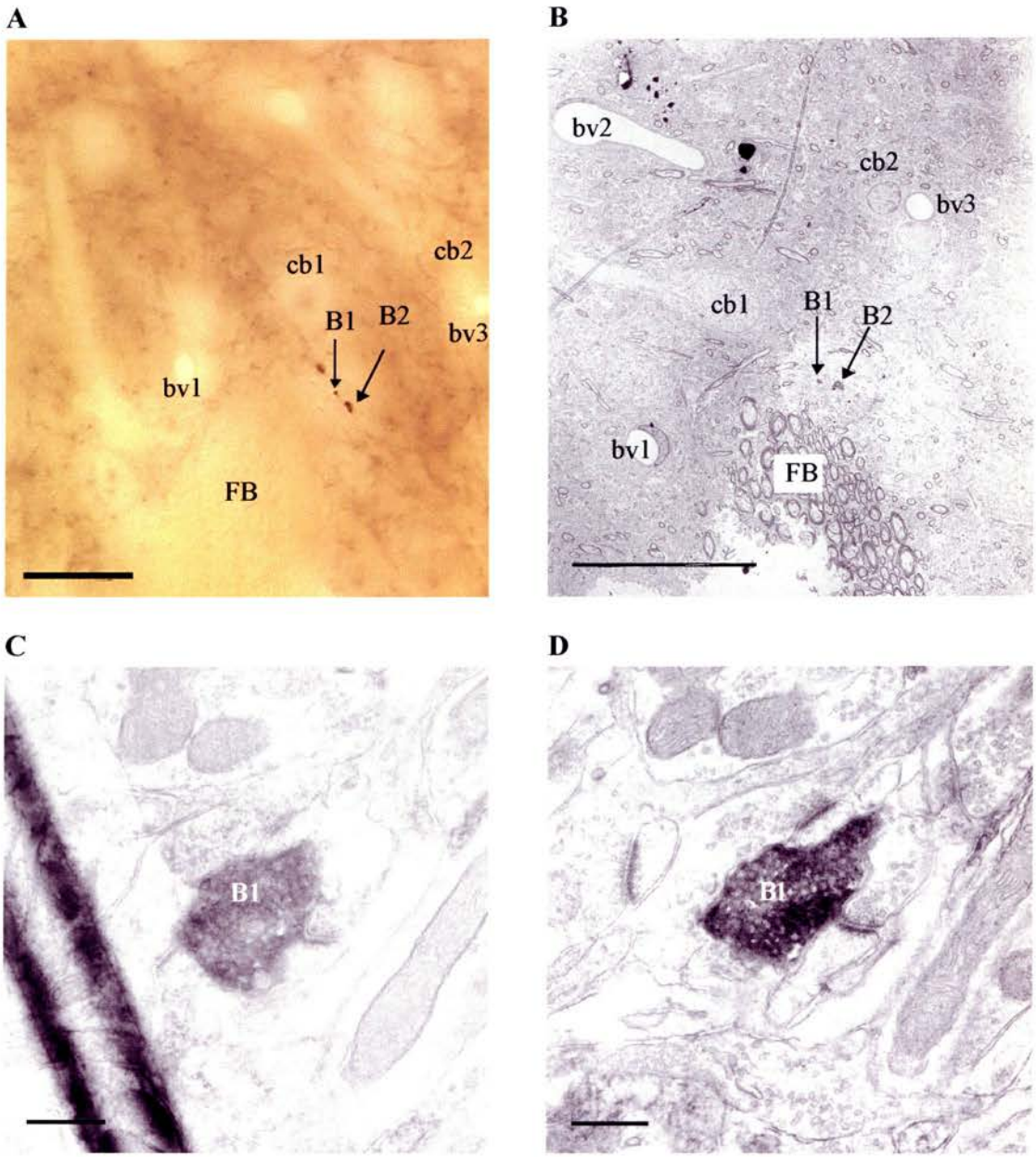

Figure 2. 15. Immunoreactive targets of the projection from the barrel cortex to the striatum.

A The histogram illustrates the total number of synapses examined, made by the different fibres. Thick fibres made contact with equal number of immunopositive and negative spines, while thin fibres, both those in the ipsilateral and contralateral striatum contacted immunonegative spines more frequently.

B The histogram shows the connectivity of the two input pathways from the cortex to the two output pathways of the striatum. Even with the pooling of data from thin fibres from both striata, the thin fibres contacted D_1 immunonegative spines with greater frequency than thick fibres.

C The histogram represents the ratio of D_1 immunopositive to D_1 immunonegative contacts made by both fibre type. The ratio of the type of contacts made by both fibre types is significantly (*) different ($p < 0.05$, Fisher's exact test).

A

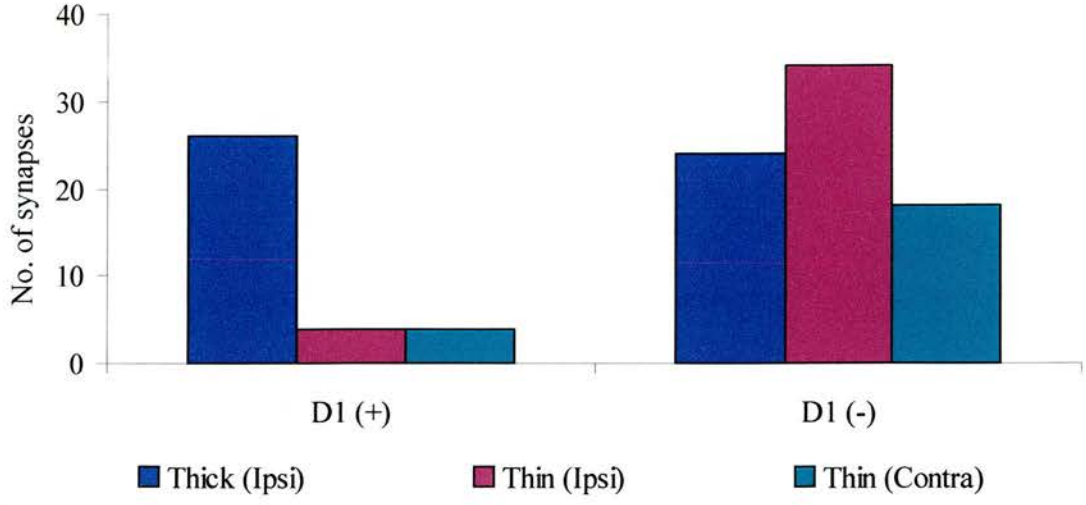
40
30
20
10
0
No. of synapses
D1 (+)
D1 (-)
Thick (Ipsi)
Thin (Ipsi)
Thin (Contra)

B

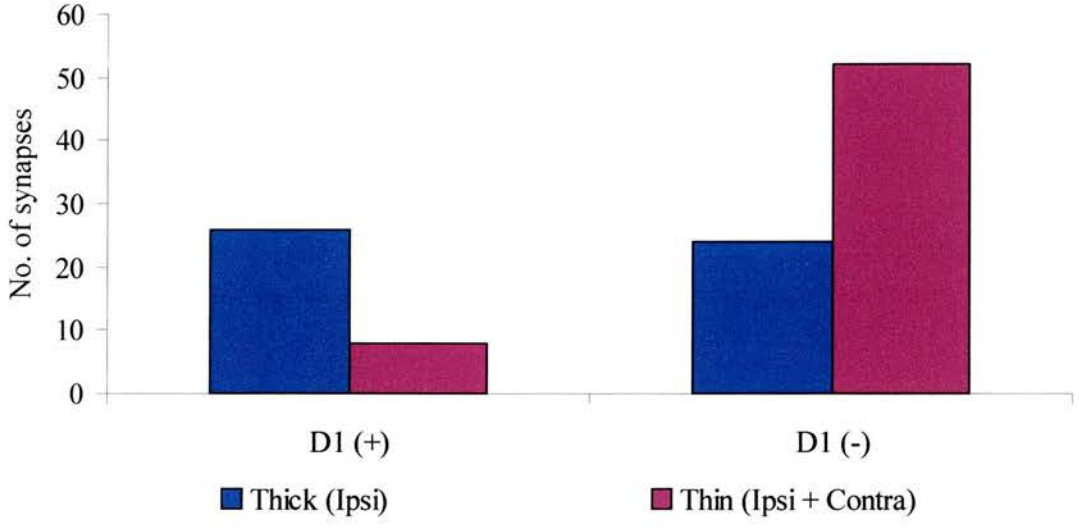
60
50
40
30
20
10
0
No. of synapses
D1 (+)
D1 (-)
Thick (Ipsi)
Thin (Ipsi + Contra)

C

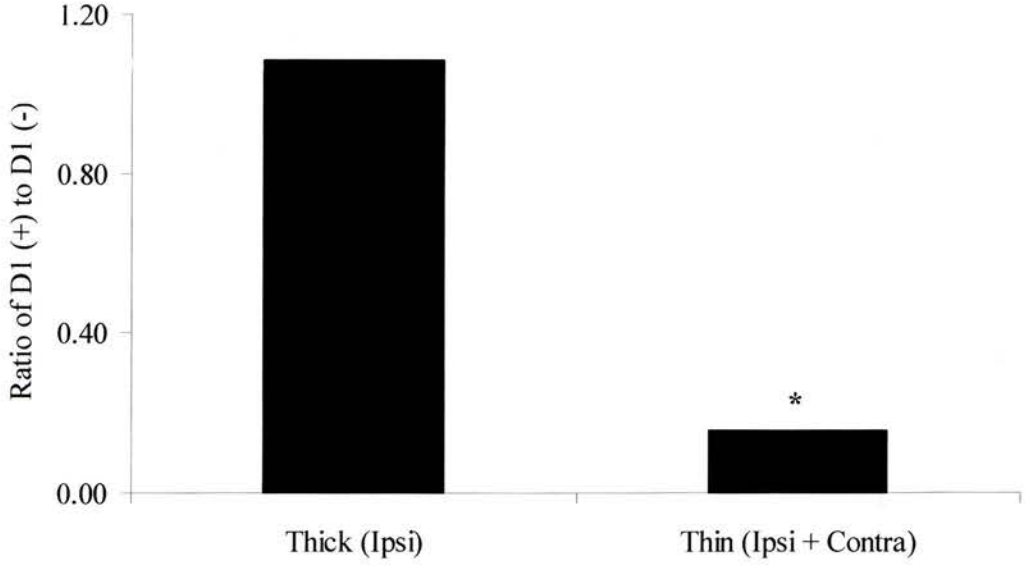
1.20
0.80
0.40
0.00
Ratio of D1 (+) to D1 (-)
*
Thick (Ipsi)
Thin (Ipsi + Contra)

Figure 2. 16. Simple vs. complex synapses made by the projections from the barrel cortex to the striatum.

A The histogram illustrates the total number of complex and simple synapses made by the different fibres. Thick fibres made equal numbers of simple and complex synapses, while thin fibres, both those in the ipsilateral and contralateral striatum made fewer complex synapses.

B The histogram shows the complexity of synapses made by the two input pathways from the cortex. Even with the pooling of data from thin fibres from both striata, thick fibres make a larger number of complex synapses.

C The histogram represents the ratio of simple to complex contacts made by both fibre types. The ratio of the type of contacts made by both fibre types is significantly (*) different, with thick fibres forming equal numbers of both types of synapses ($p < 0.05$, Fisher's exact test).

A

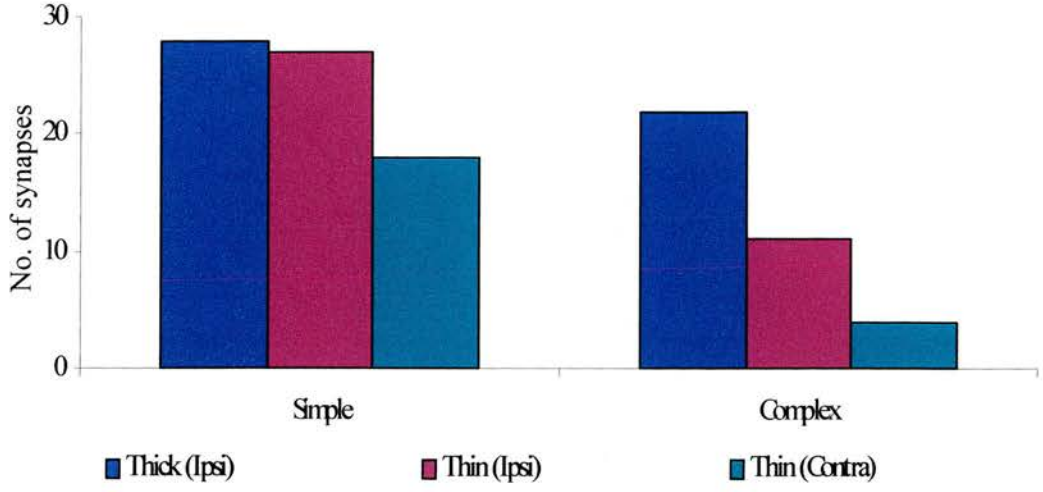
30
20
10
0
No. of synapses
Simple
Complex
Thick (Ipsi)
Thin (Ipsi)
Thin (Contra)

B

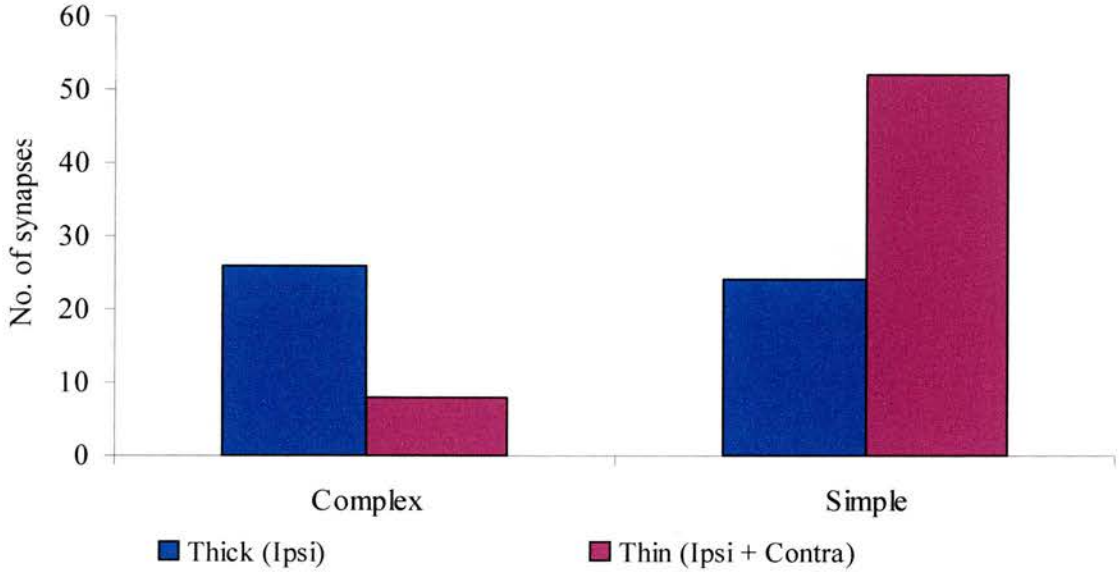
60
50
40
30
20
10
0
No. of synapses
Complex
Simple
Thick (Ipsi)
Thin (Ipsi + Contra)

C

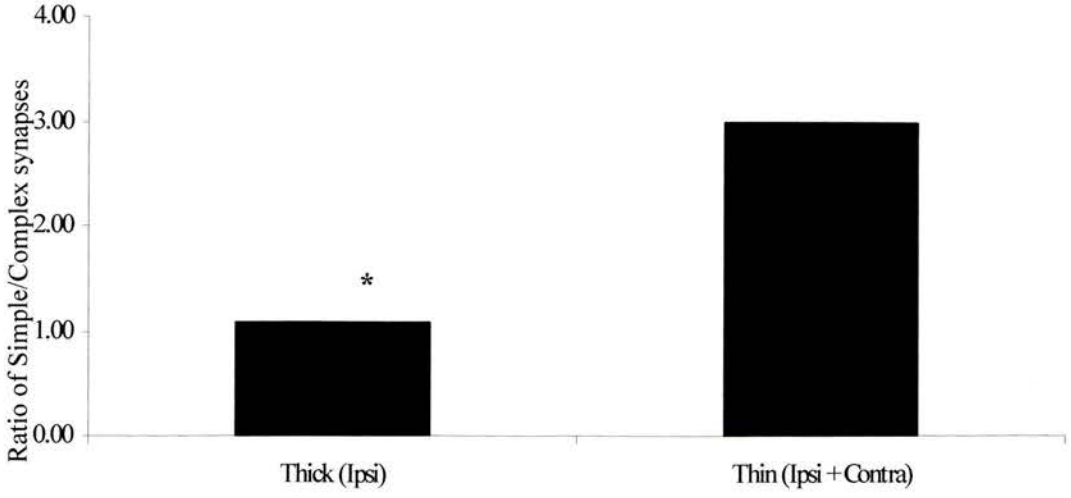
4.00
3.00
2.00
1.00
0.00
Ratio of Simple/Complex synapses
*
Thick (Ipsi)
Thin (Ipsi + Contra)

this group. A summary of the number and types of contacts made by both fibres is summarised in Figs. 2.9, 2.15, 2.16.

Two main differences between the two types of fibres were observed. The proportion of D_1 immunopositive to D_1 immunonegative contacts made by both types of fibres was significantly different (Fisher's exact test, $p < 0.05$) (Fig. 2.15C). The ratio of simple to complex synaptic contacts made by boutons of thick fibres (1.00) was significantly different to that made by boutons of thin fibres (3.00) (Fisher's exact test, $p < 0.05$) (Fig. 2.16C).

2.4) Discussion

The main findings of this study confirm previous findings and extend the knowledge of the synaptology of the two corticostriatal pathways originating from the barrel cortex. In confirmation of previous findings (Wright et al., 1999) (Alloway et al., 1998; Alloway et al., 1999), a distinct pattern of arborisation was seen in the striatum after injection of an anterograde tracer into the barrel cortex. Thick calibre fibres that belong to the topographic pathway (Wright et al., 1999) were found only in the ipsilateral striatum and formed a dense arc of terminals that ran parallel to the corpus callosum. Thin calibre fibres, which belong to the second diffuse pathway (Wright et al., 1999) were observed in both striata. The fibres did not maintain a strict topography and their terminals meandered throughout the striatum. Antibodies against D_1 receptors led to intense staining of the striatum as well as other basal ganglia structures. Both fibre types make synaptic contact with dendritic spines, agreeing with previous data (Wright et al., 1999). Boutons arising from fibres giving rise to the topographic pathway tended to be larger and many had more than one postsynaptic target. The boutons contacted D_1 immunopositive and immunonegative structures with equal frequency and formed equal numbers of simple and complex synapses. Boutons arising from the diffuse pathway were generally smaller and usually had only one postsynaptic target with which they formed, in most cases, simple synapses. This pathway also tended to contact D_1 immunonegative structures more frequently then D_1 immunopositive structures indicating that the pathway arising from cells below the septa make contact with neurones of the striatopallidal pathway more often than the fibres of the topographic system.

2.4.1) Technical considerations

Due to the need for double labelling as a means to address the issue of connectivity of the two input pathways to the two output pathways, the possibility of cross reaction has to be addressed (Bolam and Ingham, 1990). The omission of the D_1 antibody in the immunohistochemical process led to labelling by only one chromogen suggesting that cross reaction was minimal.

The classification of the fibres into the two groups was based purely on the thickness of the axons. This would not have caused any problems in the contralateral striatum as this structure only received input from the bilaterally projecting diffuse pathway which is composed of thin fibres (Wright et al., 1999). However there might have been misclassifications in the ipsilateral striatum which contained both fibre types, despite the fact that only fibres that clearly fell into one of the groups were chosen for the study. Detailed study of the projections revealed that some thick fibres branched off to form thinner calibre axons containing varicosities. Thus each thin fibre chosen for the ultrastructural study was traced back to confirm that it was not a branch of a thick fibre. However this was not always possible due to the density of arborisation which made it difficult to follow an axon for an extended distance. Also, most fibres chosen for the correlated light and electron microscope study were found either at the top or bottom of the section (see below) and the axons were not traced from one section to another. To further ensure that the fibres were indeed part of the diffuse pathway, only axons that did not follow the curvature of the corpus callosum were regarded as thin fibres. Despite this it is possible that fibres classified as ipsilateral, thin fibres in this study might represent a mix of both thick and thin fibres. Even with the possibility of misclassification, there was a significant

difference in the synaptology and connectivity of the 2 fibres, strongly suggesting that the two input pathways do in fact differentiate between the 2 groups of striatal neurones.

Another major concern of this study is the possibility of false negatives. To ensure that a D_1 immunonegative classification reflected the lack of D_1 receptors rather than the lack of penetration of immunohistochemical reagents, two internal control methods were employed. Firstly, the section with the bouton was scanned to ensure that there was D_1 immunoreactivity in surrounding structures. Secondly, each bouton from a fibre was labelled according to depth e.g. A1 to A5 with A1 representing the bouton on the top of the section (strongest immunoreactivity) and A5 the deepest in the section (weakest immunoreactivity). Thus a larger number of deeper boutons would be expected to be immunonegative if immunonegativity was due to the lack of penetration of immunohistochemical reagents. However this was not the case. In support of this, in one animal both thin and thick fibres were present on a region of striatum resectioned for EM. The thick fibres contacted a larger number of D_1 immunopositive structures than the thin fibres, despite being deeper in the striatal section. This suggests that the observation that thin fibres contact a higher proportion of immunonegative postsynaptic structures is not due to an artefact of the immunohistochemical method employed.

However a false negative could have also arisen if D_1 immunoreactivity was present but not observed in spines. The D_1 antibody used was similar to the antibody used by Hersch and colleagues (Hersch et al., 1995). They and others report that D_1 immunoreactivity is localised more often with dendrites rather than spines (Yung et al., 1995) (Hersch et al., 1995). They show examples where immunopositive

dendrites give rise to immunonegative spines (Hersch et al., 1995; Yung et al., 1995). In this study, no attempt was made to identify and record the immunoreactivity of the dendrite giving rise to the spine that formed the contact with the identified bouton. Thus some of immunonegative spines might be false negatives. Even if there was a high proprtion of false negatives, it should be safe to assume that false negatives would occur with equal frequency postsynaptic to both fibre types and thus would not influence the proportion of contacts made by each fibre type.

2.4.2) Cortical input to striatal neurones

Dendritic spines were the only postsynaptic targets of the two corticostriatal systems. This agrees with other data showing corticostriatal systems contacting dendritic spines of the striatal projection neurones (Kemp and Powell, 1971; Frotscher et al., 1981; Somogyi et al., 1981a; Dube et al., 1988; Wright et al., 1999). The excitatory connection of the pathways, as evidenced by the asymmetric nature of all synapses formed, is supported by the electrophysiological data which shows striatal neurones responding with an excitatory postsynaptic potential (EPSP) and in some cases action potentials to the stimulation of both these pathways (Wright et al., 2001).

While a small number of axodendritic synapses were reported in a study looking at input from the barrel cortex to the striatum (Wright et al., 1999), none were observed in this study. Ingham and associates, in a stereological study (Ingham et al., 1998) estimated that 5% of all synapses in the rat striatum were dendritic asymmetric synapses. In this study the synapses were not labelled and also could arise from regions other than the cortex, such as the thalamus. This input can also arise from cortical inputs synapsing onto either the proximal dendrites, interspine dendritic regions of spiny projection neurones or onto the dendrites of interneurones

(Lapper et al., 1992; Bennett and Bolam, 1994; Hersch et al., 1995; Thomas et al., 2000). Although there was no evidence of either input pathway synapsing with interneurones in this study, anterograde labelling of the somatosensory cortex and immunohistochemistry for parvalbumin-positive GABAergic interneurones revealed that this class of interneurones do synapse with boutons that have a similar morphology to boutons belonging to the topographic pathway (see Chapter 6)(Ramanathan et al., 2002). Due to the small percentage of axodendritic synapses predicted to occur in the striatum overall (Ingham et al., 1998), their lack in the present study could be due to the small numbers sampled (110-total, 50-thick fibres, 38-thin ipsilateral fibres, 22-thin contralateral fibres). Hersch and colleagues report that contralateral motor cortical boutons contact dendrites more often than an ipsilateral projection (Hersch et al., 1995) and the lack of this observation here could either reflect differences between the motor and sensory cortices or as discussed above, the small sample size. The differential connectivity of the ipsilateral and the contralateral pathways as observed by Hersch may translate to the different effects of the two projections on striatal neurones (Hersch et al., 1995). Even though little is known about how axodendritic and axospinous projections affect striatal cell physiology, it has been proposed that axodendritic synapses may serve a 'modulatory or gating function' (Hersch et al., 1995). Spines on the other hand, are thought to aid the stabilisation of excitatory synaptic transmission while playing a major role in cellular mechanisms such as long term potentiation (LTP) and cytotoxicity (Harris and Kater, 1994). It has to be noted however that others could not replicate the findings of Hersch (Hanley and Bolam, 1997).

Boutons from both fibres had similar ultrastructural features. Boutons contained numerous synaptic vesicles and in some cases, mitochondria; and are similar to a previous study (Wright et al., 1999). Boutons originating from thick fibres tended to be larger then those originating from the thin fibres. Larger boutons are believed to be more effective in transmitting synaptic information (Lisman and Harris, 1993; Pierce and Lewin, 1994), and the difference in size of the boutons might highlight the different roles played by the two pathways in the transmission of information to the striatum. Boutons of the topographic pathway also contacted more than one postsynaptic target per bouton, while the smaller boutons from thin fibres usually had only a single postsynaptic target. This fits in with the ultrastructural size principle postulated by Pierce and Lewin (Pierce and Lewin, 1994), which states that the size/volume of the bouton is related to its physiological strength.

A major difference between the two inputs is the number of complex synapses made, with thick fibres making three times as many complex synapses as thin fibres. Based on the utrastructural size principal and on work done in the hippocampus, larger boutons contact bigger postsynaptic structures which have larger postsynaptic densities (PSDs) that are often seen to have a perforation (Lisman and Harris, 1993; Pierce and Lewin, 1994), suggesting that the topographic pathway, composed of thick fibres is more efficacious.

2.4.3) Connectivity of the two input pathways to the two output pathways

The combined anterograde labelling and immunohistochemistry for D_1 revealed that the thin fibres of the diffuse pathway contacted more D_1 immunonegative structures compared to the thick fibres of the topographical pathway which did not differentiate

between immuno-positive and -negative spines. This suggests that the fine system influences the striatopallidal pathway more than the striatonigral pathway. However these results have to be interpreted with caution, as the validity of the notion of 2 fully segregated pathways has been questioned (Uchimura et al., 1986; Kawaguchi et al., 1989; Surmeier et al., 1992b; Cepeda et al., 1993; Surmeier et al., 1993; Parent et al., 1995; Surmeier et al., 1996; Wu et al., 2000; Sadek et al., 2002). The finding of the present study is contradictory to that of Hersch (Hersch et al., 1995), whose contralateral projection synapsed equally with both striatal output pathways (Hanley and Bolam, 1997). This could be due to the fact that different areas of cortex were studied in both these experiments. A bilateral projection has been well documented in the motor cortex (Wilson, 1987; Cowan and Wilson, 1994; Kincaid and Wilson, 1996) with the projection in the striatum contralateral to the injection being similar to the thick fibres of the topographic system studied here (Wright et al., 1999). However no thick fibres were found in the contralateral striatum in this and previous studies (Wright et al., 1999). Thus the barrel cortex may represent an ideal system to study the cortical input to the striatum, as the 'pure' corticostriatal input which arises from cells below septa is present bilaterally and this contralateral involvement separates it from the topographic system, that originates from cells below the barrels and is present only ipsilaterally (Wright et al., 1999; Wright et al., 2001).

2.4.4) Functional significance

In experimental models of Parkinson's disease, with the loss of dopamine induced by 6-hydroxydopamine (6-OHDA) lesions, a 19% decrease in spine density is observed in striatal neurones (Ingham et al., 1989, 1993). This loss of spines is associated with a loss of asymmetric synapses but is also accompanied by an increase in the number

of complex synapses (Ingham et al., 1998). Interestingly manipulations that increase the release of glutamate in the striatum result in a proliferation of complex synapses. Increased excitation as a result of direct stimulation of hippocampal afferents (Geinisman et al., 1988; Geinisman et al., 1991), LTP (Geinisman et al., 1991; Lisman and Harris, 1993; Harris and Kater, 1994) and the exposure of rats to sensory enriched environments (Greenough et al., 1978), have all resulted in the increase of perforated postsynaptic densities (PSDs). In the striatum, activation of the thalamocortical and corticostriatal pathways (Meshul et al., 1996b) and haloperidol treatment, which increases extracellular glutamate (See and Chapman, 1994; Yamamoto and Cooperman, 1994), results in an increase in complex synapses, possibly through an increased activity of glutamatergic synapses (Meshul and Casey, 1989; Meshul et al., 1996b; Meshul et al., 1996a). Given that this increase in perforated synapses reflects a selective sparing of a set of corticostriatal inputs, rather than the remodelling of synapses, the results of this study would suggest that the thin fibres would be more likely affected by the loss of dopamine, as they posses fewer complex synapses. This hypothesis disagrees with findings that show an increased activity in the striatopallidal pathway following dopamine depletion. 6-OHDA treatment results in an increase in biosynthesis and immunoreactivity of enkephalin (Thal et al., 1983; Young et al., 1986; Gerfen et al., 1991) and is likely due to the fact that neuropeptide expression is regulated by dopamine which differentially affects proenkephalin mRNA (messenger ribonucleic acid) (inhibits mRNA production) and SP and dynorphin mRNA (stimulates mRNA production) (Gerfen et al., 1990; Gerfen et al., 1991). Dopamine depletion also increases enkephalin immunoreactivity in the GP which is the target of the enkephalin expressing striatal projection neurones

(Voorn et al., 1987; Ingham et al., 1991) which is partly due to the increase in the size of the boutons (Ingham et al., 1997). In the same manner, dopamine depleted animals show reduction in substance P mRNA levels which is matched by parallel reductions in substance P immunoreactivity in the striatum and in the striatonigral terminals at substantia nigra level (Voorn et al., 1987; Cruz and Beckstead, 1989; Gerfen et al., 1991). In accordance with this observation is the increased activity of striatopallidal terminals, which is believed to underlie pathological increases in the firing rate of STN and GABAergic output neurones (Pan and Walters, 1988; Albin et al., 1989; Tremblay et al., 1989; DeLong, 1990). However, the change in behaviour of the output nuclei cannot be solely attributed to the change in flow of information via the indirect pathway. The loss of dopamine also exerts influences directly on to the STN via the hyperdirect pathway and has profound influences on the activity of the STN and GP network (Pan and Walters, 1988; Rothblat and Schneider, 1995; Kreiss et al., 1997; Magill et al., 2001). The inconsistency of the results of the present study and the changes that occur after dopamine depletion might be reconciled by the fact that the increase in complex synapses might reflect a remodelling of synapses. There is also a possibility that this alteration in the synaptology might be different for the two inputs, and this is an issue that has to be addressed in future experiments.

2.5) Conclusions

The thick fibres that arise from cells below the barrels are collaterals of the corticofugal fibres and project to the ipsilateral striatum in a topographic manner. The thin fibres arise from cells below the septa, are collaterals of corticocortical projections and project bilaterally to the striatum in a diffuse manner. Both pathways

form synapses onto the heads of dendritic spines belonging to medium sized densely spiny striatal projection neurones. They differ in their contacts, with boutons belonging to the topographic pathway making more complex synapses and contacting both output pathways of the striatum with similar frequencies. Thin fibres which are present bilaterally, make fewer synapses and contact D_1 immunonegative spines more often than D_1 immunopositive spines and therefore are assumed to contact predominantly striatal neurones of the indirect pathway. These findings suggest that the two input pathways transmit different information to the striatum and that they might be differentially regulated by dopamine.

CHAPTER 3

RESPONSE OF CORTICAL AND STRIATAL CELLS TO ELECTRICAL STIMULATION OF WHISKER PAD AND CONTRALATERAL CORTICAL STIMULATION

3.1) Introduction

3.1.1) Corticostriatal projections

The striatum is the main input nucleus in the basal ganglia and makes an important contribution to the control of mood and movement. In order to carry out this function it is evident that the striatum must receive afferents from a wide range of sensory and motor systems. All major regions of the cerebral cortex, including motor, primary and secondary sensory, premotor, prelimbic and limbic cortical areas project onto the striatum (Alexander and Crutcher, 1990; Gerfen and Wilson, 1996).

The corticostriatal projection arises from collaterals of glutamatergic pyramidal neurones whose cell bodies are found in layers II to VI (Donoghue and Kitai, 1981; Royce, 1983; Tanaka, 1987; Wilson, 1987; McGeorge and Faull, 1989; Cowan and Wilson, 1994). All corticostriatal neurones can be divided into at least three major classes based on their intracortical connections, laminar origin and pattern of striatal arborisation. The three classes are (1) pyramidal tract neurones in deep layer V; (2) bilaterally projecting corticocortical corticostriatal neurones in superficial layer V and deep layer III and (3) corticothalamic neurones in superficial layer VI (Wilson, 1986; Cowan and Wilson, 1994; Kincaid et al., 1998).

Based on laminar layer of origin the corticostriatal pathway can be divided into two separate pathways (Cowan and Wilson, 1994), i.e. the pathways that arise from deep layers verses superficial layers. The corticostriatal pathway that arises from deep layer V neurones, projects to the brainstem (Wilson, 1987; Cowan and Wilson, 1994). These neurones send axon collaterals to the striatum as they pass through the internal capsule and these collaterals make excitatory synaptic contacts on striatal spiny neurones (Donoghue and Kitai, 1981; Wilson et al., 1983b; Landry

et al., 1984; Wilson, 1987; Cowan and Wilson, 1994). Single cell filling experiments done by Cowan and Wilson (Wilson, 1987; Cowan and Wilson, 1994) identify two morphologically distinct cell types in the agranular cortex that give rise to brainstem projecting pyramidal neurones. Both types have dendritic arborisations in layer I and differences are seen in the axonal field size and distribution as well as the pattern of arborisation in the striatum. Despite these differences both these classes of pyramidal cells have the same electrophysiological characteristics when antidromically stimulated from the pyramidal tract (Cowan and Wilson, 1994). A second type of corticostriatal neurone, the corticothalamic neurone is also part of the corticostriatal projection arising from deep layers of cortex. These corticothalamic neurones arise in superficial layer VI of somatosensory cortex and send axon collaterals to the striatum (Wise and Jones, 1977; Royce, 1983). However these neurones have been documented only by a retrograde double labelling method.

This projection arising from deep layer cells (deep layer V and superficial layer VI) is not thought to be the main corticostriatal projection, as the response of striatal cells to stimulation of the brainstem is small in comparison to the excitatory response evoked by stimulation of even a small area of the motor cortex (Wilson et al., 1983b; Wilson, 1986; Wilson, 1987; Cowan and Wilson, 1994; Wilson, 1995). Retrograde studies have also shown a more superficial location for the majority of corticostriatal projections (Jones et al., 1977; McGeorge and Faull, 1989). The neurones that provide the majority of cortical input to the striatal circuitry are the medium sized pyramidal cells that have cells bodies in deep layer III to superficial layer V (Wilson, 1987; Cowan and Wilson, 1994). This slowly conducting population of neurones that is not activated by stimulation of the cerebral peduncle,

(Kitai et al., 1976; Jinnai and Matsuda, 1979) have apical dendrites that are thin and sparsely branched, and basilar dendrites that are small but more branched. The axonal field is extensive and collaterals are seen in the region of the parent neurone as well as extending to more superficial layers including layer I. The axons are also seen to branch in layer VI close to the white matter giving rise to branches for the collateral hemisphere as well as the ipsilateral striatum. As cortical neurones that contribute to the corpus callosum do not have branches that descend to the brain stem, (Wilson, 1987) this bilaterally projecting corticostriate pathway may provide the circuitry for the interhemispheric co-ordination of the basal ganglia (McGeorge and Faull, 1987). This projection does not follow the internal capsule fascicles, but moves laterally along the white matter before entering the striatum at a more acute angle. There is extensive arborisation in the striatum with frequent bifurcation of the axons and many varicosities en passant. Electrophysiological experiments show that these corticostriatal neurones are also commissural corticocortical neurones and these cells posses axons that do not extend beyond the striatum (Wilson, 1986; Wilson, 1987). The existence of a solely corticostriatal pathway contradicts findings of Levesque and colleagues (Levesque et al., 1996; Levesque and Parent, 1998). They propose a rule of striatal organisation, stating that corticostriatal pathways always arise as collaterals of corticofugal axons arborising elsewhere in the brain (Levesque and Parent, 1998), implying that the striatum receives an efferent copy of cortical information that is conveyed to various other brain regions including the brain stem and thalamus (Levesque and Parent, 1998). They have identified several types corticostriatal neurones and have shown that none of them have the striatum as the sole target (Levesque et al., 1996; Levesque and Parent, 1998). This apparent

discrepancy could be due to the different areas of cortex being studied i.e. prefrontal cortex and SII by Levesque and colleagues as apposed to the medial agranular cortex by Wilson and associates (Wilson, 1986; Cowan and Wilson, 1994; Levesque et al., 1996; Kincaid et al., 1998; Levesque and Parent, 1998).

Consistent with the asymmetrical nature of corticostriatal synapses onto spiny projection neurones; electrophysiological studies have shown that stimulation of the corticostriatal pathway evokes a monosynaptic excitatory postsynaptic potential (EPSP) (Wilson, 1986; Calabresi et al., 1990; Tepper and Trent, 1993; Calabresi et al., 1996) which is mediated by both α-amino-3-hydroxy-5-methyl-4-isoxazoleproprionic acid (AMPA)/kainite receptors and N-methyl-D-aspartate (NMDA) receptors (Kita, 1996). Cortical input plays a major role in the complex activity that is observed in striatal neurones during movement. Intracellular recordings *in vivo* have shown that striatal neurones display spontaneous shifts in membrane potential from a hyperpolarised (down) state (~ -75 to -90 mV) to a depolarised (up) state (~ -45 to -50 mV). The transition to the up state has been shown to be necessary for the firing of action potentials in striatal neurones (Calabresi et al., 1990; Wilson and Kawaguchi, 1996; Wickens and Wilson, 1998) and are caused by the spontaneous discharge of corticostriatal neurones (Cowan and Wilson, 1994; Wilson and Kawaguchi, 1996; Stern et al., 1997). Early experiments done by Wilson and his associates (Wilson et al., 1983a) have highlighted the importance of the contribution of the cortex to the generation of firing patterns in the striatal cells. Acute decortication, with or without a thalamic knife cut abolished the late phase of the response to all afferent inputs and caused the disappearance of the spontaneous firing of spiny neurones (Wilson et al., 1983a). In the absence of

cortical input, the potassium current I_{Kir} ensures that the membrane potential remains in the down state, well below the threshold for action potential generation and this is seen as a low rate of spontaneous activity in striatal neurones in awake animals that are behaviourally inactive (Schultz and Ungerstedt, 1978; Wilson and Groves, 1981; Kawaguchi et al., 1989; Groves et al., 1995). However the preparation, initiation and execution or termination of movement is associated with an increased corticostriatal input, which results in brief episodes of bursts of action potentials in striatal neurones (Schultz and Romo, 1988; Jaeger et al., 1993; Kiyatkin and Rebec, 1999).

Striatal cell activity is also strongly linked to and dependent on convergent inputs from the cortex. Striatal neurones possess a strong rectifying potassium current that shunts weak excitatory activity preventing the firing of action potentials. This rectification is overcome when the neurones are strongly depolarised by excitatory inputs over large portions of their dendritic fields. Each striatal neurone is thought to receive only a few synapses from a single corticostriatal axon (Kincaid et al., 1998) and it stands to reason that many corticostriatal neurones must discharge to evoke striatal activity (Wilson, 1995). Thus activity in striatal neurones may signal co-activation of specific cortical regions (Houk, 1995). To activate common postsynaptic targets the cortical regions must exhibit synchronous or near coincident discharges. One substrate for this synchronisation could be direct corticocortical connectivity and studies have shown that interconnected cortical areas project to overlapping portions of the striatum (Yeterian and Van Hoesen, 1978; Van Hoesen et al., 1981; Cavada and Goldmanrakic, 1991; Flaherty and Graybiel, 1991; Parthasarathy et al., 1992; Inase et al., 1996). However corticocortical connectivity and corticostriatal convergence are not always associated (Selemon and Goldman-

Rakic, 1985; Flaherty and Graybiel, 1993; Takada et al., 1998) and synchronisation can occur by subcortical or multisynaptic corticocortical pathways.

To further elucidate the functional significance of cortical input to the striatum, metabolic mapping studies of the rat striatum have been carried out (Brown, 1992; Brown and Sharp, 1995; Brown et al., 1996). As glucose utilization visualised by [^{14}C]deoxyglucose (DG) autoradiography primarily reflects presynaptic axon terminal activity, striatal areas with greatest afferent input from the cortex were identified via electrical stimulation of the cortex (Brown, 1992; Brown and Sharp, 1995; Brown et al., 1996). These studies have shown that there is a rough striatal somatotopy (Brown, 1992; Brown and Sharp, 1995; Brown et al., 1996) and the major characteristics of the activation agrees with the pattern of projections from sensory and motor cortex to striatum in primates (Flaherty and Graybiel, 1991, 1993) and rat (McGeorge and Faull, 1989), suggesting that the anatomical features observed are physiologically relevant. Electrophysiological studies have also confirmed this striatal somatotopy (Richards and Taylor, 1982; West et al., 1990; Carelli and West, 1991; Mittler et al., 1994; Cho and West, 1997; Glynn and Ahmad, 2002). An interesting observation of the DG studies was the activation of both striata after unilateral cortical activation (Brown, 1992; Brown and Sharp, 1995). This bilateral activation is to be expected as both the motor and sensory cortices have a bilateral projection as seen in anatomical studies in primates (Kunzle, 1975) and rats (Canteras et al., 1988; McGeorge and Faull, 1989). Asymmetrical peaks of activity were observed in both striata (Brown, 1992) with peak activation in striatum ipsilateral to movement being located in a region different from the area of peak activation in striatum contralateral to movement (Brown and Sharp, 1995). This

pattern of activity can be attributed to the non-overlapping projections observed from the motor cortex in primates (Flaherty and Graybiel, 1993). An asymmetrical, bilateral projection from the sensory cortex however was not observed until recently. One reason could be due to large injection sites employed by anatomical tracing studies. These non-specific injections might have masked asymmetrical corticostriatal projections, which could account for the asymmetrical striatal activity observed as a result of specific functional cortical activation. Recent anterograde tracing studies involving the SI cortex in rats (Wright et al., 1999) show that there is an asymmetrical projection arising from the barrel cortex to rat somatosensory striatum.

The corticostriatal projection plays an important role in the behaviour of striatal neurones. The whisker system in the rats is an ideal system to study corticostriatal information processing. By using this system, the input to the striatum can be stimulated easily. Much work has been done on the relay of whisker information from the periphery to the cortex (see below) and anatomical experiments have identified corticostriatal projections arising from the barrel cortex and are discussed below.

3.1.2) Whiskers

Facial whiskers of rodents provide the animals tactile information on space and nearby objects, motion of self relative to an object as well as discrimination of different textures (Schiffman et al., 1970; Carvell and Simons, 1995). Rats use their whiskers to explore the environment and on doing so use the sensory information to guide their locomotion (Carvell and Simons, 1990).

Whiskers are large tactile hairs in mechanically isolated hair follicles, which get an input from the trigeminal nerve (Dorfl, 1985). The nerves that innervate the whisker pad code for direction, velocity, frequency, magnitude as well as duration of whisker movement. Two sets of striated muscles, the extrinsic and intrinsic muscles work to control whisking(Dorfl, 1982; Wineski, 1985). These contract to cause the protraction and retraction of the vibrissae at frequencies of about 7 Hz in rats and 15 Hz in mice (Carvell and Simons, 1990). This sensory information is transmitted via intermediate nuclei up to the barrel cortex where there is a precise topographic anatomical co-relation between the sensory periphery and the barrel cortex (Woolsey and Van der Loos, 1970).

3.1.3) Information relay

Activity is conveyed from the whiskers to the barrel cortex over two parallel pathways, each crossing three synapses. Afferent cell bodies are in the trigeminal ganglion and central processes of these neurones terminate mainly in two separate ipsilateral brain stem nuclei: the principal trigeminal nucleus (PrV) and the spinal trigeminal nucleus (SpV) which is further subdivided into three subnuclei where whisker-like patterns of afferents and neurones are termed barrelettes (Belford and Killackey, 1979). Cells from these two nuclei project to two contralateral somatosensory thalamic nuclei, the architectonically homogenous posterior nucleus (Po) and the venteroposterior nucleus (VPM), where whisker like patterns of afferents and neurones are termed barreloids (van der Loos, 1976; Land et al., 1995). Neurones in the thalamus project to the somatosensory cortex of the same side.

In the first pathway, afferent terminals in each locus are grouped in whisker like patterns and the target cells are strongly activated by movement of a single

whisker, the principal whisker (Durham and Woolsey, 1978; McCasland and Woolsey, 1988). PrV is the main brain stem relay and the main thalamic nuclei is VPM. Thalamocortical axons from the VPM end in clusters in barrels in layer IV and in upper layers VI in register beneath them (Killackey, 1983; Jensen and Killackey, 1987; Armstrong-James and Callahan, 1991). This pathway is coined the lemniscal pathway and is fast and mainly activated by single whiskers (Welker, 1971; Simons, 1978).

In contrast, the second pathway originates mainly from large cells in SpVi (subnucleus interpolaris) on which afferents from many whiskers converge. These project to the Po in the thalamus which then projects between the barrels (septae) in layer IV as well as to layers III and V of the barrel cortex (Koralek et al., 1988; Lu and Lin, 1993). This paralemniscal pathway is slower than the lemniscal pathway and is activated by several to many adjacent whiskers (Armstrong-James and Fox, 1987).

3.1.4) Barrels and septae

The information from the whiskers is processed in layer IV of the cortex by groups of neurones arranged in discrete functional units known as barrels (Woolsey and Van der Loos, 1970). The areas of cortex above and below a barrel are known as barrel columns and each barrel processes input obtained from a single whisker. The barrel cortex can be differentiated into the cytochrome rich barrel centres and the septal cells surrounding the barrels. As discussed earlier both these domains receive inputs from different thalamic regions and thus might play different roles in information processing. Neurones in the septa have a weaker response than barrel neurones to the stimulation of principal whiskers (Armstrong-James and Fox, 1987) and display

short latency responses to deflection of surround whiskers, a characteristic not observed in barrel neurones (Armstrong-James and Fox, 1987). This difference is mainly due to the different responses of the two thalamic nuclei providing them with the input. Cells in the VPM respond most robustly to stimulation of whiskers (Simons and Carvell, 1989; Armstrong-James and Callahan, 1991; Chiaia et al., 1991b; Chiaia et al., 1991a; Diamond et al., 1992b; Diamond et al., 1992a) and have a principal whisker to which response is maximal (Diamond et al., 1992b; Diamond et al., 1992a). The response of these cells is independent of the integrity of the cortex (Diamond et al., 1992b). In contrast neurones of the Po respond to stimulation of skin, hairs and muscle related afferents in addition to whiskers (Chiaia et al., 1991b; Chiaia et al., 1991a). Spike generation in these cells is dependent on a functional cortex, indicating that the response of these cells might be due to feedback from layer V, as these cells get an insignificant input from the trigeminal nucleus (Diamond et al., 1992b). Po cells do not have a principal whisker but respond with the same amplitude to several whiskers and require more intense whisker stimulation to generate responses (Chiaia et al., 1991b; Chiaia et al., 1991a; Diamond et al., 1992a). In addition to the different response profiles of the inputs to the barrels and septae anatomical studies have shown that these two cortical domains have different outputs and connections.

Projections from a barrel column extend to the home barrel and encompass the most immediate neighbouring barrel columns and surrounding septae (Kim and Ebner, 1999). These projections tend to be sparse indicating that the main input to the barrels arises from the principal whisker and that the barrel is less activated by surrounding whiskers via intracortical circuitry (Kim and Ebner, 1999). The barrels

also send projections to SII (Alloway et al., 1999; Kim and Ebner, 1999; Alloway et al., 2000). Projections from the septae form dense terminals preferentially in septal areas at least two barrel columns away (Chapin et al., 1987 and are the source of the projections to the posterior parietal, dysgranular and SII cortices {Fabri, 1991 #74; Koralek et al., 1990; Hoeflinger et al., 1995; Kim and Ebner, 1999).

The responses and connections of the two pathways strongly suggest that they code for different information. The lemniscal pathway might convey information about what is touched by the whisker (Ahissar et al., 2000) while the paralemniscal pathway, by virtue of its connection to the posterior parietal cortex which is involved in spatial perception for eye and limb movements, (Chapin and Lin, 1984; Andersen et al., 1997) might convey information about the spatial location of the object touched by the whiskers (Ahissar et al., 2000). Thus it would be interesting to see if these two pathways remain segregated in the subcortical targets of the barrel cortex which are involved in bringing about a behaviourally relevant movement. There are both ipsilateral and contralateral projections of the vibrissae region of SI to the thalamus (Royce, 1983; Carretta et al., 1996), striatum (McGeorge and Faull, 1989; Alloway et al., 1998; Alloway et al., 1999; Wright et al., 1999) as well as an ipsilateral projection to brainstem (Mercier et al., 1990). The corticostriatal projection is important as the striatum is the input nucleus of the basal ganglia and is heavily involved in the sensorimotor aspects of movement programming (Graybiel, 1995).

3.1.5) Projections from the barrel cortex to the striatum

Unlike mice, where the terminal field from the barrel cortex is spread over the whole area of the striatum (Hoogland et al., 1987), anterograde studies (Alloway et al.,

1998; Alloway et al., 1999; Wright et al., 1999) show that in the rat, the majority of projections from the barrel cortex terminate in the dorsolateral part of the posterior striatum which is consistent with electrophysiological data that indicates that this is also the whisker sensitive region of the striatum (Carelli and West, 1991; Mittler et al., 1994; Brown and Sharp, 1995). These anatomical studies have shown two different corticostriatal pathways arising from the barrel cortex. The majority of labelled terminals aggregate in curved lamellar-shaped strips along the lateral margin of the ipsilateral striatum just below the corpus callosum (Alloway et al., 1998; Alloway et al., 1999; Wright et al., 1999). Unlike the study done by Wright and associates, Alloway and colleagues observed that these lamellae did not occupy a continuous region but were separated by regions of unlabelled neuropil, which could have been due to the intervening fibre fascicles (Alloway et al., 1998; Alloway et al., 1999). This discrete pathway which gives rise to a crude topographic organisation in the striatum is made up of thick fibres and found only ipsilaterally (Wright et al., 1999). The topographic organisation is such that row A whiskers are represented laterally and row E whiskers more medially (Alloway et al., 1999; Wright et al., 1999). Posterior whiskers terminate in more dorsal regions of each crescent shaped strip, while projections from anterior whiskers are more ventral (Alloway et al., 1999). These projections were however found to be overlapping i.e. neighbouring barrels from the same row had greater corticostriatal overlap compared to projections originating from different barrel rows (Alloway et al., 1999; Wright et al., 1999). This lends support to the view that interconnected cortical areas are more likely to send convergent projections to the striatum as barrel columns in the same row are more strongly interconnected than barrel columns in different rows (Bernardo et al.,

1990a; Bernardo et al., 1990b; McCasland et al., 1991; Hoeflinger et al., 1995; Kim and Ebner, 1999). This pattern of innervation fits in with the natural use of whiskers during exploratory behaviour in rats. Due to the organisation of the whiskers, experiments involving tactile discrimination indicate that adjacent whiskers within a row often contact an external stimulus in sequential order and thus the pattern of within-row whisker contact with an object is less likely to vary then the pattern of activation across different whisker rows (Carvell and Simons, 1990). This has been supported by DG experiments which indicate a preferential relay of information within rows than between arcs (Durham and Woolsey, 1978; McCasland and Woolsey, 1988).

These thick fibres of the discrete pathway which are present only in the ipsilateral striatum, are similar to the large diameter corticostriatal axons (0.6-0.7 μm) observed by Kincaid and Wilson (Kincaid and Wilson, 1996). These fibres arise as collaterals of corticothalamic and pyramidal tract neurones and are similar to the type of corticostriatal neurone described by Cowan and Wilson (Cowan and Wilson, 1994). In both cases the axons leave the fibre bundles at right angles and have a restricted terminal field in the striatum (Cowan and Wilson, 1994; Wright et al., 1999). Retrograde studies (Wright et al., 2001) have shown that these fibres arise from layer V neurones, below the barrel centres themselves.

Diffuse was the name coined for the second corticostriatal pathway. It is made up of thin calibre fibres and is present bilaterally (Wright et al., 1999). This diffuse system has a sparsely branching widely distributed fibre pattern which does not maintain the topography of the discrete pathway suggesting that fine spatial resolution is not required for its function (Wright et al., 1999). Septal cells which are

the source of corticocortical connectivity in the barrel cortex (Olavarria et al., 1984; Chapin et al., 1987) give rise to this system (Wright et al., 2001). This system of fine fibres travel along the edge of the corpus callosum before entering the striatum at a more acute angle (Wright et al., 1999).

A smaller projection area more medial and anterior in a zone distinctly separate from the topographically ordered dorsolateral striatum was also identified in anatomical studies (Alloway et al., 1998; Alloway et al., 1999; Wright et al., 1999). This area is composed of fine fibres which would imply that they are part of the diffuse system (Wright et al., 1999). However in some animals there appeared a topography consisting of a curved lamellae of fibres that are similar to the arcs of terminalisation found just beneath the corpus callosum (Alloway et al., 1998; Alloway et al., 1999). However in this instance the more lateral strip belongs to row E whiskers while row A is most medial (Alloway et al., 1999). This topography would suggest that either the diffuse pathway gives rise to both a non-topographical as well as a topographical projection with the latter confined to the ipsilateral striatum. The other possibility is that the large diameter axons belonging to the discrete pathway give rise to branches of smaller diameter which make up the second whisker map in the striatum.

Deoxyglucose experiments focusing on striatal activity in conscious rats have shown that there is peak activation of striatum contralateral to movement (Brown and Sharp, 1995; Brown et al., 1996). There is a patchy distribution with peak areas of activation surrounded by areas of lower activation (Brown and Sharp, 1995; Brown et al., 1996). In accordance with the anatomical data there are two areas of activation, a large medial area as well as a lateral strip of activation below the external capsule

(Brown and Sharp, 1995). Areas anterior to the projections observed anatomically are also activated by SI stimulation (Brown and Sharp, 1995; Brown et al., 1996). Interestingly peak activation is seen in the medial striatum while there is a much lower activation in the lateral strips below the corpus callosum (Brown and Sharp, 1995). This is opposite to the density of projection from the barrel cortex (Alloway et al., 1998; Alloway et al., 1999; Wright et al., 1999). Brown and associates demonstrated that the sites of lower activation overlap with areas activated by stimulation of other cortical areas (Brown and Sharp, 1995). Anatomical data confirms that dorsolateral striatum receives convergent projections from vibrissal motor cortex (Hoffer and Alloway, 2001) as well as the SII (Alloway et al., 2000). These lend strength to Brown and associates' postulate that areas of low activation are areas where information from various cortical areas are integrated (Brown and Sharp, 1995). However when single whiskers are stimulated, the peak activity in contralateral striatum is restricted mainly to dorsolateral edge of striatum just below the corpus callosum (Brown et al., 1996). This inconsistency could be due to global activation of the SI in earlier experiments (Brown and Sharp, 1995) which could cause changes in cortical, sub-cortical afferents as well as intra-striatal activity, causing increases or decreases in glucose utilisation over areas of striatum shown not to receive projections in anatomical studies or areas not activated by stimulation of a single whisker. This global activation study is important in understanding the role of the striatum during natural whisking which involves all whiskers protracting synchronously during exploratory behaviour (Carvell et al., 1991). Figure 3.1 is a schematic illustrating the flow of information from the whisker pad to the ipsilateral striatum.

Figure 3. 1. Flow of information from the whisker pad to the striatum.

The figure illustrates the flow of information from the whisker pad to the ipsilateral striatum. There are two parallel whisker pathways. The pattern of the whiskers seen on the face can be seen in the brain stem as well as the thalamus. The information from the whisker pad is transmitted to the brain stem barrelettes and then onto the contralateral thalamus. In the VPM which is part of the lemniscal pathway, there is an exact representation of the whiskers forming what is known as barreloids. The Po nucleus on the other hand does not receive such a topographically precise input but receives inputs from other structures such as fur in addition to whiskers. The VPM projects to the barrel centres maintaining the topography, while the Po projects to the septal cells surrounding the barrel centres. The barrel cortex sends 2 types of projections to the striatum. One pathway has a topography with Row A whiskers more dorsal and Row E more medial. Posterior whiskers are found more dorsal and anterior whiskers more ventral. Projections from the septa are more diffuse and do not have the topography of the first pathway. There have been reports of a second more medial topographic pathway in the ipsilateral striatum and in this pathway Row A whiskers are the most ventral and medial (Adapted from Alloway, 1999).
(PrV: principal sensory nucleus of the trigeminal nerve; SpV: spinal nucleus of the trigeminal nerve, subnuclei o-oralis, i-interpolaris, c-caudalis; VPM: venteroposterior nucleus of the thalamus; Po: venteroposterior nucleus of the thalamus)

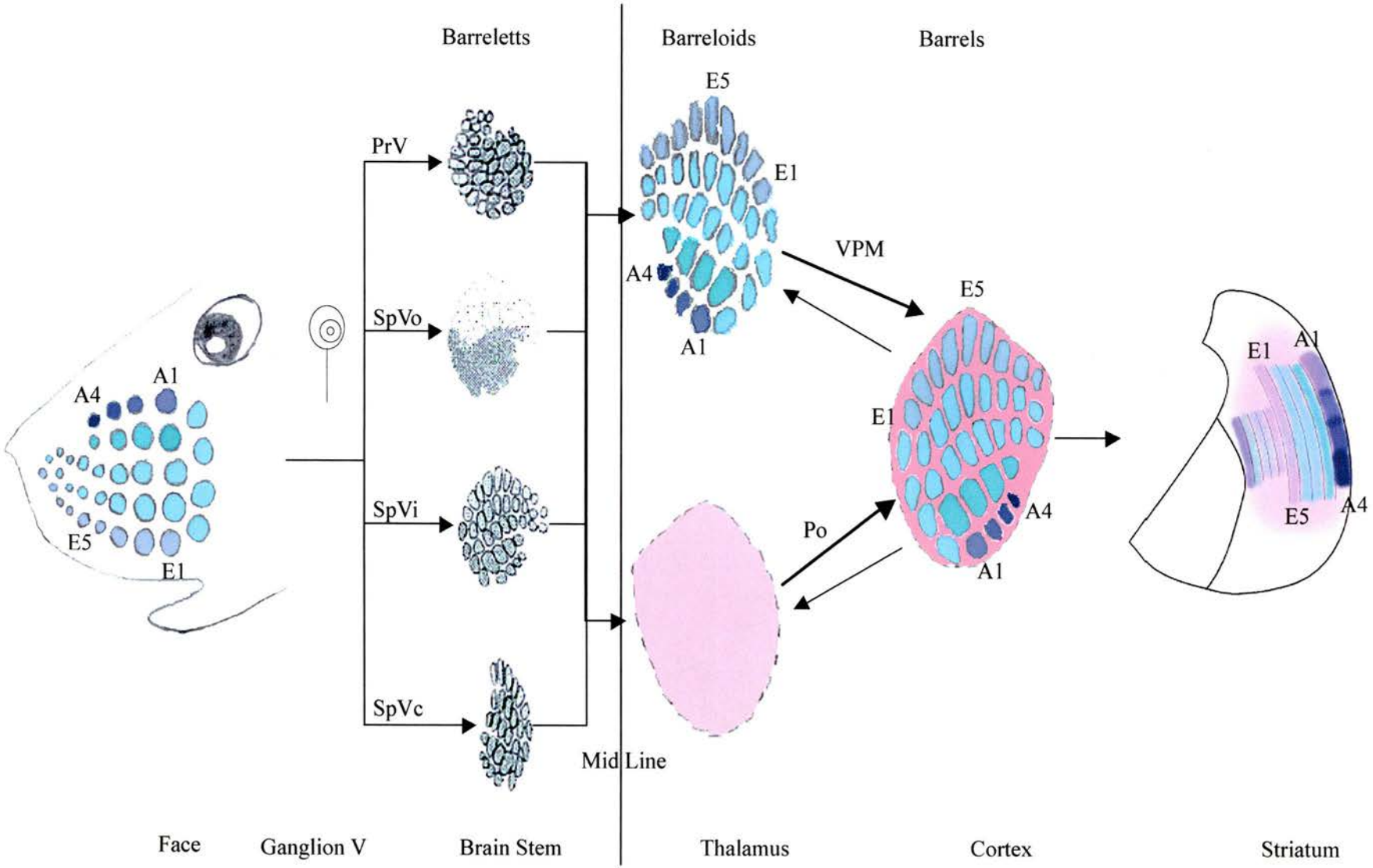
Barreletts
Barreloids
Barrels
PrV
SpVo
SpVi
SpVc
E5
E1
A4
A1
VPM
Po
Mid Line
Face
Ganglion V
Brain Stem
Thalamus
Cortex
Striatum

3.1.6) Aim

Anatomical studies have shown that there are two different pathways from the barrel cortex to the striatum and the distribution, pattern and area of innervation in the striata are distinct (Alloway et al., 1998; Alloway et al., 1999; Wright et al., 1999). This fits in with observations that there is an asymmetrical distribution of ipsilateral and contralateral striatal loci activated from deflection of a single whisker (Brown et al., 1996). Injections in anterior cortex (Kincaid and Wilson, 1996) have shown both fibre types in both striata which implies that the projections from the barrel cortex to striatum might have some unique properties. Both pathways arise from different parts of the barrel cortex i.e. the discrete pathway from the barrel centres and the diffuse pathway from the septal cells (Wright et al., 2001). Barrel and septal cells differ in the inputs they receive (Koralek et al., 1988; Lu and Lin, 1993), in their response to whisker stimulation (Armstrong-James and Fox, 1987) as well in their connections to other brain regions (Olavarria et al., 1984; Koralek et al., 1988; Lu and Lin, 1993). This would indicate that the barrel and septal domains in the barrel field play different roles in whisker information processing. As these two areas give rise to the two inputs to the striatum, which are for the most part kept distinct, it would suggest that the discrete and the diffuse pathway convey either different information or are processed differently in the striatum. The aim of this part of the study was to examine the response of striatal cells to stimulation of both pathways and to compare and contrast the responses. As cells in layer V of barrel cortex give rise to the corticostriatal projection, the response of the cortical cells to the stimulation paradigm was also recorded to determine if the response profiles of the cortical cells is mirrored by striatal neurones.

3.2) Experimental Procedures

3.2.1) Extracellular recording

3.2.1.1) Anaesthesia

A total of 13 male Sprague Dawley rats (240-350 g) were used. The rats were anaesthetised intra-peritoneally with 1ml/100g body weight of a 10% urethane (Sigma Chemicals, St Louis) 1% α-chloralose (Sigma Chemicals, St Louis) mix in distilled water. Stable levels of anaesthesia were maintained throughout with additional anaesthetic (10% of original dose) administered approximately four to six hours after the initial injection to ensure the absence of a foot withdrawal reflex.

3.2.1.2) Surgical procedures

Xyclocain (Astra Pharmaceuticals, Hertfordshire, U.K.) was sprayed on the neck and a tracheotomy was performed. The animal was then transferred to a stereotaxic apparatus and the head was secured in a stereotaxic frame via ear and tooth bars. The tail was taped to the rear of the frame in order to keep the spine straight to ensure no blockage of the trachea. Body temperature was maintained at 37^0C throughout using a homeothermic blanket and rectal probe.

The scalp was cut from the anterior of the Bregma to the base of the skull. The overlying tissue was pulled back and the skull surface cleaned to reveal the Bregma and the midline. The levator duris longus muscle at the base of the skull was pulled back to reveal the atlanto-occipital membrane. A slit was made in the membrane to expose the brain stem. An incision was made from the base of the skull to a cut created in the skin above the forepaw. Pulling a saline soaked cotton wool

strip through this passage and inserting it under the base of the skull created a cerebrospinal fluid (CSF) drain, which reduced intracerebral pressure.

The anterior superficial and posterior deep masseter muscles were teased away from the skull so as to expose the lateral parietal bone. The scalp and the masseter muscles were secured using silk suture to a brass ring situated above the skull to keep the area clear. The skull was drilled 2.1 mm posterior and 5.0 mm lateral on both sides relative to the Bregma (Paxinos and Watson, 1986). The area of the skull above the cortex on both sides was then gently picked away to ensure that no skull fragments entered the cortex. A hole was created in the dura to expose the cortical surface on the recording site to facilitate the passage of the recording electrode. An amplifier earth was secured to the scalp. The entire preparation was isolated from ground vibration by floating the table with Nitrogen.

3.2.1.3) Whisker stimulus

To activate the ipsilateral topographic pathway arising from the barrel centres, the left whisker pad was stimulated. Stimulation to the contralateral snout in the region of the whiskers was carried out using an electrical stimulator. This consisted of a pair of exposed wires attached to pins. The pins were pushed into the whisker pad and an electric current (usually 5 V) was passed across the pins in order to elicit a muscular twitch in the whisker pad. The duration of the stimulus was 0.2 ms and the cells were usually stimulated subthreshold to prevent the firing of action potentials.

3.2.1.4) Contralateral stimulating electrode

A stimulating electrode (Harvard Apparatus, UK) was placed contralateral to the recording electrode (AP-2.1 mm, L-5.0 mm) to stimulate the bilateral corticostriatal

fibres that arise as collaterals of corticocortical projection. The concentric bipolar stimulating electrode (1 mm tip separation) was lowered to a depth of 2.0 mm with respect to the cortical surface such that the tip straddled Layer V of the primary somatosensory cortex. Stimuli were rectangular pulses 0.2 ms in duration and ranging in amplitude from 4.5 to 10 mV which was subthreshold for the cells. The experimental set up is illustrated in Figure 3.2.

3.2.1.5) Extracellular recordings

Extracellular recordings were carried out using borosilicate glass microelectrodes (1.5 mm OD, 0.86 mm ID with inner filament, Harvard Apparatus, U.K.) filled with pontamine sky blue (2% in 0.5M sodium acetate). The electrode was advanced into the cortex at an angle of 90^0 to the cortical surface. It was then advanced 200-300 μm into the cortex using a manual micromanipulator and the electrode resistance and capacitance compensation balanced, before flooding the surface with warmed physiological saline or artificial cerebrospinal fluid (aCSF at 40^0C). The microelectrode was then advanced to a depth of 2,500 μm, with constant 'buzzing' to keep the electrode tip clear. The electrode resistance was typically 4-8 MΩ.

The electrode was then advanced through the striatum in 2 μm steps using a Burleigh inchworm motor stepper. Neuronal activity was searched for using electrical stimulation of the whisker pad (0.4 Hz). Once a cell was recorded extracellularly, the response to contralateral cortical stimulation was established. The electrode was advanced to a maximum depth of 5,000 μm for each tract. After each recording session the top and bottom of the tract was marked by applying a 20 μA current for approximately twenty minutes in order to make a small discrete deposition of pontamine sky blue as a stereotaxic mark. After marking the positions

Figure 3. 2. Experimental set-up.

Schematic representation (modified from Paxinos and Watson 1996) of the sites of stimulation and recording. The contralateral whisker pad was stimulated by passing an electrical current through a pair of insect pins inserted into the snout of the rat. This impulse is carried to the trigeminal nucleus, crosses the midline to activate the ipsilateral thalamic nuclei involved and then the barrel centres. The activated lemniscal pathway leads to excitation of the ipsilateral topographic pathway (at least initially) which arises from the barrel centres (Blue pathway). Stimulation of the contralateral barrel cortex was done using a stimulating electrode. This leads to activation of both pathways ipsilaterally but only activation of the diffuse pathway which arises from the septa contralaterally (Red pathway). The responses of cortical and striatal neurones were studied to both forms of stimulation. Cortical neurones were recorded from a depth of 1500 to 2200 μm with respect to the cortical surface. This was followed by a period where no cells were recorded from (passage through white matter). The electrode was then advanced to the striatum where records were obtained from depths of 2500 to 5000 μm. In experiments where no recordings were searched for from the cortex, the electrode was advanced manually to 2500 μm before striatal records were taken.

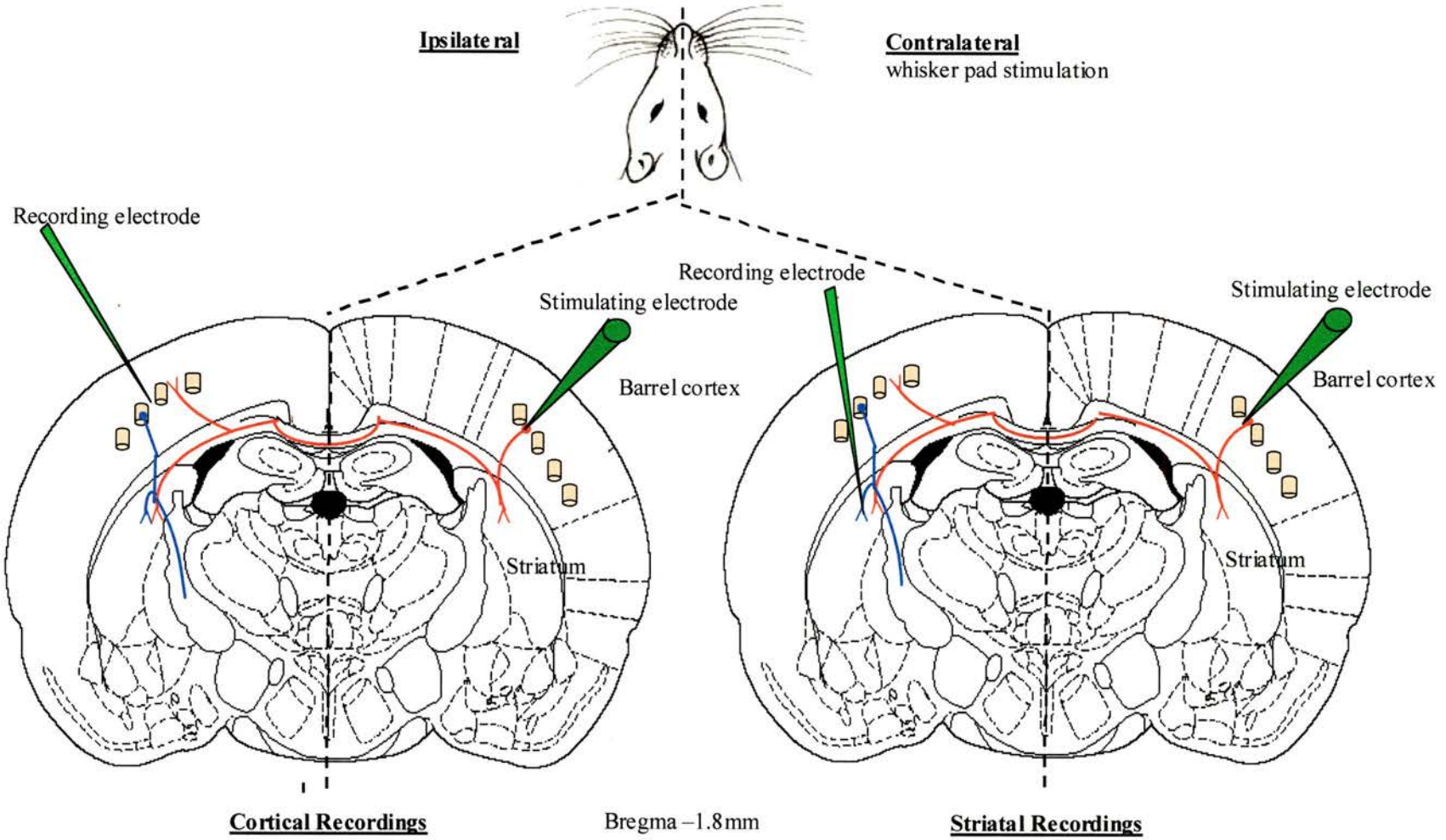
Ipsilateral
Contralateral
whisker pad stimulation
Recording electrode
Stimulating electrode
Barrel cortex
Striatum
Recording electrode
Stimulating electrode
Barrel cortex
Striatum
Cortical Recordings
Bregma –1.8mm
Striatal Recordings

the electrode was slowly brought back up to the cortical surface and moved to a different position. A maximum of two tracts were made in any one animal.

3.2.1.6) Perfusion and histology

The animals were given a terminal dose of the chloralose urethane anaesthetic. The thoracic cavity was exposed and the animal was perfused transcardially with 25 mls of heparinised (10 μ/ml) saline (90%) followed by 300 mls of 4% paraformaldehyde, 0.05% glutaraldehyde in 0.1M PBS pH 7.4. The brain was removed and stored in a 10% sucrose buffered fixative overnight at 4^0C. The brain was then cut into 50 μm coronal sections on a freezing microtome.

The sections were washed in PBS four times (5 min each) after which they were mounted on subbed slides and oven dried for one week. The sections were dehydrated in ethanol in the following concentrations (70%, 90%, 95%, 100%, 100%, 100%, 5 min each), cleared in xylene (10 min) and rehydrated through to water (100%, 100%, 100%, 95%, 90%, 70%, 50%, distilled water, 5 min each). The sections were then counterstained in Cresyl Fast Violet (0.1%) for 15 min at room temperature. They were rinsed briefly in distilled water and 50% and 70% ethanol, differentiated in 90% ethanol and then dehydrated rapidly through 95% and 100% alcohol (15-20 s each). The sections were then cleared in two changes of xylene (5 min each) and coverslipped with DPX (BDH Laboratory Supplies).

Sections were reconstructed using a drawing tube in order to determine the position of the pontamine sky blue deposits. Positions of neurones from which records were obtained were then marked on the section drawings.

3.2.2) Intracellular recording

3.2.2.1) Anaesthesia

A total of 53 male Sprague Dawley rats (240-350 g) were used for intracellular recordings. The anaesthetic composition and dose were same as the extracellular electrophysiology experiments.

3.2.2.2) Surgical procedures

A tracheotomy was performed and the animal was set up in the stereotaxic apparatus as previously described (see Section 3.2.1.2). A cotton ball soaked with aCSF (artificial cerebrospinal fluid) or saline was then placed over the hole on the recording site to protect the cortex and to prevent the cortical surface from drying up. The stimulating electrode was then lowered to a depth of 2.0 mm.

A dental cement well (Simplex Rapid, Associated Dental Products, Swindon, U.K.) approximately 1 cm tall was built around the site of the recording electrode placement (Fig. 3.3). When the well was dry, the cotton ball was removed and the dura was deflected just before the recording electrode was lowered.

3.2.2.3) Stimulus protocol

The whisker pad and contralateral cortex were stimulated as previously described. In five of the animals in addition to the whisker pad stimulus, single vibrissae were deflected using a piezoelectric stimulator. The tips of whiskers A1 to E1 were trimmed and three whiskers were fed into the electrode glass holders at any one time. The glass tubes were adjusted so that the whiskers lay close to a natural resting position as possible. The other whiskers were trimmed to prevent their accidental deflection (Fig. 3.3).

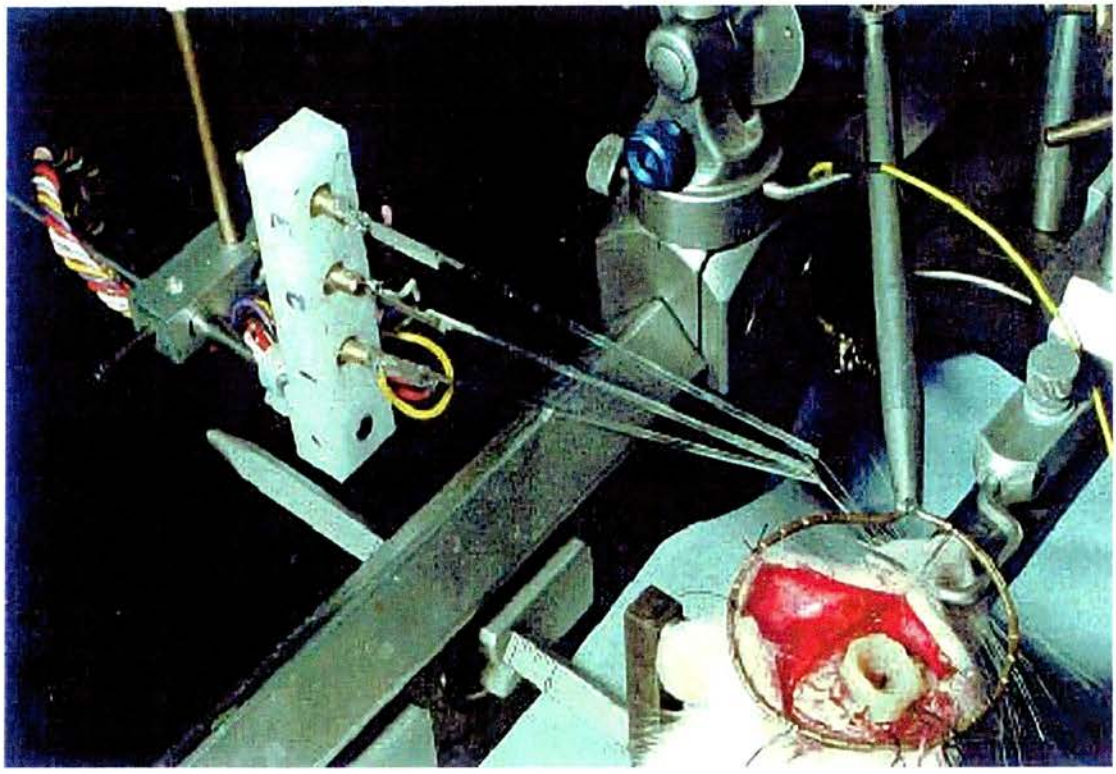

Figure 3. 3. Experimental set-up for deflection of individual whiskers.

This photograph shows a typical experimental set up. The skin and muscle were pulled back and tied to the overlying ring to keep the area clean allowing easy drilling of the skull. The cement wall built to stabilise the electrode during intracellular recordings is illustrated. In most experiments a pair of insect pins were used to stimulate the whisker pad. The photograph illustrates the piezoelectric stimulator used to deflect individual whiskers. During the use of the piezoelectric stimulator all whiskers were trimmed except those belonging to arc 1 (A1 to D1). Each piezoelectric chip was able to operate independently. (Reproduced from Hutton, 1999).

3.2.2.4) Intracellular recordings

Borosilicate glass microelectrodes (1.5 mm OD, 0.86 mm ID with inner filament, Harvard Apparatus, U.K.) containing either 3M potassium acetate or biocytin (Sigma, UK, 5% in 1M potassium acetate) with resistances of between 50-110 MΩ were used. The electrode was advanced into the cortex at an angle of 90^0 to the cortical surface. It was then advanced 100 μm into the cortex using a manual micromanipulator and the electrode resistance and capacitance compensation balanced. The dental cement well was then filled with liquid paraffin wax (Physiowax, TAAB, England) to stabilise the electrode. Neuronal activity was searched for using electrical stimulation of the whisker pad (0.4 Hz). The electrode was advanced in 2 μm steps, until a neurone was impaled either by advancement alone or by a combination of advancement and electrode 'buzzing' with high current, voltage or capacitance, to gain entry to the cell. The presence of cells was detected by a drop in membrane potential and changes in electrode resistance.

Once a cell was successfully impaled its response to contralateral cortical stimulation and individual vibrissae deflection was determined. Input resistance was estimated by passing a series of small amplitude hyperpolarising and depolarising (subthreshold) current pulses through the recording electrode (maximum of 1.5 nA to –1.5 nA in 0.5 nA steps). All pulses and measurements of cellular properties were made by triggering data acquisition regularly. Cells were either in the up or down state and no attempt was made to distinguish between the two states. The spontaneous activity of the cells was also recorded. When electrodes filled with biocytin were used, once the records were obtained the cells were filled by injecting hyperpolarising current (-2 nA in 200 ms pulses for up to 20 min). The membrane

potential was monitored during filling and for some neurones a holding current was used to stabilise the intracellular filling. If there was any sudden change in the membrane potential, filling was stopped and the electrode was carefully removed from the striatum. A maximum of three neurones were filled in any one animal. In experiments where no cells were filled or when biocytin free electrodes were used, pontamine sky blue markings were made at the top and bottom of the electrode tracts at the end of the experiment.

If no cells were impaled the electrode was advanced to a maximum depth of 5,000 μm and extracellular records were taken. The electrode was then slowly brought back up to the cortical surface and a new penetration made in a different position.

3.2.2.5) Perfusion and histology

The animal was allowed to survive at least 1 1/2 h post-filling to maximise biocytin transportation. The animals were given a terminal dose of the chloralose urethane anaesthetic. The thoracic cavity was exposed and the animal was perfused transcardially with 25 mls of heparinised (10 μ/ml) saline (90%) followed by 300 mls of 2% paraformaldehyde, 1.25% glutaraldehyde in 0.1M PBS pH 7.4. The brain was removed and stored in a 10% sucrose buffered fixative overnight at 4^0C, and then cut into 50 μm coronal sections on a freezing microtome.

The sections were washed in PBS four times (10 min each), to remove fixative. The sections were then incubated in a quenching solution, made up of 70% PBS, 30% methanol, 0.03% hydrogen peroxide, for 30 min. This was done to reduce endogenous peroxidase activity. The sections were then washed in PBS eight times (10 min each) to remove the peroxide reaction mixture. The sections were then

incubated for 5 h in 0.3% Triton-X in PBS (PBS-TX) at room temperature with gentle agitation, to increase binding between the biocytin and the ABC molecule. The sections were then incubated in ABC Elite (1:50 in PBS-TX, Vector Laboratories) at 4^0C for 60 h.

The sections were washed three times (10 min each), in PBS and reacted with DAB for 10 min. They were then well rinsed in PBS before being mounted on subbed slides. The slides were oven dried for 1 week. The sections were dehydrated in ethanol (as described in Section 3.2.1.6), cleared in xylene (10 min) and rehydrated through to water (as described in Section 3.2.1.6) before counterstaining in Methyl Green for 15 min at room temperature. They were rinsed briefly in distilled water and 50% and 70% ethanol, differentiated in 90% ethanol and then dehydrated rapidly through 95% and 100% alcohol (15-20 s each). The sections were then cleared in two changes of xylene (5 min each) and coverslipped with DPX (BDH Laboratory Supplies). Cases where only pontamine sky blue markings were made, the perfusion and histological methods employed were similar to those of the extracellular experiments.

Sections were reconstructed using a drawing tube in order to determine the position of the filled cells. Filled cells were photographed. Positions of neurones from which extracellular records were obtained were also calculated from the marked ends of the tracts.

3.2.3) Acquisition and analysis of data

3.2.3.1) Data acquisition - MacLab and Signal

All experimental data was recorded on either a Macintosh based data acquisition package (MacLab Scope) or a PC based data acquisition system (Signal 2.04). Eight

consecutive sweeps were taken for each of the stimuli. Twelve sweeps each lasting 5 s were taken for the spontaneous activity of the striatal neurones. The sweeps were later analysed off-line.

3.2.3.2) Data analysis

For extracellular records the latency of the response of the cell (as determined by the firing of an action potential, post-stimulus) was measured manually for both types of stimuli.

For intracellular data the latency, rise-time and peak amplitude of the response of the neurone to each stimulus was measured. The latency of the response was defined as the time taken from the onset of the stimulus to the start of the EPSP (Fig. 3.4). The rise time was defined as the time from the start till the first inflection in the rising phase of the EPSP (Fig. 3.4). Most of the stimuli were delivered sub-threshold and thus there were no action potentials. However when the cells fired action potentials, they were present at the peak of the EPSP. In these cases the rise time was defined as the first inflection in the rising phase of the EPSP before the firing of the action potential (Fig. 3.4). The peak amplitude was the difference between the resting membrane potential of the cell and the point of maximal response to the stimulus (not including action potentials (Fig. 3.4). Input resistance was determined from the slope of a regression line fitted to the membrane potential produced by a series of hyperpolarising and subthreshold depolarising current pulses.

3.2.3.3) Statistical analysis

The values obtained for the three variables from the two different stimuli were compared using a one-way analysis of varience (ANOVA) and Tukey's pairwise

Figure 3. 4. Definition of measurements.

The representative traces illustrate the response of 2 striatal cells to subthreshold (**A**, **B**) and suprathreshold stimulation (**C**) and the measurements (a) latency, (b) rise time and (c) peak amplitude taken. Latency (a) is defined as the time taken from the delivery of the stimulus, illustrated as a stimulus artefact (▲) in the traces to the start of the rising phase of the EPSP. Rise time (b) is defined as the time taken from the onset of the EPSP to the first inflection in the rising phase of the EPSP. Peak amplitude (c) is measured as the maximal change in membrane potential in response to delivery of a stimulus.

A illustrates the response of a striatal cell to subthreshold whisker pad stimulation. The first inflection in the EPSP occurs when the maximal response occurs and the rise time is equal to the time to peak amplitude (d).

B illustrates the response of a striatal cell to subthreshold contralateral cortical stimulation. The rise time here is not equal to the time to peak amplitude as the inflection in the EPSP occurs in the early phase of the response. Time to peak amplitude is measured from time of onset of response to point at which the EPSP reaches it maximal amplitude (d).

C illustrates the response of a striatal cell to suprathreshold whisker pad stimulation resulting in the generation of action potentials. In this case rise time (b) is measured at the peak of the EPSP before generation of an action potential. In most cases the stimuli were delivered subthreshold so there were only few instances when action potentials were generated.

A

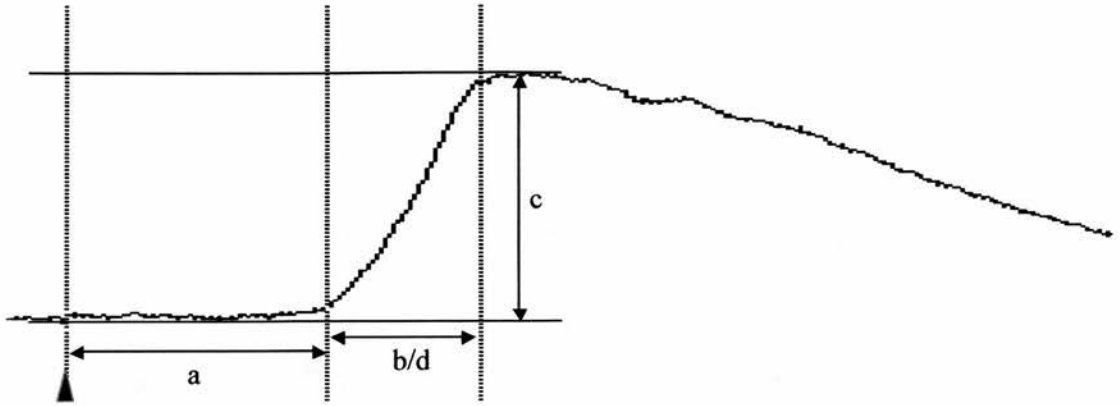

B

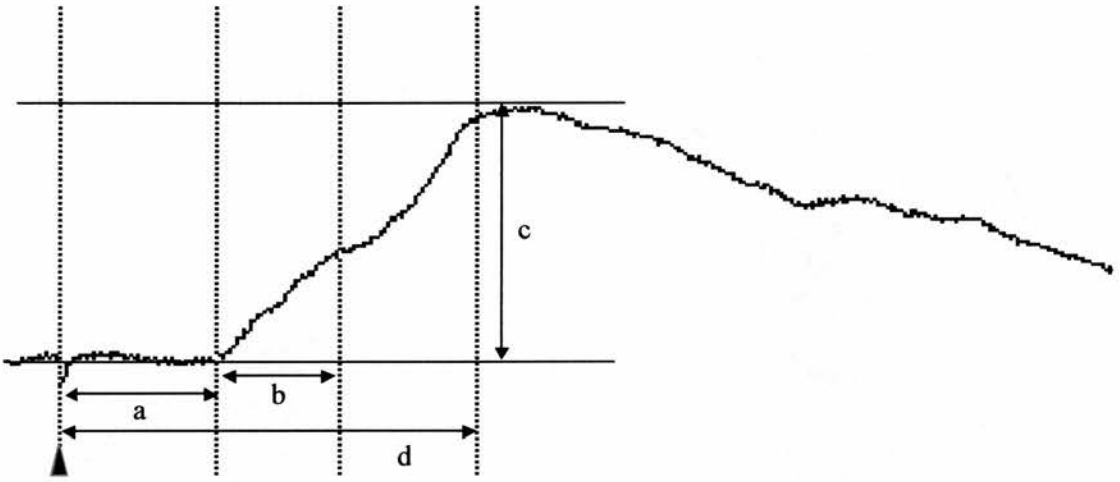

C

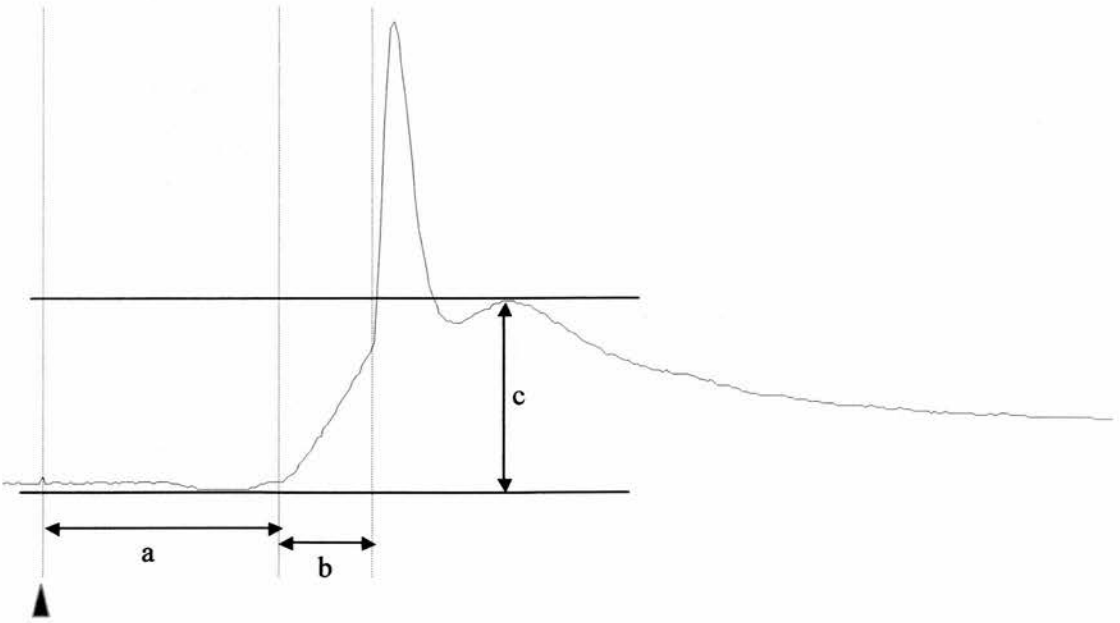

comparisons. Numerical values are given as mean ± standard deviation (S.D) unless otherwise stated. The probability level for statistical significance was set at $p < 0.05$.

3.2.4) Electroencephalogram

In some experiments, intracellular recording of striatal cells (n = 7) was coupled with electroencephalograms (EEGs) of the somatosensory cortex on both sides. The EEG was recorded using sliver wires which were placed on the dura and held in place by placing it under the skull (stimulating site) or building the dental cement well over it (recording site). The EEG was referenced against an earth which was secured to the scalp. The raw cortical signal was filtered (0.8-250 Hz), amplified 2 times, sent to an analogue digital converter (Micro 1401, CED, UK) and collected on computer together with concurrent spiking activity.

3.2.5) Cortical spreading depression

In some experiments once records from a striatal cell (n = 3) had been obtained cortical spreading depression was elicited by the topical application of 3M potassium acetate solution unilaterally either to the recording or stimulating site. In these experiments an extra hole was drilled on the recording site. This hole was as close as possible to the recording hole and allowed the application of the solution directly to the cortical surface without disturbance of the recording electrode. Spreading depression experiments were done in conjunction with experiments where cortical EEGs were recorded. Only 1 cortical shutdown was done per animal and it was done at the end of a successful recording session.

3.2.6) Acute and chronic callosal cuts

To confirm the input from the contralateral cortex and to study the contribution of the crossed corticostriatal projection to the ipsilaterally evoked EPSP acute (n = 2) and chronic (n = 4) callosal cuts were carried out. In chronic experiments 4 male Sprague Dawley rats (300-350 g) were anaesthetised with halothane in O_2 and following a craniotomy, the corpus callosum was transected under stereotaxic control. A razor blade was run along the left hemisphere from 2.5 mm anterior to 6.5 mm posterior to Bregma, 0.9 mm lateral to the midline and 5 mm dorsoventral. The animals were allowed to recover from the anaesthetic before being returned to their home cage. The animals were then used for electrophysiology experiments 3-4 days post-transection. In acute experiments the callosum was transected at the same co-ordinates just before the start of recording session. At the end of both sets of experiments the animals were given a terminal dose of the chloralose urethane anaesthetic. The thoracic cavity was exposed and the animal was perfused transcardially with 25 mls of heparinised (10 μ/ml) saline (90%) followed by 300 mls of 2% paraformeldehyde, 1.25% glutaraldehyde in 0.1M PBS pH 7.4. The brain was removed and stored in a 10% sucrose buffered fixative overnight at 4^0C. The brain was then cut into 50 μm coronal sections on a freezing microtome and the cortical transection thus verified histologically.

3.3) Results

3.3.1) Cortical cells

3.3.1.1) Extracellular electrophysiology

Extracellular recordings were obtained from 5 animals. A cortical cell that responded to whisker stimulation was identified by the occurrence of an action potential with a relatively fixed latency. Turning the stimulus off, stopped firing of the cell. All five cortical cells from which records were obtained, responded to both stimulation of the whisker pad and contralateral cortex. The cells were recorded from a depth of 1650 to 2048 μm with respect to the cortical surface and were found –0.8 mm to –2.30 mm posterior with respect to Bregma (Fig. 3.5). Figure 3.6 shows the typical response of a cortical cell to both forms of stimulation. The latency of the response of cortical neurones to stimulation of the whisker pad (7.75 ± 2.48 ms) was not significantly different from the latency of the response to stimulation of the contralateral cortex pathway (12.49 ± 6.71 ms) (ANOVA, $p > 0.05$). There was no significant correlation between the latency of the response to both forms of stimuli and the depth of the cell (Pearson correlation coefficient = 0.128, $p > 0.05$).

3.3.1.2) Intracellular electrophysiology

Intracellular recordings were carried out on 13 animals. A total of 22 cortical cells were recorded intracellularly from depths of 1642 till 2108 μm with respect to the cortical surface. A neurone was considered to be successfully impaled if the membrane potential was lower than –50 mV and/or the cell could be made to fire an action potential by applying a depolarising current. The amplitude of the action potentials had to be greater than 40 mV. As before all cortical cells responded to both

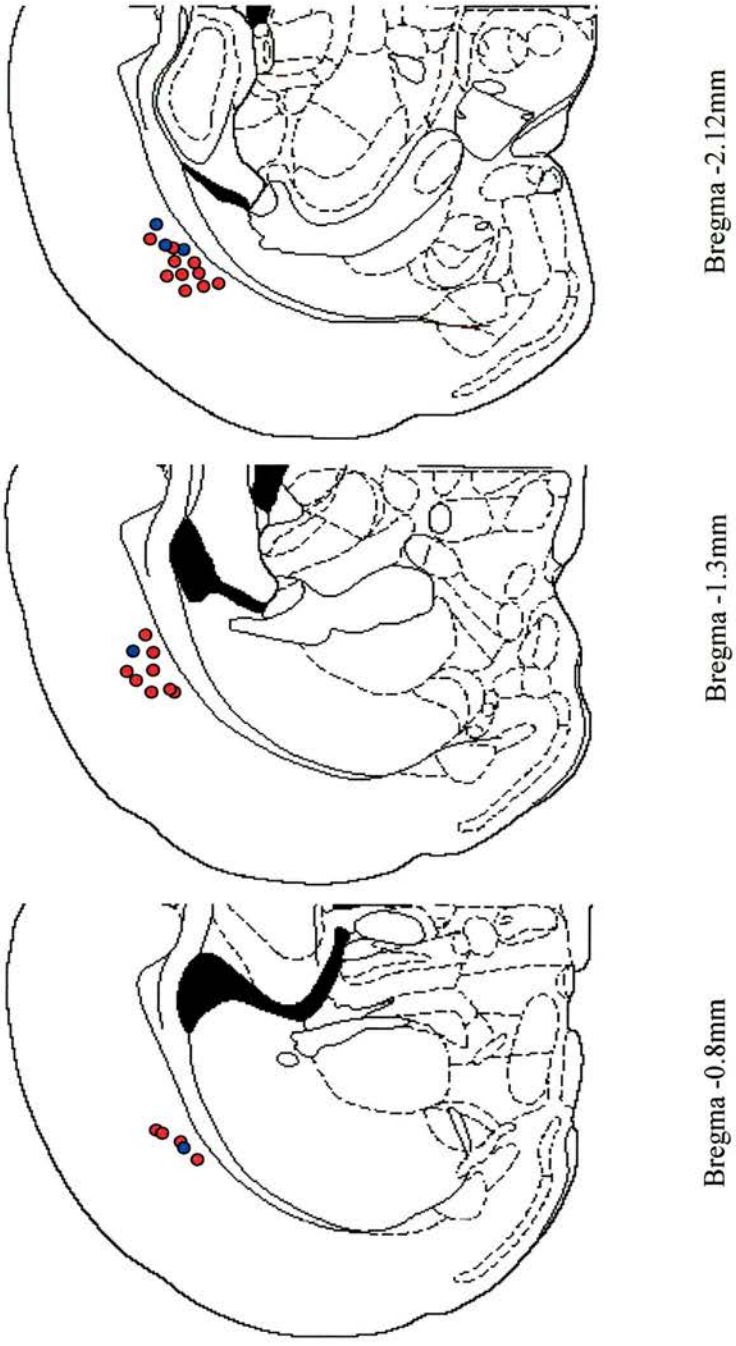

Figure 3. 5. Distribution of cortical neurones from which records were obtained.

Schematic representation (modified from Paxinos and Watson 1996) of the recording sites of cortical neurones. The approximate positions of the cortical neurones from which records were obtained were extrapolated using either pontamine sky blue markings or filled neurones. All cortical neurones recorded both extracellularly (●) and intracellularly (●) were found in 0.8 mm to 2.12 mm posterior with respect to Bregma. All neurones responded to both forms of stimuli.

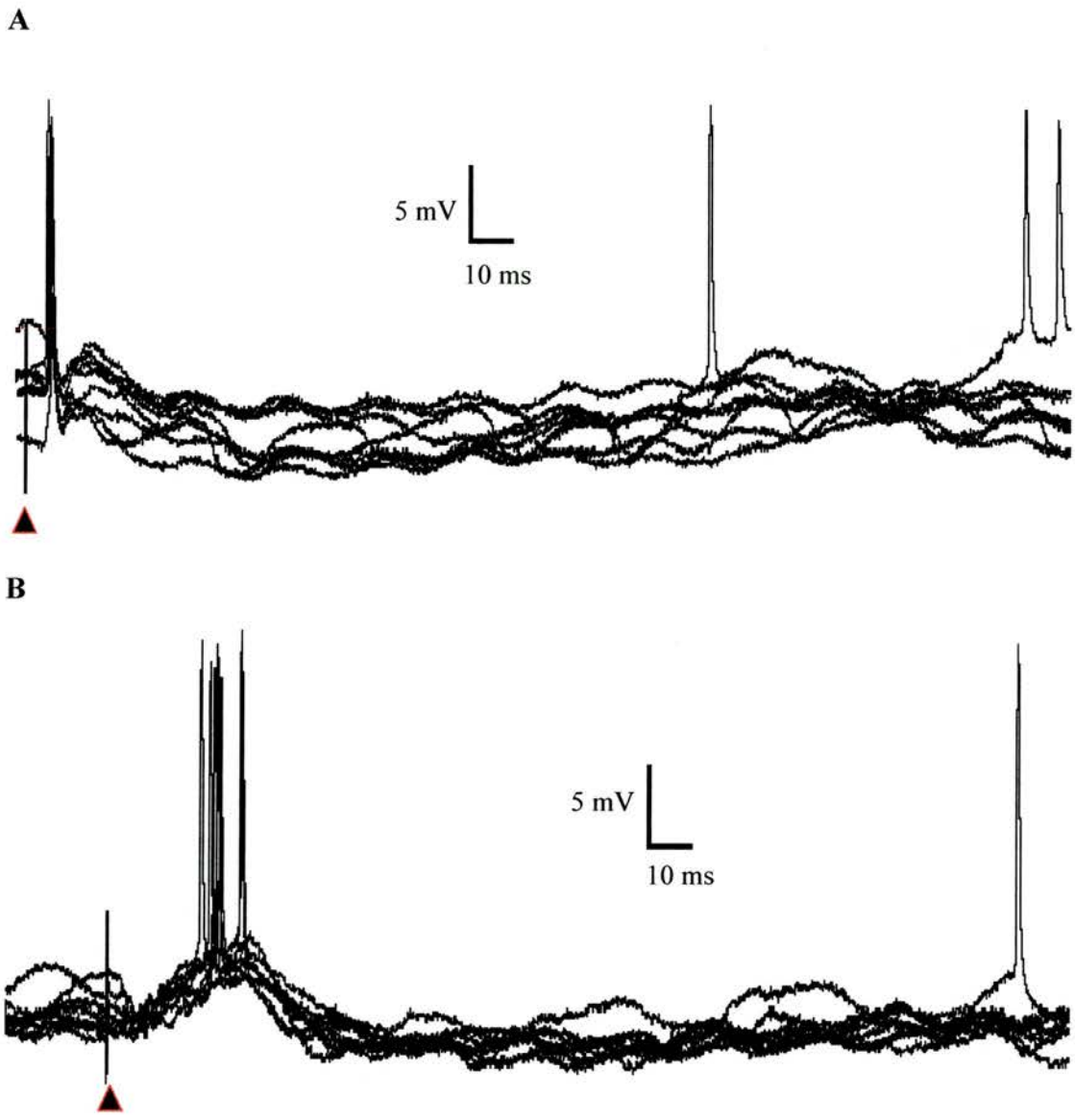

Figure 3. 6. Extracellular traces of responding cortical neurones.

Representative traces obtained from a cortical cell at a depth of 1708 μm responding to both forms of stimuli. The traces are an overlay of 8 sweeps. The stimulus artefact is highlighted by (▲). The cell responded to both forms of stimulation with action potentials of relatively fixed latencies. Turning the stimulus off, abolished this pattern of response. **A** illustrates the response of the cortical cell to whisker pad stimulation. The cell responded with the firing of action potentials (usually single action potentials) with an average latency of 6.19 ms.

B is the response of the cell to contralateral cortical stimulation. The action potentials had an average latency of 17.84 ms. After a response to both forms of stimuli the cell was silent (did not fire any action potentials) for about 150 to 200 ms after which it resumed firing of action potentials.

stimuli and were found in cortex 0.92 mm to 2.12 mm posterior to the Bregma. The positions of the cells recorded from are shown in Figure 3.5.

All cells displayed spontaneous synaptic activity (Fig. 3.7). Spontaneous events included both EPSPs and inhibitory postsynaptic potentials (IPSPs). However spontaneous IPSPs were very small at the resting membrane potential. The resting membrane potential of the cells averaged -68.07 mV and ranged from -73.57 to -60.04 mV. The peak EPSP amplitude was approximately 15 mV or less and had a membrane potential of about –50.07 mV (range -55.57 to -46.04 mV). In some cells spontaneous EPSPs were large enough to reach threshold which led to the firing of action potentials. A frequency histogram of the membrane potential shows a bimodal distribution with a peak at -69 and -51 mV (Fig. 3.7). corresponding to the depolarised or up state and a down or hyperpolarized state. Cortical cells spent most of the time in these two preferred membrane potential state and relatively little time in the transition between the two.

The cortical neurones recorded from can be classified as regular spiking (RS) cells. Current was injected into 12 of the 22 cortical cells (Fig. 3.8) and in none of the cells was high frequency firing or burst firing observed which is characteristic of fast spiking and intrinsically bursting cells respectively (Zhu and Connors, 1999). When the stimulus produced an action potential the response consisted mostly of a single action potential and occasionally a second action potential which is another feature of RS neurones (Zhu and Connors, 1999). However no attempt was made to distinguish between the three anatomically defined classes of cortical neurones.

All responses recorded in cortical neurones were a result of orthodromic activation. No antidromic activation from the contralateral cortex, characterised by

Figure 3. 7. Spontaneous activity of cortical neurones.

A The spontaneous activity of a cortical neurone recorded over a period of 5 s is displayed. The cell which was recorded at a depth of 2078 μm. Membrane potentials of the up and down state are labelled at the left of the traces (arrows). The cell tended to fire action potentials when it was in its up state. The maximal amplitude shifts were approximately 15 mV.

B A frequency histogram showing the amount of time spent by cortical neurones at any given membrane potential. When the peak amplitude was measured for each cell, a corresponding resting membrane potential (membrane potential of the cell before arrival of the stimulus) was recorded for each cell and for each sweep per cell. From a single cell, 16 traces were analysed and a total of 22 cells were analysed. The frequency of the cells sitting at a particular membrane potential was then calculated and used to plot the histogram. The histogram illustrates that the cells spent most of the time in either a hyperpolarized state (membrane potential $\approx$ -69 mV) or a depolarised state (membrane potential $\approx$ -51 mV) and little time in the transition between the two.

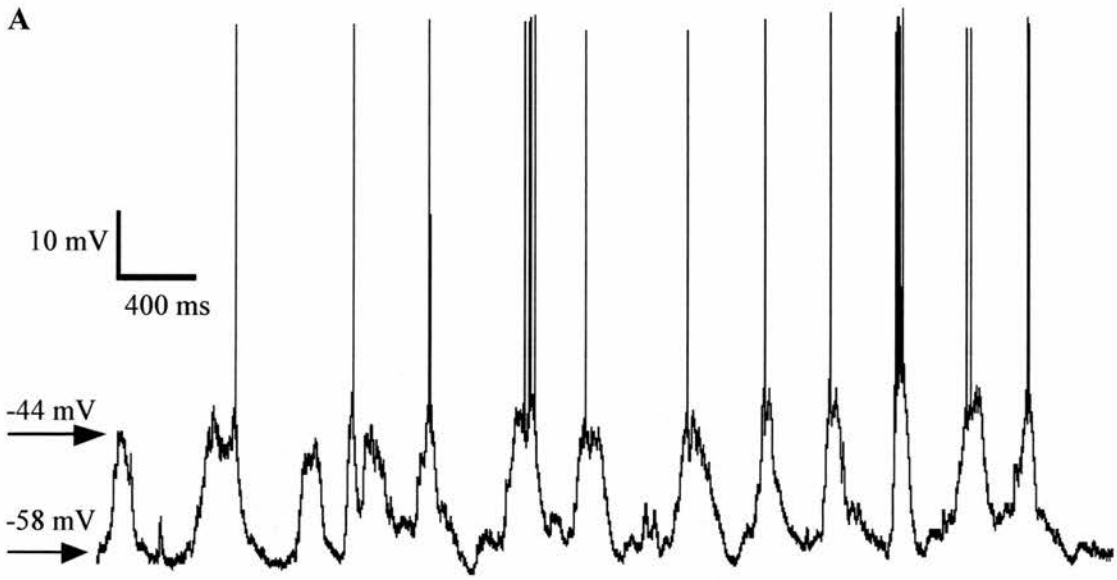
A
10 mV
400 ms
-44 mV
-58 mV

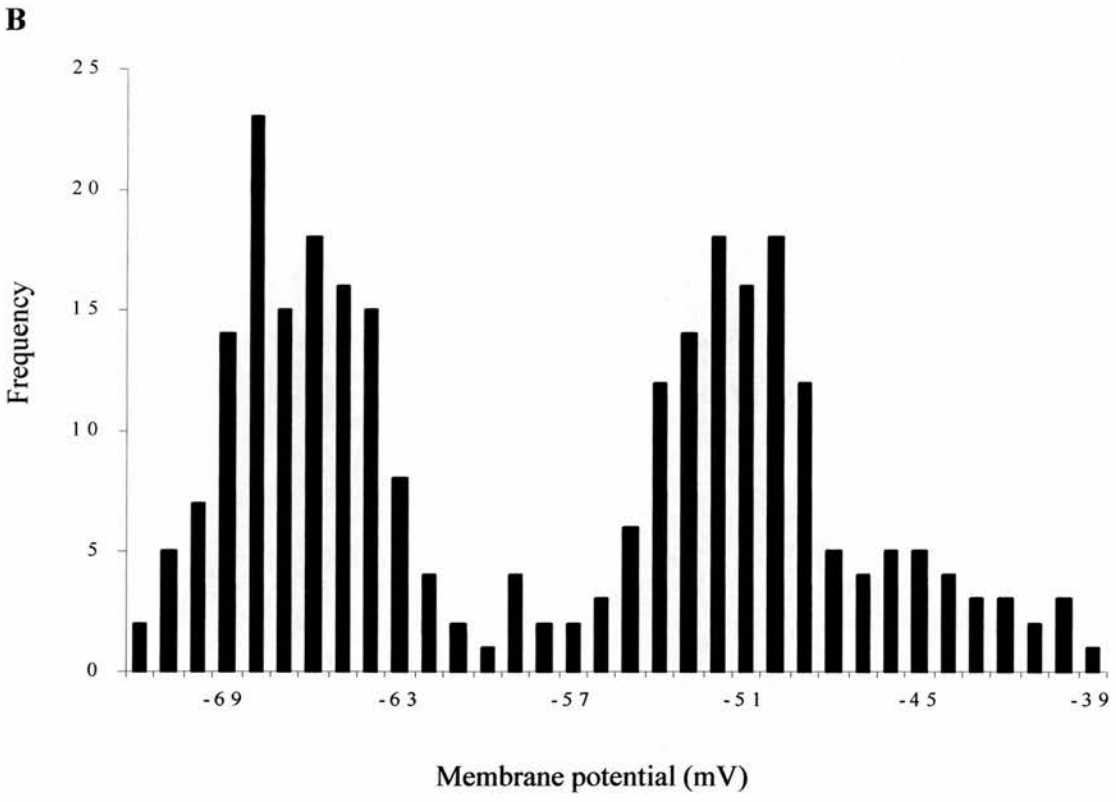
B
25
20
15
10
5
0
Frequency
-69
-63
-57
-51
-45
-39
Membrane potential (mV)

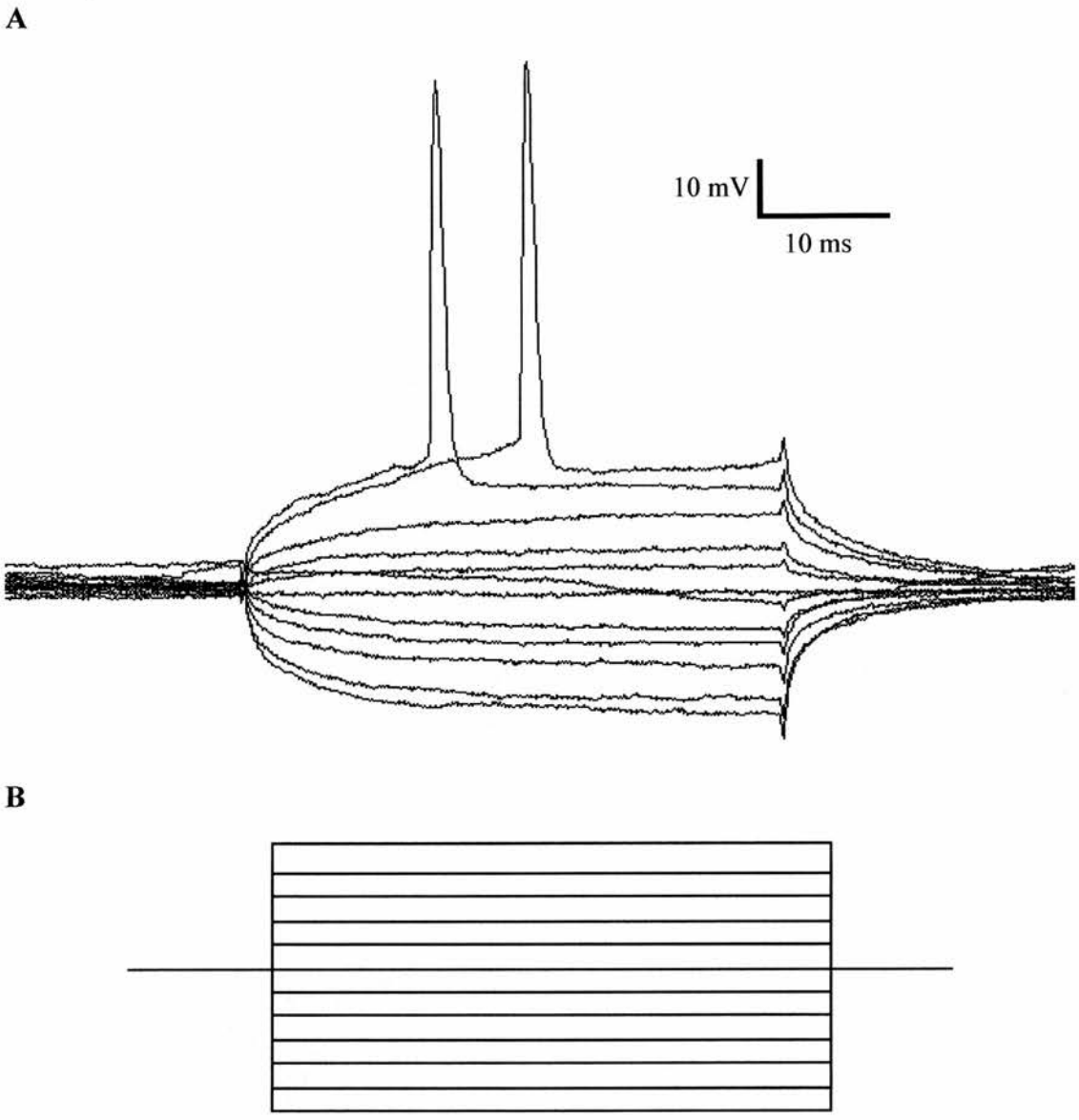

Figure 3. 8. Current injection into cortical neurones.

A The traces illustrate the characteristic response of cortical neurones to current injection. Currents, which lead to spike generation, resulted in the firing of a single or a double action potential but never bursting behaviour. There was no inward rectification observed in cortical neurones.

B The current injection was a simple rectangular pulse, with a width of 40 ms. Each step represents an increase of 0.1nA of current.

the occurrence of fixed latency action potentials at threshold with no underlying EPSP was observed. The response of cortical cells to stimulation of the whisker pad and contralateral cortex consisted of an initial EPSP followed by an IPSP (Fig. 3.9). Following this was a delayed EPSP the latency of which was highly variable (Fig. 3.9). The IPSP component was more prominent when the cell was depolarised and had very small amplitudes when the cells were near resting potential. Depolarised cells responded with an EPSP followed by a slow return of the membrane potential back to baseline values. This was followed by a period of prolonged hyperpolarisation that lasted from 150 ms to longer than 240 ms while cells close to resting potential responded with similar duration EPSPs followed by a period of inactivity lasting for about 200 ms (Fig. 3.10). The amplitude of the response of the cells to the stimuli was also was affected by the depolarisation. There was a significant negative correlation between the membrane potential and peak amplitude (Pearson correlation coefficient = -0.310, $p < 0.05$). Up to 9.6% of the variability observed in the peak amplitude can be accounted for by the difference in membrane potential when the stimulus arrived (regression analysis, R-SQ = 9.6%).

The electrophysiological characteristics of the 22 cells to both forms of stimuli is summarised in Table 3.1. The average latency of the response to both forms of stimuli is not significantly different despite very different path lengths. The depth of the cell did not affect the latency of the response (Pearson correlation coefficient = -0.209, $p > 0.05$). Both forms of stimuli were able to raise the cortical cells to firing threshold. The main difference between the two forms of stimulation was the rise time of the EPSP. Electrical stimulation of the whisker pad gave rise to rapidly rising EPSPs with little variation while activation of the cortico-cortical

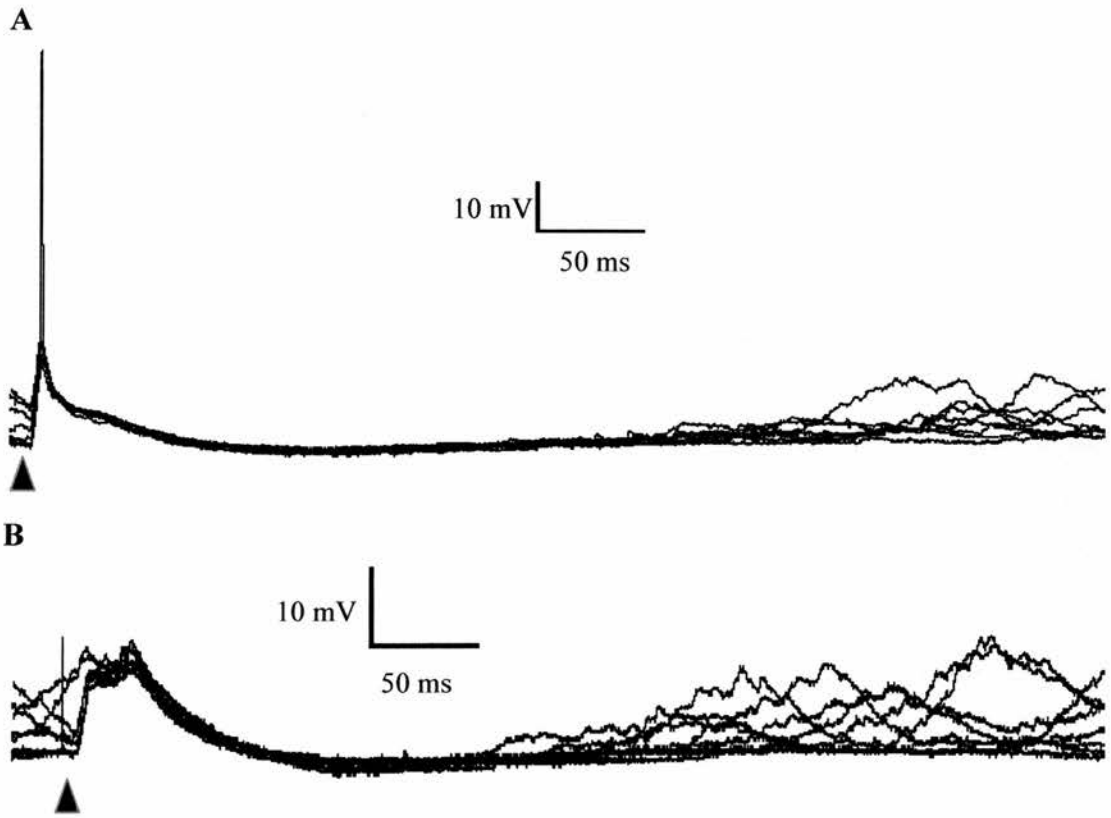

Figure 3. 9. Intracellular traces of a responding cortical neurone.

The traces illustrate the typical behaviour of cortical neurones to whisker pad and contralateral cortical stimulation. This cell was recorded at a depth of 1805 μm and is the same as that illustrated in figure 3.8. This cell had a resting membrane potential of approximately –68 mV and when it was depolarised at approximately –52 mV it sometimes fired action potentials. Traces in A and B are 8 overlaid sweeps and the values reported are the average value for the cell. The stimulus artefact is marked by a (▲).

A Response of the neurone to whisker pad stimulation. The cell responded with an EPSP with an average latency of 6.30 ms. In one of the 8 sweeps an action potential was fired. The rise time was 5.20 ms and the peak amplitude was 13.51 mV. The duration of the EPSP was 45.00 ms followed by a hyperpolarisation that lasted 264.00 ms. Following this was a switch in the membrane potential to the upstate. Note that the stimulus was delivered when the cell's membrane potential was either depolarised or hyperpolarised.

B Response of the neurone to contralateral cortical stimulation. The cell responded with an EPSP with an average latency of 6.50 ms. In none of the sweeps was an action potential was fired. The rise time was 8.42 ms and the peak amplitude was 8.84 mV. The duration of the EPSP was 55.0 ms followed by a hyperpolarisation that lasted 135.60 ms. This was followed by a switch to the upstate that was highly variable.

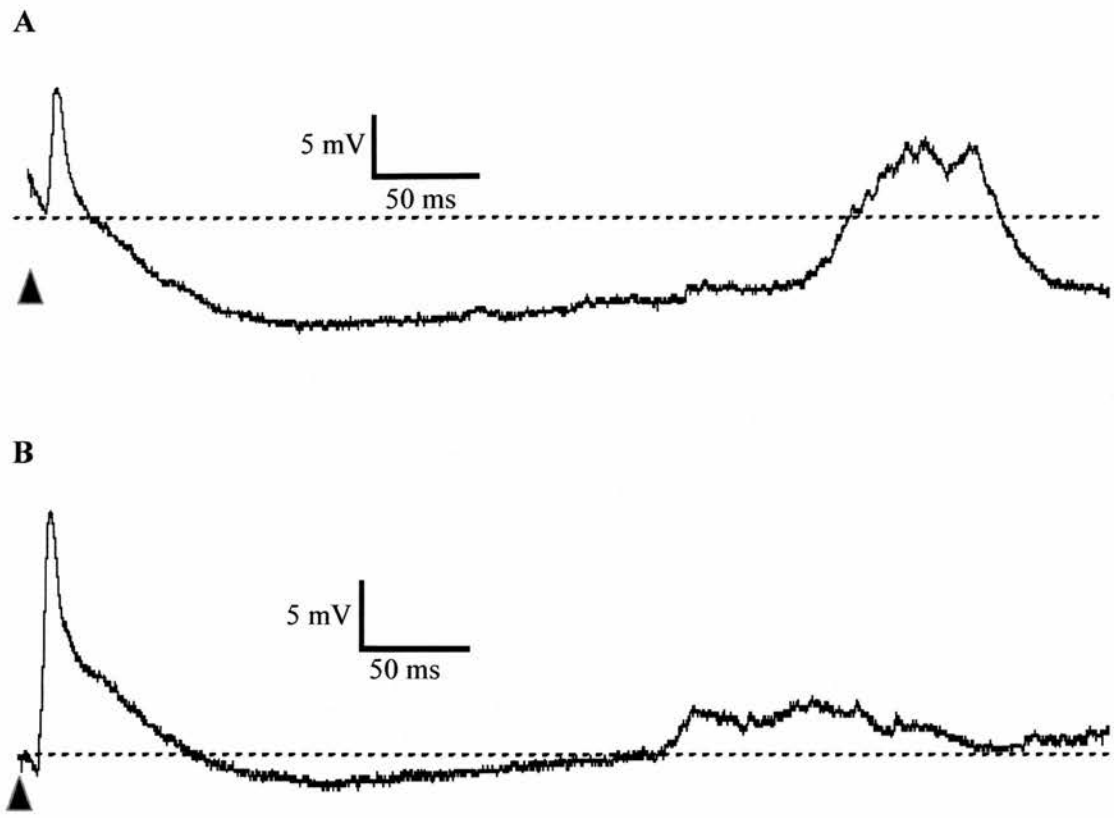

Figure 3. 10. Influence of membrane potential on the size of the EPSP and the size and duration of the IPSP in cortical neurones.

To illustrate the influence of the membrane potential on the size of the EPSP and size and duration of the IPSP, two traces from concurrent sweeps of the response of a cell to whisker pad stimulation are shown. This cell is the same cells as shown in figures 3.8 and 3.9. This cell has responses which are typical of the cortical neurones recorded from. The stimulus artefact is marked by a (▲). The dashed lines mark out the membrane potential of the neurone when the stimulus arrived.

A shows the response of the cell in its depolarised state. The cell had a membrane potential of -56.8 mV. The peak amplitude was 9.5 mV. Following the EPSP a clearly defined IPSP was observed which lasted 276 ms after which the membrane potential switched back to its depolarised state.

B This shows the next recorded response of the cell after the sweep in **A**. The cell was hyperpolarsied when the stimulus arrived. The cell which had a resting membrane potential of –69.25 mV responded with an EPSP of 18.91 mV magnitude. The cell then switched into a period of inactivity lasting 153.00 ms.

connections by stimulation of the contralateral cortex led to slow rising and variable EPSPs (Fig. 3.11).

	Stimulus type		
Variables	Whisker pad	Contralateral cortex	No. of cells
Latency (ms)	6.805 ± 1.771	8.255 ± 3.674	22
Rise time (ms)	4.097 ± 1.284	8.548 ± 4.101*	10
Peak amplitude (mV)	9.746 ± 6.601	6.271 ± 3.258	10

Table 3. 1. Summary of electrophysiological characteristics of cortical cells to electrical whisker pad stimulation and contralateral cortical stimulation.

Mean values (± standard deviation) of responding cortical cells to electrical whisker pad and contralateral cortical stimulation. The asterisk (*) denotes a statistically significant difference (ANOVA, $p < 0.05$).

3.3.2) Striatal cells

3.3.2.1) Extracellular electrophysiology

Extracellular recordings were carried out on 29 animals and a total of 108 cells were recorded from. The results obtained from 2 of the animals were not included in the analysis as histology showed that the recording electrode was in the reticular thalamus and the internal capsule.

A striatal cell that responded to whisker stimulation was identified by the occurrence of an action potential with a relatively fixed latency. Turning the stimulus off, stopped firing of the cell. Neurones that did not respond fired spontaneously and randomly at different time intervals after the stimulus and this pattern of firing did not change with turning the stimulus off. A cell was classified as a non responding cell if it did not respond to either of the stimuli. Response to just one form of

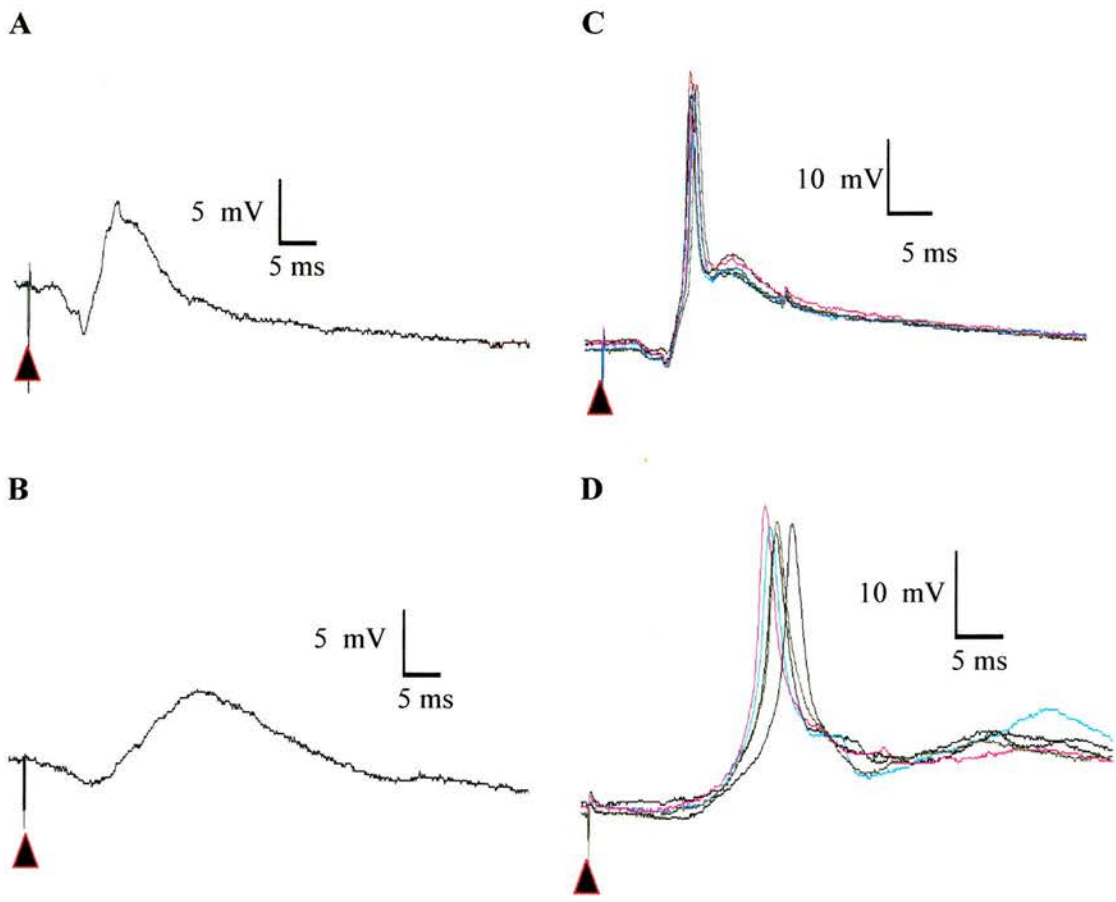

Figure 3. 11. Whisker pad vs. contralateral cortical stimulation in cortical neurones.

A and **B** illustrate the difference in the rise time of the EPSP in response to whisker pad (**A**) and contralateral cortical stimulation (**B**). The cortical cell recorded at a depth of 2078 μm was stimulated subthreshold to prevent the firing of action potentials. The stimulus artefact is marked by a (▲). The traces displayed are the average of 8 sweeps.
A The rise time to whisker pad stimulation was 3.6 ± 1.23 ms. Note the rapid rise of the EPSP with relatively no inflection in the EPSP till the peak amplitude was reached.
B Contralateral cortical stimulation gave rise to an EPSP with a rise time of 12.06 ± 1.05 ms. The rising phase of the EPSP was more gradual with a greater number of inflections before maximal response to the stimulus was reached.
C and **D** illustrate the response of another cortical neurone stimulated supratheshold so as to generate action potential firing.
C Action potential firing in response to whisker pad stimulation was fairly consistent and latency to spike initiation was similar from sweep to sweep.
D Spike initiation latency was more variable in response to contralateral cortical stimulation. There is a greater jitter in the traces when compared to **C**.

stimulation was considered a responding cell. Out of the 108 cells recorded extracellularly 26 were non responding cells. Neurones that responded were found in the striatum 0.9 mm to 2.12 mm posterior to the Bregma, whilst more anterior striatal neurones did not respond (Fig. 3.12).

Although the majority of cells responded to both stimuli, there were 3 cells that had no response to whisker pad stimulation but responded to stimulation of the contralateral cortex. All 3 cells were from three different animals. In these animals other cells which were recorded from were responsive to both stimuli. When this occurred the placement of the insect pins was checked to ensure that all whiskers were moved when a pulse was delivered. Histology later revealed that these cells were found in the region of striatum that did receive projection from the barrel cortex (Fig. 3.12). Fourteen neurones responded only to stimulation of the whisker pad. These neurones were from 8 experimental animals. In two of the 8 animals histology revealed that the stimulating electrode was too lateral and not in Layer V of the somatosensory cortex. In the remaining 6 animals the placement of the stimulating electrode was correct as verified by histological means, and the stimulating electrode was working as other cells recorded from the same animals responded to stimulation of the contralateral cortex (Fig. 3.12).

The latency of the first action potential after the stimulus was recorded for each cell. The mean latency of the response of the cell was calculated by calculating the average latency of 8 sweeps. The mean time to first action potentials of non-responding cells ranged from 60 ms to 300 ms (Table 3.2). The mean values had large standard deviations suggesting a random pattern of firing.

Figure 3. 12. Distribution of striatal neurones recorded extracellularly.

Schematic representation (modified from Paxinos and Watson 1996) of the location of striatal neurones recorded extracellularly. The approximate positions of the striatal neurones from which records were obtained were extrapolated using pontamine sky blue markings. Non responding neurones were located in the anterior striatum and no responding neurones were recorded until -0.92mm with respect to Bregma. The majority of neurones responding to both forms of stimulation were located in the dorsolateral edge of striatum. The three neurones which only responded to contralateral cortical stimulation but not whisker pad stimulation were located in more ventral and medial striatum. Neurones which did not respond to contralateral cortical stimuli (not due to misplacement of stimulating electrode) were located amongst neurones responding to both forms of stimuli.

- Location of non-responding neurones.
- Location of neurones responding to both forms of stimulation.
- Location of neurones responding to contralateral cortical stimulation but not whisker pad stimulation.
- Location of neurones responding to whisker pad but not contralateral cortical stimulation.
- Location of neurones responding to whisker pad but not contralateral cortical stimulation due to misplacement of stimulating electrode.

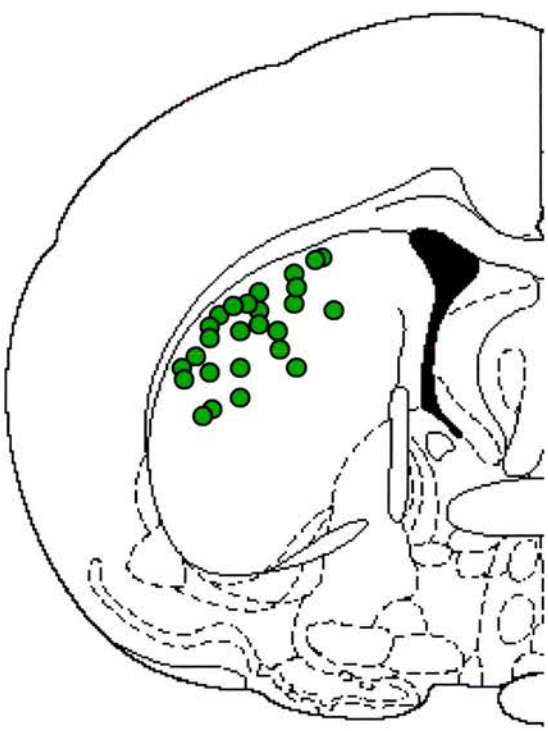

Bregma -0.4 mm

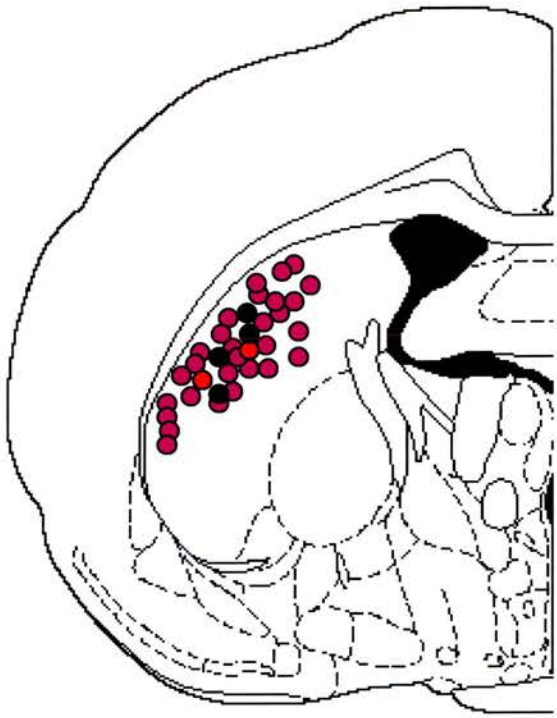

Bregma -0.92 mm

Bregma -1.80 mm

Bregma -2.12 mm

Units that had latencies less than 5 ms were disregarded as these were most probably recordings from axons. These units were hard to hold and the action potentials lasted for less than 0.5 ms. For cells that responded, individual records with responses that occurred very close (less than 5 ms) to the stimulus, were omitted from the analysis. Even though both stimuli used a cycle duration of 2.5 s in order to ensure that there was full electrical recovery of the cortex between stimuli there were instances when the response of the cell occurred very close (less than 5 ms) to the stimulus. These records were omitted from the analysis as the cell was either spontaneously firing or still firing in response to the previous stimuli and thus the latency would not represent the latency of the response to the stimulus.

The average latency of response for the two forms of stimulation is summarised in Table 3.2.

	Responding cells (ms)	No. of cells	Non-responding cells (ms)	No. of cells
Whisker pad	12.653 ± 4.756	79	95.280 ± 88.090	26
C. cortex	13.555 ± 6.065	68	126.200 ± 95.100	26

Table 3. 2. Mean latencies of extracellularly recorded striatal cells to electrical whisker pad stimulation and contralateral cortical stimulation.

Mean latencies (± standard deviation) of non-responding and responding striatal cells to electrical whisker pad stimulation (whisker) and contralateral cortical stimulation (c. cortex).

The response of striatal neurones to both forms of stimuli was over a wide range (whisker pad: 5.850 – 27.770 ms, contralateral cortex: 5.900 – 28.190 ms). The striatal cells could be roughly divided into 3 groups based on the latency of their response. The first group had a short latency ranging from 6.0 to 10.0 ms, the second

11 ms to 17 ms and the third 18 ms to 28 ms. Figure 3.13 illustrates these three groups. This wide range of latencies is partly due to the depth of the cell. There was a significant positive correlation between the depth of the cell and the latency of response (whisker pad: Pearson correlation coefficient = 0.344, $p < 0.05$, contralateral cortex: Pearson correlation coefficient = 0.486, $p < 0.05$). Up to 15.6% of variability seen in the latencies could be accounted for by the depth of the cell (regression analysis, R-SQ = 15.6%).

3.3.2.2) Intracellular electrophysiology

Intracellular records were obtained from 115 striatal neurones from 33 animals. Cells had to have a resting membrane potential of -55 mV and below with the amplitude of the action potentials greater than 45 mV from threshold and action potential duration of less then 2 ms, to be included in the study. Striatal neurones exhibited an average membrane potential of -79.34 ± 7.93 mV which ranged between -50.40 and -95.82 mV. The cells exhibited spontaneous membrane potential fluctuations of amplitudes of approximately 20 mV (Fig. 3.14). A frequency histogram of the membrane potential shows a bimodal distribution with a peak at -69 and -85 mV (Fig. 3.14). These peaks in membrane potential correspond to an up or a depolarised state and a down or hyperpolarized state. The up state potential ranged from -45 to -70 mV. During these episodes small changes in membrane potential occurred causing threshold to be reached resulting in the firing of action potentials with average spike heights of 45 mV. Membrane potential of the hyperpolarised state ranged from -80 to -95 mV and in this phase fluctuations in membrane potential were diminished. The membrane current – voltage relationship of neurones was obtained from measurements of membrane potential in response to a series of intracellular current

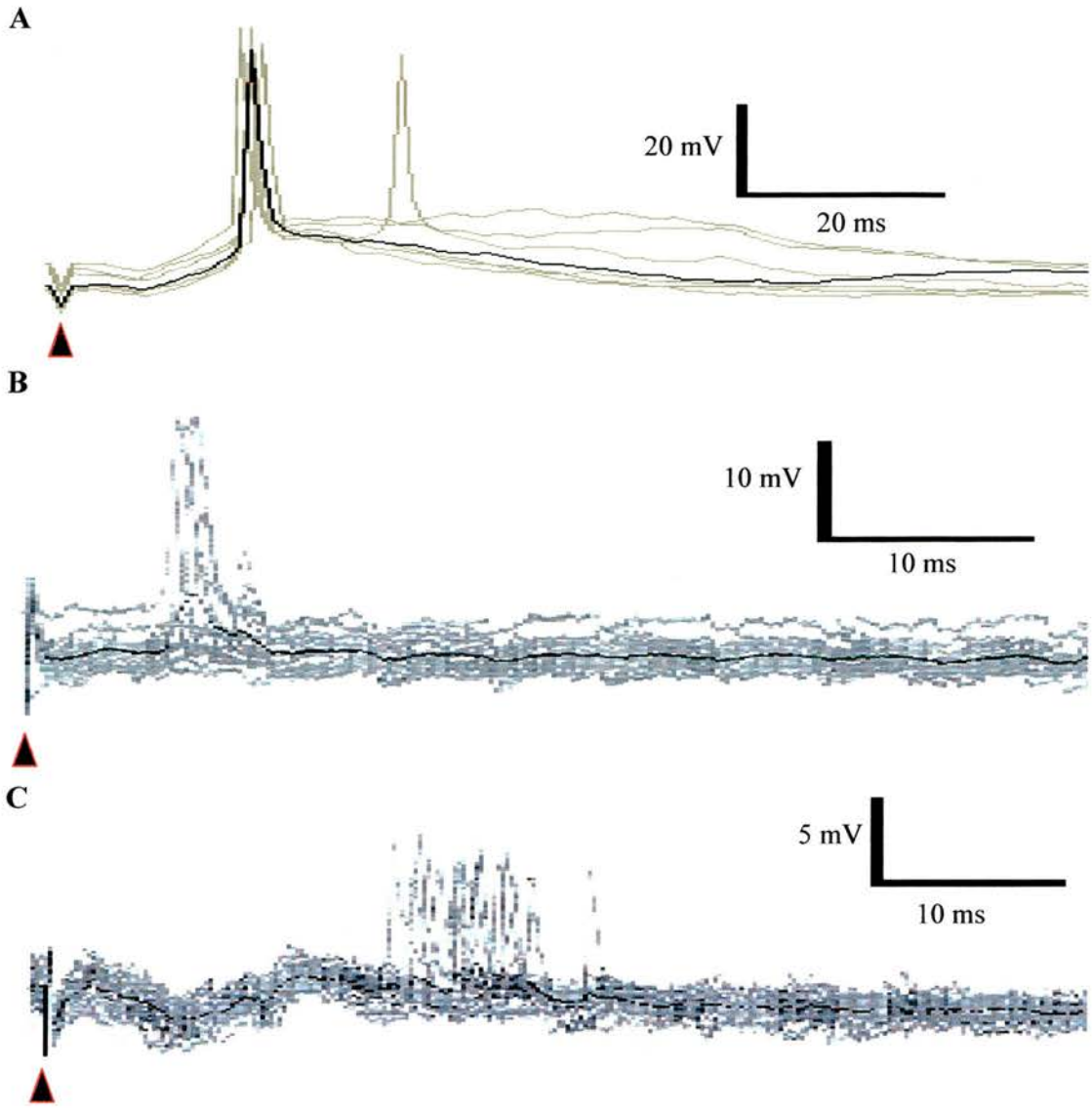

Figure 3. 13. Extracellular traces of responding striatal neurones.

The figures are 3 representative traces from 3 striatal neurones responding to whisker pad stimulation. The traces are an overlay of 8 sweeps. The stimulus artefact is marked by a (▲). The traces in A were recorded using Signal while those in B and C were recorded using MacLab Scope. The responses of the cells were clearly distinguished by their relative fixed latency to firing action potentials and cessation of fixed latency firing when the stimulus was turned off.

A This cell was recorded at a depth of 3078 μm and had an average latency of 7.94 ± 0.25 ms.

B This cell was recorded at a depth of 3744 μm and had an average latency of 14.50 ± 2.01 ms.

C This cell was recorded at a depth of 4626 μm and had an average latency of 21.13 ± 4.50 ms.

Figure 3. 14. Spontaneous activity of striatal neurones.

A The spontaneous activity of a striatal neurone recorded over a period of 5 s is displayed. The cell was recorded at a depth of 3394 μm. Membrane potentials of the up and down state are labelled at the left of the traces (arrows). The cell tended to stay in one state for approximately 200 ms before switching. The maximal amplitude shifts were approximately 20 mV. The cell fired fewer action potentials compared to cortical neurones (Compare with Fig. 3.7A). The cell only fired action potentials when it was in its up state and high frequency fluctuations in the membrane potential reached spike generation threshold.

B A frequency histogram showing the amount of time spent by striatal neurones at any given membrane potential. When the peak amplitude was measured for each cell, a corresponding resting membrane potential (membrane potential of the cell before arrival of the stimulus) was recorded for each cell and for each sweep per cell. From a single cell, 16 traces were analysed and a total of 80 cells were analysed. The frequency of the cells sitting at a particular membrane potential was the calculated and used to plot the histogram. The histogram illustrates a bimodal distribution of membrane potential. On average cells tended to spend more time in a hyperpolarised state (membrane potential ≈ -85 mV). Cells also had a preferred depolarised state (membrane potential ≈ -68 mV) and spent little time in the transition between the two.

A

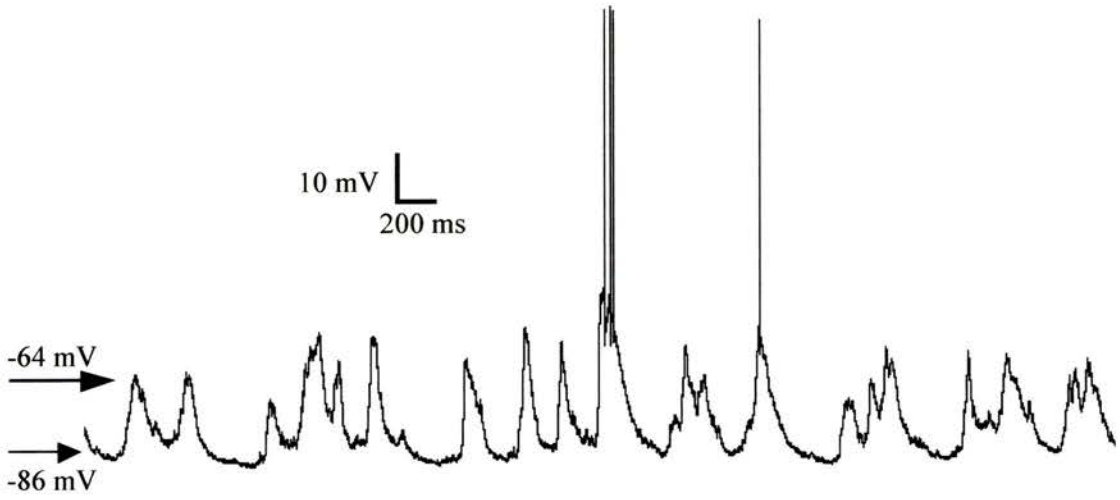
10 mV
200 ms
-64 mV
-86 mV

B

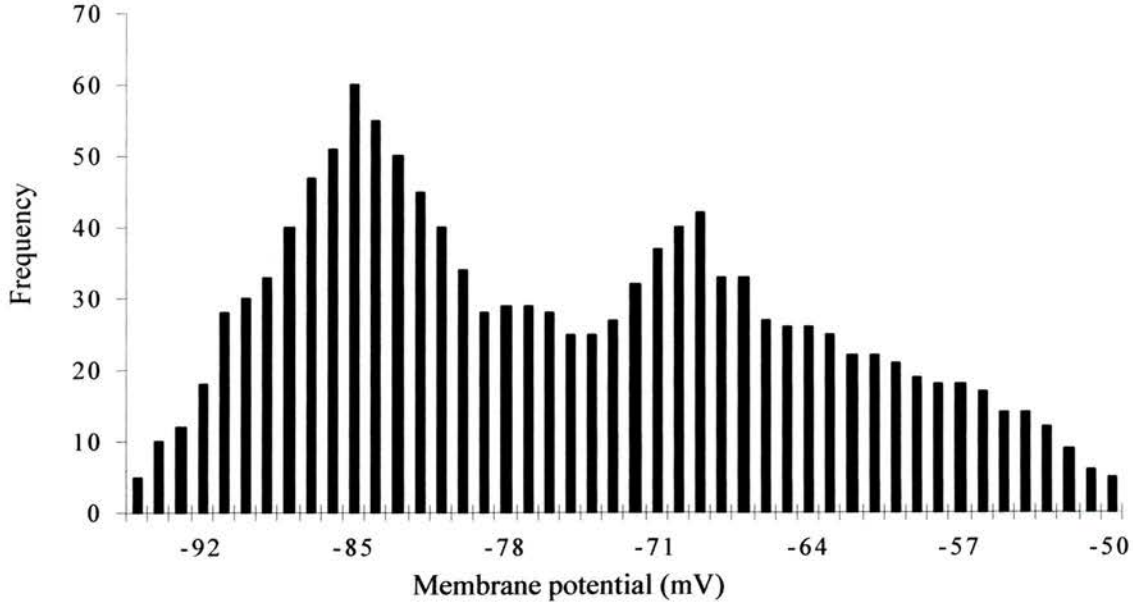
Frequency
70
60
50
40
30
20
10
0
-92
-85
-78
-71
-64
-57
-50
Membrane potential (mV)

pulses. There was an inward rectification as seen by the saturation of the hyperpolarising responses to current pulses of increasing negative intensity. Positive current pulses evoked a slowly developing ramp depolarisation which in some cases lead to a long latency spike discharge (Fig. 3.15). Input resistance was measured from the slope of a regression line fitted to a graph of membrane potential against current injected. Average input resistance was 9.925 (± 5.830) MΩ and ranged from 1.179 to 33.856 MΩ. The input resistance values obtained in this study showed a large variability and are not typical of striatal neurones *in vivo*. This is due to the fact that current was not injected when the cell was in the down state alone. Figure 3.15 shows intracellular records from two cells showing membrane potential responses to current pulses and the resulting current-voltage response graphs. Current was injected into cell A usually when the cell was in the down state. The input resistance of this cell is 26.18 MΩ. Cell B however has an input resistance of 1.179 MΩ. The traces illustrate that in some instances the cell was in the up state during the delivery of the pulses while other times, the cell switched between the two states during the current injection. As a result of this input resistance was not used as a criteria to identify striatal cells.

The positions of the cells recorded from are shown in Figure 3.16. Cells that responded were found in the region of striatum that received projections from the barrel cortex while non-responding cells were found anterior to it (Fig. 3.16). The average latency for the two forms of stimulation in both groups of cells is summarised in Table 3.3.

Figure 3. 15. Current injection into striatal neurones.

To illustrate the influence of the membrane potential on the input resistance representative traces from two striatal neurones are shown. The current pulse was a simple rectangular pulse, with a width of 40ms, similar to that used for cortical neurones and is displayed in Figure 3.8.

A Hyperpolarising and depolarising current pulses were delivered when the cell was in the down state (approximately –90 mV). Looking at the corresponding change in membrane potential, there is an inward rectification present as seen by the small changes in membrane potential with increasing injection of hyperpolarising current compared with the large changes in membrane potential with increasing injection of depolarising current. At maximal current injection the membrane potential was still below threshold for action potential generation. The input resistance was determined from the slope of a regression line fitted to the membrane potential and was 26.18 MΩ.

B Current injection into this cell occurred over both states as well as during the transition between the states. At maximal current injection the membrane potential reached threshold for action potential generation leading to the firing of a long latency action potential. Comparing **A** and **B** the inward rectification easily identifiable in **A** is not visible in **B**. The input resistance for this cell calculated from the traces was 1.179 MΩ.

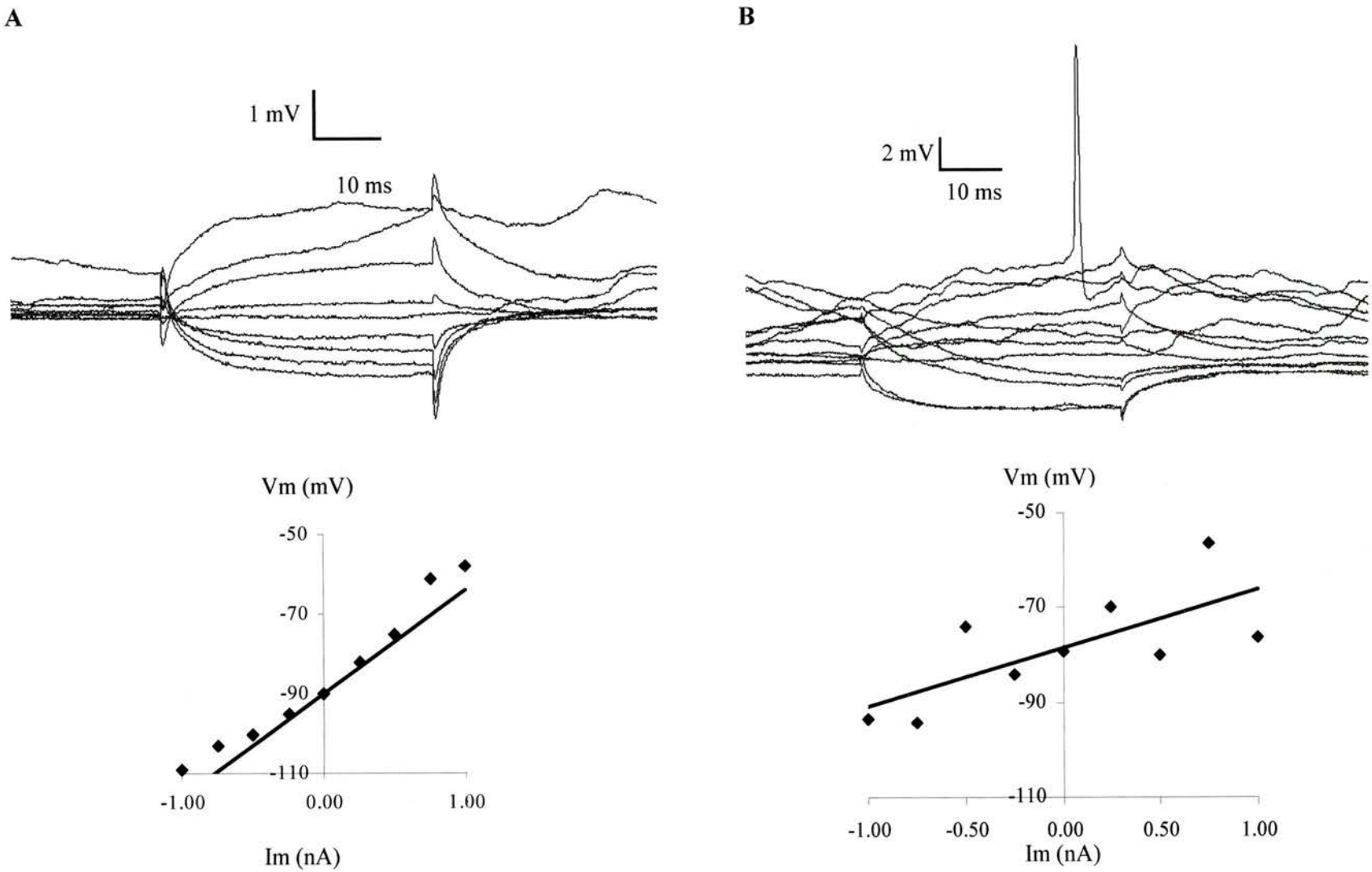
A
1 mV
10 ms
Vm (mV)
-50
-70
-90
-110
-1.00
0.00
1.00
Im (nA)
B
2 mV
10 ms
Vm (mV)
-50
-70
-90
-110
-1.00
-0.50
0.00
0.50
1.00
Im (nA)

Figure 3. 16. Distribution of striatal neurones recorded intracellularly.

Schematic representation (modified from Paxinos and Watson, 1996) of the location of striatal neurones recorded intracellularly. The approximate positions of the striatal neurones from which records were obtained were extrapolated using either pontamine sky blue markings or from biocytin filled neurones. The distribution of the different groups of neurones is similar to that observed extracellularly (Fig. 3.12). Non responding neurones were located in the anterior striatum and no responding neurones were recorded until -0.92mm with respect to Bregma. The majority of neurones responding to both forms of stimulation were located in the dorsolateral edge of striatum. The two neurones which only responded to contralateral cortical stimulation but not whisker pad stimulation were located in more ventral and medial striatum. Neurones which did not respond to contralateral cortical stimuli (not due to misplacement of stimulating electrode) were located amongst neurones responding to both forms of stimuli. The single neurone that responded strongly to a deflection of whisker A1 (Fig. 3.21) was located just below the corpus callosum

- Location of non-responding neurones.
- Location of neurones responding to both forms of stimulation.
- Location of neurones responding to contralateral cortical stimulation but not whisker pad stimulation.
- Location of neurones responding to whisker pad but not contralateral cortical stimulation.
- Location of neurones responding to whisker pad but not contralateral cortical stimulation due to misplacement of stimulating electrode.
- Location of neurone responding to deflection of whisker A1.

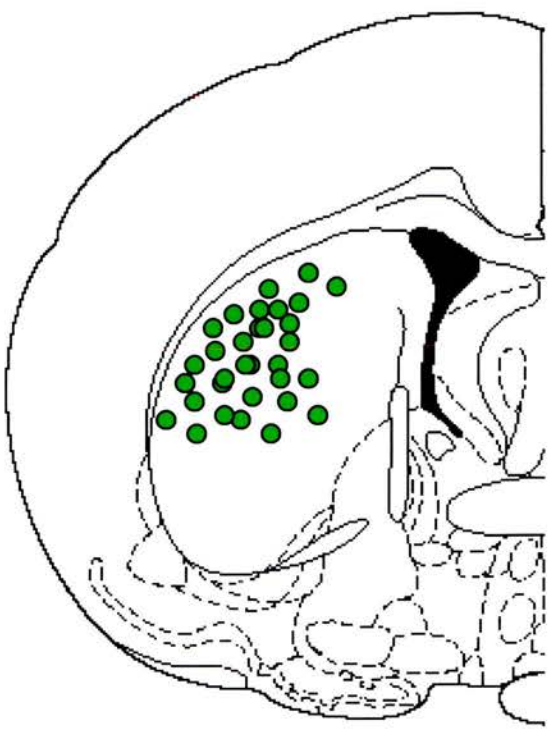

Bregma -0.4 mm

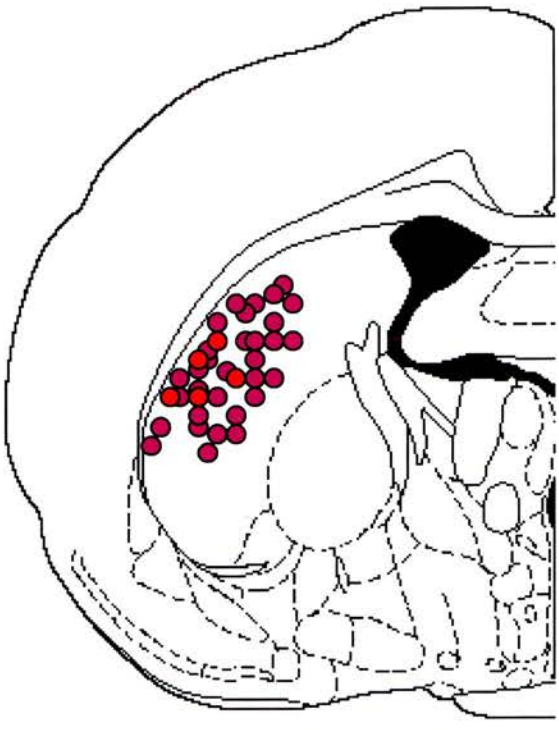

Bregma -0.92 mm

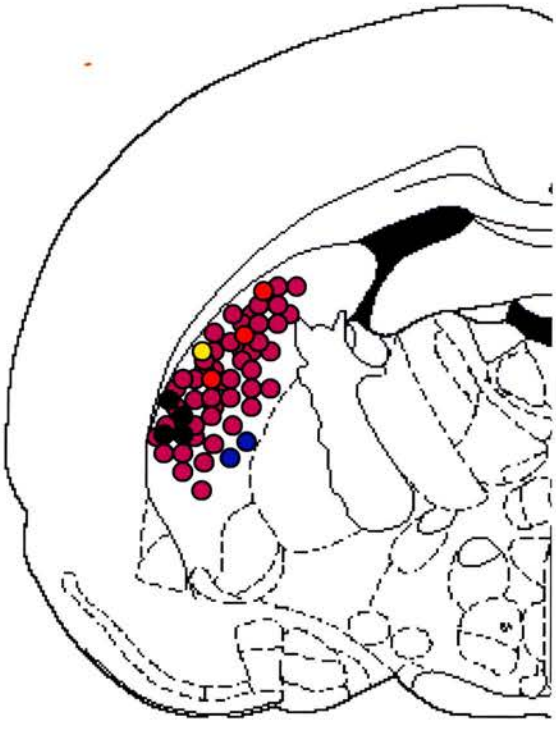

Bregma -1.80 mm

Bregma -2.12 mm

	Responding cells (ms)	No. of cells	Non-responding cells (ms)	No. of cells
Whisker pad	10.914 ± 3.695	113	105.360 ± 78.263	32
C. cortex	11.832 ± 5.488	100	96.849 ± 95.020	32

Table 3. 3. Mean latencies of intracellularly recorded striatal cells to electrical whisker pad stimulation and contralateral cortical stimulation.

Mean latencies (± standard deviation) of non-responding and responding striatal cells to electrical whisker pad stimulation (whisker) and contralateral cortical stimulation (c. cortex).

Non-responding striatal cells showed spontaneous shifts in membrane in potential and did not change their behaviour when the stimulus was turned off. Responding neurones responded with an EPSP with a relatively fixed latency which was abolished when the stimulus was turned off. Two striatal neurones from two different animals did not respond to whisker pad stimulation. These cells were found in the area of striatum that did receive input from the barrel cortex (Fig. 3.16). In these animals records were obtained from other striatal cells that responded to electrical stimulation of the whisker pad. Seven striatal neurones did not respond to contralateral cortex as a result of misplacement of the stimulating electrode. The remaining eight cells from eight different animals did not respond to the stimulus even though other cells in the same recording tract were responsive.

A comparison of the responses of striatal cells to both forms of stimulation is summarised below.

	Stimulus type	
Variables	Whisker pad	Contralateral cortex
Latency (ms)	10.914 ± 3.695	11.832 ± 5.488
Rise time (ms)	8.857 ± 1.675	18.645 ± 6.449*
Peak amplitude (mV)	11.115 ± 6.948	8.973 ± 6.964

Table 3. 4. Summary of electrophysiological characteristics of striatal cells to electrical whisker pad and contralateral cortical stimulation.

Mean values (± standard deviation) of responding striatal cells to electrical whisker pad and contralateral cortical stimulation. The asterisk (*) denotes a statistically significant difference (ANOVA, $p < 0.05$).

Striatal cells responded to the stimuli with an EPSP followed by a period of inactivity that lasted up to 250 ms. In most cases the stimuli did not produce action potentials as they were delivered sub-threshold, however in some cases, when the stimuli were delivered when the cell was in the up state, single action potentials were fired. Representative responses of 2 spiny projection striatal neurones are shown in Figure 3.17. Stimulation produced short latency EPSPs. The latency of the response to both stimuli is not significantly different (whisker pad: range 5.980 – 29.970 ms; contralateral cortex: 6.390 – 28.450 ms) and is not correlated with the depth of the cell (Pearson correlation coefficient = 0.097, $p > 0.05$). The amplitude of EPSPs (whisker pad: range 5.010 – 29.230 mV; contralateral cortex: 5.000 – 27.690 mV) was significantly correlated to the state of the cell when the stimulus was delivered (Pearson correlation coefficient = -0.730, $p < 0.05$). Regression analysis showed that up to half of the variability (R-SQ = 53.3%) was due to the membrane potential (Fig. 3.18). As seen in cortical cells the only difference between the 2 stimuli was the rise time of EPSPs (Fig. 3.19). Stimulation of the contralateral cortex gave rise to slow

Figure 3. 17. Intracellular traces of responding striatal neurones.

The traces illustrate the typical behaviour of striatal neurones to whisker pad and contralateral cortical stimulation. **A** and **B** were obtained from the same cell recorded at a depth of 3586 μm which was stimulated subthreshold for action potential generation. The cell in **C** was recorded at a depth of 3320 μm. Traces represent an overlay of 8 sweeps and the values reported are the average value for the cell. The stimulus artefact is marked by a (▲).

A Response of the neurone to whisker pad stimulation. The cell responded with an EPSP with an average latency of 7.64 ms. The rise time was 5.59 ms and the peak amplitude was 15.81 mV. The duration of the EPSP was 100.00 ms followed by a period of inactivity that lasted 198.00 ms. Following that, the membrane potential was seen to switch to the upstate. Note that the stimulus was delivered when the cell's membrane potential was either depolarised or hyperpolarised.

B Response of the neurone to contralateral cortical stimulation. The cell responded with an EPSP with an average latency of 12.98 ms. The rise time was 19.37 ms and the peak amplitude was 14.77 mV. The duration of the EPSP was 101.60 ms followed by a period of inactivity that lasted 175.00 ms after which the cell switched to the up state.

C Response of a neurone to whisker pad stimulation. The cell was stimulated suprathreshold to generate action potentials. The cell which was usually in the down state (≈-90 mV) when the stimulus was delivered switched to the up state (≈-50 mV) and fired single action potentials. The action potentials were usually located at the peak of EPSP and overshot 0 mV. The cell responded with an EPSP of latency 8.65 ms, rise time 5.46 ms and peak amplitude of 11.30 mV. The EPSP which lasted 47.00 ms was followed by a period of inactivity that lasted 135.00 ms. Following that, the membrane potential was seen to switch to the upstate where sometimes action potentials were fired.

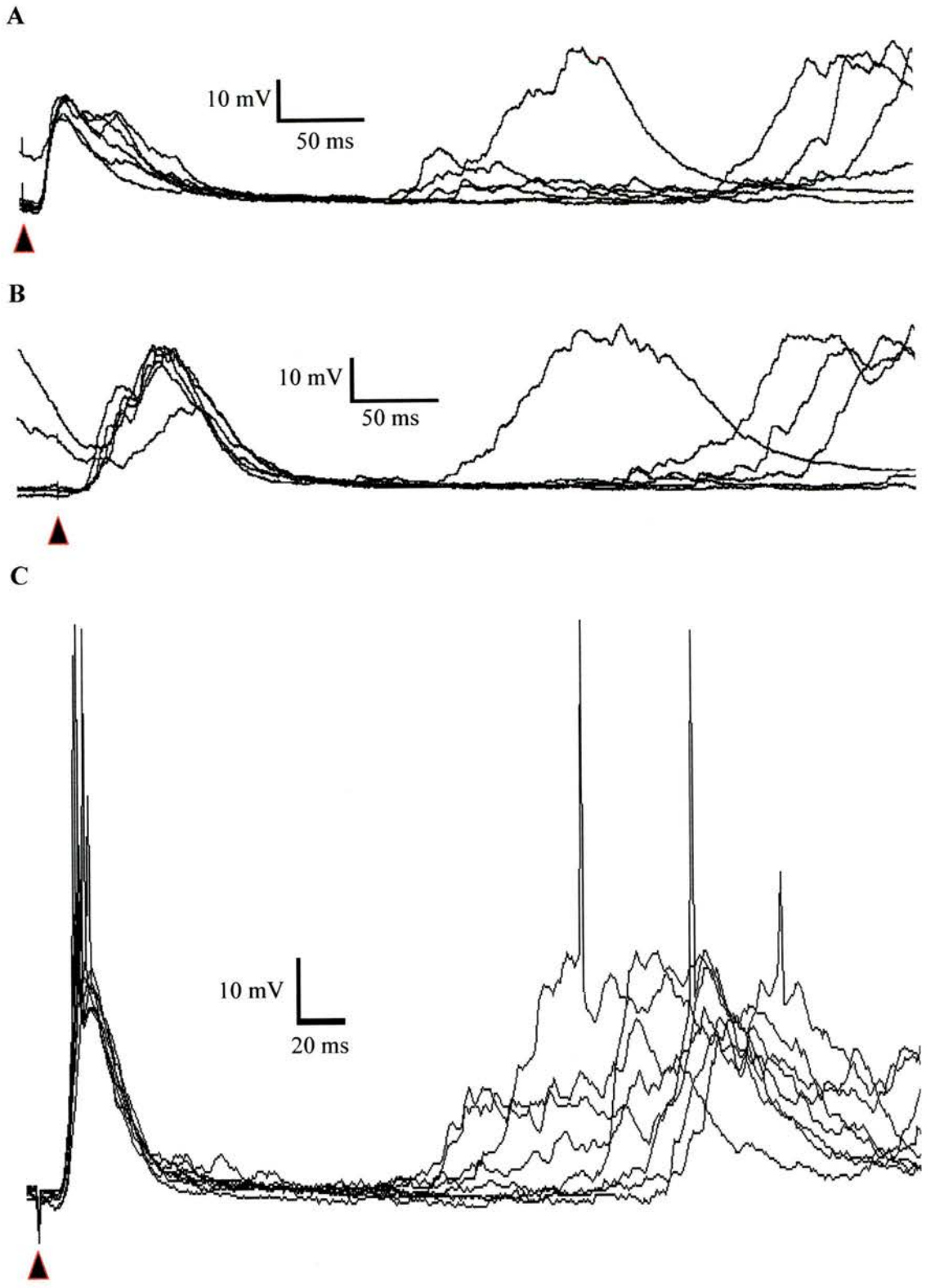
A
10 mV
50 ms
B
10 mV
50 ms
C
10 mV
20 ms

Figure 3. 18. Influence of the membrane potential on the size of the EPSP in striatal neurones.

To illustrate the influence of the membrane potential on the size of the peak amplitude, two traces from concurrent sweeps of the response of a cell to whisker pad stimulation are shown (**A**, **B**). This cell has responses which are typical of striatal neurones. The average peak amplitude of this cell is 9.9 mV and has a range 7.37 mV to 17.19 mV. The stimulus artefact is marked by a (▲).

A shows the response of the cell in its depolarised state. The cell had a membrane potential of –73 mV when the stimulus arrived and gave rise to a peak amplitude of 8.9 mV. There is a pronounced hyperpolarisation following the EPSP.

B The next sweep following **A** shows the cell in a hyperpolarised membrane potential (-87 mV) when the stimulus arrived. The cell responded with a short latency EPSP with a peak amplitude of 16.97 mV followed by a slow return of membrane potential to it hyperpolarised potential. The 'hyperpolarisation' is not as pronounced as **A** and can be classified as a period of inactivity as the membrane potential does not go below the membrane potential when the stimulus was delivered.

C A scatter plot of the membrane potential of the all striatal cells when the stimulus arrived versus the peak amplitude of the response to the stimulus shows that that the two variables are negatively correlated (Pearson correlation coefficient = -0.730, P = 0.000). Thus the more hyperpolarised the cell was, the bigger was its response to the stimuli.

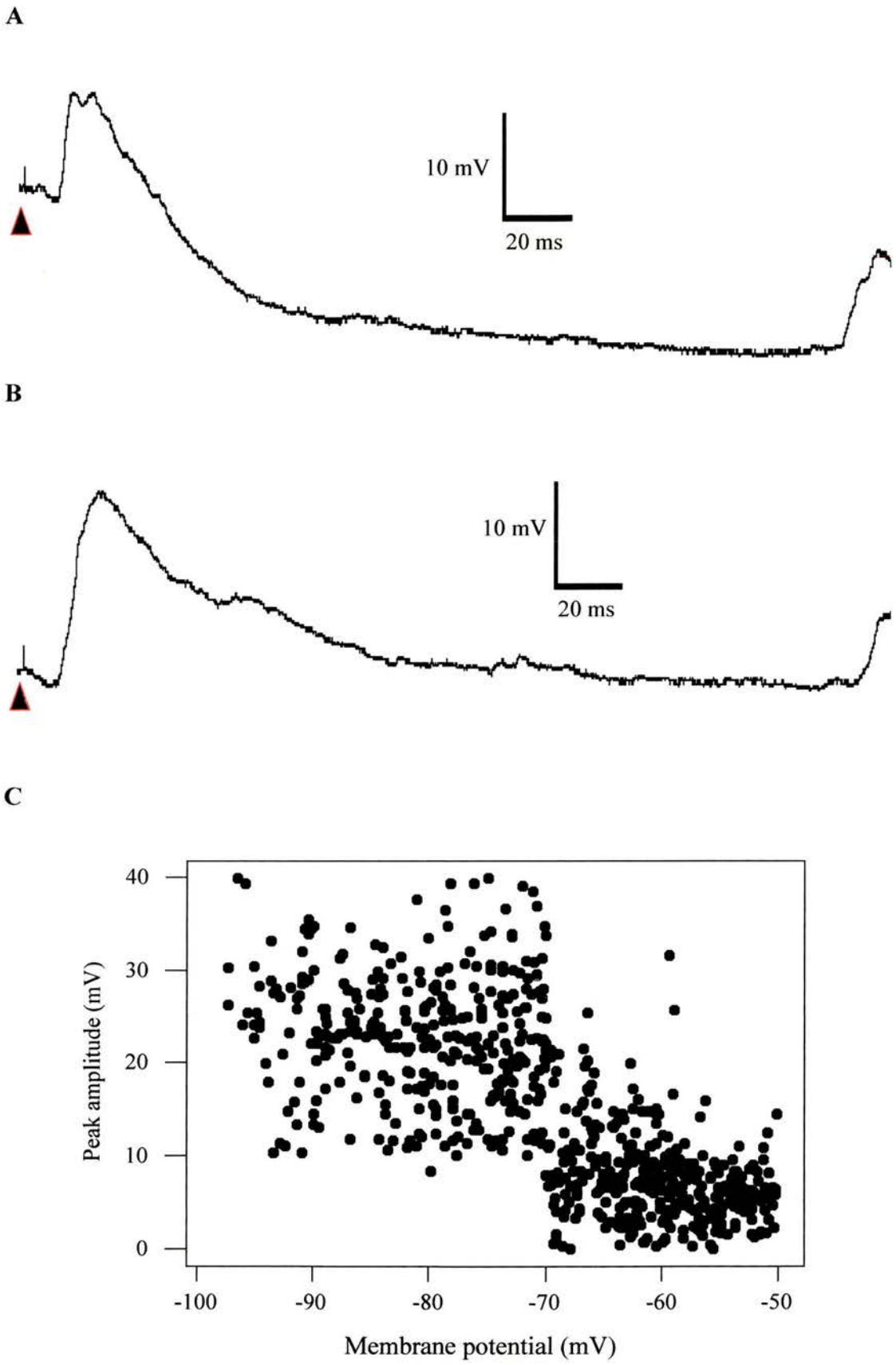
A
10 mV
20 ms
B
10 mV
20 ms
C
Peak amplitude (mV)
40
30
20
10
0
-100
-90
-80
-70
-60
-50
Membrane potential (mV)

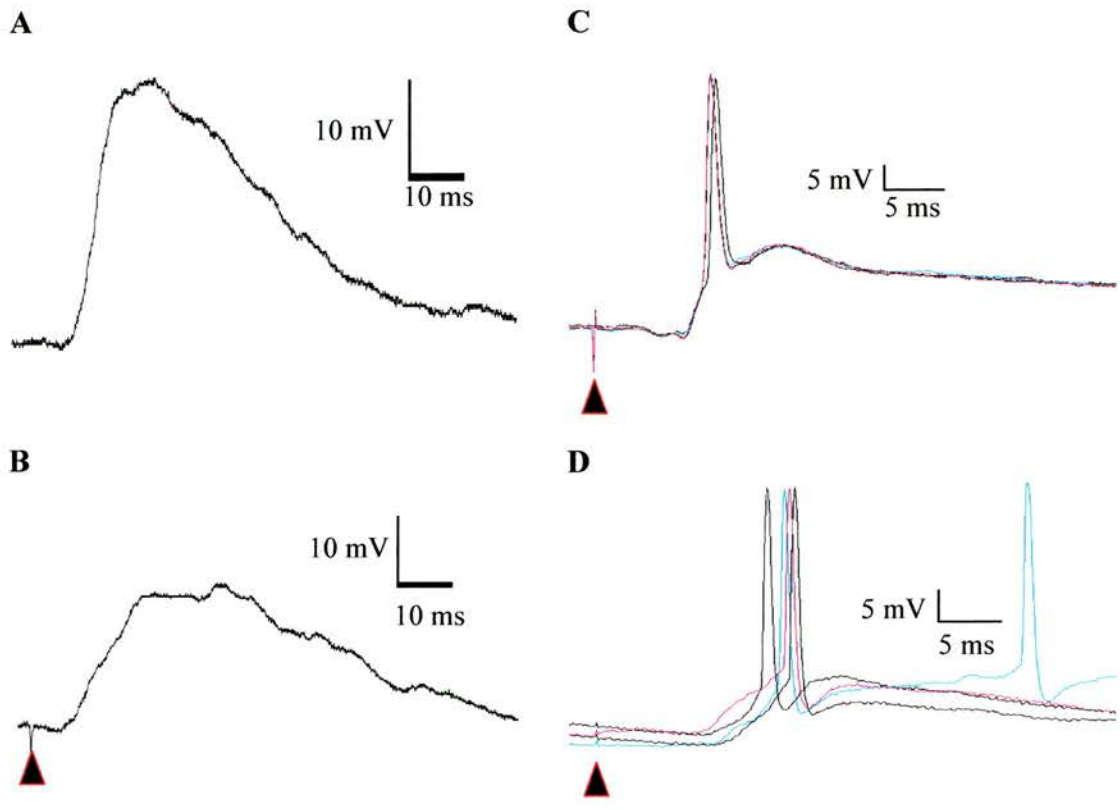

Figure 3. 19. Whisker pad vs. contralateral cortical stimulation in striatal neurones.

A B illustrate the difference in the rise time of the EPSPs in response to whisker pad (**A**) and contralateral cortical stimulation (**B**). The striatal cell recorded at a depth of 2934 μm was stimulated subthreshold to prevent the firing of action potentials. The stimulus artefact is marked by a (▲). The traces displayed are the average of 8 sweeps.
A The rise time to whisker pad stimulation was 8.89 ± 0.96 ms. There was a rapid rise of the EPSP with relatively little inflection till the peak amplitude was reached.
B Contralateral cortical stimulation gave rise to an EPSP with a rise time of 14.83 ± 3.05 ms. The rising phase of the EPSP was more gradual with a greater number of inflections before maximal response to the stimulus was reached.
C D illustrate the response of another striatal neurone stimulated supratheshold so as to generate action potential firing. The traces consist of 4 overlaid sweeps.
C Action potential firing in response to whisker pad stimulation was very consistent and latency to spike initiation was similar from sweep to sweep. This is seen by the fact that even though 4 traces were overlaid only 2 action potentials are visible as 3 of them have almost identical spike initiation latencies.
D Spike initiation latency was more variable in response to contralateral cortical stimulation. There is a greater jitter in the traces when compared to **C**.

rising EPSPs with variable action potential latencies while whisker pad stimulation resulted in EPSPs that had a rapid rise time and showed little variation in latency to spike generation.

Two cells were stimulated with increasing stimulus intensities to see if there was a polysynaptic component in the response of the cells (Fig. 3.20). Each trace represents the average of 8 sweeps at a particular stimulus intensity. The averaged responses were then offset manually so that the membrane potential was the same in all traces (-80 mV) allowing easy comparison of inflections in the response. In the averaged traces, inflections on the rising phase of the EPSP were prominent and were seen over a range of stimulus intensities. In addition, the latency to onset of the EPSP in these cells appeared to decrease with an increase in the stimulus intensity, which suggests that there might be a significant polysynaptic contribution in the response of the neurones to whisker pad stimulation. There is less jitter in the latency of the neurones to contralateral cortical stimulation. An increase in the stimulus intensity does not increase the latency of the response. This suggests that this might be a monosynaptic pathway or at least fewer pathways are involved in the response.

3.3.2.3) Individual whisker deflection

In 5 experiments individual whisker deflection was carried together with electrical whisker pad and contralateral cortical stimulation. One cell responded strongly to a single whisker deflection while 6 cells responded to the whisker pad and cortical stimulation but had no response to the movement of single vibrissae.

Figure 3.21 shows the one cell that responded to the piezoelectric whisker deflection. The cell was at a depth of 2508 μm. cell was filled for 20 min and histology revealed that the striatal cell lay just below the corpus callosum. The

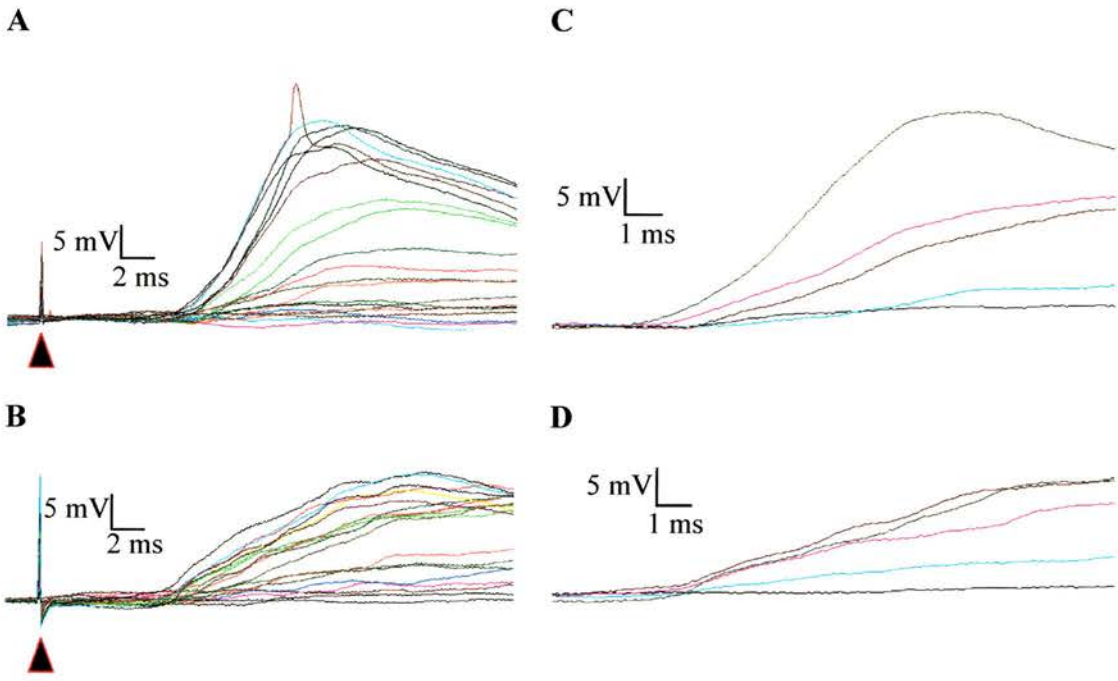

Figure 3. 20. Response of striatal neurones to increasing intensities of whisker pad and contralateral cortical stimuli.

The traces illustrate the response of a striatal neurone at a depth of 3125 μm to increasing whisker pad (**A, C**) and contralateral cortical (**B, D**) stimulation. The latter traces **C** and **D** are expanded traces of **A** and **B** respectively and have fewer overlaid sweeps making the identification of the start of the response easier. The traces consist of overlaid sweeps that were individually offset so as to have the same membrane potential. Note the difference in rise time to both forms of stimulation. The stimulus artefact is marked by a (▲).

A C show the response of the cell to increasing whisker pad stimulation. There is a considerable shortening in the latency of the response to increasing intensity of stimulation indicating that this pathway involves more than one synapse.

B D show the response of the cell to increasing contralateral cortical stimulation. Even with increasing stimulus intensities there seems to be a relatively fixed latency to the onset of the response. This indicates that at least the earliest excitatory response is due to a monosynaptic input.

Figure 3. 21. Individual whisker deflection.

In addition to responding to electrical stimulation of the whisker pad (**A**) and contralateral cortex (**B**) one cell responded to the deflection of an individual whisker (**C**). The neurone which responded robustly to piezoelectric deflection of whisker A 1 was at a depth of 2508μm and histology revealed that this cell was located just below the corpus callosum. The traces are an overlay of 8 sweeps (grey) and the averaged trace is shown in black. These traces were obtained using the MacLab Scope acquisition package. The stimulus artefact is marked by a (▲). The response to all 3 forms of stimulation was very similar.

A Response of the cell to whisker pad stimulation. The mean latency was 6.85 ± 0.53msec. This was followed by a period of inactivity lasting over 200 ms.

B Response of the cell to contralateral cortical stimulation. The mean latency was 8.14 ± 0.72msec. This was followed by a period of inactivity lasting over 200 ms.

C Response of the cell to deflection of the whisker A1. The mean latency was 8.52 ± 0.54msec. This was followed by a period of inactivity lasting over 200 ms.

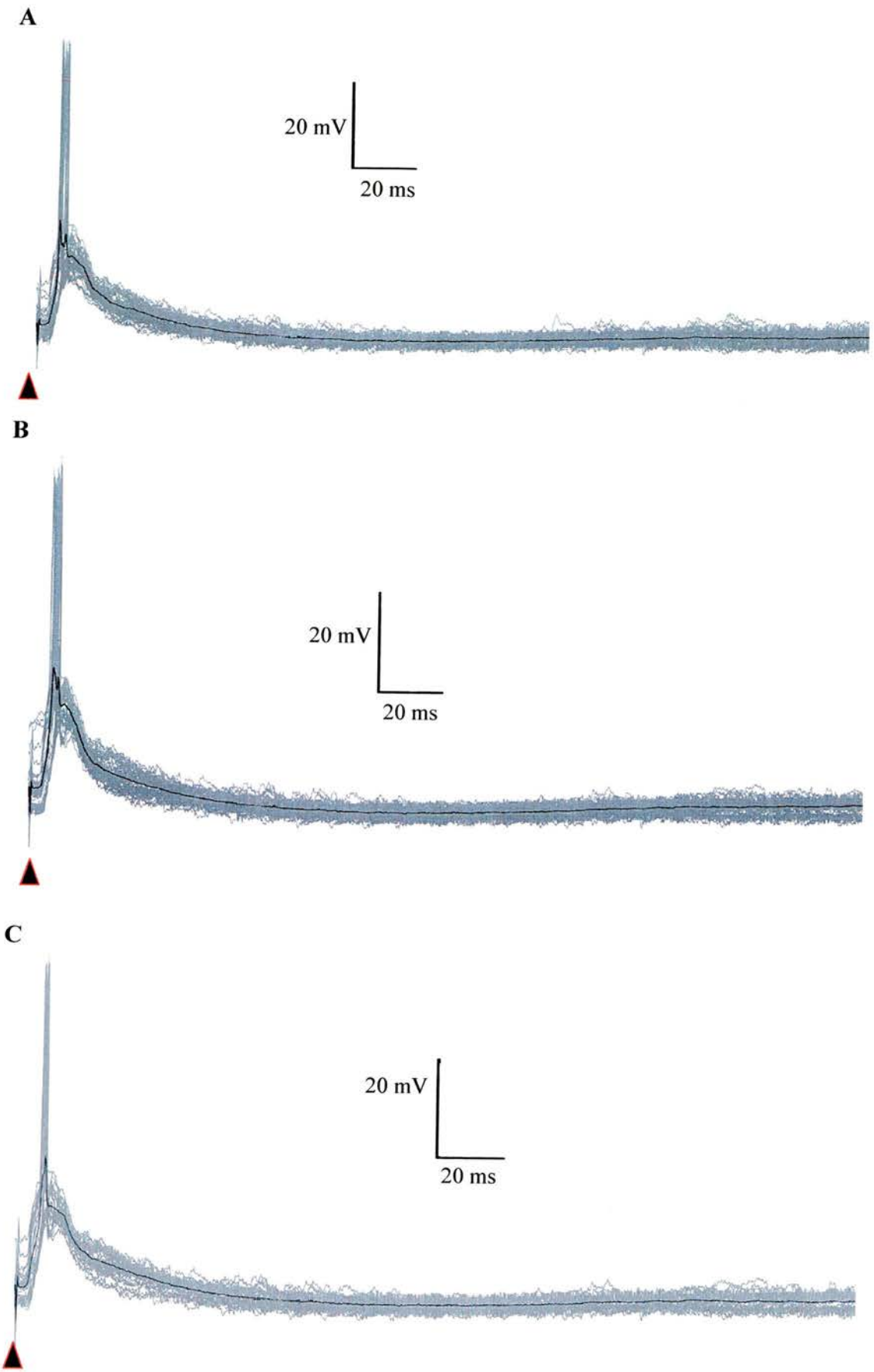
A
20 mV
20 ms
B
20 mV
20 ms
C
20 mV
20 ms

detailed morphology of the cell is discussed in the later sections. The cell responded to the deflection of whisker A1 that is the most dorsal whisker. The cell had a average membrane potential of –72 mV. Looking at the overlay of the 16 sweeps taken and the relatively small standard deviation values, the consistency of the responses of the cell to all 3 types of stimuli is evident.

3.3.3) Electroencephalogram

To investigate the relationship between cortical and striatal activity, focal EEGs were taken from both the sides of the cortex simultaneously with intracellular recordings of striatal neurones (n = 7) (Fig. 3.22). Concurrent recordings of the membrane potential of striatal neurones and cortical EEGs indicated that the two waveforms were oscillating synchronously. Further analysis such as cross-correlograms could not be carried out due to the lack of long periods (> 5 s) of data due to the method of data acquisition.

3.3.4) Cortical spreading depression

The relationship between cortical and striatal activity was further analysed by spreading depression via application of 3M potassium acetate to the cortical surface. Spreading depression was carried out in 6 animals but records were only obtained from 3 cells from 3 animals. Application of the solution usually caused a burst of activity in the striatal cell and loss of the cell. In the 3 cells transient cortical inactivation resulted in a loss of rhythmic, coherent activity in the cortex which was associated with the loss of the spontaneous shifts in membrane potential in the striatal cells. Once the cortex was shutdown striatal cells did not respond to either whisker pad or contralateral cortical stimulation (Fig. 3.23). In all 3 cases the

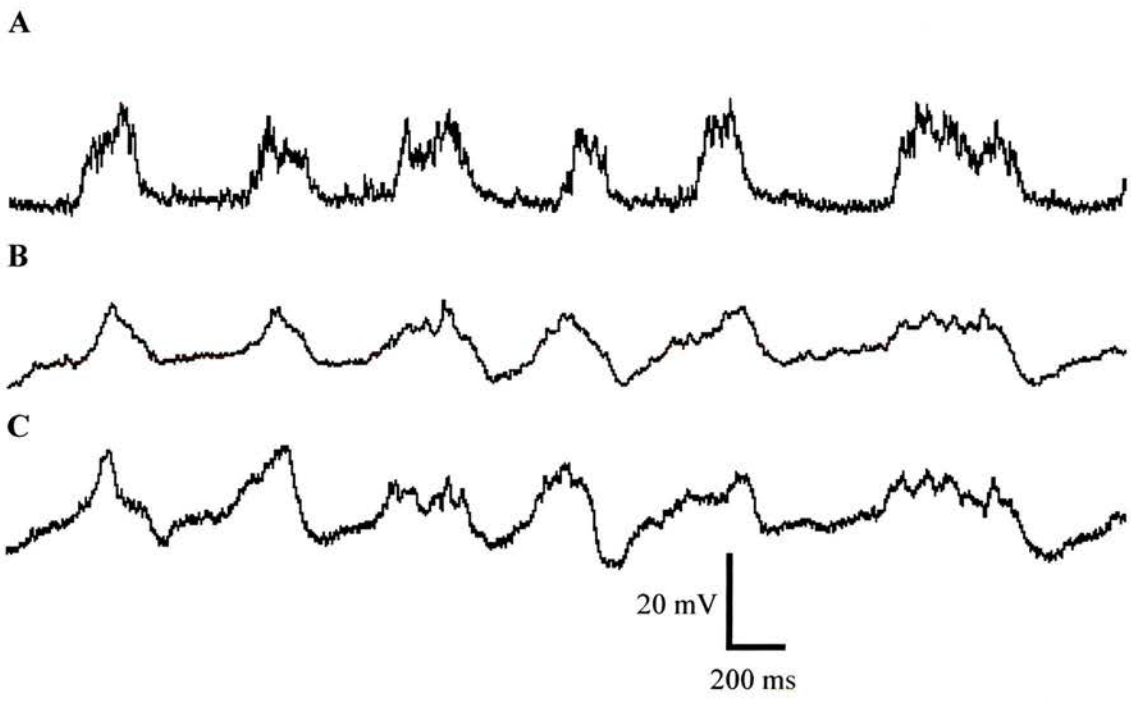

Figure 3. 22. Cortical EEG and spontaneous striatal activity.

Simultaneous recordings of the cortical EEGs and striatal neurones were taken. Visual inspection of the recordings of the spontaneous membrane potential fluctuations of striatal neurones (**A**), cortical EEG on the recording side (ipsilateral cortex, **B**) and stimulating side (contralateral cortex, **C**) indicated that spontaneous membrane potential fluctuations of striatal neurones were correlated with the slow oscillatory activity in the cortical EEG.

Figure 3. 23. Cortical shutdown.

Cortical shutdown was achieved by local application of potassium acetate (same solution as recording electrode). Application of potassium acetate was marked time zero and records were taken at 5 minute intervals until the spontaneous activity resumed and the response of the striatal neurone to both forms of stimulation returned. Shutdown of one side of the cortex was not possible and application of the solution to the cortical surface caused an electrical shut down on both sides of the cortex at the same time. The stimulus artefact is marked by a (▲).

A Whisker pad stimulation gave rise to a response consisting of an EPSP with an average amplitude of 8.95 mV. The cortical EEG of the ipsilateral cortex is displayed below.

B Response of the same cell to whisker pad stimulation 5 minutes after application of potassium acetate. The EEG shows no electrical activity in the cortex and even maximal stimulation of the whisker pad gave rise to no discernable response.

C Contralateral cortical stimulation gave rise to a response consisting of an EPSP with an average amplitude of 6.78 mV. The cortical EEG of the contralateral cortex is displayed below.

D Response of the same cell to contralateral cortical stimulation 5 minutes after application of potassium acetate. The EEG shows no electrical activity in the cortex and even maximal stimulation of the contralateral cortex gave rise to no discernable response.

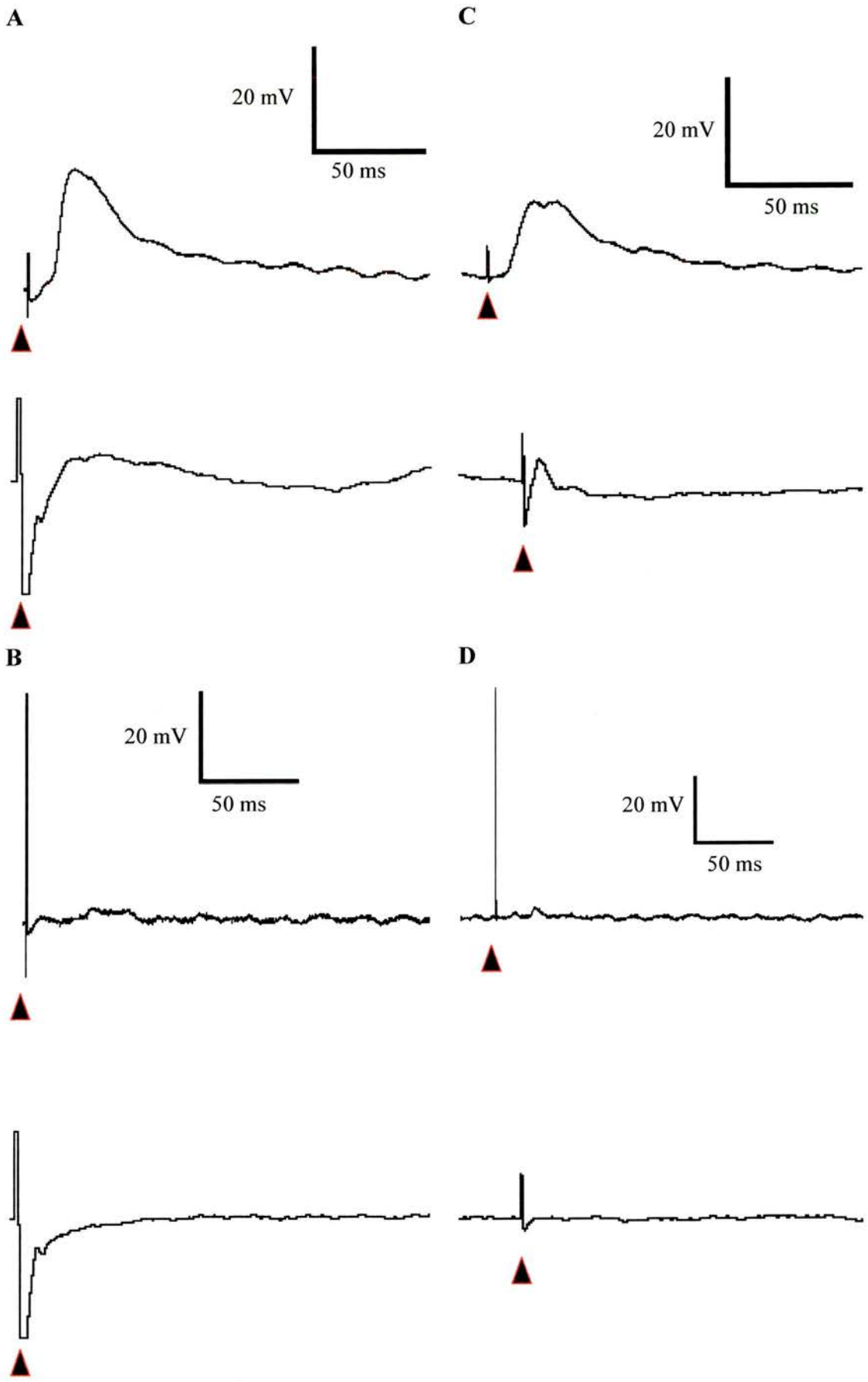
A
20 mV
50 ms
C
20 mV
50 ms
B
20 mV
50 ms
D
20 mV
50 ms

depression of cortical activity was fully reversible and there was full recovery of cortical and striatal activity approximately 35 min after cortical shutdown. There was a resurgence of cortical waves and an increase in striatal depolarisation. The response of the cells to both forms of stimuli before depression and after full recovery of the cortex was not significantly different (whisker pad: control - 11.115 ± 6.948 mV, after cortical shutdown – 10.925 ± 2.356 mV, ANOVA, $p > 0.05$; contralateral cortex: control - 8.973 ± 6.964 mV, after cortical shutdown – 9.087 ± 1.990 mV, ANOVA, $p > 0.05$)

3.3.5) Acute and chronic callosal cuts

To confirm that the response seen as a result of stimulation of the contralateral cortex is due to activation of fibres arising from the contralateral cortex acute callosal cuts were carried out. The extent of the callosal cut was verified histologically after the experiment (Fig. 3.24). The callosal cut extended from 1.00 mm to –6.00 mm with respect to Bregma. In all callosal cuts there was considerable damage to the underlying thalamic nuclei. The spontaneous behaviour of striatal neurones was similar to that of control animals. All responses to contralateral cortical stimulation were abolished (control - 8.973 ± 6.964 mV, acute callosal cut – 0.635 ± 0.855 mV; ANOVA, $p < 0.05$) (Fig 3.25). As in most cells there was no indication of an EPSP in response to contralateral cortical stimulation, the amplitude of the response was measured using mean latency of control striatal neurones to contralateral cortical stimulation as a guide. Consequently no measurements of latency and rise time were taken. The response to whisker pad stimulation however was unaltered in magnitude (control - 11.115 ± 6.948 mV, acute callosal cut – 11.148 ± 1.150 mV; ANOVA, $p >$

Figure 3. 24. Extent and histological verification of callosal cuts.

A Schematic representation (modified from Paxinos and Watson 1996) of the extent of the callosal cut. The saggital section is 0.9 mm lateral to Bregma. The callosal cut extends from 1.0 mm to –6.0 mm (arrows) with respect to Bregma completely cutting the corpus callosum.

B Low power photographs of a brain from an animal on which acute callosal transactions had been carried out. These representative coronal sections spanning most of the striatum show a cut in the corpus callosum. These sections also illustrate the destruction of part of the thalamus as a result of the depth of the knife cut. Scale bar 1000 μm.

A

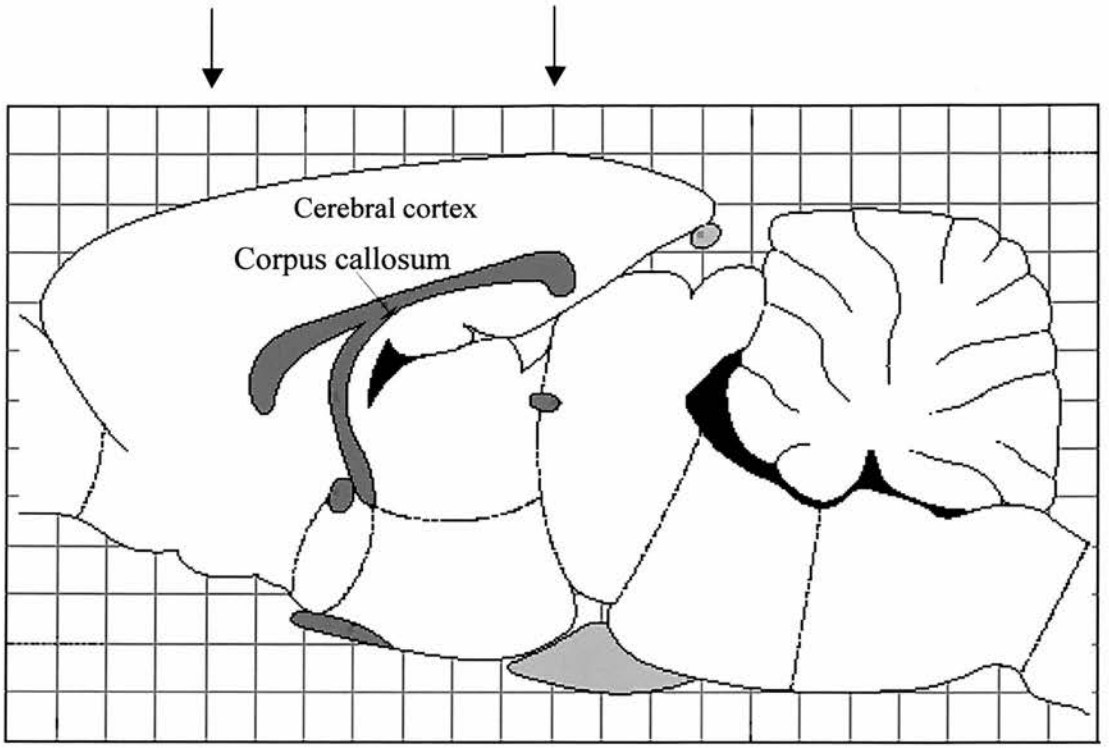

B

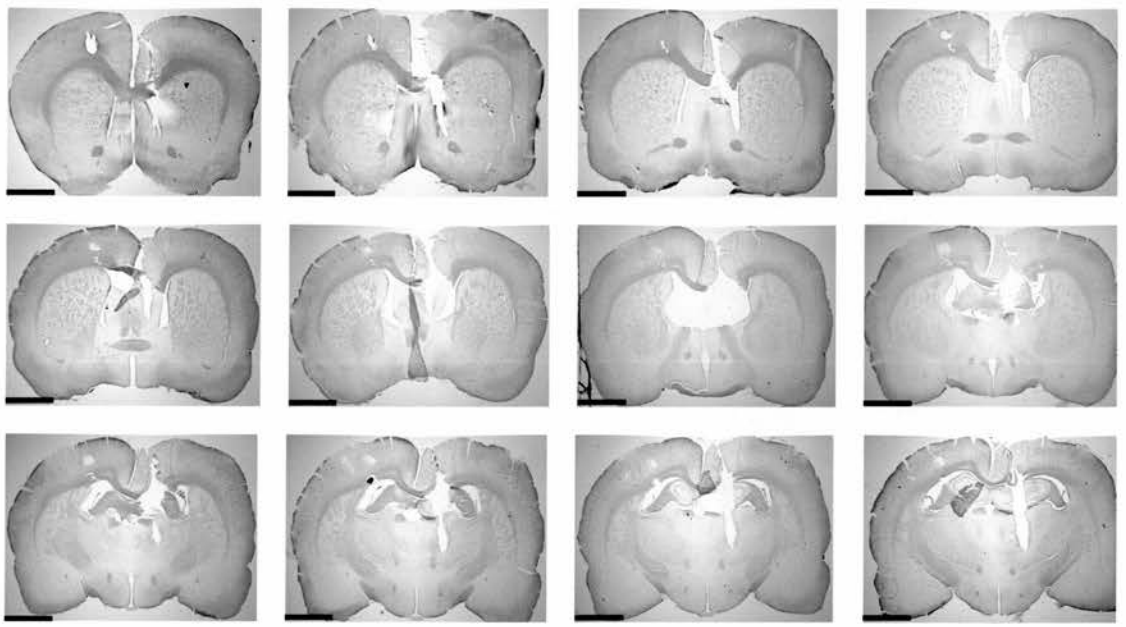

Figure 3. 25. Response to both forms of stimulation in control vs. acute callosal cut animals.

A B C illustrate the spontaneous activity and response of a striatal neurone to both forms of stimulation recorded from an animal with an acute callosal cut. The traces are an overlay of 8 sweeps and the stimulus artefact is marked by a (▲).

A Response of the cell to stimulation of the whisker pad. The EPSP had a latency of 8.05 ms, rise time of 5.71 ms and a peak amplitude of 10.13 mV.

B Response of the cell to stimulation of the contralateral cortex. No discernable response was present even at very high stimulus intensities.

C Spontaneous activity of the cell. The spontaneous behaviour of the cell is very similar to the behaviour of the neurone to contralateral cortical stimulation.

D Graphs illustrating the response properties (latency, rise time, peak amplitude) of striatal neurones in controls (■) and after acute callosal cuts (■). The only statistically significant change is seen in the peak amplitude of the EPSP in response to contralateral cortical stimulation in acute callosally transected animals (*, ANOVA, $p < 0.05$) . The response properties due to the whisker stimulus are unaffected.

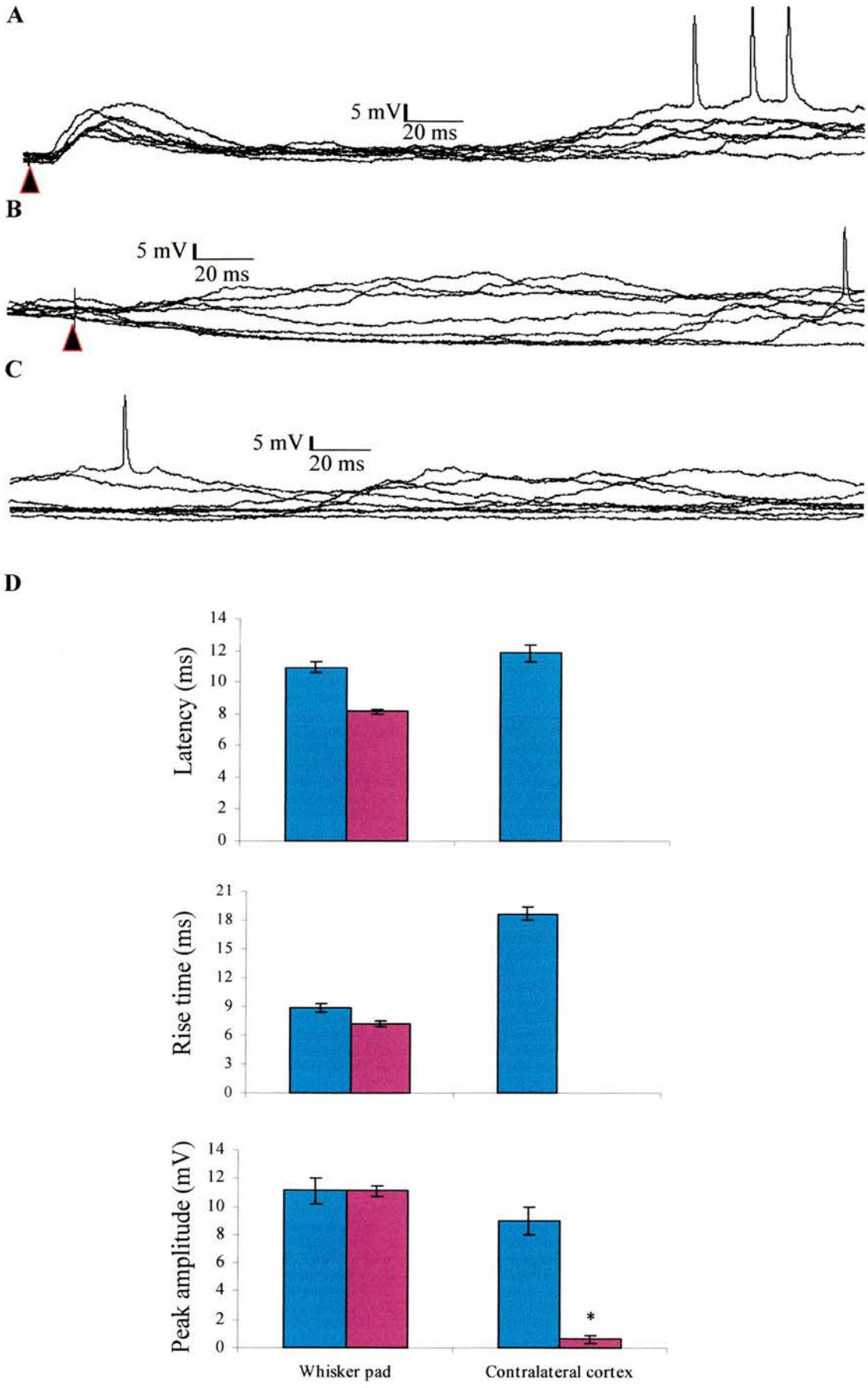
A
5 mV
20 ms
B
5 mV
20 ms
C
5 mV
20 ms
D
Latency (ms)
14
12
10
8
6
4
2
0
Rise time (ms)
21
18
15
12
9
6
3
0
Peak amplitude (mV)
14
12
10
8
6
4
2
0
*
Whisker pad
Contralateral cortex

0.05). The latency and rise time were also unaffected (Fig. 3.25). Four animals underwent chronic callosal transections and 9 cells were recorded from. The extent of the callosal cut was comparable to that of acute callosal cuts. Once again all response to contralateral cortical stimulation was abolished (Fig.3.26) The rise time and latency of response to whisker pad stimulation were unaltered (Fig. 3.26). The amplitude of response to whisker pad stimulation however was significantly reduced (control - 11.115 ± 6.948 mV, chronic callosal cut – 7.891 ± 2.069 mV; ANOVA, $p < 0.05$). In both acute and chronic experiments, the placement of the stimulating electrode was checked to ensure that the lack of response was not due to misplacement of the electrode. Also the same stimulating electrode was used in another experiment where the callosum was intact. This was done to verify that the electrode was still able to give rise to comparable response characteristics in normal animals. This confirmed that the lack of response in these experiments was a result of the callosal cuts and not due to damage of the electrode.

3.3.6) Morphology of cells

A total of 36 cells were filled. However 4 could not be histologically identified. This was due to the use of fixative with a low glutaraldehyde concentration and the presence of large amounts of blood in the brain, which could not be removed by quenching and thus lead to a very high degree of background staining. All the filled cells were of the spiny projection neurone type. Figure 3.27A shows a cell filled for 2 min before the membrane potential increased and the electrode withdrawn. A 'ghost' cell was seen with little dendritic detail visible. When a cell was filled for longer than 2 min the dendrites could be seen more easily (Fig. 3.27B). Figure 3.27C shows a cell that was filled with biocytin for 20 min. At higher magnification (Figure 3.27D)

Figure 3. 26. Response to both forms of stimulation in control vs. chronic callosal cut animals.

A B illustrate the response of a striatal neurone to both forms of stimulation recorded from an animal with a chronic callosal cut. The traces are an overlay of 8 sweeps and the stimulus artefact is marked by a (▲).

A Response of the cell to stimulation of the whisker pad. The EPSP has a latency of 8.65 ms, rise time of 7.21 ms and a peak amplitude of 5.28 mV.

B Response of the cell to stimulation of the contralateral cortex. No discernable response was present even at very high stimulus intensities.

C Graphs illustrating the response properties (latency, rise time, peak amplitude) of striatal neurones in controls (■) and after chronic callosal cuts (■). A statistically significant change is seen in the peak amplitude of the EPSP in response to both forms of stimulation (whisker pad -control - 11.115 ± 6.948 mV, chronic callosal cut – 7.891 ± 2.069 mV; ANOVA, $p < 0.05$, contralateral cortex –control - 8.973 ± 6.964 mV, chronic callosal cut – 0.135 ± 0.698 mV; ANOVA, $p < 0.05$).

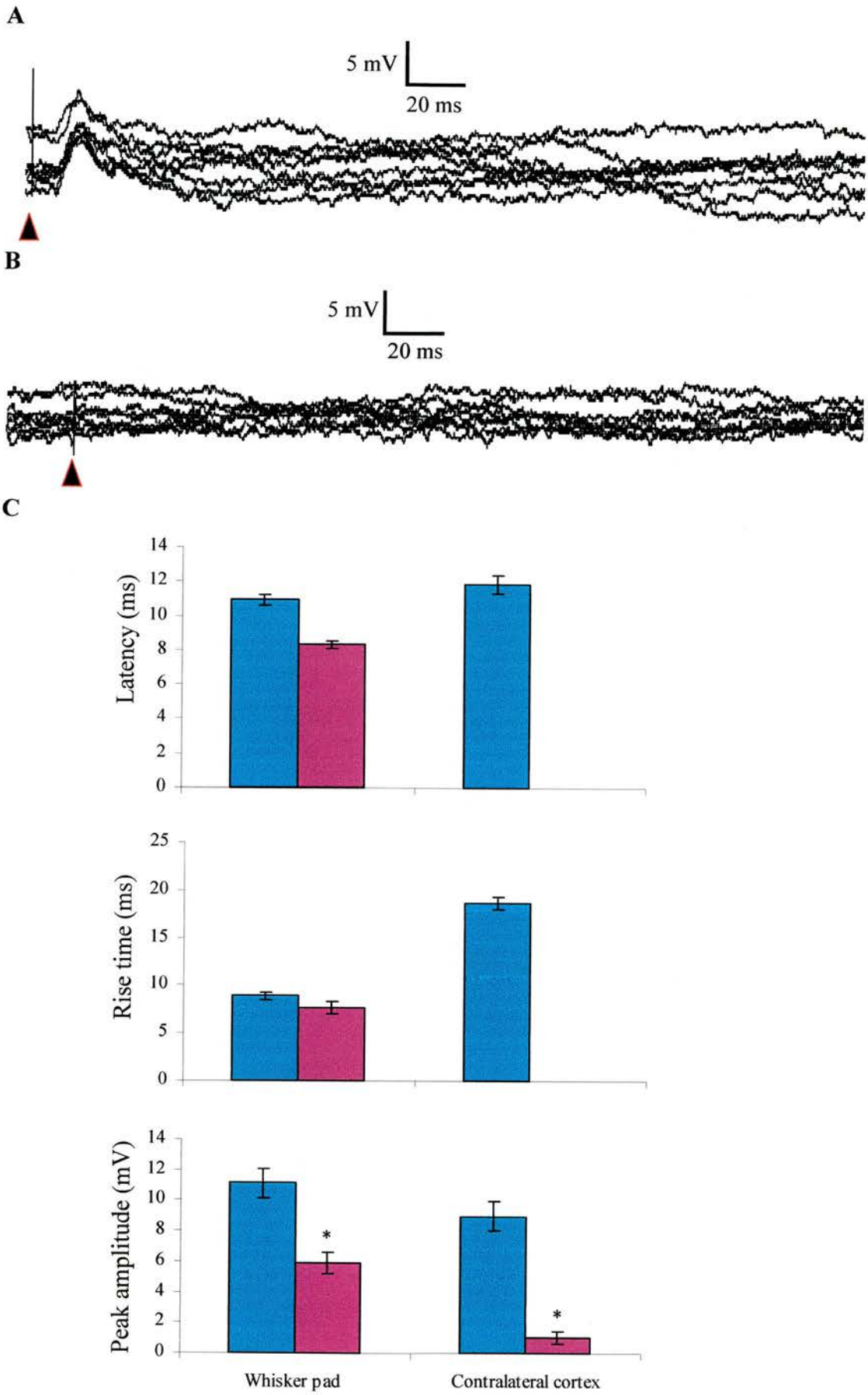
A
5 mV
20 ms
B
5 mV
20 ms
C
Latency (ms)
14
12
10
8
6
4
2
0
Rise time (ms)
25
20
15
10
5
0
Peak amplitude (mV)
14
12
10
8
6
4
2
0
*
*
Whisker pad
Contralateral cortex

Figure 3. 27. Morphology of filled striatal neurones.

Cells were filled with biocytin and the sections were cross-reacted with avidin biotin and DAB was used to visualise the product. Sections were counterstained with methyl green. All cells had morphological features characteristic of spiny striatal projection neurones.

A A cell at a depth of 3132 μm which was filled for 2 min. This is an example of a ghost cell where the detailed morphology of the cell is not visible. Scale bar 30 μm.

B A cell at a depth of 3242 μm was filled for 15 min. There is more morphological detail seen compared to **A**. Scale bar 30 μm.

C A cell at a depth of 2508 μm which was filled with biocytin for 20 min. This was the striatal neurone that responded to individual whisker deflection. The spines on the dendrite are more clearly visible. Scale bar 30 μm.

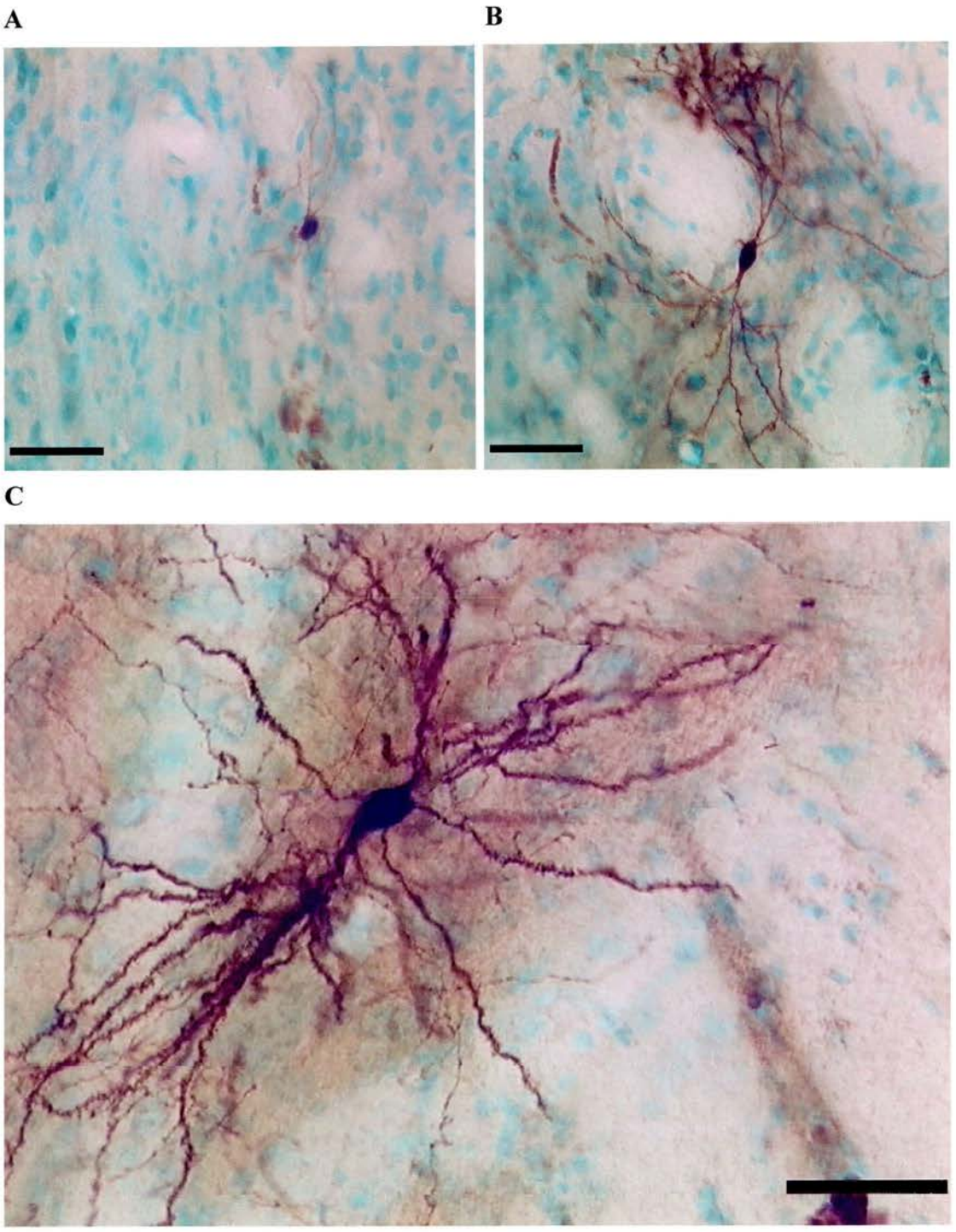
A
B
C

it is possible to see the spines on the dendrites. In general, the cell bodies of all 32 neurones were similar in size.

3.4) Discussion

3.4.1) Cortical cells

Using the depth reading from the Burleigh Inchworm and subsequent histology, the majority of cortical recordings were obtained from layer V cortical neurones. This suggestion is consistent with the fact that the latency of the responses to stimulation was not dependent in anyway on the depth of the cell, as Carvell and Simon (Carvell and Simons, 1988) have demonstrated that cortical cells of different layers have dissimilar response latencies to whisker stimulation. Layer IV cortical neurones have the shortest latency (5-7 ms) (Zhu and Connors, 1999) which is a reflection of the fact these cells are the first to receive ascending sensory information, via the fast thalamocortical axons from the VB thalamus (Woolsey and Van der Loos, 1970; Simons, 1978; Armstrong-James and Fox, 1987; Armstrong-James et al., 1993). The longer latencies observed in this study are likely to be due to activation of this direct ascending pathway relayed by a slower group of thalamocortical fibres, or due to the intracortical transfer of activation (Gazzara et al., 1986; Armstrong-James et al., 1992; Brett et al., 1994). The anterior-posterior extent of the recordings fall within the boundaries of the SI cortex in rodents (Paxinos and Watson, 1986). As the cortical extracellular recordings did not provide any more information than the intracellular data, the majority of the discussion will focus on the latter.

Intracellular recordings of barrel cortical neurones under urethane chloralose anaesthesia showed membrane potential shifts. This spontaneous activity was composed of rhythmic depolarising components separated by prolonged hyperpolarisation and agrees with previous data obtained from other cortical areas (Steriade et al., 1993b; Cowan and Wilson, 1994; Stern et al., 1997; Zhu and

Connors, 1999). Dual recordings of intracellular cortical recordings and cortical field potentials shows that cells in large areas of the cortex undergo these shifts of membrane potential synchronously (Steriade et al., 1993b). In the present study, depolarised membrane potentials were about -45 mV and the increase in amplitude of high frequency fluctuations in the depolarised state sometime crossed the spike threshold, resulting in the generation of action potentials. However in most cases the cells were subthreshold to spike generation and this is likely to be partly due to the presence of subthreshold potassium currents in cortical pyramidal neurones (Foehring and Surmeier, 1993). The main mechanism behind the hyperpolarisation is thought to be disfacilitation (Cowan and Wilson, 1994). Cowan and Wilson suggest that episodes of depolarisation and hyperpolarisation represent periods of increased and decreased synaptic input to neurones respectively (Cowan and Wilson, 1994). An increase in input resistance occurs during this prolonged hyperpolarisation suggesting that there is a removal of synaptic input, which manifests as a suppression of neuronal discharge (Cowan and Wilson, 1994). There is also a small $GABA_A$ mediated component (Connors et al., 1988) as seen by the decrease in amplitude and duration of hyperpolarisation following intracellular infusion of chloride (Steriade et al., 1993b). However the inhibitory postsynaptic potentials have a short latency and cannot fully account for the long lasting hyperpolarisation (Contreras et al., 1996). Furthermore these inhibitory cells oscillate in phase with pyramidal neurones (Contreras and Steriade, 1995). Other mechanisms responsible for generation of hyperpolarisation could involve intrinsic membrane properties. Inhibition of slow calcium and sodium activated potassium currents found in cortical neurones (Schwindt et al., 1988; Schwindt et al., 1989) via activation of cholinergic circuits

leads to suppression of the lasting hyperpolarisation in cortical neurones (Steriade et al., 1993a).

The lack of antidromic activation would strongly suggest that all of layer V cortical cells that were recorded from in the current study were found below the barrel centres and were not cells below the septa as septal cells are the corticocortical neurones in the barrel cortex (Olavarria et al., 1984). Stimulation of the whisker pad resulted in an EPSP-IPSP-EPSP response profile in cortical neurones that is in agreement with previous studies (Simons, 1978; Armstrong-James and Fox, 1987; Nicolelis et al., 1995; Fee et al., 1997; Zhu and Connors, 1999). It involves an initial short excitatory postsynaptic response with a latency of about 7 ms lasting for approximately 40-80 ms, followed by a hyperpolarisation lasting 150-250 ms. This is followed by several delayed and more variable EPSP's over the next few hundred milliseconds. This triphasic excitation-inhibition-delayed excitation is very characteristic of the response generated by VPM to barrel thalamocortical inputs when activated by the principal whisker. As thalamocortical fibres make only excitatory synaptic terminals, (White, 1979) and the VPM itself has no inhibitory interneurones, (Barbaresi et al., 1986; Harris and Hendrickson, 1987) and inhibitory interactions are less frequently observed (Simons and Carvell, 1989), the inhibitory portion of the response is most likely to be cortical in origin, arising from local intracortical circuits.

The barrel cortex has non-spiny i.e. smooth non pyramidal cells that have been identified as interneurones, and these use GABA as their neurotransmitter. These GABAergic cells make up approximately 15% of total neuronal population in the barrel cortex and are present in high numbers in the layer IV (Beaulieu, 1993),

the main input layer for thalamocortical projections. Distribution of these cells with respect to the barrel and septal domains is highly variable and depends on the antibodies used. Antisera against glutamic acid decarboxylase show a preferential distribution of immunopositive somata and terminals along the sides of barrels (Lin et al., 1985) while Chimelowska and Celio using antibodies against GABA and parvalbumin (PV) respectively show a higher proportion of cells along the sides of barrels with the terminals confined to the barrel centres (Chmielowska et al., 1988; Celio, 1990). Furthermore this different localisation pattern observed in the above three studies was not always reproduced (Akhtar and Land, 1991; Staiger et al., 1996). Up to 8% of VPM efferents target GABAergic structures with single PV neurones receiving multiple thalamic synapses (Staiger et al., 1996). The majority of VPM efferents synapse onto the cell body and proximal dendritic shafts of interneurones while impinging on dendritic spines of excitatory neurones (White et al., 1984; Keller and White, 1987), suggesting that there is considerably stronger thalamocortical synaptic currents in inhibitory interneurones. A stronger thalamocortical thalamocortical synaptic current may also be attributed to the higer single channel conductance of AMPA-subtype glutamate receptors in inhibitory interneurones (Angulo et al., 1997; Swanson et al., 1997). The numbers, locations and types of thalamocortical synapses leads to a strong and rapid excitation of these inhibitory interneurones when the thalamocortical pathway is activated (Agmon and Connors, 1992). These thalamically driven inhibitory cells which are more excitable than excitatory pyramidal and stellate cells (Porter et al., 2001) make direct inhibitory contact onto spiny cells (Porter et al., 2001). These interneurones are fast spiking, have high frequency bursts and can repolarise quickly (Zhu and Connors,

1999), leading to temporal summation of IPSPs and thus giving rise to long lasting inhibition. This disynaptic feedforward circuit can thus act as a possible route for the generation of whisker evoked EPSP-IPSP. A $GABA_B$ receptor mediated response has been shown to be involved in the generation of hyperpolarisation (Connors et al., 1988). However its involvement is likely to be confined to the initial portion of the inhibition and as observed in spontaneous membrane potential fluctuations, the hyperpolarisation is mainly caused by disfacilitation (Cowan and Wilson, 1994). The origin of the delayed whisker evoked EPSP is not clear, though there is much evidence to suggest that it is probably due to the recurrent activation of cortical and subcortical circuitry (Armstrong-James et al., 1991; Castro-Alamancos and Connors, 1996).

In addition to the reported EPSP-IPSP-EPSP profile, inhibition alone as well as excitation alone responses have been reported (Carvell and Simons, 1988; Sachdev et al., 2000). Inhibition alone has been reported to occur only in septal cells (Sachdev et al., 2000) and could imply that septal cells are more densely innervated by interneurones although the cause of this inhibition has yet to be identified (Sachdev et al., 2000). These stimulus evoked IPSPs may play a crucial role in sensory transmission as they are able to terminate EPSPs before they reach threshold and generate action potentials (Pei et al., 1994). Excitation alone has only been reported in one study (Carvell and Simons, 1988) but neither of these response profiles were observed in the current study.

While the response of cortical neurones to the stimulation of the contralateral whisker pad has been well characterised in awake, awake-paralysed as well as anaesthetised rats, to date there are only two known studies which have looked at the

responses of these cortical cells to stimulation of the ipsilateral whisker pad (Pidoux and Verley, 1979; Shuler et al., 2001). The current study has shown that cortical cells can respond to both forms of stimulation i.e. electrical stimulation of the whisker pad which activates the lemniscal pathway and direct stimulation of the contralateral cortex which activates interhemispherically projecting corticocortical neurones. While stimulation of the contralateral cortex like that carried out in this study cannot be considered to be equivalent to stimulation of the ipsilateral whisker pad both would result in activation of only the corticocortical connections contralaterally. Studies looking at primary sensory cortices after ipsilateral activation have identified transcallosal pathways as being responsible for the responses of cortical cells to stimulation of the ipsilateral whisker pad (Pidoux and Verley, 1979; Manzoni et al., 1989; Swadlow and Hicks, 1997; Shuler et al., 2001). Unlike other cortical areas where ipsilateral pathways exist subcortically (Armstrong-James and George, 1988) there have been no reports on responses in the contralateral whisker trigeminal and ipsilateral thalamic nuclei to whisker stimulation. Also there is no anatomical evidence for subcortical whisker related pathways. Thus at least in rodents input from whiskers on both sides of the snout remain segregated up to the barrel cortex where intracortical connections can act as a means by which this bilateral information is integrated. As no records from cortical cells were obtained from the callosal cuts and cortical shutdown experiments, it can be said with some degree of certainty that the response to contralateral cortical stimulation is due to activation of callosally projecting cells.

The study done by Shuler and associates (Shuler et al., 2001) is the first known report that looks at the extracellular responses to ipsilateral whisker

deflection. In their study about 75% of the neurones recorded from responded to deflection of the whisker on both sides of the snout compared to 100% of cells in this study. This could reflect the sample size of the study but is most likely to be due to the different stimulation paradigms. Shuler and co-workers used a physiologically relevant stimulus while here, a stimulating electrode was placed in the contralateral cortical field. So even if the same corticocortical pathways are activated, the relay of information as a result of the two forms of stimuli are highly different. Deflection of individual whiskers would require the information to be transmitted up to the cortex via the trigeminal nucleus and then the thalamus. As it is the septal cells that give rise to the corticocortical projection (Olavarria et al., 1984), activation of these cells would only occur if the Po nucleus which provides the input is activated (Koralek et al., 1988; Lu and Lin, 1993). Electrophysiological studies show that Po neurones require more intense whisker stimulation to generate responses (Chiaia et al., 1991b; Chiaia et al., 1991a; Diamond et al., 1992a). As a result, single whisker deflections may not be sufficient to activate these corticocortical neurones. Supporting this, is the finding that as the strength of the stimulus increased, the proportion of cortical neurones responding to ipsilateral whisker stimulation increased (Shuler et al., 2001). In the present study all cortical neurones responded and this is most likely due to the fact that septal cells were directly stimulated without having the information relayed via the Po nucleus.

The response to contralateral cortical stimulation had a similar response profile to whisker pad stimulation i.e. EPSP-IPSP-EPSP. This agrees with anatomical and histological studies showing corticocortical connections making excitatory synaptic connections (Cipolloni and Peters, 1983). Thus the inhibitory phase

observed is most likely to be caused by local intracortical inhibitory interneurones and not directly by callosal inputs. This finding is somewhat different to that of Cowan and Wilson (Cowan and Wilson, 1994) who orthodromically activated their crossed corticostriatal neurones shown to have corticocortical connections. The response consisted of a very low amplitude depolarisation which could be made to fire action potentials via injection of depolarising current followed by hyperpolarisation, a partial recovery of the membrane potential and a subsequent second hyperpolarisation (Cowan and Wilson, 1994). The first hyperpolarisation is sensitive to both hyperpolarising current and chloride injection suggesting that it is an IPSP, while the second hyperpolarisation is insensitive to the injections and is likely to be due to disfacilitation (Cowan and Wilson, 1994). This dual hyperpolarisation disrupted by a partial recovery of membrane potential is not seen in barrel cortical neurones suggesting that in this area of cortex transcallosal projections might make different connections. One possibility is that interhemispheric corticocortical fibres arising from the barrel cortex avoid contacting interneurones thus providing an explanation for the lack of the short latency IPSP observed by Cowan and Wilson (Cowan and Wilson, 1994). As yet all anatomical studies show input from callosal projections synapsing onto dendritic spines with none contacting onto cell bodies (Cipolloni and Peters, 1983). As the fast spiking interneurones do not posses spines (Porter et al., 2001) they are not likely to be the main target of the corticocortical projections. In agreement with this Swadlow observed interneurones responding to callosal stimulation in SI forelimb cortex but did not observe this phenomenon in the vibrissae cortex of rabbits even though the same experimental procedures were used (Swadlow, 1989, 1990).

The main difference in the responses of cortical cells to both forms of stimulation was in the rise time. Stimulation of the contralateral cortex gave rise to EPSPs with statistically significant slower rise times, compared to EPSPs in response to whisker pad stimulation. This difference could be because a cortical neurone receives more thalamocortical input compared to crossed corticocortical input. Thus when a massive synchronous input arrives via the thalamus the response is an EPSP with a rapid rise time compared to the input from the septal cells. Different EPSP shapes are thought to indicate a different localisation for the respective synapses. Predictions based on the cable theory suggest that synapses located distally on dendrites produce EPSPs of slower rise times than those located nearer or on the soma (Brown, 1991). However the reason for the difference in rise times has not been conclusively proven.

The amplitude of the response of the neurones to both forms of stimuli was similar and partly related to the membrane potential of the cell when the stimulus was delivered. Large amplitude EPSPs were usually observed when the cell was hyperpolarised. In this state action potentials were rarely observed. Action potentials were produced when the stimulus arrived when the cell was at a more depolarised resting membrane potential even though the EPSPs were of smaller amplitude. This dependence of the response on the state of the cell is similar to that reported by Sachdev and colleagues (Sachdev and Wilson, 2001), where a whisker deflection in spite of producing a larger EPSP was less effective in producing an action potential. This variability is thought to mainly reflect changes in either cortical network activity and/or thalamocortical pathways and is not a result of intrinsic membrane properties of single cortical neurones (Sachdev and Wilson, 2001). However in the

present study the dependence of the amplitude on membrane potential was not as large as that reported by Sachdev (Sachdev and Wilson, 2001) and might be due to the different anaesthetics used. The use of ketamine and xylazine seems to produce larger membrane potential shifts than when urethane chloralose is used. However the reason for the larger amplitude changes are unknown.

Anaesthetics have a strong influence on the activity of cortical cells. Different types of anaesthetics induce distinct cortical rhythms which are unique to different sleep stages (Steriade, 1997). The influence of the anaesthetics is thought to modulate synaptic activity within the cortical as well as corticothalamic loops without influencing the intrinsic membrane properties of the neurones. Urethane alters the bursting behaviour of cortical neurones (Simons et al., 1992) and decreases neuronal firing. The use of urethane is preferred to that of ketamine, a known blocker of the NMDA receptor (Anis et al., 1983), even though both anaesthetics produce synchronised slow oscillations of about 1 Hz in the cortex (Steriade et al., 1993b) which resembles slow wave sleep. Urethane might be responsible for uncovering horizontal connections in the cortex (Simons et al., 1992) and as that is one of the connections explored in this thesis, its use was preferred to that of ketamine. The use of α-chloralose, a $GABA_A$ receptor potentiator (Lovinger et al., 1993) preserved peripheral input to the cortex, and its use has been suggested in fMRI studies permitting detection of cortical responses to peripheral input (Ueki et al., 1992). The receptive fields of barrel cortical neurones are also larger then those observed under urethane or barbiturate anaesthesia. (Harding et al., 1979). The urethane chloralose mixture has been used in *in vivo* recordings (Hutton, 1999) and the barrel cortical responses are similar to those reported previously (Zhu and Connors, 1999).

3.4.2) Striatal cells

Records were obtained from striatal projection neurones. Although the main neuronal type in the striatum is the GABAergic medium spiny projection neurone, which in rodents make up 90-95% of the neuronal population (Bolam and Bennett, 1995; Gerfen and Wilson, 1996), three main classes of aspiny striatal interneurones have been described based on their chemical, physiological, and morphological characteristics (reviewed by (Kawaguchi et al., 1995; Kawaguchi, 1997). All the cells filled with biocytin in the present study, were histologically verified to be striatal projection neurones. However it was not always possible to fill all cells recorded from and in many experiments biocytin free electrodes were used (see below). Thus in an attempt to identify the type of striatal neurone recorded from intracellular current pulses were injected into the cell allowing the study of the membrane current – voltage relationship of neurones. As current pulses of increasing negative intensity were injected there was a saturation of the hyperpolarising responses indicative of a inward rectification which has been identified in striatal projection neurones (Jiang and North, 1991) and accumbens neurones (Uchimura et al., 1989) *in vitro*. Injection of a threshold pulse evoked a slowly developing ramp depolarisation leading to a long latency spike discharge is likely to be mediated by the calcium independent slowly inactivating potassium A current (I_{AS}). This current studied in striatal slices is activated by depolarisation and inactivates over a long time course permitting the membrane to depolarise towards spike threshold giving rise to the ramp response to depolarising current (Bargas et al., 1989; Surmeier et al., 1991; Surmeier et al., 1992a). Input resistance was also calculated. However the cells tended to switch between the up and down states during current injection, the values

obtained were atypical. Activation of outwardly rectifying conductances and the inactivation of inward rectification at depolarising membrane potentials give rise to a higher input resistance at the up state unlike the down state, where the cell has a low input resistance which is mainly due to powerful inward rectification (Kita et al., 1985; Wilson, 1995). Thus the input resistance is highly affected by the state of the cell.

A relatively large number of striatal cells were recorded in this study. This is despite the fact that striatal neurones exhibit a low rate of firing activity. This has been attributed to a set of voltage dependent potassium currents (Nisenbaum et al., 1994; Nisenbaum and Wilson, 1995; Wilson, 1995) which shunt excitatory activity. The reason for the large numbers of neurones detected in this study is because these cells were detected during ongoing whisker pad (and as a result corticostriatal) stimulation, which has been shown to be a useful method of detecting and recording from striatal cells (Schultz and Ungerstedt, 1978). The areas in which neurones responded match the areas that contain the topographical projection from the ipsilateral barrel cortex (Wright et al., 1999). The clear "cut off" mark of responding and non-responding cells show that the neurones in the striatum receive their inputs from specific regions in the cortex. The location of the neurone responding robustly to the deflection of whisker A1 also confirms the functionality of the topography. The anterior-posterior extent of responsive striatal neurones is different to that of the anterior-posterior extent of activation seen in DG experiments after whisker stimulation (Brown and Sharp, 1995; Brown et al., 1996). The patches of activation observed in DG experiments tended to be more medial and ventral, and might not have been recorded from due to sampling methods. If 5 or more non-responding

striatal cells were encountered on a single tract then the electrode was withdrawn and was moved caudally. The deeper neurones which might have responded to stimulation were not recorded from. However a recent study by Sachdev and associates (Sachdev and Wilson, 2002) showed recordings of whisker responsive striatal neurones more anterior than this study. However these cells were rare (Sachdev, R., personal communication) compared to the number of responsive neurones found in the anterior-posterior extent of striatum shown to receive the densest projection from the barrel cortex.

Unlike cortical neurones, striatal neurones that only responded to one stimulus were observed. An initial study looking at striatal responses to stimulation of both these pathways did not describe any singly responsive cells (Wright et al., 2001). A larger number of singly responsive cells were observed in extracellular studies compared to initial intracellular studies and this is mainly due to sampling bias. In extracellular recordings the electrode sampled the full dorso-ventral extent unlike intracellular experiments where up to a maximum of 3 cells were filled in a single animal. This electrode tracking biased dorsal sampling, resulted in intracellular recordings from a larger number of neurones in the dorsolateral striatum. The detailed plot of the location of striatal neurones responding to single stimuli revealed that most of the cells had a more ventral location in the striatum. To overcome this sampling bias in latter intracellular experiments, cells were not filled with biocytin thus allowing sampling of more ventrally located striatal neurones. However as a result of decreased electrode resistance due to breakage of the electrode tip, more ventrally located striatal neurones were rarely recorded from.

There was no noticeable difference between the striatal cells that responded to both forms of stimuli. The cells did not differ in either their spontaneous behaviour or in their response to stimulation. There seemed to be three groups of striatal neurones based on the latency of response in extracellular recordings. However this difference in latency was partly due to the depth of the cell which has been shown to have an influence on the latency (Schultz and Ungerstedt, 1978).

Although no cross correlogram analysis had been carried out, visual inspection of simultaneous recordings of the cortical EEG and the membrane potential of striatal neurones indicated that spontaneous membrane potential fluctuations of striatal neurones were correlated with the slow oscillatory activity in the cortical EEG. Intracellular *in vivo* recordings of cortical neurones in this and previous studies show that cortical neurones display rhythmic depolarisation and hyperpolarisation (Wilson, 1987; Cowan and Wilson, 1994). These shifts in membrane potential are strongly correlated with EEG slow oscillatory activity (Amzica and Steriade, 1995). Previous studies have revealed a strong correlation between the 1 Hz rhythm of the cortical EEG and the fluctuations in striatal neurones' membrane potential (Stern et al., 1998; Mahon et al., 2001; Tseng et al., 2001; Kasanetz et al., 2002). Thus the synchronisation is a reflection of the spreading of the cortical rhythms to the striatum (Tseng et al., 2001).

Cortical neurones which send axons to the striatum fire in a manner similar to striatal neurones (Cowan and Wilson, 1994; Stern et al., 1997) and thus the membrane potential of the striatal neurone reflects the pattern of synaptic input to the cell. Up states are induced by strongly synchronous afferent input as shown by the lack of depolarising states in experiments where the integrity of the cortex has been

compromised both in this study with the cortical spreading depression and by others (Wilson, 1993) and the persistent down state in brain slices but not in chronic organotypic cortex-striatum co-cultures (Plenz and Aertsen, 1996a). The down state was thought to be caused by GABAergic inhibition among spiny neurones. Supporting this systemic administration of GABA antagonists blocked the inhibitory phase (Bernardi et al., 1975) leading to the further assumption that spontaneous quiet periods were due to the action of feedback inhibition among striatal neurones. However despite electron microscopic studies showing that the main target of the large axonal arborisations of striatal neurones were other striatal neurones (Wilson and Groves, 1980), electrophysiological studies did not find direct evidence for inhibitory synaptic interactions among striatal neurones (Jaeger et al., 1994; Stern et al., 1998) until recently (Czubayko and Plenz, 2002; Tunstall et al., 2002). These latter studies have shown that striatal projection neurones are interconnected by functional inhibitory synapses and this lateral inhibition may be important in synaptic plasticity, the development of matrisomes and the control of temporal firing of action potentials (Czubayko and Plenz, 2002; Tunstall et al., 2002).

The spontaneous behaviour of striatal neurons is brought about not only by the patterning of synaptic input to the cells but by the presence of synaptic conductances intrinsic to the neurones. In the down state the membrane potential was highly polarised at –85 mV and the fluctuations in membrane potential were diminished. This has been attributed to the inwardly rectifying potassium conductance which keeps the neuronal membrane close to that of the potassium reversal potential (Kita et al., 1985; Kawaguchi et al., 1989; Uchimura et al., 1989; Jiang and North, 1991). It has been proposed that this inward rectifier is present not

only on the soma but on the dendrites of the cell also, thus altering the electrotonic length of the dendritic tree (Wilson, 1995). Coherent synaptic input to a cell which is capable of depolarising the cell can deactivate the inward rectifier and drastically reduce the electrotonic length and lead to the cell switching to the upstate (Wilson, 1993, 1995). In the up state, outwardly rectifying potassium conductances activated by depolarisation come into play and keep the membrane potential of the striatal neurone just below threshold and thus explains the low spontaneous activity of the neurone (Calabresi et al., 1987a; Calabresi et al., 1990; Surmeier et al., 1991; Surmeier et al., 1992a; Nisenbaum et al., 1994; Nisenbaum et al., 1996). Substantial additional input is necessary to impel the neurones to threshold (Kasanetz et al., 2002). Once excitation decreases, it leads to the reactivation of the inward rectifier making the cell switch to its down state.

Stimulation of either pathway lead to a response consisting of a short latency large amplitude membrane depolarisation followed by a long lasting hyperpolarisation. When action potentials were generated they tended to be few and had relatively long latencies and corresponded to the peak amplitude of depolarisation. This effect of cortical stimulation either via electrical stimulation of the whisker pad or by direct stimulation of the contralateral cortex on striatal neurones has been described by a large number of investigators (Buchwald et al., 1973; Kitai et al., 1976; Wilson, 1986; Kita, 1996; Vilagi et al., 1998). The initial excitatory response has been shown to be an EPSP mediated by the excitatory neurotransmitter glutamate (Herrling, 1985; Cherubini et al., 1988; Jiang and North, 1991). Four major subtypes of glutamate receptors have been identified i.e. AMPA, NMDA, kainate and metabotropic receptors and spiny striatal neurones possess all

four types of glutamate receptors (Tallaksen-Greene et al., 1992; Tallaksen-Greene and Albin, 1994). AMPA and kainate responses constitute the main component of the postsynaptic potential in neurones at resting membrane potential, while the NMDA mediated response becomes the significant component at subthreshold membrane potentials due to the removal of the magnesium block of the NMDA channel (Kita, 1996). The long and slow nature of the NMDA response is suited for the temporal summation of excitatory afferent inputs from the cortex (Kita, 1996).

Comparing the responses of cortical and striatal neurones to whisker pad stimulation, it is clearly evident that both types of neurones have very similar response profiles. The earliest response in cortical cell was around 7 ms while that in striatal cells was 8 ms. From this it can be postulated that the responding striatal cells receive their excitatory drive from cortical neurones present in layer V of the ipsilateral somatosensory cortex as the results are consistent with the well characterised monsynaptic glutamatergic cortically evoked synaptic potentials in striatal neurones (Jiang and North, 1991; Charpier et al., 1999). However it is important to consider the role played by other inputs to the striatum which might be activated by whisker pad stimulation as the variation in the onset of the response to whisker pad stimulation with increasing stimulus intensity was indicative of a polysynaptic pathway.

A major source of excitatory input to the striatum arises from the thalamus (Kemp and Powell, 1971; Buchwald et al., 1973; Kunze et al., 1979; Wilson et al., 1983b). Stimulation of the thalamostriatal pathway results in either an EPSP alone (Buchwald et al., 1973) or an EPSP-IPSP response in striatal neurones (Wilson et al., 1983b). The inhibition is however is not a direct action of thalamostriatal fibres as

destruction of the cortex which abolishes the orthodromic activation of thalamocortical and subsequently corticostriatal pathways, results in a smaller amplitude EPSP-only response in striatal neurones (Wilson et al., 1983b). Based on conduction velocities a striatal cell could respond to activation of a direct thalamostriatal projection and the activation of the collaterals of the brainstem projecting cortical neurones at roughly the same time and in roughly the same manner (Wilson et al., 1983b). As the projection activated by the whisker pad stimulation is part of the fast conducting brainstem projecting cortical neurones (Jinnai and Matsuda, 1979; Wright et al., 1999), the extent of stimulation of striatal neurones due to direct thalamostriatal activation was determined by electrically shutting down the cortex. Shutting the cortex as confirmed by EEG traces, totally abolished the response in striatal neurones indicating that in this experimental set up most of the information conveyed to the striatal neurone is through the cortex and not directly from the thalamus.

To ensure that the response classified here as response due to the activation of the contralateral cortex, does in fact originate in the contralateral cortex, cortical shutdown and callosal cuts were carried out. All experiments abolished the response of striatal cells to contralateral cortical stimulation. In support of this the invariant latency of response to increasing stimulus intensity suggest that the input from the contralateral cortex is a monosynaptic one.

One of the main aims of this study was to compare the responses of striatal neurones to both forms of stimulation. Response to contralateral cortical stimulation tended to have a longer latency than the response to whisker pad stimulation, but the difference was not statistically different. This was despite different path lengths (3

synapses versus 1) and can be accounted for by the conduction velocities. The striatal collaterals of descending brain stem projecting cortical neurones have a high conduction velocity (Jinnai and Matsuda, 1979). In the current study when this pathway was activated by whisker pad stimulation and hence via 3 synapses, a response in striatal neurones had a similar latency to the directly stimulated contralateral corticostriatal projection. This can be explained by the fine calibre of the fibres (Wright et al., 1999) that make up this system, which therefore has a slow conduction velocity (Swadlow, 1989, 1990). This is supported by findings of Wilson and associates who show that contralateral cortical stimulation gave rise to longer latency EPSP than ipsilateral cortical stimulation (Wilson, 1986). As in cortical neurones, there was no difference in the response profile to both forms of stimulation which consisted of an EPSP-IPSP. A recent study has reported that striatal neurones tended to stay in the up state, after an EPSP in response to a single whisker stimulus (Sachdev and Wilson, 2002). However no such state transitions were observed in this study which could reflect the effect of using different anaesthetics or a different stimulation method. In the one cell where a response was obtained by piezoelectric deflection of a single whisker, the cell displayed a pronounced hyperpolarisation rather than a prolonged up state, suggesting the difference between the two studies is more likely to be due to anaesthetics. As reported before (Wright et al., 2001), both pathways gave rise to large amplitude EPSPs which were able to generate action potentials when spike generation threshold was reached. When the density of the projection from both cortices is considered, it seems highly likely that the ipsilateral cortex plays some role in the response of striatal neurones to contralateral cortical stimulation. Chronic hemidecortication has shown that at least as half of the EPSP in

response to contralateral cortical stimulation is derived from an axon reflex from projections of ipsilateral corticostriatal terminals arising from cells that have a bilateral striatal projection as well as a projection to the contralateral cortex (Wilson, 1986). The response was highly dependent on the state of the cell when the stimulus arrived and is a reflection of the change in the input resistance between the two states. The main difference between the responses was once again in the rise time of the EPSP. Wilson and associates reported that response to stimulation of contralateral cortex takes a significantly longer time to reach peak amplitude compared to ipsilateral cortical stimulation (Wilson, 1986). This difference in rise time might reflect a difference in the anatomy of connectivity of the two pathways to striatal neurones (Brown, 1991).

Another possible explanation for the difference in the rise time could be that the type of cortical neurones mediating the response. Cowan and Wilson did not report a difference in the type of cortical cells giving rise to the crossed corticostriatal projection (diffuse projection with respect to barrel cortical projections) and pyramidal tract cells (topographic projection with respect to barrel cortical projections) (Cowan and Wilson, 1994). All the cortical neurones obtained in this study were orthodromically activated and none were antidromically activated from the contralateral cortex and this strongly suggest that the recordings were of barrel cortical neurones and not septal cells and just like the study of Cowan all recorded cells were regular spiking cells (Cowan and Wilson, 1994). Regular spiking neurones which receive a direct input form the thalamus (Agmon and Connors, 1992) have a limited input to the striatum where they form a simple and restricted input (Cowan and Wilson, 1994; Gerfen and Wilson, 1996). These short latency

responsive neurones have axons and dendrites generally confined to the parent barrel (Chagnac-Amitai and Connors, 1989a, b) and thus are likely to convey information principally about a whisker to their targets. Intrinsically bursting neurones on the other hand do not receive a direct thalamic input (Agmon and Connors, 1992) and are more likely to be under the control of cortical influences as their dendrites are located in the layers V and VI; the output layers of the cortex (Chagnac-Amitai et al., 1990; Connors and Gutnick, 1990). These neurones have longer latencies and longer conduction velocities when compared to regular spiking cells (Hutton, 1999). Thus it is possible to conceive that the projection giving rise to the topographic projection could primarily arise from regular spiking, while the majority of septal cells might be intrinsically bursting neurones. However intrinsically bursting neurones were speculated to be the type of neurones giving rise to the topographic projection (Hutton, 1999). However some regular spiking neurones were also recorded in this study and these were also part of the topographic projection (Hutton, 1999). The ability of intrinsically bursting neurones to act as a network and co-ordinate and amplify cortical firing patterns (Connors, 1984; Chagnac-Amitai and Connors, 1989a) make them an ideal candidate to influence the neuronal activity of striatal neurones which have been shown to require a synchronous coherent cortical input to generate firing (Kincaid et al., 1998; Zheng and Wilson, 2002). The proportion of these two cell groups in the two cortical domains (barrel centres and septae) would strongly influence the response of striatal neurones to their activation. To date no known study has addressed this issue and might be due in part to the difficulty in locating antidromically activating crossed corticostriatal (septal) neurones.

What is considered in this study as a response to whisker pad stimulation is not stimulation of the topographic pathway alone. The massive synchronous movement of whiskers by the electrical stimulation of the whisker pad ensures that the response obtained is initially caused by stimulation of the barrel columns and therefore the topographic pathway. However the stimulus spreads beyond the barrel column to surrounding barrels as well as septa and as the diffuse pathway projects ipsilaterally, some component of the response to whisker pad stimulation would include activation of the diffuse pathway ipsilaterally. Chronic callosal cuts which have been shown to destroy cell bodies, dendrites and axons of bilaterally projecting neurones (Wilson, 1986) were carried out to ascertain the extent of the contribution of the septal cells to whisker pad stimulation. The only difference was in the amplitude of the EPSP, and all other parameters were similar to cells from normal animals. Thus ipsilaterally projecting septal cells seem to have a small contribution to whisker pad evoked responses in the striatum.

As anaesthetics play an important part in the physiology of recordings performed *in vivo*, the choice of anaesthetics in this experiment was important. The normal functioning of central dopamine neurones was critical, as they have been shown to play a role in the spatial navigation in the rat (Whishaw and Dunnett, 1985) and degeneration of ascending dopamine neurones produced by 6-hydroxydopamine lesions causes sensory inattention (Ungerstedt and Ljungberg, 1974; Ljungberg and Ungerstedt, 1976). Experiments involving measurements of dopamine metabolism *in vivo* (by measuring the oxidation of dihydroxyphenylacetic acid (DOPAC)) have shown that anaesthetics such as chloral hydrate and pentobarbitone depress dopaminergic activity (Ford and Marsden, 1986). The use of α-chloralose gave

stable baseline DOPAC levels and this suggested that the mechanism of α-chloralose action involved little or no depressive influence on central dopamine metabolism and neurotransmission (Ford and Marsden, 1986). Sedgwick and Williams also suggested that the effect of α chloralose in cats was to emphasise the basic rhythmic pattern of caudate nucleus activity (Sedgwick and Williams, 1967). They found that in conscious cats, caudate cells present an irregular rhythmic activity, which grouped into bursts after chloralose injection. However the effects were not specific for chloralose as a similar activity was observed in cats anaesthetised with pentobarbitone.

Experiments carried out to demonstrate the effects of urethane have shown that urethane administered intraperitoneally at commonly used doses (around 1.5 g/kg) depressed spontaneous firing rates of striatal neurones (Warenycia and McKenzie, 1984). This could account for the low spontaneous firing rate of striatal neurones during urethane anaesthesia (Wilson, 1993) i.e. 0.1 Hz to 3.0 Hz compared to firing rates ranging from 4.4 Hz to 18.4 Hz in freely moving animals (Trulson and Jacobs, 1979). Urethane does not block the depolarising corticostriatal synaptic input produced by natural somatosensory stimulation but it can stop striatal cells discharging in response to it. So while the membrane potential of striatal cells still spontaneously shift between the up and down states, the number of times the cell fires in the up state decreases (Wilson and Kawaguchi, 1996). Thus it can be speculated that anaesthetics such as urethane may alter certain striatal mechanisms such as GABAergic chloride currents that could interact with voltage dependent potassium currents during the upstate to reduce the likelihood of reaching the threshold for action potentials. Comparisons of the activity of individual neurones in

the lateral striatum between periods of wakefulness and anaesthesia showed that urethane suppressed spontaneous firing and eliminated somatosensory-evoked firing (West, 1998).

3.5) Conclusions

The main findings of the study show that cortical and striatal neurones are able to respond to whisker stimulation under chloralose-urethane anaesthesia. Comparisons of contralateral cortical stimulation and ipsilateral cortical activation via the whisker pad show that for both cells types, while the mean latencies of the responses were the same, the EPSP rise time for contralateral cortical stimulation was significantly longer than whisker pad stimulation. The behaviour of the striatal cells mirrors that of layer V cortical neurones indicating that these cells provide the main excitatory drive to striatal neurones. The segregation of the two parallel pathways up to cortex (lemniscal, paraleminscal) is somewhat maintained both anatomically and physiologically in the striatum indicating a different role for the two pathways.

CHAPTER 4

INTERACTION OF THE TWO CORTICOSTRIATAL SYSTEMS IN RAT SOMATSENSORY CORTEX AND STRIATUM

4.1) Introduction

The results from Chapters 2 and 3 strongly suggest that the two input pathways arising from the barrel cortex are involved in transmitting different types of information to the striatum. The pathway that arises from cells below the barrels has a topographical pattern of termination in the striatum (Alloway et al., 1998; Alloway et al., 1999; Wright et al., 1999), makes more complex synaptic contacts onto dendritic spines and when stimulated, gives rise to rapidly rising EPSPs (Wright et al., 2001). The second pathway that arises from cells below the septa has a diffuse distribution in both striata (Wright et al., 1999; Wright et al., 2001), makes simple synapses with dendritic spines and has a slow EPSP rise time (Wright et al., 2001). The differences observed are likely to be due to the different functions of these two corticostriatal systems. The inputs coming from below the barrel centres are highly efficacious in stimulating the postsynaptic targets and thus provide an efficient system that may quickly bring about a relevant motor behaviour in response to sensory information gathered from the whiskers. The function of the diffuse pathway however is not known. The diffuse pattern of projection would imply that this pathway does not play a role in conveying fine spatial somatosensory information (Wright et al., 1999). A possible function of this pathway comes from studies looking at the function of the different inputs to the nucleus accumbens in the ventral striatum.

4.1.1) Gating of inputs to the nucleus accumbens

The nucleus accumbens receives an input from a wide range of structures, namely the prefrontal and entorhinal cortex, the hippocampus and the amygdala

(Groenewegen et al., 1980; Kelley and Domesick, 1982; DeFrance et al., 1985; Sesack et al., 1989; Kita and Kitai, 1990), suggesting that this nucleus is involved in the coordination of limbic and motor systems (Mogenson et al., 1980). Accumbens neurones have been shown to receive convergent input from these afferents both anatomically and physiologically (O'Donnell and Grace, 1995; Finch, 1996; French and Totterdell, 2002). The spontaneous activity of these cells is similar to that displayed by striatal projection neurones and is composed of periodical shifts in membrane potential from a hyperpolarised resting membrane potential or down state, to a depolarised up state (Yim and Mogenson, 1988; O'Donnell and Grace, 1995). Hippocampal afferents that are carried to the nucleus accumbens via the fimbria-fornix, are the source of the synaptic inputs that cause bistable cells to show depolarising plateaus because transection of the fimbria-fornix abolishes up state transitions, while lidocaine injections into the fimbria-fornix lead to temporary suppression of up events (O'Donnell and Grace, 1995). Simultaneous recordings of field potentials in the hippocampus and *in vivo* intracellular recordings of accumbens neurones indicate that transitions to the up state are correlated with population activity in the hippocampus (Goto and O'Donnell, 2001a, b).

In vivo, accumbens cells that are bistable respond to both prefrontal cortical and hippocampal stimulation (O'Donnell and Grace, 1995). The amplitude of response to prefrontal cortical stimulation is correlated with the membrane potential of the cell when the stimulus is delivered, with a large amplitude EPSP when the cell is stimulated in the down state and a small amplitude EPSP when the stimulus is delivered when the cell is depolarised (O'Donnell and Grace, 1995). The generation of action potentials in response to prefrontal cortical stimulation however only occurs

when the stimulus is delivered in the up state and requires an intact hippocampal input (O'Donnell and Grace, 1995). This is due to the fact that stimulation of hippocampal afferents forces cells to stay in the up state (seen as a prolonged EPSP) and trains of stimuli result in depolarising plateaus that are similar in amplitude and duration to spontaneously occurring depolarising membrane shifts (O'Donnell and Grace, 1995). Thus when prefrontal cortical stimulation occurs following hippocampal stimulation, it results in action potential generation for a stimulus intensity that is sub-threshold for action potential generation when delivered in the hyperpolarised state (O'Donnell and Grace, 1995). These results have lead to the hypothesis that hippocampal afferents gate prefrontal cortical information in accumbens neurones by switching cells into the up state (O'Donnell and Grace, 1995). Thus context sensitive inputs from the hippocampus gate cortical inputs into a pattern of neuronal activity in the nucleus accumbens which then influences its targets, the ventral pallidum and substantia nigra (Nauta and Domesick, 1984; Zahm et al., 1996; O'Donnell, 1999). This information is then relayed to the mediodorsal thalamic nucleus and up to the prefrontal cortex where the latter structure's activity is defined by the pattern of activation of accumbal neurones (Lavin and Grace, 1994). Thus the inputs from the hippocampus, by controlling some aspects of the timing of the up events, may determine the spatiotemporal pattern of thalamoprefrontal cortical activity.

4.1.2) Diffuse pathway from the barrel cortex is a gating pathway

There exists some similarities between nucleus accumbens and striatal neurones. Striatal neurones exhibit spontaneous membrane fluctuations *in vivo* and there is a negative correlation between the membrane potential of the cell and the size of its

response to stimulation as shown both in this thesis and previous studies (Hull et al., 1970; Wilson and Groves, 1981). The lack of a topographical pattern of terminalisation would suggest that the diffuse pathway conveys information that does not require fine spatial resolution (Wright et al., 2001) and one role for this corticostriatal pathway could be that of gating inputs that arrive via the topographic pathway. Activation of the diffuse pathway leads to an EPSP which has a longer rise time (Wright et al., 2001) which might imply that the cells have a longer EPSP duration in response to contralateral cortical stimulation. Thus activation of the diffuse pathway could lead to striatal projection neurones switching to the up state, allowing the generation of action potentials in response to stimulation of the topographic pathway and thus affecting down stream structures.

4.1.3) Aim

The aim of the study was to look into the possible roles of the two pathways and to test the hypothesis that one of these corticostriatal pathways gates the other. Pairs of stimuli were delivered and the effect of one pathway on the other and on itself was investigated in striatal neurones. Emphasis was placed on both the duration of the EPSPs caused by the two forms of stimulation and effect of the state of the cell on its response to the paired stimulus. If the difference in conduction velocities of the two pathways observed in these experiments, occurs in unanaesthetised, naturally behaving animals, one would expect the stimuli to arrive asynchronously despite simultaneous stimulation of both pathways. As before, stimulation of the left whisker pad would stimulate neurones in the right striatum via activation of the topographic pathway arising from the right barrel cortex. The neurones in the right striatum will also be stimulated if the right whisker pad is stimulated. Stimulus applied to the right

whisker pad will lead to activation of the left barrel cortex and consequently lead to the activation of the bilateral diffuse pathway which would lead to activation of neurones in the right striatum. Stimulation of the right whisker pad would mean that the stimuli would have to cross at least three more synapses than when the left barrel cortex is directly stimulated, increasing the latency of the response of striatal neurones to activation of the diffuse pathway. The response of striatal neurones to asynchronous stimulation of the two pathways was also studied. The same experimental protocols were also carried out on layer V cortical neurones, which provide the main excitatory input to the striatal neurones.

4.2) Experimental Procedures

4.2.1) Anaesthesia

A total of 25 male Sprague Dawley rats (240-350 g) were used. The anaesthetic make-up and dose were similar to the electrophysiology experiments described in Chapter 3. All rats received intra-peritoneal injections of a 10% urethane, (Sigma Chemicals, St Louis) 1% α-chloralose (Sigma Chemicals, St Louis) mix in distilled water (1 ml/100 g of body weight). Stable levels of anaesthesia were maintained throughout with additional anaesthetic (10% of original dose) administered approximately four to six hours after the initial injection to ensure the absence of a foot withdrawal reflex.

4.2.2) Surgical procedures

A tracheotomy was performed and the animal was set up in the stereotaxic apparatus as previously described (Chapter 3.2). Briefly, the scalp was cut from the base of the skull to the anterior of the Bregma and the overlying tissue and skull surface cleared as before. The CSF drain was put in place and the masseter muscles and scalp were secured to a brass ring. The skull was drilled bilaterally at 2.1 mm posterior and 5.0 mm lateral to Bregma (Paxinos and Watson, 1986). The area of the skull above the cortex was gently picked away to prevent skull fragments from entering the cortex. A cotton ball soaked with saline was placed over the hole on the recording site. The stimulating electrode was then lowered to a depth of 2.0 mm. A dental cement well (Simplex Rapid, Associated Dental Products, Swindon, U.K.) was built around the site of the recording electrode placement. When the well was dry, the cotton ball was

removed and the dura was deflected just before the recording electrode was lowered (refer to Figure. 3.2).

4.2.3) Stimulus protocol

The whisker pad and contralateral cortex were stimulated as previously described (Section 3.2.1.3 and 3.2.1.4). However all stimuli were adjusted to be subthreshold so that no action potentials were fired in response to activation of the two pathways. No individual whisker deflections were carried out in these experiments.

4.2.4) Intracellular recordings and pairing protocols

Borosilicate glass microelectrodes (1.5 mm OD, 0.86 mm ID with inner filament, Harvard Apparatus, U.K.) containing 3M potassium acetate with resistances of between 60-110 MΩ were used. The electrode was advanced into the cortex at an angle of 90^0 to the cortical surface. It was then advanced 100 μm into the cortex using a manual micromanipulator and the electrode resistance and capacitance compensation balanced. The dental cement well was then filled with liquid paraffin wax (Physiowax, TAAB, England) to stabilise the electrode. Neuronal activity was searched for using electrical stimulation of the whisker pad (0.4 Hz). The electrode was advanced in 2 μm steps, until a neurone was impaled either by advancement alone or by a combination of advancement and electrode 'buzzing' with high current, voltage or capacitance, to gain entry to the cell. The presence of cells was detected by a drop in membrane potential and changes in electrode resistance and capacitance.

Once a cell was successfully impaled its response to contralateral cortical stimulation was determined and only cells that responded to both forms of stimuli were chosen for the interaction study. The input resistance of cells was estimated by

passing a series of small amplitude hyperpolarising and depolarising (subthreshold) current pulses through the recording electrode (1.5 nA to –1.5 nA in 0.5 nA steps). These pulses were delivered both before and after the pairing protocols. All pulses and measurements of cellular properties were made by triggering data acquisition when the cell was either in the up or down state and no attempt was made to distinguish between the two states. The spontaneous activity of the cells was also recorded.

All cells were subjected to 4 pairing protocols which were designed to investigate the interaction of the two pathways as well as the effect of a pathway on itself. A pairing protocol consisted of an initial stimulus (first stimulus), followed by a second stimulus, which was delivered after a time interval. The time intervals were fixed and were 10 ms, 20 ms, 40 ms up to 380 ms with intervals of 20 ms. Thus for each protocol there were 20 time intervals, and for each time interval 8 sweeps were taken. The four protocols were numbered 1 to 4 and the order of the stimuli for each of them is shown in Table 4.1. Protocol 1 investigated the effects of an initial whisker pad stimulation on the response of the cell to contralateral cortical stimulation while protocol 2 looked at the effects of a preceding cortical stimulus on the response of the cell to whisker pad stimulation. Protocols 3 and 4 were designed to investigate the effects of a pathway on itself.

When data acquisition was carried out using MacLab Scope (n=12), the pulses were delivered via a D100 digitimer and the time interval between the two pulses was manually increased, from 10 ms to 380 ms, for each pairing protocol. In the remaining cells (n=13), data was acquired using Signal 2.04 and the delivery of the pulses was via a digital signal from the computer and completely randomised.

Once again all pulses were delivered when the cell was either in the up or down state and no attempt was made to distinguish between the two states. Only cells that were held long enough to enable all 4 pairing protocols to be carried out were included in the study.

Protocol number	First Stimulus	Second Stimulus	No. of time intervals	No. of sweeps per time interval
1	Whisker pad	Contralateral cortex	20	8
2	Contralateral cortex	Whisker pad	20	8
3	Whisker pad	Whisker pad	20	8
4	Contralateral cortex	Contralateral cortex	20	8

Table 4. 1. Summary of the pairing protocols.

As only biocytin-free electrodes were used to maximise the number of cells recorded from, (see Chapter 3.4) pontamine sky blue markings were made at the top and bottom of the electrode tracts at the end of the experiment. The electrode was advanced to a maximum depth of 5,000 μm and if no cells were impaled, the electrode was slowly brought back up to the cortical surface and a new penetration made in a different position.

4.2.5) Perfusion and histology

Animals from which interaction data was obtained were transcaridally perfused. The perfusion and subsequent processing of the brains from all animals was similar to the process described in Chapter 3.3. Sections were reconstructed using a drawing tube and the positions of neurones from which interaction records were obtained were calculated from the marked ends of the tracts.

4.2.6) Acquisition and analysis of data

4.2.6.1) Data acquisition - MacLab and Signal

All experimental data was recorded on either a Macintosh based data acquisition package (MacLab Scope) or a PC based data acquisition system (Signal 2.04). Eight consecutive sweeps were taken for each stimuli and at each time interval for each pairing protocol. Twelve sweeps each lasting 5 s were taken for the spontaneous activity of the striatal neurones. The sweeps were later analysed off-line.

4.2.6.2) Data analysis

The latency, rise-time, and peak amplitude of the response of the neurone to each stimulus was measured as before (see Chapter 3.2 and Fig. 3.4 for definition of measurements). In addition the duration of the EPSPs was also measured. The duration of the EPSP was defined as the time taken from the onset of the EPSP to the time at which the membrane potential returned to baseline values (Fig 4.1). The baseline value for each sweep was the membrane potential of the cell pre-stimulus. These measurements were taken from all traces (i.e. from responses when one stimulus was delivered and from responses to both stimuli in the pairing protocols). In addition the time to peak amplitude was also measured when neurones were given only the whisker or contralateral cortical stimulus. Figure 4.2 illustrates 2 traces, where in one, the response to the second stimulus is clearly visible i.e. not inhibited (**A**) and the other where the response to the second stimulus is inhibited (**B**). In the first instance, the measurements were taken in the same manner as before. However when no response to the second stimuli was visible, the average latency of the response of the cell, and the average time to peak amplitude to the particular stimulus were used as guides to aid measurements. Using the stimulus artefact as a reference,

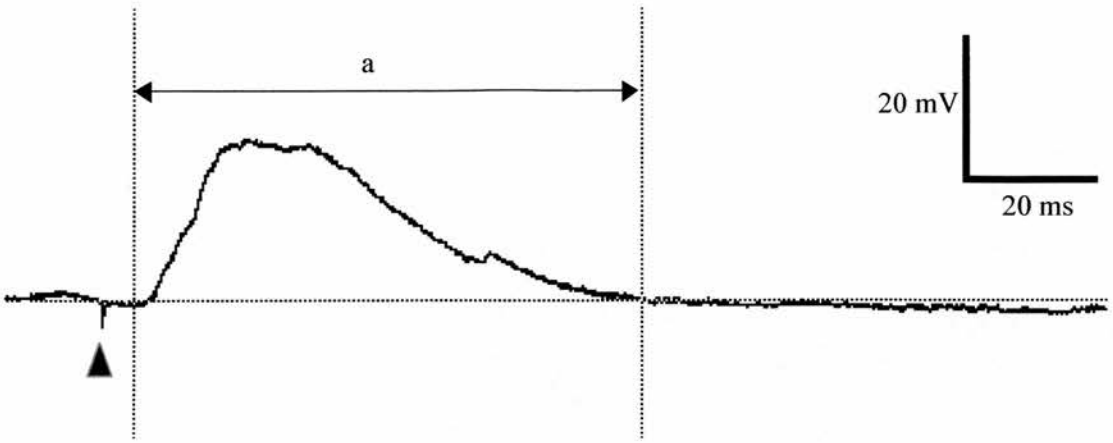

Figure 4. 1. Measurement of the duration of an EPSP.

The representative trace illustrates the response of a striatal cell to subthreshold whisker pad stimulation. The duration of the EPSP (a) is defined as the time taken from the start of the rising phase of the EPSP to the point at which the EPSP returns to baseline value. The baseline membrane potential of the cell is marked with a horizontal line. The stimulus artefact is marked with a (▲).

Figure 4. 2. Measurement of the response characteristics of EPSPs as a result of the second stimulus in the pairing protocol.

The representative traces illustrates the response of a striatal cell to 2 subthreshold whisker pad stimuli. The stimulus artefacts are marked with (▲)

A The trace illustrates the response of the striatal cell to 2 whisker pad stimuli delivered 10 ms apart. The EPSP in response to the second whisker pad stimuli is clearly visible. The latency (a), rise time (b) and peak amplitude (c) are marked on the trace. The start of the onset of the 2nd EPSP coincides with the peak amplitude of the 1st EPSP in response to the first whisker pad stimulus. The duration of the EPSP (d) is measured from the start of the first EPSP to the point at which the membrane potential returns to baseline level.

B The trace illustrates the response of the striatal cell to 2 whisker pad stimuli delivered 20 ms apart. The response to the second whisker pad stimuli is not visible. The latency (a) and peak amplitude (b) are marked on the trace. As no visible response is seen, the average latency of the cell to whisker pad stimulation is used as a guide to mark the approximate position (*) of an EPSP if it would have occurred. Using the time to peak amplitude as a guide, another cursor (#) is placed in the position which is the approximate time at which the EPSP reaches its peak amplitude. The change in membrane potential between theses two points is considered the peak amplitude of the 'EPSP' in response to the second whisker stimulus. In this case the response has a negative value. The duration of the EPSP (c) is measured from the start of the first EPSP to the point at which the membrane potential returns to baseline level.

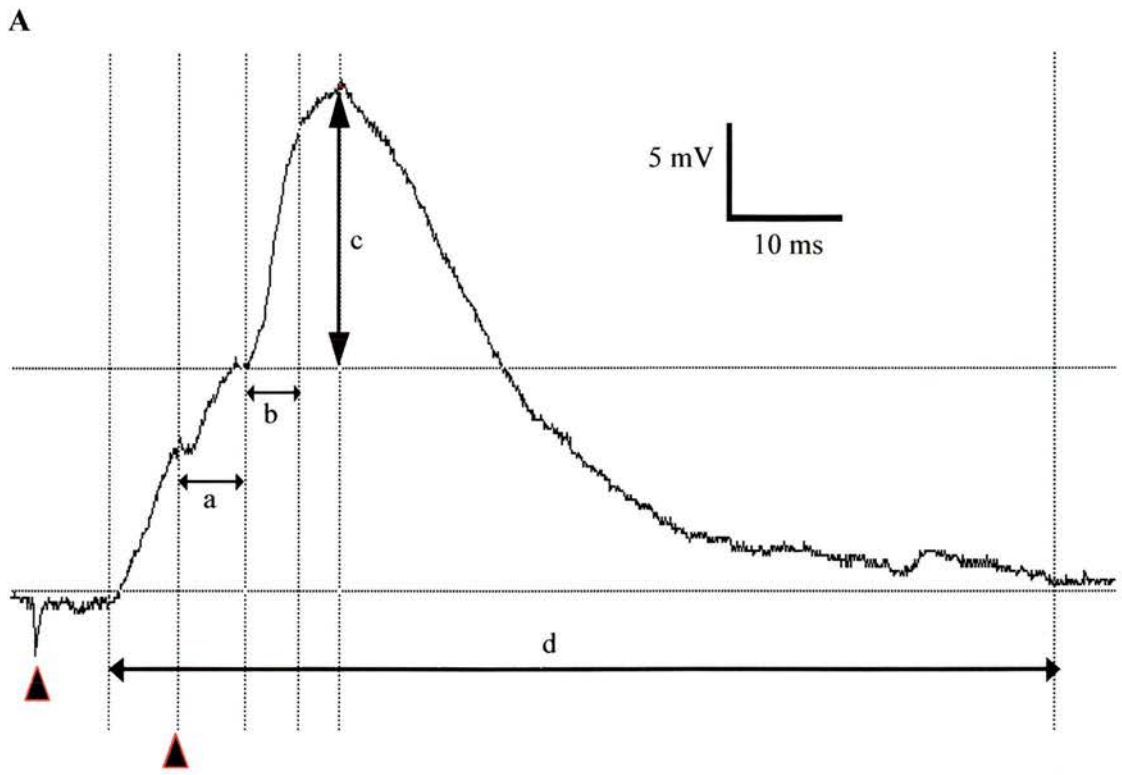
A
5 mV
10 ms
c
b
a
d

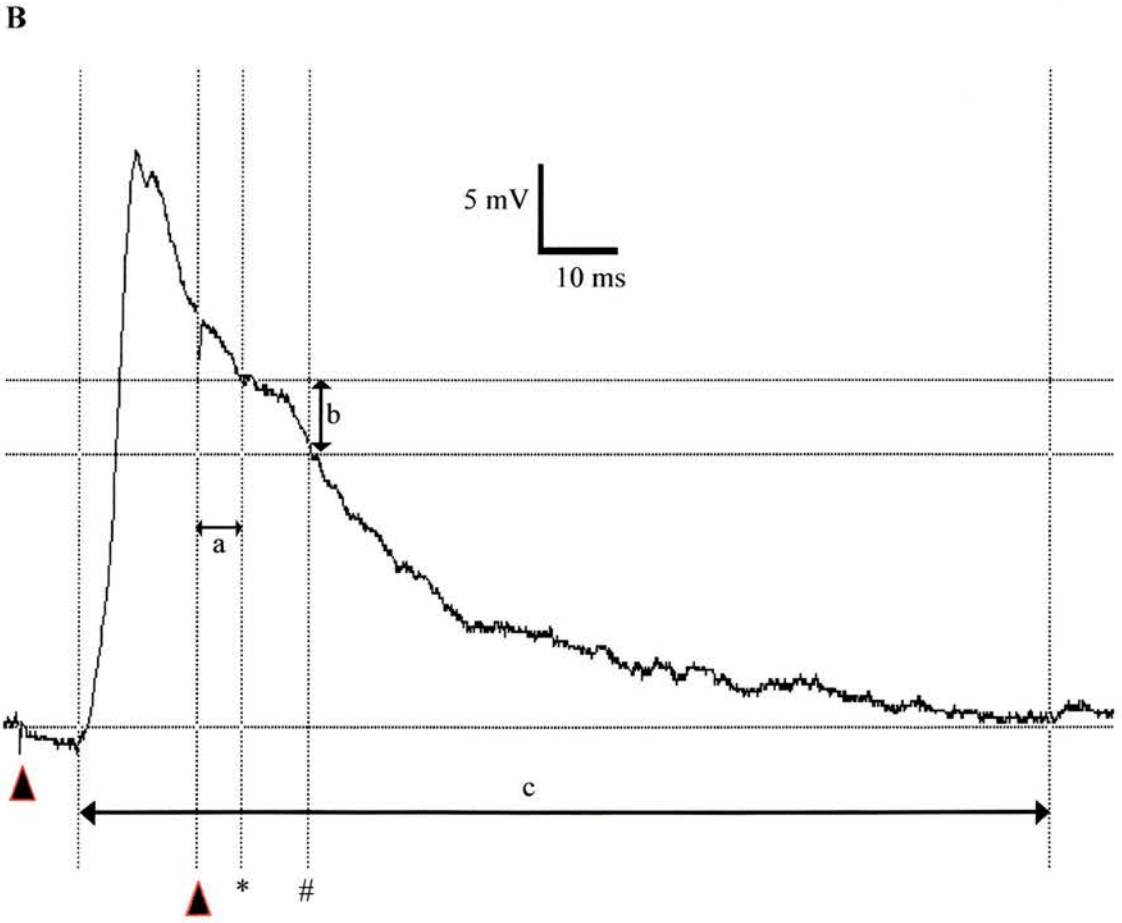
B
5 mV
10 ms
b
a
c
*
#

vertical markers were placed at the point which the response was thought to start and at the point at which it was thought to reach its peak (using the average values for the cell). The change in membrane potential between these two points was considered to be the peak amplitude. Due to this method of measurement, some negative values of peak amplitude were attained. In circumstances when there was no clear response to the second stimuli, no rise time values or EPSP duration times were taken. These values were only taken when the response of the cell to the second stimulus reached a value that was 10% of the average peak amplitude (of that cell) when the correponding stimulus was delivered singly. Input resistance was determined from the slope of a regression line fitted to the membrane potential produced by a series of hyperpolarising and subthreshold depolarising current pulses.

As one of the aims of the experiments was to see if the state of the cell affected its response to the paired stimulus, each trace was analysed and the state of the cell when the first stimulus was delivered, was recorded. If the first stimulus was delivered during a transition state - up to down or down to up, the trace was excluded from analysis.

4.2.6.3) Statistical analysis

For each cell the average value of the eight sweeps were calculated for the variables i.e. latency, rise time, peak amplitude and time to peak amplitude (only when one stimulus was delivered). This was done for the response of the cell to the stimulus when only one was given and the response of the cell to the both stimuli during the pairing protocol. The values for all cells were then pooled and compared using a one-way ANOVA and Tukey's pairwise comparisons. Numerical values are given as

mean ± standard deviation (S.D) unless otherwise stated. The probability level for statistical significance was set at $p < 0.05$.

4.3) Results

4.3.1) Cortical cells

Intracellular records were obtained from 12 cortical cells, from 12 animals. The cells were located -1.3 to -2.12 mm posterior to Bregma and were recorded at a depth of 1783 to 1999 μm from the cortical surface. The positions of the cells recorded from are shown in Figure 4.3.

The spontaneous behaviour of the cells and their response to stimulation of the whisker pad and the contralateral cortex were similar to the cells described in Chapter 3. Briefly cortical cells displayed spontaneous shifts in membrane potential. The resting membrane potential averaged -73.04 mV and ranged from -68.00 to -79.36 mV. Episodes of depolarisation which lasted approximately 200 ms had membrane potentials of -54.5 mV (range: -50.62 to -60.01 mV) The cells sometimes fired action potentials when they were in the depolarised state. The injection of subthreshold depolarising and hyperpolarising current pulses, showed a distinct lack of inward rectification. As before no attempt was made to distinguish between the three physiologically defined classes of cortical neurones.

All responses recorded in cortical neurones were a result of orthodromic activation. No antidromic activation from the contralateral cortex was observed, as evidenced by the occurrence of a fixed latency action potential at threshold with no underlying EPSP. All cells responded with an initial EPSP followed by an IPSP. The response characteristics of the cortical cells to electrical stimulation of the whisker pad and the contralateral cortex is summarised in Table 4.2. As before the only difference was observed in the rise time of the EPSP, which was significantly longer in the response of the cell to contralateral cortical stimulation.

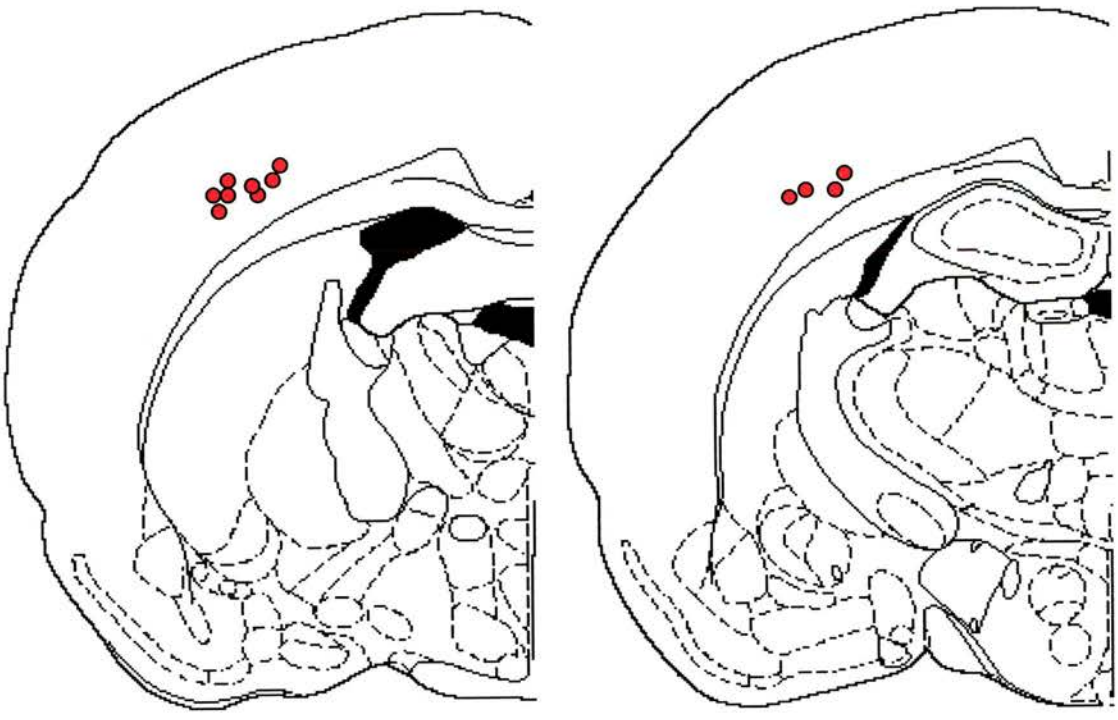

Bregma -1.3 mm

Bregma -2.12 mm

Figure 4. 3. Distribution of cortical neurones from which records were obtained.

Schematic figures of the rat brain (modified from Paxinos and Watson 1996) with the location of cortical neurones from which data was obtained (●). The approximate positions of the cortical neurones were extrapolated using pontamine sky blue markings.

	Stimulus type		
Variable	Whisker pad	Contralateral cortex	No. of cells
Latency (ms)	7.880 ± 2.447	7.675 ± 2.238	12
Rise Time (ms)	4.976 ± 1.708	7.75 ± 4.72 *	12
Peak amplitude (mV)	15.114 ± 6.48	8.875 ± 4.63	12
EPSP duration (ms)	87.380 ± 59.28	106.300 ± 47.34	12

Table 4. 2. Summary of electrophysiological characteristics of cortical cells to electrical stimulation of the whisker pad and contralateral cortical stimulation.
Mean values of responding cortical neurones. The asterisk (*) denotes a statistically significant difference (ANOVA, $p < 0.05$, Tukey's pairwise comparisons).

There was no significant correlation between the latency of the response to both forms of stimuli and the depth of the cell (Pearson correlation coefficient = 0.267, $p > 0.05$). The peak amplitude was significantly negatively correlated to the membrane potential of the cell (Pearson correlation coefficient = -0.825, $p < 0.05$) and up to 66.6% of the variability observed in peak amplitude can be accounted for by the difference in membrane potential when the stimulus arrived. The duration of the EPSP was highly variable and this was due firstly, to the delivery of the stimulus in either an up or down state (see below) and secondly, to the short duration pre-stimulus time that was recorded which might not have been an accurate representation of the baseline membrane potential of the cell (Fig 4.4).

All the data analysis that was carried out on the 12 cells was also carried out on individual cells and no differences between individual cells were observed. Thus the results from all cortical neurones were pooled. It was not possible to study the response of the cells to these pairing protocols with respect to the two states of the

Figure 4. 4. Influence of the state of the cell on the duration of the EPSP.

To illustrate the influence of the membrane potential on the duration of the EPSP, two traces from consecutive sweeps of the response of a cortical cell to whisker pad stimulation is shown. This cell has responses which are typical of the cortical neurones recorded from. The stimulus artefact is marked by a (▲). The dashed lines mark out the baseline membrane potential.

A This shows the response of the cell in its depolarised state. The cell had a membrane potential of -50.5 mV. The peak amplitude was 7.85 mV. The EPSP had a duration of 23.31 ms.

B This shows the next recorded response of the cell in **A** after the sweep illustrated in **A** was recorded. The cell was hyperpolarsied when the stimulus arrived. The cell which had a resting membrane potential of -73.4 mV responded with an EPSP of 17.93 mV magnitude and 75.5 ms duration.

A

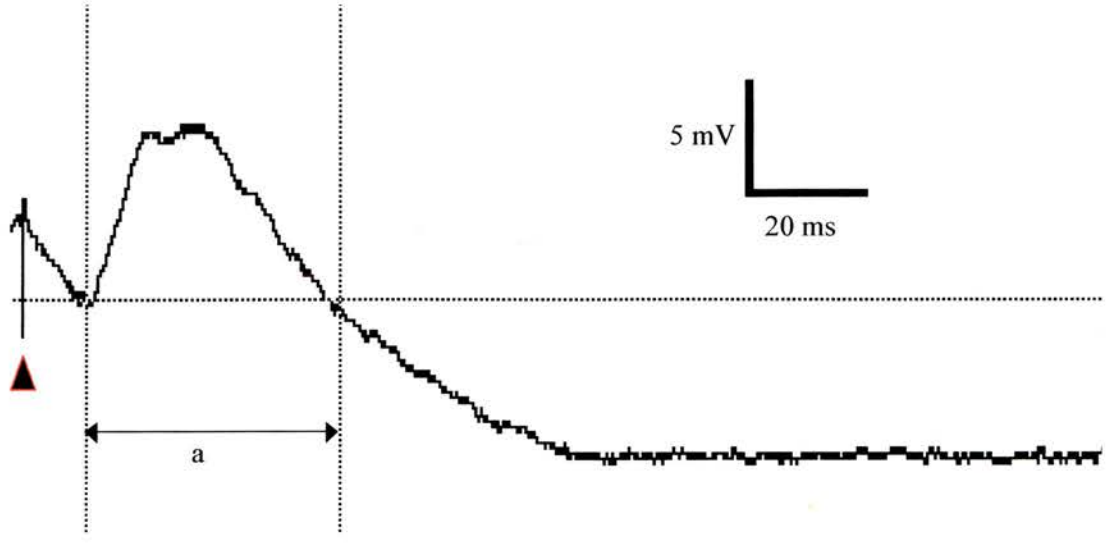

B

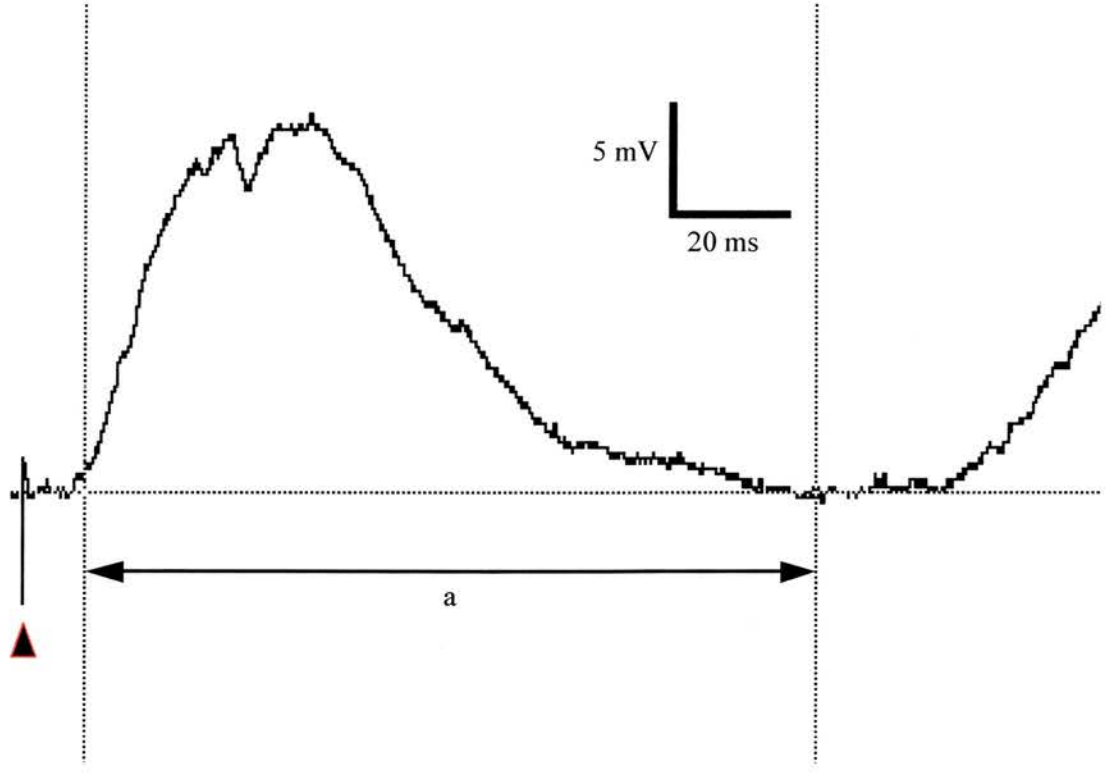

cells due to the small number of cells and the fact that most of the stimuli were delivered when the cell was in a transition state. To elucidate the effect of the state of the cell on the response, correlation between the membrane potential and size of the response of the cell to the second stimulus was carried out for each time interval and is presented below together with the results obtained from each pairing protocol.

4.3.1.1) Protocol 1: Whisker pad – contralateral cortex interaction (Fig. 4.5)

An initial whisker pad stimulus inhibited the response of the cell to contralateral cortical stimulation when the contralateral cortical stimulus was delivered either 10 or 20 ms after the whisker pad stimulation (ANOVA, $p < 0.05$, Tukey's pairwise comparisons). From time intervals of 40 ms to 380 ms, the response of the cell to the stimulation of the contralateral cortex was unaffected by the preceding whisker pad stimulation. The EPSPs to the second cortical stimulus from time intervals from 40 ms to 380 ms had response characteristics that did not significantly differ from the response of neurones to contralateral cortical stimulation alone (all 4 variables - ANOVA, $p > 0.05$, Tukey's pairwise comparisons). Visual inspection of the traces revealed that a large EPSP in response to whisker pad stimulation usually gave rise to a smaller sized cortically derived EPSP compared to the large response following a moderate sized EPSP as a result of stimulating the whisker pad (Fig. 4.6). To determine if the size of the response to the second stimulus was affected by the magnitude of the initial response, the correlation coefficient was calculated for each time interval (Appendix 1). The sizes of the two EPSPs were found to be negatively correlated only at time intervals of 100 ms and 140 ms, while the remaining time intervals showed no significant correlation. The discrepancy between the qualitative and quantitative data is probably due to the method of sampling, which disregards

Figure 4. 5. Response of cortical neurones to whisker pad-contralateral cortex pairing protocol.

A The overlaid traces illustrate the response of a cortical neurone to the whisker pad-contralateral cortex pairing protocol. Each coloured trace is the averaged response of the cell to the second stimulus at a particular time interval. The EPSP in response to whisker pad stimulation is highlighted with a **red** arrow. The response of the cell to a single contralateral cortical stimulation is marked with a **black** arrow. Note the difference in the rise time of the EPSPs. The traces show that the response of the cortical neurone to the second stimulus is inhibited at time intervals of 10 and 20 ms after which the cell is able to the respond to the contralateral cortical stimulus with a peak amplitude that is similar to when the contralateral cortex is stimulated on its own.

B The histogram illustrates the averaged peak amplitude of the EPSPs in response to the contralateral cortical stimuli across all time intervals for all 12 cortical neurones. The values are the average ± standard error. Time 0 is the average peak amplitude of the response to single contralateral cortical stimulation. The asterisks (*) denote a significant difference from the value at time 0 (ANOVA, $p < 0.05$, Tukey's pairwise comparisons).

C The histogram illustrates the averaged EPSP duration for the time intervals when the second EPSP occurred during the first EPSP. The values are the average ± standard error. The value at time 0 is the average EPSP duration following whisker pad stimulation. There is no significant increase in the EPSP duration at any of the time intervals (ANOVA, $p > 0.05$, Tukey's pairwise comparisons).

A

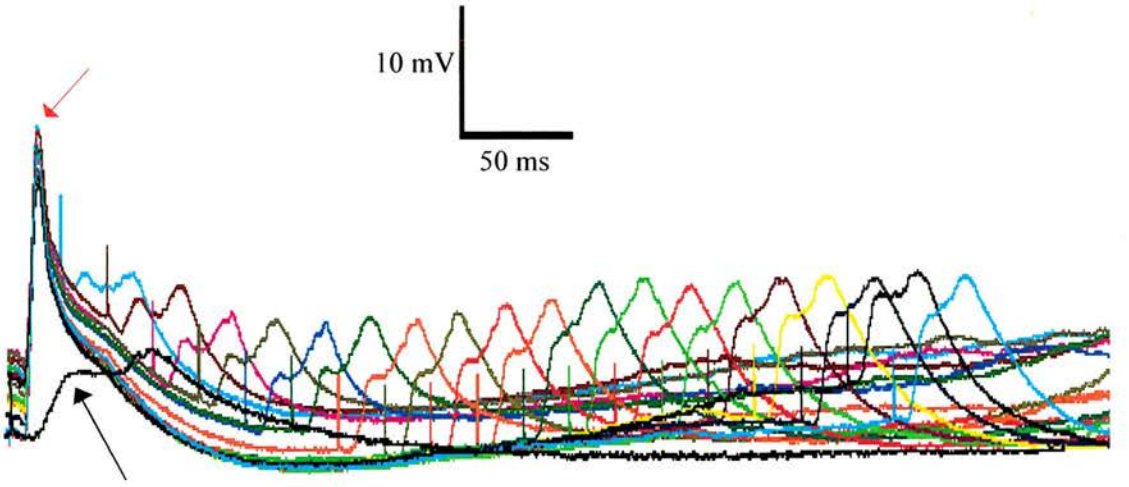
10 mV
50 ms

B

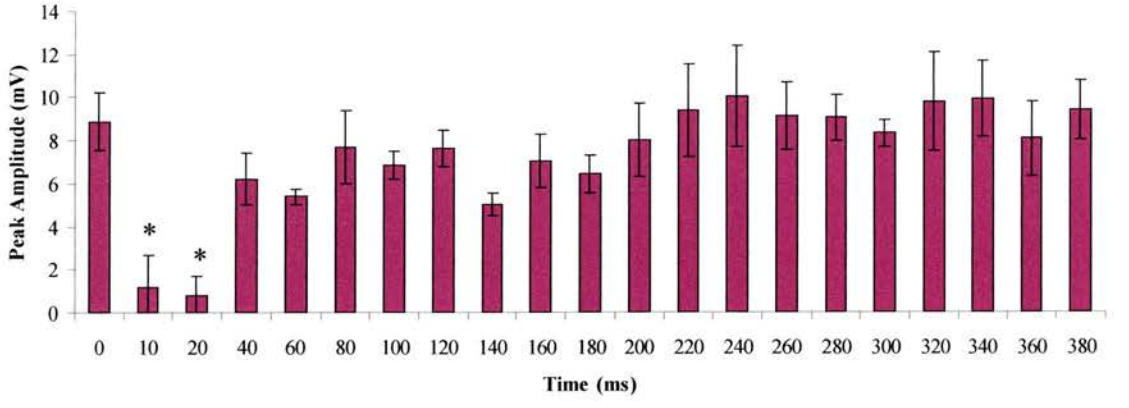
Peak Amplitude (mV)
14
12
10
8
6
4
2
0
*
*
0
10
20
40
60
80
100
120
140
160
180
200
220
240
260
280
300
320
340
360
380
Time (ms)

C

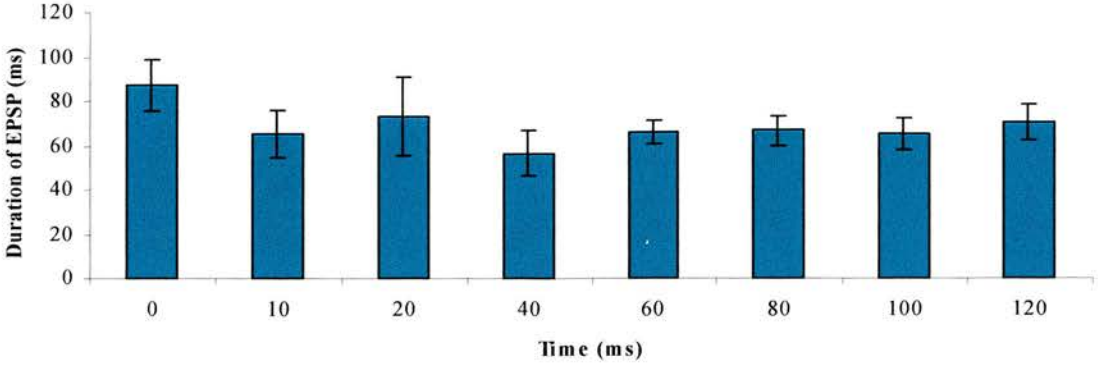
Duration of EPSP (ms)
120
100
80
60
40
20
0
0
10
20
40
60
80
100
120
Time (ms)

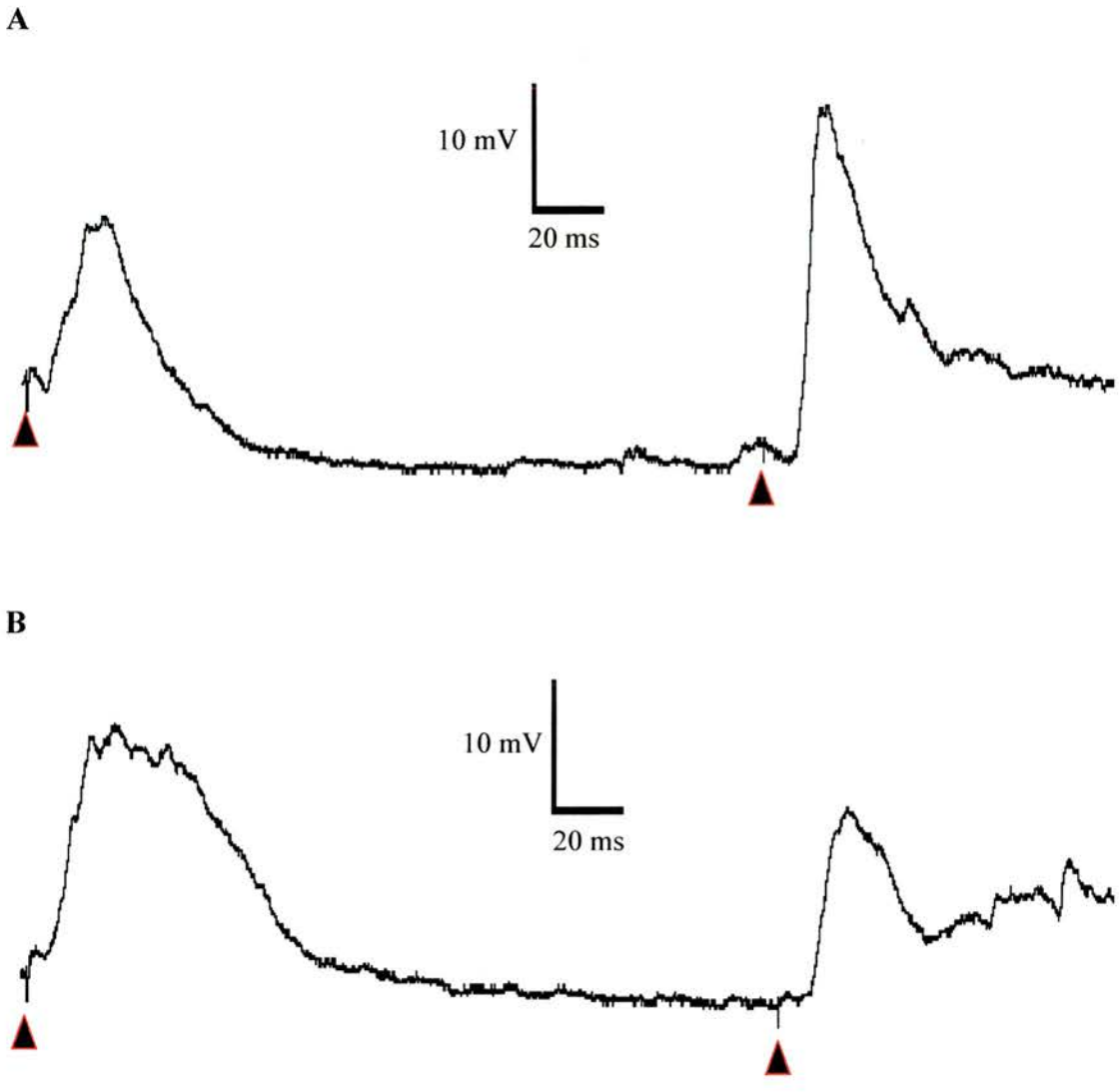

Figure 4. 6. Amplitude of the second EPSP is partly dependent on the size of the first EPSP.

To illustrate the influence of the size of the first EPSP on the amplitude of the second EPSP, two traces from consecutive sweeps of the response of a cortical cell to whisker pad-contralateral cortex pairing protocol at a time interval of 200 ms is shown. The stimulus artefacts are marked by a (▲).

A In this trace the amplitude of the response to whisker pad stimulation is 12.52 mV, while contralateral cortical stimulation gives rise to an EPSP with an amplitude of 26.17 mV.

B This shows the next recorded response of the cell in **A** after the sweep illustrated in **A** was recorded. The cell now responds to the whisker pad stimulus with a larger amplitude EPSP (18.65 mV), but a smaller amplitude EPSP in response to contralateral cortical stimulation (13.73 mV).

the state of the cell when either stimulus is delivered. To see the effect of the membrane potential on the amplitude of the response to the second stimulus the correlation coefficient and the R-squared value from regression analysis were calculated for each time interval and the results are shown in Appendix 2. Both values are highly correlated and up to 67% of the variability observed in the size of the EPSP can be attributed to membrane potential. When the second (contralateral cortical) stimulus was delivered at time intervals that were within the EPSP in response to the whisker pad stimulation (10 to 120 ms), the duration of the EPSP in response to whisker pad stimulation was measured and found not to be significantly different (ANOVA, $p > 0.05$, Tukey's pairwise comparisons). The second response was not different from single contralateral cortical stimulation in terms of latency and rise time and EPSP duration for all the time intervals.

4.3.1.2) Protocol 2: Contralateral cortex – whisker pad interaction (Fig. 4.7)

An initial contralateral cortical stimulus did not affect the peak amplitude of the response to whisker pad stimulation at any of the time intervals (ANOVA, $p > 0.05$, Tukey's pairwise comparisons) and when the second stimulus was delivered within the EPSP in response to contralateral cortical stimulation there was a clear summation of EPSPs. This lack of inhibition was not observed in any other pairing protocol. The response to whisker pad stimulation was not significantly different from single whisker pad stimulation in terms of latency and rise time and EPSP duration for all the time intervals. When the contralateral cortical stimulus was delivered at time intervals that were within the EPSP in response to the whisker pad stimulation (10 to 80 ms), the duration of the EPSP in response to whisker pad stimulation was measured and found not to be significantly different (ANOVA, $p >$

Figure 4. 7. Response of cortical neurones to contralateral cortex-whisker pad pairing protocol.

A The overlaid traces illustrate the response of a cortical neurone to the contralateral cortex-whisker pad pairing protocol. Each coloured trace is the averaged response of the cell to the second stimulus at a particular time interval. The EPSP in response to contralateral cortex stimulation is highlighted with a **red** arrow. The response of the cell to a single whisker pad stimulation is marked with a **black** arrow (the green trace). The traces show that the response of the cortical neurone to the second stimulus is not inhibited at any of the time intervals.

B The histogram illustrates the averaged peak amplitude of the EPSPs in response to the whisker pad stimulus across all time intervals for all 12 cortical neurones. The values are the average ± standard error. Time 0 is the average peak amplitude of the response to single whisker pad stimulation. There is no significant decrease in the EPSP amplitude at any of the time intervals (ANOVA, $p > 0.05$, Tukey's pairwise comparisons).

C The histogram illustrates the averaged EPSP duration for the time intervals when the second EPSP occurred during the first EPSP. The values are the average ± standard error. The value at time 0 is the average EPSP duration following contralateral cortical stimulation. There is no significant increase in the EPSP duration at any of the time intervals (ANOVA, $p > 0.05$, Tukey's pairwise comparisons).

A

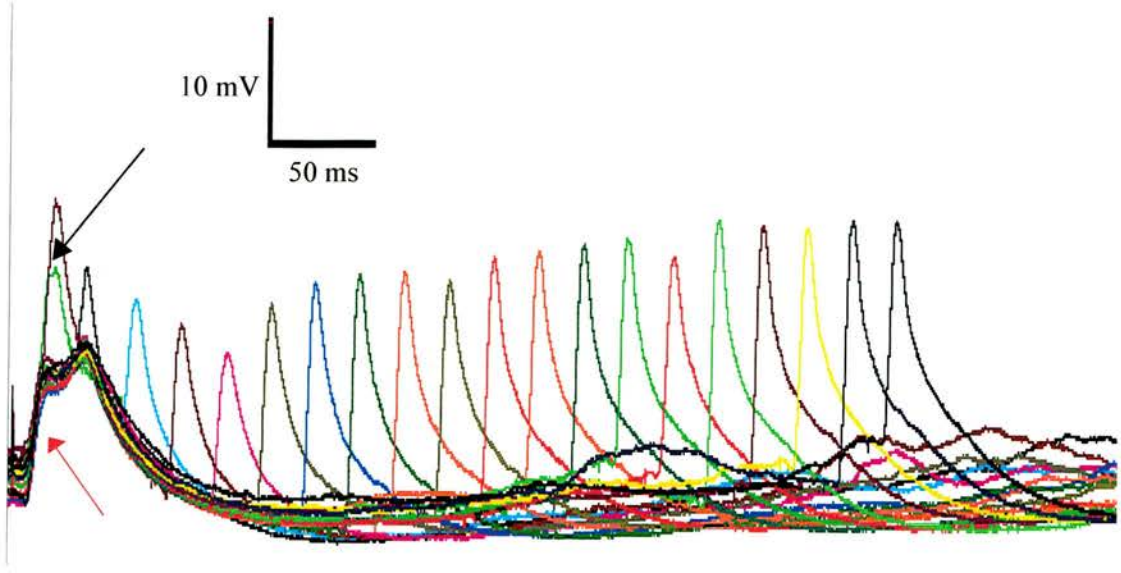
10 mV
50 ms

B

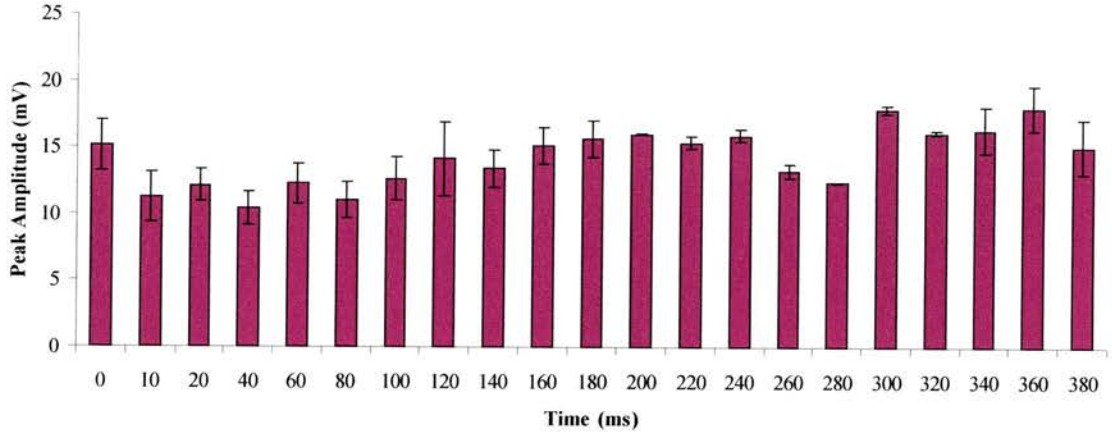
Peak Amplitude (mV)
25
20
15
10
5
0
0 10 20 40 60 80 100 120 140 160 180 200 220 240 260 280 300 320 340 360 380
Time (ms)

C

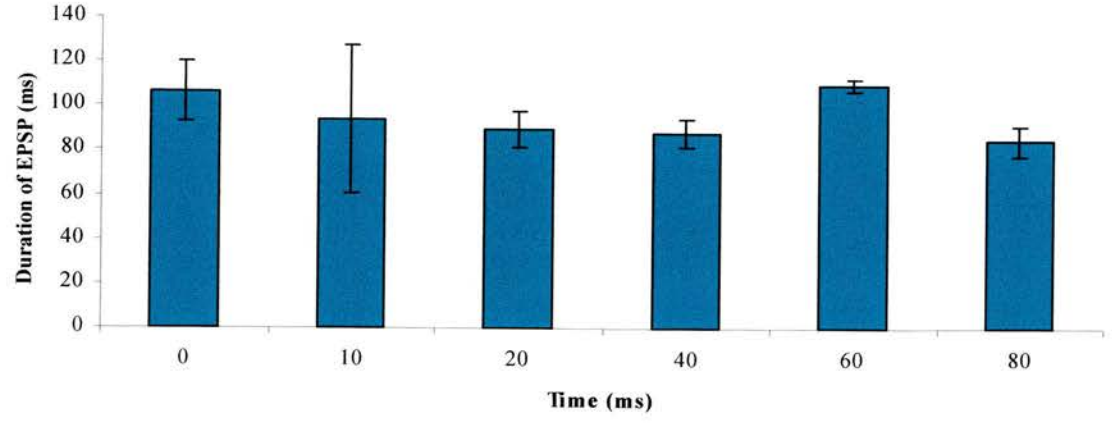
Duration of EPSP (ms)
140
120
100
80
60
40
20
0
0 10 20 40 60 80
Time (ms)

0.05, Tukey's pairwise comparisons).There was a significant negative correlation between the membrane potential of a cell when the stimulus was delivered, and the peak amplitude of its response (Appendix 2).

4.3.1.3) Protocol 3: Whisker pad – whisker pad interaction (Fig. 4.8)

An initial whisker pad stimulus inhibited the response of cortical cells to a second whisker pad stimulus. This inhibition was seen up to a time interval of 160 ms after which the neurones responded to the second whisker pad stimulus with an amplitude, rise time and latency that were statistically similar to the response of the neurones to single whisker pad stimulation. From Figure 4.8 it can be seen that at time intervals of 10 to 120 ms the response to the second stimulus is strongly inhibited and from 100 to 160 ms a small amplitude EPSP is visible. The size of response was partly dependent on the membrane potential of a cell when the stimulus was delivered (Appendix 2). There was no significant change in the duration of the EPSP at anytime interval (ANOVA, $p > 0.05$, Tukey's pairwise comparisons).

4.3.1.4) Protocol 4: Contralateral cortex – contralateral cortex interaction (Fig. 4.9)

Increasing the time interval between the two contralateral cortical stimuli lead to inhibition followed by a recovery of the cells' response to the second contralateral cortical stimulation. Inhibition was seen up to when the stimuli were delivered 120 ms apart. When a second response was detected, it has response characteristics that were no different from single contralateral cortical stimulation in terms of latency and rise time for all the time intervals There was a significant negative correlation between the membrane potential of a cell when the stimulus was delivered and the

Figure 4. 8. Response of cortical neurones to whisker pad-whisker pad pairing protocol.

A The overlaid traces illustrate the response of a cortical neurone to the whisker pad-whisker pad pairing protocol. Each coloured trace is the averaged response of the cell to the second stimulus at a particular time interval. The traces show that the response of the cortical neurone to the second stimulus is inhibited up to the time interval of 180 ms.

B The histogram illustrates the averaged peak amplitude of the EPSPs in response to the whisker pad stimulus across all time intervals for all 12 cortical neurones. The values are the average ± standard error. Time 0 is the average peak amplitude of the response to single whisker pad stimulation. The asterisks (*) denote a significant difference from the value at time 0 (ANOVA, $p < 0.05$, Tukey's pairwise comparisons).

C The histogram illustrates the averaged EPSP duration for the time intervals when the second EPSP occurred during the first EPSP. The values are the average ± standard error. The value at time 0 is the average EPSP duration following whisker pad stimulation. There is no significant increase in the EPSP duration at any of the time intervals (ANOVA, $p > 0.05$, Tukey's pairwise comparisons).

A

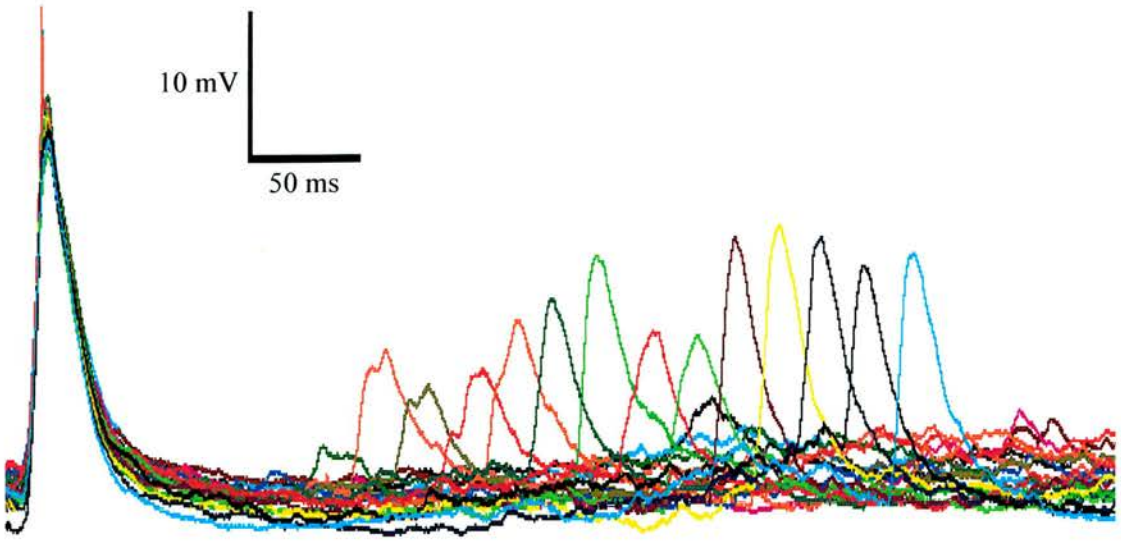
10 mV
50 ms

B

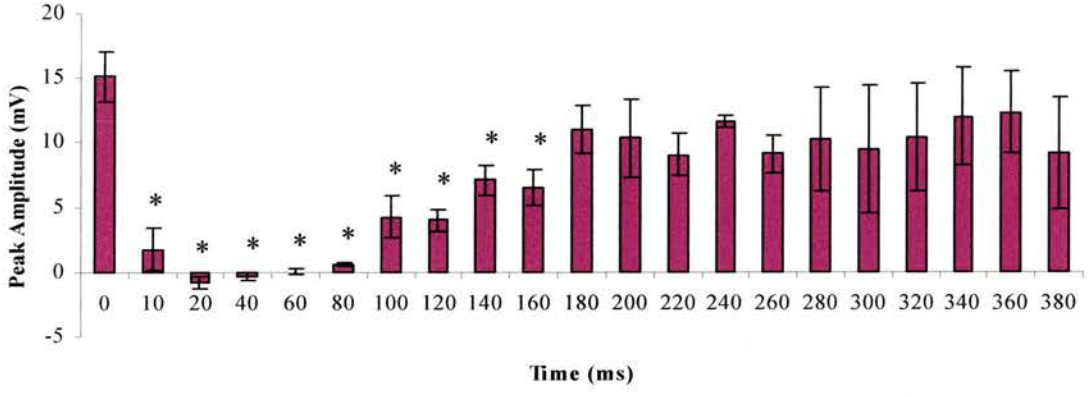
Peak Amplitude (mV)
20
15
10
5
0
-5
0 10 20 40 60 80 100 120 140 160 180 200 220 240 260 280 300 320 340 360 380
Time (ms)

C

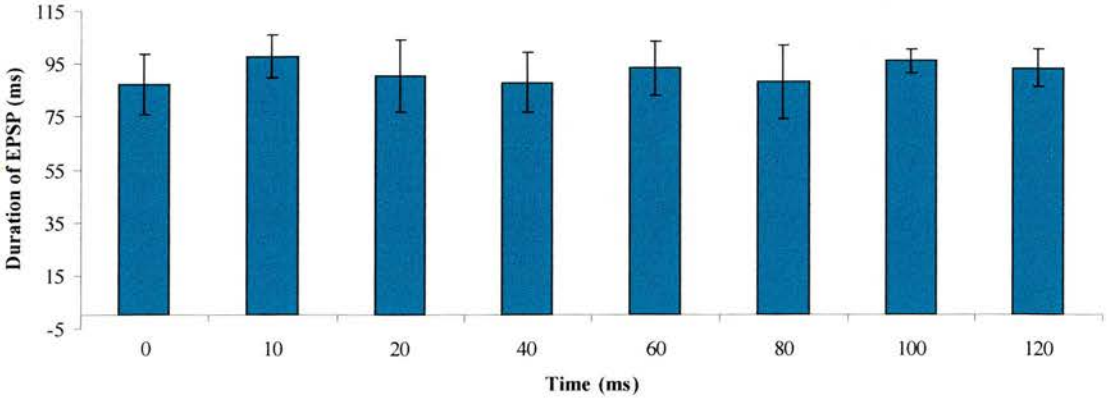
Duration of EPSP (ms)
115
95
75
55
35
15
-5
0 10 20 40 60 80 100 120
Time (ms)

Figure 4. 9. Response of cortical neurones to contralateral cortex-contralateral cortex pairing protocol.

A The overlaid traces illustrate the response of a cortical neurone to the contralateral cortex-contralateral cortex pairing protocol. Each coloured trace is the averaged response of the cell to the second stimulus at a particular time interval. The traces show that the response of the cortical neurone to the second stimulus is inhibited up to the time interval of 120 ms.

B The histogram illustrates the averaged peak amplitude of the EPSPs in response to the contralateral cortical stimulus across all time intervals for all 12 cortical neurones. The values are the average ± standard error. Time 0 is the average peak amplitude of the response to single contralateral cortical stimulation. The asterisks (*) denote a significant difference from the value at time 0 (ANOVA, $p < 0.05$, Tukey's pairwise comparisons).

C The histogram illustrates the averaged EPSP duration for the time intervals when the second EPSP occurred during the first EPSP. The values are the average ± standard error. The value at time 0 is the average EPSP duration following contralateral cortical stimulation. There is no significant increase in the EPSP duration at any of the time intervals (ANOVA, $p > 0.05$, Tukey's pairwise comparisons).

A

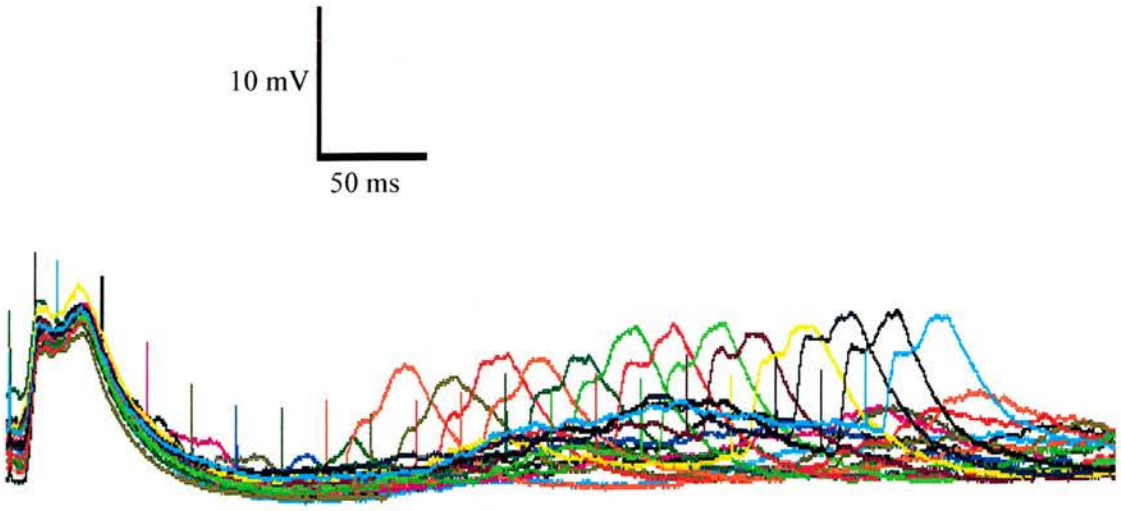
10 mV
50 ms

B

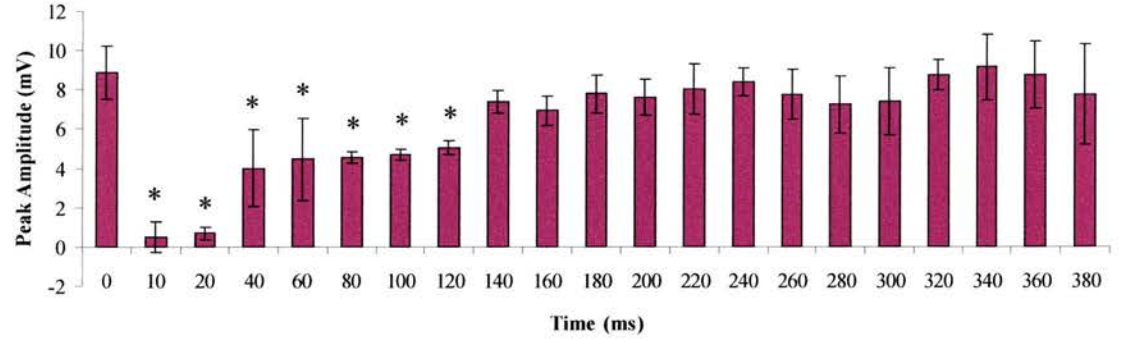
Peak Amplitude (mV)
12
10
8
6
4
2
0
-2
0
10
20
40
60
80
100
120
140
160
180
200
220
240
260
280
300
320
340
360
380
Time (ms)

C

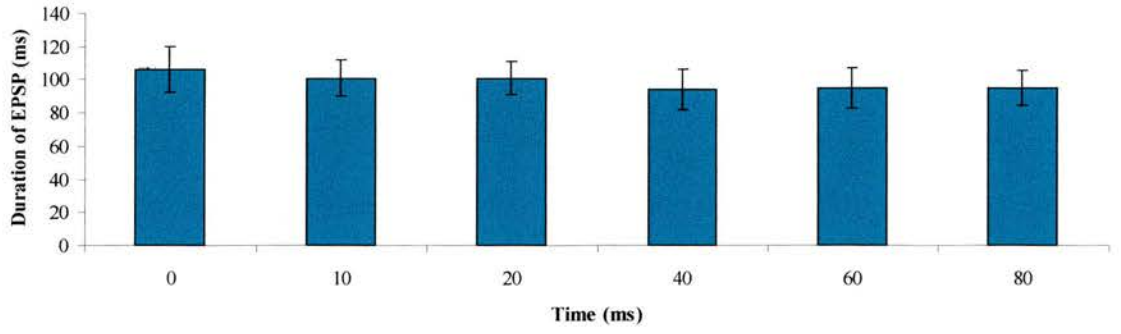
Duration of EPSP (ms)
140
120
100
80
60
40
20
0
0
10
20
40
60
80
Time (ms)

peak amplitude of its response (Appendix 2). The duration of the EPSP was not altered at any time interval.

The main findings of the pairing protocols are summarised in Table 4.3. The period of inhibition refers to the last time interval at which the response to the second stimulus was affected by the preceding stimulus.

Protocol	Period of inhibition (ms)
1: whisker pad – contralateral cortex	20
2: contralateral cortex – whisker pad	-
3: whisker pad – whisker pad	160
4: contralateral cortex – contralateral cortex	120

Table 4. 3. Summary of the results of the pairing protocols in cortical neurones.

4.3.2) Striatal cells

Records from a total of 25 striatal neurones from 19 animals were obtained. The cells were recorded from a depth of 2918 to 4695 μm with respect to the cortical surface and were found in striatum 1.8 to 2.12 mm posterior to Bregma (Fig. 4.10). The cells had similar spontaneous behaviour and response characteristics to both forms of stimuli as previously described in Chapter 3. All striatal neurones displayed spontaneous shifts in membrane potential which ranged between -49.26 and -94.22 mV. The membrane potential of the depolarised state averaged -62.36 mV (range -49.26 to -71.59 mV) and in some instances cells fired action potentials when they were in this state. The down state had an average membrane potential of -85.26 mV and in this phase fluctuations in membrane potential were diminished.

All 25 striatal neurones responded to both forms of stimulation and the results are summarised in the table below (Table 4.4). As before the only difference was in

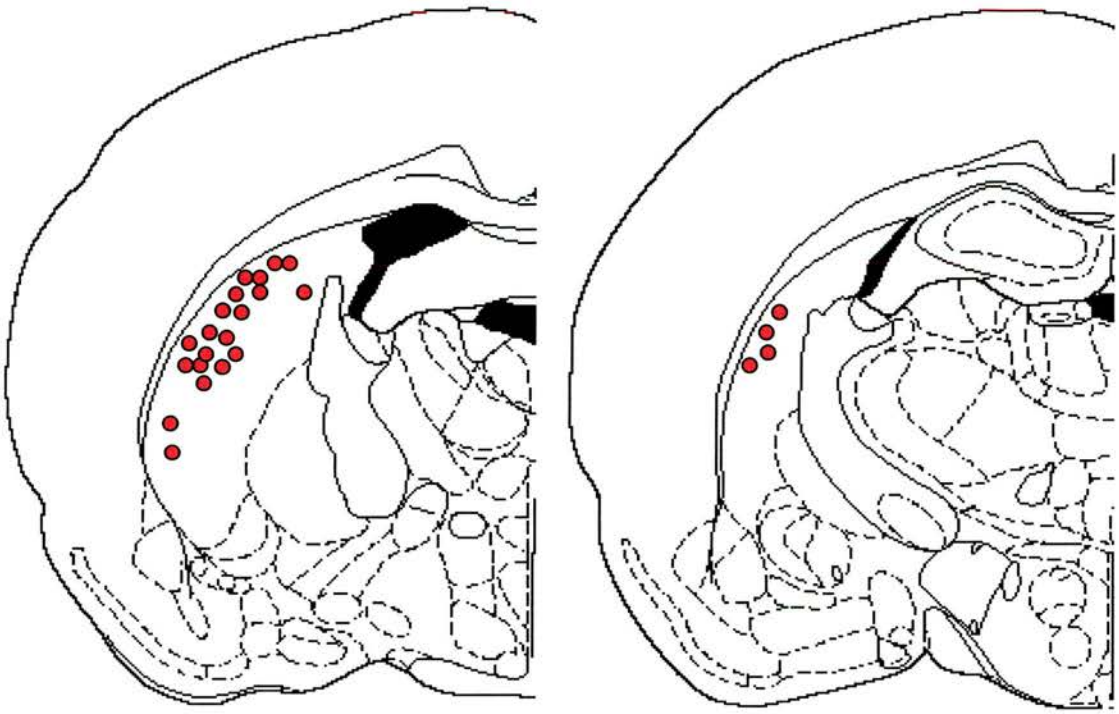

Bregma -1.3 mm

Bregma -2.12 mm

Figure 4. 10. Distribution of striatal neurones from which records were obtained.

Schematic figures of the rat brain (modified from Paxinos and Watson 1996) with the location of striatal neurones from which data was obtained (●). The approximate positions of the striatal neurones were extrapolated using pontamine sky blue markings.

the rise time of the EPSPs in response to both forms of stimuli (*, ANOVA, $p < 0.05$, Tukey's pairwise comparisons). The value of the duration of the EPSP is highly variable and is thought to reflect the method of sampling which disregards the state of the cell when the stimulus is delivered. The peak amplitude in response to both forms of stimuli was significantly negatively correlated with the membrane potential of the neurone when the stimuli were delivered (Pearson correlation coefficient = -0.895, $p < 0.05$). As the membrane potential of the cells affects both the peak amplitude and the duration of the EPSP, all the traces of the neurones responding to stimulation of the whisker pad or contralateral cortex alone were classified as either up or down based on the state of the cell when the stimuli was delivered.

	Stimulus Type	
Variables	Whisker pad	Contralateral cortex
Latency (ms)	8.798 ± 2.216	8.357 ± 2.721
Rise time (ms)	9.002 ± 2.680	22.103 ± 5.226 *
Peak amplitude (mV)	14.654 ± 6.966	12.557 ± 7.045
Duration of EPSP (ms)	102.200 ± 72.100	113.700 ± 72.300

Table 4. 4. Response characteristics of striatal neurones to whisker pad and contralateral cortical stimulation.

Mean values of responding striatal neurones. The asterisk (*) denotes a statistically significant difference (ANOVA, $p < 0.05$).

Tables 4.5 and 4.6 compares the results of the cells in both the up and down states to stimulation of the whisker pad and contralateral cortex respectively. While the state of the cells did not affect the latency of the response, the duration of the EPSP (*, ANOVA, $p < 0.05$, Tukey's pairwise comparisons) and the peak amplitude (*, ANOVA, $p < 0.05$, Tukey's pairwise comparisons) are significantly increased in the

down states compared to the up states.

	Whisker pad		
Variables	Both states	Up state	Down state
Latency (ms)	8.798 ± 2.216	8.568 ± 2.659	7.968 ± 3.256
Rise time (ms)	9.002 ± 2.680	7.001 ± 3.012	7.569 ± 2.598
Peak amplitude (mV)	14.654 ± 6.966	5.960 ± 3.580	20.703 ± 8.351 *
Duration of EPSP (ms)	102.200 ± 72.10	26.68 ± 10.110	140.300 ± 11.600 *

Table 4. 5. Comparison of the response characteristics of striatal neurones to whisker pad stimulation during up, down or averaged traces.

	Contralateral cortex		
Variables	Both states	Up state	Down state
Latency (ms)	8.357 ± 2.721	9.332 ± 4.897	8.511 ± 3.165
Rise time (ms)	22.103 ± 5.226	10.399 ± 6.887	26.474 ± 6.832 *
Peak amplitude (mV)	12.557 ± 7.045	5.211 ± 2.020	19.219 ± 5.412 *
Duration of EPSP (ms)	113.700 ± 72.300	23.38 ± 12.120	149.90 ± 24.700 *

Table 4. 6. Comparison of the response characteristics of striatal neurones to contralateral cortical stimulation during up , down or averaged traces.

All four pairing protocols were carried out on the 25 cells. For each pairing protocol the results from all traces (up, down and transition states) will be presented followed by the results of the pairing protocol when the first stimulus was delivered either during the up or down state. As the majority of the stimuli were delivered when the cells were either in a down or transition state some of the time intervals

were not analysed in this state dependent manner as there was insufficient data (a minimum of 5 cells are required to be included in the analysis).

4.3.2.1) Protocol 1: Whisker pad – contralateral cortex interaction

4.3.2.1.1) Averaged results from all (up, down and transition) states (Fig. 4.11)

Electrical stimulation of the whisker pad did not inhibit the response of striatal cells to contralateral cortical stimulation when the cortical stimulus was delivered 10 ms after whisker stimulation. The response of the neurones to contralateral cortical stimulation was significantly decreased at time intervals of 20 ms and 40 ms (ANOVA, $p < 0.05$, Tukey's pairwise comparisons). The response to contralateral cortical stimulation was not significantly different from single contralateral cortical stimulation in terms of latency and rise time and EPSP duration for all the time intervals (ANOVA, $p > 0.05$, Tukey's pairwise comparisons). When the contralateral cortical stimulus was delivered at time intervals that were within the EPSP in response to the whisker pad stimulation (10 to 120 ms), the duration of the EPSP in response to whisker pad stimulation was measured and found not to be significantly different (ANOVA, $p > 0.05$, Tukey's pairwise comparisons).

4.3.2.1.2) Averaged results from up states (Fig. 4.12)

Sufficient data was obtained for all time intervals. When the second stimulus was delivered after time intervals of 20 and 40 ms there was a significant decrease in the peak amplitude of the response (ANOVA, $p < 0.05$, Tukey's pairwise comparisons). A significant change in the peak amplitude was also observed from time intervals of 140 to 380 ms (ANOVA, $p < 0.05$, Tukey's pairwise comparisons). This is likely due to the fact that cells switch to the down state at these times and as a result, the

Figure 4. 11. Response of striatal neurones to whisker pad-contralateral cortex pairing protocol.

A The overlaid traces illustrate the response of a striatal neurone to the whisker pad-contralateral cortex pairing protocol. Each coloured trace is the averaged response of the cell to the second stimulus at a particular time interval. The response of the cell to a single contralateral cortical stimulation is marked with a **black** arrow. The summation of EPSPs seen at a time interval of 10 ms is marked with a red arrow. Note the difference in the rise time of the EPSPs. The traces show that the response of the cortical neurone to the second stimulus is inhibited up to the time intervals of 60 ms after which the cell is able to the respond to the contralateral cortical stimulus with a peak amplitude that is similar to when the contralateral cortex is stimulated on its own.

B The histogram illustrates the averaged peak amplitude of the EPSPs in response to the contralateral cortical stimuli across all time intervals for all 25 striatal neurones. The values are the average ± standard error. Time 0 is the average peak amplitude of the response to single contralateral cortical stimulation. The asterisks (*) denote a significant difference from the value at time 0 (ANOVA, $p < 0.05$, Tukey's pairwise comparisons).

C The histogram illustrates the averaged EPSP duration for the time intervals when the second EPSP occurred during the first EPSP. The values are the average ± standard error. The value at time 0 is the average EPSP duration following whisker pad stimulation. There is no significant increase in the EPSP duration at any of the time intervals (ANOVA, $p > 0.05$, Tukey's pairwise comparisons).

A

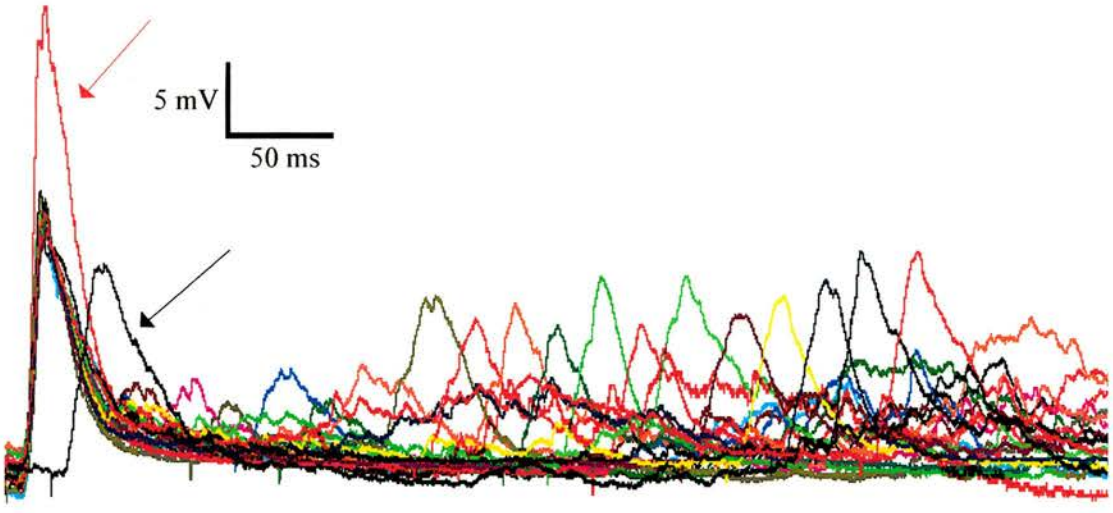
5 mV
50 ms

B

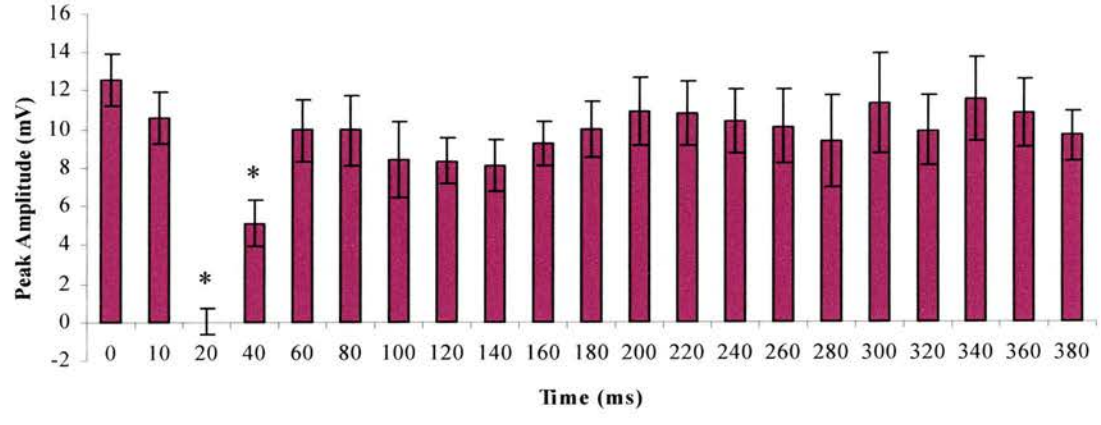
Peak Amplitude (mV)
16
14
12
10
8
6
4
2
0
-2
*
*
0 10 20 40 60 80 100 120 140 160 180 200 220 240 260 280 300 320 340 360 380
Time (ms)

C

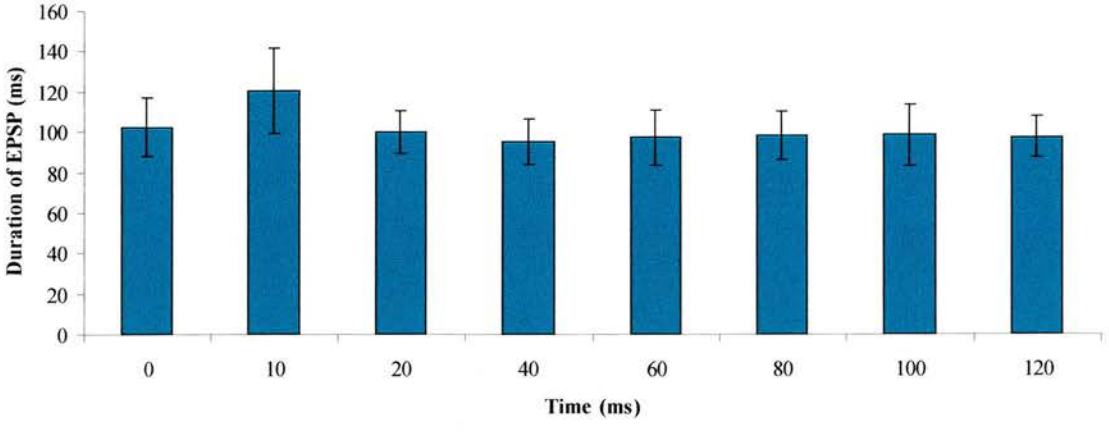
Duration of EPSP (ms)
160
140
120
100
80
60
40
20
0
0 10 20 40 60 80 100 120
Time (ms)

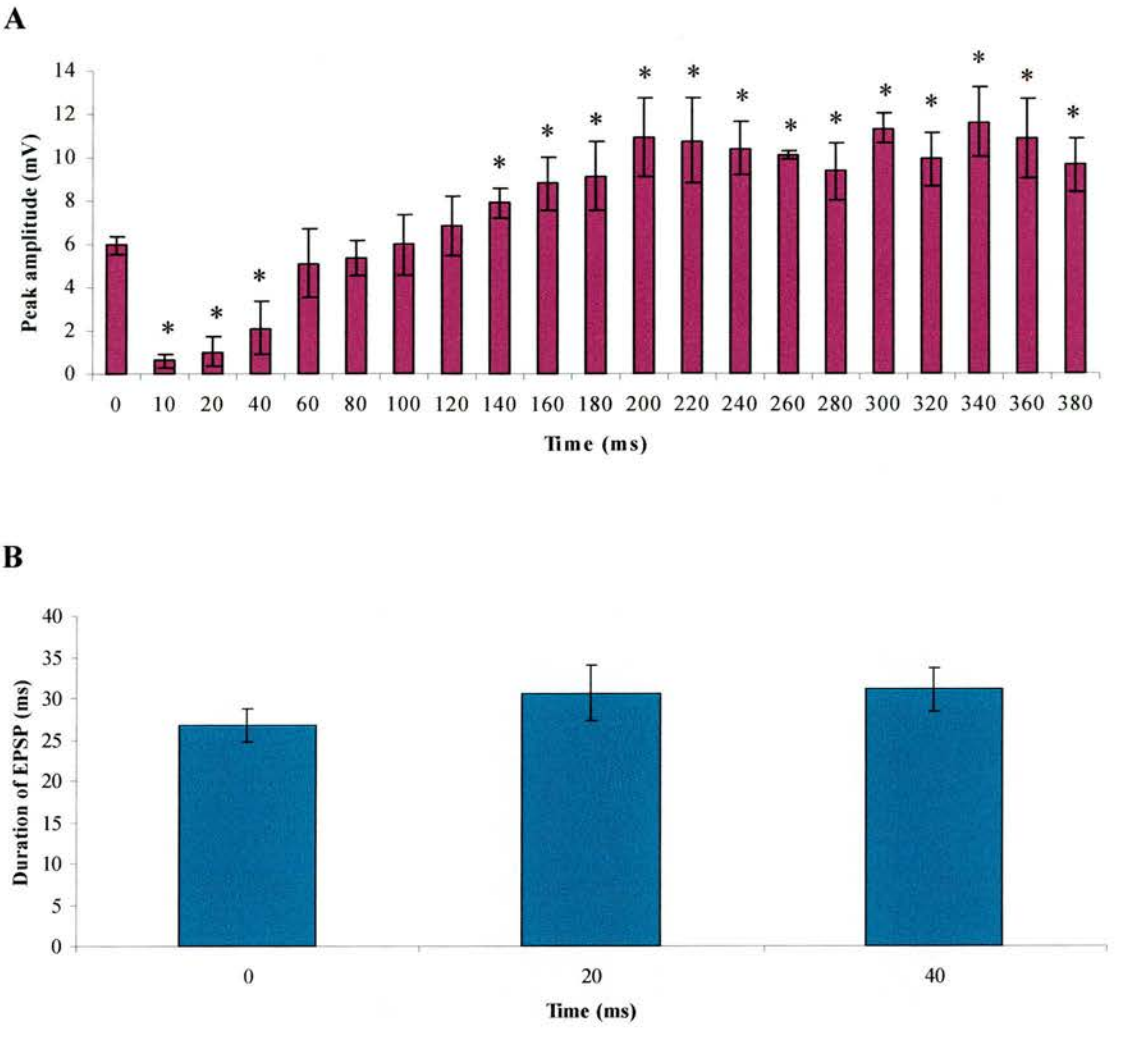

Figure 4. 12. Response of striatal neurones to whisker pad-contralateral cortex pairing protocol, when the whisker pad stimulus was delivered in the up state.

A The histogram illustrates the averaged peak amplitude of the EPSPs in response to the contralateral cortical stimuli across all time intervals for all 25 striatal neurones. The first stimulus (whisker pad) was delivered when the cell was in its up state. Time 0 is the average peak amplitude of the EPSPs in response to single contralateral cortical stimulation. The asterisks (*) denote a significant difference from the value at time 0 (ANOVA, $p < 0.05$, Tukey's pairwise comparisons).

B The histogram illustrates the averaged EPSP duration for the time intervals when the second EPSP occurred during the first EPSP. The value at time 0 is the average EPSP duration following whisker pad stimulation when the cell was in the up state. There is no significant increase in the EPSP duration at any of the time intervals (ANOVA, $p > 0.05$, Tukey's pairwise comparisons).

response to the second stimulus is greater when compared to the peak amplitude when the cell is stimulated in the up state. The duration of EPSP was not significantly different at any of the time intervals (ANOVA, $p > 0.05$, Tukey's pairwise comparisons).

4.3.2.1.3) Averaged results from down states (Fig. 4.13)

Data was obtained from all time intervals. The response of the neurones to contralateral cortical stimulation was significantly decreased at time intervals of 20 ms and 40 ms (ANOVA, $p < 0.05$, Tukey's pairwise comparisons). At all other time intervals, the peak amplitude was not significantly different from the response to single contralateral cortical stimulation (ANOVA, $p > 0.05$, Tukey's pairwise comparisons). The duration of EPSP was not significantly different at any of the time intervals (ANOVA, $p > 0.05$, Tukey's pairwise comparisons).

4.3.2.2) Protocol 2: Contralateral cortex – whisker pad interaction

4.3.2.2.1) Averaged results from all (up, down and transition) states (Fig. 4.14)

Contralateral cortical stimulation did not inhibit the response of striatal cells to whisker pad stimulation when the 2 stimuli were 10 ms apart. The EPSP of the neurones to the whisker pad stimulation was significantly decreased at time intervals of 20, 40, 60 and 80 ms (ANOVA, $p < 0.05$, Tukey's pairwise comparisons). While the latency of the response was unaltered (ANOVA, $p > 0.05$, Tukey's pairwise comparisons) the rise time of the whisker stimulus was significantly slower from 20ms to 60ms when compared to control values (ANOVA, $p < 0.05$, Tukey's pairwise comparisons). When the whisker pad stimulus was delivered at time intervals that were within the EPSP in response to the contralateral cortical

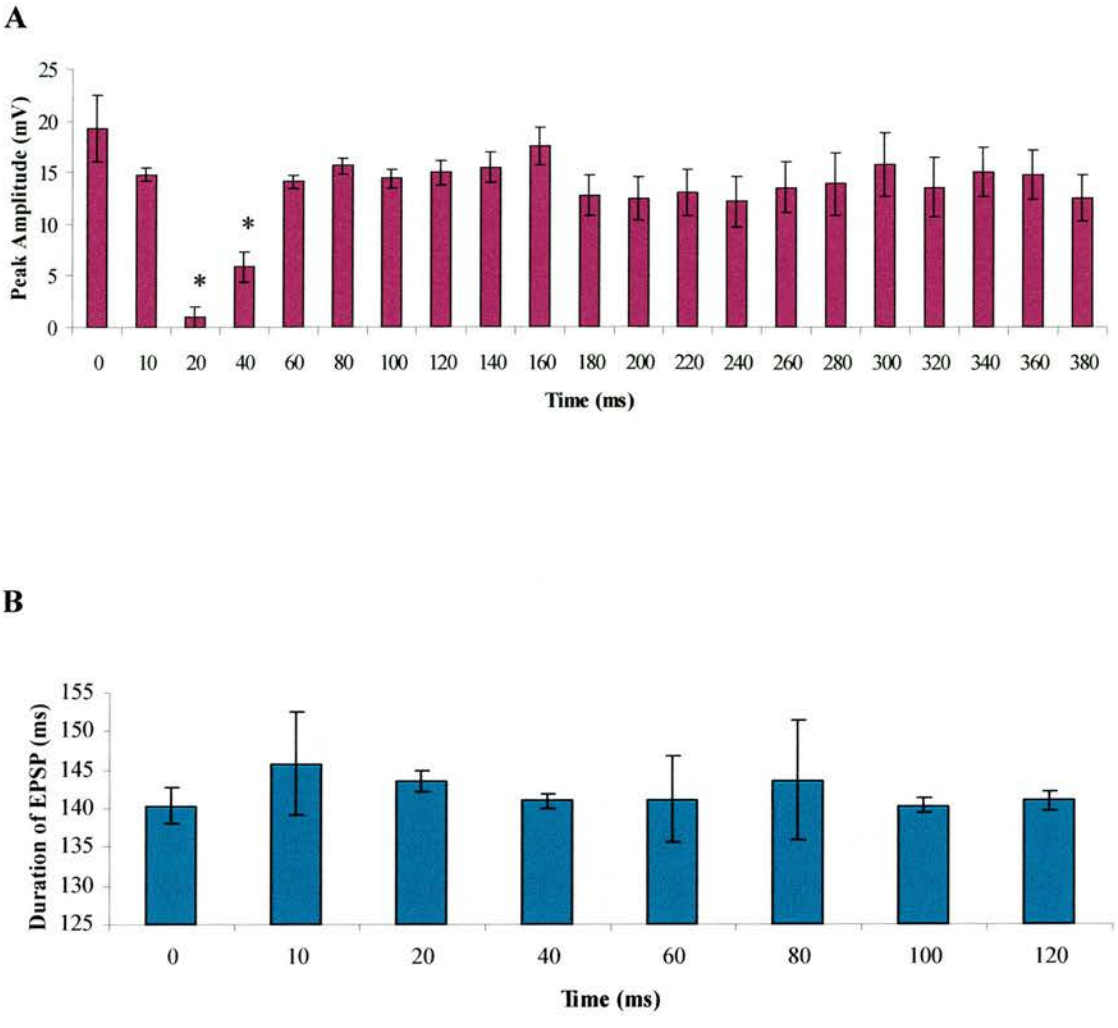

Figure 4. 13. Response of striatal neurones to whisker pad-contralateral cortex pairing protocol, when the whisker pad stimulus was delivered in the down state.

A The histogram illustrates the averaged peak amplitude of the EPSPs in response to the contralateral cortical stimuli across all time intervals for all 25 striatal neurones. The first stimulus (whisker pad) was delivered when the cell was in its down state. Time 0 is the average peak amplitude of the EPSPs in response to single contralateral cortical stimulation. There is a significant decrease in the EPSP amplitude at time intervals of 20 ms and 40 ms (ANOVA, $p < 0.05$, Tukey's pairwise comparisons).

B The histogram illustrates the averaged EPSP duration for the time intervals when the second EPSP occurred during the first EPSP. The value at time 0 is the average EPSP duration following whisker pad stimulation when the cell was in the down state. There is no significant increase in the EPSP duration at any of the time intervals (ANOVA, $p > 0.05$, Tukey's pairwise comparisons).

Figure 4. 14. Response of striatal neurones to contralateral cortex-whisker pad pairing protocol.

A The overlaid traces illustrate the response of a striatal neurone to the contralateral cortex-whisker pad pairing protocol. Each coloured trace is the averaged response of the cell to the second stimulus at a particular time interval. The response of the cell to a single whisker pad stimulation is marked with a **black** arrow. The summation of EPSPs seen at a time interval of 10 ms is marked with a red arrow. Note the difference in the rise time of the EPSPs. The traces show that the response of the striatal neurone to the second stimulus is inhibited up to time intervals of 80 ms after which the cell is able to the respond to the whisker pad stimulus with a peak amplitude that is similar to when the whisker pad is stimulated on its own.

B The histogram illustrates the averaged peak amplitude of the EPSPs in response to the whisker pad stimuli across all time intervals for all 25 striatal neurones. The values are the average ± standard error. Time 0 is the average peak amplitude of the response to single whisker pad stimulation. The asterisks (*) denote a significant difference from the value at time 0 (ANOVA, $p < 0.05$, Tukey's pairwise comparisons).

C The histogram illustrates the averaged rise time of the EPSP in response to whisker pad stimulation. The values are the average ± standard error. The value at time 0 is the average EPSP rise time following single whisker pad stimulation. There is a significant increase in the EPSP rise time at the time intervals of 20 ms to 60 ms (ANOVA, $p, < 0.05$, Tukey's pairwise comparisons).

A

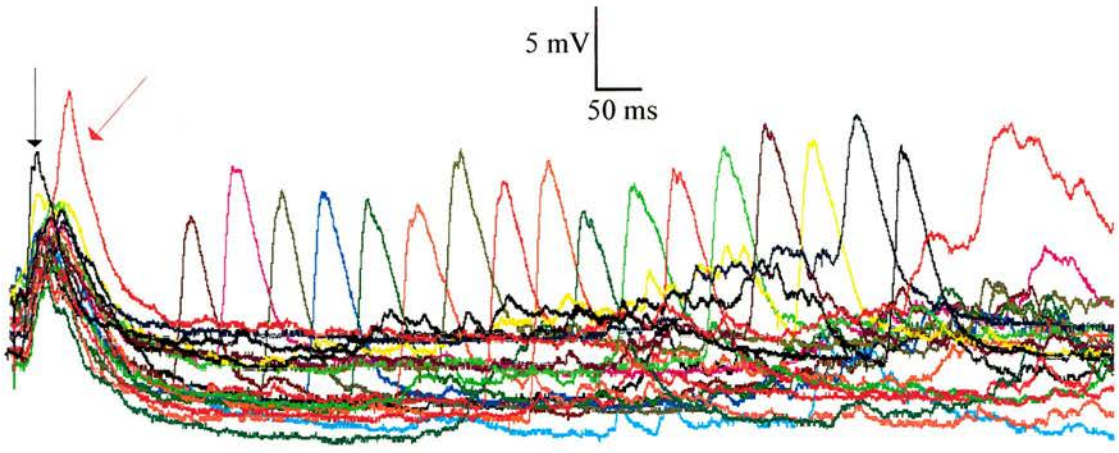
5 mV
50 ms

B

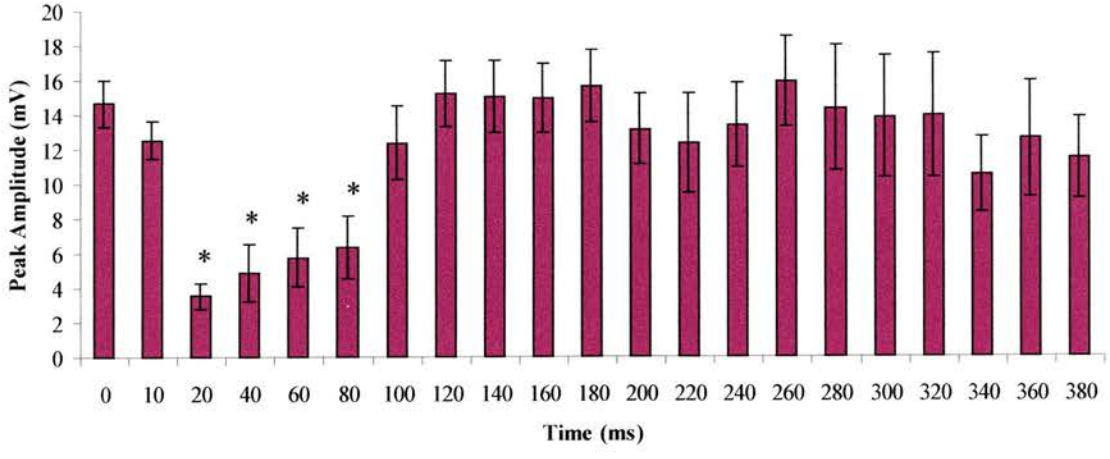
Peak Amplitude (mV)
0
2
4
6
8
10
12
14
16
18
20
0 10 20 40 60 80 100 120 140 160 180 200 220 240 260 280 300 320 340 360 380
Time (ms)

C

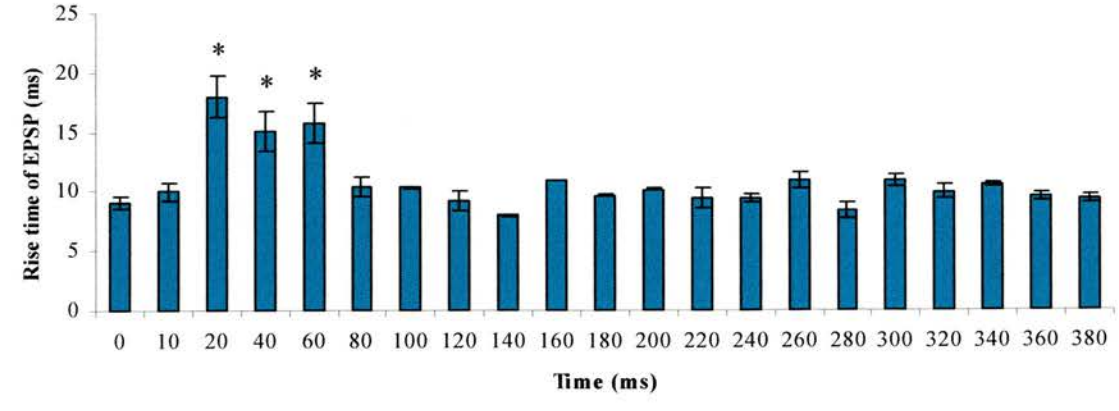
Rise time of EPSP (ms)
0
5
10
15
20
25
0 10 20 40 60 80 100 120 140 160 180 200 220 240 260 280 300 320 340 360 380
Time (ms)

stimulation (10 to 140 ms), the duration of the EPSP in response to contralateral cortical stimulation was measured and found not to be significantly different (ANOVA, $p > 0.05$, Tukey's pairwise comparisons).

4.3.2.2.2) Averaged results from up states (Fig. 4.15)

A significant decrease in the peak amplitude of the response was seen at time intervals of 20 to 80 ms (ANOVA, $p < 0.05$, Tukey's pairwise comparisons). A significant change in the peak amplitude was also observed from time intervals of 140 to 380 ms (ANOVA, $p < 0.05$, Tukey's pairwise comparisons). This is likely due to the fact that cells switch to the down state at these times and as a result, the response to the second stimulus is greater when compared to the peak amplitude when the cell is stimulated in the up state. At all other time intervals there was no significant difference in the amplitude of the response. The duration of the EPSPs was not significantly altered at any of the time intervals (ANOVA, $p > 0.05$, Tukey's pairwise comparisons). The rise time of the EPSP was significantly increased at time intervals of 20 ms to 60 ms (ANOVA, $p < 0.05$, Tukey's pairwise comparisons).

4.3.2.2.3) Averaged results from down states (Fig. 4.16)

Data was obtained from all time intervals. For time intervals of 20 to 80 ms the peak amplitude was significantly different from the peak amplitude recorded from striatal neurones when they were stimulated in the down state (ANOVA, $p < 0.05$, Tukey's pairwise comparisons). The duration of EPSP was not significantly altered at any time interval (ANOVA, $p > 0.05$, Tukey's pairwise comparisons). The rise time of the EPSP was significantly increased at time intervals of 20 ms to 60 ms (ANOVA, $p < 0.05$, Tukey's pairwise comparisons).

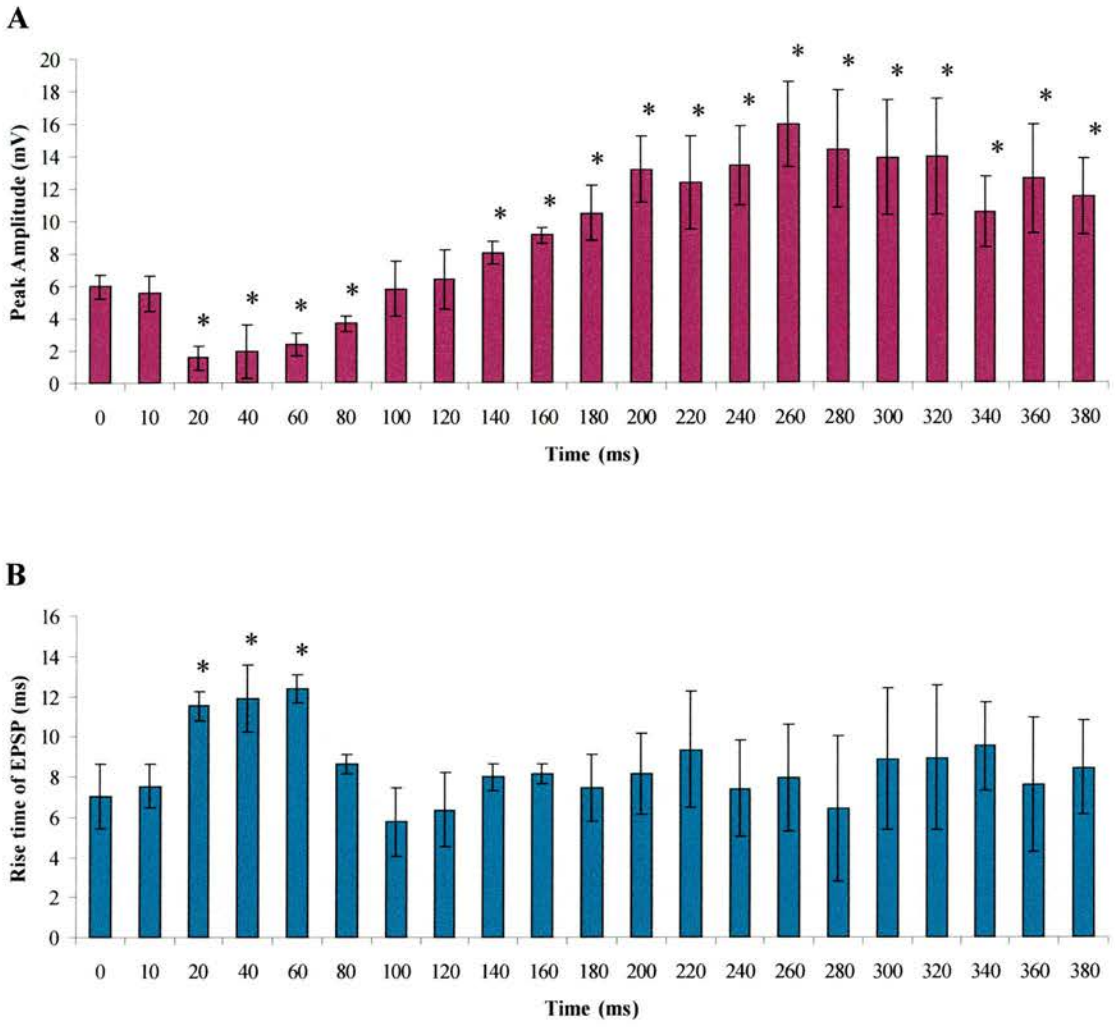

Figure 4. 15. Response of striatal neurones to contralateral cortex-whisker pad pairing protocol, when the contralateral cortical stimulus was delivered in the up state.

A The histogram illustrates the averaged peak amplitude of the EPSPs in response to the whisker pad stimuli across all time intervals for all 25 striatal neurones. The first stimulus (contralateral cortex) was delivered when the cell was in its up state. Time 0 is the average peak amplitude of the EPSPs in response to single whisker pad stimulation. The asterisks (*) denote a significant difference from the value at time 0 (ANOVA, $p < 0.05$, Tukey's pairwise comparisons).

B The histogram illustrates the averaged rise time of the EPSP in response to whisker pad stimulation. The values are the average ± standard error. The value at time 0 is the average EPSP rise time following single whisker pad stimulation. There is a significant increase in the EPSP rise time at the time intervals of 20 ms to 60 ms (ANOVA, $p , < 0.05$, Tukey's pairwise comparisons).

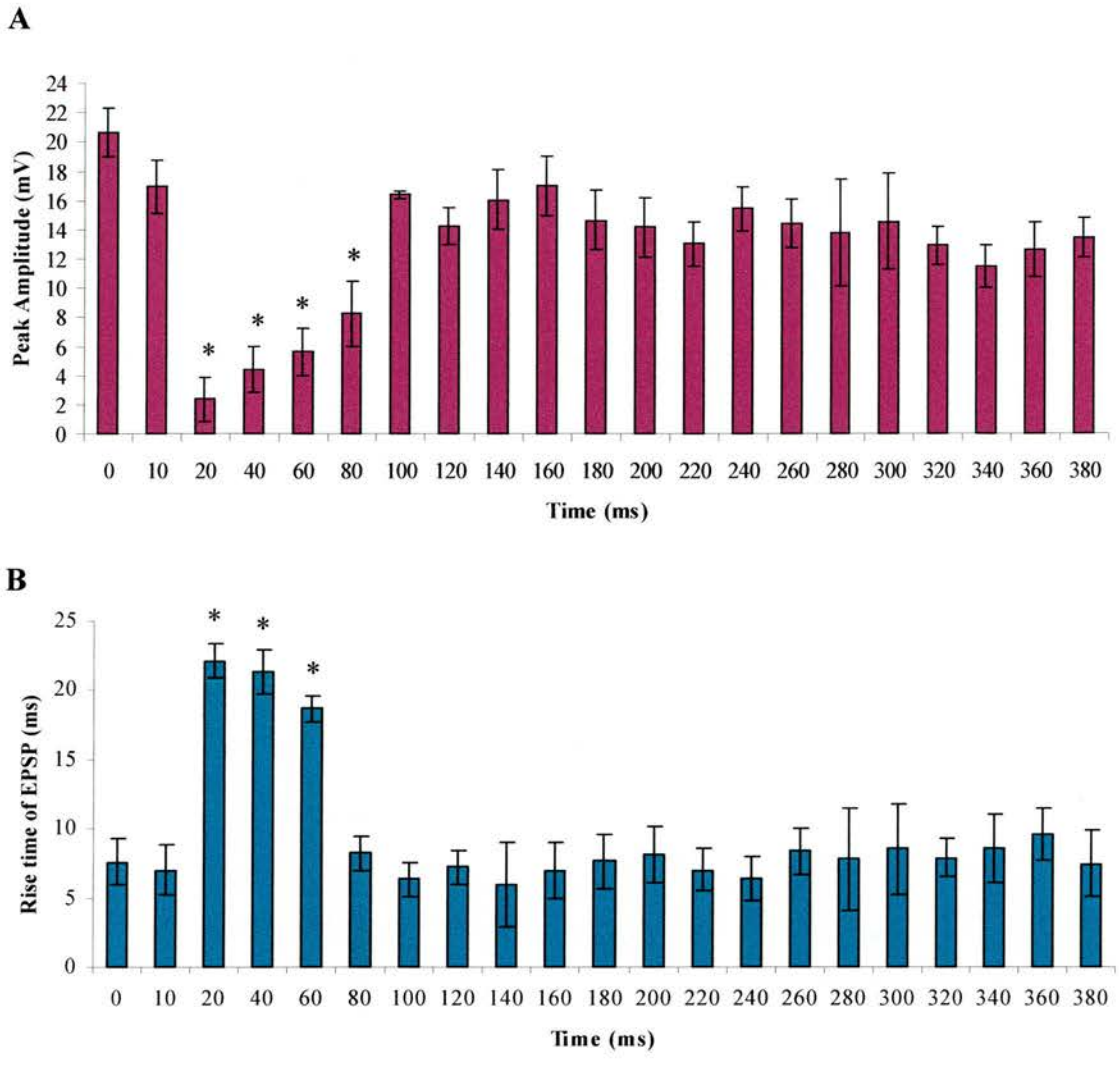

Figure 4. 16. Response of striatal neurones to contralateral cortex-whisker pad pairing protocol, when the contralateral cortical stimulus was delivered in the down state.

A The histogram illustrates the averaged peak amplitude of the EPSPs in response to the whisker pad stimuli across all time intervals for all 25 striatal neurones. The first stimulus (contralateral cortex) was delivered when the cell was in its down state. Time 0 is the average peak amplitude of the EPSPs in response to single whisker pad stimulation. The asterisks (*) denote a significant difference from the value at time 0 (ANOVA, $p < 0.05$, Tukey's pairwise comparisons).

B The histogram illustrates the averaged rise time of the EPSP in response to whisker pad stimulation. The values are the average ± standard error. The value at time 0 is the average EPSP rise time following single whisker pad stimulation. There is a significant increase in the EPSP rise time at the time intervals of 20 ms to 60 ms (ANOVA, $p < 0.05$, Tukey's pairwise comparisons).

4.3.2.3) Protocol 3: Whisker pad – whisker pad interaction

4.3.2.3.1) Averaged results from all (up, down and transition) states (Fig. 4.17)

A time interval of 10 ms lead to a summation of EPSPs in response to both whisker pad stimuli. Stimulation of the whisker pad lead to a prolonged inhibition, lasting 260 ms during which the response of the striatal cells to the second whisker stimulus was significantly decreased. As the cells recovered from the inhibition the rise time of the EPSPs was significantly slower at time intervals of 100 ms and 120ms after which the rise time was similar to control values. No rise time values were calculated before the time interval of 100 ms as the peak response of the cells was not 10% of the average peak amplitude (see Section 4.2.6.2). At no time interval was the duration of the EPSP significantly altered from values when the whisker pad was stimulated on its own (ANOVA, $p > 0.05$, Tukey's pairwise comparisons).

4.3.2.3.2) Averaged results from up states (Fig. 4.18)

Data was obtained for all time intervals except at 280 ms. The peak amplitude was significantly different up to the time interval of 240 ms (ANOVA, $p < 0.05$, Tukey's pairwise comparisons). A significant change in the peak amplitude was also observed from time intervals of 320 ms to 380 ms (ANOVA, $p < 0.05$, Tukey's pairwise comparisons). This is likely due to the fact that cells switch to the down state at these times and as a result, the response to the second stimulus is greater when compared to the peak amplitude when the cell is stimulated in the up state. The rise time of the EPSP was measured for time interval of 200 ms onwards (excluding 280 ms) and was not significantly different from the rise time of EPSPs in response to single whisker pad stimulation (ANOVA, $p > 0.05$, Tukey's pairwise comparisons). The

Figure 4. 17. Response of striatal neurones to whisker pad-whisker pad pairing protocol.

A The overlaid traces illustrate the response of a striatal neurone to the whisker pad-whisker pad pairing protocol. Each coloured trace is the averaged response of the cell to the second stimulus at a particular time interval. The summation of EPSPs seen at a time interval of 10 ms is marked with a red arrow. The traces show that the response of the striatal neurone to the second stimulus is inhibited up to time intervals of 260 ms after which the cell is able to the respond to the second whisker pad stimulus with a peak amplitude that is similar to when the whisker pad is stimulated on its own.

B The histogram illustrates the averaged peak amplitude of the EPSPs in response to the whisker pad stimuli across all time intervals for all 25 striatal neurones. The values are the average ± standard error. Time 0 is the average peak amplitude of the response to single whisker pad stimulation. The asterisks (*) denote a significant difference from the value at time 0 (ANOVA, $p < 0.05$, Tukey's pairwise comparisons).

C The histogram illustrates the averaged rise time of the EPSP in response to whisker pad stimulation. The values are the average ± standard error. The value at time 0 is the average EPSP rise time following single whisker pad stimulation. There is a significant increase in the EPSP rise time at the time intervals of 100 ms and 120 ms (ANOVA, $p, < 0.05$, Tukey's pairwise comparisons).

A

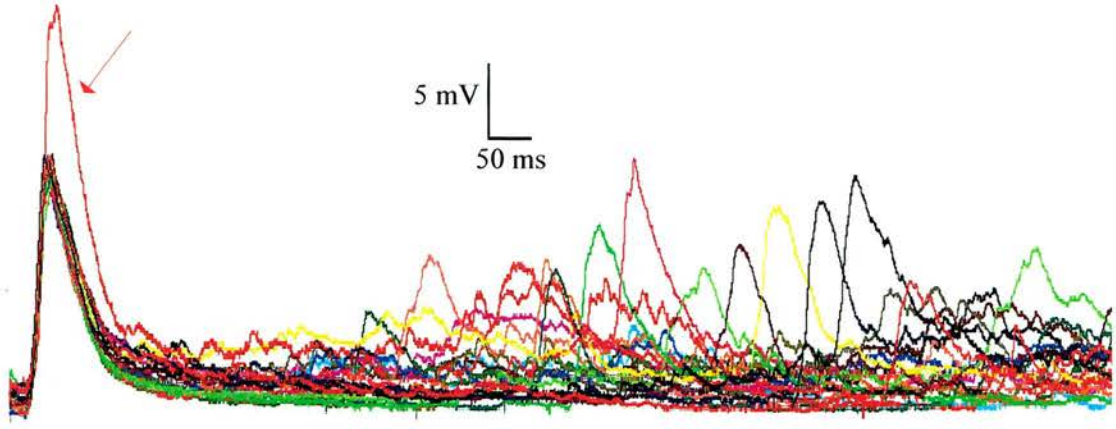
5 mV
50 ms

B

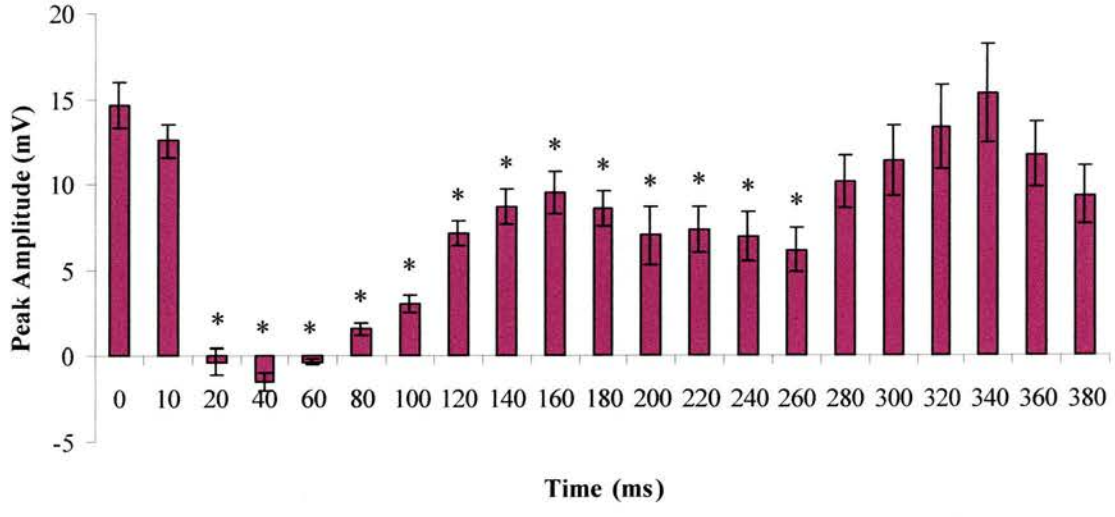
Peak Amplitude (mV)
20
15
10
5
0
-5
0 10 20 40 60 80 100 120 140 160 180 200 220 240 260 280 300 320 340 360 380
Time (ms)

C

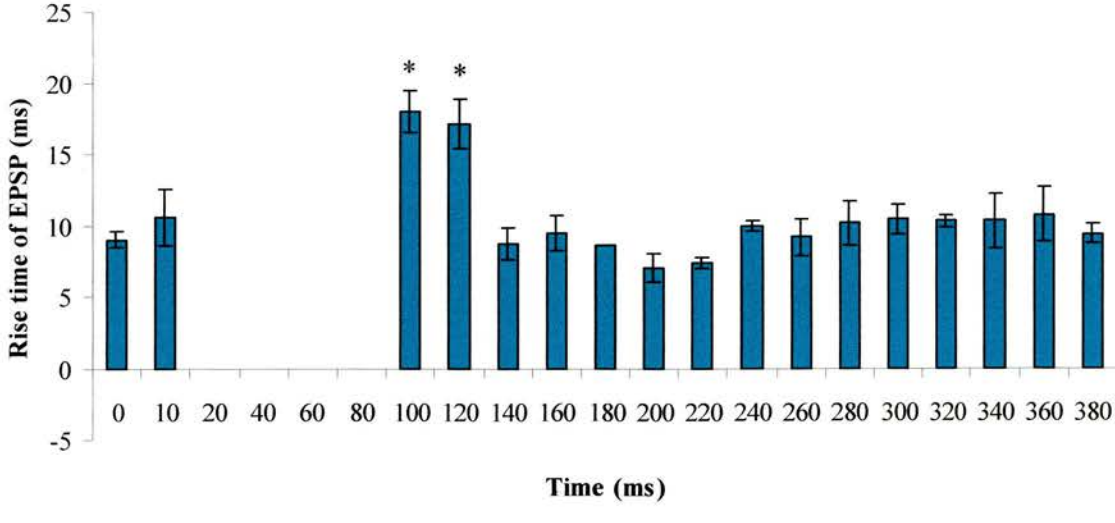
Rise time of EPSP (ms)
25
20
15
10
5
0
-5
0 10 20 40 60 80 100 120 140 160 180 200 220 240 260 280 300 320 340 360 380
Time (ms)

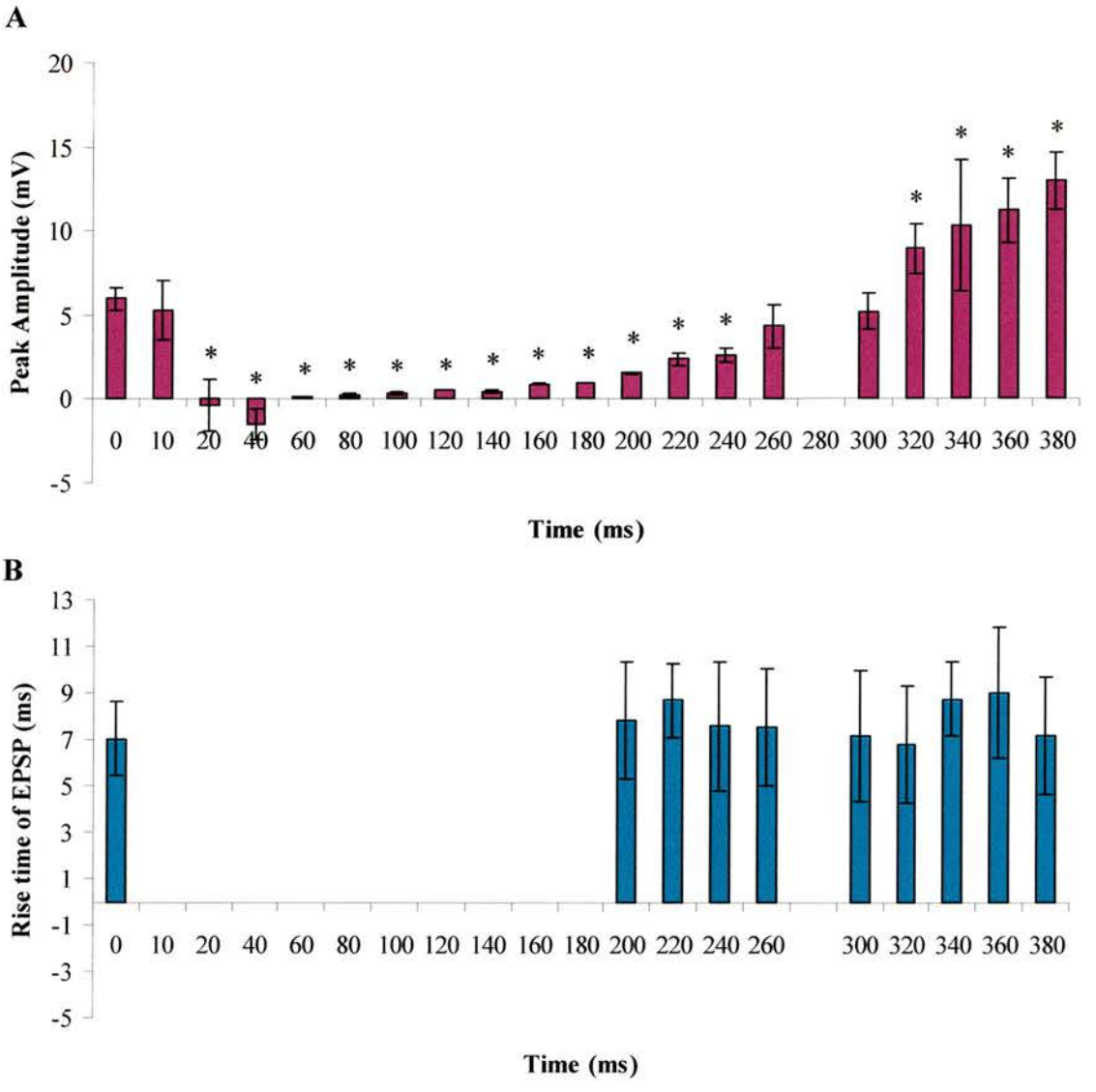

Figure 4. 18. Response of striatal neurones to whisker pad-whisker pad pairing protocol, when the whisker pad stimulus was delivered in the up state.

A The histogram illustrates the averaged peak amplitude of the EPSPs in response to the whisker pad stimuli across all time intervals for all 25 striatal neurones. The first stimulus (whisker pad) was delivered when the cell was in its up state. Time 0 is the average peak amplitude of the EPSPs in response to single whisker pad stimulation. The asterisks (*) denote a significant difference from the value at time 0 (ANOVA, $p < 0.05$, Tukey's pairwise comparisons).

B The histogram illustrates the averaged rise time of the EPSP in response to whisker pad stimulation. The values are the average ± standard error. The value at time 0 is the average EPSP rise time following single whisker pad stimulation. There is no significant change in the EPSP rise time at any of the time intervals (ANOVA, $p , < 0.05$, Tukey's pairwise comparisons).

duration of EPSP was not altered at any time interval (ANOVA, $p > 0.05$, Tukey's pairwise comparisons).

4.3.2.3.3) Averaged results from down states (Fig. 4.19)

A significant decrease in the peak amplitude of the EPSP was seen from time intervals of 20 to 240 ms after which the magnitude of the response returned to normal values (ANOVA, $p < 0.05$, Tukey's pairwise comparisons). The rise time of the whisker pad evoked EPSPs was significantly lengthened at time intervals from 80 to 140 ms (ANOVA, $p < 0.05$, Tukey's pairwise comparisons). The duration of the EPSPs was not significantly altered at any of the time intervals (ANOVA, $p > 0.05$, Tukey's pairwise comparisons).

4.3.2.4) Protocol 4: Contralateral cortex – contralateral cortex interaction

4.3.2.4.1) Averaged results from all (up, down and transition) states (Fig. 4.20)

Stimulation of the contralateral cortex inhibited the response of striatal cells to a second contralateral cortical stimulation. The cells were able to respond to the second contralateral stimuli when it was delivered at least 100 ms after the initial stimulus. This was the only pairing protocol when a summation of the EPSPs was not seen when the 2 stimuli were delivered 10 ms apart.

4.3.2.4.2) Averaged results from up states (Fig. 4.21)

Up state data was obtained for all time intervals. A significant decrease in the peak amplitude of the response was seen at time intervals of 10 ms to 80 ms (ANOVA, $p < 0.05$, Tukey's pairwise comparisons). At all other time intervals there was no significant difference in the amplitude of the response. The duration and rise time of

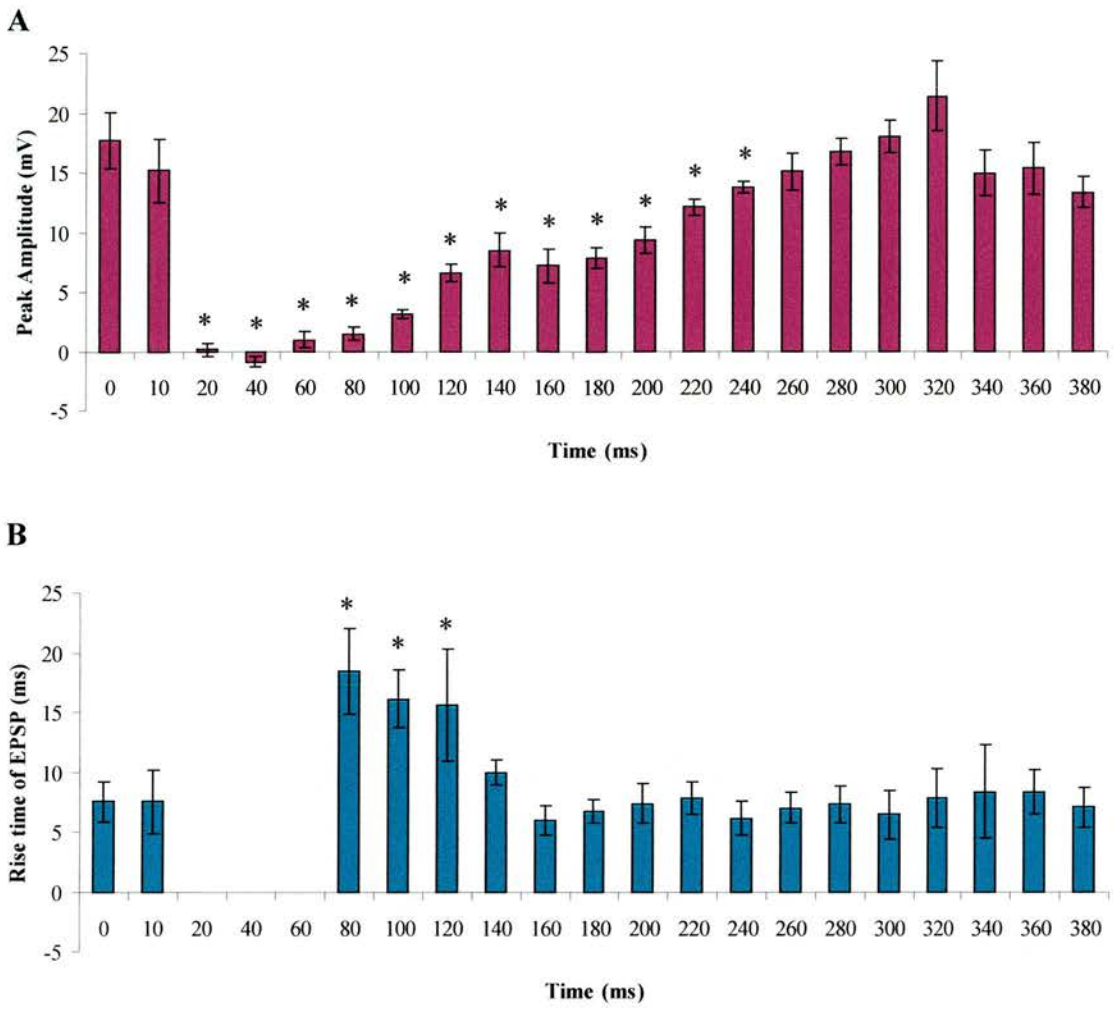

Figure 4. 19. Response of striatal neurones to whisker pad-whisker pad pairing protocol, when the whisker pad stimulus was delivered in the down state.

A The histogram illustrates the averaged peak amplitude of the EPSPs in response to the whisker pad stimuli across all time intervals for all 25 striatal neurones. The first stimulus (whisker pad) was delivered when the cell was in its down state. Time 0 is the average peak amplitude of the EPSPs in response to single whisker pad stimulation. The asterisks (*) denote a significant difference from the value at time 0 (ANOVA, $p < 0.05$, Tukey's pairwise comparisons).

B The histogram illustrates the averaged rise time of the EPSP in response to whisker pad stimulation. The values are the average ± standard error. The value at time 0 is the average EPSP rise time following single whisker pad stimulation. There EPSP rise time is significantly increased at time intervals of 80 ms, 100 ms and 120 ms (ANOVA, $p, < 0.05$, Tukey's pairwise comparisons).

Figure 4. 20. Response of striatal neurones to contralateral cortex-contralateral cortex pairing protocol.

A The overlaid traces illustrate the response of a striatal neurone to the contralateral cortex-contralateral cortex pairing protocol. Each coloured trace is the averaged response of the cell to the second stimulus at a particular time interval. There is no summation of EPSPs at a time interval of 10 ms unlike the other 3 pairing protocols (compare with Figs. 4.11, 4.14, 4.17). The traces show that the response of the striatal neurone to the second stimulus is inhibited up to time intervals of 80 ms after which the cell is able to the respond to the second whisker pad stimulus with a peak amplitude that is similar to when the contralateral cortex is stimulated on its own.

B The histogram illustrates the averaged peak amplitude of the EPSPs in response to the contralateral cortical stimuli across all time intervals for all 25 striatal neurones. The values are the average ± standard error. Time 0 is the average peak amplitude of the response to single contralateral cortical stimulation. The asterisks (*) denote a significant difference from the value at time 0 (ANOVA, $p < 0.05$, Tukey's pairwise comparisons).

C The histogram illustrates the averaged EPSP duration for the time intervals when the second EPSP occurred during the first EPSP. The values are the average ± standard error. The value at time 0 is the average EPSP duration following contralateral cortical stimulation. There is no significant increase in the EPSP duration at any of the time intervals (ANOVA, $p > 0.05$, Tukey's pairwise comparisons).

A

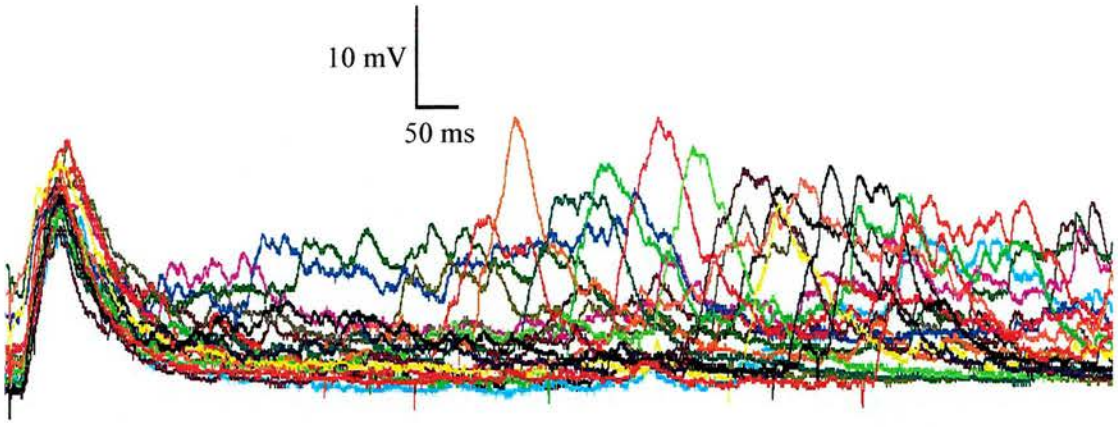
10 mV
50 ms

B

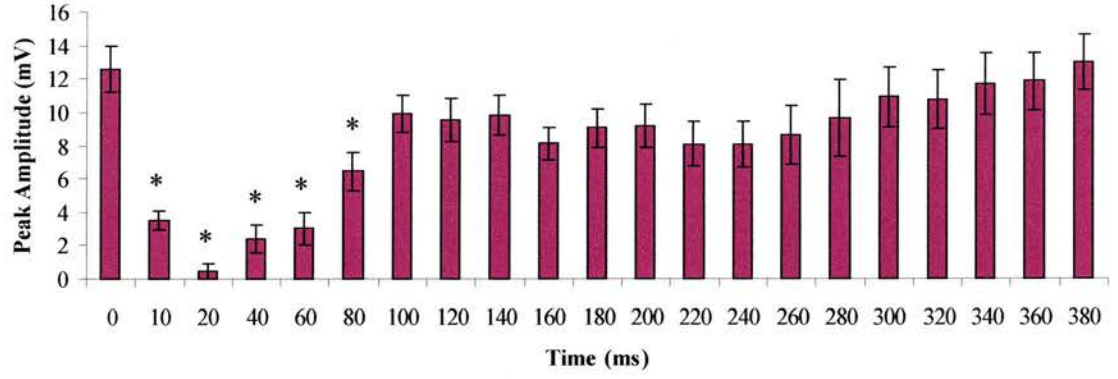
Peak Amplitude (mV)
0
2
4
6
8
10
12
14
16
0 10 20 40 60 80 100 120 140 160 180 200 220 240 260 280 300 320 340 360 380
Time (ms)

C

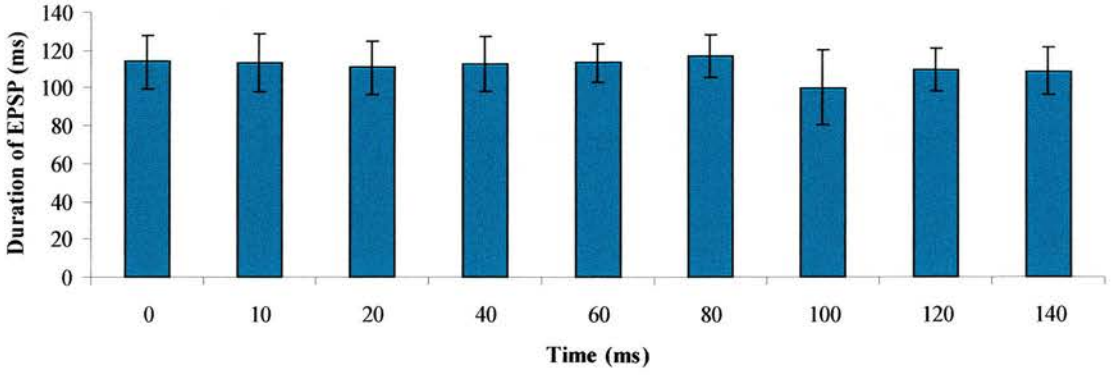
Duration of EPSP (ms)
0
20
40
60
80
100
120
140
0 10 20 40 60 80 100 120 140
Time (ms)

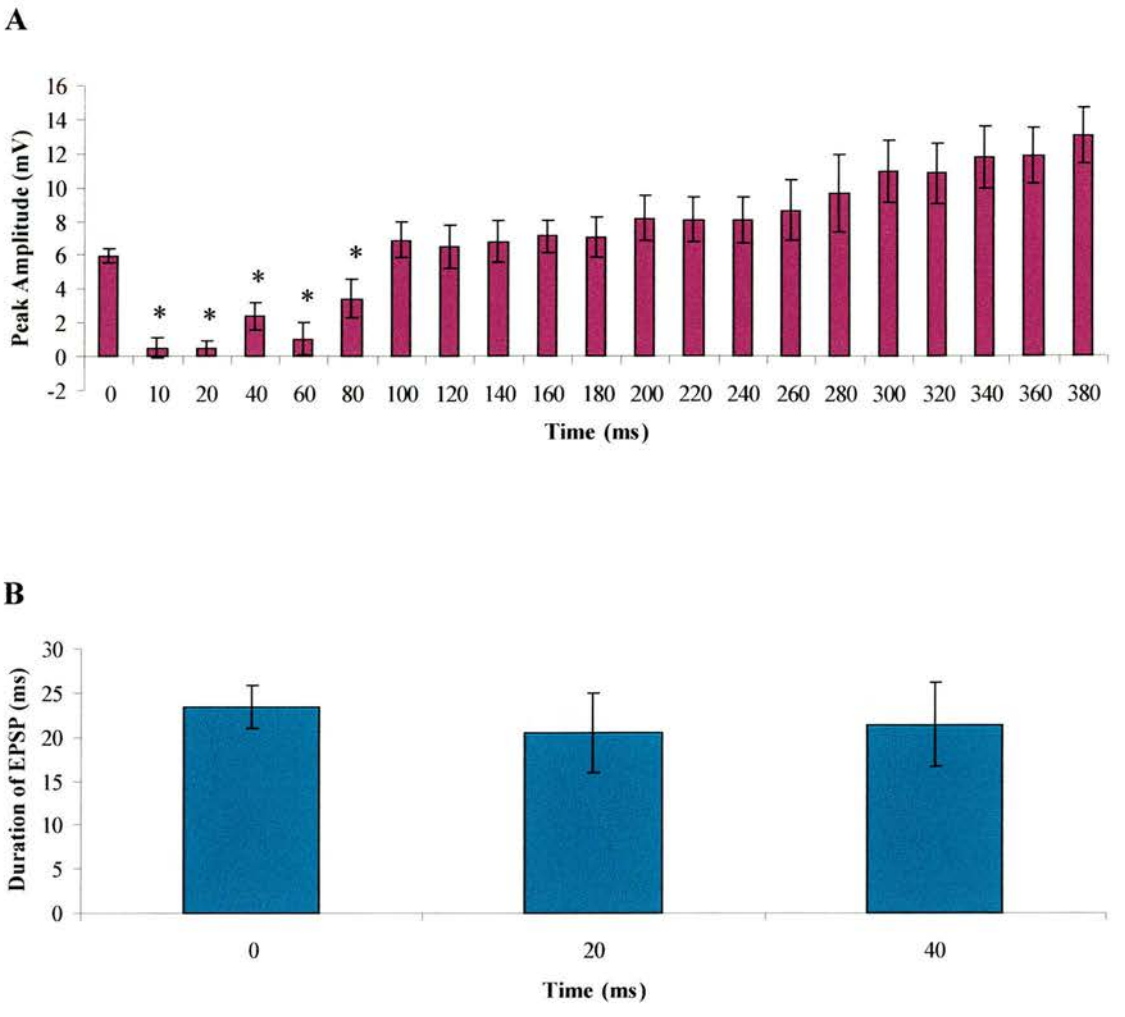

Figure 4. 21. Response of striatal neurones to contralateral cortex-contralateral cortex pairing protocol, when the contralateral cortical stimulus was delivered in the up state.

A The histogram illustrates the averaged peak amplitude of the EPSPs in response to the contralateral cortical stimuli across all time intervals for all 25 striatal neurones. The first stimulus (contralateral cortex) was delivered when the cell was in its up state. Time 0 is the average peak amplitude of the EPSPs in response to single contralateral cortical stimulation. The asterisks (*) denote a significant difference from the value at time 0 (ANOVA, $p < 0.05$, Tukey's pairwise comparisons).

B The histogram illustrates the averaged EPSP duration for the time intervals when the second EPSP occurred during the first EPSP. The value at time 0 is the average EPSP duration following contralateral cortical stimulation when the cell was in the up state. There is no significant increase in the EPSP duration at any of the time intervals (ANOVA, $p > 0.05$, Tukey's pairwise comparisons).

the EPSPs was not significantly altered at any of the time intervals (ANOVA, $p > 0.05$, Tukey's pairwise comparisons).

4.3.2.4.3) Averaged results from down states (Fig. 4.22)

The peak amplitude was significantly different from the peak amplitude recorded from striatal neurones when they were stimulated in the down state, from time interval 10 ms to 60 ms (ANOVA, $p < 0.05$, Tukey's pairwise comparisons). The duration and the rise time of the EPSP was not significantly altered at any time interval (ANOVA, $p > 0.05$, Tukey's pairwise comparisons).

Table 4.7 summarises the results from all traces for all four protocols. It highlights the period of inhibition as well as indicating if summation of EPSPs was observed at if they were the time intervals at which they occurred.

Protocol	Summation of EPSPs	Period of inhibition (ms)
1: whisker pad –contralateral cortex	Yes (10 ms)	40
2: contralateral cortex –whisker pad	Yes (10 ms)	80
3: whisker pad –whisker pad	Yes (10 ms)	260
4: contralateral cortex –contralateral cortex	No	60

Table 4. 7. Summary of the results of the pairing protocols in striatal neurones.

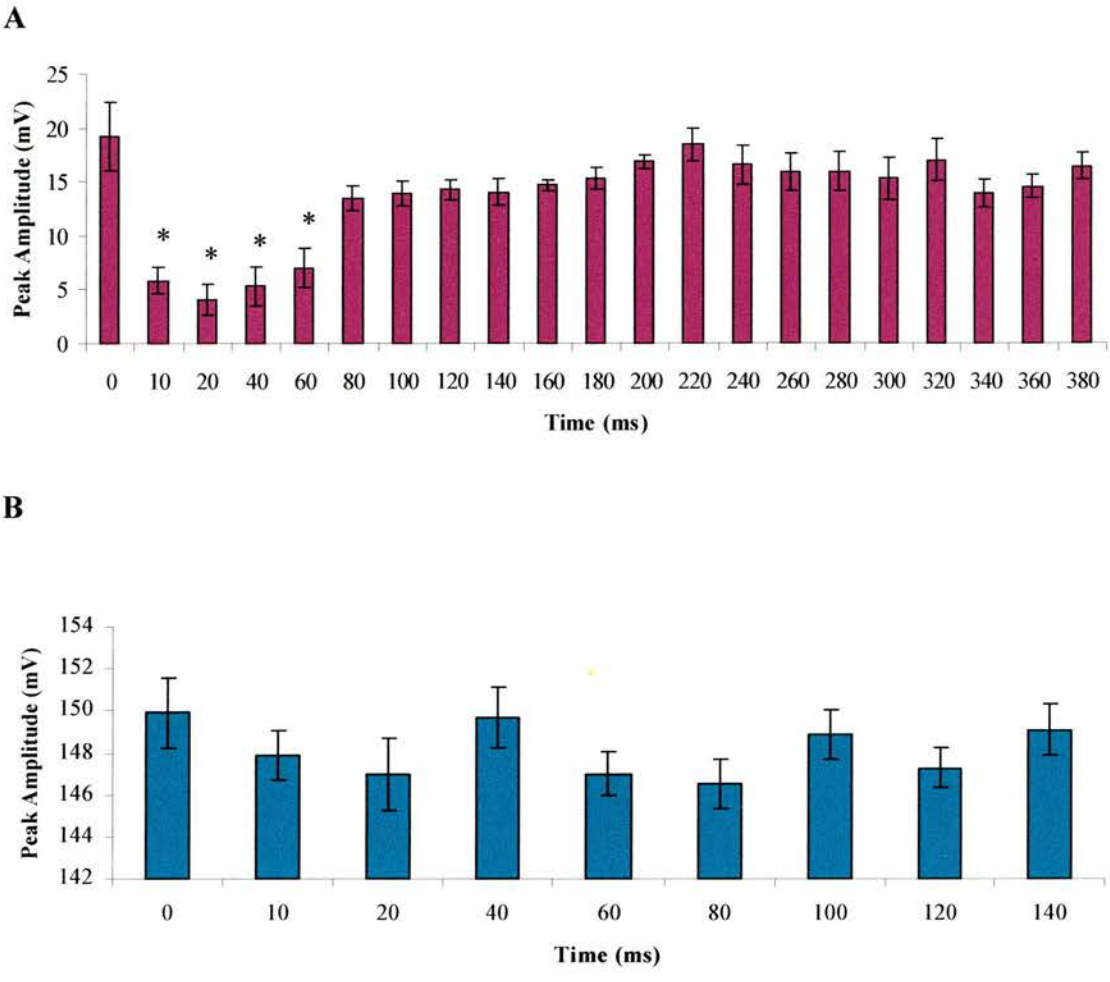

Figure 4. 22. Response of striatal neurones to contralateral cortex-contralateral cortex pairing protocol, when the contralateral cortical stimulus was delivered in the down state.

A The histogram illustrates the averaged peak amplitude of the EPSPs in response to the contralateral cortical stimuli across all time intervals for all 25 striatal neurones. The first stimulus (contralateral cortex) was delivered when the cell was in its down state. Time 0 is the average peak amplitude of the EPSPs in response to single contralateral cortical stimulation. The asterisks (*) denote a significant difference from the value at time 0 (ANOVA, $p < 0.05$, Tukey's pairwise comparisons).

B The histogram illustrates the averaged EPSP duration for the time intervals when the second EPSP occurred during the first EPSP. The value at time 0 is the average EPSP duration following contralateral cortical stimulation when the cell was in the down state. There is no significant increase in the EPSP duration at any of the time intervals (ANOVA, $p > 0.05$, Tukey's pairwise comparisons).

4.4) Discussion

4.4.1) Cortical cells

As discussed in Chapter 3, based on the average latency and depth of the records, the cells are most likely recorded from cortical layer Vb. Cortical cells in this layer project mainly to the pontine nucleus while the projection to the somatosensory striatum from the barrel cortex originates mainly in upper portions of layer V (Mercier et al., 1990; Wright et al., 2001). Cells in layer Vb have a shorter latency response to stimulation compared to layer Va neurones (Armstrong-James et al., 1992). The cells in this study most likely represent a mix of layer Va and Vb neurones. A comparison of the cells with the longest and shortest latency showed that the cells behaved in the same manner to paired stimuli and thus the data was pooled. As before these layer V cells found below the barrels will be referred to barrel centre cells and the layer V cells found below the septa as septal cells.

In cortical neurones the first stimulus inhibited the response of the cell to the second stimulus in the pairing protocol to varying degrees. This inhibition can be due to two reasons, i.e. the activation of interneurones and disfacilitation. Interneurones are found in all layers of the barrel column and make up approximately 15% of total neuronal stomata in the barrel cortex (Beaulieu, 1993). The large percentage of interneurones are found in layer IV where they play an important role in the feed-forward inhibitory circuitry and suppress spike generation in target neurones (Beaulieu, 1993; Porter et al., 2001; Swadlow, 2003). Interneurones also might play a role in feedback inhibition (Swadlow, 2003). These interneurones are also found in Layer V and these are also strongly modulated by thalamic input (Swadlow, 2000). This is in contrast to the finding that corticofugal neurones in layer V of the visual,

somatosensory and motor cortices in the rabbit and cat have a weaker thalamocortical input compared to a callosal input suggesting that these cells may be specialised for the integration of corticocortical input rather than thalamocortical input (Ferster and Lindstrom, 1983; Weyand et al., 1986a, b; Swadlow, 1988, 1990, 1991, 2000).

The pairing study carried out in this thesis explored how corticofugal neurones integrated input from the thalamus (as a result of whisker pad stimulation) and corticocortical input (as a result of contralateral cortical stimulation). In the whisker pad-contralateral cortex stimulation paradigm, the second cortical stimulus when it is delivered at time intervals of 10 and 20 ms is unable to produce an EPSP of the same amplitude compared to if it had been applied on its own. An initial whisker stimulus activates the VPM, which them activates the barrel column resulting in an EPSP in the layer V cells (Simons, 1978; Armstrong-James and Fox, 1987; Armstrong-James et al., 1992; Nicolelis et al., 1995; Fee et al., 1997; Zhu and Connors, 1999). This strong, synchronous input to the barrel centre activates recurrent inhibition mediated by cortical interneurones (Ferster and Lindstrom, 1983; Swadlow, 1989, 1990; Agmon and Connors, 1992; Gil and Amitai, 1996). This recurrent inhibition, which is meditated by the cortical interneurones, lasts for approximately 2-50 ms and is a result of the connectivity of the layer VI interneurones to other interneurones and the ability of GABAergic cortical neurones to suppress each others activity through autapses (Thomson et al., 1996; Tamas et al., 1997; Tamas et al., 1998; Gibson et al., 1999). This allows for the fast recovery of the cortex following an inhibitory volley and fits in the recovery time window of the cortical neurone to the second contralateral cortical stimulus.

In the whisker pad-whisker pad stimulation paradigm, an initial whisker stimulus leads to activation of the barrel centre neurones by activation of the VPM and due to the strength of the stimulus, sets up recurrent inhibition which suppresses the response of the cortical neurones to a second whisker pad stimulus for approximately 50 ms. However the decrease in response to the second stimulus lasted 160 ms. This could be due to disfacilitation. Periods of hyperpolarisation during slow wave sleep have been attributed to disfacilitation rather than active inhibition by intracortical interneurones (Timofeev et al., 2001). Cortical disfacilitation can be caused either by the hyperpolarisation of thalamocortical neurones or the depression of thalamocortical and intracortical synapses by low cholinergic activity which is seen during slow wave sleep (Hirsch et al., 1983; Timofeev et al., 1996; Gil et al., 1997). The hyperpolarisation seen in thalamocortical neurones prevents the firing of action potentials curbing the transmission of information up to the barrel cortex. Thus the period of inhibition seen in the present study after dual stimulation of the whisker pad is likely to be due to the inability of the thalamus to transmit incoming information from the whisker pad as a result of an initial inhibition followed by a disfacilitation.

In the contralateral cortex-whisker pad pairing protocol, stimulation of the contralateral cortex results in activation of the crossed corticocortical fibres that transmit the impulses to the ipsilateral cortex. The crossed corticocortical neurones activate barrel centre neurones resulting in an EPSP. This crossed corticocortical pathway is not dense in the somatosensory cortex and as a result, is likely to be less effective in activating interneurones resulting in the very weak or non-existent recurrent inhibition (Olavarria et al., 1984; Chapin et al., 1987; Koralek et al., 1990).

Another possibility is that these crossed cortical fibres do not contact interneurones as all anatomical studies show input from callosal projections synapsing onto dendritic spines with none contacting onto cell bodies (Cipolloni and Peters, 1983). As the fast spiking interneurones do not posses spines they are not the main target of the corticocortical projections (Porter et al., 2001). Previous studies have shown that the main driving force of the interneurones is thalamic input and the ability of a crossed callosal input to activate interneurones is unknown (Swadlow and Gusev, 2000; Porter et al., 2001). It cannot be discounted that excitation of the barrel centre neurones by the crossed corticocortical pathway will lead to activation of the thalamus (via a corticothalamic pathway) and then activation of interneurones that can potentially modulate the response of the cell to further stimuli (Bourassa et al., 1995; Wright et al., 2000). However this is a polysynaptic pathway and it is likely that any inhibition mediated through this route will be weak. Thus due to the lack of a strong inhibitory drive the barrel cortical cells are able to respond to a subsequent whisker pad stimulus with an EPSP amplitude that is similar to that observed when the whisker pad is stimulated on its own.

In the dual contralateral cortical stimulation protocol (protocol 4), an initial contralateral cortex results in an EPSP in the ipsilateral barrel cortex. The strength of the cortical stimulus that is delivered through a stimulating electrode is likely to set up recurrent inhibition that would prevent the septal cells from being excited by a second contralateral cortical stimulus. Thus the long period of inhibition seen in the barrel centres from which records were obtained, might not reflect the inability of the barrel centre cells to respond to two contralateral cortical stimuli but is likely to be

the result of the inability of the septal cells providing the input to these barrel centre neurones to respond to dual cortical stimuli.

The results of this thesis are somewhat in agreement with the study of Shuler (Shuler et al., 2001). In the latter study the responses in Layer V cortical cells to simulation of both the contralateral and ipsilateral whisker pad was studied, using extracellular electrophysiology (Shuler et al., 2001). They report that an initial stimulus (their condition stimulus) attenuated the response probability of the neurones to a second stimulus (their test stimulus) (Shuler et al., 2001). The degree of attenuation is related to both the sequence of the stimuli as well as the inter stimulus intervals between the two stimuli as is seen in the present study. Greater attenuation of the response probability is seen when the condition stimulus was the contralateral whisker pad and the test stimulus the ipsilateral whisker pad compared to vice versa and previous stimulation of the ipsilateral whisker pad inhibits cortical responses to any subsequent ipsilateral whisker stimulus (Shuler et al., 2001). The similarity in the response of the cortical neurones to asynchronous inputs in both the present study and Shuler's study is despite the fact that different anaesthetics and whisker stimuli were used. There is a considerable concern in extrapolating the results of this thesis to try and explain how the behaviour of two pathways can be interpreted in behavioural terms as the stimulation protocols are likely to be non-physiological. However the congruent results of this and Shuler's study suggest certain aspects of the interaction of the two pathways are maintained even while using non-physiologically relevant stimuli.

Previous studies indicate that the transcallosal projection might play a modulatory role (Clarey et al., 1996; Shin et al., 1997). The results of the present

study suggests that the barrel cortex is able to integrate whisker responses bilaterally and can use this information to perform tasks such as conjoint detection of left and right whisker-mediated distance information (Shuler et al., 2002). While the stimulation protocols employed in this study do not allow an investigation into the integration of information from heterologous whiskers, a previous study has demonstrated that the bilateral influence on the responses is not restricted to the homologous receptive field as previously hypothesized (Pidoux and Verley, 1979; Armstrong-James and George, 1988; Clarey et al., 1996; Shin et al., 1997; Iwamura, 2000; Shuler et al., 2001). The results of the interaction study would suggest that output of layer V cortical neurones is likely to reflect the activity of both the thalamocortical and callosal projections.

4.4.2) Striatal cells

The main hypothesis tested was that the diffuse pathway gates the response of striatal neurones to stimulation of the topographic pathway. While the role of a gating pathway fits in with its dispersed pattern of innervation, there are several factors that suggest that this might not be the function of the diffuse corticostriatal pathway. Firstly, both pathways are able to generate action potentials when stimulated suprathreshold (Chapter 3) (Wright et al., 2001) and are not dependent on the other to reach spiking threshold, unlike the nucleus accumbens (O'Donnell and Grace, 1995). It can be argued that due to the spread of excitation to septal cells, stimulation of the whisker pad activates not only cells of the topographic pathway but also involves the cells beneath the septa, which make up the diffuse projection (Wright et al., 1999; Wright et al., 2001). Thus, at least in this stimulation paradigm there is no strict topographic only projection. However in animals with chronic callosal cuts,

degeneration of the axons and cell bodies would result in a barrel centre only projection. Such experiments were carried out (Chapter 3) and in these animals stimulation of the whisker pad was able to produce action potentials when the cells were stimulated suprathreshold. However due to the bilateral projection of cells below the septa to the striatum, there is a possibility that chronic callosal cuts will result in degeneration of only the contralateral branch of the projection, while preserving the input to the ipsilateral striatum. These chronic animals still displayed spontaneous up and down states, confirming that episodes of depolarisation are not a unique feature of the diffuse pathway. This fits in with studies that have shown that the cortex drives the state transition in the striatum and it seems highly unlikely that this role is confined to a subset of cortical neurones (Wilson et al., 1983a; Wilson, 1993; Cowan and Wilson, 1994; Wilson, 1995; Wilson and Kawaguchi, 1996; Stern et al., 1997). Another feature seen in nucleus accumbens neurones responding to hippocampal stimulation is the prolonged depolarisation after trains of stimuli and the long duration EPSP after a single stimulus (O'Donnell and Grace, 1995). While no trains of stimuli were delivered in the experiments done in this thesis, there was no significant difference in the duration of the EPSP to a single stimulus. Even when the responses were separated based on the state of the cell when the stimulus was delivered, there was no significant difference in the EPSP duration between the two stimuli. Thus neither of the stimuli is able to maintain a state of prolonged depolarisation which is a feature one would expect of a response generated by a pathway that acts as a gate on another. Another important consideration is the anatomical connectivity of the two pathways to the target cell. In nucleus accumbens cells, up to 10% of hippocampal afferents terminate on the cell bodies of proximal

dendrites unlike prefrontal cortical axons which are exclusively observed at distal dendrites (Meredith et al., 1990). This anatomical arrangement would suggest that the hippocampal afferents have a greater influence on the membrane potential compared to prefrontal cortical inputs to the cells and has been shown in cross correlation studies (Goto and O'Donnell, 2001a, b). The two corticostriatal pathways originating in the barrel cortex have not been shown to connect to different portions of the striatal neurones (Chapter 2)(Wright et al., 1999). Both pathways synapse onto spines but as yet it is not known if these spines are located on the proximal or distal dendrites (Chapter 2)(Wright et al., 1999). One possible explanation of the slower rise time of the EPSP in response to stimulation of the contralateral cortex is that this pathway contacts more distal dendrites which once again would refute the idea that this pathway acts as a gate for input arriving via the topographic pathway (Chapter 3)(Wright et al., 2001).

There is a possibility that the diffuse pathways could act as an indicator of past events. A calcium independent potassium A current (I_{AS}) has been shown to play a role in the time dependent role in the facilitation of cortical inputs *in vivo* (Mahon et al., 2000a; Mahon et al., 2000b). This potassium current inactivates around –60 mV and recovers slowly from inactivation (Nisenbaum et al., 1994; Gabel and Nisenbaum, 1998). This allows time dependent facilitation after strong depolarising inputs by modification of the intrinsic excitability of striatal neurones (Mahon et al., 2000a). For the diffuse pathway to be an indicator of past events, the stimulation of the pathway has to give rise to responses with certain characteristics. Activation of the I_{AS} occurs only at –60 mV and stimuli that result in depolarisation that is below that of the threshold for I_{AS} do not result in an increase in the responsiveness of the

cell (Mahon et al., 2000a). Stimulation of the contralateral cortex does give rise to an EPSP and in some instances the threshold value of I_{AS} is reached (Nisenbaum et al., 1994). However, the mean value of the EPSPs in response to stimulation of the whisker pad, gave rise to a larger amplitude EPSP compared to contralateral cortical stimulation. An interesting area to look into would be the response of the cells to stimuli that were delivered suprathreshold as that would result in the activation of I_{AS} current and has been shown to have a facilitatory effect in both striatal and other neurones (Storm, 1988; McCormick, 1991; Mahon et al., 2000a; Mahon et al., 2000b).

Another manner in which this pathway could act as an indicator of past events would be if acted as a primer. While a striatal cell is able to fire action potentials in response to stimulation of the topographic pathway alone, this requires a high stimulus intensity enabling the cell to reach the threshold for spike generation. However if a cell responds to contralateral cortical stimulation by switching to the up state, it would increase the chances of the cell firing an action potential in response to a lower intensity stimulus. This 'priming' was observed in some of the interaction studies when a whisker pad stimulus on its own was subthreshold but when delivered 10 ms after a contralateral cortical stimulus was able to generate action potentials. However, this summation of EPSPs was also seen at the time interval of 10 ms for whisker pad – contralateral cortex and whisker pad – whisker pad interaction and is not a unique feature of the diffuse pathway. The slow conduction velocity is another feature of the diffuse pathway that would not support the hypothesis that it functions as a priming pathway (Wright et al., 2001). Using values from Chapter 3, stimulation of the left whisker pad would elicit a response in a cell in the right striatum

approximately 8 ms later (via activation of the topographic pathway that arises from the right barrel cortex). Stimulation of the right whisker pad will result elicit a response in a cell in the right striatum approximately 14 ms later (as it takes an average of 6 ms for cells in the cortex to respond to a peripheral whisker stimulus and an average of 8 ms for striatal cells to respond to stimulation of the diffuse pathway). Thus simultaneous stimulation of both whisker pads in a behaving animal would result in the cell responding to the stimulation of the topographic pathway before responding to activation of the diffuse pathway. Taking into consideration the conduction velocity it would seem that the topographic pathway would be more suitable as the priming pathway as it is the first stimulus to reach the striatal cell.

One important consideration while interpreting the results of this study is how both pathways are affected during the natural behaviour of the rodent. Thus while the experiments done in this thesis explore the behaviour of striatal neurones to stimulation of both these corticostriatal pathways, the stimuli are not physiologically relevant. An important issue that has to be considered is the strength of activation of the contralaterally projecting corticostriatal pathway during natural whisking behaviour. While studies have looked at the response of cortical neurones to stimulation of both whisker pads, there has not been an equivalent study looking at the response in striatum.

In three of the four pairing protocols, a summation of EPSPs is observed when the stimuli are delivered 10 ms apart. Thus the second stimulus is neither facilitated or depressed by the preceding stimulus. The timing of the delivery of the second stimulus is such that the striatal cells are not disfacilitated and thus are able to respond to the second stimulus. In most cases the delivery of the second stimulus

occurred when cells were in the down state and due to their increased input resistance they respond with a large amplitude EPSP. There is a possibility that the summation observed is not due to summation of EPSPs but is in part due to an IPSP. At resting membrane potentials IPSPs are depolarising. While no experiments were done to disprove this, the occasional generation of action potentials after the second stimulus would strongly suggest that the facilitation is caused by an addition of EPSPs.

The summation of EPSPs seen in the striatal cells was not mirrored in the cortical neurones subjected to the same pairing protocols. The exception is protocol 2 where a whisker pad stimulus is delivered after contralateral cortical stimulation. The response of cortical neurones to stimulation of the whisker pad followed by a contralateral cortical stimulation 10ms later was inhibition. However in striatal cells there was a summation and this can be easily attributed to the fact that in the striatal pairing protocol the contralateral cortical stimulation is able to affect the striatal cell on its own without involving the barrel cortex on the ipsilateral side and thus is not affected by the inhibition seen in the cortical neurones. However using this same argument one would expect no summation following dual whisker pad stimulation as the cortex is unable to respond to a second whisker pad stimulus delivered 10 ms after the first. As the input to the striatal cell comes from the barrel centre neurones, a corresponding inhibition is expected. The summation of the EPSP amplitudes could be due to impulses transmitted to the striatal cells via the axon reflex arising from the crossed corticostriatal pathway (Wilson, 1986). Septal cells are also activated by a whisker pad stimulus and thus the response to the second stimulus could be a summation of both the axon reflex and activation of the septal cells (Wright et al.,

2001). This hypothesis can be tested by doing the pairing protocol in animals that have undergone chronic callosal cuts and this was attempted but no cells were obtained. Dual contralateral cortical stimulation did not result in a summation of EPSP when the stimuli were delivered 10 ms apart. In this pairing protocol the response of the striatal cells mirrored that of the cortical neurones and the lack of the response to a second cortical stimulus is likely due to the fact that the cortical cells that are stimulating the striatal cell are unable to respond to dual contralateral cortical stimulation due to the strength of the cortical stimulus which activates cortical interneurons and sets up a recurrent inhibition.

Following the summation seen at 10 ms there was a period of inhibition the length of which varied between protocols and is likely due to disfacilitation (Wilson et al., 1983a). However there is difference between the period of inhibition seen in cortical cells and striatal cells to the pairing protocol and is seen in striatal neurones during protocols 1, 2 and 3. In the case of protocol 2 (contralateral cortex-whisker pad stimulation) no inhibition was seen in the cortex but striatal neurones were unable to respond to a subsequent whisker pad stimulus for time intervals up to 80 ms. An important consideration is that striatal cells are believed to receive convergent input from a large number of corticostriatal efferents and the inhibition seen could be a result of disfacilitation from other cortical inputs (Kincaid et al., 1998; Zheng and Wilson, 2002). GABAergic striatal interneurones are more easily excited by cortical stimulation and are able to exert an inhibitory influence over a large number of striatal projection neurones (Cowan et al., 1990; Kita et al., 1990; Lapper et al., 1992; Kawaguchi, 1993; Kita, 1993; Bennett and Bolam, 1994; Plenz and Aertsen, 1996a, b; Parthasarathy and Graybiel, 1997; Koos and Tepper, 1999). It

is possible that these interneurones might also increase the period of inhibition seen in striatal cells. In the dual cortical pairing protocol the striatal cells displayed a much shorter inhibition compared to cortical neurones. The reasons for this are unclear as the hyperpolarisation in the cortex would translate to a lack of activity in the striatal neurones as the prolonged periods of 'electrical silence' in the striatum have been attributed to disfacilitation (Wilson et al., 1983a).

During the recovery of the cells response to a second stimulus, the latency, EPSP duration and the rise time was measured. The only difference was observed in the rise of the EPSP in response to a second whisker stimulus i.e. protocols 2: contralateral cortex-whisker pad and 3: whisker pad-contralateral cortex. The increased rise time of the small amplitude EPSPs that were produced during the inhibitory period of the pairing protocol would suggest that the septal cells were the major contributors the EPSP, suggesting that septal cells recover from inhibition quicker than barrel centre neurones. The increased period of inhibition following dual whisker pad compared to contralateral cortical stimulation would support this.

4.5) Conclusions

Both pathways interact at the level of both a single striatal and cortical cell. EPSPs were followed by a period of inhibition, the extent of which was dependent on the order and source of the stimuli. The results of the current study indicate that the behaviour of the striatal cells to paired stimuli closely reflects the interaction seen in the layer V cortical cells that provide the main excitatory drive to striatal cells. While a summation of EPSPs is seen in striatal neurones at a time interval when the two stimuli were delivered 10 ms apart, it seems unlikely that the stimuli would arrive within this time interval in a behaving animal. Thus while the pattern of axonal

arborisation would suggest that the diffuse pathway acts as priming pathway, the electrophysiological data does not support this hypothesis.

CHAPTER 5

EFFECTS OF DOPAMINE ON INTERACTION OF THE TWO CORTICOSTRIATAL SYSTEMS IN RAT SOMATSENSORY STRIATUM

5.1) Introduction

5.1.1) Dopamine in the striatum

The substantia nigra provides a major dopaminergic input to the striatum (Anden et al., 1964; Gerfen et al., 1987; Jimenez-Castellanos and Graybiel, 1987; Hanley and Bolam, 1997). Dopamine has been implicated in pathologic conditions such as Parkinson's disease, Huntington's disease and schizophrenia. One of the consequences of the loss of dopamine as seen in Parkinson's disease is the imbalance of information flow through the two striatal pathways i.e. the direct and the indirect pathways (see Chapter 2 for a detailed discussion). This is thought to result in some of the characteristics motor impairments as seen in Parkinsonian patients, including rigidity, difficulty in the initiation of movements, akinesia, and slowness in the implementation of movements. A commonly used animal model of Parkinson's disease is the 6-hydroxydopamine (6-OHDA) model. The depletion of dopamine produces numerous changes in the behaviour of the rat including the loss of spontaneous eating and drinking and a decrease in voluntary movement (Marshall et al., 1974; Zis et al., 1974; Schallert and Whishaw, 1978; Schallert et al., 1978a; Schallert et al., 1978b; Whishaw et al., 1981). These animals also display an increase in their postural adjustments and these changes in the behaviour of the rat suggests that the 6-OHDA depleted rat provides a good animal analogue for the human Parkinson condition (Schallert and Whishaw, 1978; Schallert et al., 1978a; Schallert et al., 1978b; Whishaw et al., 1978; Schultz, 1982).

In addition to the motor impairments observed in Parkinson patients, an impairment in somatosensory processing has also been documented (Schneider et al., 1987; Schneider et al., 1992). Patients are unable to produce an appropriate motor

response to somatosensory stimuli and have impaired judgement and detection of somatosensory signals (Schneider et al., 1987; Schneider et al., 1992). Interestingly the loss of dopamine also disrupts the processing of sensory information in the 6-hydroxydopamine treated rats, which lose their ability to orientate towards tactile stimuli (Marshall et al., 1974; Ljungberg and Ungerstedt, 1976). Ungerstedt et al., (Ungerstedt and Ljungberg, 1974) reported that the responses of striatal cells to peripheral stimulation was not detected after the removal of dopamine. These results strongly suggest that dopamine plays a key role in the processing of somatosensory information in the striatum.

5.1.2) Effects of dopamine on the electrophysiological characteristics of striatal neurones

Morphological studies have shown that glutamatergic terminals from the cortex and thalamus and dopaminergic terminals from the nigra converge on the single spines of striatal projection neurones (Freund et al., 1984; Smith and Bolam, 1990a). This implies that a tight interaction exists between these two neurotransmitters and the response of striatal neurones is a reflection of this interaction. Glutamate and dopamine produce their effects by acting on a variety of receptors. Glutamate receptors can be grouped into two main classes, the ionotropic/ligand gated cation channels which includes NMDA, AMPA and kainate as well as the metabotropic glutamate receptors which are coupled to various signal transduction processes (Monaghan et al., 1989; Watkins et al., 1990; Hollmann and Heinemann, 1994). Dopamine exerts its effects via activation of dopamine receptors. The different types of dopamine receptors and the result of their activation has been described in Chapter 2.

Early extracellular experiments studying single unit records from anaesthetised animals where dopamine was applied either intophoretically or via stimulation of the nigra, report that dopamine depresses spontaneous striatal cell firing (Bloom et al., 1965; McLennan and York, 1967; York, 1967; Brown and Arbuthnott, 1983; Johnson et al., 1983; Chiodo and Berger, 1986; Hu and Wang, 1988; Nisenbaum et al., 1988). Experiments looking at the effects of dopamine on single unit activity as a result of corticostriatal activation also show that dopamine reduces evoked spike activity (Brown and Arbuthnott, 1983; Hu and Wang, 1988; Wachtel et al., 1989; Hu et al., 1990). While the majority of results suggest a inhibitory role for the effects of dopamine, some investigators have reported excitatory effects of dopamine (Hirata et al., 1984; Ohno et al., 1987; Nisenbaum and Berger, 1992). The differential effects of dopamine have been partly explained by the dosage effect. Chiodo and Berger (Chiodo and Berger, 1986) first showed that dopamine can account for both the excitatory and inhibitory effects seen. The increase or decrease in glutamate induced cell firing is dependent on the concentration of dopamine with low doses facilitating spiking via a D_1 receptor mediated mechanism that increases NMDA-receptor mediated currents and high doses of dopamine inhibiting spiking via D_2 receptors that suppress AMPA mediated currents (Chiodo and Berger, 1986; Hu and Wang, 1988; Nisenbaum et al., 1988; Cepeda et al., 1993; Gonon, 1997; Hu and White, 1997; Zheng et al., 1999).

In *in vivo* observations, where there is direct stimulation of the nigra or application of dopamine, striatal neurones respond with an EPSP suggesting that the effects of dopamine is excitatory (Hull et al., 1970; Kitai et al., 1975; Kitai et al., 1976). The apparent disagreement between extracellular and intracellular studies was

reconciled by findings that dopamine while depolarising striatal cells inhibited their glutamate induced spiking activity (Herrling and Hull, 1980). Recent studies have demonstrated that D_1 agonists inhibit striatal neurones at hyperpolarised membrane potential but enhance evoked activity at depolarised membrane potential due to dopamine mediated activation of calcium conductances (Hernandez-Lopez et al., 1997; Cepeda et al., 1998). This has provided an explanation for the differences observed between intracellular data from *in vivo* and *in vitro* studies. Due to the hyperpolarised membrane potential of striatal neurones *in vitro*, this enhancement of membrane potential is not observed.

The response of striatal neurones to dopamine is also thought to depend on the type of striatal neurone. Striatonigral neurones which are thought to be the type 1 neurones described by Onn are preferentially sensitive to D_1 receptor agonist while striatopallidal neurones (Type II) are powerfully inhibited by D_2 agonists (Nisenbaum and Berger, 1992; Nisenbaum et al., 1992; Onn et al., 1994a, b, c). Recent studies have also demonstrated that different groups of striatal neurones may have different responses to dopamine. In awake unrestrained animals, motor related striatal neurones are excited by dopamine while non-motor related neurones respond with inhibition (Haracz et al., 1989; Haracz et al., 1993; Pierce and Rebec, 1995), suggesting that while the main strongly convergent excitatory input to cells is enhanced, weakly coherent input is suppressed. This agrees with the hypotheses that dopamine increases the signal to noise ratio for evoked activity (Nicola et al., 2000).

Based on anatomical and electrophysiological evidence, dopamine is in a strong position to modulate the response of striatal neurones to corticostriatal activation. While there is substantial *in vivo* and *in vitro* experimental data that

illustrate the inhibitory action of dopamine on the responses evoked by corticostriatal activation there is no consensus on which dopamine receptor mediates this activity (Herrling and Hull, 1980; Mercuri et al., 1985; Calabresi et al., 1987b). While a large body of evidence suggests that D_2 receptors mediate this attenuation, others suggest that post-synaptic D_1 receptors are responsible (Brown and Arbuthnott, 1983; Calabresi et al., 1987b; Garcia-Munoz et al., 1991; Jiang and North, 1991; Cepeda et al., 1994; Levine et al., 1996).

In conclusion the effects of dopamine on the activity of striatal neurones has lead to numerous contradictory results and is likely to be due to a variety of reasons. Different effects are seen due to the activation of different dopamine receptors and one factor determining this is the concentration of dopamine. The altered responses can also be attributed to the different types of striatal neurones as well as to the different sites of localisation (pre and post synaptic) of the dopamine receptors. These results all point to a strong modulatory role of dopamine in the striatum.

5.1.3) Morphological changes as a result of the loss of dopamine

Besides the changes in the electrophysiological behaviour of striatal neurones as a result of dopamine, a number of morphological changes as a result of the loss of dopamine have also been have been reported. The spine density of striatal neurones decreases by 18%, 26 days after 6-OHDA treatment and remains lower than control values for up to a year (Ingham et al., 1989, 1993). The time span for the reduction of spine density coincides with electrophysiological findings that the spontaneous activity of striatal neurones increases up to 3 weeks after dopamine removal (Schultz, 1982). A similar reduction in spine density occurs in cats after cortical and thalamic input to striatal neurones is removed (Kemp and Powell, 1971).

More recently the same group (Ingham et al., 1998) have also shown that after a lesion of the dopamine system, the total number of asymmetric boutons in the striatum decrease, with an increase in the density of a sub-population of asymmetric boutons which have complex synaptic specialisations. This raises the issue as to the action of dopamine and if the loss of spines and synapses as a result of the removal of dopamine from the striatum is a global phenomenon or is limited to certain pre or post synaptic targets (Ingham et al., 1998).

5.1.4) Aim

Dopamine plays a role in the processing of somatosensory information in the striatum and the main aim of this study was to investigate the effects of the loss of dopamine by 6-OHDA, on the response of striatal neurones to stimulation and interaction of the two corticostriatal systems arising from the barrel cortex. As the two corticostriatal pathways also contact the 2 types of output striatal projection pathways with unequal frequency (Chapter 2), the loss of dopamine (if it is not a global phenomenon) might preferentially affect one pathway over the other.

5.2) Experimental Procedures

5.2.1) Unilateral lesion of midbrain dopaminergic neurones with 6-hydroxydopamine

5.2.1.1) Anaesthesia and surgery

A total of 26 male Sprague Dawley rats (200-220g) were anaesthetised with halothane in O_2. Stable levels of anaesthesia were maintained throughout the surgical procedure to ensure the absence of a foot withdrawal reflex. The rats were placed in a stereotaxic frame and the head was secured in the frame via ear and tooth bars. The scalp was cut from the anterior of the Bregma to the base of the skull and the overlaying tissue was pulled back and clamped. The skull surface was cleaned to reveal the Bregma and the midline. Rostrocaudal and mediolateral co-ordinates for the placement of the 6-OHDA was calculated using Bregma as a reference point and the stereotaxic co-ordinates were derived from the atlas of Paxinos and Watson (Paxinos and Watson, 1986). Access to the brain was made using a hand held dental drill and bit to create a burr hole. Drilling was stopped to leave a thin transparent layer of bone overlaying the brain. This was gently picked away to prevent accidental damage to the cortical surface and to ensure that no skull fragments entered the cortex. A hole was created in the dura to expose the cortical surface to facilitate the passage of the needle.

All rats were injected with 2 µl of saline containing 6 µg of 6-OHDA (Sigma, UK) and 0.4 µl of ascorbic acid into the right medial forebrain bundle (AP-3.8 mm, L-1.5, DV-8.0). The mixture was injected over a period of 2 min after which the needle was left in place for a further 5 min. After careful withdrawal of the needle, the skin overlying the exposed cranium was drawn together and sutured. The

animals were kept warm and after recovery from the anaesthetic they were returned to their home cages.

5.2.1.2) Testing for successful 6-OHDA lesions

The success of the lesion was tested 10 days after the operation by determining the number of turns the animals made in response to the administration of apomorphine (0.25 mg/kg, in H_2O, i.p., Research Biochemicals Incorporated, Massachusetts, UK) (Ungerstedt and Arbuthnott, 1970). Animals that turned more than 200 complete circles away from the injected side in 45 min were considered to have at least 90% loss of dopamine from the lesioned side and were used for electrophysiological experiments 30 days post-lesion (Hefti et al., 1980).

5.2.2) Anaesthesia

A total of 12 male Sprague Dawley rats (240-350 g) were used. The anaesthetic make-up and dose were similar to the electrophysiology experiments described in Chapters 3 and 4. All rats received intra-peritoneal injections of a 10% urethane, (Sigma Chemicals, St Louis) 1% α-chloralose (Sigma Chemicals, St Louis) mix in distilled water (1 ml/100 g of body weight). Stable levels of anaesthesia were maintained throughout with additional anaesthetic (10% of original dose) administered approximately four to six hours after the initial injection to ensure the absence of a foot withdrawal reflex.

5.2.3) Surgical procedures

A tracheotomy was performed and the animal was set up in the stereotaxic apparatus as previously described (Chapter 3.2). Briefly, the scalp was cut from the base of the skull to the anterior of the Bregma and the overlying tissue and skull surface cleared

as before. The CSF drain was put in place and the masseter muscles and scalp were secured to a brass ring. The skull was drilled 2.1 mm posterior and 5.0 mm lateral on both sides relative to the Bregma (Paxinos and Watson, 1986). The area of the skull above the cortex on both sides was then gently picked away to prevent skull fragments from entering the cortex. A cotton ball soaked with saline was then placed over the hole on the recording site. The stimulating electrode was then lowered to a depth of 2.0 mm. A dental cement well (Simplex Rapid, Associated Dental Products, Swindon, U.K.) was built around the site of the recording electrode placement. When the well was dry, the cotton ball was removed and the dura was deflected just before the recording electrode was lowered.

5.2.4) Stimulus protocol

The whisker pad and contralateral cortex were stimulated as previously described. When the pairing protocol was carried out, all stimuli were adjusted to be subthreshold so that no action potentials were fired in response to activation of the two pathways. No individual whisker deflections were carried out in these experiments.

5.2.5) Intracellular recordings and pairing protocols

The method used for the intracellular recordings and the pairing protocols were similar to those described in Chapters 3 and 4 and is briefly described below. Borosilicate glass microelectrodes (1.5 mm OD, 0.86 mm ID with inner filament, Harvard Apparatus, U.K.) containing 3M potassium acetate with resistances of between 60-110 MΩ were used. The electrode was advanced into the cortex at an angle of 90^0 to the cortical surface. It was then advanced 100 μm into the cortex

using a manual micromanipulator and the electrode resistance and capacitance compensation balanced. The dental cement well was then filled with liquid paraffin wax (Physiowax, TAAB, England) to stabilise the electrode. The electrode was than manually advanced to a depth of 2,000 μm. Neuronal activity was searched for using electrical stimulation of the whisker pad (0.4 Hz). The electrode was advanced in 2 μm steps, until a neurone was impaled either by advancement alone or by a combination of advancement and electrode 'buzzing' with high current, voltage or capacitance, to gain entry to the cell. The presence of cells was detected by a drop in membrane potential and changes in electrode resistance.

Once a cell was successfully impaled its response to contralateral cortical stimulation was determined. Only cells that responded to both forms of stimuli were chosen for the interaction study. The input resistance of cells was estimated by passing a series of small amplitude hyperpolarising and depolarising (subthreshold) current pulses through the recording electrode (1.5 nA to –1.5 nA in 0.5 nA steps). These pulses were delivered both before and after the pairing protocols. All pulses and measurements of cellular properties were made by triggering data acquisition when the cell was either in the up or down state and no attempt was made to distinguish between the two states. The spontaneous activity of the cells was also recorded.

All cells were subjected to the 4 pairing protocols which were designed to investigate the interaction of the two pathways as well as the effect of a pathway on itself (see Chapter 4.4, Table 4.1).

When data acquisition was carried out using MacLab Scope (n = 2), the pulses were delivered via a D100 digitimer and the time interval between the two pulses

was manually increased, from 10 ms to 380 ms, for each pairing protocol. In the remaining cells (n = 8), data was acquired using Signal 2.04 and the delivery of the pulses was via a digital signal from the computer and completely randomised. Once again all pulses were delivered when the cell was either in the up or down state and no attempt was made to distinguish between the two states. Only cells that were held long enough to enable all 4 pairing protocols to be carried out were included in the study.

As only biocytin-free electrodes were used to maximise the number of cells recorded from, (see Chapter 3.4) pontamine sky blue markings were made at the top and bottom of the electrode tracts at the end of the experiment. The electrode was advanced to a maximum depth of 5,000 μm and if no cells were impaled, the electrode was slowly brought back up to the cortical surface and a new penetration made in a different position.

5.2.6) Perfusion and histology

Animals from which data was obtained, were deeply anaesthetised with sodium pentobarbital (Sagatal, 200 mg/kg; Rhône Mérieux, Tallaght, Dublin). Rats were pre-perfused with 50 mls of 0.9% saline containing 150 units of heparin followed by 300 ml of 0.05% glutaraldehyde and 4% paraformaldehyde in 0.1M PB (pH 7.4). Following fixation, the brain was removed and stored in a 10% sucrose buffered fixative overnight at 4^0C. The brain was then cut into 50 μm coronal sections on a freezing microtome.

5.2.6.1) Immunocytochemistry for D_1 group of dopamine receptor

The sections were washed in PBS four times (10 min each), to remove fixative. The sections were then incubated in a quenching solution, made up of 70% PBS, 30% methanol, 0.03% hydrogen peroxide, for 30 min. This was done to reduce endogenous peroxidase activity. The sections were then washed in PBS eight times (10 min each) to remove the peroxide reaction mixture. The sections were then incubated for 2 h in 20% goat serum made in 0.3% PBS-TX at room temperature with gentle agitation. Striatal sections were then reacted with antibodies against tyrosine hydroxylase (Affinity antibodies) overnight at 4^0C with gentle agitation (1:4000 in PBS-TX). The sections were washed twice (10 min each), in PBS-TX before incubation in biotinylated goat anti-rabbit IgG (1:200 in PBS-TX, Vector Labs, UK) for an hour. Sections were washed (2 times, for 10min in PBS) and followed by ABC reaction (ABC Elite kit; 1:50 in PBS, Vector Labs, UK). Sections were washed (2 x 10 min) and the bound peroxidase was revealed with DAB. Sections were washed in PBS (three times, 10 min each) after 10 min to terminate the reaction. The sections were well rinsed in PBS before being mounted on subbed slides. The slides were oven dried for 1 week. The sections were dehydrated in ethanol in the following concentrations (70%, 90%, 95%, 100%, 100%, 100%, 5 min each), cleared in xylene (10 min) and coverslipped with DPX (BDH Laboratory Supplies). Sections were reconstructed using a drawing tube. Positions of neurones from which records were obtained were calculated from the marked ends of the tracts.

5.2.7) Acquisition and analysis of data

5.2.7.1) Data acquisition - MacLab and Signal

All experimental data was recorded on either a Macintosh based data acquisition package (MacLab Scope) or a PC based data acquisition system (Signal 2.04). Eight consecutive sweeps were taken for each stimuli and at each time interval for each pairing protocol. Twelve sweeps each lasting 5 s were taken for the spontaneous activity of the striatal neurones. The sweeps were later analysed off-line.

5.2.7.2) Data analysis

The latency, rise-time, peak amplitude, and duration of the response of the neurone to each stimulus was measured as before (see Chapter 3.2, Fig. 3.4, Chapter 4.2 and Fig. 4.1 for definition of measurements). Input resistance was determined from the slope of a regression line fitted to the membrane potential produced by a series of hyperpolarising and subthreshold depolarising current pulses.

5.2.7.3) Statistical analysis

For each cell the average value of the eight sweeps were calculated for the variables i.e. latency, rise time, peak amplitude and time to peak amplitude (only when one stimulus was delivered). This was done for the response of the cell to the stimulus when only one was given and the response of the cell to the both stimuli during the pairing protocol. The values for all cells were then pooled and compared using a one-way ANOVA and Tukey's pairwise comparisons. Numerical values are given as mean ± standard deviation (S.D) unless otherwise stated. The probability level for statistical significance was set at $p < 0.05$.

5.3) Results

5.3.1) Histological verification of 6-OHDA lesions

Animals that were used in electrophysiology experiments, were confirmed as successful 6-OHDA lesions by a near complete loss of TH-immunoreactive neurones from the right substantia nigra (Fig 5.1).

5.3.2) Striatal intracellular electrophysiology

Intracellular records were obtained from 14 striatal neurones from 12 animals. Striatal neurones exhibited an average membrane potential of -73.49 ± 6.82 mV which ranged between -46.50 and -92.69 mV. The cells exhibited spontaneous membrane potential fluctuations of amplitudes of approximately 20 mV (Fig. 5.2). A frequency histogram of the membrane potential shows a bimodal distribution with a peak at -65 and -80 mV (Fig. 5.2). These peaks in membrane potential correspond to the up or depolarised state and a down or hyperpolarized state. The up state potential ranged from -46 to -68 mV. During these episodes small changes in membrane potential occurred causing threshold to be reached resulting in the firing of action potentials with average spike heights of 45 mV. Membrane potential of the hyperpolarised state ranged from -78 to -93 mV and in this phase fluctuations in membrane potential were diminished.

The membrane current – voltage relationship of neurones was obtained from measurements of membrane potential in response to a series of intracellular current pulses. There was an inward rectification as seen by the saturation of the hyperpolarising responses to current pulses of increasing negative intensity. Positive current pulses evoked a slowly developing ramp depolarisation which in some cases

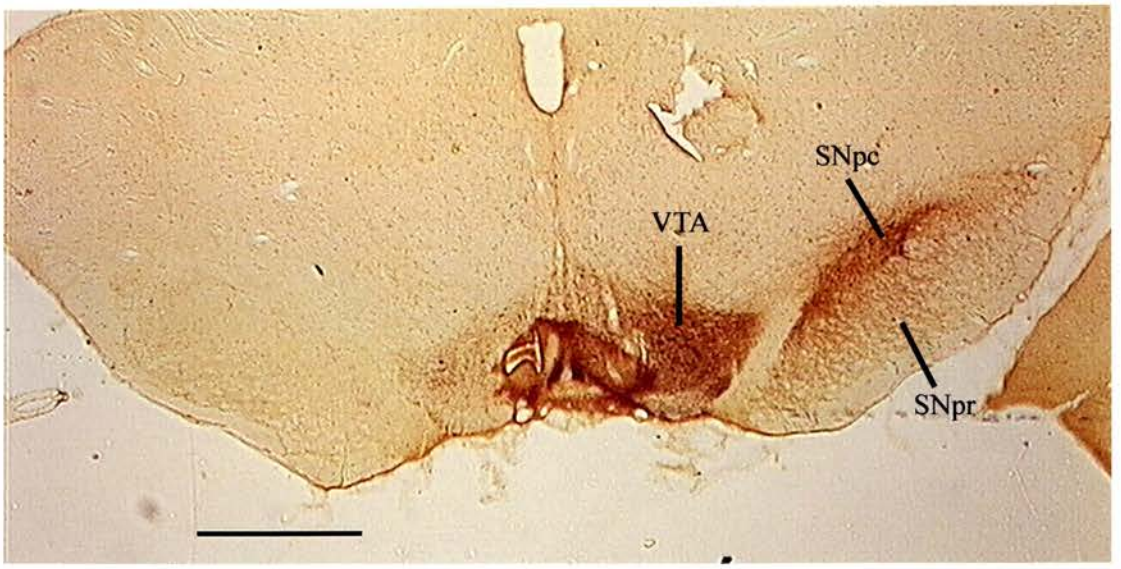

Figure 5. 1. Anatomical verification of unilateral nigral lesions.

Light micrograph of a coronal section through the nigra of a 6-OHDA lesioned rat. The section was stained to reveal tyrosine hydroxylase immunoreactivity (TH). There is intense TH staining in the right substantia nigra pars compacta (SNpc) and ventral tegmental are (VTA). Lighter immunoreactivity was obsereved in the substantia nigra pars reticulata (SNpr). Staining for TH was not detected in the left hemisphere. Scale bar: 1 mm.

Figure 5. 2. Spontaneous activity of striatal neurones.

A The spontaneous activity of a striatal neurone recorded over a period of 5 s is displayed. The cell was at a depth of 3568 μm. Membrane potentials of the up and down state are labelled at the left of the traces (arrows). The cell tended to fire action potentials when it was in its up state. The maximal amplitude shifts were approximately 20 mV. Compared with Figure 3.14, the cell illustrated here which is from a 6-OHDA lesioned animal fires more often when in the up state.

B A frequency histogram showing the amount of time spent by striatal neurones at any given membrane potential. When the peak amplitude was measured for each cell, a corresponding resting membrane potential (membrane potential of the cell before arrival of the stimulus) was recorded for each cell and for each sweep per cell. From a single cell, 656 traces were analysed and a total of 10 cells were analysed. The frequency of the cells sitting at a particular membrane potential was then calculated and used to plot the histogram. The histogram illustrates that the cells spent most of the time in either a hyperpolarized state (membrane potential $\approx$ -80 mV) or a depolarised state (membrane potential $\approx$ -65 mV) and little time in the transition between the two.

A

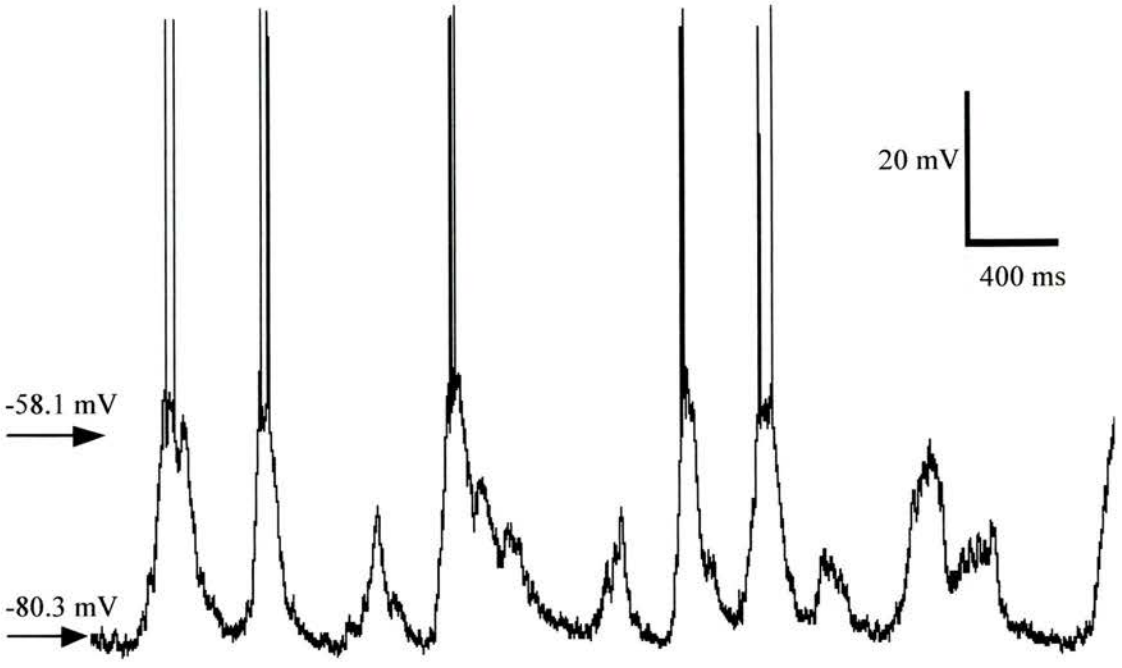
20 mV
400 ms
-58.1 mV
-80.3 mV

B

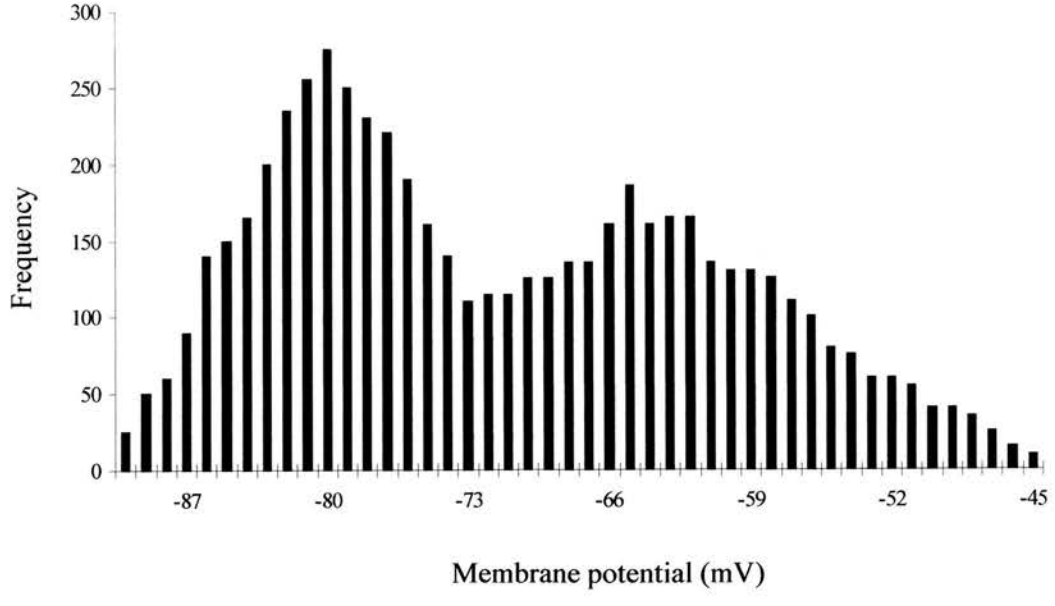
300
250
200
150
100
50
0
Frequency
-87
-80
-73
-66
-59
-52
-45
Membrane potential (mV)

lead to a long latency spike discharge (Fig. 5.3). Input resistance was measured from the slope of a regression line fitted to a graph of membrane potential against current injected. Average input resistance was 25.685 (± 8.360) MΩ and ranged from 2.561 to 49.664 MΩ. The input resistance values obtained in this study showed a large variability and are not typical of striatal neurones. As discussed earlier (Chapter 3.2) this is due to that fact that current was not injected when the cell was in the down state alone. As a result, while input resistance was calculated for each cell, it was not used as a criteria to identify striatal neurones.

A comparison of the electrophysiological properties of intracellularlly recorded striatal neurones in control (data from chapters 3 and 4) and 6-OHDA lesioned animals (Table 5.1) revealed that striatal neurones had a more depolarised membrane potential in both the up state and down states animals. Visual inspection of the traces of the spontaneous activity of the neurones seemed to suggest that neurones from lesioned animals also tended to fire more action potentials when the cell was in the up state.

5.3.3) Response characteristics to two forms of stimulation

The positions of the cells recorded from are shown in Figure 5.4. Cells that responded were found in the region of striatum that received projections from the barrel cortex i.e. -1.3 to -2.12 mm posterior with respect to Bregma . All the cells sampled in this study responded to both forms of stimulation. During the collection of data, the number of non-responsive neurones were recorded and was not significantly different from control animals. There was also no significant difference in the dorsal-ventral extent of responding neurones.

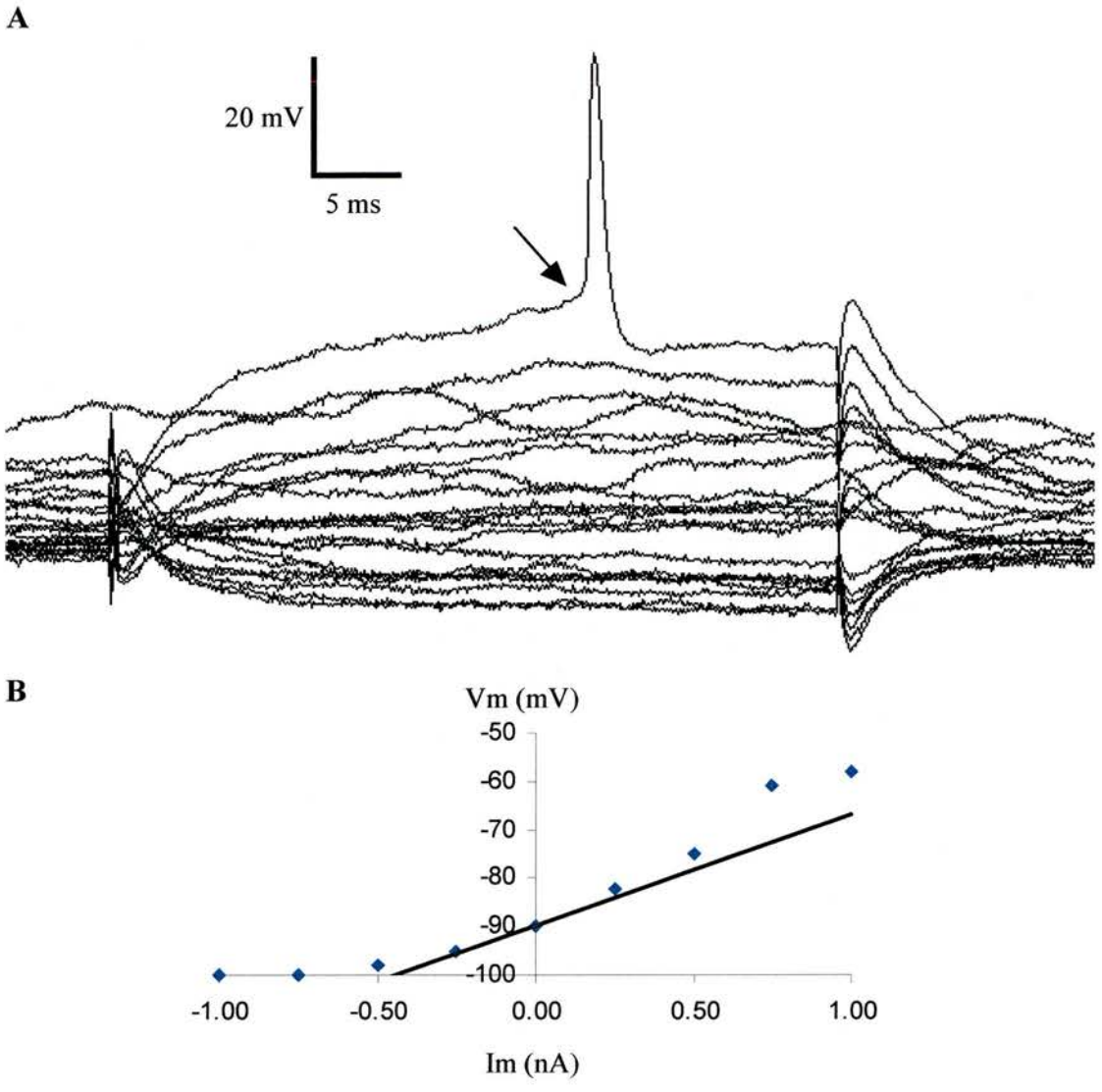

Figure 5. 3. Current injection into striatal neurones.

To illustrate the influence of the membrane potential on the input resistance representative traces from a striatal neurone is shown. The current pulse was a simple rectangular pulse, with a width of 40ms.

A Hyperpolarising and depolarising current pulses were delivered when the cell was in the down state (approximately -90 mV). Looking at the corresponding change in membrane potential, there is an inward rectification present as seen by the small changes in membrane potential with increasing injection of hyperpolarising current compared with the large changes in membrane potential with increasing injection of depolarising current. At maximal current injection the membrane potential reached threshold for action potential generation leading to the firing of a long latency action potential (arrow).

B The input resistance was determined from the slope of a regression line fitted to the membrane potential and was 22.84 MΩ.

.

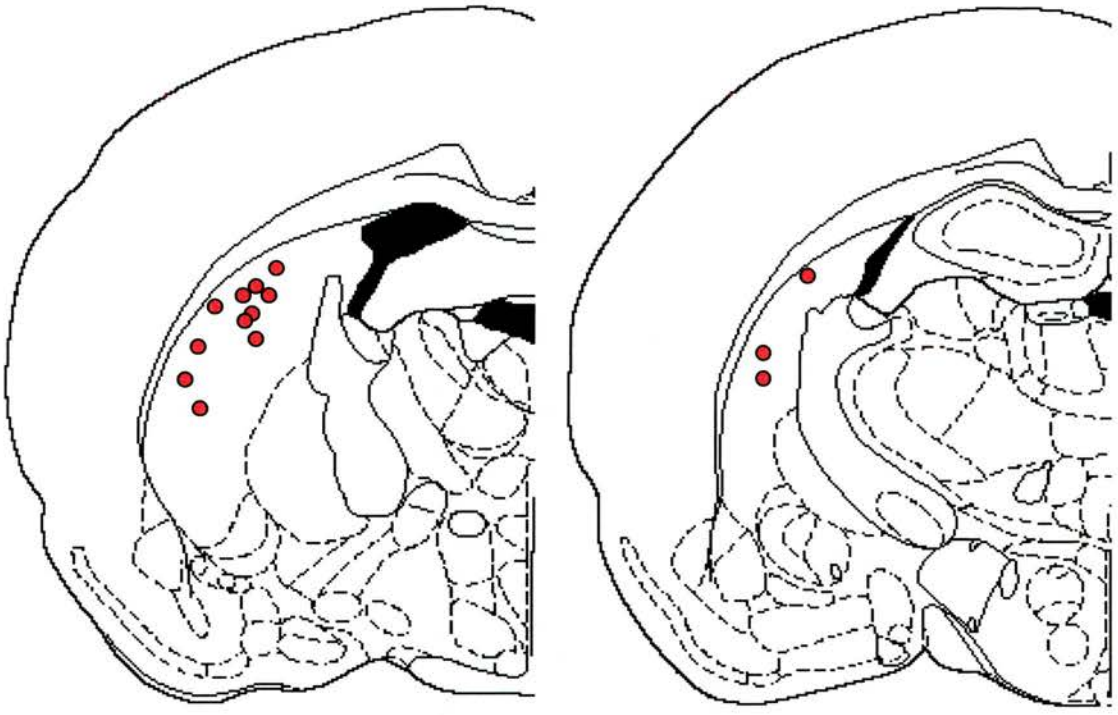

Bregma -1.3 mm

Bregma -2.12 mm

Figure 5. 4. Distribution of striatal neurones from which records were obtained.

Schematic figures of the rat brain (modified from Paxinos and Watson 1996) with the location of striatal neurones from which data was obtained (●). The approximate positions of the striatal neurones from which records were obtained were extrapolated using pontamine sky blue markings.

Variable	Control	6-OHDA lesioned
No. of cells	135	14
Input resistance (MΩ)	9.925 ± 5.830	25.685 ± 8.360 *
Average membrane potential (mV)	-79.340 ± 7.930	-73.49 ± 6.82 *
Average up-state membrane potential (mV)	-68.752 ± 1.250	-63.230 ± 1.359 *
Average down-state membrane potential (mV)	-85.014 ± 1.269	-80.300 ± 1.690 *

Table 5. 1. Comparison of electrophysiological properties of striatal neurones from control and lesioned animals.

Mean values (± standard deviation) of striatal cells in normal and lesioned animals. The asterisks (*) denotes a statistically significant difference (two tailed t-test, $p < 0.05$).

Striatal cells responded to both stimuli with an EPSP followed by a period of inactivity. In most cases the stimuli did not produce action potentials as they were delivered sub-threshold, however in some cases, when the stimuli were delivered when the cell was in the up state, single action potentials were fired. Representative responses of 2 spiny projection striatal neurones are shown in Figure 5.5. A comparison of the responses of striatal cells to both forms of stimulation is summarised below (Table 5.2).

The latency of the response to both stimuli is significantly different but is not correlated with the depth of the cell (Pearson correlation coefficient = 0.1.23, $p > 0.05$). The amplitude of EPSPs was significantly correlated to the state of the cell when the stimulus was delivered (Pearson correlation coefficient = -0.507, $p < 0.05$). Regression analysis showed that up to quarter of the variability (R-SQ = 25.7%) was due to the membrane potential (Fig. 5.6). In contrast to control animals there was no

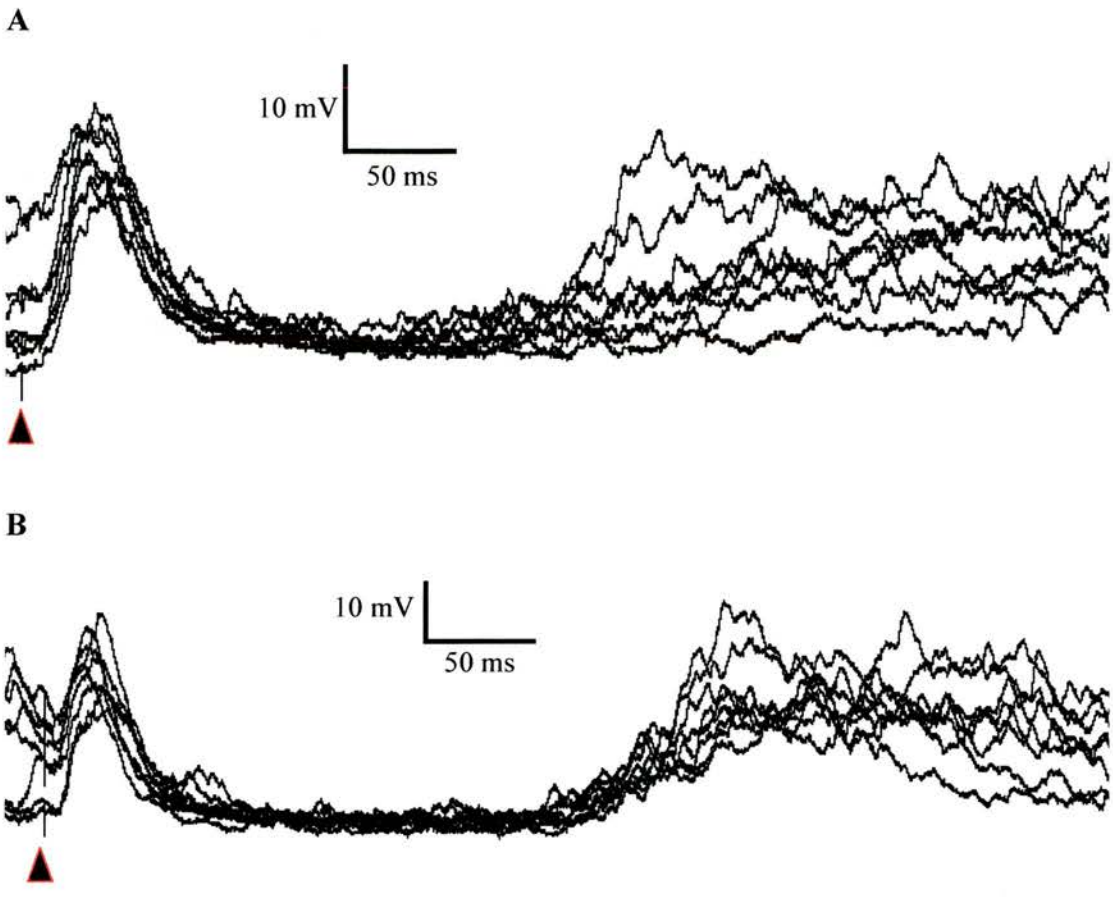

Figure 5. 5. Intracellular traces of responding striatal neurones.

The traces illustrate the typical behaviour of striatal neurones to whisker pad and contralateral cortical stimulation. **A** and **B** were obtained from the same cell recorded at a depth of 4066 μm which was stimulated subthreshold for action potential generation. Traces represent an overlay of 8 sweeps and the values reported are the average value for the cell. The stimulus artefacts are marked by a (▲).

A Response of the neurone to whisker pad stimulation. The cell responded with an EPSP with an average latency of 9.20 ms. The rise time was 16.99 ms and the peak amplitude was 15.31 mV. The duration of the EPSP was 75.50 ms followed by a period of inactivity that lasted 165 ms. Following that, the membrane potential was seen to switch to the upstate. Note that the stimulus was delivered when the cell's membrane potential was either depolarised or hyperpolarized.

B Response of the neurone to contralateral cortical stimulation. The cell responded with an EPSP with an average latency of 8.70 ms. The rise time was 18.41 ms and the peak amplitude was 12.23 mV. The duration of the EPSP was 66 ms followed by a period of inactivity that lasted 139.00 ms after which the cell switched to the up state.

Figure 5. 6. Influence of the membrane potential on the size of the EPSP in striatal neurones.

To illustrate the influence of the membrane potential on the size of the peak amplitude, two traces from concurrent sweeps of the response of a cell to whisker pad stimulation are shown (**A**, **B**). This cell has responses which are typical of striatal neurones. The average peak amplitude of this cell is 29.36 mV and has a range 12.37 mV to 40.19 mV. The stimulus artefact is marked by a (▲).

A shows the response of the cell in its depolarised state. The cell had a membrane potential of –62 mV when the stimulus arrived and gave rise to a peak amplitude of 15.31 mV. There is a pronounced hyperpolarisation following the EPSP.

B The next sweep following **A** shows the cell in a hyperpolarised membrane potential (-95.1 mV) when the stimulus arrived. The cell responded with a short latency EPSP with a peak amplitude of 40.10 mV followed by a slow return of membrane potential to it hyperpolarised potential.

C A scatter plot of the membrane potential of the all striatal cells when the stimulus arrived versus the peak amplitude of the response to the stimulus shows that that the two variables are negatively correlated (Pearson correlation coefficient = -0.507, $p < 0.05$). Thus the more hyperpolarised the cell was the bigger was its response to the stimuli.

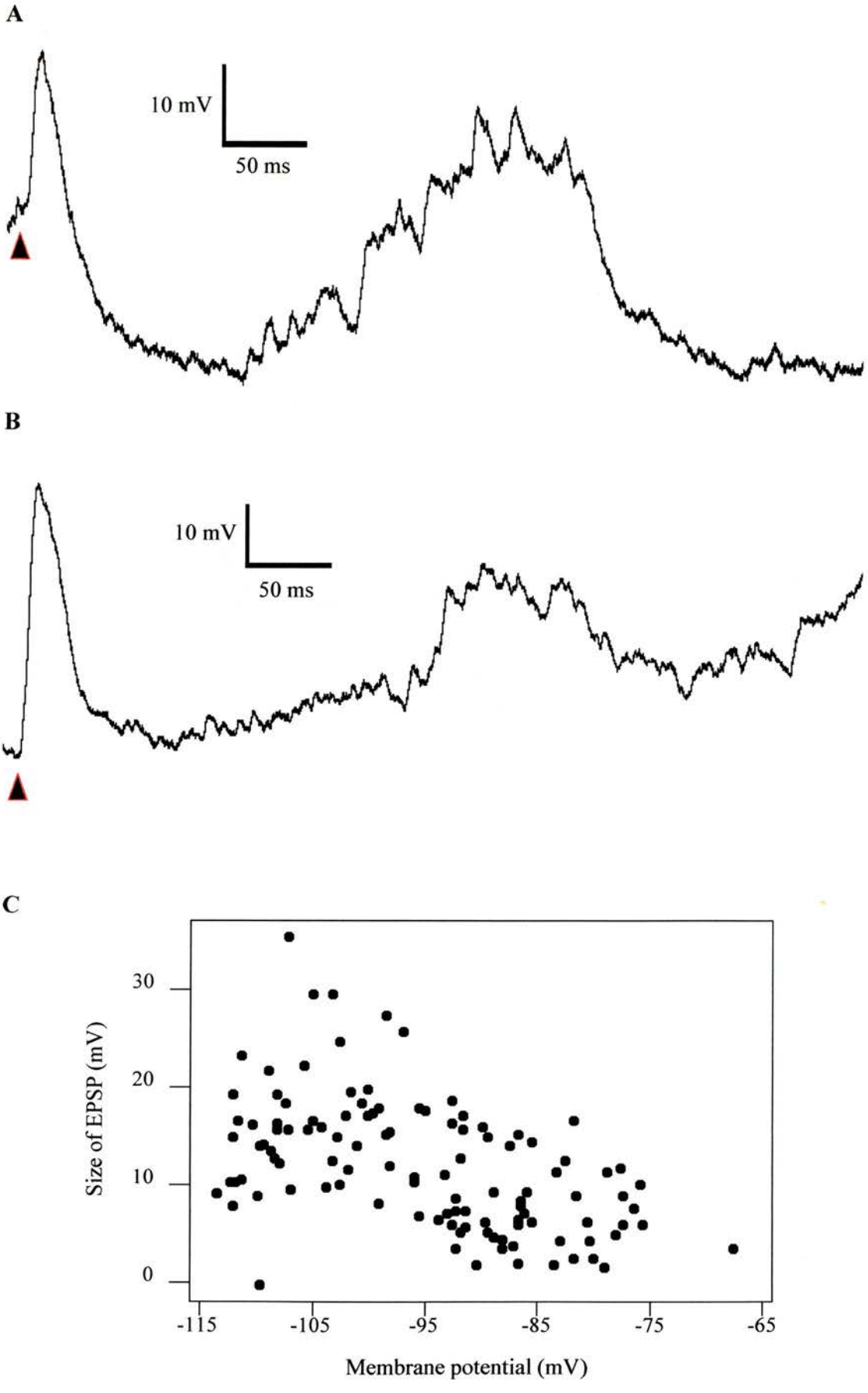
A
10 mV
50 ms
B
10 mV
50 ms
C
Size of EPSP (mV)
30
20
10
0
-115
-105
-95
-85
-75
-65
Membrane potential (mV)

significant difference in the rise times in the response of the cell to whisker pad and contralateral cortical stimulation (ANOVA, $p > 0.05$) (Fig. 5.7).

	Stimulus type	
Variables	Whisker pad	Contralateral cortex
Latency (ms)	11.130 ± 1.073	8.247 ± 2.760 *
Rise time (ms)	18.340 ± 4.820	23.156 ± 4.964
Peak amplitude (mV)	11.589 + 5.389	10.698 ± 6.378
Duration of EPSP	104.881 ± 80.480	135.945 ± 84.296

Table 5. 2. Summary of electrophysiological characteristics of striatal cells to electrical whisker pad and contralateral cortical stimulation.

Mean values (± standard deviation) of responding striatal cells to electrical whisker pad and contralateral cortical stimulation. The asterisk (*) denotes a statistically significant difference (ANOVA, $p < 0.05$).

Comparing the response characteristics of striatal neurones in control and lesioned animals, the only differences were observed in the response of striatal neurones in lesioned animals to whisker pad stimulation. There was a significant difference in the latency and rise time of the EPSP in response to whisker pad stimulation (Table 5.3). The response to contralateral cortical stimulation was not altered for any of the variables in lesioned animals (Table 5.4).

Figure 5. 7. Whisker pad vs. contralateral cortical stimulation in striatal neurones.

A B illustrate the rise time of the EPSP in response to whisker pad (**A**) and contralateral cortical stimulation (**B**). The striatal cell recorded at a depth of 3029 μm was stimulated subthreshold to prevent the firing of action potentials. The stimulus artefact is marked by a (▲). The traces displayed are the averaged responses to 8 sweeps.

A The rise time to whisker pad stimulation was 15.32 ± 3.86 ms. The rising phase (◄—►) of the EPSP was gradual with a number of inflections before maximal response to the stimulus was reached.

B Contralateral cortical stimulation gave rise to an EPSP with a rise time of 19.914 ± 3.10 ms. The rising phase (◄—►) of the EPSP is similar to the EPSP in response to whisker pad stimulation.

C D illustrate the response of another cortical neurone stimulated supratheshold so as to generate action potential firing. The traces consist of 4 overlaid traces.

C Action potential firing in response to whisker pad stimulation was variable in response and latency to spike initiation was differed from sweep to sweep. Compared with spike initiation in control animals (see Figure 3.19), there is greater variability in 6-OHDA animals.

D Spike initiation latency was variable in response to contralateral cortical stimulation. There is a similar jitter in the traces when compared to **C**.

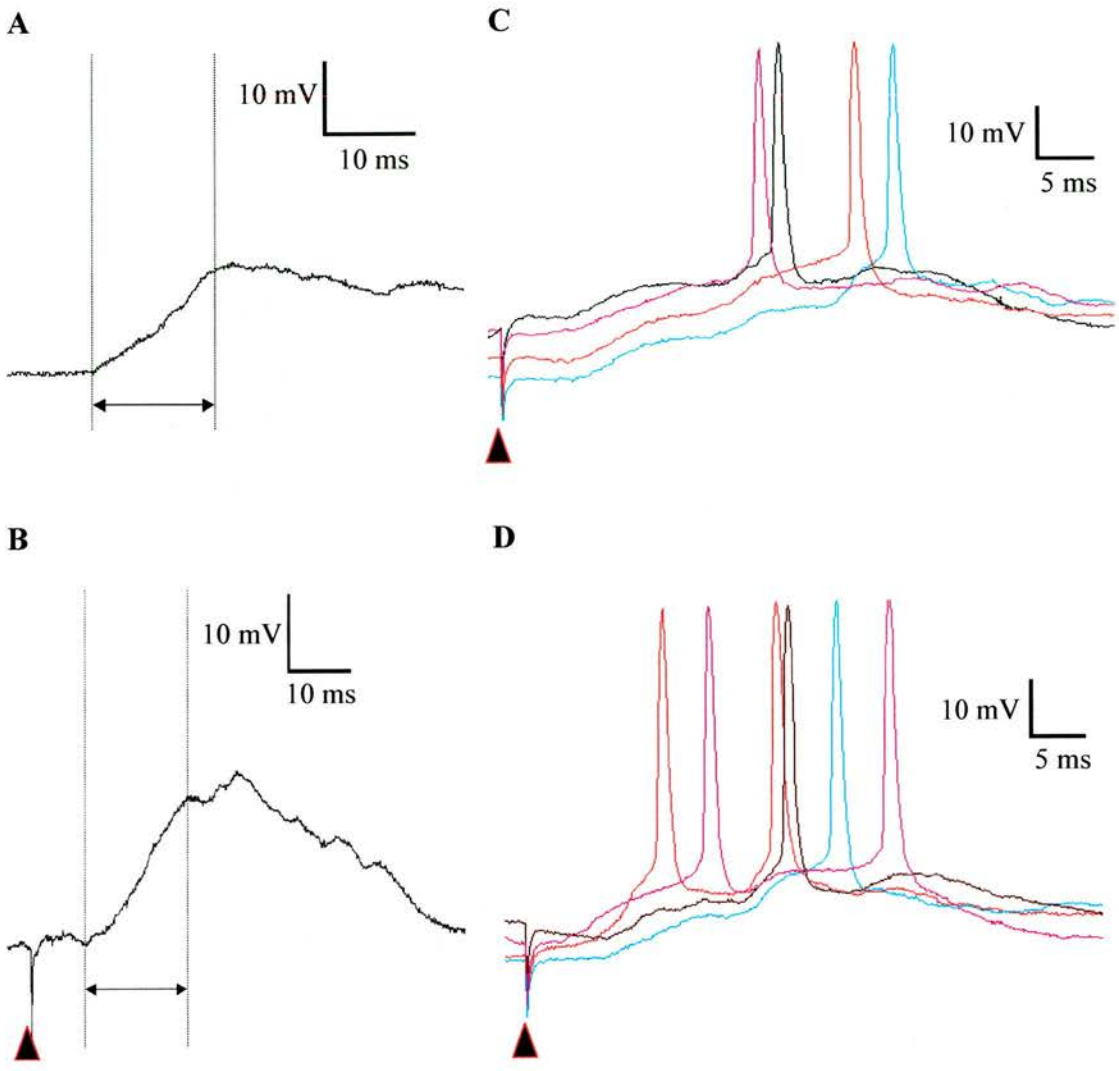
A
10 mV
10 ms
C
10 mV
5 ms
B
10 mV
10 ms
D
10 mV
5 ms

Variables	Whisker pad			
	Control	n	6-OHDA lesioned	n
Latency (ms)	9.856 ± 3.357	138	11.130 ± 1.073 *	14
Rise Time (ms)	8.929 ± 9.660	138	18.340 ± 4.820 *	14
Peak amplitude (mV)	12.880 ± 6.115	138	11.589 + 5.389	14
Duration of EPSP	102.200 ± 72.100	25	104.881 ± 80.480	14

Table 5. 3. Comparison of the of electrophysiological characteristics of striatal cells in control and 6-OHDA lesioned animals to electrical whisker pad stimulation.

Mean values (± standard deviation) of responding striatal cells to electrical whisker pad. The asterisks (*) denote a statistically significant difference (two tailed t-test, $p < 0.05$).

Variables	Contralateral cortex			
	Control	n	6-OHDA lesioned	n
Latency (ms)	9.095 ± 2.731	136	8.247 ± 2.760	14
Rise Time (ms)	20.374 ± 6.254	136	23.156 ± 4.964	14
Peak amplitude (mV)	10.795 ± 4.075	136	10.698 ± 6.378	14
Duration of EPSP	113.700 ± 72.300	25	135.945 ± 84.296	14

Table 5. 4. Comparison of the electrophysiological characteristics of striatal cells in control and 6-OHDA lesioned animals to contralateral cortical stimulation.

Mean values (± standard deviation) of responding striatal cells to contralateral cortical stimulation. None of the variables are statistically different (two tailed t-test, $p > 0.05$).

5.3.4) Pairing protocols in 6-OHDA treated animals

Ten of the 14 striatal cells described above were subjected to the 4 pairing protocols. Due to small number of cells, the separation of traces into an up and down state (based on when the first stimuli was delivered) was not attempted and the results using all the traces are presented below.

5.3.4.1) Protocol 1: Whisker pad – contralateral cortex interaction (Fig. 5.8)

Electrical stimulation of the whisker pad inhibited the response of striatal cells up to the time interval of 20 ms (ANOVA, $p < 0.05$, Tukey's pairwise comparisons) after which the response of the cell to the second stimulus (contralateral cortical stimulation) was similar to the response of striatal neurones to single contralateral cortical stimulation. The response to contralateral cortical stimulation was not significantly different from single contralateral cortical stimulation in terms of latency and rise time for all the time intervals (ANOVA, $p > 0.05$, Tukey's pairwise comparisons). When the contralateral cortical stimulus was delivered at time intervals that were within the EPSP in response to the whisker pad stimulation (10 to 120 ms), the duration of the EPSP in response to whisker pad stimulation was measured and found not to be significantly different (ANOVA, $p > 0.05$, Tukey's pairwise comparisons).

5.3.4.2) Protocol 2: Contralateral cortex – whisker pad interaction (Fig. 5.9)

Contralateral cortical stimulation inhibited the response of striatal cells to whisker pad stimulation up to time intervals of 200 ms (ANOVA, $p < 0.05$, Tukey's pairwise comparisons). The response to whisker pad stimulation was not significantly different from single whisker pad stimulation in terms of latency and rise time for all

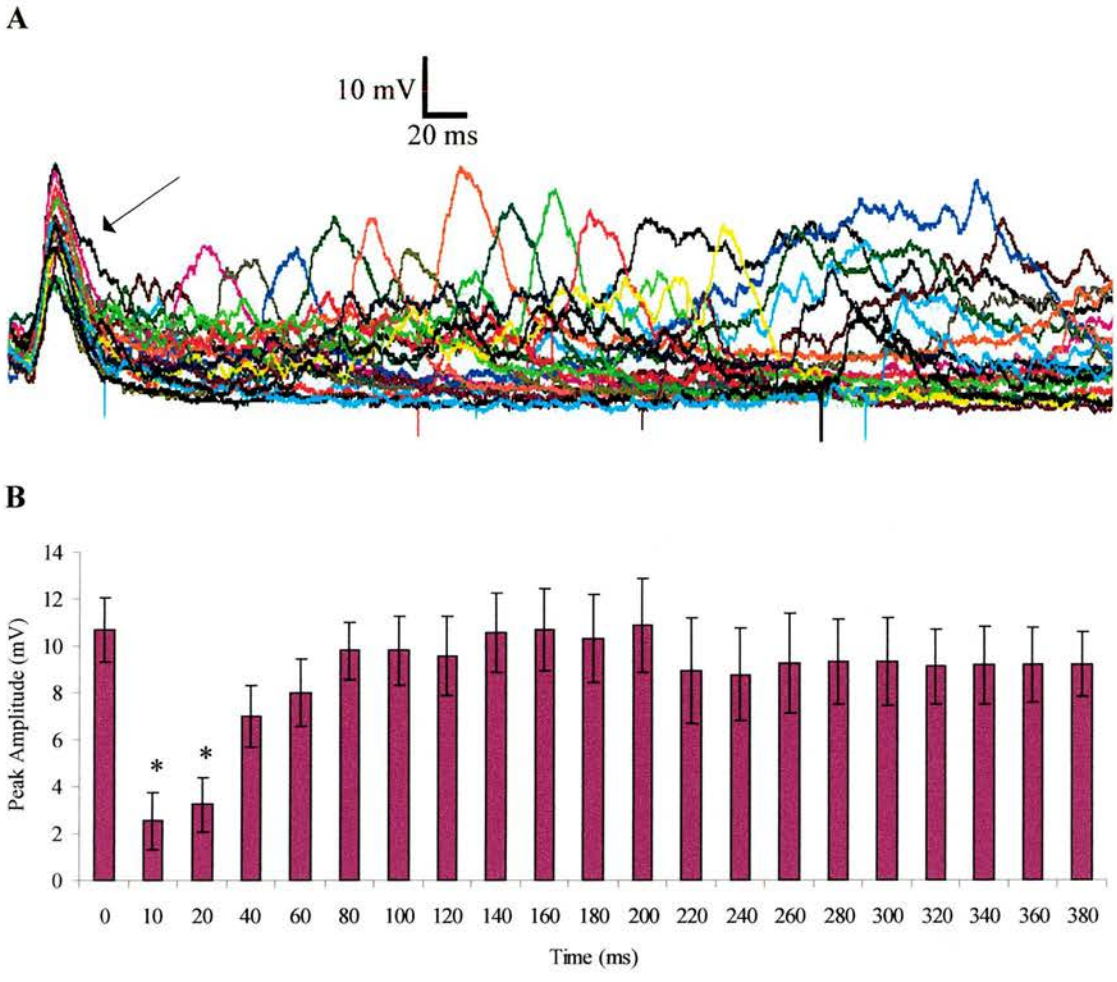

Figure 5. 8. Response of striatal neurones to whisker pad-contralateral cortex pairing protocol.

A The overlaid traces illustrate the response of a striatal neurone to the whisker pad-contralateral cortex pairing protocol. Each coloured trace is the averaged response of the cell to the second stimulus at a particular time interval. The response of the cell to a single contralateral cortical stimulation is marked with a **black** arrow. The traces show that the response of the striatal neurone to the second stimulus is inhibited up to the time intervals of 20 ms after which the cell is able to the respond to the contralateral cortical stimulus with a peak amplitude that is similar to when the contralateral cortex is stimulated on its own.

B The histogram illustrates the averaged peak amplitude of the EPSPs in response to the contralateral cortical stimuli across all time intervals for all 10 striatal neurones. The values are the average ± standard error. Time 0 is the average peak amplitude of the response to single contralateral cortical stimulation. The asterisks (*) denote a significant difference from the value at time 0 (ANOVA, $p < 0.05$, Tukey's pairwise comparisons).

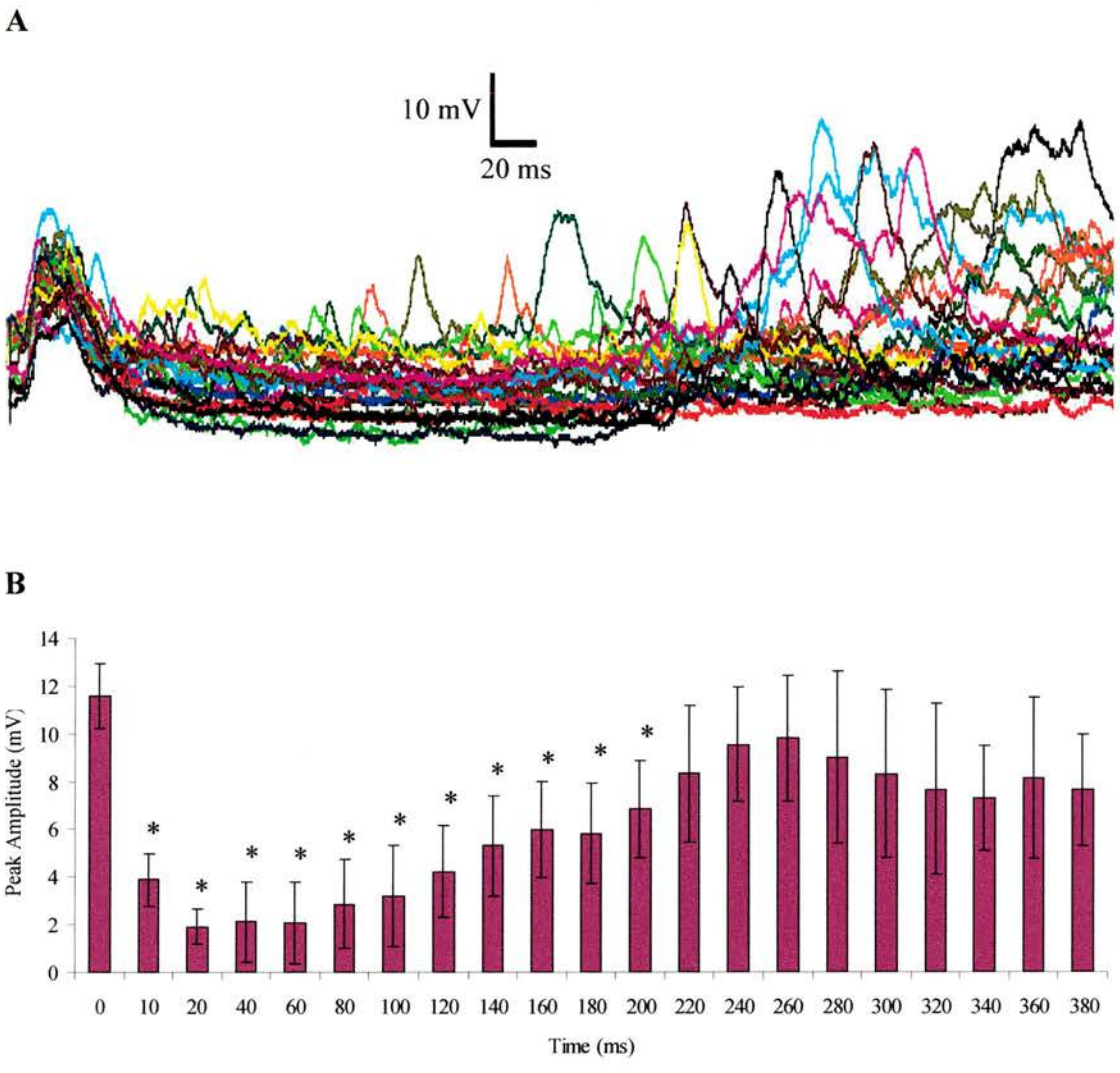

Figure 5. 9. Response of striatal neurones to contralateral cortex-whisker pad pairing protocol.

A The overlaid traces illustrate the response of a striatal neurone to the contralateral cortex-whisker pad pairing protocol. Each coloured trace is the averaged response of the cell to the second stimulus at a particular time interval. The traces show that the response of the striatal neurone to the second stimulus is inhibited up to time intervals of 200 ms after which the cell is able to the respond to the whisker pad stimulus with a peak amplitude that is similar to when the whisker pad is stimulated on its own.
B The histogram illustrates the averaged peak amplitude of the EPSPs in response to the whisker pad stimuli across all time intervals for all 10 striatal neurones. The values are the average ± standard error. Time 0 is the average peak amplitude of the response to single whisker pad stimulation. The asterisks (*) denote a significant difference from the value at time 0 (ANOVA, $p < 0.05$, Tukey's pairwise comparisons).

the time intervals (ANOVA, $p > 0.05$, Tukey's pairwise comparisons). When the whisker pad stimulus was delivered at time intervals that were within the EPSP in response to the contralateral cortical stimulation (10 to 140 ms), the duration of the EPSP in response to contralateral cortical stimulation was measured and found not to be significantly different (ANOVA, $p > 0.05$, Tukey's pairwise comparisons).

5.3.4.3) Protocol 3: Whisker pad – whisker pad interaction (Fig. 5.10)

Stimulation of the whisker pad lead to a prolonged inhibition, during which the response of the striatal cells to the second whisker stimulus was significantly decreased. The cells did not recover from the inhibition when the stimuli were delivered 380 ms apart. In two animals after all 4 pairing protocols were completed, the second whisker pad stimulus was manually moved out to 600 ms using the D-100 digitimer (Fig. 5.11) and at these time intervals a significant response to the whisker pad stimulus was not observed. In these two cells when the second stimulus was at 600 ms, the first whisker pad stimulus was switched off to check if the cell was still able to respond and an EPSP due to the stimulus at 600 ms was observed (Fig. 5.11). At no time interval was the duration of the EPSP significantly altered from values when the whisker pad was stimulated on it own (ANOVA, $p > 0.05$, Tukey's pairwise comparisons).

5.3.4.4) Protocol 4: Contralateral cortex – contralateral cortex interaction (Fig. 5.12)

Stimulation of the contralateral cortex inhibited the response of striatal cells to a second contralateral cortical stimulation. The cells were able to respond to the second contralateral stimuli when it was delivered at least 160 ms after the initial stimulus. The response to contralateral cortical stimulation was not significantly different from

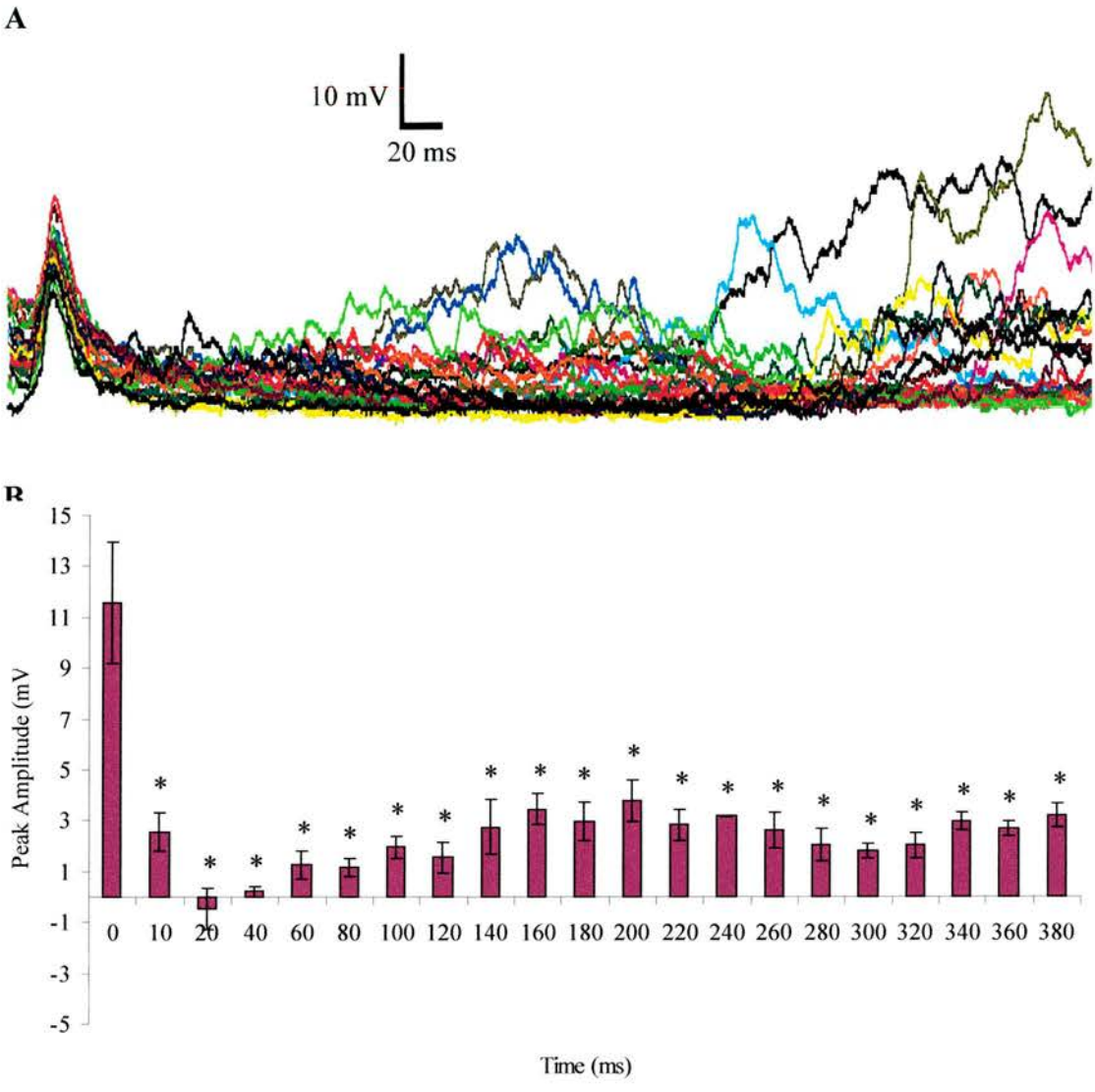

Figure 5. 10. Response of striatal neurones to whisker pad-whisker pad pairing protocol.

A The overlaid traces illustrate the response of a striatal neurone to the whisker pad-whisker pad pairing protocol. Each coloured trace is the averaged response of the cell to the second stimulus at a particular time interval. The traces show that the response of the striatal neurone to the second stimulus is inhibited beyond 380 ms. The cell is unable to respond to the second whisker pad stimulus with a peak amplitude that is similar to when the whisker pad is stimulated on its own.

B The histogram illustrates the averaged peak amplitude of the EPSPs in response to the whisker pad stimuli across all time intervals for all 10 striatal neurones. The values are the average ± standard error. Time 0 is the average peak amplitude of the response to single whisker pad stimulation. The asterisks (*) denote a significant difference from the value at time 0 (ANOVA, $p < 0.05$, Tukey's pairwise comparisons).

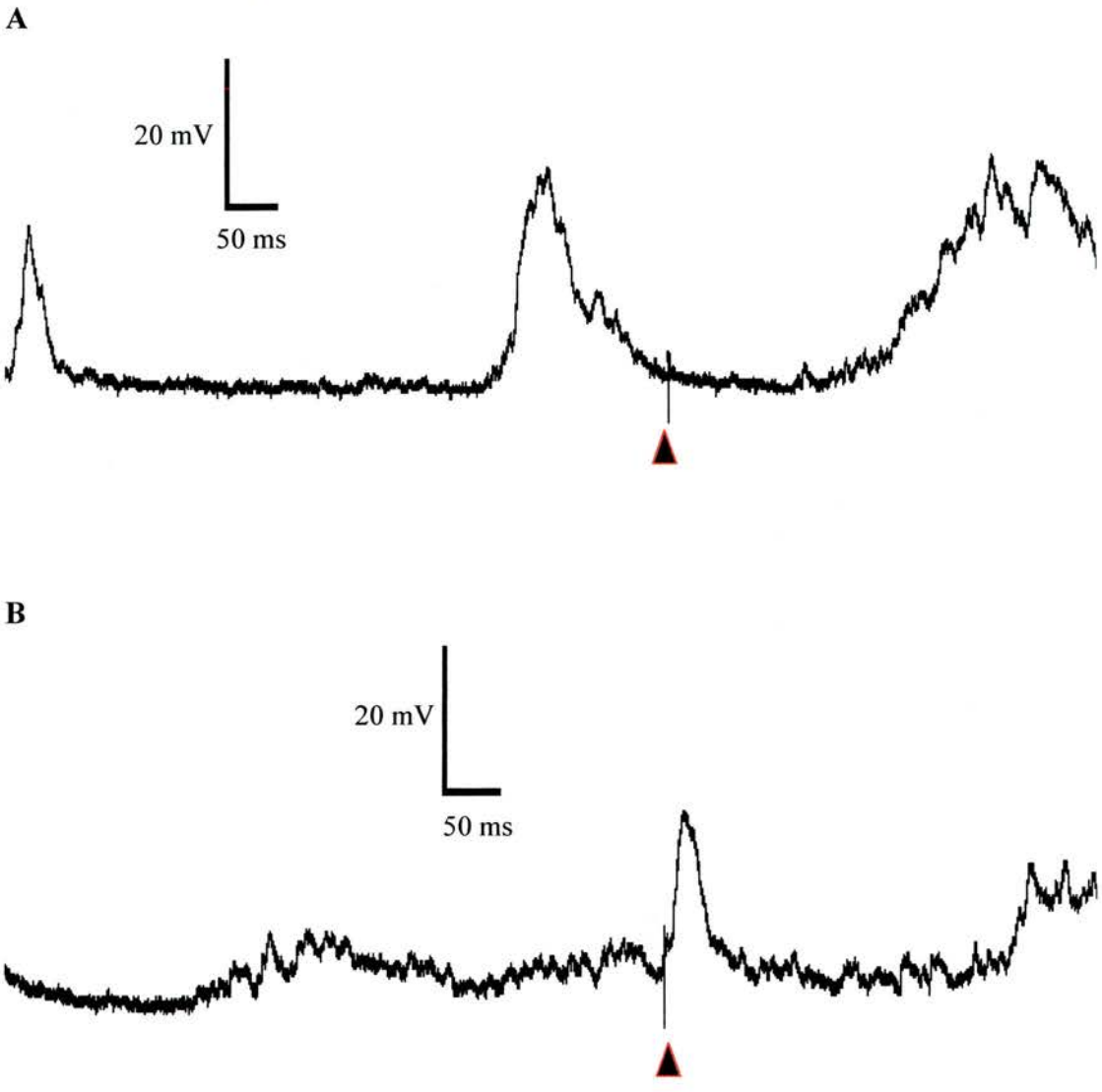

Figure 5. 11. Prolonged inhibition of striatal neurones to dual whisker pad stimuli.

A The trace is the averaged response (of 8 sweeps) of a striatal cell to two whisker pad stimuli delivered 600 ms apart. The response of the cell to the first stimulus elicited a response with an average peak amplitude of 20.3 mV, while the average response to the second stimulus was 0.23 mV.

B Following the delivery of the second stimulus at a time interval of 600 ms, the first stimulus was switched off. The trace is the averaged response (of 8 sweeps) of the striatal cell, and has an amplitude of 15.69 mV, strongly suggesting that the lack of response is a result of inhibition as a result of the first stimulus.

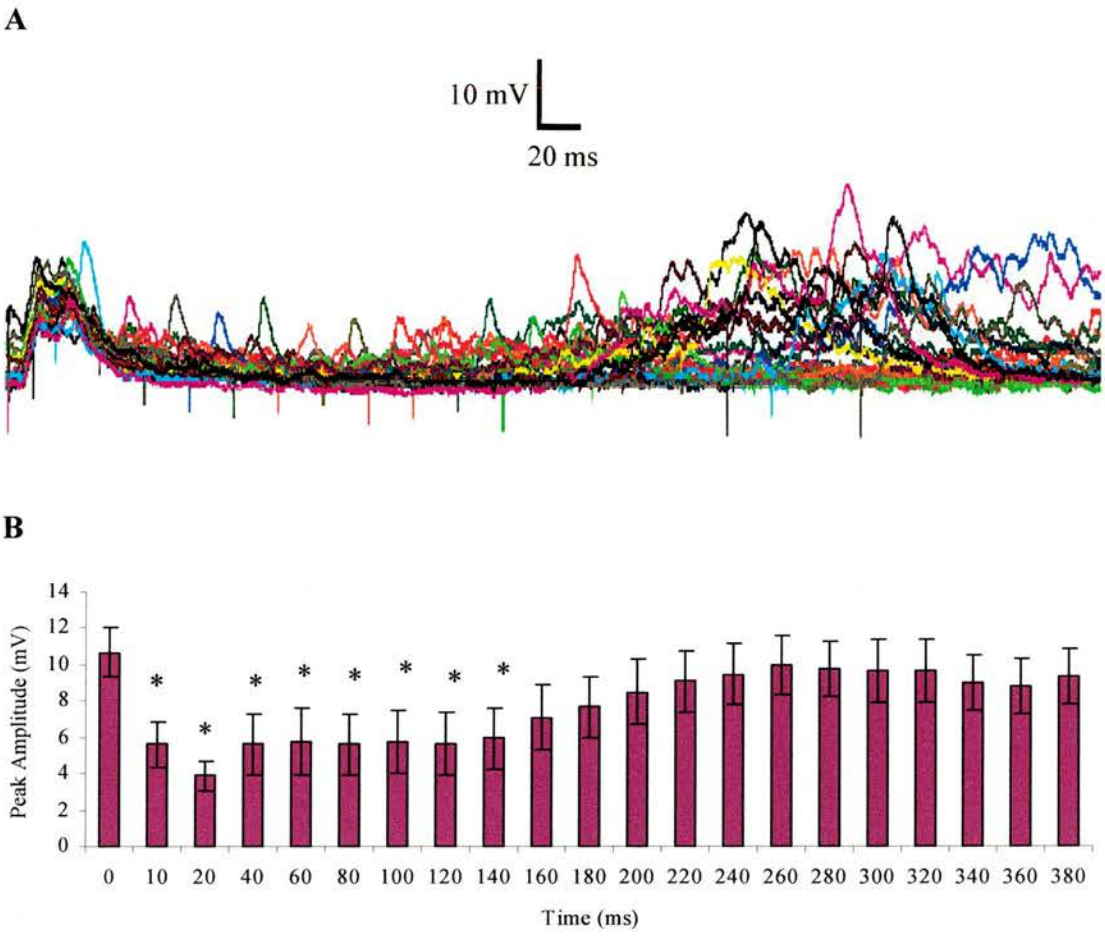

Figure 5. 12. Response of striatal neurones to contralateral cortex-contralateral cortex pairing protocol.

A The overlaid traces illustrate the response of a striatal neurone to the contralateral cortex-contralateral cortex pairing protocol. Each coloured trace is the averaged response of the cell to the second stimulus at a particular time interval. The traces show that the response of the striatal neurone to the second stimulus is inhibited up to time intervals of 140 ms after which the cell is able to the respond to the second contralateral cortical stimulus with a peak amplitude that is similar to when the contralateral cortex is stimulated on its own.

B The histogram illustrates the averaged peak amplitude of the EPSPs in response to the contralateral cortical stimuli across all time intervals for all 10 striatal neurones. The values are the average ± standard error. Time 0 is the average peak amplitude of the response to single contralateral cortical stimulation. The asterisks (*) denote a significant difference from the value at time 0 (ANOVA, $p < 0.05$, Tukey's pairwise comparisons).

single contralateral cortical stimulation in terms of latency and rise time for all the time intervals (ANOVA, $p>0.05$, Tukey's pairwise comparisons). At no time interval was the duration of the EPSP significantly altered from values when the contralateral cortex was stimulated on it own (ANOVA, $p > 0.05$, Tukey's pairwise comparisons).

A summary of the main findings of the pairing protocols are shown in Table 5.5. The period of inhibition refers to the last time interval at which the response to the second stimulus was affected by the preceding stimulus.

Protocol	Period of inhibition (ms)
1: whisker pad – contralateral cortex	20
2: contralateral cortex – whisker pad	200
3: whisker pad – whisker pad	> 380
4: contralateral cortex – contralateral cortex	140

Table 5. 5. Summary of the results of the pairing protocols in striatal neurones.

5.3.5) Pairing protocol in control vs. 6-OHDA animals

The effects of the loss of dopamine on interaction of the two stimuli at the level of a single striatal cells were investigated by comparing the average peak amplitude of the response from both groups of animals (control and lesion) for all 82 time intervals (2 single stimulus and 20 times intervals for each pairing protocol). Due to the unbalanced nature of the data (25 cells vs. 10 cells), a 2 way analysis of variance (ANOVA) could not be used and a general liner model (GLM) was employed. There was a significant difference between the 2 groups and between the 82 treatments (GLM, $p < 0.05$). Individual time points, between control and lesioned animals were compared using a t-test. To compare the period of inhibition, the length of inhibition

for each cell was calculated and the mean values, between control and lesioned animals were compared.

5.3.5.1) Protocol 1: Whisker pad – contralateral cortex interaction

There is a significant difference in the peak response of the two groups at the time interval of 10 ms. At this time point, the summation of EPSPs observed in control animals is no longer present in the lesioned animals subjected to the same pairing protocol (two tailed t-test, $p < 0.05$). While in control animals the first whisker pad stimulus inhibited the response of the cell to a second contralateral cortical stimulus up to time intervals of 40 ms, in 6-OHDA animals the inhibition was seen up to time intervals of 20 ms. This difference in the period of inhibition could have occurred by chance and was not significantly different between the two groups (two tailed t-test, $p > 0.05$).

5.3.5.2) Protocol 2: Contralateral cortex – whisker pad interaction

The summation of EPSP seen at a time interval of 10 ms in control animals is not seen in lesioned animals and correspondingly the peak response between the two groups at a time interval of 10 ms is significantly different (two tailed t-test, $p < 0.05$). The period of inhibition is increased from 78.40 ± 12.80 ms in control animals to 202.00 ± 11.35 ms in lesioned animals and this difference is statistically different (two tailed t-test, $p < 0.05$).

5.3.5.3) Protocol 3: Whisker pad – whisker pad interaction

There is a significant difference in the peak response of the two groups at a time interval of 10 ms. At this time point, the summation of EPSPs observed in control animals is no longer present in the lesioned animals subjected to the same pairing

protocol (two tailed t-test, $p < 0.05$). While in control animals the first whisker pad stimulus inhibited the response of the cell to a second whisker pad stimulus up to time intervals of 261.60 ± 13.78 ms, in 6-OHDA animals the inhibition was seen to exceed time intervals of 380 ms (two tailed t-test, $p < 0.05$).

5.3.5.4) Protocol 4: Contralateral cortex – contralateral cortex interaction

No significant difference was observed at time a time interval of 10 ms between the two stimuli (two tailed t-test, $p > 0.05$). The period of inhibition is significantly increased from 62.56 ± 14.23 ms to 142.00 ± 11.35 ms when comparing control and lesioned animals.

A summary of the comparisons of the pairing protocols in control and lesioned animals is shown in Table 5.6. The period of inhibition refers to the last time interval at which the response to the second stimulus was affected by the preceding stimulus. The values are the group mean, and are the average of the individual values calculated for each cell. The summation of EPSPs if observed and the time intervals at which they occurred are also highlighted.

	Summation of EPSP		Period of inhibition (ms)	
Pairing protocol	Control	Lesion	Control	Lesion
1: whisker pad – contralateral cortex	Yes (10 ms)	No	41.60 ± 17.24	28.00 ± 10.32
2: contralateral cortex – whisker pad	Yes (10 ms)	No	78.40 ± 12.80	202.00 ± 11.35 *
3: whisker pad – whisker pad	Yes (10 ms)	No	261.60 ± 13.78	> 380.00 *
4: contralateral cortex – contralateral cortex	No	No	62.56 ± 14.23	142.00 ± 11.35 *

Table 5. 6. Summary of the results of the pairing protocols in striatal neurones.

Mean values of striatal neurones to pairing protocols from control and 6-OHDA animals. The asterisk (*) denotes a statistically significant difference (Two tailed t-test, $p < 0.05$).

5.4) Discussion

5.4.1) Striatal neurones

As in control animals, 6-OHDA lesioned animals displayed spontaneous shifts in membrane potential. However in contrast to control animals, the cells tended to have a less hyperpolarised membrane potential in both the up and down states. Although no quantitative analysis was carried out, striatal neurones from dopamine depleted animals also fired more action potentials when they were in the up state. This increased spontaneous activity fits in with previous *in vitro* and *in vivo* observations, where striatal neurones from 6-OHDA lesioned rats have an increased firing rate (Arbuthnott, 1974; Schultz, 1982; Nisenbaum et al., 1986; Kish et al., 1999; Chen et al., 2001; Tseng et al., 2001). This increased corticostriatal transmission is likely to involve both pre and postsynaptic mechanisms. D_2 receptors on cortical afferent terminals have been shown to reduce cortically elicited EPSPs in up to 60% of striatal neurones (Brown and Arbuthnott, 1983; O'Donnell and Grace, 1994; Sesack et al., 1994; Levine et al., 1996) and the inactivation of this mechanism could account for the more depolarised up states. Postsynaptically, dopamine modulates the activity of a wide variety of channels and currents. Inwardly rectifying potassium channels, which keep the resting potential of striatal neurones near the potassium equilibrium are activated by dopamine and their reduced activity in dopamine depleted animals, might account for the more depolarised membrane potential of striatal neurones (Pacheco-Cano et al., 1996; Waszczak et al., 1998). L-type calcium channels are also affected by dopamine and D_2 agonists have been shown to suppress these currents (Hernandez-Lopez et al., 2000). As blockers of these L-type channels reduce glutamate induced bursts, the lack of activation of these currents in chronic

nigrostriatal lesioned animals may also account for the increased corticostriatal transmission (Cooper and White, 2000). This increased excitability of striatal neurones is thought in part to account for the switching in the firing pattern of SNpr neurones from tonic regular firing in normal animals to rhythmic burst firing in lesioned animals (Pan and Walters, 1988; MacLeod et al., 1990; Murer et al., 1997; Ni et al., 2000). Tseng and colleagues postulated that due to their low firing probability, striatal neurones in control animals were unable to transmit slow cortical rhythms to the target nuclei unlike striatal neurones in lesioned animals that as a result of their increased excitability were able to transmit the cortical rhythm downstream to both the GP and the SNpr (Tseng et al., 2001).

All striatal neurones that responded to both forms of stimulation were found in areas of striatum that receive a projection from the barrel cortex (Alloway et al., 1998; Alloway et al., 1999; Wright et al., 1999). Previous experiments looking at striatal organisation, have shown that both striatal and pallidal neurones change their responsiveness following dopamine depletion (Filion et al., 1988; Schneider, 1991; Rothblat and Schneider, 1993, 1995; Cho et al., 2002). This reorganisation of the striatum is thought to reflect the loss of spines, synapses, and possible corticostriatal sprouting following 6-OHDA treatment (Ingham et al., 1989, 1993; Ingham et al., 1998; Cho et al., 2002). The increase in the rise time of EPSPs in response to whisker pad stimulation in lesioned animals also suggests that there has been some striatal reorganisation. The increase in rise time is only seen following whisker pad stimulation while the response to contralateral cortical stimulation remains unchanged. One possibility is that only a subset of synapses are modified following the loss of dopamine. The thin fibres that make up the bilaterally projecting diffuse

pathway, and are activated by contralateral cortical stimulation preferentially contact striatal neurones that are part of the indirect pathway (Chapter 2). The thick fibres of the ipsilateral topographic pathway that are activated by whisker pad stimulation, contact both pathways with equal frequency (Chapter 2). The electrophysiological data would suggest that, as the responses to stimulation of the diffuse are unchanged after dopamine depletion, the topographic pathway is preferentially affected by the loss of dopamine. The effect of dopamine could therefore be targeted at either the presynaptic or postsynaptic structure. Fibres that make up the diffuse pathway are collaterals of corticocortical fibres while those that are part of the topographic pathway are collaterals of corticofugal pathways (Wright et al., 1999; Wright et al., 2001). There is a possibility that the dopamine exerts a greater influence on one of these subsets of corticostriatal pathways and spines that contact collaterals of corticofugal fibres are preferentially lost over spines synapsing with collaterals of corticocortical fibres.

If the actions of dopamine are dependent on the postsynaptic targets of the two corticostriatal pathways, it would seem that the directly projecting striatal neurones are affected by the loss of dopamine due to the fact that the response as a result of activation of the diffuse pathway (which contacts D_1 negative structures preferentially) is unaltered in the lesioned animal. Preliminary work looking at the type of target made by corticostriatal pathways before and after the loss of dopamine, shows a decrease (though not significant) in the number of D_1 immunonegative targets (Ingham et al., 2002). This taken together with increase seen in the number of complex synapses (Ingham et al., 1998) would suggest that the topographic pathway is preserved and it is the diffuse pathways that is affected. However there are two

factors that have to be considered. The topographic pathways also contacts D_1 immunonegative structures and these might be the synapses that are lost. Also the increase in the number of complex synapses observed in dopamine depleted animals (Ingham et al., 1998) might not necessarily represent a preservation of these synapses, but could indicate a remodelling of simple asymmetric synapses into complex synapses in the dopamine depleted animal. As yet, there is no anatomical evidence for the specific action of dopamine on certain pre or post-synaptic targets. Thus there is a need to look at the postsynaptic targets of both corticostriatal pathways following 6-OHDA treatment which would shed light on the actions of dopamine.

From the data obtained from the pairing protocols, one of the main differences observed between lesioned and normal animals was the summation of EPSPs observed when the two stimuli were delivered 10 ms apart, in 3 of the 4 pairing protocols (i.e. whisker pad-contralateral cortex, contralateral cortex-whisker pad, whisker pad-whisker pad). The only pairing protocol, where summation was not observed in control animals, was dual stimulation of the contralateral cortex. Thus one possible explanation is that whisker pad stimulation in lesioned animals gives rise to a response that is similar to when the contralateral cortex is stimulated. While the response to single stimuli and the lack of summation of EPSPs would support this hypothesis, there are other possible explanations.

The results from the interaction study done in Chapter 3 would suggest that the lack of summation of EPSPs seen in the dual contralateral cortical stimulation is likely to be the inability of cortical cells providing the input to closely timed stimuli and not due to the inability of the striatal neurone to respond to the second

contralateral cortical stimulus. While there is a possibility that 6-OHDA treatment changes the response of cortical neurones to the two stimuli and the interaction of both pathways, the scarcity of dopaminergic projections to this area of cortex would suggest that the changes are striatal in origin (Berger et al., 1991).

The lack of summation seen in lesioned animals might be due to changes in the activation of the D1 receptor. Application of dopamine in anaesthetised preparations and in freely moving animals has shown dopamine to have a facilitatory effect on glutamatergic transmission in striatal neurones, and is likely to be mediated by the D_1 receptor (Hu and Wang, 1988; Kiyatkin and Rebec, 1996; Gonon, 1997; Hu and White, 1997). D1 receptor activation enhances NMDA receptor mediated currents and L-type calcium currents and the lack of activation of these currents is likely to decrease the excitability of striatal neurones (Surmeier et al., 1995; Cepeda et al., 1998; Cepeda and Levine, 1998).

If the lack of summation was only due to the fact that whisker pad stimulation elicited responses that were similar to the contralateral cortically derived responses, it would follow on that the length of inhibition would be the same for all the four pairing protocols and should be similar in duration to the length of inhibition following dual contralateral cortical stimulation in control animals. However this was not the case, and for all four pairing protocols the time at which the response to the second stimulus was not significantly affected by the first was significantly increased. The effect of dopamine on inhibitory synaptic transmission has not been widely examined and there might be numerous factors behind the increased inhibition that was observed.

In the previous chapter (Chapter 4), the inhibition seen in the striatal cells to the second stimulus, was thought to reflect the inability of cortical neurones to the respond to the second stimulus as a result of recurrent inhibition. However the increased inhibition seen following 6-OHDA might be due to striatal mediated mechanisms. While it is believed that IPSPs generated in striatal neurones is mainly due to GABAergic interneurones, recent studies have shown that the dense recurrent axon collaterals of spiny neurones are functional but weak (Jaeger et al., 1994; Czubayko and Plenz, 2002; Tunstall et al., 2002). This synaptic transmission is dynamic and modifiable and GABAergic synapses in the striatum show synaptic augmentation and paired pulse depression (Radnikow et al., 1997; Fitzpatrick et al., 2001; Czubayko and Plenz, 2002; Tunstall et al., 2002). This lateral inhibition among striatal cells has been used in computational models of learning, where the increased inhibition after dopamine depletion has been proposed to result in Parkinsonian motor dysfunction (Wickens et al., 1995). As yet, there is little physiological evidence for the modification of the inhibitory interactions between striatal neurones following dopamine depletion, and Nicola and associates, report that dopamine has little effect on IPSPs evoked by electrical stimulation of the striatum (Nicola and Malenka, 1998).

Another manner in which dopamine might modulate inhibitory synaptic transmission in the striatum, is by directly acting on striatal interneurones. Due to the low occurrence of interneurones, and the difficulty in identifying these cells (based on cell size), there are few reports on the effects of dopamine on this class of cells. The exception is the large aspiny cholinergic interneurones. These cells express a high level of D_2 and D5 receptor mRNA (Le Moine et al., 1990; Bergson et al., 1995;

Yan et al., 1997; Yan and Surmeier, 1997) and the activation of these receptors, suppresses acetylcholine release. Striatal parvalbumin (PV) interneurones express the mRNA for D_2 receptors (Lenz et al., 1994) and are known to receive a dopaminergic innervation (Kubota et al., 1987). Dopamine is able to directly activate these GABAergic interneurons and the loss of dopamine is thought to result in a reduced activity of these cells (Bracci et al., 2002). Dopamine depletion results in a reduced activation of PV interneurons after corticostriatal stimulation, measured by c-fos expression (Trevitt and Marshall, 2002). While PV interneurons are present only in low numbers (3-5% of total striatal cell population) in the striatum, they are the main source of inhibition are able to strongly modulate the activity of striatal output neurones (Bolam and Bennett, 1995; Koos and Tepper, 1999). Parvalbumin interneurons display neurotensin immunoreactivity following dopamine depletion and are thought to account for some of the changes seen in the acute stages of nigral denervation (Schuller and Marshall, 2000; Martorana et al., 2001). While the reduced activity of the GABAergic interneurons would aid in the explanation of the increased activity of the striatal neurones, it goes against the observation of the increased inhibition in pairing protocols, following dopamine depletion.

Another important consideration is the effect of dopamine on the pallidostriatal pathway. Cells in the GP, can be divided into two groups based on their targets. Approximately two thirds of pallidal cells, send projections to down stream targets, which includes the STN, EP and SNpr (Kita, 1994; Rajakumar et al., 1994b). These cells contain the calcium binding protein, parvalbumin (Kita, 1994; Rajakumar et al., 1994b). The remainder one third of cells, which do not contain PV, express preproenkephalin mRNA and make up the pallidostriatal projection (Hoover and

Marshall, 1999, 2002). Both these classes of pallidal neurones are differentially regulated by dopamine (Ruskin and Marshall, 1997). Infusion of sulpiride, a D_2 antagonist into the GP, induces Fos expression in only PV immunonegative pallidal cells (Billings and Marshall, 2003). These pallidostriatal neurones have been shown to selectively innervate striatal interneurons, and there is a possibility that the loss of dopamine can influence striatal output cells, by modulating the behaviour of striatal interneurons via the pallidostriatal pathway (Bevan et al., 1998). Nigral 6-OHDA lesions increase the level of GAD_{67} mRNA, which is the precursor for the enzyme in GABA synthesis, in pallidal neurones (Herrero et al., 1996). This increase is believed to be mediated by subthalamic projections to the GP, as there is an increased activity in STN neurones following dopamine depletion. The PV immunonegative pallidal neurones, that project back to the striatum have a significant increase in GAD_{67} mRNA expression compared to PV immunopositive neurones, indicating that the pallidostriatal pathway is preferentially affected by the loss of dopamine (Marshall and Billings, 2002). The increased activity in this pathway, would increase the inhibition of interneurons, resulting in the dishinhibition of striatal output neurones. The increased activation of the pallidostriatal pathway following 6-OHDA would therefore not account for the increased inhibition, observed in the pairing protocols and the reason for the increase in inhibition is still unclear.

5.5) Conclusions

The removal of the dopaminergic projection from the nigra, affects the responses of striatal neurones to stimulation of the two corticostriatal pathways originating from the barrel cortex. Stimulation of both pathways results in EPSPs or action potentials when suprathreshold stimuli are delivered. The response of striatal neurones to

whisker pad stimulation is altered, with an increase in the rise time of the EPSP, while the response to contralateral cortical stimuli is unaltered suggesting that the effects of dopamine depletion are targeted at specific pre or post synaptic targets. Dopamine depletion might preferentially target either collaterals of corticofugal pathways or striatal cells that are D_1 immunopositive. The interaction of the two pathways at the level of a single striatal cell are also altered. The summation of EPSPs observed when stimuli were delivered 10 ms apart in control animals, are no longer seen and could once again reflect the preferential loss of a subset of synapses. The period of inhibition seen in the pairing protocols is significantly lengthened in the lesioned animals, indicating that dopamine modulates inhibitory synaptic mechanisms in the striatum.

CHAPTER 6

SYNAPTIC CONVERGENCE OF MOTOR AND SENSORY CORTICAL AFFERENTS ONTO GABAergic INTERNEURONES IN THE RAT STRIATUM

6.1) Introduction

6.1.1) Information processing in the basal ganglia

There is growing evidence that the functions of the basal ganglia involve not only strictly sensorimotor aspects of movement programming, but also conditional aspects of planning movements, programme selection, motor memory and retrieval (Graybiel, 1990). Thus a major role of these nuclei is to integrate sensorimotor, associative and limbic information in the production of context-dependent behaviours (Graybiel, 1990, 1995). Work done in the 1970s postulated that the basal ganglia acted as 'funnels' for information of diverse origin (Alexander et al., 1986; Goldman-Rakic and Selemon, 1990). Subsequent experimental data led to the concept of parallel processing, where the basal ganglia was thought to be composed of 'loops', with each 'loop' getting information from a specific cortical area (Alexander et al., 1986; Alexander et al., 1990; Alexander and Crutcher, 1990; DeLong, 1990; Goldman-Rakic and Selemon, 1990). Anatomical and physiological data suggest that cortical information that is transmitted to the basal ganglia via the corticostriatal projection, is channelled into parallel functional circuits (somatic, motor and limbic) that remain segregated at each level of the basal ganglia-thalamo-cortical loops (Alexander et al., 1986; Alexander et al., 1990; Alexander and Crutcher, 1990; DeLong, 1990; Hoover and Strick, 1993; Parent and Hazrati, 1995; Middleton and Strick, 2000). However this view of "segregated information channelling" has been disputed (Francois et al., 1987; Chevalier and Deniau, 1990; Graybiel and Kimura, 1995) and computational principles such as convergence, recurrence and competition have emerged as common themes of information processing (Beiser et al., 1997). The main reason for this is that in addition to the

organisation underlying 'parallel processing', the anatomical substrate also exists for integration of diverse information within and between these loops (Nauta and Domesick, 1984; Francois et al., 1987; Flaherty and Graybiel, 1991; Parthasarathy et al., 1992; Flaherty and Graybiel, 1993, 1995; Graybiel, 1995; Beiser et al., 1997; Maurin et al., 1999; Haber et al., 2000; Hoffer and Alloway, 2001; Kolomiets et al., 2001). Indeed, anatomical connects that may underlie the integration of diverse information within the basal ganglia at the synaptic level have been identified (Somogyi et al., 1981b; Bevan et al., 1996; Bevan et al., 1997). For instance, neurones of the substantia nigra pars compacta that project to the dorsal (motor and associative) striatum receive synaptic input from neurones located in the ventral (limbic pole) striatum (Somogyi et al., 1981b). Similarly, although there is a clear topography of the caudal projections of the ventral pallidum (limbic pole) and the globus pallidus (motor and associative), there are regions of overlap in which synaptic convergence of the two divisions of the pallidal complex occurs at the single cell level (Bevan et al., 1996; Bevan et al., 1997).

6.1.2) Organisational principles of the corticostriatal projections

The striatum is the largest nucleus in the basal ganglia and has a representation of each area of the cortex (McGeorge and Faull, 1989). It was discovered that acetylcholinesterase (AChE) poor striosomes (patches) receive inputs from neural structures affiliated with the limbic system, while the AChE rich extrastriosomal matrix receive cortical inputs most directly related to sensorimotor processing (Graybiel and Ragsdale, 1978; Ragsdale and Graybiel, 1981; Gerfen, 1984; Donoghue and Herkenham, 1986). A study in the rat demonstrated that the striosome-matrix compartmentalisation was found to be specific to the cortical layer

of origin rather than the cortical area of origin (Gerfen, 1989). Patches receive input from deep layer V cortical areas while the matrix areas receive input from superficial layer V and III. However, this laminar organisation of cortical projections to patch and matrix compartments has not been widely studied in species such as cats and primates. The output of the two compartments were also found to be segregated. Neurones in the matrix project to the globus pallidus and substantia nigra pars reticulata, and neurones of the striosomes project to the substantia nigra pars compacta and adjacent regions (Gerfen, 1984; Gerfen, 1985; Jimenez-Castellanos and Graybiel, 1989). Matrix directed corticostriatal projections were also found to innervate discrete zones within the matrix rather than having a homogenous innervation pattern (Selemon and Goldman-Rakic, 1985; Alexander et al., 1986; Fotuhi et al., 1989; Flaherty and Graybiel, 1993). The axonal arborisations from the cortex terminates in small clusters and these matrisomes reflect striatal modules (Flaherty and Graybiel, 1991; Graybiel et al., 1993; Parthasarathy and Graybiel, 1997). This topographic projection pattern as well as the striosome matrix compartmentalisation has lead to speculations that parallel processing is a central feature of information processing in corticostriatal circuits. However, evidence that convergence of corticostriatal inputs does occur has been found.

The cortex projects to the striatum in a distributed, discontinuous and topographic manner (Goldman and Nauta, 1977; Selemon and Goldman-Rakic, 1985). These corticostriatal projections overlap, interdigitate and remain separate (Malach and Graybiel, 1986; Gerfen, 1989; Flaherty and Graybiel, 1991; Parthasarathy et al., 1992; Flaherty and Graybiel, 1993, 1995; Brown et al., 1998; Takada et al., 1998; Hoffer and Alloway, 2001). This interdigitaion and overlap

would allow significant integration of diverse cortical information. Several anatomical experiments suggested that corticostriatal projections from distinct cortical regions are more likely to have overlapping terminal areas if the cortical areas are reciprocally connected (Yeterian and Van Hoesen, 1978; Pearson et al., 1983; Flaherty and Graybiel, 1993). However, this was found not to be a general principle of organisation of the corticostriatal projections by Selemon and associates (Selemon and Goldman-Rakic, 1985). They showed that the overlap of cortical terminal fields did not always represent corticocortical connectivity but could signify a functional interaction between distinct cortical centres. Projections from two functionally related but distinct cortical regions (primary motor cortex and primary somatosensory cortex) converge in the striatum (Flaherty and Graybiel, 1993; Hoffer and Alloway, 2001). Using electrophysiology to guide tracer deposition, Flaherty and associates showed that there were large areas of overlap in the ipsilateral corticostriatal projections. The overlapping areas included both matrisomes and striosomes and were somatotopically restricted (Flaherty and Graybiel, 1993). This anatomical data strongly suggests that integration of information from various cortical regions can occur within the striatum. Electrophysiological studies have shown striatal neurones to respond to both somatosensory and auditory stimuli in rats (Chudler et al., 1995) and tactile, auditory and visual stimuli in cats (Wilson et al., 1983c; Schneider, 1991). However, in these experiments, the stimuli were applied locally and it cannot be concluded that the convergence and integration of different sensory information observed, were a direct result of converging cortical input onto a single striatal cell. Thus both anatomical and electrophysiological data strongly imply that convergence of inputs from diverse cortical regions might occur in the

striatum. However, this form of integration has not been shown at the level of a single striatal cell.

6.1.3) Cortical input to the striatum

The main target of corticostriatal terminals are the spines of the GABAergic medium sized densely spiny projection neurones, which in rodents make up 90-95% of the neuronal population (Kemp and Powell, 1971; Frotscher et al., 1981; Somogyi et al., 1981a; Dube et al., 1988; Smith et al., 1994). This cortical input shapes the activity of these neurones(Wilson et al., 1983a; Wilson, 1995; Wilson and Kawaguchi, 1996; Mahon et al., 2001). The second major target of the cortical input to the striatum is the class of GABAergic interneurone(Lapper et al., 1992; Bennett and Bolam, 1994; Koos and Tepper, 1999).

6.1.4) GABAergic parvalbumin interneurones

Immunohistochemical studies using antibodies against glutamic acid decarboxylase (GAD); the synthetic enzyme for GABA, revealed that a small subset of striatal neurones stained strongly for the antibody (Ribak et al., 1979; Bolam et al., 1985). These cells are also more effective at taking up exogenous GABA and are specifically labelled in experiments that employ the uptake of radioactively labelled GABA (Bolam et al., 1983). Examination of these structures at the light and electron microscope levels revealed that they were interneurones (Bolam et al., 1983; Bolam et al., 1985). Work done by Gerfen and associates (Gerfen et al., 1985) demonstrated that these neurones stained positively for parvalbumin (PV), a calcium binding protein. This allowed convenient and reliable detection of this group of GABAergic interneurones by conventional immunocytochemical methods (Cowan et al., 1990).

Anatomical and physiological data has demonstrated that PV-positive GABAergic interneurones receive a direct input from the cortex (Kita et al., 1990; Lapper et al., 1992; Bennett and Bolam, 1994) and are easily excitable by cortical stimulation (Kawaguchi, 1993; Plenz and Aertsen, 1996a, b; Parthasarathy and Graybiel, 1997). These interneurones are connected by both gap junctions and chemical synapses (Kita et al., 1990; Chang and Kita, 1992; Bennett and Bolam, 1994; Koos and Tepper, 1999). The major target of these interneurones are the soma and the proximal dendritic regions of spiny projection neurones (Kita, 1993; Bennett and Bolam, 1994). Parvalbumin interneurones form basket-like synaptic arborisations on medium spiny projection neurones and an individual interneurone may contact hundreds of spiny neurones (Cowan et al., 1990; Kita et al., 1990; Kita, 1993; Bennett and Bolam, 1994). These fast spiking interneurones fire at high rates with little adaptation to spike frequency (Kawaguchi, 1993; Plenz and Kitai, 1998) and generate inhibitory synaptic potentials that are able to curb the generation of action potentials in spiny projection neurones (Koos and Tepper, 1999). It has been proposed that fast spiking parvalbumin interneurones provide a feed-forward inhibition of medium spiny neurones following cortical stimulation and thus regulate excitability or threshold of the output cells (Pennartz and Kitai, 1991; Jaeger et al., 1994; Plenz and Kitai, 1998). In addition these PV cells are selectively innervated by a subclass of neurones of the globus pallidus (Bevan et al., 1998). Thus GP neurones which are activated directly by the cortex or via activation of the STN pathway (Ryan and Clark, 1991; Kita, 1992) are able to modulate the effect of cortical excitation on parvalbumin interneurones.

6.1.5) Aim

The aim of the present study was to determine whether projections from distinct but functionally related cortical areas converge at the level of the single striatal neurone. In view of the critical position of PV-positive, GABA interneurones in the circuitry of the striatum, and the fact that they are activated more easily, and over a larger volume of striatum following cortical stimulation, than are spiny neurones (Parthasarathy and Graybiel, 1997), cortical input to these neurones was analysed. Thus, the aim was to determine whether cortical afferents from the primary motor cortex (M1) and primary somatosensory cortex (S1) converge on PV-positive interneurones and to provide insight into the pattern of innervation of these neurones by individual cortical axons.

6.2) Experimental Procedures

6.2.1) Preparation of animals

Twelve adult female Wistar rats (200-350g, Charles River, Margate, Kent, UK) were used in the present study. They were maintained on a 12 hour light/12 hour dark cycle with free access to food and water. Procedures involving animals were carried out in strict accordance with the Animals (Scientific Procedures) Act, 1986. They were anaesthetised by intraperitoneal injections of a mixture of fentanyl/fluanisone (0.135 mg/ml and 10 mg/ml respectively; Hypnorm®; Janssen-Cilag Ltd., High Wycombe, U.K.) and midazolam (5 mg/ml; Hypnovel®; Roche Products Ltd., Welwyn Garden City, U.K.)(1:1:2 with sterile water: 2.7 ml/kg). Stable levels of anaesthesia were maintained throughout the surgical procedure to ensure the absence of a foot withdrawal reflex. The rats were placed in a stereotaxic frame and the head was secured in the frame via ear and tooth bars. The scalp was cut from the anterior of the Bregma to the base of the skull and the overlaying tissue was pulled back and clamped. The skull surface was cleaned to reveal the Bregma and the midline. Rostrocaudal and mediolateral co-ordinates for the placement of the neuronal tracers were calculated using Bregma as a reference point and the stereotaxic co-ordinates were derived from the atlas of Paxinos and Watson (Paxinos and Watson, 1986). Access to the brain was made using a hand held dental drill and bit to create a burr hole. Drilling was stopped to leave a thin transparent layer of bone overlaying the brain. This was gently picked away to prevent accidental damage to the cortical surface and to ensure that no skull fragments entered the cortex. A hole was created in the dura to expose the cortical surface to facilitate the passage of the glass micropipette and to prevent the tip becoming blocked by adhering dura. The animals

received unilateral deposits of *Phaseolus vulgaris* Leucoagglutinin (PHAL; 2.5% in 0.1M phosphate buffer; PB pH 8.0: Vector Labs, Peterborough, UK) in the primary motor cortex (M1) and Biotinylated dextran amine (BDA; 10% in 0.9% NaCl; Molecular Probes, U.S.A.) in the primary somatosensory cortex (S1). In some cases the delivery of the 2 tracers was reversed i.e. PHAL in S1 and BDA in M1. The anterograde tracers were delivered by iontophoresis via glass micropipettes of 7-50μm internal tip diameter using a pulsed (7s on/7s off) positive cathodal current (7-10μA) over 10-15 min. Three deposits were made in each region. After careful withdrawal of the micropipette, the skin overlying the exposed cranium was drawn together and sutured. The animals were kept warm and after recovery from the anaesthetic they were returned to their home cages.

6.2.2) Perfusion fixation

Following a survival time of 5-8 days, the rats were deeply anaesthetised with sodium pentobarbital (Sagatal, 200 mg/kg; Rhône Mérieux, Tallaght, Dublin) and perfused transcardially with 50-100 mls of phosphate buffered saline (PBS, 0.1M pH 7.4) followed by 300 mls of 0.1%-.0.2% glutaraldehyde and 3% paraformaldehyde in 0.1M PB. Some animals were post-perfused with approximately 100 ml of PBS. Following fixation, the brain was removed from the skull and stored in PBS at 4°C prior to further processing. Coronal sections including tracer injection sites, and the thalamus as well as the transport sites in the striatum were cut on a vibrating microtome at 70 μm. All sections were washed several times in PBS.

6.2.3) Preparation of tissue for light microscopy

6.2.3.1) Localisation of anterograde tracers

Sections of the injection sites, thalamus and striatum were incubated for 30 min in 0.3% Triton-X in PBS (PBST), followed by multiple washes in PBS and an incubation in 1% bovine serum albumin in PBS for 2 hours at room temperature (PBS-BSA). Injected and transported BDA was revealed by incubation overnight at room temperature in an avidin-biotin-peroxidase complex (ABC; 1:100 in PBST-BSA, Vector Labs, UK). Sections were washed and equilibrated in Tris buffer (0.05M, pH 7.6) for 5-10 min. BDA was visualised by reacting the sections in a solution containing diaminobenzidine (DAB, 25 mg/100 ml Tris buffer; Sigma, Dorset, UK) and 0.006% hydrogen peroxide for 10-15 min. The reaction was terminated by rinsing several times in Tris buffer. To reveal the injected and transported PHAL, sections were incubated in rabbit anti-PHAL (1:1000 in PBST-BSA, Vector Labs, UK) overnight at room temperature. After several washes in PBS, the sections were incubated in a solution of goat anti-rabbit immunoglobulin (IgG) (1:200 in PBST-BSA, Dako, UK) for 2 hours at room temperature followed by a 1 hour incubation in rabbit peroxidase-antiperoxidase (PAP) (1:100 in PBST-BSA, Dako, UK). The bound peroxidase was then revealed by equilibrating in Tris buffer (0.05M pH 8.0) for 5-10 min and then placing them in Tris buffer containing 0.025% DAB in the presence of nickel ions (nDAB) and 0.006% hydrogen peroxide for 10-15 min. The reaction was terminated by rinsing several times in Tris buffer. In some animals BDA was revealed with nDAB and PHAL with DAB. On completion of the immunostaining the sections containing the injection sites and thalamus were processed for light microscopy while striatal sections were further processed to reveal parvalbumin-positive neurones. Sections processed for light microscopy were mounted on gelatine-coated microscope slides, air dried overnight at room

temperature, rapidly dehydrated through a graded series of dilutions of acetone, and a coverslipped using XAM (Merck, UK) as the mounting medium.

6.2.3.2) Immunocytochemistry for parvalbumin

Parvalbumin-immunoreactive structures were revealed by incubation in mouse anti-PV (1:1000 in PBST-BSA, Swant, Bellinzona, Switzerland) for 24-36 hours at 4°C. After several washes in PBS, the sections were incubated in goat-antimouse IgG (1:200 in PBST-BSA, Jackson Immunoresearch, West Grove, PA, USA) for 2 hours at room temperature and mouse PAP (1:100, Dako, UK) for an hour at room temperature. Bound peroxidase was revealed using chromogen Vector SG for 5-15 min and processed for light microscopy as described above.

6.2.4) Preparation of tissue for electron microscopy

The striata of six animals were processed for electron microscopy. To increase the penetration of reagents sections were equilibrated in a cryoprotectant consisting of 25% (w/v) sucrose and 10% (v/v) glycerol in 0.05M phosphate buffer (pH 7.4) for a minimum of 2 hours. They were then freeze-thawed in isopentane (BDH, UK) and cooled in liquid nitrogen for up to 3 times. The sections were washed several times in PBS before the tracers and parvalbumin positive cells were revealed as described above. As these sections were processed for electron microscopy, Triton X-100 was omitted from the protocol. The labelled sections of the striatum were placed flat at the bottom of a petri dish and post fixed in 1% osmium tetroxide (Oxkem, UK), 5% βD-Glucose (BDH Labs, Poole, UK) in 0.1M PB at pH 7.4 for 60-70 min (Acsady et al., 1996). The sections were dehydrated through a graded series of dilutions of acetone (with 1% uranyl acetate in the 70% solution) and infiltrated with resin

overnight (Durcupan, Fluka Chemicals, UK). They were then mounted in resin on glass microscope slides and polymerised in a 60°C oven for 48 hours.

6.2.5) Analysis of material

All sections containing the sites of injection of the tracers were examined to ensure that they were correctly placed. The locations of the injection sites were also confirmed by analysis of sections of the thalamus for anterogradely and retrogradely labelled structures. Sections of the striatum from those animals in which the injections were correctly located were examined in the light microscope for the anterograde tracers and PV immunoreactivity. In some animals the anterograde labelling was plotted and recorded schematically. Particular attention was paid to regions of overlap of the two tracers. In these areas, PV-immunoreactive neuronal perikarya and emerging dendrites were examined at high magnification and the positions of anterogradely labelled terminals closely apposed to them was noted. In some cases PV-positive neurones and individual cortical axons were drawn with the aid of a drawing tube and photographed digitally.

In a semi-quantitative analysis, a single section of the striatum from each of three rats that were prepared for light microscopy (i.e. Triton X100 included in the incubations) was analysed at high magnification. The selected sections were those in which the region of overlap of the anterograde labelling from the two regions of the cortex was the most extensive. The location of each PV-positive perikaryon and emerging dendrites was noted. The proportion apposed by anterogradely labelled terminals derived from either region of the cortex was noted.

From the tissue that was processed for electron microscopy, 8 PV-immunoreactive neurones (from 4 animals) whose cell bodies and/or dendrites were

identified as being apposed by anterogradely labelled terminals from both regions of the cortex in the light microscope, were selected for further study. The cells were drawn and photographed at high magnification and examined by correlated light and electron microscopy. The coverslip overlying the tissue was removed using a razor blade. The area of interest was cut from the microscope slide and glued to the top of a blank cylinder of resin using cyanoacrylate glue. Serial ultrathin sections of 40-60 nm thickness were cut on a Reichert-Jung Ultracut E ultramicrotome (Leica) and collected on Pioloform-coated single slot copper grids. The ultrathin sections were then contrasted with lead citrate for 2-3 min and examined in a Philips CM 10 electron microscope.

6.3) Results

6.3.1) Light microscopic observations

6.3.1.1) Appearance of the reaction products

The anterogradely labelled and immunolabelled structures were visualised with different chromogens for the peroxidase reactions that were distinguishable at the light microscopic level. Structures visualised with DAB as the chromogen for the peroxidase reaction were characterised by the presence of the typical reddish-brown amorphous reaction product (Fig. 6.5) and those visualised with nDAB contained the typical blue-black reaction product (Fig. 6.5). Parvalbumin-immunoreactive structures were visualised using Vector SG as the chromogen and were characterised by the presence of a greyish blue reaction product that was less homogeneous than the DAB reaction products (Fig. 6.5). The use of osmium tetroxide solution supplemented with glucose maintained colour separation between different reaction products in the sections that were prepared for electron microscopy (Acsady et al., 1996)(Figs. 6.8A, D; 6.9A, D; 6.10A, D).

6.3.1.2) Injection sites

The location of the injection sites of the two anterograde tracers (PHAL and BDA) was confirmed by visualisation of the tracers in the M1 and S1 cortices (Fig. 6.1). In the majority of cases the deposits of the two tracers were clearly separated. They spanned most of the cortical laminae without inclusion of the underlying corpus callosum. In some cases there were retrogradely labelled neurones of S1 close to the M1 injection site. However these retrogradely labelled neurones were clearly separate from the filled neurones at the injection site.

Figure 6. 1. Injection sites.

A, B Schematic representation (modified from Paxinos and Watson 1996) of the sites of injection of PHAL in M1 (vertical hatching) and BDA in S1 (horizontal hatching) and the corresponding labelling in the thalamus in two animals used in the electron microscope analysis. The deposits of PHAL were confined to frontal cortex areas 1 and 3 (Fr1 and Fr3 respectively) with slight encroachment in area 2 (Fr2). In each animal, the thalamic labelling was confined to the ventrolateral nucleus of the thalamus. The BDA deposits were confined to parietal cortex, area 1 (Par 1) and labelling in the thalamus was confined to the lateral and medial aspects of the posterior nucleus. The numbers denote the position in millimetres with respect to Bregma (Paxinos and Watson, 1986). (AI – agranular insular cortex, Po – posterior thalamic group, VL - ventrolateral nucleus of thalamus; VM - ventromedial nucleus of thalamus; VPL – lateral aspect of ventroposterior nucleus of thalamus; VPM – medial aspect of ventroposterior nucleus of thalamus.)

C Deposit of BDA in S1 cortex visualised using nDAB giving rise to a bluish black reaction product. The injection spans most of the cortical layers with no involvement of the corpus callosum (CC) (NS – neostriatum). Scale bar 400 μm.

D Deposit of PHAL in M1 cortex visualised using DAB giving a brown reaction product. Scale bar 400 μm. Adjacent to the PHAL injection sites are retrogradely labelled BDA (nDAB) blue neurones (black arrows). These neurones are found in the upper layers of the cortex. The insert which is the same area in D at a higher magnification, shows that these retrogradely labelled cells are clearly separate from those of the PHAL deposit The asterisk (*) marks the same blood vessel in both pictures. Scale bar 165 μm

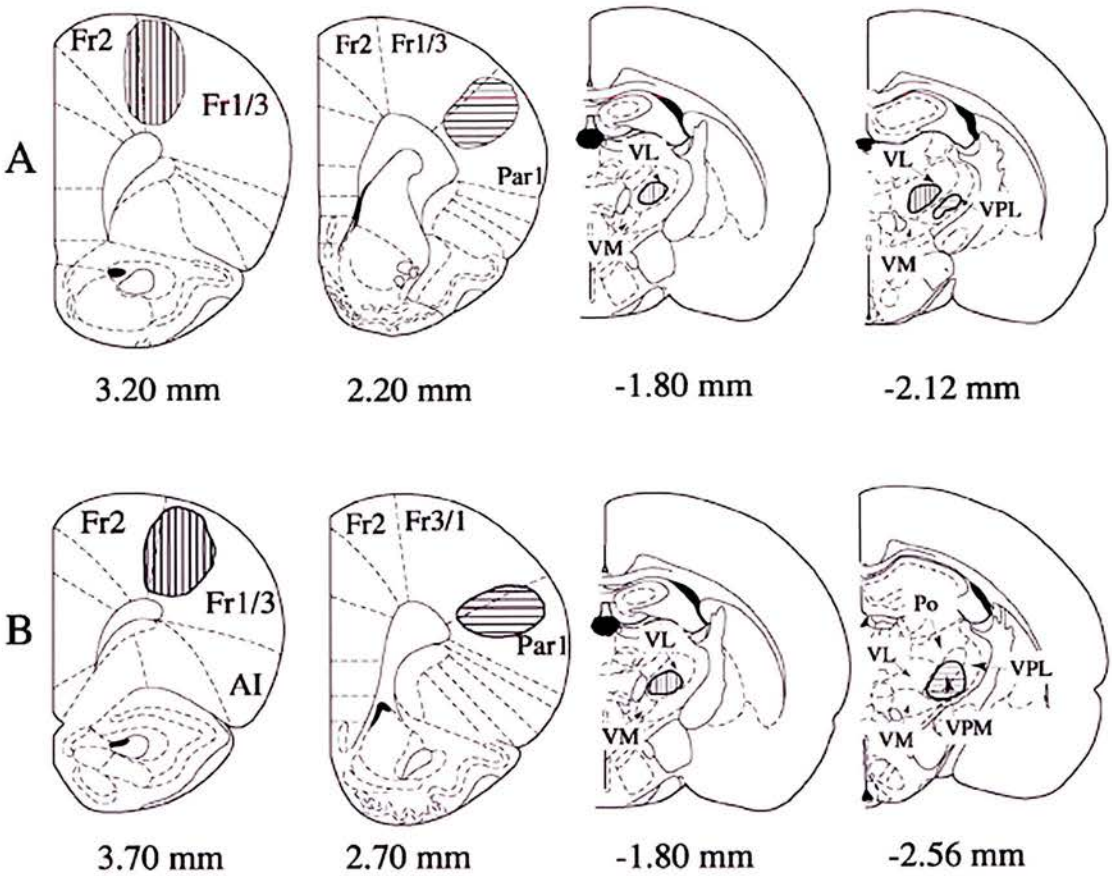
A
Fr2
Fr1/3
Fr2
Fr1/3
Par1
VL
VM
VL
VPL
VM
3.20 mm
2.20 mm
-1.80 mm
-2.12 mm
B
Fr2
Fr1/3
AI
Fr2
Fr3/1
Par1
VL
VM
Po
VL
VPL
VPM
VM
3.70 mm
2.70 mm
-1.80 mm
-2.56 mm

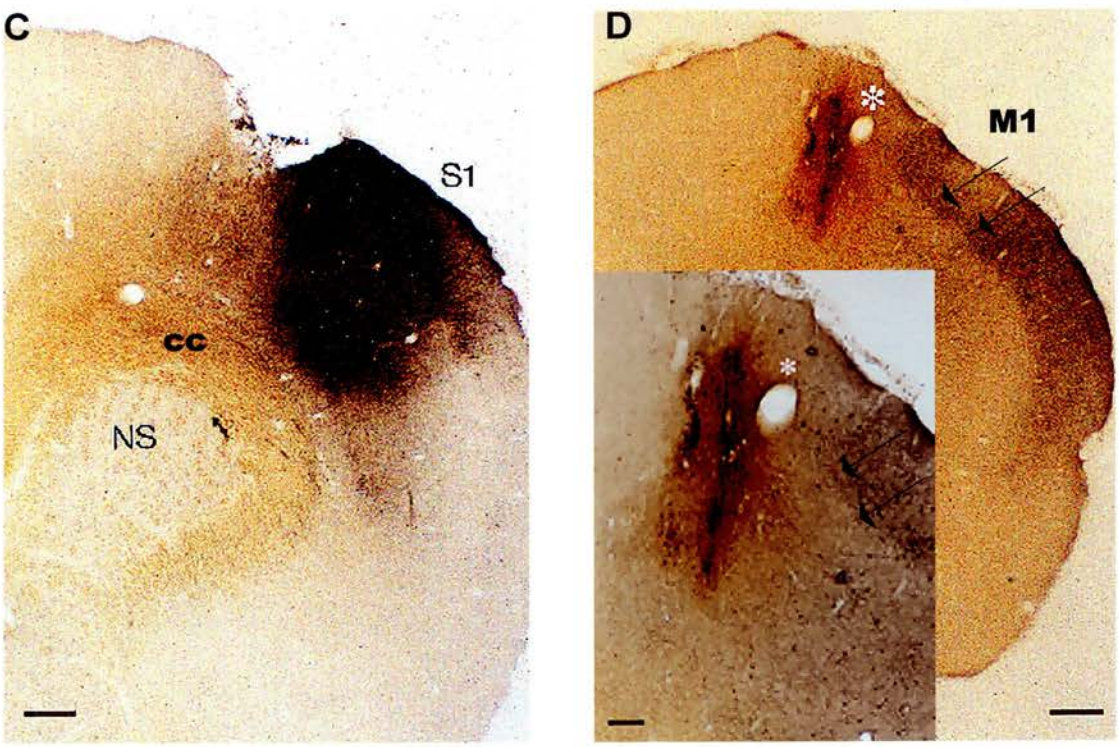
C
S1
cc
NS
D
M1

In these experiments large amounts of tracers were injected into the cortices to ensure that the entire striatal terminal field of each cortical projection was labelled, thus maximising the possibility of terminal overlap. To ensure that there was no overlap of injection sites and to confirm the location of the injections the coincidental anterograde and retrograde labelling of thalamic nuclei was analysed. The motor cortex is innervated by thalamocortical projections mainly from the ventromedial and ventrolateral thalamic nuclei and in turn sends projections back to these motor nuclei (Cicirata et al., 1986; Cicirata et al., 1990). The somatosensory cortex is reciprocally connected to the ventrobasal nuclei, the intralaminal nucleus centralis lateralis and the medial portion of the posterior thalamic group (Price and Webster, 1972; Nothias et al., 1988; Bourassa et al., 1995). In 4 out of the 6 animals prepared for electron microscopy the labelling of thalamic nuclei was distinct for both the injection sites and cells from these animals were studied at the ultrastructural level (Fig. 6.2). In the remaining two animals there was clearly an overlap of the two injection sites in the different cortical territories as indicated by the thalamic labelling. These animals, and those prepared for light microscopy in which overlap of injections occurred, were excluded from the analysis.

6.3.1.3) Distribution of anterograde labelling

The deposits of PHAL and BDA in the M1 and S1 cortices respectively, led to intense labelling of corticostriatal projections which were topographically organised and largely consistent with previous observations (McGeorge and Faull, 1989). The corticostriatal axons were collected in the fascicles of axon bundles traversing the striatum and axonal arbours were primarily located around the fibre fascicles. The typical pattern of innervation of the striatum from M1 is illustrated in Figure 6.3.

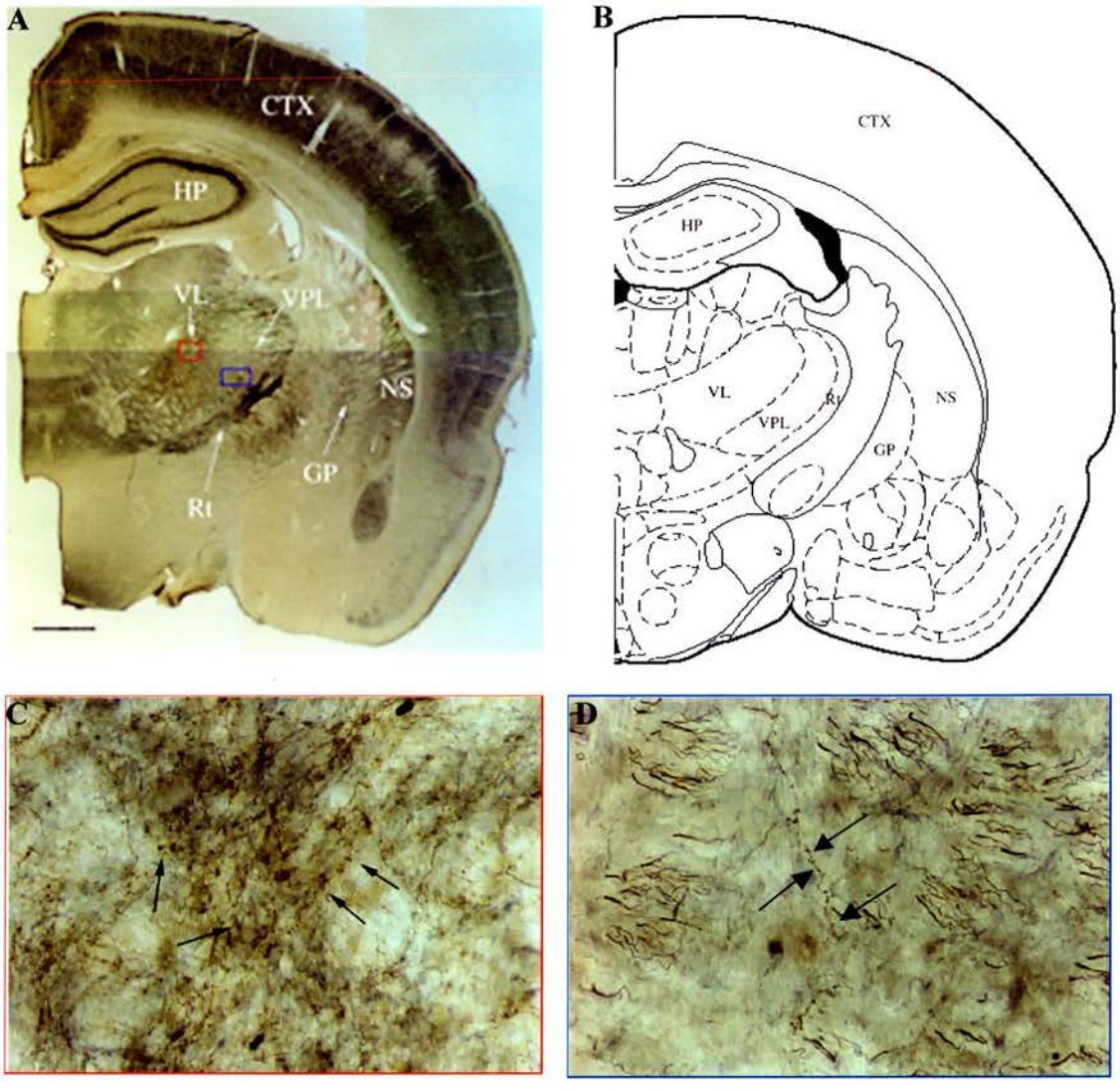

Figure 6. 2. Anterograde labelling in the thalamus.

A Light micrograph showing the anterograde labelling in the thalamus following injection of different tracers in the M1 (PHAL; DAB, brown reaction product) and S1 (BDA; nDAB, blue reaction product) cortices (Mag. 1.6X) (CTX – cortex; GP – globus pallidus; HP – hippocampus; NS – neostriatum; Rt – reticular thalamus; VL – ventrolateral thalamic nuclei; VPL – ventral posteriolateral thalamic nuclei). Scale bar 610 μm.
B Schematic showing coronal sections of rat brain approximately –2.12mm relative to Bregma (Adapted from the atlas of Paxinos and Watson, 1986).
C Higher magnification of anterograde labelling in VL. Arrows indicate PHAL, DAB (brown) labelled axon terminals.
D Higher magnification of anterograde labelling in VPL. Arrows indicate BDA, nDAB (blue) labelled axon terminals.

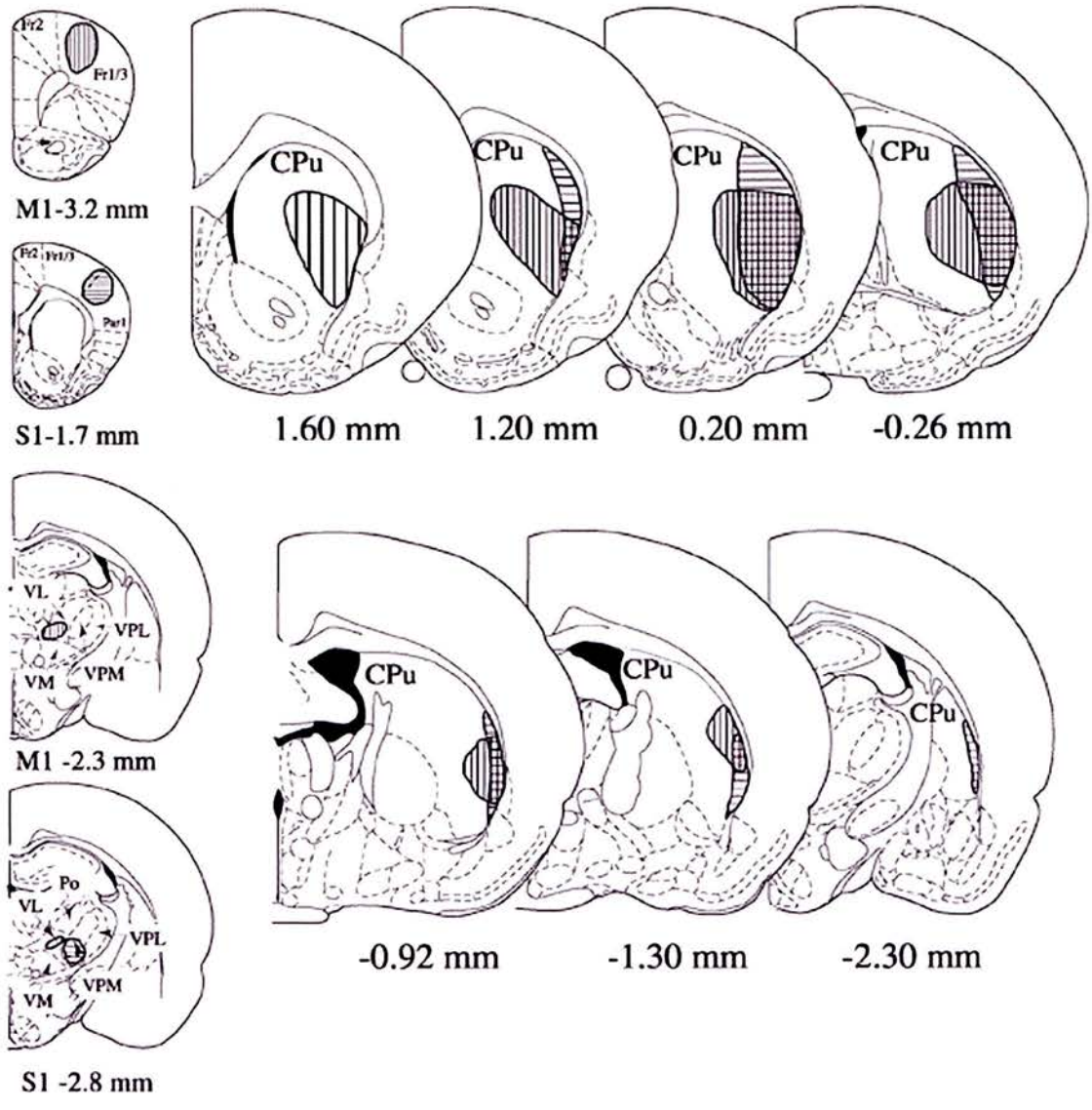

Figure 6. 3. Axonal arborisation of corticostriatal projections.

Schematic representations (modified from Paxinos and Watson 1996) of the sites of injection of PHAL in M1 cortex and BDA in the S1 cortex, the corresponding labelling in the thalamus and the anterograde labelling in the striatum. In each diagram the PHAL injection and the corresponding transport sites are indicated by vertical hatching and the BDA injection and transport sites by horizontal hatching. The figures denote the position in millimetres with respect to Bregma (Paxinos and Watson, 1986) (AI – agranular insular cortex, CPu – caudate putamen, Fr1 – frontal cortex, area 1, Fr2 – frontal cortex, area 2, Fr3 – frontal cortex, area 3, Par 1 – parietal cortex, area 1, Po – posterior thalamic group, VL - ventrolateral nucleus of thalamus; VM - ventromedial nucleus of thalamus; VPL – lateral aspect of ventroposterior nucleus of thalamus; VPM – medial aspect of ventroposterior nucleus of thalamus).

Anterogradely labelled fibres occurred in a band of striatum extending from approximately 1.6 mm rostral to about 1.3 mm caudal of Bregma. Anterograde labelling from S1 occurred in a band in the lateral aspects of the striatum extending from approximately 1.2 mm rostral to approximately 2.3 mm caudal of Bregma. The band extended over a large part of the striatum in the dorsoventral plane and, at its maximum extent, occupied about one third of the striatum in the mediolateral plane (Fig. 6.3). The axonal arbours from the S1 cortex had a distinctive pattern of axonal arbourisation in the caudal aspects of the striatum which was similar to the thick and thin corticostriatal fibre system arising from the barrel cortex (Wright et al., 1999)(Fig. 6.4).

A large part of the more lateral and caudal aspects of the projection from M1 overlapped with the projection from S1. In these regions the two sets of anterogradely labelled terminals were intermixed to such an extent that axonal varicosities derived from the different cortical territories were often observed in close proximity (Figs. 6.5, 6.6B, 6.8A, D; 6.9A, D; 6.10A, D).

6.3.1.4) Parvalbumin-positive GABAergic interneurones

Parvalbumin-positive interneurones were identified by the grey reaction product formed by the Vector SG. Perikarya and proximal dendrites, as well as isolated dendrites, were labelled. Their morphology and distribution were consistent with previous studies (Cowan et al., 1990; Kita et al., 1990; Bennett and Bolam, 1994). The labelled neurones had medium sized cell bodies, which were oval, or fusiform in shape. In some cases, indentations of the nuclear membrane were visible (Fig. 6.10D). Labelled primary dendrites branched close to the cell body and the secondary dendrites were generally smooth, but sometimes gave rise to varicosities.

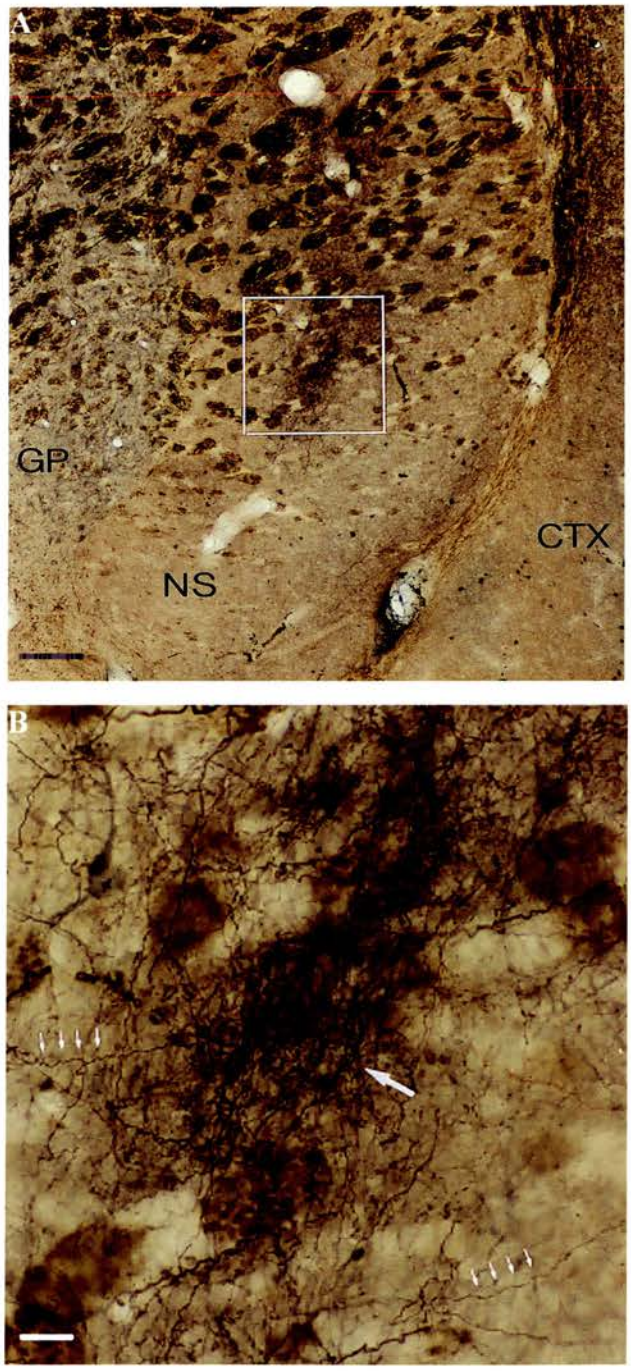

Figure 6. 4. Pattern of anterograde labelling from S1 in caudal striatum.

A A low power micrograph showing the focused arborisation of anterogradely labelled axons from the somatosensory cortex (BDA, nDAB, blue reaction product) within a more diffuse arbor. The boxed area is shown at higher magnification in B (CTX – cortex; GP – globus pallidus; NS - neostriatum). Scale bar 0.75 μm.

B The focused arbour (large arrow) consists of a mass of large calibre axons following the dorsoventral axis. Surrounding it is a more diffuse arbour (small arrows) consisting of fine calibre axons, which in general follow the mediolateral axis. Scale bar 10 μm.

Higher order dendrites were usually not labelled. The heaviest labelling of PV-positive structures was in the dorsolateral aspect of the striatum. Although the striatum is known to possess a dense network of PV-positive local axons and axonal boutons, PV-positive axonal fields were usually not labelled in the present study.

6.3.1.5) Light microscopic analysis of convergence.

Parvalbumin-positive neuronal perikarya and dendrites were intermingled amongst axons and axonal boutons anterogradely labelled from both M1 and S1 cortices (Fig. 6.5). The PV-positive structures were often closely apposed by the anterogradely labelled boutons consistent with previous observations of cortical input to this class of neurone (Lapper and Bolam, 1992; Bennett and Bolam, 1994). Single axons anterogradely labelled from either M1 or S1 were frequently found to form multiple appositions with individual PV-positive interneurones within a few microns (Fig. 6.6). They commonly gave rise to 2-3 boutons apposed to an individual PV-positive neurone, although as many as 6 were observed (Fig. 6.6). In many cases, an individual PV-positive neuronal perikaryon or isolated dendrite was closely apposed by terminals anterogradely labelled from M1 and S1 (Fig. 6.5). Examination of all PV-positive perikarya and emerging dendrites (but not isolated dendrites) in single sections at the level of the greatest extent of overlap of the two projections, revealed that up to 51% (range: 35.4-50.9) of PV-positive neurones were apposed by terminals derived from the cortex. Up to 46% (range: 24.7-46.2) of those that were apposed by cortical terminals were apposed by terminals derived from both cortical regions which represents up to 23% (range: 8.8-23.5) of all PV-positive neurones in the single sections.

Figure 6. 5. Apposition of cortical terminals from M1 and S1 cortices onto PV interneurones.

Light micrograph illustrating convergence of motor and somatosensory afferents in the striatum. Parvalbumin-immunostained perikarya (PV) and axons anterogradely labelled with PHAL from the motor cortex (M1) and axons anterogradely labelled with BDA from the somatosensory cortex (S1). In these cases the PHAL containing motor cortical afferents were revealed using DAB as the chromogen for the peroxidase reaction giving a brown reaction product. The BDA-containing axons were labelled with nickel DAB as the chromogen giving the blue reaction product. These digital images and those in Figures 6.8A, D ; 6.9A, D; 6.10A, D were prepared from scanned images of colour photomicrographs and have been colour balanced in Adobe Photoshop 6.0. They are derived from sections that were prepared for light microscope analysis only.

A This parvalbumin-immunolabelled neurone (PV) is in a region containing many PHAL and BDA labelled axons, many of which are closely apposed to the labelled neurone (arrows). At this focal depth there are several BDA labelled boutons apposed to the perikaryon and proximal dendrite and a PHAL labelled bouton also closely apposes the dendrite. Scale bar 10 μm.

B Montage of a second parvalbumin-immunolabelled neurone (PV) that is apposed by boutons derived from both the motor cortex (PHAL) and the somatosensory cortex (BDA) (arrows). The PHAL labelled axon gives rise to several boutons that are apposed to the PV-positive perikaryon. Scale bar 10 μm.

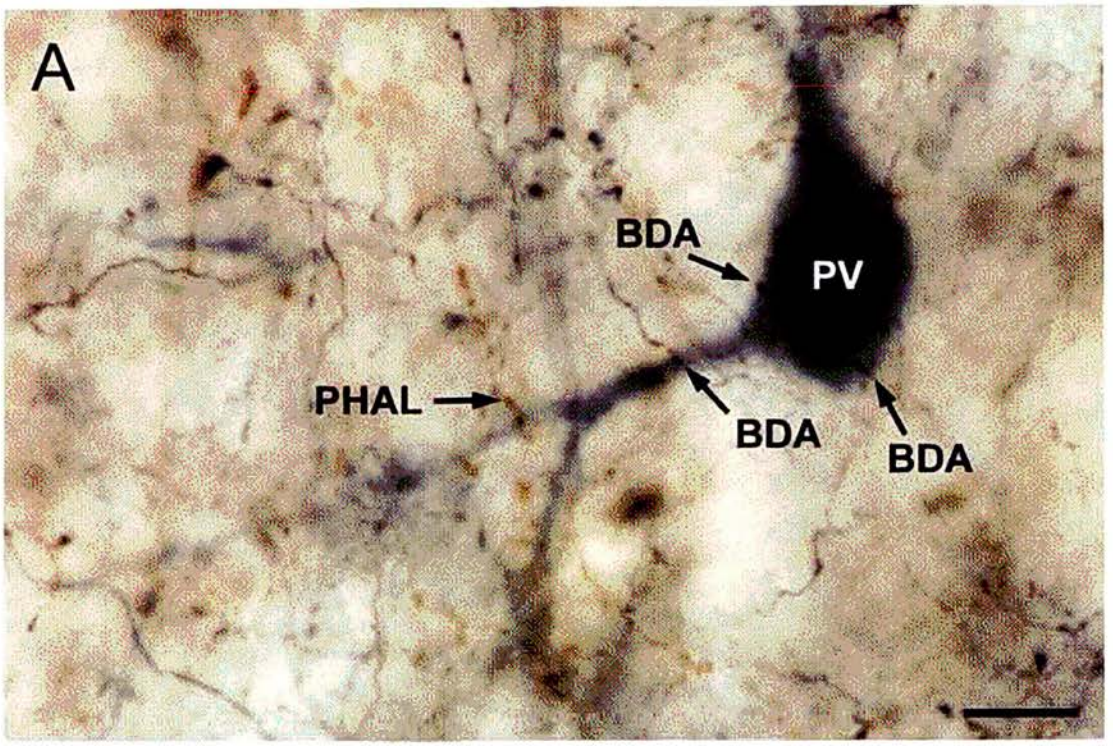
A
BDA
PV
PHAL
BDA
BDA

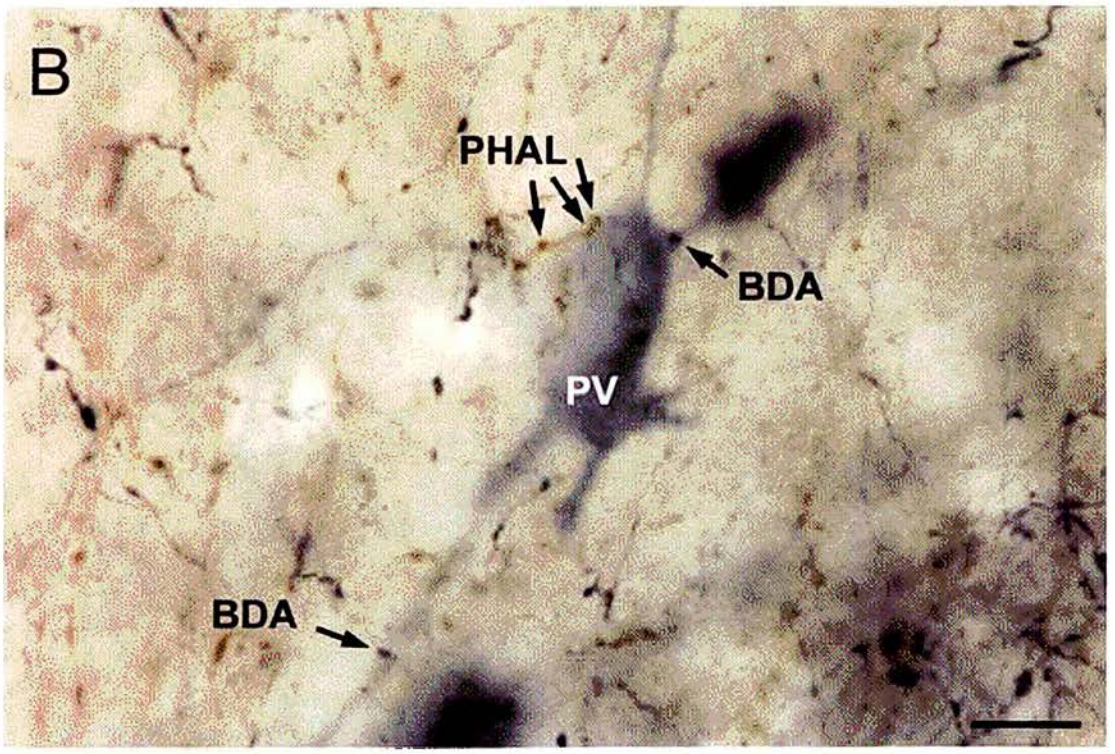
B
PHAL
BDA
PV
BDA

Figure 6. 6. Multiple contacts of corticostriatal axons onto PV-positive interneurones.

Light microscopic digital images and corresponding camera lucida drawings of striatal parvalbumin-positive neurones and individual cortical axon forming multiple appositions.

A, B Digital montage **(A)** and drawing **(B)** of a parvalbumin-positive interneurone and anterogradely labelled cortical fibres in the striatum. The PV-positive neurone gave rise to several immunolabelled dendrites, one of which was closely apposed by an axon anterogradely labelled with BDA from the sensorimotor cortex. The axon gave rise to six varicosities that closely apposed the dendrite (small arrows, 1-6), five of which were visible in the light micrograph (1-5). The neurone was also apposed by two varicosities of an axon anterogradely labelled with PHAL from the motor cortex (two arrows, upper right), only visible in the camera lucida drawing.

C, D A parvalbumin-positive neurone apposed by an axon anterogradely labelled with PHAL from the motor cortex giving rise to five boutons that closely appose the dendrites and perikaryon of the labelled neurone.

E, F A parvalbumin-positive neurone apposed by an axon anterogradely labelled with BDA from the sensorimotor cortex giving rise to five boutons that closely appose the perikaryon and dendrites of the labelled neurone.

Scales: **A, C & E** = 10 μm; **B, D & F** = 10 μm

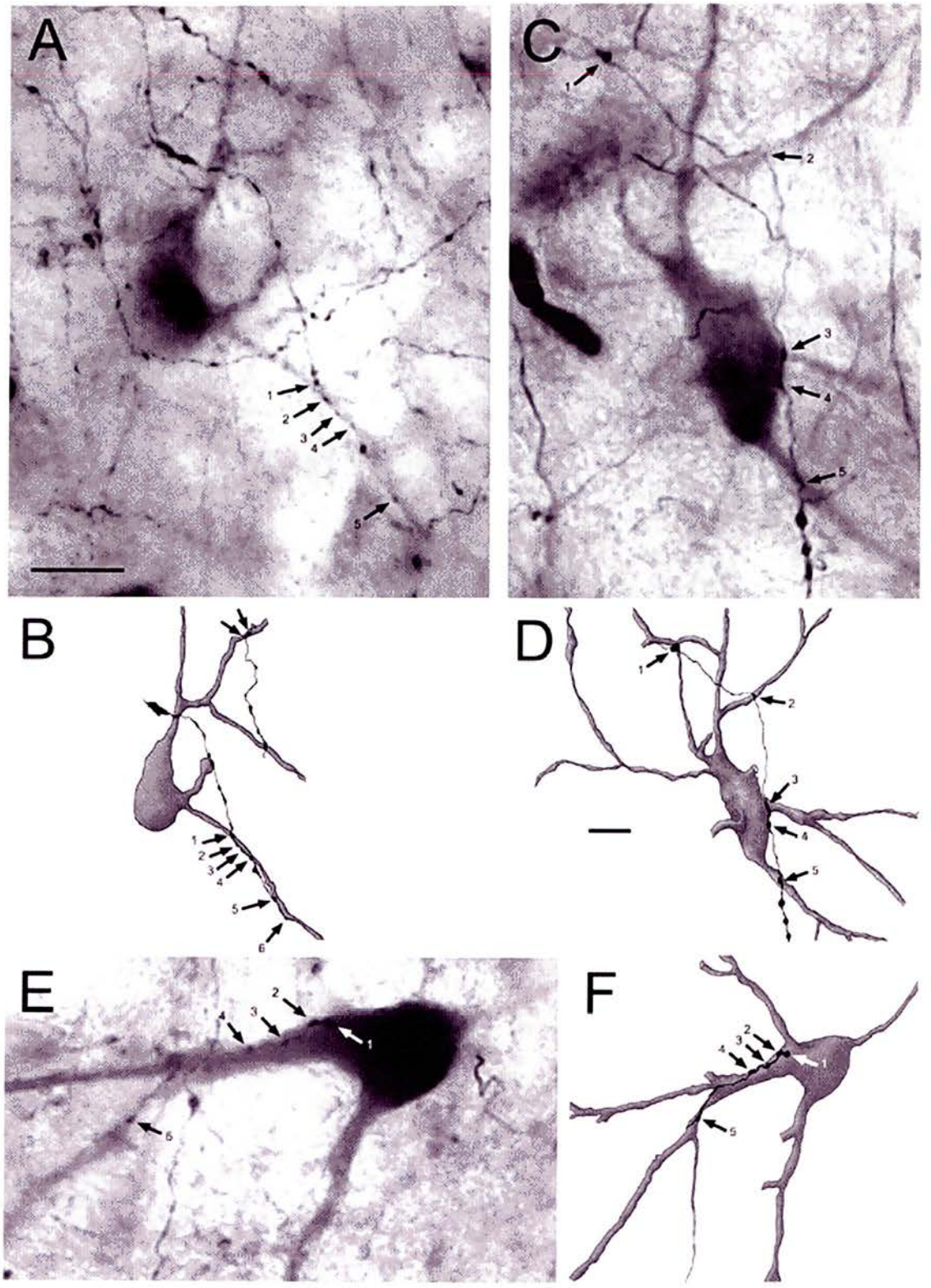
A
C
B
D
E
F

6.3.2) Electron microscopic observations

In order to confirm that the appositions observed in the light microscopic analysis were indeed synapses, PV-positive neurones were examined by electron microscopy. Correlated light and electron microscopy was carried out because the extent and quality of immunohistochemical and histochemical staining is reduced in material prepared for electron microscopy. A total of 8 PV-positive neurones (2 from each of the 4 rats) that were apposed by terminals from both M1 and S1, were selected at the light microscopic level for study in the electron microscope.

In the electron microscope the cell bodies and dendrites of the labelled PV-positive structures contained an amorphous, electron dense reaction product similar to that previously reported for Vector SG (Hussain et al., 1996; Hanley and Bolam, 1997). Ultrastructural features of the PV-immunoreactive structures were consistent with previous descriptions (Kita et al., 1990; Lapper et al., 1992; Bennett and Bolam, 1994). They possessed a relatively large volume of cytoplasm that was rich in organelles such as mitochondria, ribosomes and Golgi apparatus (Figs. 6.8B, C, E, F; 6.9B, C, E, F; 6.10B, C, E, F). The nuclear membrane possessed indentations (Figs. 6.10E) and intranuclear inclusions were often observed (Fig. 6.8E). Anterogradely labelled axon terminals were identified by the presence of reaction product as well as by their position in relation to landmarks such as blood vessels, unstained neurones and glial cells (Figs 6.8B, C, E, F; 6.9B, C, E, F; 6.10B, C, E, F; 6.11B). Axons and terminals which were visualised using nDAB were more intensely stained than DAB-labelled structures (compare Figs 6.8C & F and 6.9C & F). Consistent with previous studies (Kemp and Powell, 1971; Somogyi et al., 1981a; Dube et al., 1988; Smith et al., 1994; Hersch et al., 1995) the anterogradely labelled corticostriatal boutons were

packed with round vesicles and usually contained one or more mitochondria (Figs. 6.8C, F; 6.9C, F; 6.10C, F; 6.11C). They formed asymmetric synapses with dendritic spines and with dendritic shafts (Fig. 6.7). The terminals were variable in size and some of the larger boutons were similar in morphology to the boutons of the 'discrete' corticostriatal projection from the barrel cortex (Wright et al., 1999). The correlated light and electron microscopy revealed that they also formed asymmetric synapses on the cell body and proximal dendrites of PV-positive interneurones (Figs. 6.8; 6.9; 6.10). Of the 8 cells studied, 5 of them (from 3 rats) were found to receive convergent synaptic input from both the M1 and S1 cortices (Figs. 6.8; 6.9; 6.10). In one of the neurones that received the convergent input, three synapses from the motor cortex arose from a single axon (Fig. 6.10).

Of the three neurones that were examined by correlated light and electron microscopy and failed to reveal convergent input from the cortex, two were abandoned because of poor ultrastructural preservation. In only one case was a labelled bouton identified at the light microscopic level found not to make contact with the PV-positive neurone; the bouton, anterogradely labelled from S1, made synaptic contact with an adjacent, unstained spine.

In addition to the labelled boutons identified at both the light and electron microscopic levels, additional labelled boutons were observed in contact with the PV-positive neurones. These boutons (n=6) had the morphology of corticostriatal boutons and formed asymmetric synapses and were usually obscured by the overlying the PV-labelled cell bodies (Fig. 6.11). In addition to these, many unlabelled boutons formed asymmetric synaptic contacts with PV-immunolabelled cell bodies and dendrites (Fig. 6.11). The results are summarised in Table 6.1.

Figure 6. 7. Synaptic contact of an anterogradely labelled corticostriatal terminal.

Electron micrograph of a PHAL, DAB labelled axon terminal from the M1 cortex (*) making a synapse with a dendritic spine (SP). The bouton is packed with round vesicles which are a characteristic feature of corticostriatal terminals. The arrowheads indicate the postsynaptic density associated with an asymmetric synapse. Scale bar 0.25 μm.

Figure 6. 8. Synaptic convergence of motor and somatosensory cortical afferents onto a parvalbumin-positive, GABAergic interneurone in the striatum: correlated light and electron microscopy.

A Light micrograph of a parvalbumin-immunostained neurone (PV) labelled using Vector SG as the substrate for the peroxidase reaction. The neurone was located in a region containing fibres anterogradely labelled with PHAL from the motor cortex (PHAL, nDAB as chromogen; blue fibre indicated by small arrows on the left) and with BDA from the somatosensory cortex (BDA, DAB as chromogen; brown fibre indicated by small arrows on the right). The axon from the somatosensory cortex gives rise to several varicosities, one of which, closely apposes the perikaryon (BDA, large arrow). The capillary, c, is labelled as a landmark between the light and electron microscope levels.

B Low power electron micrograph of part of the same perikaryon and the BDA-labelled, somatosensory cortical bouton closely apposed to it (BDA, arrow).

C High power electron micrograph of the BDA-labelled bouton from the somatosensory cortex. The labelled terminal forms an asymmetrical synaptic contact (arrowhead) with the parvalbumin-immunolabelled neurone.

D Light micrograph of the same parvalbumin-immunolabelled neurone (PV) at a deeper focal depth. At this level the neurone is apposed by a PHAL-positive bouton (PHAL, arrow) derived from the motor cortex.

E Low power electron micrograph at about the same level as in **D**. The perikaryon, part of a dendrite and the PHAL-labelled bouton (arrow) derived from the M1 cortex are present. Note the position of the capillary, c, for correlation between light and electron microscopic levels. The immunostained neurone possesses an intranuclear inclusion (small arrow), a feature typical of striatal GABAergic interneurones.

F High power electron micrograph of the PHAL-positive bouton forming an asymmetrical synapse (arrowhead) with the parvalbumin-positive dendritic shaft. Note that the reaction product formed by the nDAB is more intense than that formed by the DAB as seen in **C**. Two unlabelled boutons are indicated by asterisks.

Scales: **A**, **D** = 12.5 μm; **B**, **E** = 5 μm; **C**, **F** = 0.25 μm

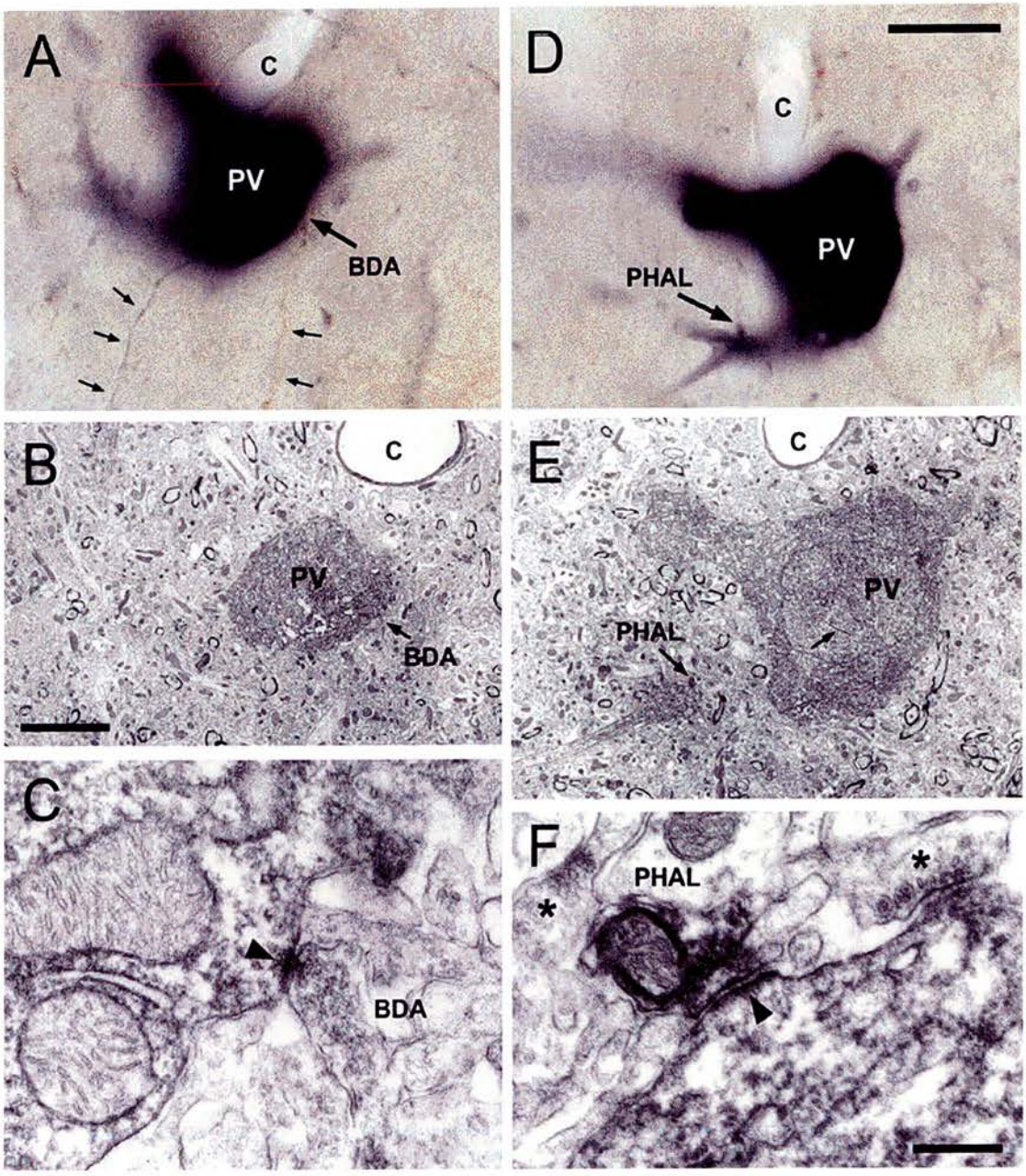
A
C
PV
BDA
D
C
PV
PHAL
B
C
PV
BDA
E
C
PV
PHAL
C
BDA
F
PHAL
*
*

Figure 6. 9. Synaptic convergence of motor and somatosensory cortical afferents onto a parvalbumin-immunolabelled, GABAergic interneurone in the striatum: correlated light and electron microscopy.

A Light micrograph of a parvalbumin-immunostained neurone (PV; Vector SG as a chromogen) that is closely apposed by a BDA-positive bouton (BDA, arrow) that was anterogradely labelled from the somatosensory cortex (DAB as chromogen, brown reaction product). Note the additional axon anterogradely labelled from the somatosensory cortex in the upper right of the micrograph (small arrows). An unstained neurone (n) and a capillary (c) are labelled for correlation between the light and electron microscopic levels.

B Low power electron micrograph of the same neurone and the bouton anterogradely labelled with BDA from the somatosensory cortex.

C High power electron micrograph of the BDA-labelled bouton forming an asymmetric synapse (arrowhead) with the parvalbumin-positive neurone.

D The same neurone at a deeper focal depth. The proximal dendrite of the neurone is apposed by two boutons derived from two axons that were anterogradely labelled with PHAL from the motor cortex.

E Low power electron micrograph at about the same level of the perikaryon and dendrite and the two PHAL-labelled boutons from the motor cortex. The unstained neurone (n) and capillary (c) are labelled for correlation between the light and electron microscope levels.

F High power electron micrograph of the two PHAL-positive boutons (b_1 and b_2), derived from the motor cortex, forming asymmetric synapses (arrowheads) with the proximal dendrite of the parvalbumin-positive GABAergic interneurone.

Scales: **A**, **D** = 12.5 μm; **B**, **E** = 5 μm; **C**, **F** = 0.5 μm

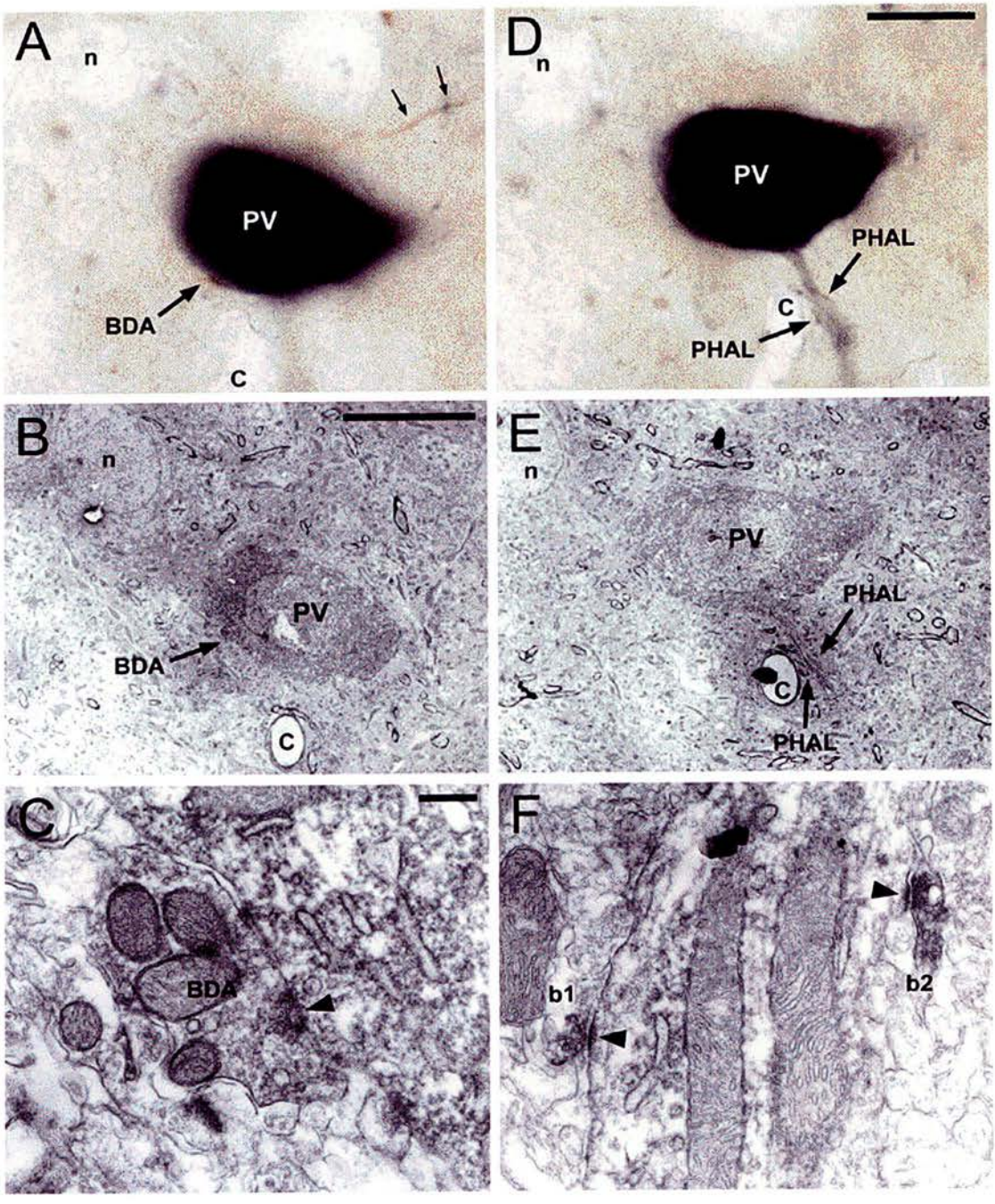
A
n
PV
BDA
C
D
n
PV
PHAL
C
PHAL
B
n
PV
BDA
C
E
n
PV
PHAL
C
PHAL
C
BDA
F
b1
b2

Figure 6. 10. Multiple synaptic contact of a single motor cortical axon onto a parvalbumin-positive GABAergic interneurone in the striatum: correlated light and electron microscopy.

A Light micrograph of a parvalbumin-immunostained neurone (PV; Vector SG as a chromogen) labelled using Vector SG as the substrate for the peroxidase reaction. It is closely apposed by fibres anterogradely labelled with PHAL from the sensory cortex (PHAL, nDAB as chromogen; blue fibre indicated by arrow on the left) and with a BDA-positive bouton from the motor cortex (BDA, DAB as chromogen; brown fibre indicated by arrow on the right). The capillary, (c) and an unstained neurone (n) are labelled as landmarks for correlation between the light and electron microscope levels.

B Low power electron micrograph of the same neurone and the bouton anterogradely labelled with BDA from the motor cortex.

C High power electron micrograph of the BDA-labelled bouton from the motor cortex. The labelled terminal forms an asymmetrical synaptic contact (arrowheads) with the parvalbumin-immunolabelled neurone.

D The same neurone at a deeper focal depth. The perikaryon of the neurone is apposed by another BDA labelled bouton from the same motor cortical axon as that seen in **A**. The immunostained neurone possesses an intranuclear inclusion (white arrowhead), a feature typical of GABAergic interneurones in the striatum.

E Low power electron micrograph at about the same level as in D. The perikaryon, part of a dendrite and two PHAL-labelled boutons derived from the somatosensory cortex and the BDA labelled bouton derived from the motor cortex are present. Note the position of the capillary (c) and unstained neurone (n) for correlation between light and electron microscopic levels. The immunostained neurone possesses an intranuclear inclusion (white arrowhead), a feature typical of GABAergic interneurones in the striatum.

F High power electron micrograph of the BDA-positive bouton derived from the motor cortex, forming an asymmetric synapse (arrowheads) with the cell body of the parvalbumin-positive GABAergic interneurone.

Scales: **A**, **D** = 10.5 μm; **B**, **E** = 5 μm; **C**, **F** = 0.3 μm

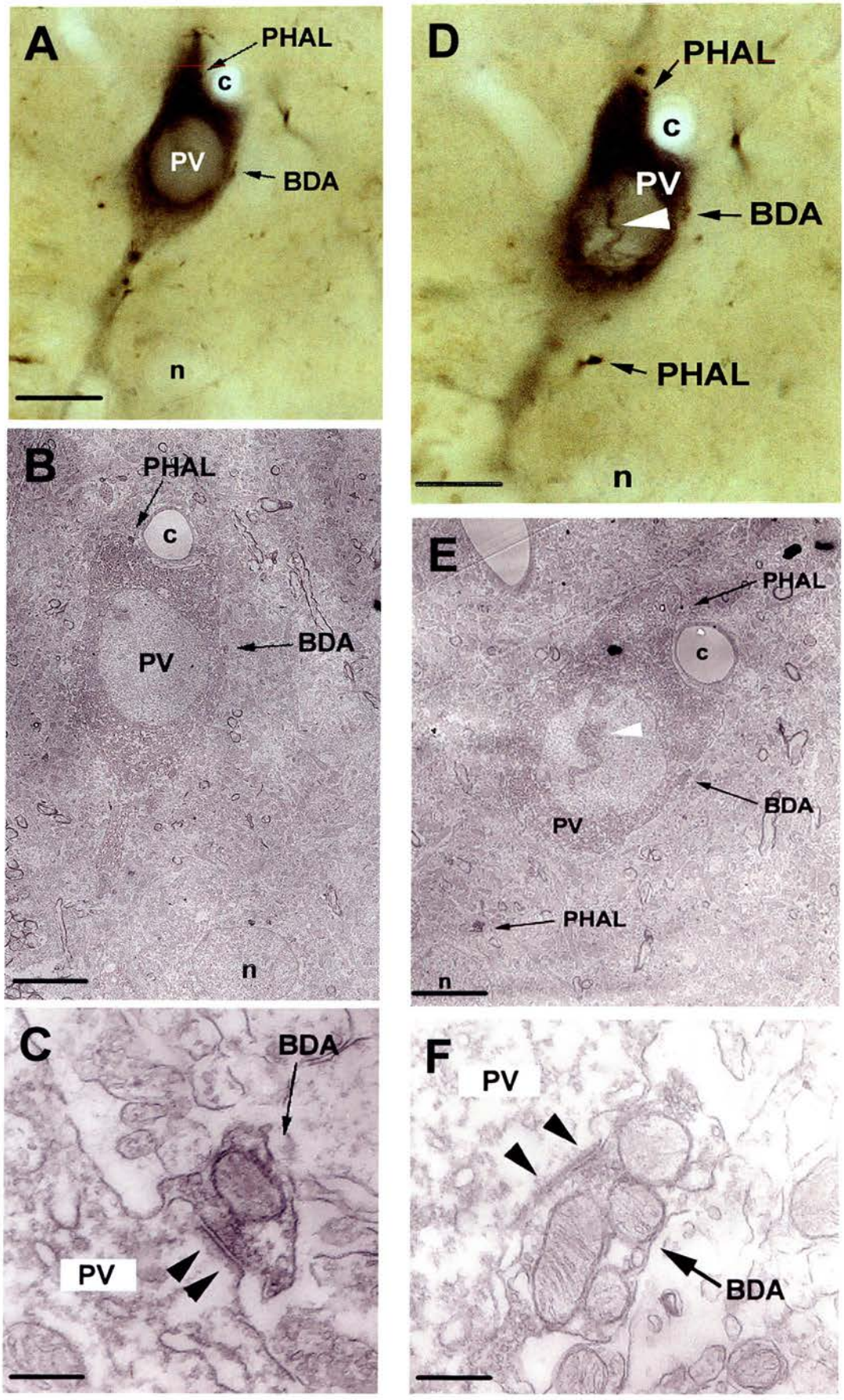
A
PHAL
c
PV
BDA
n
D
PHAL
c
PV
BDA
PHAL
n
B
PHAL
c
BDA
PV
n
E
PHAL
c
BDA
PV
PHAL
n
C
BDA
PV
F
PV
BDA

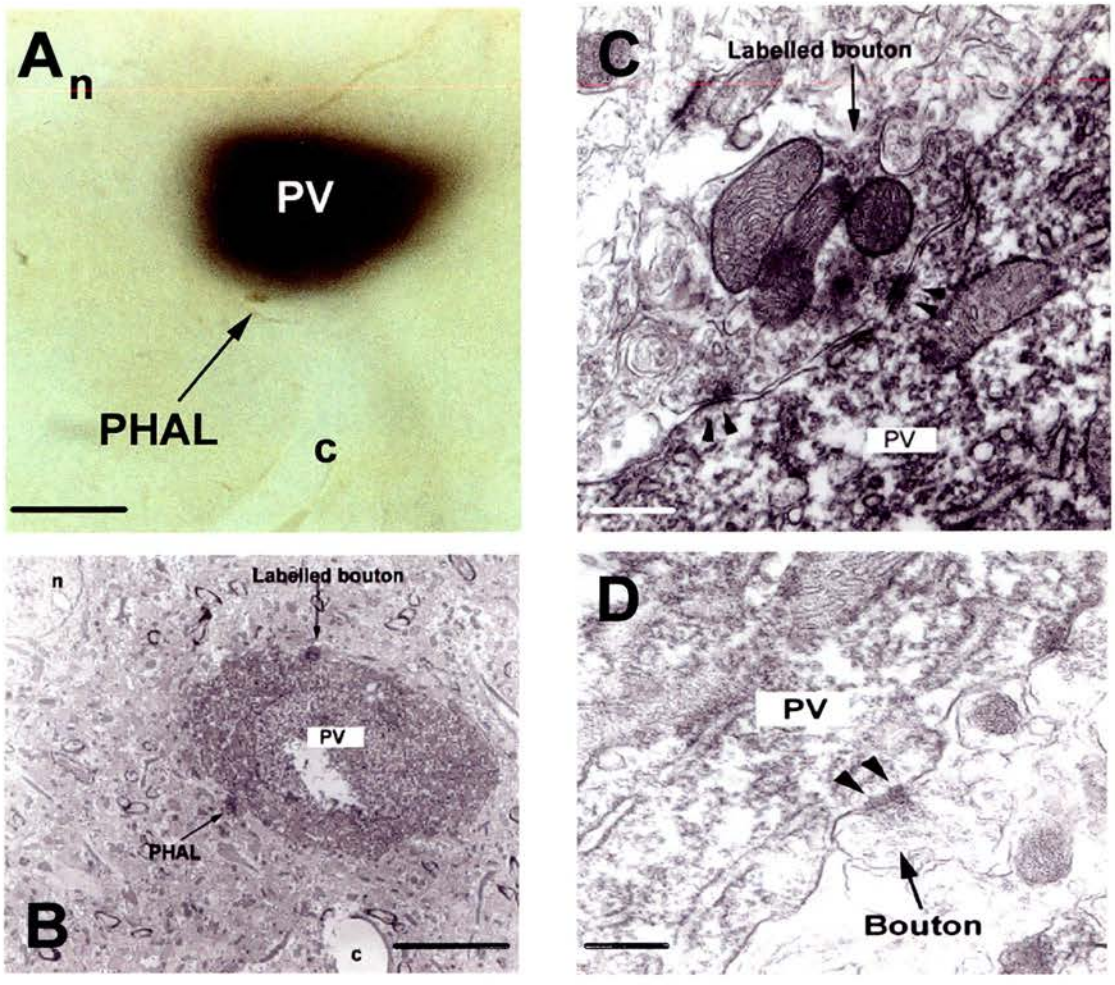

Figure 6. 11. Other synaptic contacts of PV interneurones.

A Light micrograph of a PV-immunolabelled interneurone apposed by a PHAL-labelled, (DAB as chromogen, brown reaction product) axon terminal from the motor cortex. The position of a capillary, (c) and an unstained neurone (n) has been marked for correlation between light and electron microscopic levels. Scale bar 10 μm

B Low power electron micrograph of the PV-positive interneurone in **A**. In addition to the PHAL bouton (PHAL arrow) identified at the light microscope level there is an additional labelled bouton (labelled bouton arrow) making synaptic contact with the perikaryon of the interneurone. Scale bar 5 μm

C High power electron micrograph of the labelled bouton making an asymmetric synaptic contact (arrowheads) with the immunolabelled interneurone. Scale bar 0.25 μm

D High power electron micrograph of an example of an unlabelled bouton making an asymmetric synaptic contact with the soma of a PV-positive interneurone. Scale bar 0.25 μm

Animal	Cell	No. of DAB-labelled boutons forming asymmetrical synapses.	No. of nDAB-labelled boutons forming asymmetrical synapses.	Convergence	Presence of labelled but unidentified boutons	Presence of unlabelled boutons forming asymmetrical synapses.
1	1	1	2	Yes	Yes	Yes
	2	1	1	Yes	No	Yes
2	3	2	3	Yes	Yes	Yes
	4	4	2	Yes	No	Yes
3	5	1	1	Yes	No	Yes
	6	1	0	No	No	Yes
4	7	Poor preservation of ultrastructure				
	8					
5	9	Overlap of injection sites				
	10					
6	11	Overlap of injection sites				
	12					

Table 6. 1. Summary of correlated light and electron microscopy results.

6.4) Discussion

The primary objective was to determine whether synaptic convergence of somatosensory and motor corticostriatal projections occurs at the single cell level in the areas of overlap of these projections. The main finding is that somatosensory and motor corticostriatal afferents do indeed form convergent synapses with individual striatal neurones indicating that one aspect of sensory-motor integration performed by the basal ganglia occurs at the level of single cells in the striatum.

6.4.1) Parvalbumin immunoreactivity

A small set of striatal neurones was parvalbumin immunoreactive. These neurones had an oval or fusiform shaped cell body with aspiny dendrites that ramified extensively close to the cell body. Ultrastructural analysis showed these cells to have deep nuclear indentations and in some a nuclear rod or inclusion body was seen. The thin layer of cytoplasm surrounding the large nucleus was rich in organelles. These features at both the LM and EM levels are characteristic of parvalbumin interneurones (Cowan et al., 1990; Kita et al., 1990; Lapper et al., 1992; Bennett and Bolam, 1994). These PV interneurones have been identified as GABAergic by their uptake of [^{3}H] GABA, as well as being positively labelled for GAD and GABA (Ribak et al., 1979; Bolam et al., 1983; Bolam et al., 1985; Kita and Kitai, 1988). Colocalisation studies showed overlap of GABA positive and parvalbumin interneurones (Cowan et al., 1990). There was a tendency for densely stained parvalbumin immunoreactive neurones to be located in the lateral striatum, while medial areas had few immunopositive cells. This finding is in agreement with previous results (Celio, 1990; Cowan et al., 1990; Bennett and Bolam, 1994). This

preferential distribution suggests that these neurones are involved in mediating cortical information that projects to this area.

6.4.2) Anterograde labelling

Deposits of BDA and PHAL in the S1 and M1 cortices respectively led to intense labelling of corticostriatal projections. These were topographically organised as shown by previous studies (Donoghue and Herkenham, 1986; McGeorge and Faull, 1989; Ebrahimi et al., 1992). The caudal most aspect of the S1 projection formed discrete axonal foci. These foci are reminiscent of previous descriptions of striatal matrisomes and of the recently demonstrated "discrete and diffuse" corticostriatal projection from the barrel cortex (Flaherty and Graybiel, 1993; Wright et al., 1999). The anterograde labelling showed large areas of overlap between the M1 and S1 axonal arbours with the greater overlap in the rostral dorsolateral striatum. This region of overlap coincides with the area of greatest PV immunoreactivity.

6.4.3) Anterograde labelling and parvalbumin immunoreactivity

The major targets of corticostriatal axons are the dendritic spines of spiny projection neurones and the dendritic shafts of PV-positive, GABAergic interneurones (Kemp and Powell, 1971; Somogyi et al., 1981a; Lapper et al., 1992; Bennett and Bolam, 1994). This study was confined to the latter class of neurone and light microscopy revealed that the dendrites and perikarya of PV-positive, GABAergic interneurones were apposed by terminals derived from both the primary motor and somatosensory cortices. The analysis of sections at the level of the densest overlap of the two projections revealed that this was a common phenomenon.

6.4.4) Quantification of convergence

An attempt was made at the light microscope level to quantify the percentage of parvalbumin interneurones receiving convergent input. Up to half of the PV-positive neurones that were apposed by terminals derived from the cortex had convergent appositions from both regions of the cortex. This value is likely to be an underestimate of the true incidence of convergence as numerous isolated PV-positive dendrites were apposed by both sets of terminals and at least some of these may have arisen from the PV-positive perikarya and proximal dendrites that were not found to be apposed by both sets of cortical terminals. Furthermore, the entire projection from the areas of cortex that received the deposits of the tracers is unlikely to have been labelled, nor is the entire dendritic arbour of a PV-positive neurone likely to be labelled. Also, as these experiments required the use of three sets of chromogens each with differential penetration to localise BDA, PHAL and parvalbumin, there may be a high number of false negatives. Thus, the number of PV interneurones receiving a convergent input may be significantly higher. One indication of this was the observation that PV neurones received asymmetric synaptic input from unlabelled boutons. These could be axons from the M1 and S1 region of the cortex which did not transport the tracer, or where the histochemical reaction did not reveal the tracer. However, these could be inputs from other regions of the cortex or thalamus which have been shown to make asymmetric synapses onto PV interneurones (Rudkin and Sadikot, 1999). The striatum also receives excitatory input from the dorsal raphe nucleus and these may contact PV interneurones forming asymmetric synapses (Pasik et al., 1984; Corvaja et al., 1991). In some sections

labelled boutons were seen at the EM level, but these were not identified in the LM photographs or drawings. These terminals were usually found directly above or below the cell body and the intense staining of the cell might have obscured the view of the bouton. This inability to detect boutons at the LM level also hampers quantification of the amount of convergence.

6.4.5) Pattern of cortical innervation of PV-positive interneurones

An additional observation that was made in the present study has a bearing on the principles of organisation of the corticostriatal projections. At the light microscopic level, single axons from M1 or S1 were often seen to form multiple appositions (up to 6 were observed) within a small distance on a single PV-positive interneurone. In one case it was confirmed by electron microscopy that the closely spaced multiple appositions do form synaptic contacts. It has been calculated that a single cortical axon will form approximately 40 synapses within the volume of striatum occupied by a single spiny neurone. Since that same volume of striatum will contain 2845 spiny neurones (each of which receive about 5000 cortical synapses), the probability of an individual cortical axon contacting a spiny neurone is low (Kincaid et al., 1998). The same volume of striatum will contain approximately 18 PV-positive neurones, based on the estimate of 16875 PV-positive neurones (Luk and Sadikot, 2001) and 2.72 million spiny neurones (Oorschot, 1996) in the striatum and assuming an even distribution which may in fact not be the case (Cowan et al., 1990; Kita et al., 1990). If cortical axons innervate striatal neurones in a non-selective way, then the probability of a cortical axon contacting a PV-positive neurone is very low and the probability of it forming more than one contact is even lower (Kincaid et al., 1998; Zheng and Wilson, 2002). Since multiple appositions were observed in contact

with an individual PV-positive neurone then cortical axons, must in some way, show selectivity for the PV-positive neurones. Given that the same volume of striatum contains 381,180 cortical axons (Kincaid et al., 1998; Zheng and Wilson, 2002), those that selectively contact the 18 PV-positive neurones must therefore be a subpopulation. It remains to be established which of the several classes of cortical neurones that innervate the striatum provides this selective innervation (Gerfen and Wilson, 1996; Kincaid and Wilson, 1996).

From the light microscopic analysis it was apparent that an individual cortical axon that was apposed to a PV-positive structure also gave rise to boutons not apposed to PV-positive structures. This implies that individual cortical axons contact both PV-positive interneurones and spiny neurones and/or other classes of interneurones. An intriguing possibility is that the PV-positive, GABA interneurones and the population of spiny neurones contacted by the same cortical axons are bound together by the axon collaterals of the interneurone thereby forming some type of modular arrangement. It should be noted, however, that the influence of GABA interneurones is likely to extend beyond their axonal field as they are interconnected by gap junctions (Kita et al., 1990; Kita, 1993; Koos and Tepper, 1999).

The finding that PV-positive interneurones receive multiple contacts from a single axon suggests that they may be activated by a weaker and/or less synchronised cortical input than is required to activate a striatal projection neurone (Wilson, 1995; Stern et al., 1997; Charpier et al., 1999). Thus GABAergic interneurones are likely to be more responsive to cortical inputs than spiny neurones. This suggestion is consistent with the studies of Parthasarathy and Graybiel (Parthasarathy and Graybiel, 1997) who showed that weak cortical stimulation that was unable to

activate a large number of projection neurones was able to induce immediate early gene expression in PV-positive interneurones. It may be that while many corticostriatal neurones need to fire synchronously in order to evoke activity in spiny projection neurones (Wilson, 1995; Stern et al., 1997; Charpier et al., 1999), input from fewer corticostriatal neurones, albeit from different cortical regions, is needed to activate PV-positive interneurones. Thus, PV-interneurones may shunt coincident cortical activity in suboptimally excited striatal spiny cells (Parthasarathy and Graybiel, 1997; Plenz and Kitai, 1998; Koos and Tepper, 1999). Only when cortical input to the spiny neurones is sufficiently large will the shunting be overcome and the selected population of spiny neurones be allowed to reach firing threshold.

6.4.6) Functional significance

The results of this study provides evidence that PV-positive, GABA interneurones play a role in sensorimotor integration in the striatum. Although their precise role remains undetermined, it is likely that the sensory and motor information integrated by PV-positive, GABA interneurones is transmitted to spiny projection neurones in such a form as to control the output of a selected group of spiny neurones by shunting cortical excitation and/or by synchronization of their activity (Plenz and Kitai, 1998; Koos and Tepper, 1999). This finding is coincident with the view that parvalbumin interneurones play a role in feed forward inhibition of medium spiny cells (Kawaguchi, 1993; Bennett and Bolam, 1994; Plenz and Kitai, 1998). *In vitro* slice experiments and organotypic co-cultures have shown PV interneurones to be fast spiking cells. These cells have a characteristic low input resistance, short duration spike and abrupt repetitive firing (Kawaguchi, 1993; Plenz and Aertsen, 1996b; Plenz and Kitai, 1998). While spiny cells receive cortical input mainly onto

their dendritic spines (Somogyi et al., 1981a; Dube et al., 1988), parvalbumin interneurones receive innervation on their cell bodies, proximal and distal dendrites (Kita et al., 1990; Lapper et al., 1992; Bennett and Bolam, 1994). This difference in spatial organisation as well as our data, which shows that PV interneurones get convergent cortical inputs and multiple contacts from a single axon, suggests that these interneurones are more sensitive to cortical input than spiny neurones. Parvalbumin interneurones have also been shown to be connected via gap junctions (Kita et al., 1990; Chang and Kita, 1992; Koos and Tepper, 1999). Thus these cells can act as a syncytium and strongly modulate the firing of a large number of spiny projection neurones simultaneously (Koos and Tepper, 1999). The firing pattern of PV positive GABAergic interneurones plus the anatomical connection allows inhibitory potentials generated in one PV neurone to modulate the activity of a large number of projection neurones. Thus, cortical input which is unable to produce an EPSP in a medium spiny neurone could activate the PV interneurones. These neurones via their basket like arborisations on to the spiny cells can thus inhibit suboptimally excited striatal cells, while selectively allowing striatal projection cells that receive coherent cortical input to fire. This hypothesis fits in with the studies done by Parthasarathy and associates (Parthasarathy and Graybiel, 1997) who showed that micro-stimulation of the sensorimotor cortex led to immediate early gene expression in localised enkephalin positive cell clusters as well as a second group of neurones which were stimulated over a larger area and co-localised with parvalbumin. Thus, while a weak stimulus was unable to activate a large number of medium spiny projection neurones it was able to induce immediate early gene expression in parvalbumin interneurones.

A sub-population of GP neurones are known to innervate the striatum (Shu and Peterson, 1988; Walker et al., 1989; Spooren et al., 1996). The selective innervation of PV interneurones by a subclass of neurones in the GP (Bevan et al., 1998) indicates that these neurones are able to modulate the effect of cortical excitation on parvalbumin interneurones as a result of their direct or indirect activation by the cortex (Ryan and Clark, 1991; Kita, 1992). This connection plays an important role in synchronising the activity of the spiny projection neurones. A similar role for interneurones in the cortex has been suggested (Cobb et al., 1995).

Parvalbumin positive interneurones have also been shown to be contacted by other structures within the basal ganglia. Parvalbumin interneurones express the mRNA for D_2 receptors (Lenz et al., 1994) and to receive a dopaminergic innervation (Kubota et al., 1987). Striatal cholinergic interneurones synapse onto somata and dendrites of PV neurones (Chang and Kita, 1992) and PV interneurones contact varicose dendrites with could belong to somatostatin containing striatal interneurones (Kita et al., 1990). Thus PV interneurones receive more than cortical input and play an important role in integrating information from many regions of the basal ganglia and in turn help control local neuronal circuits in the striatum.

Experiments by Cowan and colleagues (Cowan et al., 1990) showed that the distribution of these GABAergic interneurones was not restricted to either the patch or the matrix, and the axons and dendrites of the cells cross the boundaries between compartments. So, while this study has shown that PV interneurones integrate information from different cortical areas that project to the same compartment, i.e. matrix, these neurones may also mediate the integration of information from cortical areas that project to different compartments, e.g. prelimbic cortex and sensory cortex

(Gerfen, 1984; Donoghue and Herkenham, 1986) as well as combining information from different cortical layers (Gerfen, 1989). The dendritic and local axonal fields of striatal projection neurones, however, stay within the boundaries of the patch matrix compartmentalisation (Penny et al., 1988; Kawaguchi et al., 1989). These interneurones therefore, may mediate the flow of cortical information between the patch matrix compartments.

Since spiny projection neurones are the major target of the corticostriatal projection there are additional possibilities for the synaptic convergence of corticostriatal afferents. It remains to be established whether the input from the two regions of the cortex converge on the same spiny projection neurones and/or target distinct populations of spiny neurones projecting to particular regions.

6.5) Conclusions

The overlapping corticostriatal projections from primary motor and somatosensory cortices do not remain segregated at the single cell level of the striatum, but rather, give rise to convergent synapses on individual PV-positive GABA interneurones. Thus, one mechanism by which the basal ganglia integrates somatosensory and motor information is through convergent cortical inputs to parvalbumin positive GABAergic interneurones. This integrated information is then transmitted to spiny projection neurones whereupon it shunts excitatory inputs to these cells and synchronises their activity, thereby achieving selective flow of information through the basal ganglia.

CHAPTER 7
GENERAL DISCUSSION

7.1) Discussion

7.1.1) Main findings

The findings of this thesis extend the knowledge of the anatomy and physiology of two corticostriatal pathways arising from the barrel cortex (Alloway et al., 1998; Alloway et al., 1999; Wright et al., 1999; Wright et al., 2001). Previous studies showed that these pathways differ in several aspects;

(i) Cells of origin

(ii) Projection sites onto the striatum

(iii) Morphology of the fibres

(iv) Patterns of axonal arborisation in the striatum

In this thesis I have extended these findings and discovered that the two corticostriatal pathways differ in their striatal postsynaptic targets and give rise to different striatal and cortical responses when stimulated (Alloway et al., 1998; Alloway et al., 1999; Wright et al., 1999; Wright et al., 2001). In addition if the dopaminergic input to the striatum is removed via 6-OHDA injections into the medial forebrain bundle, one of these corticostriatal pathway is modified preferentially and could be reflected the loss of synapses from a subset of striatal neurones (Ingham et al., 1998).

The experiments carried out in this thesis allowed the five aims set out in Chapter 1 to be realised. The aims were,

1. **To localise precisely, the postsynaptic targets of the topographic and diffuse pathways.**

   Both, the ipsilateral topographic pathway (made up of thick fibres) and the bilateral diffuse pathway (made up of thin fibres) form synapses onto the

heads of spines belonging to medium sized densely spiny striatal projection neurones. Boutons belonging to the topographic pathway make more complex synapses and contact both output pathways of the striatum with similar frequencies. Thin fibres make fewer synapses and contact D_1 immunonegative spines more often than D_1 immunopositive spines and therefore are assumed to contact predominantly striatal neurones of the indirect pathway.

2. **To compare and contrast the physiological responses of striatal and Layer V barrel cortical neurones to stimulation of the topographic and diffuse pathways.**

   Cortical and striatal neurones are able to respond to stimulation of both pathways under chloralose-urethane anaesthesia. Comparisons of stimulation of the diffuse pathway (via contralateral cortical stimulation) and topographic pathway (via stimulation of the whisker pad) show that for both cells types, while the mean latencies of the responses were the same, the EPSP rise time for contralateral cortical stimulation was significantly longer than whisker pad stimulation. The behaviour of the striatal cells mirrors that of cortical neurones indicating that these cells provide the main excitatory drive to striatal neurones.

3. **To study the physiological responses of striatal and Layer V barrel cortical neurones to asynchronously delivered pairs of stimuli to the topographic and diffuse pathways.**

   Both pathways interact at the level of both a single striatal and cortical cell. EPSPs were followed by a period of inhibition, the extent of which was

dependent on the order and source of the stimuli. The behaviour of the striatal cells to paired stimuli closely reflects the interaction seen in the layer V cortical cells that provide the main excitatory drive to striatal cells.

4. **To understand the response of striatal neurones in Parkinson's disease, the physiological response of striatal neurones to stimulation of the topographic and diffuse pathways and asynchronously delivered pairs of stimuli to the topographic and diffuse pathways when the dopaminergic input to striatal neurones was destroyed.**

   The removal of the dopaminergic projection from the nigra, affects the responses of striatal neurones to stimulation of the two corticostriatal pathways originating from the barrel cortex. The response of striatal neurones to whisker pad stimulation is altered, with an increase in the rise time of the EPSP, while the response to contralateral cortical stimuli is unaltered. The interaction of the two pathways at the level of a single striatal cell is also altered. The summation of EPSPs observed when stimuli were delivered 10 ms apart in control animals, are no longer seen and the period of inhibition seen in the pairing protocols is significantly lengthened in the lesioned animals, indicating that dopamine modulates inhibitory synaptic mechanisms in the striatum.

5. **To localise precisely, the motor and somatosensory cortical input to GABAergic interneurones in the striatum with the specific aim of examining possibility of convergence.**

   The overlapping corticostriatal projections from primary motor and somatosensory cortices do not remain segregated at the single cell level of the

striatum, but rather, give rise to convergent synapses on individual PV-positive GABA interneurones. Multiple appositions from individual cortical axons observed in contact with individual PV-positive neurones indicate that organisation of the corticostriatal projections varies between striatal projection neurones and striatal interneurones.

Both, the ipsilateral topographic pathway (made up of thick fibres) and the bilateral diffuse pathway (made up of thin fibres) form synapses onto the heads of spines belonging to medium sized densely spiny striatal projection neurones. In agreement with this, stimulation of either corticostriatal pathway, (topographic ipsilateral pathway by electrical stimulation of the whisker pad and diffuse bilateral pathway by stimulation of the contralateral cortex via a stimulating electrode) gave rise to EPSPs in striatal neurones and in some instances action potentials when the cells were stimulated suprathreshold. A difference was observed in the rise time of the EPSPs, in response to stimulation of either corticostriatal pathway in striatal neurones. The EPSP rise time in response to contralateral cortical stimulation was significantly longer than whisker pad stimulation and is likely a reflection of the difference in the the anatomy of connectivity of the two pathways to striatal neurones (Brown, 1991).

Boutons belonging to the topographic pathway, make complex synapses onto the head of the spines more frequently than boutons belonging to the diffuse pathway. The topographic pathway as its name suggests, also maintains a 'map' of the whiskers in the striatum, a characteristic that is not observed in the axonal arborisation pattern of the diffuse pathway (Wright et al., 1999). These data suggests

that the topographic pathway, as a result of its pattern of arborisation and contacts with spiny projection striatal neurones is an ideal pathway involved in transmitting whisker information to the striatum. However the function of the diffuse pathway is less clear and the lack of a topographic pattern of axonal arborisation suggests that, the role of this corticostriatal pathways might be one of a primer. This hypothesis was tested by stimulating both corticostriatal pathways asynchronously and looking to see if an initial stimulus facilitated or attenuated the response of the striatal cells to the second stimulus. While both pathways interact at the level a single striatal cell, the diffuse pathway did not have a clear facilitatory effect on the response of striatal cells to activation of the topographic pathway by stimulation of the whisker pad. Thus while the pattern of axonal arborisation would suggest that the diffuse pathway acts as priming pathway, the electrophysiological data does not support this hypothesis.

The loss of dopamine, alters the response of striatal neurones to stimulation of the topographic pathway, while the response of the cells to contralateral cortical stimulation (activation of the diffuse pathway) is unchanged. There is an increase in the rise time of the EPSP, and the spike initiation latency following suprathreshold whisker pad stimulation is more variable. As removal of dopamine results in the loss of spines (Ingham et al., 1989, 1993), the changes in the response of striatal neurones to corticostriatal stimulation, could reflect the loss of a specific set of spines i.e. spines contacted by the topographic pathway. The interaction of the two corticostriatal pathways at the level of a single striatal cell is also altered. The summation of EPSPs observed when the stimuli were delivered 10 ms apart in control animals, is no longer observed and could once again reflect the preferential

loss of a subset of synapses. As the loss of summation of EPSPs observed in lesioned animals, is likely to be mediated by D_1 set of dopamine receptors, and these receptors are contacted more often by the topographic pathway, it would seem that this corticostriatal pathway is more affected by dopamine loss. The period of inhibition seen in the pairing protocols is significantly lengthened in the lesioned animals, indicating that dopamine powerfully modulates inhibitory synaptic mechanisms in the striatum.

There is also a direct cortical input to interneurones in the striatum (Lapper and Bolam, 1992; Lapper et al., 1992; Kawaguchi, 1993, 1997; Thomas et al., 2000). Striatal projection neurones are likely to be affected by the cortical input to these interneurones via polysynaptic connections. Parvalbumin positive, GABAergic interneurones are the main source of inhibition in the striatum, the activity of these cells strongly modulates the behaviour of striatal neurones (Kawaguchi, 1997; Koos and Tepper, 1999). Thus the connectivity of these cells to different cortical areas was investigated and PV positive interneurones receive convergent input from functionally related cortical areas. Multiple appositions from individual cortical axons were observed in contact with individual PV-positive neurones indicating that organisation of the corticostriatal projections varies between striatal projection neurones and striatal interneurones (Kincaid et al., 1998; Ramanathan et al., 2002; Zheng and Wilson, 2002).

One surprising finding of this thesis was the difference in the anatomical and physiological results. There was a clear difference in the postsynaptic targets of the two input pathways from the barrel cortex to the striatum (Chapter 2), and changes in the response of striatal neurones to corticostriatal stimulation, after 6-OHDA was

confined to one pathway, strongly suggesting that the two pathways contact different striatal cells. Thus based on these results, a higher number of singly responsive striatal neurones would be expected. However, the majority of striatal cells (163 responding to both stimuli vs. 5 responding to contralateral cortical stimulation alone and 18 to whisker pad stimulation alone) responded to stimulation of both pathways.

While the results of this thesis might be further evidence that dopamine receptors are colocalised on the same striatal cell, it could also be due to technical difficulties in classifying D_1 receptor immunostaining as previously discussed (Chapter 2, see discussion). Another possibility is sampling error, in the anatomical study done in Chapter 2. Even though every attempt was made to select thin fibres (belonging to the diffuse pathway) in an area of striatum containing fibres of both pathways, there was a bias in selecting fibres that were relatively isolated, due to the ease of their identification at the electron microscope level. Thus there is a possibility that the thin fibres of the anatomical study were not the thin fibres that were part of the diffuse pathway, but were another corticostriatal projection. In addition to the main topographic corticostriatal pathway described, a second type of topographic projection arising from the barrel cortex (Alloway et al., 1999; Wright et al., 1999) has been observed and thin fibres sampled in the anatomical study could arise form this pathway. This projection is found more medial and is composed of thin fibres (Alloway et al., 1999; Wright et al., 1999). Interestingly, all neurones responsive only to contralateral cortical stimulation were found to be located more medially and at depths of 4200 to 4538. Based on the thickness of the fibres present in medial striatum and the fact that the neurones found in that area of striatum responded only to contralateral cortical stimulation it would seem that the second topographic

pathway might be part of the previously described 'diffuse' pathway (Wright et al., 1999). However, the position of all the fibres studied in the anatomical study were plotted and they corresponded to the area of striatum that receives the majority of the projections from the barrel cortex, and was similar to area from which electrophysiological records were obtained.

Another possibility for the small number of singly responsive neurones observed, could be the strength of the stimulus used. One possibility is that striatal neurones did not receive any information from the barrel cortex and were responding to stimulation of other areas of cortex, as the stimuli used in this study were not focal. However in experiments where the contralateral stimulating electrode had been misplaced, cells histologically verified to be located in the whisker area of striatum did not respond to contralateral cortical stimulation suggesting that while other cortical areas might be activated, the response of the cells is most likely to be from stimulation of the contralateral barrel cortex. The areas in which neurones responded match the areas that contain the topographical projection from the ipsilateral barrel cortex (Wright et al., 1999). The clear "cut off" mark of responding and non-responding cells confirms that neurones in the striatum receive their inputs from specific regions in the cortex.

7.1.2) Future work

One important finding of this thesis is that dopamine affects collaterals of brain stem projecting corticostriatal more strongly than 'pure' corticostriatal pathways. While there is physiological evidence for this, no anatomical work has been carried out. Thus one area where further work has to be carried out is, investigating the changes

in the connectivity of the two corticostriatal pathways to the output pathways of the striatum following dopamine depletion.

The differential connectivity of the two pathways can be exploited in the understanding of the interplay between dopamine and corticostriatal synaptic plasticity. Striatal neurones display both long term potentiation (LTP) and long term depression (LTD) (Reynolds and Wickens, 2002) (Cepeda and Levine, 1998). The variability in results among the different groups has been partly attributed to the different experimental approaches, such as *in vivo* vs. *in vitro*, pulsatile vs. bath application (reviewed by (Reynolds and Wickens, 2002) (Cepeda and Levine, 1998)). In addition to this, variation in the type of plasticity is attributed to the location of the neurones, with more medially located striatal neurones displaying potentiation compared to synaptic depression as expressed by lateral neurones (Akopian et al., 2000; Partridge et al., 2000). This has been partially explained by a decreasing gradient in D2 receptor expression lateral to medial (Joyce and Marshall, 1987; Russell et al., 1992), which fits in with electrophysiological studies that show LTP following high frequency stimulation (HFS) in both D2 knockout mice and flowing application of D2 receptor blockade (Calabresi et al., 1992; Calabresi et al., 1997). Another regional difference observed in, *in vivo* studies has been related to the hemisphere of cortical stimulation. LTP has been demonstrated after HFS of the ipsilateral cortex (Charpier et al., 1999), while LTD is seen after contralateral cortical stimulation (Reynolds and Wickens, 2000). While it is tempting to link the discrepancy with the results of this thesis, it has to be remembered that the above studies were performed in the motor cortex. Unlike the barrel cortex, it sends both pure corticostriatal and collaterals of brain stem projecting to both striata and the

connectivity of its corticostriatal projection is different (Hersch et al., 1995; Kincaid and Wilson, 1996). With this in mind, it begs the question what type of synaptic plasticity that would be obtained by stimulation of both corticostriatal pathways arising from the barrel cortex. As the connectivity of these two pathways to specific striatal neurones has been studied, the contribution of the specific dopamine receptors to striatal synaptic plasticity can be investigated.

As discussed in Chapter 6, the probability of a striatal GABAergic interneurone receiving multiple appositions from a single cortical afferent is very low. However multiple appositions were often observed and in one case, the cortical axon was verified under the EM to form multiple synapses with a single parvalbumin interneurone. This suggests that the connectivity of cortical area and parvalbumin interneurones is a selective process. However, it is not known if this selective innervation is provided by one class of corticostriatal projection. This question can be answered by looking at the connectivity of the two types of corticostriatal projection arising from the barrel cortex, to the GABAergic interneurones.

7.2) Conclusions

The projections from the barrel cortex to the striatum are unique in that, the pathways arising from 2 classes of cortical neurones that innervate the striatum can be stimulated separately and have unique anatomical and physiological properties. Thus the barrel-corticostriatal system is an ideal model to study the influence of the cortex on striatal behaviour and has provided clues as to how this pathway is modulated by dopamine.

REFERENCES

Acsady L, Gorcs TJ, Freund TF (1996) Different populations of vasoactive intestinal polypeptide-immunoreactive interneurons are specialized to control pyramidal cells or interneurons in the hippocampus. Neuroscience 73:317-334.

Agmon A, Connors BW (1992) Correlation between firing pattern and thalamocortical synaptic responses of neurons in the mouse barrel cortex. JNeurosci 12:319-329.

Ahissar E, Sosnik R, Haidarliu S (2000) Transformation from temporal to rate coding in a somatosensory thalamocortical pathway. Nature 406:302-306.

Akhtar NE, Land PW (1991) Activity-dependant regualtion of glutamic acid decarboxylase in the rat barrel cortex: Effects of neonatal versus adult sensory deprivation. JCompNeurol 307:200-213.

Akopian G, Musleh W, Smith R, Walsh JP (2000) Functional state of corticostriatal synapses determines their expression of short- and long-term plasticity. Synapse 38:271-280.

Albin RL, Young AB, Penney JB (1989) The functional anatomy of basal ganglia disorders. Trends Neurosci 12:366-375.

Alexander GE, Crutcher ME (1990) Functional architecture of basal ganglia circuits: neural substrates of parallel processing. Trends Neursoci 13:266-271.

Alexander GE, DeLong MR, Strick PL (1986) Parallel organization of functionally segregated circuits linking basal ganglia and cortex. Annu Rev Neurosci 9:357-381.

Alexander GE, Crutcher MD, DeLong MR (1990) Basal ganglia-thalamocortical circuits - parallel substrates for motor, oculomotor, 'prefrontal' and 'limbic' functions Uylings, H.B.M..//Vaneden, C.G.//Debruin, J.P.C.//Corner, M.A.//Feenstra, M.G.P. Edition: Elsevier Science Publishers.

Alloway KD, Mutic JJ, Hoover JE (1998) Divergent corticostriatal projections from a single cortical column in the somatosensory cortex of rats. Brain Res 785:341-346.

Alloway KD, Crist J, Mutic JJ, Roy SA (1999) Corticostriatal projections from rat barrel cortex have an anisotropic organization that correlates with vibrissal whisking behavior. J Neurosci 19:10908-10922.

Alloway KD, Mutic JJ, Hoffer ZS, Hoover JE (2000) Overlapping corticostriatal projections from the rodent vibrissal representations in primary and secondary somatosensory cortex. J Comp Neurol 426:51-67.

Amzica F, Steriade M (1995) Short- and long-range neuronal synchronization of the slow (< 1 Hz) cortical oscillation. J Neurophysiol 73:20-38.

Anden NE, Magnusson T, Rosengren E (1964) On the presence of dihydroxyphenylalanine decarboxylase in nerves. Experientia 20:328-329.

Andersen RA, Snyder LH, Bradley DC, Xing J (1997) Multimodal representation of space in the posterior parietal cortex and its use in planning movements. Annu Rev Neurosci 20:303-330.

Angulo MC, Lambolez B, Audinat E, Hestrin S, Rossier J (1997) Subunit composition, kinetic, and permeation properties of AMPA receptors in single neocortical nonpyramidal cells. J Neurosci 17:6685-6696.

Anis NA, Berry SC, Burton NR, Lodge D (1983) The dissociative anaesthetics, ketamine and phencyclidine, selectively reduce excitation of central mammalian neurones by N-methyl-aspartate. Br J Pharmacol 79:565-575.

Aosaki T, Kawaguchi Y (1996) Actions of substance P on rat neostriatal neurons in vitro. J Neurosci 16:5141-5153.

Arbuthnott GW (1974) Proceedings: Spontaneous activity of single units in the striatum after unilateral destruction of the dopamine input. J Physiol 239:121P-122P.

Armstrong-James M, Fox K (1987) Spatiotemporal convergence and divergence in the rat S1 "barrel" cortex. J Comp Neurol 263:265-281.

Armstrong-James M, George MJ (1988) Bilateral receptive fields of cells in rat Sm1 cortex. Exp Brain Res 70:155-165.

Armstrong-James M, Callahan C (1991) Thalamocortical mechamisms in the formation of receptive fields of rat barrel cortex neurons. II. The contribution of ventroposterior medial thalamic (VPm) neurones. JCompNeurol 303:211-224.

Armstrong-James M, Callahan CA, Friedman M (1991) Thalamocortical mechanisms in the formation of receptive fields of rat barrel cortex neurons. I. Intracortical mechanisms. JCompNeurol 303:193-210.

Armstrong-James M, Fox K, Das-Gupta A (1992) Flow of excitation within rat barrel cortex on striking a single vibrissa. J Neurophysiol 68:1345-1358.

Armstrong-James M, Welker E, Callahan CA (1993) The contribution of NMDA and non-NMDA receptors to fast and slow transmission of sensory information in the rat SI barrel cortex. JNeurosci 13:2149-2160.

Aronin N, Chase K, DiFiglia M (1986) Glutamic acid decarboxylase and enkephalin immunoreactive axon terminals in the rat neostriatum synapse with striatonigral neurons. Brain Res 365:151-158.

Barbaresi P, Spreafico R, Frassoni C, Rustioni A (1986) GABA-ergic neurons are present in the dorsal column nucleui but not in the ventroposterior complex of rats. Brain Res 382:305-326.

Bargas J, Galarraga E, Aceves J (1989) An early outward conductance modulates the firing latency and frequency of neostriatal neurons of the rat brain. Exp Brain Res 75:146-156.

Bates MD, Senogles SE, Bunzow JR, Liggett SB, Civelli O, Caron MG (1991) Regulation of responsiveness at D2 dopamine receptors by receptor desensitization and adenylyl cyclase sensitization. Mol Pharmacol 39:55-63.

Beaulieu C (1993) Numerical data on neocortical neurons in adult rat, with special reference to the GABA population. Brain Res 609:284-292.

Beiser DG, Hua SE, Houk JC (1997) Network models of the basal ganglia. Curr Opin Neurobiol 7:185-190.

Belford GR, Killackey HP (1979) The development of vibrissae representation in subcortical trigeminal centres of the neonatal rat. JCompNeurol 188:63-74.

Bennett BD, Bolam JP (1994) Synaptic input and output of parvalbumin-immunoreactive neurones in the neostriatum of the rat. Neuroscience 62:707-719.

Berendse HW, Galis-de Graaf Y, Groenewegen HJ (1992) Topographical organization and relationship with ventral striatal compartments of prefrontal corticostriatal projections in the rat. J Comp Neurol 316:314-347.

Berger B, Gaspar P, Verney C (1991) Dopaminergic innervation of the cerebral cortex: unexpected differences between rodents and primates. Trends Neurosci 14:21-27.

Bergman H, Wichmann T, DeLong MR (1990) Reversal of experimental parkinsonism by lesions of the subthalamic nucleus. Science 249:1436-1438.

Bergson C, Mrzljak L, Smiley JF, Pappy M, Levenson R, Goldman-Rakic PS (1995) Regional, cellular, and subcellular variations in the distribution of D1 and D5 dopamine receptors in primate brain. J Neurosci 15:7821-7836.

Bernardi G, Marciani MG, Morocutti C, Giacomini P (1975) The action of GABA on rat caudate neurones recorded intracellularly. Brain Res 92:511-515.

Bernardo KL, McCasland JS, Woolsey TA (1990a) Local axonal trajectories in mouse barrel cortex. Exp Brain Res 82:247-253.

Bernardo KL, McCasland JS, Woolsey TA, Strominger RN (1990b) Local intra- and interlaminar connections in mouse barrel cortex. J Comp Neurol 291:231-255.

Bertrand PP, Galligan JJ (1994) Contribution of chloride conductance increase to slow EPSC and tachykinin current in guinea-pig myenteric neurones. J Physiol 481 (Pt 1):47-60.

Bevan MD, Bolam JP (1995) The glutamate-enriched cortical and thalamic input to neurons in the subthalamic nucleus of the rat: convergence with GABA-positive terminals. J Comp Neurol 361:491-511.

Bevan MD, Smith AD, Bolam JP (1996) The substantia nigra as a site of synaptic integration of functionally diverse information arising from the ventral pallidum and the globus pallidus in the rat. Neuroscience 75:5-12.

Bevan MD, Clarke NP, Bolam JP (1997) Synaptic integration of functionally diverse pallidal information in the entopeduncular nucleus and subthalamic nucleus in the rat. J Neurosci 17:308-324.

Bevan MD, Booth PAC, Eaton SA, Bolam JP (1998) Selective innervation of neostriatal interneurons by a subclass of neuron in the globus pallidus of the rat. J Neurosci 18:9438-9452.

Billings LM, Marshall JF (2003) D2 antagonist-induced c-fos in an identified subpopulation of globus pallidus neurons by a direct intrapallidal action. Brain Res 964:237-243.

Bley KR, Tsien RW (1990) Inhibition of Ca2+ and K+ channels in sympathetic neurons by neuropeptides and other ganglionic transmitters. Neuron 4:379-391.

Bloom FE, Costa E, Salmoiraghi GC (1965) Anesthesia and the responsiveness of individual neurons of the caudate nucleus of the cat to acetylcholine, norepinephrine and dopamine administered by microelectrophoresis. J Pharmacol Exp Ther 150:244-252.

Bolam JP, Izzo PN (1988) The postsynaptic targets of substance P-immunoreactive terminals in the rat neostriatum with particular reference to identified spiny striatonigral neurons. Expl Brain Res 70:361-377.

Bolam JP, Ingham CA (1990) Combined morphological and histochemical techniques for the study of neuronal microcircuits. In: Analysis of Neuronal Microcircuits and Synaptic Interactions. (Bjorklund A, Hokfelt T, Wouterlood FG, van den Pol AN, eds), pp 125-198. Amsterdam: Elsevier Science Publishers B.V.

Bolam JP, Bennett B (1995) The microcircuitry of the neostriatum. Austin: R.G. Landes Company.

Bolam JP, Clarke DJ, Smith AD, Somogyi P (1983) A type of aspiny neuron in the rat neostriatum accumulates (^{3}H) γ aminobutyric acid: combination of Golgi-staining, autoradiography and electron microscopy. J Comp Neurol 213:121-134.

Bolam JP, Powell JF, Wu J-Y, Smith AD (1985) Glutamate decarboxylase-immunoreactive structures in the rat neostriatum. A correlated light and electron microscopic study including a combination of Golgi-impregnation with immunocytochemistry. J Comp Neurol 237:1-20.

Bourassa J, Pinault D, Deschenes M (1995) Corticothalamic projections from the cortical barrel field to the somatosensory thalamusin rats : a single fiber study using biocytin as an anterograde tracer. European Journal of Neuroscience 7:19-30.

Bracci E, Centonze D, Bernardi G, Calabresi P (2002) Dopamine excites fast-spiking interneurons in the striatum. J Neurophysiol 87:2190-2194.

Brett B, Di S, Watkins L, Barth DS (1994) A horseradish peroxidase study of parallel thalamocortical projections responsible for the generation of mid-latency auditory-evoked potentials. Brain Res 647:65-75.

Brown AG (1991) Nerve cells and nervous systems. An introduction to neuroscience. London: Springer-Verlag.

Brown JR, Arbuthnott GW (1983) The electrophysiology of dopamine (D2) receptors: a study of the actions of dopamine on corticostriatal transmission. Neuroscience 10:349-355.

Brown LL (1992) Somatotopic organization in rat striatum: evidence for a combinational map. Proc Natl Acad Sci U S A 89:7403-7407.

Brown LL, Sharp FR (1995) Metabolic mapping of rat striatum: somatotopic organization of sensorimotor activity. Brain Res 686:207-222.

Brown LL, Hand PJ, Divac I (1996) Representation of a single vibrissa in the rat neostriatum: peaks of energy metabolism reveal a distributed functional module. Neuroscience 75:717-728.

Brown LL, Smith DM, Goldbloom LM (1998) Organizing principles of cortical integration in the rat neostriatum: Corticostriate map of the body surface is an ordered lattice of curved laminae and radial points. J Comp Neurol 392:468-488.

Buchwald NA, Price DD, Vernon L, Hull CD (1973) Caudate intracellular response to thalamic and cortical inputs. Exp Neurol 38:311-323.

Calabresi P, Misgeld U, Dodt HU (1987a) Intrinsic membrane properties of neostriatal neurons can account for their low level of spontaneous activity. Neuroscience 20:293-303.

Calabresi P, Mercuri NB, Stefani A, Bernardi G (1990) Synaptic and intrinsic control of membrane excitability of neostriatal neurons. I. An in vivo analysis. J Neurophysiol 63:651-662.

Calabresi P, Pisani A, Mercuri NB, Bernardi G (1996) The corticostriatal projection: from synaptic plasticity to dysfunctions of the basal ganglia. Trends Neurosci 19:19-24.

Calabresi P, Mercuri N, Stanzione P, Stefani A, Bernardi G (1987b) Intracellular studies on the dopamine-induced firing inhibition of neostriatal neurons in vitro: evidence for D1 receptor involvement. Neuroscience 20:757-771.

Calabresi P, Maj R, Pisani A, Mercuri NB, Bernardi G (1992) Long-term synaptic depression in the striatum: physiological and pharmacological characterization. J Neurosci 12:4224-4233.

Calabresi P, Saiardi A, Pisani A, Baik JH, Centonze D, Mercuri NB, Bernardi G, Borrelli E (1997) Abnormal synaptic plasticity in the striatum of mice lacking dopamine D2 receptors. J Neurosci 17:4536-4544.

Canteras RD, Shammah-Lagnado SJ, Silva BA, Ricardo JA (1988) Somatosensory inputs to the subthalamic nucleus: a combined retrograde and anterograde horseradish peroxidase study in the rat. Brain Res 458:53-64.

Carelli RM, West MO (1991) Representation of the body by single neurons in the dorsolateral striatum of the awake, unrestrained rat. J Comp Neurol 309:231-249.

Carretta D, Sbriccoli A, Santarelli M, Pinto F, Granato A, Minciacchi D (1996) Crossed thalamo-cortical and cortico-thalamic projections in adult mice. Neurosci Lett 204:69-72.

Carvell GE, Simons DJ (1988) Membrane Potential changes in Rat Sm1 Cortical Neurons evoked by Controlled Stimulation of Mystacial Vibrissae. Brain Res 448:186-191.

Carvell GE, Simons DJ (1990) Biometric analyses of vibrissal tactile discrimination in the rat. J Neurosci 10:2638-2648.

Carvell GE, Simons DJ (1995) Task- and subject-related differences in sensorimotor behavior during active touch. Somatosens Mot Res 12:1-9.

Carvell GE, Simons DJ, Lichtenstein SH, Bryant P (1991) Electromyographic activity of the mystacial pad musculature during whisking behaviour in the rat. SomatosenMotor Res 8:159-164.

Castro-Alamancos MA, Connors BW (1996) Cellular mechanisms of the augmenting response: short-term plasticity in a thalamocortical pathway. J Neurosci 16:7742-7756.

Cavada C, Goldmanrakic PS (1991) Topographic Segregation of Corticostriatal Projections from Posterior Parietal Subdivisions in the Macaque Monkey. Neuroscience 42:683-696.

Celio MR (1990) Calbindin D-28k and parvalbumin in the rat nervous system. Neuroscience 35:375-475.

Cepeda C, Levine MS (1998) Dopamine and N-methyl-D-aspartate receptor interactions in the neostriatum. Dev Neurosci 20:1-18.

Cepeda C, Buchwald NA, Levine MS (1993) Neuromodulatory actions of dopamine in the neostriatum are dependent upon the excitatory amino acid receptor subtypes activated. Proc Natl Acad Sci U S A 90:9576-9580.

Cepeda C, Walsh JP, Peacock W, Buchwald NA, Levine MS (1994) Neurophysiological, pharmacological and morphological properties of human caudate neurons recorded in vitro. Neuroscience 59:89-103.

Cepeda C, Colwell CS, Itri JN, Chandler SH, Levine MS (1998) Dopaminergic modulation of NMDA-induced whole cell currents in neostriatal neurons in slices: contribution of calcium conductances. J Neurophysiol 79:82-94.

Chagnac-Amitai Y, Connors BW (1989a) Synchronised excitation and inhibition driven by intrinsically bursting neurons in neocortex. JNeurophysiol 62:1149-1162.

Chagnac-Amitai Y, Connors BW (1989b) Horizontal spread of synchronised activity in neocortex and its control by GABA-mediated inhibition. JNeurophysiol 61:747-758.

Chagnac-Amitai Y, Luhman HJ, Prince DA (1990) Burst generating and regular spiking layer 5 pyramidal neurons of rat neocortex have different morphological features. JCompNeurol 296:598-613.

Chang HT, Kita H (1992) Interneurons in the rat striatum: relationships between parvalbumin neurones and cholinergic neurons. Brain Res 574:307-311.

Chapin JK, Lin C-S (1984) Mapping the body representation in the SI cortex of the anaesthatised and awake rat. JCompNeurol 229:199-213.

Chapin JK, Sadeq M, Guise LU (1987) Corticocortical connections within the primary somatosensory cortex of the rat. JCompNeurol 263:326-346.

Charpier S, Mahon S, Deniau JM (1999) *In vivo* induction of striatal long-term potentiation by low-frequency stimulation of the cerebral cortex. Neuroscience 91:1209-1222.

Chatterjie N, Sechzer JA, Lieberman KW, Alexander GJ (1998) Dextro-naloxone counteracts amphetamine-induced hyperactivity. Pharmacol Biochem Behav 59:271-274.

Chen MT, Morales M, Woodward DJ, Hoffer BJ, Janak PH (2001) In vivo extracellular recording of striatal neurons in the awake rat following unilateral 6-hydroxydopamine lesions. Exp Neurol 171:72-83.

Cherubini E, Herrling PL, Lanfumey L, Stanzione P (1988) Excitatory amino acids in synaptic excitation of rat striatal neurones in vitro. J Physiol 400:677-690.

Chevalier G, Deniau JM (1990) Disinhibition as a basic process in the expression of striatal functions. Trends Neurosci 13:277-280.

Chevalier G, Vacher S, Deniau JM, Desban M (1985) Disinhibition as a basic process in the expression of striatal functions. I. The striato-nigral influence on tecto-spinal/tecto-diencephalic neurons. Brain Res 334:215-226.

Chiaia NL, Rhoades RW, Fish SE, Killackey HP (1991a) Thalamic processing of vibrissal information in the rat: II. Morphological and functional properties of medial ventral posterior nucleus and posterior nucleus neurons. JCompNeurol 314:217-236.

Chiaia NL, Rhoades RW, Bennett-Clarke CA, Fish SE, Killackey HP (1991b) Thalamic processing of vibrissal information in the rat: I. Afferent iput to the medial ventral and posterior nuclei. JCompNeurol 314:201-216.

Chiodo LA, Berger TW (1986) Interactions between dopamine and amino acid-induced excitation and inhibition in the striatum. Brain Res 375:198-203.

Chmielowska J, Stewart MG, Bourne RC (1988) gamma-Aminobutyric acid (GABA) immunoreactivity in mouse and rat first somatosensory (SI) cortex: description and comparison. Brain Res 439:155-168.

Cho J, West MO (1997) Distributions of single neurones related to body parts in the lateral striatum of the rat. Brain research 756:241-246.

Cho J, Duke D, Manzino L, Sonsalla PK, West MO (2002) Dopamine depletion causes fragmented clustering of neurons in the sensorimotor striatum: Evidence of lasting reorganization of corticostriatal input. J Comp Neurol 452:24-37.

Choi EJ, Xia Z, Villacres EC, Storm DR (1993) The regulatory diversity of the mammalian adenylyl cyclases. Curr Opin Cell Biol 5:269-273.

Chudler EH, Sugiyama K, Dong WK (1995) Multisensory convergence and integration in the neostriatum and globus pallidus of the rat. Brain Res 674:33-45.

Cicirata F, Angaut P, Serapide MF, Panto MR (1990) Functional organization of the direct and indirect projection via the reticularis thalami nuclear complex from the motor cortex to the thalamic nucleus ventralis lateralis. Experimental Brain Research 79:325-337.

Cicirata F, Angaut P, Cioni M, Serapide MF, Papale A (1986) Functional organization of thalamic projections to the motor cortex. An anatomical and electrophysiological study in the rat. Neuroscience 19:81-99.

Cipolloni PB, Peters A (1983) The termination of callosal fibres in the auditory cortex of the rat. A combined Golgi--electron microscope and degeneration study. J Neurocytol 12:713-726.

Clarey JC, Tweedale R, Calford MB (1996) Interhemispheric modulation of somatosensory receptive fields: evidence for plasticity in primary somatosensory cortex. Cereb Cortex 6:196-206.

Cobb SR, Buhl EH, Halasy K, Paulsen O, Somogyi P (1995) Synchronization of neuronal activity in hippocampus by individual GABAergic interneurons. Nature 378:75-78.

Connors BW (1984) Initiation of synchronised neuronal bursting in neocortex. Nature 310:685-687.

Connors BW, Gutnick MJ (1990) Intrinsic firing patterns of diverse neocortical neurons. Trends neurosci 13:99-104.

Connors BW, Malenka RC, Silva LR (1988) Two inhibitory postsynaptic potentials, and GABAA and GABAB receptor-mediated responses in neocortex of rat and cat. J Physiol 406:443-468.

Contreras D, Steriade M (1995) Cellular basis of EEG slow rhythms: a study of dynamic corticothalamic relationships. J Neurosci 15:604-622.

Contreras D, Timofeev I, Steriade M (1996) Mechanisms of long-lasting hyperpolarizations underlying slow sleep oscillations in cat corticothalamic networks. J Physiol 494 (Pt 1):251-264.

Cooper DC, White FJ (2000) L-type calcium channels modulate glutamate-driven bursting activity in the nucleus accumbens in vivo. Brain Res 880:212-218.

Corvaja M, Doucet G, Bolam JP (1991) Characterization of the postsynaptic targets of serotonergic terminals in the substantia nigra and striatum of the rat. . Eur J Neurosci Suppl 4:150.

Cowan RL, Wilson CJ (1994) Spontaneous firing patterns and axonal projections of single corticostriatal neurons in the rat medial agranular cortex. J Neurophysiol 71:17-32.

Cowan RL, Wilson CJ, Emson PC, Heizmann CW (1990) Parvalbumin-containing GABAergic interneurons in the rat neostriatum. J Comp Neurol 302:197-205.

Cruz CJ, Beckstead RM (1989) Nigrostriatal dopamine neurons are required to maintain basal levels of substance P in the rat substantia nigra. Neuroscience 30:331-338.

Czubayko U, Plenz D (2002) Fast synaptic transmission between striatal spiny projection neurons. Proc Natl Acad Sci U S A 99:15764-15769.

De Camilli P, Macconi D, Spada A (1979) Dopamine inhibits adenylate cyclase in human prolactin-secreting pituitary adenomas. Nature 278:252-254.

Dearry A, Gingrich JA, Falardeau P, Fremeau RT, Jr., Bates MD, Caron MG (1990) Molecular cloning and expression of the gene for a human D1 dopamine receptor. Nature 347:72-76.

DeFrance JF, Marchand JF, Sikes RW, Chronister RB, Hubbard JI (1985) Characterization of fimbria input to nucleus accumbens. J Neurophysiol 54:1553-1567.

DeLong MR (1990) Primate models of movement disorders of basal ganglia origin. Trends Neurosci 13:281-285.

Deniau JM, Chevalier G (1985) Disinhibition as a basic process in the expression of striatal functions. II. The striato-nigral influence on thalamocortical cells of the ventromedial thalamic nucleus. Brain Res 334:227-233.

Diamond ME, Armstrong-James M, Ebner FF (1992a) Somatic sensory responses in the rostral sector of the posterior group (POm) and in the ventral posterior medial nucleus (VPm) of the rat thalamus. JCompNeurol 318:462-476.

Diamond ME, Armstrong-James M, Budway MJ, Ebner FF (1992b) Somatic sensory responses in the rostral sector of the posterior group (POm) and in the ventral posterior medial nucleus (VPm) of the rat thalamus: Dependance on barrel cortex. JCompNeurol 319:66-84.

Donoghue JP, Kitai ST (1981) A collateral pathway to the neostriatum from corticofugal neurons of the rat sensory-motor cortex: an intracellular HRP study. J Comp Neurol 201:1-13.

Donoghue JP, Herkenham M (1986) Neostriatal projections from individual cortical fields conform to histochemically distinct striatal compartments in the rat. Brain Res 365:397-403.

Dorfl J (1982) The musculature of the mystacial vibrissae of the white mouse. J Anat 135:147-154.

Dorfl J (1985) The innervation of the mystacial region of the white mouse. A topographical study. Journal of Anatomy 142:173-184.

Dube L, Smith AD, Bolam JP (1988) Identification of synaptic terminals of thalamic or cortical origin in contact with distinct medium size spiny neurons in the rat neostriatum. J Comp Neurol 267:455-471.

Durham D, Woolsey TA (1978) Acute whisker removal reduces neuronal activity in barrels of mouse SmL cortex. J Comp Neurol 178:629-644.

Ebrahimi A, Pochet R, Roger M (1992) Topographical organization of the projections from physiologically identified areas of the motor cortex to the striatum of the rat. Neurosci Res 14:39-60.

Fee MS, Mitra PP, Kleinfeld D (1997) Central versus peripheral determinants of patterned spike activity in rat vibrissa cortex during whisking. J Neurophysiol 78:1144-1149.

Ferster D, Lindstrom S (1983) An intracellular analysis of geniculo-cortical connectivity in area 17 of the cat. J Physiol 342:181-215.

Filion M, Tremblay L, Bedard PJ (1988) Abnormal influences of passive limb movement on the activity of globus pallidus neurons in parkinsonian monkeys. Brain Res 444:165-176.

Finch DM (1996) Neurophysiology of converging synaptic inputs from the rat prefrontal cortex, amygdala, midline thalamus, and hippocampal formation onto single neurons of the caudate/putamen and nucleus accumbens. Hippocampus 6:495-512.

Finnerty GT, Roberts LS, Connors BW (1999) Sensory experience modifies the short-term dynamics of neocortical synapses. Nature 400:367-371.

Fitzpatrick JS, Akopian G, Walsh JP (2001) Short-term plasticity at inhibitory synapses in rat striatum and its effects on striatal output. J Neurophysiol 85:2088-2099.

Flaherty AW, Graybiel AM (1991) Corticostriatal transformations in the primate somatosensory system. Projections from physiologically mapped body-part representations. J Neurophysiol 66:1249-1263.

Flaherty AW, Graybiel AM (1993) Two input systems for body representations in the primate striatal matrix: experimental evidence in the squirrel monkey. J Neurosci 13:1120-1137.

Flaherty AW, Graybiel AM (1995) Motor and somatosensory corticostriatal projection magnifications in the squirrel monkey. J Neurophysiol 74:2638-2648.

Foehring RC, Surmeier DJ (1993) Voltage-gated potassium currents in acutely dissociated rat cortical neurons. J Neurophysiol 70:51-63.

Ford AP, Marsden CA (1986) Influence of anaesthetics on rat striatal dopamine metabolism in vivo. Brain Res 379:162-166.

Fotuhi M, Koliatos VE, Alexander GE, Delong MR (1989) Patterns of sensorimotor integration in the primate neostriatum: primary somatosensory cortex (SC) and motor cortex (MC) project to coextensive territories in the putamen. In: Society of Neuroscience Abstracts, p 15:285.

Fox K (2002) Anatomical pathways and molecular mechanisms for plasticity in the barrel cortex. Neuroscience 111:799-814.

Francois C, Yelnik J, Percheron G (1987) Golgi study of the primate substantia nigra II. Spatial organization of dendritic arborizations in relation to the cytoarchitectonic boundaries and to the striatonigral bundle. J Comp Neurol 265:473-493.

Fremeau RT, Jr., Duncan GE, Fornaretto MG, Dearry A, Gingrich JA, Breese GR, Caron MG (1991) Localization of D1 dopamine receptor mRNA in brain supports a role in cognitive, affective, and neuroendocrine aspects of dopaminergic neurotransmission. Proc Natl Acad Sci U S A 88:3772-3776.

French SJ, Totterdell S (2002) Hippocampal and prefrontal cortical inputs monosynaptically converge with individual projection neurons of the nucleus accumbens. J Comp Neurol 446:151-165.

Freund TF, Powell J, Smith AD (1984) Tyrosine hydroxylase-immunoreactive boutons in synaptic contact with identified striatonigral neurons, with particular reference to dendritic spines. Neuroscience 13:1189-1215.

Frotscher M, Rinne U, Hassler R, Wagner A (1981) Termination of cortical afferents on identified neurons in the caudate nucleus of the cat. A combined Golgi-EM degeneration study. Exp Brain Res 41:329-337.

Fujimoto K, Kita H (1993) Response characteristics of subthalamic neurons to the stimulation of the sensorimotor cortex in the rat. Brain Res 609:185-192.

Fuller TA, Russchen FT, Price JL (1987) Sources of presumptive glutamergic/aspartergic afferents to the rat ventral striatopallidal region. J Comp Neurol 258:317-338.

Gabel LA, Nisenbaum ES (1998) Biophysical characterization and functional consequences of a slowly inactivating potassium current in neostriatal neurons. J Neurophysiol 79:1989-2002.

Garcia-Munoz M, Young SJ, Groves PM (1991) Terminal excitability of the corticostriatal pathway. I. Regulation by dopamine receptor stimulation. Brain Res 551:195-206.

Gazzara RA, Fisher RS, Levine MS, Hull CD, Buchwald NA (1986) Physiological and morphological analyses of ventral anterior and ventral lateral thalamic neurons in the cat. Brain Res 397:225-237.

Geinisman Y, Morrell F, deToledo-Morrell L (1988) Remodeling of synaptic architecture during hippocampal "kindling". Proc Natl Acad Sci U S A 85:3260-3264.

Geinisman Y, deToledo-Morrell L, Morrell F (1991) Induction of long-term potentiation is associated with an increase in the number of axospinous synapses with segmented postsynaptic densities. Brain Res 566:77-88.

Gerfen CR (1984) The neostriatal mosaic: compartmentalization of corticostriatal input and striatonigral output systems. Nature 311:461-464.

Gerfen CR (1985) The neostriatal mosaic. I. compartmental organization of projections from the striatum to the substantia nigra in the rat. J Comp Neurol 236:454-476.

Gerfen CR (1989) The neostriatal mosaic: striatal patch-matrix organization is related to cortical lamination. Science 246:385-388.

Gerfen CR (1992) The neostriatal mosaic: multiple levels of compartmental organization in the basal ganglia. Annu Rev Neurosci 15:285-320.

Gerfen CR, Young WS, 3rd (1988) Distribution of striatonigral and striatopallidal peptidergic neurons in both patch and matrix compartments: an in situ hybridization histochemistry and fluorescent retrograde tracing study. Brain Res 460:161-167.

Gerfen CR, Wilson CJ (1996) The Basal Ganglia: Elsevier Science.

Gerfen CR, Baimbridge KG, Miller JJ (1985) The neostriatal mosaic: Compartmental distribution of calcium binding protein and parvalbumin in the basal ganglia of the rat and monkey. Proc Natl Acad Sci 82:8780-8784.

Gerfen CR, Herkenham M, Thibault J (1987) The neostriatal mosaic: II. Patch- and matrix-directed mesostriatal dopaminergic and non-dopaminergic systems. J Neurosci 7:3915-3934.

Gerfen CR, McGinty JF, Young WS, 3rd (1991) Dopamine differentially regulates dynorphin, substance P, and enkephalin expression in striatal neurons: in situ hybridization histochemical analysis. J Neurosci 11:1016-1031.

Gerfen CR, Keefe KA, Steiner H (1998) Dopamine-mediated gene regulation in the striatum. Adv Pharmacol 42:670-673.

Gerfen CR, Engber TM, Mahan LC, Susel Z, Chase TN, Monsma FJ, Jr., Sibley DR (1990) D1 and D2 dopamine receptor-regulated gene expression of striatonigral and striatopallidal neurons. Science 250:1429-1432.

Gibson JR, Beierlein M, Connors BW (1999) Two networks of electrically coupled inhibitory neurons in neocortex. Nature 402:75-79.

Gil Z, Amitai Y (1996) Properties of convergent thalamocortical and intracortical synaptic potentials in single neurons of neocortex. J Neurosci 16:6567-6578.

Gil Z, Connors BW, Amitai Y (1997) Differential regulation of neocortical synapses by neuromodulators and activity. Neuron 19:679-686.

Gingrich JA, Caron MG (1993) Recent advances in the molecular biology of dopamine receptors. Annu Rev Neurosci 16:299-321.

Glazewski S, Barth AL, Wallace H, McKenna M, Silva A, Fox K (1999) Impaired experience-dependent plasticity in barrel cortex of mice lacking the alpha and delta isoforms of CREB. Cereb Cortex 9:249-256.

Glynn G, Ahmad SO (2002) Three-dimensional electrophysiological topography of the rat corticostriatal system. J Comp Physiol A Neuroethol Sens Neural Behav Physiol 188:695-703.

Goldman PS, Nauta WJH (1977) An intricately patterned prefronto-caudate projection in the rhesus monkey. J Comp Neurol 171:369-374.

Goldman-Rakic PS, Selemon LD (1990) New frontiers in basal ganglia research. Trends in Neuroscience 13:241-244.

Gonon F (1997) Prolonged and extrasynaptic excitatory action of dopamine mediated by D1 receptors in the rat striatum in vivo. J Neurosci 17:5972-5978.

Goto Y, O'Donnell P (2001a) Network synchrony in the nucleus accumbens in vivo. J Neurosci 21:4498-4504.

Goto Y, O'Donnell P (2001b) Synchronous activity in the hippocampus and nucleus accumbens in vivo. J Neurosci 21:RC131.

Graybiel AM (1990) Neurotransmitters and neuromodulators in the basal ganglia. Trends Neurosci 13:244-254.

Graybiel AM (1995) Building action repertoires: memory and learning functions of the basal ganglia. Current Opinion Neurobiol 5:733-741.

Graybiel AM, Ragsdale CW, Jr. (1978) Histochemically distinct compartments in the striatum of human, monkeys, and cat demonstrated by acetylthiocholinesterase staining. Proc Natl Acad Sci U S A 75:5723-5726.

Graybiel AM, Kimura M (1995) Adaptive neural networks in the basal ganglia. In: Models of Information Processing in the Basal Ganglia (Houk JC, Davis JL, Beiser DG, eds), pp 103-116: The MIT Press.

Graybiel AM, Flaherty AW, Gimenez-Amaya JM (1993) Striosomes and matrisomes. In: The Basal Gnaglia (Bernardi G, Carpenter M, Di Chiara G, Morelli G, Stanzione P, eds), pp 3-12. New York: Plenum Press.

Greenough WT, West RW, DeVoogd TJ (1978) Subsynaptic plate perforations: changes with age and experience in the rat. Science 202:1096-1098.

Greif GJ, Lin YJ, Liu JC, Freedman JE (1995) Dopamine-modulated potassium channels on rat striatal neurons: specific activation and cellular expression. J Neurosci 15:4533-4544.

Groenewegen HJ, Becker NE, Lohman AH (1980) Subcortical afferents of the nucleus accumbens septi in the cat, studied with retrograde axonal transport of horseradish peroxidase and bisbenzimid. Neuroscience 5:1903-1916.

Groenewegen HJ, Berendse HW, Haber SN (1993) Organization of the output of the ventral striatopallidal system in the rat: ventral pallidal efferents. Neuroscience 57:113-142.

Groves PM, Garcia-Munoz M, Linder JC, Manley MS, Martone ME, Young SJ (1995) Elements of the intrinsic organization and information processing in the neostriatum. In: Models of Information Processing in the Basal Ganglia (Houk JC, Davis JL, Beiser DG, eds), pp 51-96: The MIT Press.

Haber SN, Lynd-Balta E, Mitchell SJ (1993) The organization of the descending ventral pallidal projections in the monkey. J Comp Neurol 329:111-128.

Haber SN, Fudge JL, McFarland NR (2000) Striatonigrostriatal pathways in primates form an ascending spiral from the shell to the dorsolateral striatum. J Neurosci 20:2369-2382.

Haber SN, Groenewegen HJ, Grove EA, Nauta WJ (1985) Efferent connections of the ventral pallidum: evidence of a dual striato pallidofugal pathway. J Comp Neurol 235:322-335.

Hanley JJ, Bolam JP (1997) Synaptology of the nigrostriatal projection in relation to the compartmental organization of the neostriatum in the rat. Neuroscience 81:353-370.

Haracz JL, Tschanz JT, Greenberg J, Rebec GV (1989) Amphetamine-induced excitations predominate in single neostriatal neurons showing motor-related activity. Brain Res 489:365-368.

Haracz JL, Tschanz JT, Wang Z, White IM, Rebec GV (1993) Striatal single-unit responses to amphetamine and neuroleptics in freely moving rats. Neurosci Biobehav Rev 17:1-12.

Harding G, Stogsdill RM, Towe AL (1979) Relative effects of pentobarbitol and chloralose on the responsiveness of the neurones in sensorimotor cerebral cortex of the domestic cat. Neurosci 4:369-378.

Harris KM, Kater SB (1994) Dendritic spines: cellular specializations imparting both stability and flexibility to synaptic function. Annu Rev Neurosci 17:341-371.

Harris RM, Hendrickson AE (1987) Local circuit neurons in the rat ventrobasal thalamus--a GABA immunocytochemical study. Neuroscience 21:229-236.

Hefti F, Melamed E, Wurtman RJ (1980) Partial lesions of the dopaminergic nigrostriatal system in rat brain: biochemical characterization. Brain Res 195:123-137.

Heimer L, Zahm DS, Churchill L, Kalivas PW, Wohltmann C (1991) Specificity in the projection patterns of accumbal core and shell in the rat. Neuroscience 41:89-125.

Hernandez-Lopez S, Bargas J, Surmeier DJ, Reyes A, Galarraga E (1997) D1 receptor activation enhances evoked discharge in neostriatal medium spiny neurons by modulating an L-type Ca2+ conductance. J Neurosci 17:3334-3342.

Hernandez-Lopez S, Tkatch T, Perez-Garci E, Galarraga E, Bargas J, Hamm H, Surmeier DJ (2000) D2 dopamine receptors in striatal medium spiny neurons reduce L-type Ca2+ currents and excitability via a novel PLC[beta]1-IP3-calcineurin-signaling cascade. J Neurosci 20:8987-8995.

Herrera-Marschitz M, Meana JJ, Hokfelt T, You ZB, Morino P, Brodin E, Ungerstedt U (1992) Cholecystokinin is released from a crossed corticostriatal pathway. Neuroreport 3:905-908.

Herrero MT, Levy R, Ruberg M, Luquin MR, Villares J, Guillen J, Faucheux B, Javoy-Agid F, Guridi J, Agid Y, Obeso JA, Hirsch EC (1996) Consequence of nigrostriatal denervation and L-dopa therapy on the expression of glutamic acid decarboxylase messenger RNA in the pallidum. Neurology 47:219-224.

Herrling PL (1985) Pharmacology of the corticocaudate excitatory postsynaptic potential in the cat: evidence for its mediation by quisqualate- or kainate-receptors. Neuroscience 14:417-426.

Herrling PL, Hull CD (1980) Iontophoretically applied dopamine depolarizes and hyperpolarizes the membrane of cat caudate neurons. Brain Res 192:441-462.

Hersch SM, Ciliax BJ, Gutekunst CA, Rees HD, Heilman CJ, Yung KKL, Bolam JP, Ince E, Yi H, Levey AI (1995) Electron microscopic analysis of D1 and D2 dopamine receptor proteins in the dorsal striatum and their synaptic relationships with motor corticostriatal afferents. J Neurosci 15:5222-5237.

Hikosaka O, Wurtz RH (1983a) Visual and oculomotor functions of monkey substantia nigra pars reticulata. IV. Relation of substantia nigra to superior colliculus. J Neurophysiol 49:1285-1301.

Hikosaka O, Wurtz RH (1983b) Visual and oculomotor functions of monkey substantia nigra pars reticulata. III. Memory-contingent visual and saccade responses. J Neurophysiol 49:1268-1284.

Hirata K, Yim CY, Mogenson GJ (1984) Excitatory input from sensory motor cortex to neostriatum and its modification by conditioning stimulation of the substantia nigra. Brain Res 321:1-8.

Hirsch JC, Fourment A, Marc ME (1983) Sleep-related variations of membrane potential in the lateral geniculate body relay neurons of the cat. Brain Res 259:308-312.

Hoeflinger BF, Bennett-Clarke CA, Chiaia NL, Killackey HP, Rhoades RW (1995) Patterning of local intracortical projections within the vibrissae representation of rat primary somatosensory cortex. J Comp Neurol 354:551-563.

Hoffer ZS, Alloway KD (2001) Organization of corticostriatal projections from the vibrissal representations in the primary motor and somatosensory cortical areas of rodents. J Comp Neurol 439:87-103.

Hollmann M, Heinemann S (1994) Cloned glutamate receptors. Annu Rev Neurosci 17:31-108.

Hoogland PV, Welker E, van der Loos H (1987) Organizations of the projections from barrel cortex to thalamus in mice studied with Phaseolus vulgaris-leucoagglutinin and HRP. ExpBrain Res 68:73-87.

Hoover BR, Marshall JF (1999) Population characteristics of preproenkephalin mRNA-containing neurons in the globus pallidus of the rat. Neurosci Lett 265:199-202.

Hoover BR, Marshall JF (2002) Further characterization of preproenkephalin mRNA-containing cells in the rodent globus pallidus. Neuroscience 111:111-125.

Hoover JE, Strick PL (1993) Multiple output channels in the basal ganglia. Science 259:819-821.

Houk JC (1995) Information processing in modular circuits linking basal ganglia and cerebral cortex. In: Models of Information Processing in the Basal Ganglia (Houk JC, Davis JL, Beiser DG, eds), pp 3-9: The MIT Press.

Hu XT, Wang RY (1988) Comparison of effects of D-1 and D-2 dopamine receptor agonists on neurons in the rat caudate putamen: an electrophysiological study. J Neurosci 8:4340-4348.

Hu XT, White FJ (1997) Dopamine enhances glutamate-induced excitation of rat striatal neurons by cooperative activation of D1 and D2 class receptors. Neurosci Lett 224:61-65.

Hu XT, Wachtel SR, Galloway MP, White FJ (1990) Lesions of the nigrostriatal dopamine projection increase the inhibitory effects of D1 and D2 dopamine agonists on caudate-putamen neurons and relieve D2 receptors from the necessity of D1 receptor stimulation. J Neurosci 10:2318-2329.

Hull CD, Bernardi G, Buchwald NA (1970) Intracellular responses of caudate neurons to brain stem stimulation. Brain Res 22:163-179.

Hussain Z, Johnson LR, Totterdell S (1996) A light and electron microscopic study of NADPH-diaphorase-, calretinin- and parvalbumin-containing neurons in the rat nucleus accumbens. J Chem Neuroanat 10:19-39.

Hutton EAM (1999) Somatosensory cortical input to the striatum. In: Department of preclinical veterinary sciences, p 245. Edinburgh: University of Edinburgh.

Inase M, Sakai ST, Tanji J (1996) Overlapping corticostriatal projections from the supplementary motor area and the primary motor cortex in the macaque monkey: an anterograde double labeling study. J Comp Neurol 373:283-296.

Ingham CA, Hood SH, Arbuthnott GW (1989) Spine density on neostriatal neurones changes with 6-hydroxydopamine lesions and with age. Brain Res 503:334-338.

Ingham CA, Hood SH, Arbuthnott GW (1991) A light and electron microscopical study of enkephalin- immunoreactive structures in the rat neostriatum after removal of the nigrostriatal dopaminergic pathway. Neuroscience 42:715-730.

Ingham CA, Hood SH, Arbuthnott GW (1993) Correlated light and electron microscopy of golgi impregnated neostriatal neurons after 6-hydroxydopamine lesions in the rat. In: The Basal Ganglia III (Bernardi G, Carpenter M, Di Chiara G, Morelli G, Stanzione P, eds), pp 21-28. New York: Plenum Press.

Ingham CA, Stephens B, Arbuthnott GW (2002) Structural plasticity in parkinson's disease. In: The Basal Ganglia VII (Nicholson LFB, Faull RL, eds), pp 333-340. New York: Kluwer Academic/Plenum Publishers.

Ingham CA, Hood SH, Taggart P, Arbuthnott GW (1998) Plasticity of synapses in the rat neostriatum after unilateral lesion of the nigrostriatal dopaminergic pathway. J Neurosci 18:4732-4743.

Ingham CA, Hood SH, Mijnster MJ, Baldock RA, Arbuthnott GW (1997) Plasticity of striatopallidal terminals following unilateral lesion of the dopaminergic nigrostriatal pathway: a morphological study. Exp Brain Res 116:39-49.

Iwamura Y (2000) Bilateral receptive field neurons and callosal connections in the somatosensory cortex. Philos Trans R Soc Lond B Biol Sci 355:267-273.

Jackson DM, Westlind-Danielsson A (1994) Dopamine receptors: molecular biology, biochemistry and behavioural aspects. Pharmacol Ther 64:291-370.

Jaeger D, Gilman S, Aldridge JW (1993) Primate basal ganglia activity in a precued reaching task: preparation for movement. Exp Brain Res 95:51-64.

Jaeger D, Kita H, Wilson CJ (1994) Surround inhibition among projection neurons is weak or nonexistent in the rat neostriatum. JNeurophysiol 72:2555-2558.

Jensen KF, Killackey HP (1987) Terminal arbors of axons projecting to the somatosensory cortex of the adult rat. 1.The normal morphology of specific thalamocortical afferents. JNeurosci 7:3529-3543.

Jiang ZG, North RA (1991) Membrane properties and synaptic responses of Rat Striatal Neurones In Vitro. JPhysiol 443:533-553.

Jimenez-Castellanos J, Graybiel AM (1987) Subdivisions of the dopamine-containing A8-A9-A10 complex identified by their differential mesostriatal innervation of striosomes and extrastriosomal matrix. Neuroscience 23:223-242.

Jimenez-Castellanos J, Graybiel AM (1989) Compartmental origins of striatal efferent projections in the cat. Neuroscience 32:297-321.

Jinnai K, Matsuda Y (1979) Neurons of the motor cortex projecting commonly on the caudate nucleus and the lower brain stem in the cat. Neurosci Lett 13:121-126.

Johnson SW, Palmer MR, Freedman R (1983) Effects of dopamine on spontaneous and evoked activity of caudate neurons. Neuropharmacology 22:843-851.

Jones EG, Coulter JD, Burton H, Porter R (1977) Cells of origin and terminal distribution of corticostriatal fibers arising in the sensory-motor cortex of monkeys. JCompNeurol 173:53-80.

Joyce JN, Marshall JF (1987) Quantitative autoradiography of dopamine D2 sites in rat caudate-putamen: localization to intrinsic neurons and not to neocortical afferents. Neuroscience 20:773-795.

Kasanetz F, Riquelme LA, Murer MG (2002) Disruption of the two-state membrane potential of striatal neurones during cortical desynchronisation in anaesthetised rats. J Physiol 543:577-589.

Kawaguchi Y (1993) Physiological, morphological, and histochemical characterization of three classes of interneurons in rat neostriatum. J Neurosci 13:4908-4923.

Kawaguchi Y (1997) Neostriatal cell subtypes and their functional roles. Neurosci Res 27:1-8.

Kawaguchi Y, Wilson CJ, Emson PC (1989) Intracellular recording of identified neostriatal patch and matrix spiny cells in a slice preparation preserving cortical inputs. J Neurophysiol 62:1052-1068.

Kawaguchi Y, Wilson CJ, Emson PC (1990) Projection subtypes of rat neostriatal matrix cells revealed by intracellular injection of biocytin. J Neurosci 10:3421-3438.

Kawaguchi Y, Wilson CJ, Augood SJ, Emson PC (1995) Striatal interneurones: chemical, physiological and morphological characterization. Trends Neurosci 18:527-535.

Keller A, White EL (1987) Synaptic organization of GABAergic neurons in the mouse SmI cortex. J Comp Neurol 262:1-12.

Kelley AE, Domesick VB (1982) The distribution of the projection from the hippocampal formation to the nucleus accumbens in the rat: an anterograde- and retrograde-horseradish peroxidase study. Neuroscience 7:2321-2335.

Kemp JM, Powell TPS (1971) The termination of fibres from the cerebral cortex and thalamus upon dendritic spines in the caudate nucleus: A study with the golgi method. PhilTransRSocLondB 262:429-439.

Killackey HP (1983) The somatosensory cortex of the rodent. TINS 6:425-429.

Kim U, Ebner FF (1999) Barrels and septa: separate circuits in rat barrels field cortex. J Comp Neurol 408:489-505.

Kincaid AE, Wilson CJ (1996) Corticostriatal innervation of the patch and matrix in the rat neostriatum. J Comp Neurol 374:578-592.

Kincaid AE, Zheng T, Wilson CJ (1998) Connectivity and convergence of single corticostriatal axons. J Neurosci 18:4722-4731.

Kish LJ, Palmer MR, Gerhardt GA (1999) Multiple single-unit recordings in the striatum of freely moving animals: effects of apomorphine and D-amphetamine in normal and unilateral 6-hydroxydopamine-lesioned rats. Brain Res 833:58-70.

Kita H (1992) Responses of globus pallidus neurons to cortical stimulation: intracellular study in the rat. Brain Res 589:84-90.

Kita H (1993) GABAergic circuits of the striatum.

Kita H (1994) Parvalbumin-immunopositive neurons in rat globus pallidus: a light and electron microscopic study. Brain Res 657:31-41.

Kita H (1996) Glutamatergic and GABAergic postsynaptic responses of striatal spiny neurons to intrastriatal and cortical stimulation recorded in slice preparations. Neuroscience 70:925-940.

Kita H, Kitai ST (1988) Glutamate decarboxylase immunoreactive neurons in rat neostriatum: their morphological types and populations. Brain Res 447:346-352.

Kita H, Kitai ST (1990) Amygdaloid projections to the frontal cortex and the striatum in the rat. J Comp Neurol 298:40-49.

Kita H, Kitai ST (1994) The morphology of globus pallidus projection neurons in the rat: an intracellular staining study. Brain Res 636:308-319.

Kita H, Chang HT, Kitai ST (1983) Pallidal inputs to subthalamus: intracellular analysis. Brain Res 264:255-265.

Kita H, Kita T, Kitai ST (1985) Active membrane properties of rat neostriatal neurons in an in vitro slice preparation. Exp Brain Res 60:54-62.

Kita H, Kosaka T, Heizmann CW (1990) Parvalbumin-immunoreactive neurons in the rat neostriatum: a light and electron microscopic study. Brain Res 536:1-15.

Kitai ST, Deniau JM (1981) Cortical inputs to the subthalamus: intracellular analysis. Brain Res 214:411-415.

Kitai ST, Surmeier DJ (1993) Cholinergic and dopaminergic modulation of potassium conductances in neostriatal neurons. Adv Neurol 60:40-52.

Kitai ST, Kocsis JD, Wood J (1976) Origin and characteristics of the cortico-caudate afferents: an anatomical and electrophysiological study. Brain Res 118:137-141.

Kitai ST, Wagner A, Precht W, Ono T (1975) Nigro-caudate and caudato-nigral relationship: an electrophysiological study. Brain Res 85:44-48.

Kiyatkin EA, Rebec GV (1996) Dopaminergic modulation of glutamate-induced excitations of neurons in the neostriatum and nucleus accumbens of awake, unrestrained rats. J Neurophysiol 75:142-153.

Kiyatkin EA, Rebec GV (1999) Modulation of striatal neuronal activity by glutamate and GABA: iontophoresis in awake, unrestrained rats. Brain Res 822:88-106.

Kolomiets BP, Deniau JM, Mailly P, Menetrey A, Glowinski J, Thierry AM (2001) Segregation and convergence of information flow through the cortico-subthalamic pathways. J Neurosci 21:5764-5772.

Koos T, Tepper JM (1999) Inhibitory control of neostriatal projection neurons by GABAergic interneurons. Nature *Neurosci* 2:467-472.

Koralek KA, Olavarria J, Killackey HP (1990) Areal and laminar organization of corticocortical projections in the rat somatosensory cortex. J Comp Neurol 299:133-150.

Koralek K-A, Jensen KF, Killackey HP (1988) Evidence for two complementary patterns of thalamic input to the rat somatosensory cortex. Brain Res 463:346-351.

Kreiss DS, Mastropietro CW, Rawji SS, Walters JR (1997) The response of subthalamic nucleus neurons to dopamine receptor stimulation in a rodent model of Parkinson's disease. J Neurosci 17:6807-6819.

Kubota Y, Inagaki S, Kito S, Wu J-Y (1987) Dopaminergic axons directly make synapses with GABAergic neurons in the rat neostriatum. Brain Res 406:147-156.

Kunze W, McKenzie JS, Bendrups AP (1979) An electrophysiological study of thalamo-caudate neurones in the cat. Exp Brain Res 36:233-244.

Kunzle H (1975) Bilateral projections from precentral motor cortex to the putamen and other parts of the basal ganglia. An autoradiographic study in Macaca fascicularis. Brain Res 88:195-209.

Laitinen JT (1993) Dopamine stimulates K+ efflux in the chick retina via D1 receptors independently of adenylyl cyclase activation. J Neurochem 61:1461-1469.

Land PW, Buffer SA, Yaskosky JD (1995) Barreloids in Adult Rat Thalamus: Three-Dimensional Architecture and Relationship to Somatosensory Cortical Barrels. The Journal of Comparative Neurology 355:573-588.

Landry P, Wilson CJ, Kitai ST (1984) Morphological and electrophysiological characteristics of pyramidal tract neurons in the rat. Exp Brain Res 57:177-190.

Lapper SR, Bolam JP (1992) Input from the frontal cortex and the parafascicular nucleus to cholinergic interneurones in the dorsal striatum of the rat. Neuroscience 51:533-545.

Lapper SR, Smith Y, Sadikot AF, Parent A, Bolam JP (1992) Cortical input to parvalbumin-immunoreactive neurones in the putamen of the squirrel monkey. Brain Res 580:215-224.

Lavin A, Grace AA (1994) Modulation of dorsal thalamic cell activity by the ventral pallidum: its role in the regulation of thalamocortical activity by the basal ganglia. Synapse 18:104-127.

Lavoie B, Parent A (1991) Dopaminergic neurons expressing calbindin in normal and parkinsonian monkeys. Neuroreport 2:601-604.

Le Moine C, Tison F, Bloch B (1990) D2 dopamine receptor gene expression by cholinergic neurons in the rat striatum. Neurosci Lett 117:248-252.

Le Moine C, Normand E, Bloch B (1991) Phenotypical characterization of the rat striatal neurons expressing the D1 dopamine receptor gene. Proc Natl Acad Sci U S A 88:4205-4209.

Lenz S, Perney TM, Qin Y, Robbins E, Chesselet M-F (1994) GABA-ergic interneurons of the striatum express the Shaw-like potassium channel Kv3.1. Synapse 18:55-66.

Levesque M, Parent A (1998) Axonal arborization of corticostriatal and corticothalamic fibers arising from prelimbic cortex in the rat. Cereb Cortex 8:602-613.

Levesque M, Charara A, Gagnon S, Parent A, Deschenes M (1996) Corticostriatal projections from layer V cells in rat are collaterals of long-range corticofugal axons. Brain Res 709:311-315.

Levey AI, Hersch SM, Rye DB, Sunahara RK, Niznik HB, Kitt CA, Price DL, Maggio R, Brann MR, Ciliax BJ, et al. (1993) Localization of D1 and D2 dopamine receptors in brain with subtype-specific antibodies. Proc Natl Acad Sci U S A 90:8861-8865.

Levine MS, Li Z, Cepeda C, Cromwell HC, Altemus KL (1996) Neuromodulatory actions of dopamine on synaptically-evoked neostriatal responses in slices. Synapse 24:65-78.

Lin CS, Lu SM, Schmechel DE (1985) Glutamic acid decarboxylase immunoreactivity in layer IV of barrel cortex of rat and mouse. J Neurosci 5:1934-1939.

Lisman JE, Harris KM (1993) Quantal analysis and synaptic anatomy--integrating two views of hippocampal plasticity. Trends Neurosci 16:141-147.

Ljungberg T, Ungerstedt U (1976) Sensory inattention produced by 6-hydorxy-dopamine-induced degeneration of ascending dopamine neurones in the brain. Exp Neurol 53:585-600.

Loopuijt LD, van der Kooy D (1985) Organization of the striatum: collateralization of its efferent axons. Brain Res 348:86-99.

Lovinger DM, Zimmerman SA, Levitin M, Jones MV, Harrison NL (1993) Trichloroethanol potentiates synaptic transmission mediated by gamma-aminobutyric acidA receptors in hippocampal neurons. J Pharmacol Exp Ther 264:1097-1103.

Lu SM, Lin CS (1993) Thalamic afferents of the rat barrel cortex: A light - and electron- microscopic study using phaseolus vulgaris leucoagglutinin as an anterograde tracer. SomatosenMotor Res 10:1-16.

Luk KC, Sadikot AF (2001) GABA promotes survival but not proliferation of parvalbumin-immunoreactive interneurons in rodent neostriatum: an in vivo study with stereology. Neuroscience 104:93-103.

MacLeod NK, Ryman A, Arbuthnott GW (1990) Electrophysiological properties of nigrothalamic neurons after 6-hydroxydopamine lesions in the rat. Neuroscience 38:447-456.

Magill PJ, Bolam JP, Bevan MD (2001) Dopamine regulates the impact of the cerebral cortex on the subthalamic nucleus-globus pallidus network. Neuroscience 106:313-330.

Mahon S, Deniau JM, Charpier S (2001) Relationship between EEG potentials and intracellular activity of striatal and cortico-striatal neurons: an in vivo study under different anesthetics. Cereb Cortex 11:360-373.

Mahon S, Delord B, Deniau JM, Charpier S (2000a) Intrinsic properties of rat striatal output neurones and time-dependent facilitation of cortical inputs in vivo. J Physiol 527 Pt 2:345-354.

Mahon S, Deniau JM, Charpier S, Delord B (2000b) Role of a striatal slowly inactivating potassium current in short-term facilitation of corticostriatal inputs: a computer simulation study. Learn Mem 7:357-362.

Malach R, Graybiel AM (1986) Mosaic architecture of the somatic sensory-recipient sector of the cat's striatum. J Neurosci 6:3436-3458.

Manzoni T, Barbaresi P, Conti F, Fabri M (1989) The callosal connections of the primary somatosensory cortex and the neural bases of midline fusion. Exp Brain Res 76:251-266.

Marshall JF, Billings LM (2002) Dopamine cell injury-induced increases in gad67 mrna in rat globus pallidus (gp): neuron population differences. In: Society for Neuroscience, p 63.11. Orlando, Florida.

Marshall JF, Richardson JS, Teitelbaum P (1974) Nigrostriatal bundle damage and the lateral hypothalamic syndrome. J Comp Physiol Psychol 87:808-830.

Martorana A, Fusco FR, Picconi B, Massa R, Bernardi G, Sancesario G (2001) Dopamine denervation induces neurotensin immunoreactivity in GABA-parvalbumin striatal neurons. Synapse 41:360-362.

Maurice N, Deniau JM, Glowinski J, Thierry AM (1999) Relationships between the prefrontal cortex and the basal ganglia in the rat: physiology of the cortico-nigral circuits. J Neurosci 19:4674-4681.

Maurice N, Deniau JM, Menetrey A, Glowinski J, Thierry AM (1998) Prefrontal cortex-basal ganglia circuits in the rat: involvement of ventral pallidum and subthalamic nucleus. Synapse 29:363-370.

Maurin Y, Banrezes B, Menetrey A, Mailly P, Deniau JM (1999) Three-dimensional distribution of nigrostriatal neurons in the rat: Relation to the topography of striatonigral projections. Neuroscience 91:891-909.

McCasland JS, Woolsey TA (1988) High-resolution 2-deoxyglucose mapping of functional cortical columns in mouse barrel cortex. J Comp Neurol 278:555-569.

McCasland JS, Carvell GE, Simons DJ, Woolsey TA (1991) Functional Asymmetries in the Rodent Barrel Cortex. SomatosenMotor Res 8:111-116.

McCormick DA (1991) Functional properties of a slowly inactivating potassium current in guinea pig dorsal lateral geniculate relay neurons. J Neurophysiol 66:1176-1189.

McDonald AJ (1991a) Topographical organization of amygdaloid projections to the caudatoputamen, nucleus accumbens, and related striatal-like areas of the rat brain. Neuroscience 44:15-33.

McDonald AJ (1991b) Organization of amygdaloid projections to the prefrontal cortex and associated striatum in the rat. Neuroscience 44:1-14.

McDonald WM, Sibley DR, Kilpatrick BF, Caron MG (1984) Dopaminergic inhibition of adenylate cyclase correlates with high affinity agonist binding to anterior pituitary D2 dopamine receptors. Mol Cell Endocrinol 36:201-209.

McGeorge AJ, Faull RLM (1987) The organization and collateralization of corticostriate neurones in the motor and sensory cortex of the rat brain. Brain Res 423:318-324.

McGeorge AJ, Faull RL (1989) The organization of the projection from the cerebral cortex to the striatum in the rat. Neuroscience 29:503-537.

McLennan H, York DH (1967) The action of dopamine on neurones of the caudate nucleus. J Physiol 189:393-402.

Medina AE, Liao DS, Mower AF, Ramoa AS (2001) Do NMDA receptor kinetics regulate the end of critical periods of plasticity? Neuron 32:553-555.

Mercier BE, Legg CR, Glickstein M (1990) Basal ganglia and cerebellum receive different somatosensory information in rats. ProcNatlAcadSci(USA) 87:4388-4392.

Mercuri N, Bernardi G, Calabresi P, Cotugno A, Levi G, Stanzione P (1985) Dopamine decreases cell excitability in rat striatal neurons by pre- and postsynaptic mechanisms. Brain Res 358:110-121.

Meredith GE, Wouterlood FG, Pattiselanno A (1990) Hippocampal fibers make synaptic contacts with glutamate decarboxylase-immunoreactive neurons in the rat nucleus accumbens. Brain Res 513:329-334.

Meshul CK, Casey DE (1989) Regional, reversible ultrastructural changes in rat brain with chronic neuroleptic treatment. Brain Res 489:338-346.

Meshul CK, Bunker GL, Mason JN, Allen C, Janowsky A (1996a) Effects of subchronic clozapine and haloperidol on striatal glutamatergic synapses. J Neurochem 67:1965-1973.

Meshul CK, Buckman JF, Allen C, Riggan JP, Feller DJ (1996b) Activation of corticostriatal pathway leads to similar morphological changes observed following haloperidol treatment. Synapse 22:350-361.

Micheva KD, Beaulieu C (1997) Development and plasticity of the inhibitory neocortical circuitry with an emphasis on the rodent barrel field cortex: a review. Can J Physiol Pharmacol 75:470-478.

Middleton FA, Strick PL (2000) Basal ganglia and cerebellar loops: motor and cognitive circuits. Brain Res Brain Res Rev 31:236-250.

Mirabella G, Battiston S, Diamond ME (2001) Integration of multiple-whisker inputs in rat somatosensory cortex. Cereb Cortex 11:164-170.

Missale C, Nash SR, Robinson SW, Jaber M, Caron MG (1998) Dopamine receptors: from structure to function. Physiol Rev 78:189-225.

Mittler T, Cho J, Peoples LL, West MO (1994) Representation of the body in the lateral striatum of the freely moving rat: single neurons related to licking. Exp Brain Res 98:163-167.

Mogenson GJ, Jones DL, Yim CY (1980) From motivation to action: functional interface between the limbic system and the motor system. Prog Neurobiol 14:69-97.

Monaghan DT, Bridges RJ, Cotman CW (1989) The excitatory amino acid receptors: their classes, pharmacology, and distinct properties in the function of the central nervous system. Annu Rev Pharmacol Toxicol 29:365-402.

Monakow KH, Akert K, Kunzle H (1978) Projections of the precentral motor cortex and other cortical areas of the frontal lobe to the subthalamic nucleus in the monkey. Exp Brain Res 33:395-403.

Monsma FJ, Jr., Mahan LC, McVittie LD, Gerfen CR, Sibley DR (1990) Molecular cloning and expression of a D1 dopamine receptor linked to adenylyl cyclase activation. Proc Natl Acad Sci U S A 87:6723-6727.

Morino P, Herrera-Marschitz M, Meana JJ, Ungerstedt U, Hokfelt T (1992) Immunohistochemical evidence for a crossed cholecystokinin corticostriatal pathway in the rat. Neurosci Lett 148:133-136.

Morino P, Herrera-Marschitz M, Castel MN, Ungerstedt U, Varro A, Dockray G, Hokfelt T (1994) Cholecystokinin in cortico-striatal neurons in the rat: immunohistochemical studies at the light and electron microscopical level. Eur J Neurosci 6:681-692.

Murer MG, Riquelme LA, Tseng KY, Pazo JH (1997) Substantia nigra pars reticulata single unit activity in normal and 60HDA-lesioned rats: effects of intrastriatal apomorphine and subthalamic lesions. Synapse 27:278-293.

Nambu A, Tokuno H, Takada M (2002) Functional significance of the cortico-subthalamo-pallidal 'hyperdirect' pathway. Neurosci Res 43:111-117.

Nambu A, Takada M, Inase M, Tokuno H (1996) Dual somatotopical representations in the primate subthalamic nucleus: evidence for ordered but reversed body-map transformations from the primary motor cortex and the supplementary motor area. J Neurosci 16:2671-2683.

Nambu A, Tokuno H, Inase M, Takada M (1997) Corticosubthalamic input zones from forelimb representations of the dorsal and ventral divisions of the premotor cortex in the macaque monkey: comparison with the input zones from the primary motor cortex and the supplementary motor area. Neurosci Lett 239:13-16.

Nauta WJH, Domesick VB (1984) Afferent and efferent relationships of the basal ganglia.3-23.

Ng GY, Mouillac B, George SR, Caron M, Dennis M, Bouvier M, O'Dowd BF (1994) Desensitization, phosphorylation and palmitoylation of the human dopamine D1 receptor. Eur J Pharmacol 267:7-19.

Ni ZG, Gao DM, Benabid AL, Benazzouz A (2000) Unilateral lesion of the nigrostriatal pathway induces a transient decrease of firing rate with no change in the firing pattern of neurons of the parafascicular nucleus in the rat. Neuroscience 101:993-999.

Nicola SM, Malenka RC (1998) Modulation of synaptic transmission by dopamine and norepinephrine in ventral but not dorsal striatum. J Neurophysiol 79:1768-1776.

Nicola SM, Surmeier DJ, Malenka RC (2000) Dopaminergic modulation of neuronal excitability in the striatum and nucelus accumbens. Annual Review of Neuroscience 23:185-215.

Nicolelis MA, Baccala LA, Lin RC, Chapin JK (1995) Sensorimotor encoding by synchronous neural ensemble activity at multiple levels of the somatosensory system. Science 268:1353-1358.

Nisenbaum ES, Berger TW (1992) Functionally distinct subpopulations of striatal neurons are differentially regulated by GABAergic and dopaminergic inputs-I. In vivo analysis. Neuroscience 48:561-578.

Nisenbaum ES, Wilson CJ (1995) Potassium currents responsible for inward and outward rectification in rat neostriatal spiny projection neurons. JNeurosci 15:4449-4463.

Nisenbaum ES, Orr WB, Berger TW (1988) Evidence for two functionally distinct subpopulations of neurons within the rat striatum. J Neurosci 8:4138-4150.

Nisenbaum ES, Grace AA, Berger TW (1992) Functionally distinct subpopulations of striatal neurons are differentially regulated by GABAergic and dopaminergic inputs--II. In vitro analysis. Neuroscience 48:579-593.

Nisenbaum ES, Xu ZC, Wilson CJ (1994) Contribution of a slowly inactivating potassium current to the transition to firing of neostriatal spiny projection neurons. JNeurophysiol 71:1174-1189.

Nisenbaum ES, Stricker EM, Zigmond MJ, Berger TW (1986) Long-term effects of dopamine-depleting brain lesions on spontaneous activity of type II striatal neurons: relation to behavioral recovery. Brain Res 398:221-230.

Nisenbaum ES, Wilson CJ, Foehring RC, Surmeier DJ (1996) Isolation and characterization of a persistent potassium current in neostriatal neurons. J Neurophysiol 76:1180-1194.

Nothias F, Peschanski M, Besson JM (1988) Somatotopic reciprocal connections between the somatosensory cortex and the thalamic Po nucleus in the rat. Brain Research 447:169-174.

O'Donnell P (1999) Ensemble coding in the nucleus accumbens. Psychobiology 27:187-197.

O'Donnell P, Grace AA (1994) Tonic D2-mediated attenuation of cortical excitation in nucleus accumbens neurons recorded in vitro. Brain Res 634:105-112.

O'Donnell P, Grace AA (1995) Synaptic interactions among excitatory afferents to nucleus accumbens neurons: hippocampal gating of prefrontal cortical input. J Neurosci 15:3622-3639.

Ohno Y, Sasa M, Takaori S (1987) Coexistence of inhibitory dopamine D-1 and excitatory D-2 receptors on the same caudate nucleus neurons. Life Sci 40:1937-1945.

Olavarria J, Van Sluyters RC, Killackey HP (1984) Evidence for the comlementary organization of callosal and thalamic connections within rat somatosensory cortex. Brain Res 291:364-368.

Onali P, Schwartz JP, Costa E (1981) Dopaminergic modulation of adenylate cyclase stimulation by vasoactive intestinal peptide in anterior pituitary. Proc Natl Acad Sci U S A 78:6531-6534.

Onali P, Olianas MC, Gessa GL (1985) Characterization of dopamine receptors mediating inhibition of adenylate cyclase activity in rat striatum. Mol Pharmacol 28:138-145.

Onn SP, Berger TW, Grace AA (1994a) Identification and characterization of striatal cell subtypes using in vivo intracellular recording and dye-labeling in rats: III. Morphological correlates and compartmental localization. Synapse 16:231-254.

Onn SP, Berger TW, Grace AA (1994b) Identification and characterization of striatal cell subtypes using in vivo intracellular recording in rats: II. Membrane factors underlying paired-pulse response profiles. Synapse 16:195-210.

Onn SP, Berger TW, Grace AA (1994c) Identification and characterization of striatal cell subtypes using in vivo intracellular recording in rats: I. Basic physiology and response to corticostriatal fiber stimulation. Synapse 16:161-180.

Onn SP, West AR, Grace AA (2000) Dopamine-mediated regulation of striatal neuronal and network interactions. Trends Neurosci 23:S48-56.

Oorschot DE (1996) Total number of neurons in the neostriatal, pallidal, subthalamic, and substantia nigral nuclei of the rat basal ganglia: a stereological study using the cavalieri and optical disector methods. J Comp Neurol 366:580-599.

Pacheco-Cano MT, Bargas J, Hernandez-Lopez S, Tapia D, Galarraga E (1996) Inhibitory action of dopamine involves a subthreshold Cs(+)-sensitive conductance in neostriatal neurons. Exp Brain Res 110:205-211.

Pan HS, Walters JR (1988) Unilateral lesion of the nigrostriatal pathway decreases the firing rate and alters the firing pattern of globus pallidus neurons in the rat. Synapse 2:650-656.

Parent A, Hazrati LN (1995) Functional anatomy of the basal ganglia. II. The place of subthalamic nucleus and external pallidum in basal ganglia circuitry. Brain Res Rev 20:128-154.

Parent A, Charara A, Pinault D (1995) Single striatofugal axons arborizing in both pallidal segments and in the substantia nigra in primates. Brain Res 698:280-284.

Parthasarathy HB, Graybiel AM (1997) Cortically driven immediate-early gene expression reflects modular influence of sensorimotor cortex on identified striatal neurons in the squirrel monkey. J-Neurosci 17:2477-2491.

Parthasarathy HB, Schall JD, Graybiel AM (1992) Distributed but convergent ordering of corticostriatal projections - analysis of the frontal eye field and the supplementary eye field in the macaque monkey. J Neurosci 12:4468-4488.

Partridge JG, Tang KC, Lovinger DM (2000) Regional and postnatal heterogeneity of activity-dependent long-term changes in synaptic efficacy in the dorsal striatum. J Neurophysiol 84:1422-1429.

Pasik P, Pasik T, Holstein GR, Pecci Saavedra J (1984) Serotoninergic innervation of the monkey basal ganglia: an immunocytochemical, light and electron microscopy study: Plenum Pub Corp.

Paxinos G, Watson C (1986) The rat brain in sterotaxic coordinates. Sydney: Academic Press.

Pearson RCA, Gatter KC, Powell TPS (1983) The cortical relationships of certain basal ganglia and the cholinergic basal forebrain nuclei. Brain Res 261:327-330.

Pei X, Vidyasagar TR, Volgushev M, Creutzfeldt OD (1994) Receptive field analysis and orientation selectivity of postsynaptic potentials of simple cells in cat visual cortex. J Neurosci 14:7130-7140.

Pennartz CM, Kitai ST (1991) Hippocampal inputs to identified neurons in an in vitro slice preparation of the rat nucleus accumbens: evidence for feed-forward inhibition. J Neurosci 11:2838-2847.

Pennartz CM, Boeijinga PH, Kitai ST, Lopes da Silva FH (1991) Contribution of NMDA receptors to postsynaptic potentials and paired-pulse facilitation in identified neurons of the rat nucleus accumbens in vitro. Exp Brain Res 86:190-198.

Penny GR, Afsharpour S, Kitai ST (1986) The glutamate decarboxylase-, leucine enkephalin-, methionine enkephalin- and substance P-immunoreactive neurons in the neostriatum of the rat and cat: evidence for partial population overlap. Neuroscience 17:1011-1045.

Penny GR, Wilson CJ, Kitai ST (1988) Relationship of the axonal and dendritic geometry of spiny prejection neurons to the compartmental organization of the neostriatum. J Comp Neurol 269:275-289.

Pidoux B, Verley R (1979) Projections on the cortical somatic I barrel subfield from ipsilateral vibrissae in adult rodents. Electroencephalogr Clin Neurophysiol 46:715-726.

Pierce JP, Lewin GR (1994) An ultrastructural size principle. Neuroscience 58:441-446.

Pierce RC, Rebec GV (1995) Iontophoresis in the neostriatum of awake, unrestrained rats: differential effects of dopamine, glutamate and ascorbate on motor- and nonmotor-related neurons. Neuroscience 67:313-324.

Plenz D, Aertsen A (1996a) Neural dynamics in cortex-striatum co-cultures. I. Anatomy and electrophysiology of neuronal cell types. Neuroscience 70:861-892.

Plenz D, Aertsen A (1996b) Neural dynamics in cortex-striatum co-cultures. II. Spatiotemporal characteristics of neuronal activity. Neuroscience 70:893-924.

Plenz D, Kitai ST (1998) Up and down states in striatal medium spiny neurons simultaneously recorded with spontaneous activity in fast-spiking interneurons studied in cortex-striatum-substantia nigra organotypic cultures. J Neurosci 18:266-283.

Porter JT, Johnson CK, Agmon A (2001) Diverse types of interneurons generate thalamus-evoked feedforward inhibition in the mouse barrel cortex. J Neurosci 21:2699-2710.

Price TR, Webster KE (1972) The cortico-thalamic projection form the primary somatosensory cortex of the rat. Brain Research 44:636-640.

Radnikow G, Rohrbacher J, Misgeld U (1997) Heterogeneity in use-dependent depression of inhibitory postsynaptic potentials in the rat neostriatum in vitro. J Neurophysiol 77:427-434.

Ragsdale CW, Jr., Graybiel AM (1981) The fronto-striatal projection in the cat and monkey and its relationship to inhomogeneities established by acetylcholinesterase histochemistry. Brain Res 208:259-266.

Rajakumar N, Elisevich K, Flumerfelt BA (1994a) The pallidostriatal projection in the rat: a recurrent inhibitory loop? Brain Res 651:332-336.

Rajakumar N, Rushlow W, Naus CC, Elisevich K, Flumerfelt BA (1994b) Neurochemical compartmentalization of the globus pallidus in the rat: an immunocytochemical study of calcium-binding proteins. J Comp Neurol 346:337-348.

Ramanathan S, Hanley JJ, Deniau JM, Bolam JP (2002) Synaptic convergence of motor and somatosensory cortical afferents onto GABAergic interneurons in the rat striatum. J Neurosci 22:8158-8169.

Rawls SM, McGinty JF (2000) Delta opioid receptors regulate calcium-dependent, amphetamine-evoked glutamate levels in the rat striatum: an in vivo microdialysis study. Brain Res 861:296-304.

Reynolds JN, Wickens JR (2002) Dopamine-dependent plasticity of corticostriatal synapses. Neural Netw 15:507-521.

Reynolds JNJ, Wickens JR (2000) Substantia nigra dopamine regulates synaptic plasticity and membrane potential fluctuations in the rat neostriatum, in vivo. Neuroscience 99:199-203.

Ribak CE, Vaughn JE, Roberts E (1979) The GABA neurons and their axon terminals in rat corpus striatum as demonstrated by GAD immunocytochemistry. J Comp Neurol 187:261-284.

Richards CD, Taylor DCM (1982) Electrophysiological evidence for a somatotopic sensory projection to the striatum of the rat. Neurosci Lett 30:235-240.

Rothblat DS, Schneider JS (1993) Response of caudate neurons to stimulation of intrinsic and peripheral afferents in normal, symptomatic, and recovered MPTP-treated cats. J Neurosci 13:4372-4378.

Rothblat DS, Schneider JS (1995) Alterations in pallidal neuronal responses to peripheral sensory and striatal stimulation in symptomatic and recovered parkinsonian cats. Brain Res 705:1-14.

Rouzaire-dubois B, Hammond C, Hamon B, Feger J (1980) Pharmacological blockade of the globus palidus-induced inhibitory response of subthalamic cells in the rat. Brain Res 200:321-329.

Royce GJ (1983) Cortical neurons with collateral projections to both the caudate nucleus and the centromedian-parafascicular thalamic complex: a fluorescent retrograde double labeling study in the cat. Exp Brain Res 50:157-165.

Rudkin TM, Sadikot AF (1999) Thalamic input to parvalbumin-immunoreactive gabaergic interneurons: Organization in normal striatum and effect of neonatal decortication. Neuroscience 88:1165-1175.

Ruskin DN, Marshall JF (1997) Differing influences of dopamine agonists and antagonists on Fos expression in identified populations of globus pallidus neurons. Neuroscience 81:79-92.

Russell VA, Allin R, Lamm MC, Taljaard JJ (1992) Regional distribution of monoamines and dopamine D1- and D2-receptors in the striatum of the rat. Neurochem Res 17:387-395.

Ryan LJ, Clark KB (1991) The role of the subthalamic nucleus in the response of globus pallidus neurons to stimulation of the prelimbic and agranular frontal cortices in rats. Exp Brain Res 86:641-651.

Sachdev RN, Wilson CJ (2001) Mechanisms underlying the trial to trial variability in response to whisker stimulation in rat barrel cortex. In: Society for Neuroscience, p 393.317. San Diego, CA.

Sachdev RN, Wilson CJ (2002) State dependence of neostriatal response to whisker stimulation. In: Society for Neuroscience, p 765.765. Orlando, Florida.

Sachdev RN, Sellien H, Ebner FF (2000) Direct inhibition evoked by whisker stimulation in somatic sensory (SI) barrel field cortex of the awake rat. J Neurophysiol 84:1497-1504.

Sadek AR, Magill PJ, Bolam JP (2002) Substance P immunostaining in the globus pallidus of the rat. In: 3rd Forum of European Neuroscience, p 091.021. Paris, France.

Schad CA, Justice JB, Jr., Holtzman SG (1995) Naloxone reduces the neurochemical and behavioral effects of amphetamine but not those of cocaine. Eur J Pharmacol 275:9-16.

Schallert T, Whishaw IQ (1978) Two types of aphagia and two types of sensorimotor impairment after lateral hypothalamic lesions: observations in normal weight, dieted, and fattened rats. J Comp Physiol Psychol 92:720-741.

Schallert T, Whishaw IQ, De Ryck M, Teitelbaum P (1978a) The postures of catecholamine-depletion catalepsy: their possible adaptive value in thermoregulation. Physiol Behav 21:817-820.

Schallert T, Whishaw IQ, Ramirez VD, Teitelbaum P (1978b) Compulsive, abnormal walking caused by anticholinergics in akinetic, 6-hydroxydopamine-treated rats. Science 199:1461-1463.

Schiffman HR, Lore R, Passafiume J, Neeb R (1970) Role of vibrissae for depth perception in the rat (Rattus norvegicus). Anim Behav 18:290-292.

Schinelli S, Paolillo M, Corona GL (1994) Opposing actions of D1- and D2-dopamine receptors on arachidonic acid release and cyclic AMP production in striatal neurons. J Neurochem 62:944-949.

Schlaggar BL, O'Leary DD (1993) Patterning of the barrel field in somatosensory cortex with implications for the specification of neocortical areas. Perspect Dev Neurobiol 1:81-91.

Schlaggar BL, Fox K, O'Leary DD (1993) Postsynaptic control of plasticity in developing somatosensory cortex. Nature 364:623-626.

Schneider JS (1991) Responses of striatal neurons to peripheral sensory stimulation in symptomatic MPTP-exposed cats. Brain Research 544:297-302.

Schneider JS, Diamond SG, Markham CH (1987) Parkinson's disease: sensory and motor problems in arms and hands. Neurology 37:951-956.

Schneider JS, McLaughlin WW, Roeltgen DP (1992) Motor and nonmotor behavioral deficits in monkeys made hemiparkinsonian by intracarotid MPTP infusion. Neurology 42:1565-1572.

Schuller JJ, Marshall JF (2000) Acute immediate-early gene response to 6-hydroxydopamine infusions into the medial forebrain bundle. Neuroscience 96:51-58.

Schultz W (1982) Depletion of dopamine in the striatum as an experimental model of Parkinsonism: direct effects and adaptive mechanisms. Prog Neurobiol 18:121-166.

Schultz W, Ungerstedt U (1978) A method to detect and record from striatal cells of low spontaneous activity by stimulating the corticostriatal pathway. Brain Res 142:357-362.

Schultz W, Romo R (1988) Neuronal activity in the monkey striatum during the initiation of movements. Exp Brain Res 71:431-436.

Schwindt PC, Spain WJ, Crill WE (1989) Long-lasting reduction of excitability by a sodium-dependent potassium current in cat neocortical neurons. J Neurophysiol 61:233-244.

Schwindt PC, Spain WJ, Foehring RC, Stafstrom CE, Chubb MC, Crill WE (1988) Multiple potassium conductances and their functions in neurons from cat sensorimotor cortex in vitro. J Neurophysiol 59:424-449.

Sedgwick EM, Williams TD (1967) The response of single units in the caudate nucleus to peripheral stimulation. J Physiol, Lond 189:281-298.

See RE, Chapman MA (1994) Chronic haloperidol, but not clozapine, produces altered oral movements and increased extracellular glutamate in rats. Eur J Pharmacol 263:269-276.

Selemon LD, Goldman-Rakic PS (1985) Longitudinal topography and interdigitation of corticostriatal projections in the rhesus monkey. J Neurosci 5:776-794.

Sesack SR, Aoki C, Pickel VM (1994) Ultrastructural localization of D2 receptor-like immunoreactivity in midbrain dopamine neurons and their striatal targets. J Neurosci 14:88-106.

Sesack SR, Deutch AY, Roth RH, Bunney BS (1989) Topographical organization of the efferent projections of the medial prefrontal cortex in the rat: an anterograde tract-tracing study with Phaseolus vulgaris leucoagglutinin. J Comp Neurol 290:213-242.

Shen KZ, North RA (1992) Substance P opens cation channels and closes potassium channels in rat locus coeruleus neurons. Neuroscience 50:345-353.

Shin HC, Won CK, Jung SC, Oh S, Park S, Sohn JH (1997) Interhemispheric modulation of sensory transmission in the primary somatosensory cortex of rats. Neurosci Lett 230:137-139.

Shu SY, Peterson GM (1988) Anterograde and retrograde axonal transport of Phaseolus vulgaris leucoagglutinin (PHA-L) from the globus pallidus to the striatum of the rat. J Neurosci Methods 25:175-180.

Shuler MG, Krupa DJ, Nicolelis MA (2001) Bilateral integration of whisker information in the primary somatosensory cortex of rats. J Neurosci 21:5251-5261.

Shuler MG, Krupa DJ, Nicolelis MA (2002) Integration of bilateral whisker stimuli in rats: role of the whisker barrel cortices. Cereb Cortex 12:86-97.

Simons DJ (1978) Response properties of vibrissa units in the rat S1 somatosensory neocortex. JNeurophysiol 41:798-820.

Simons DJ, Carvell GE (1989) Thalamocortical Response Transformation in the Rat Vibrissa/Barrel System. JNeurophysiol 61:311-330.

Simons DJ, Carvell GE, Hershey AE, Bryant DP (1992) Responses of barrel cortex neurons in awake rats and effects of urethane anesthesia. Exp Brain Res 91:259-272.

Smith AD, Bolam JP (1990a) The neural network of the basal ganglia as revealed by the study of synaptic connections of identified neurones. Trends Neurosci 13:259-265.

Smith Y, Bolam JP (1990b) The output neurones and the dopaminergic neurones of the substantia nigra receive a GABA-containing input from the globus pallidus in the rat. J Comp Neurol 296:47-64.

Smith Y, Bolam JP, Von Krosigk M (1990) Topographical and Synaptic Organization of the GABA-Containing Pallidosubthalamic Projection in the Rat. Eur J Neurosci 2:500-511.

Smith Y, Bevan MD, Shink E, Bolam JP (1998) Microcircuitry of the direct and indirect pathways of the basal ganglia. Neuroscience 86:353-387.

Smith Y, Bennett BD, Bolam JP, Parent A, Sadikot AF (1994) Synaptic relationships between dopaminergic afferents and cortical or thalamic input in the sensorimotor territory of the striatum in monkey. J Comp Neurol 344:1-19.

Soghomonian JJ, Descarries L, Watkins KC (1989) Serotonin innervation in adult rat neostriatum. II. Ultrastructural features: a radioautographic and immunocytochemical study. Brain Res 481:67-86.

Somogyi P, Bolam JP, Smith AD (1981a) Monosynaptic cortical input and local axon collaterals of identified striatonigral neurons. A light and electron microscopic study using the Golgi-peroxidase transport-degeneration procedure. J Comp Neurol 195:567-584.

Somogyi P, Bolam JP, Totterdell S, Smith AD (1981b) Monosynaptic input from the nucleus accumbens-ventral striatum region to retrogradely labelled nigrostriatal neurones. Brain Res 217:245-263.

Somogyi P, Priestley JV, Cuello AC, Smith AD, Takagi H (1982) Synaptic connections of enkephalin-immunoreactive nerve terminals in the neostriatum: a correlated light and electron microscopic study. J Neurocytol 11:779-807.

Spooren WPJM, LyndBalta E, Mitchell S, Haber SN (1996) Ventral pallidostriatal pathway in the monkey: evidence for modulation of basal ganglia circuits. J Comp Neurol 370:295-312.

Staiger JF, Zilles K, Freund TF (1996) Distribution of GABAergic elements postsynaptic to ventroposteromedial thalamic projections in layer IV of rat barrel cortex. Eur J Neurosci 8:2273-2285.

Steiner H, Gerfen CR (1998) Role of dynorphin and enkephalin in the regulation of striatal output pathways and behavior. Exp Brain Res 123:60-76.

Steiner H, Gerfen CR (1999) Enkephalin regulates acute D2 dopamine receptor antagonist-induced immediate-early gene expression in striatal neurons. Neuroscience 88:795-810.

Steriade M (1997) Synchronized activities of coupled oscillators in the cerebral cortex and thalamus at different levels of vigilance. Cereb Cortex 7:583-604.

Steriade M, Amzica F, Nunez A (1993a) Cholinergic and noradrenergic modulation of the slow (approximately 0.3 Hz) oscillation in neocortical cells. J Neurophysiol 70:1385-1400.

Steriade M, Contreras D, Curro Dossi R, Nunez A (1993b) The slow (< 1 Hz) oscillation in reticular thalamic and thalamocortical neurons: scenario of sleep

rhythm generation in interacting thalamic and neocortical networks. J Neurosci 13:3284-3299.

Stern EA, Kincaid AE, Wilson CJ (1997) Spontaneous subthreshold membrane potential fluctuations and action potential variability of rat corticostriatal and striatal neurons in vivo. J Neurophysiol 77:1697-1715.

Stern EA, Jaeger D, Wilson CJ (1998) Membrane potential synchrony of simultaneously recorded striatal spiny neurons *in vivo*. Nature 394:475-478.

Storm JF (1988) Temporal integration by a slowly inactivating K+ current in hippocampal neurons. Nature 336:379-381.

Sunahara RK, Guan HC, O'Dowd BF, Seeman P, Laurier LG, Ng G, George SR, Torchia J, Van Tol HH, Niznik HB (1991) Cloning of the gene for a human dopamine D5 receptor with higher affinity for dopamine than D1. Nature 350:614-619.

Surmeier DJ, Song WJ, Yan Z (1996) Coordinated expression of dopamine receptors in neostriatal medium spiny neurons. J Neurosci 16:6579-6591.

Surmeier DJ, Stefani A, Foehring RC, Kitai ST (1991) Developmental regulation of a slowly-inactivating potassium conductance in rat neostriatal neurons. Neurosci Lett 122:41-46.

Surmeier DJ, Reiner A, Levine MS, Ariano MA (1993) Are neostriatal dopamine receptors co-localized? Trends Neurosci 16:299-305.

Surmeier DJ, Xu ZC, Wilson CJ, Stefani A, Kitai ST (1992a) Grafted neostriatal neurons express a late-developing transient potassium current. Neuroscience 48:849-856.

Surmeier DJ, Bargas J, Hemmings HC, Jr., Nairn AC, Greengard P (1995) Modulation of calcium currents by a D1 dopaminergic protein kinase/phosphatase cascade in rat neostriatal neurons. Neuron 14:385-397.

Surmeier DJ, Eberwine J, Wilson CJ, Cao Y, Stefani A, Kitai ST (1992b) Dopamine receptor subtypes colocalize in rat striatonigral neurons. Proc Natl Acad Sci U S A 89:10178-10182.

Swadlow HA (1988) Efferent neurons and suspected interneurons in binocular visual cortex of the awake rabbit: receptive fields and binocular properties. J Neurophysiol 59:1162-1187.

Swadlow HA (1989) Efferent neurons and suspected interneurons in S-1 vibrissa cortex of the awake rabbit: receptive fields and axonal properties. J Neurophysiol 62:288-308.

Swadlow HA (1990) Efferent neurons and suspected interneurons in S-1 forelimb representation of the awake rabbit: receptive fields and axonal properties. J Neurophysiol 63:1477-1498.

Swadlow HA (1991) Efferent neurons and suspected interneurons in second somatosensory cortex of the awake rabbit: receptive fields and axonal properties. J Neurophysiol 66:1392-1409.

Swadlow HA (2000) Descending corticofugal neurons in layer 5 of rabbit S1: evidence for potent corticocortical, but not thalamocortical, input. Exp Brain Res 130:188-194.

Swadlow HA (2003) Fast-spike interneurons and feedforward inhibition in awake sensory neocortex. Cereb Cortex 13:25-32.

Swadlow HA, Hicks TP (1997) Subthreshold receptive fields and baseline excitability of "silent" S1 callosal neurons in awake rabbits: contributions of AMPA/kainate and NMDA receptors. Exp Brain Res 115:403-409.

Swadlow HA, Gusev AG (2000) The influence of single VB thalamocortical impulses on barrel columns of rabbit somatosensory cortex. J Neurophysiol 83:2802-2813.

Swanson GT, Kamboj SK, Cull-Candy SG (1997) Single-channel properties of recombinant AMPA receptors depend on RNA editing, splice variation, and subunit composition. J Neurosci 17:58-69.

Takada M, Tokuno H, Nambu A, Inase M (1998) Corticostriatal projections from the somatic motor areas of the frontal cortex in the macaque monkey: segregation versus overlap of input zones from the primary motor cortex, the supplementary meter area, and the premotor cortex. Exp Brain Res 120:114-128.

Tallaksen-Greene SJ, Albin RL (1994) Localization of AMPA-selective excitatory amino acid receptor subunits in identified populations of striatal neurons. Neurosci 61:509-519.

Tallaksen-Greene SJ, Wiley RG, Albin RL (1992) Localization of striatal excitatory amino acid binding site subtypes to striatonigral projection neurons. Brain Res 594:165-170.

Tamas G, Buhl EH, Somogyi P (1997) Massive autaptic self-innervation of GABAergic neurons in cat visual cortex. J Neurosci 17:6352-6364.

Tamas G, Somogyi P, Buhl EH (1998) Differentially interconnected networks of GABAergic interneurons in the visual cortex of the cat. J Neurosci 18:4255-4270.

Tanaka D (1987) Differential laminar distribution of corticostriatal neurons in the prefrontal and pericruciate gyri of the dog. J Neurosci 7:4095-4106.

Tepper JM, Trent F (1993) In vivo studies of the postnatal development of rat neostriatal neurons, Progress in Brain Research Edition: Elsevier science publishers.

Tepper JM, Sawyer SF, Groves PM (1987) Electrophysiologically identified nigral dopaminergic neurons intracellularly labeled with HRP: light-microscopic analysis. J Neurosci 7:2794-2806.

Thal LJ, Sharpless NS, Hirschhorn ID, Horowitz SG, Makman MH (1983) Striatal met-enkephalin concentration increases following nigrostriatal denervation. Biochem Pharmacol 32:3297-3301.

Thomas TM, Smith Y, Levey AI, Hersch SM (2000) Cortical inputs to m2-immunoreactive striatal interneurons in rat and monkey. Synapse 37:252-261.

Thomson AM, West DC, Hahn J, Deuchars J (1996) Single axon IPSPs elicited in pyramidal cells by three classes of interneurones in slices of rat neocortex. J Physiol 496 (Pt 1):81-102.

Timofeev I, Contreras D, Steriade M (1996) Synaptic responsiveness of cortical and thalamic neurones during various phases of slow sleep oscillation in cat. J Physiol 494 (Pt 1):265-278.

Timofeev I, Grenier F, Steriade M (2001) Disfacilitation and active inhibition in the neocortex during the natural sleep-wake cycle: an intracellular study. Proc Natl Acad Sci U S A 98:1924-1929.

Tremblay L, Filion M, Bedard PJ (1989) Responses of pallidal neurons to striatal stimulation in monkeys with MPTP-induced parkinsonism. Brain Res 498:17-33.

Trevitt JT, Marshall JF (2002) The effect of central dopamine (DA) depletion on corticostriatal-induced fos expression in the striatum. In: Society for Neuroscience, p 264.213. Orlando, Florida.

Trulson ME, Jacobs BL (1979) Effects of D-amphetamine on striatal unit activity and behavior in freely moving cats. Neuropharm 18:735-738.

Tseng KY, Kasanetz F, Kargieman L, Riquelme LA, Murer MG (2001) Cortical slow oscillatory activity is reflected in the membrane potential and spike trains of striatal neurons in rats with chronic nigrostriatal lesions. J Neurosci 21:6430-6439.

Tunstall MJ, Oorschot DE, Kean A, Wickens JR (2002) Inhibitory interactions between spiny projection neurons in the rat striatum. J Neurophysiol 88:1263-1269.

Uchimura N, Higashi H, Nishi S (1986) Hyperpolarizing and depolarizing actions of dopamine via D-1 and D-2 receptors on nucleus accumbens neurons. Brain Res 375:368-372.

Uchimura N, Cherubini E, North RA (1989) Inward rectification in rat nucleus accumbens neurons. J Neurophysiol 62:1280-1286.

Ueki M, Mies G, Hossmann KA (1992) Effect of alpha-chloralose, halothane, pentobarbital and nitrous oxide anesthesia on metabolic coupling in somatosensory cortex of rat. Acta Anaesthesiol Scand 36:318-322.

Ungerstedt U, Arbuthnott GW (1970) Quantitative recording of rotational behavior in rats after 6-hydroxy-dopamine lesions of the nigrostriatal dopamine system. Brain Res 24:485-493.

Ungerstedt U, Ljungberg T (1974) Central dopamine neurons and sensory processing. J Psychiatr Res 11:149-150.

van der Loos H (1976) Barreloids in the Mouse Somatosensory Thalamus. NeurosciLett 2:1-6.

Van Hoesen GW, Yeterian EH, Lavizzo Mourey R (1981) Widespread corticostriate projections from temporal cortex of the rhesus monkey. J Comp Neurol 199:205-219.

Vilagi I, Kocsis P, Tarnawa I, Banczerowski-Pelyhe I (1998) Effect of glutamate receptor antagonists on excitatory postsynaptic potentials in striatum. Brain Res Bull 46:483-486.

Voorn P, Roest G, Groenewegen HJ (1987) Increase of enkephalin and decrease of substance P immunoreactivity in the dorsal and ventral striatum of the rat after midbrain 6-hydroxydopamine lesions. Brain Res 412:391-396.

Wachtel SR, Hu XT, Galloway MP, White FJ (1989) D1 dopamine receptor stimulation enables the postsynaptic, but not autoreceptor, effects of D2 dopamine agonists in nigrostriatal and mesoaccumbens dopamine systems. Synapse 4:327-346.

Walker RH, Arbuthnott GW, Wright AK (1989) Electrophysiological and anatomical observations concerning the pallidostriatal pathway in the rat. Exp Brain Res 74:303-310.

Wallace H, Fox K (1999a) Local cortical interactions determine the form of cortical plasticity. J Neurobiol 41:58-63.

Wallace H, Fox K (1999b) The effect of vibrissa deprivation pattern on the form of plasticity induced in rat barrel cortex. Somatosens Mot Res 16:122-138.

Warenycia MW, McKenzie GM (1984) Responses of striatal neurons to anesthetics and analgesics in freely moving rats. Gen Pharmacol 15:517-522.

Waszczak BL, Martin LP, Greif GJ, Freedman JE (1998) Expression of a dopamine D2 receptor-activated K+ channel on identified striatopallidal and striatonigral neurons. Proc Natl Acad Sci U S A 95:11440-11444.

Watkins JC, Krogsgaard-Larsen P, Honore T (1990) Structure-activity relationships in the development of excitatory amino acid receptor agonists and competitive antagonists. Trends Pharmacol Sci 11:25-33.

Welker C (1971) Microelectrode delineation of fine grain somatotopic organisation of SmI cerebral neocortex in albino rat. Brain Res 26:259-275.

West MO (1998) Anesthetics eliminate somatosensory-evoked discharges of neurons in the somatotopically organized sensorimotor striatum of the rat. J Neurosci 18:9055-9068.

West MO, Carelli RM, Pomerantz M, Cohen SM, Gardner JP, Chapin JK, Woodward DJ (1990) A region in the dorsolateral striatum of the rat exhibiting single-unit correlations with specific locomotor limb movements. J Neurophysiol 64:1233-1246.

Weyand TG, Malpeli JG, Lee C, Schwark HD (1986a) Cat area 17. IV. Two types of corticotectal cells defined by controlling geniculate inputs. J Neurophysiol 56:1102-1108.

Weyand TG, Malpeli JG, Lee C, Schwark HD (1986b) Cat area 17. III. Response properties and orientation anisotropies of corticotectal cells. J Neurophysiol 56:1088-1101.

Whishaw IQ, Dunnett SB (1985) Dopamine depletion, stimulation or blockade in the rat disrupts spatial navigation and locomotion dependent upon beacon or distal cues. Behavioural Brain Research 18:11-29.

Whishaw IQ, Schallert T, Kolb B (1981) An analysis of feeding and sensorimotor abilities of rats after decortication. J Comp Physiol Psychol 95:85-103.

Whishaw IQ, Robinson TE, Schallert T, De Ryck M, Ramirez VD (1978) Electrical activity of the hippocampus and neocortex in rats depleted of brain dopamine and norepinephrine: relations to behavior and effects of atropine. Exp Neurol 62:748-767.

White EL (1979) Thalamocortical synaptic relations:A review with emphasis on the projections of specific thalamic nuclei to the primary sensory areas of the neocortex. Brain ResRev 1:275-311.

White EL, Benshalom G, Hersch SM (1984) Thalamocortical and other synapses involving nonspiny multipolar cells of mouse SmI cortex. J Comp Neurol 229:311-320.

Wickens JR, Wilson CJ (1998) Regulation of action-potential firing in spiny neurons of the rat neostriatum in vivo. J Neurophysiol 79:2358-2364.

Wickens JR, Kotter R, Alexander ME (1995) Effects of local connectivity on striatal function: stimulation and analysis of a model. Synapse 20:281-298.

Wilson CJ (1986) Postsynaptic potentials evoked in spiny neostriatal projection neurons by stimulation of ipsilateral and contralateral neocortex. Brain Res 367:201-213.

Wilson CJ (1987) Morphology and synaptic connections of crossed corticostriatal neurons in the rat. J Comp Neurol 263:567-580.

Wilson CJ (1993) The generation of natural firing patterns in neostriatal neurons: Elsevier science publishers.

Wilson CJ (1995) The contribution of cortical neurones to the firing pattern of striatal spiny neurones. In: Models of Information Processing in the Basal Ganglia (Houk JC, Davis JL, Beiser DG, eds), pp 29-50: The MIT Press.

Wilson CJ, Groves PM (1980) Fine structure and synaptic connections of the common spiny neuron of the rat neostriatum: a study employing intracellular injection of horseradish peroxidase. J Comp Neurol 194:599-615.

Wilson CJ, Groves PM (1981) Spontaneous firing patterns of identified spiny neurons in the rat neostriatum. Brain Res 220:67-80.

Wilson CJ, Kawaguchi Y (1996) The origins of two-state spontaneous membrane potential fluctuations of neostriatal spiny neurons. J Neurosci 16:2397-2410.

Wilson CJ, Chang HT, Kitai ST (1983a) Disfacilitation and long-lasting inhibition of neostriatal neurons in the rat. Exp Brain Res 51:227-235.

Wilson CJ, Chang HT, Kitai ST (1983b) Origins of post synaptic potentials evoked in spiny neostriatal projection neurons by thalamic stimulation in the rat. Exp Brain Res 51:217-226.

Wilson JS, Hull CD, Buchwald NA (1983c) Intracellular studies of the convergence of sensory input on caudate neurons of cat. Brain Res 270:197.

Wineski LE (1985) Facial morphology and vibrissal movement in the golden hamster. J Morphol 183:199-217.

Wise SP, Jones EG (1977) Cells of origin and terminal distribution of descending projections of the rat somatic sensory cortex. JCompNeurol 175:129-158.

Woolsey TA, Van der Loos H (1970) The structural organization of layer IV in the somatosensory region (SI) of mouse cerebral cortex. The description of a cortical field composed of discrete cytoarchitectonic units. Brain Res 17:205-242.

Wright AK, Norrie L, Arbuthnott GW (2000) Corticofugal axons from adjacent 'barrel' columns of rat somatosensory cortex: cortical and thalamic terminal patterns. J Anat 196 (Pt 3):379-390.

Wright AK, Ramanathan S, Arbuthnott GW (2001) Identification of the source of the bilateral projection system from cortex to somatosensory neostriatum and an exploration of its physiological actions. Neuroscience 103:87-96.

Wright AK, Norrie L, Ingham CA, Hutton EAM, Arbuthnott GW (1999) Double anterograde tracing of outputs from adjacent "barrel columns" of rat somatosensory cortex. Neostriatal projection patterens and terminal ultarstructure. Neuroscience 88:119-113.

Wu Y, Richard S, Parent A (2000) The organization of the striatal output system: a single-cell juxtacellular labeling study in the rat. Neurosci Res 38:49-62.

Yamamoto BK, Cooperman MA (1994) Differential effects of chronic antipsychotic drug treatment on extracellular glutamate and dopamine concentrations. J Neurosci 14:4159-4166.

Yan Z, Surmeier DJ (1997) D5 dopamine receptors enhance Zn2+-sensitive GABA(A) currents in striatal cholinergic interneurons through a PKA/PP1 cascade. Neuron 19:1115-1126.

Yan Z, Song WJ, Surmeier J (1997) D2 dopamine receptors reduce N-type Ca2+ currents in rat neostriatal cholinergic interneurons through a membrane-delimited, protein-kinase-C-insensitive pathway. J Neurophysiol 77:1003-1015.

Yeterian EH, Van Hoesen GW (1978) Cortico-striate projections in the rhesus monkey: the organization of certain cortico-caudate connections. Brain Res 139:43-63.

Yim CY, Mogenson GJ (1988) Neuromodulatory action of dopamine in the nucleus accumbens: an in vivo intracellular study. Neuroscience 26:403-415.

York DH (1967) The inhibitory action of dopamine on neurones of the caudate nucleus. Brain Res 5:263-266.

You ZB, Herrera-Marschitz M, Brodin E, Meana JJ, Morino P, Hokfelt T, Silveira R, Goiny M, Ungerstedt U (1994) On the origin of striatal cholecystokinin release: studies with in vivo microdialysis. J Neurochem 62:76-85.

Young WS, 3rd, Bonner TI, Brann MR (1986) Mesencephalic dopamine neurons regulate the expression of neuropeptide mRNAs in the rat forebrain. Proc Natl Acad Sci U S A 83:9827-9831.

Yung KK, Smith AD, Levey AI, Bolam JP (1996) Synaptic connections between spiny neurons of the direct and indirect pathways in the neostriatum of the rat:

evidence from dopamine receptor and neuropeptide immunostaining. Eur J Neurosci 8:861-869.

Yung KK, Bolam JP, Smith AD, Hersch SM, Ciliax BJ, Levey AI (1995) Immunocytochemical localization of D1 and D2 dopamine receptors in the basal ganglia of the rat: light and electron microscopy. Neuroscience 65:709-730.

Zahm DS, Williams E, Wohltmann C (1996) Ventral striatopallidothalamic projection: IV. Relative involvements of neurochemically distinct subterritories in the ventral pallidum and adjacent parts of the rostroventral forebrain. J Comp Neurol 364:340-362.

Zheng P, Zhang XX, Bunney BS, Shi WX (1999) Opposite modulation of cortical N-methyl-D-aspartate receptor-mediated responses by low and high concentrations of dopamine. Neuroscience 91:527-535.

Zheng T, Wilson CJ (2002) Corticostriatal combinatorics: the implications of corticostriatal axonal arborizations. J Neurophysiol 87:1007-1017.

Zhou QY, Grandy DK, Thambi L, Kushner JA, Van Tol HH, Cone R, Pribnow D, Salon J, Bunzow JR, Civelli O (1990) Cloning and expression of human and rat D1 dopamine receptors. Nature 347:76-80.

Zhu JJ, Connors BW (1999) Intrinsic firing patterns and whisker-evoked synaptic responses of neurons in the rat barrel cortex. J Neurophysiol 81:1171-1183.

Zis AP, Fibiger HC, Phillips AG (1974) Reversal by L-dopa of impaired learning due to destruction of the dopaminergic nigro-neostriatal projection. Science 185:960-962.

APPENDIX

Appendix 1. Correlation between the size of the EPSPs in response to the initial stimulus and second stimulus, for each time interval for all 4 paring protocols in cortical neurones.

Whisker-Cortex				
Time interval	Size of first EPSP	Size of Second EPSP	Correlation coefficient	*P* - value
10ms	14.560	1.198	-0.395	0.381
20ms	15.89	0.798	-0.175	0.707
40ms	14.67	4.198	0.727	0.067
60ms	14.92	3.382	0.403	0.37
80ms	12.21	4.697	-0.66	0.107
100ms	14.98	3.842	0.36	0.047
120ms	13.94	4.605	0.28	0.543
140ms	16.98	5.014	-0.965	0.002
160ms	14.76	7.025	0.238	0.65
180ms	13.27	6.429	0.368	0.543
200ms	14.12	8.001	-0.032	0.959
220ms	12.46	9.394	0.653	0.598
240ms	13.38	10.029	0.381	0.563
260ms	17.3	9.128	-0.408	0.128
280ms	16.7	9.026	0.289	0.852
300ms	14.2	8.31	-0.548	0.423
320ms	13.6	9.763	0.835	0.384
340ms	16.74	9.926	-0.325	0.793
360ms	16.369	8.054	-0.765	0.284
380ms	21.255	9.374	0.025	0.065

Cortex-Whisker				
Time interval	Size of first EPSP	Size of Second EPSP	Correlation coefficient	*P* - value
10ms	10.34	9.204	-0.394	0.382
20ms	9.97	8.124	-0.091	0.847
40ms	8.16	8.415	-0.102	0.828
60ms	7.06	9.258	-0.575	0.177
80ms	8.41	11.03	-0.491	0.263
100ms	7.51	12.631	-0.596	0.158
120ms	7.01	14.145	-0.936	0.064
140ms	10.2	17.423	-0.55	0.45
160ms	9.07	19.112	0.629	0.371
180ms	9.85	19.638	0.56	0.335
200ms	8.22	19.986	-0.89	0.048
220ms	9.74	19.352	-0.38	0.205
240ms	9.58	19.894	0.636	0.205
260ms	7.48	18.267	-0.255	0.351
280ms	9.492	17.346	-0.75	0.054
300ms	9.6	21.828	-0.534	0.142
320ms	8.32	20.089	0.561	0.133
340ms	10.79	20.334	0.25	0.303
360ms	7.145	21.992	-0.71	0.698
380ms	9.8	19.055	0.46	0.468

Whisker-Whisker				
Time interval	Size of first EPSP	Size of Second EPSP	Correlation coefficient	*P* - value
10ms	14.96	1.711	-0.685	0.089
20ms	14.25	-0.766	-0.416	0.354
40ms	15.4	-0.318	-0.492	0.262
60ms	13.39	0.007	-0.061	0.897
80ms	13.92	0.596	-0.002	0.996
100ms	14.18	4.223	-0.818	0.025
120ms	16.17	3.929	-0.764	0.045
140ms	15.5	7.061	-0.791	0.034
160ms	16.57	10.46	0.532	0.219
180ms	13.47	9.039	0.546	0.341
200ms	14.95	8.308	-0.874	0.053
220ms	13.6	9.045	0.819	0.09
240ms	14.05	11.574	-0.746	0.048
260ms	17.47	9.108	0.653	0.589
280ms	19.075	10.193	0.532	0.219
300ms	18.76	8.422	-0.426	0.326
320ms	21.05	10.325	-0.656	0.075
340ms	22.534	11.984	-0.819	0.09
360ms	17.561	12.301	-0.575	0.177
380ms	18.942	9.108	-0.829	0.0853

Cortex-Cortex				
Time interval	Size of first EPSP	Size of Second EPSP	Correlation coefficient	*P* - value
10ms	6.25	2.245	0.306	0.504
20ms	7.1	1.742	-0.979	0
40ms	6.97	3.001	-0.567	0.184
60ms	6.85	3.437	-0.707	0.076
80ms	7.03	0.517	0.519	0.233
100ms	7.78	0.684	-0.476	0.28
120ms	7.82	1.018	-0.393	0.441
140ms	6.61	1.376	0.157	0.767
160ms	6.32	1.939	0.412	0.417
180ms	8.113	2.778	-0.091	0.909
200ms	10.98	2.595	-1	0
220ms	7.04	4.015	0.738	0.262
240ms	9.46	4.736	-0.812	0.188
260ms	9.69	6.179	-0.413	0.587
280ms	8.832	7.215	0.519	0.233
300ms	8.55	7.379	0.5	0.169
320ms	8.32	6.723	-0.568	0.186
340ms	8.76	9.139	-0.48	0.287
360ms	7.91	8.729	0.412	0.417
380ms	9.21	7.716	-0.426	0.326

Appendix 2. Correlation coefficient and the R-squared value from regression analysis of the membrane potential on the amplitude of the response to the second stimulus for each time interval for all 4 paring protocols in cortical neurones.

Whisker-Cortex					
Time interval	Membrane pot	Size of Second EPSP	Correlation coeff	*P* - value	R-Sq
10ms	-55.150	1.198	-0.591	0.000	33.70%
20ms	-58.920	0.798	-0.434	0.001	17.30%
40ms	-62.530	4.198	-0.334	0.012	9.50%
60ms	-64.540	3.382	-0.502	0.000	23.80%
80ms	-65.040	4.697	-0.546	0.000	28.50%
100ms	-65.360	3.842	-0.607	0.000	35.70%
120ms	-66.120	4.605	-0.492	0.000	22.80%
140ms	-69.010	5.014	-0.504	0.000	23.80%
160ms	-69.300	7.025	-0.589	0.000	33.20%
180ms	-66.110	6.429	-0.553	0.000	28.80%
200ms	-67.310	8.001	-0.585	0.000	32.50%
220ms	-76.245	9.394	-0.748	0.000	54.40%
240ms	-75.611	10.029	-0.230	0.280	1.00%
260ms	-74.936	9.128	-0.528	0.008	24.60%
280ms	-75.048	9.026	-0.407	0.049	12.70%
300ms	-73.626	8.31	-0.727	0.000	50.80%
320ms	-75.457	9.763	-0.832	0.000	67.90%
340ms	-75.519	9.926	-0.724	0.000	50.30%
360ms	-72.889	8.054	-0.720	0.000	49.70%
380ms	-75.150	9.374	-0.662	0.000	41.20%

Cortex-Whisker					
Time interval	Membrane pot	Size of Second EPSP	Correlation coeff	*P* - value	R-Sq
10ms	-58.670	9.204	-0.680	0.000	45.300%
20ms	-57.440	8.124	-0.080	0.560	0.000%
40ms	-60.520	8.415	0.017	0.901	0.000%
60ms	-64.990	9.258	0.165	0.225	0.900%
80ms	-64.830	11.030	0.345	0.009	10.300%
100ms	-67.170	12.631	0.301	0.024	7.400%
120ms	-78.047	14.145	0.227	0.211	2.000%
140ms	-79.236	17.423	0.306	0.089	6.300%
160ms	-80.196	19.112	0.391	0.027	12.500%
180ms	-77.310	19.638	-0.553	0.005	27.500%
200ms	-77.494	19.986	-0.192	0.368	0.000%
220ms	-75.826	19.352	-0.615	0.001	34.900%
240ms	-76.297	19.894	-0.898	0.000	79.800%
260ms	-74.803	18.267	-0.755	0.000	55.100%
280ms	-75.058	17.346	-0.431	0.035	14.900%
300ms	-76.348	21.828	-0.716	0.000	49.000%
320ms	-75.365	20.089	-0.592	0.002	32.000%
340ms	-74.301	20.334	-0.907	0.000	81.500%
360ms	-74.884	21.992	-0.899	0.000	79.900%
380ms	-73.140	19.055	-0.948	0.000	89.300%

Whisker-Whisker					
Time interval	Membrane pot	Size of Second EPSP	Correlation coeff	*P* - value	R-Sq
10ms	-56.170	1.711	-0.615	0.000	36.700%
20ms	-57.580	-0.766	-0.035	0.796	0.000%
40ms	-62.420	-0.318	0.051	0.709	0.000%
60ms	-65.400	0.007	-0.272	0.042	5.700%
80ms	-67.800	0.596	-0.095	0.486	0.000%
100ms	-68.680	4.223	-0.396	0.003	14.100%
120ms	-69.380	3.929	-0.807	0.000	64.500%
140ms	-68.860	7.061	-0.906	0.000	81.800%
160ms	-67.100	10.46	-0.323	0.015	8.800%
180ms	-61.660	9.039	0.010	0.953	0.000%
200ms	-60.790	8.308	0.165	0.310	0.200%
220ms	-60.690	9.045	-0.406	0.009	14.200%
240ms	-75.990	11.574	-0.619	0.001	35.500%
260ms	-75.283	9.108	-0.825	0.000	66.600%
280ms	-74.843	10.193	-0.470	0.021	18.500%
300ms	-74.987	8.422	-0.335	0.109	7.200%
320ms	-74.803	10.325	-0.780	0.000	59.100%
340ms	-75.191	11.984	-0.814	0.000	64.700%
360ms	-73.257	12.301	-0.883	0.000	77.000%
380ms	-68.860	7.061	-0.906	0.000	81.800%

Cortex-Cortex					
Time interval	Membrane pot	Size of Second EPSP	Correlation coeff	*P* - value	R-Sq
10ms	-57.250	2.245	-0.271	0.044	5.600%
20ms	-56.080	1.742	0.141	0.300	0.200%
40ms	-58.230	3.001	-0.476	0.000	21.200%
60ms	-61.820	3.437	-0.013	0.923	0.000%
80ms	-61.500	0.517	-0.348	0.008	10.500%
100ms	-62.160	0.684	-0.305	0.022	7.600%
120ms	-59.470	1.018	0.386	0.007	13.000%
140ms	-59.920	1.376	-0.493	0.000	22.600%
160ms	-60.160	1.939	-0.543	0.000	28.000%
180ms	-74.432	2.778	0.16	0.381	0.000%
200ms	-74.048	2.595	0.162	0.376	0.000%
220ms	-73.894	4.015	-0.496	0.004	22.000%
240ms	-74.301	4.736	0.079	0.667	0.000%
260ms	-73.541	6.179	0.261	0.149	3.700%
280ms	-74.117	7.215	-0.503	0.012	21.900%
300ms	-73.482	7.379	-0.462	0.023	17.800%
320ms	-73.390	6.723	-0.341	0.103	7.600%
340ms	-72.930	9.139	-0.786	0.000	60.100%
360ms	-74.055	8.729	-0.738	0.000	52.400%
380ms	-72.380	7.716	-0.843	0.000	69.700%

Appendix 3. Publications.

Pergamon

www.elsevier.com/locate/neuroscience

PII: S0306-4522(00)00564-9

Neuroscience Vol. 103, No. 1, pp. 87–96, 2001

0306-4522/01 $20.00+0.00

IDENTIFICATION OF THE SOURCE OF THE BILATERAL PROJECTION SYSTEM FROM CORTEX TO SOMATOSENSORY NEOSTRIATUM AND AN EXPLORATION OF ITS PHYSIOLOGICAL ACTIONS

A. K. WRIGHT, S. RAMANATHAN and G. W. ARBUTHNOTT*

University of Edinburgh Centre for Neuroscience, Department of Preclinical Veterinary Sciences, Summerhall, Edinburgh EH9 1QH, UK

Abstract—Microinjections of cholera toxin B subunit were made into the area of the neostriatum that receives input from the primary somatosensory barrel cortex (SI) in the rat. Studies of the cortices then allowed retrograde identification of the cortical cells supplying the striatal input. When injections were restricted to the neostriatum, retrograde labelling was found in layer V of both SI cortices. Ipsilateral to the injection, cells were retrogradely filled with toxin in all parts of the barrel field, in adjacent parietal cortex, in the motor cortex and in prefrontal areas. A similar distribution across cortical areas was seen contralaterally; however, the stained cells in the SI were between rather than within barrel columns. An earlier anterograde study suggested two inputs from the SI to the neostriatum. The present results indicate that one input to the somatosensory area of the neostriatum arises bilaterally from neurons between the barrels of the SI, while the topographic pathway from below the barrels is present only ipsilaterally. These anatomical results indicate that separate stimulation of the two corticostriatal pathways from the barrel cortex is possible. Electrical stimulation of the contralateral cortex will activate the bilateral pathway, while electrical stimulation of the whisker pads activates the barrels and hence the topographic pathway. Neurons in the somatosensory region of the striatum responded to stimuli in the contralateral cortex and in the contralateral whisker pad. In spite of very different path lengths, stimuli via the two routes gave rise to excitatory postsynaptic potentials in the striatal cells with similar latencies. The excitatory postsynaptic potentials to whisker pad stimulation had a rapid rise time and usually resulted in at least one action potential. Responses to stimulation of the contralateral cortex rose to a peak more slowly and were more variable in latency, but also gave rise to an action potential in the majority of cases. All the neurons had the physiological characteristics of medium-sized densely spiny cells and after intracellular filling with biocytin had the appropriate morphology.

In summary, we propose that two corticostriatal pathways arise from layer V cells in the barrel area of the somatosensory cortex; one is bilateral and arises from cells mainly below the septa, while a topographical pathway arises from cells below the barrels. Both pathways can raise the spiny output cells of the striatum to firing threshold. The latencies from the contralateral cortex imply slowly conducting fibres with considerably more temporal dispersion than the pathway from below the barrels, which we excited from the contralateral periphery. © 2001 IBRO. Published by Elsevier Science Ltd. All rights reserved.

Key words: corticostriatal, whiskers, barrel cortex, cortico-cortical.

The neostriatum is usually thought of as the major input structure of the basal ganglia, and it receives a massive input from all of the cerebral cortex.[10,11,14,17,19–23,26,28,34,37,39,41,45] Many current ideas about how the basal ganglia might be involved in behaviour depend upon the neostriatum somehow selecting a subset of the cortical input to become the basis of the behavioural output of the animal.[29,36] The corticostriatal pathway is a major source of the excitation which leads to output from the neostriatum and it seems likely that the ability of cortical inputs to fire striatal output cells depends on a considerable convergence of cortical fibres on to each striatal neuron.[17,18] The input from the cortex is arranged in a loose topographical order, with frontal areas mainly represented in the anterior and medial neostriatum and more posterior cortex projecting caudally and laterally.[23] In some areas, there is an additional input from supragranular layers of the cortex,[23] and it seems likely that at least one way of dividing the neostriatum might be the result of the input from deeper layers being targeted to matrix and more superficial layers to striosomes.[12,13]

In a previous anatomical study, we identified two morphologically distinct corticostriatal pathways from the barrel cortex in the rat.[44] One was topographically arranged and showed the typical morphology of collateral branches from the corticofugal fibres in the rat, including the corticothalamic systems.[43] The second pathway was not topographically arranged and fine fibres with many varicosities innervated the striatum diffusely over a wider area.[44] We speculated that this diffuse system might project bilaterally to the striatum, like the cortico-cortical fibres from the agranular cortex,

*Corresponding author. Tel.: +44-131-650-6177; fax: +44-131-650-6177.

E-mail address: g.arbuthnott@ed.ac.uk (G. W. Arbuthnott).

Abbreviations: EPSP, excitatory postsynaptic potential; LTP, long-term potentiation; PBS, phosphate-buffered saline; PBS–TX, phosphate-buffered saline containing Triton X-100; SI, primary somatosensory cortex.

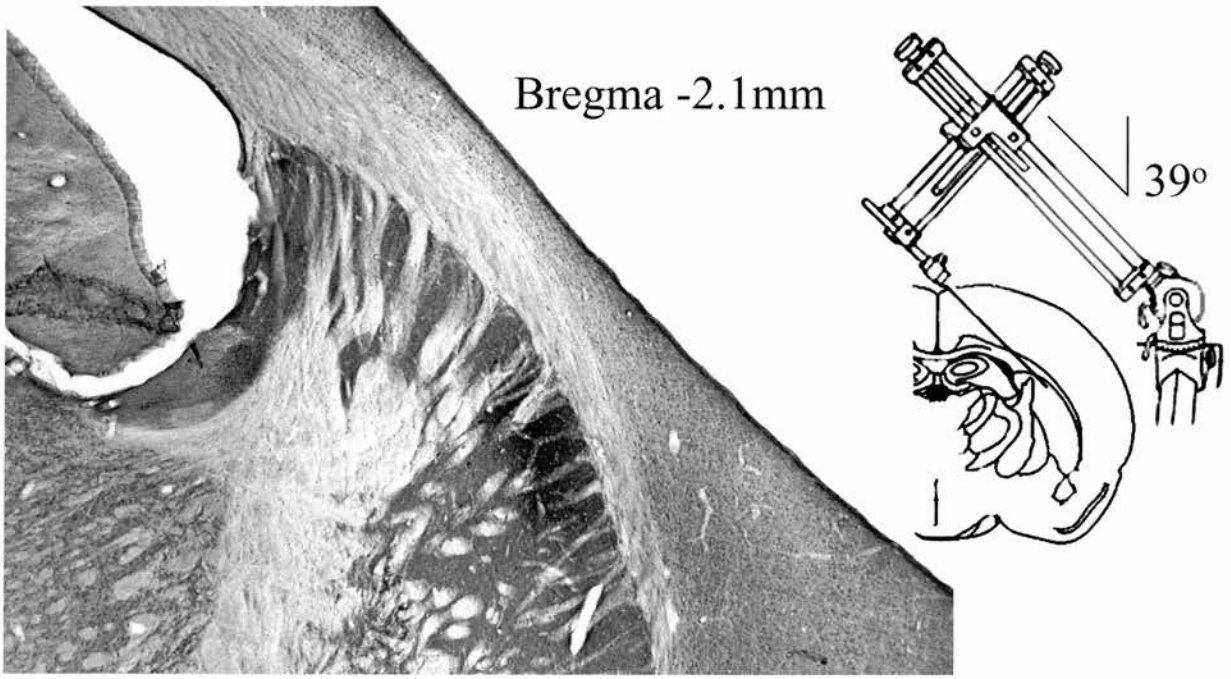

Fig. 1. The injection angle and a typical injection site. A low-magnification photomicrograph of an injection site in the area of the striatum which receives input from the barrel cortex. The drawing inset shows the angle of approach used in the experiments. The cortex has been removed so that the barrel field can be studied in sections parallel to the pia.

high current, voltage or capacitance. Once a cell was successfully impaled, its response to contralateral cortical stimulation and whisker pad stimulation was then determined. Injecting hyperpolarising current (−2 nA in 200-ms pulses for up to 20 min) filled the cells with biocytin. The membrane potential was monitored during filling, and for some neurons a holding current was used to stabilise the cell during intracellular filling. If there was any sudden change in the membrane potential, filling was stopped and the electrode carefully removed from the striatum. No more than three neurons were filled in any one animal. At the end of the experiment, all the animals were perfused with fixative containing 2% paraformaldehyde and 1.25% glutaraldehyde, and the brains postfixed as for the anatomical investigations.

Statistical tests

Responses of single cells to the two stimuli were compared using a paired *t*-test, with $P < 0.05$ accepted as the level of significance. Latencies were measured to the beginning of the excitatory postsynaptic potential (EPSP) in intracellular records and the rise time measured from there to the peak of the EPSP. Measurements are quoted as mean ± S.D.

Biocytin histology

Fifty-micrometre sections were washed four times in phosphate-buffered saline (PBS; 10 min each), to remove fixative, before quenching for 30 min, in 30% methanol and 0.03% hydrogen peroxide in PBS. After eight more washes in PBS, the sections were then incubated for 5 h in PBS–TX at room temperature with gentle agitation, followed by 60 h at 4°C in ABC Elite (1:50 in PBS–TX; Vector Laboratories). The sections were then washed three times in PBS, and reacted with 3,3′-diaminobenzidine for 10 min to visualise the biocytin, well rinsed in PBS and then mounted on subbed slides that were then oven dried for a week. Dehydration in ethanol, de-fatting in xylene and rehydrating through to water allowed the sections to be counterstained in 5% Methyl Green, dehydrated and coverslipped with DPX. Camera lucida drawings of the sections were made in order to determine the position of the filled cells.

RESULTS

Technical considerations

Injections that resulted in successful labelling of cortical cells in the barrel field filled the region of the striatum shown previously to receive from the barrel cortex (Fig. 1). Owing to the angle of approach (Fig. 1), such injections do not invade the overlying cortex, and only neurons in layer V were labelled in adjacent cortex. Occasionally, the spread from the injection site did involve the callosum below the SI or parts of the cortex itself. In these cases, cells in layer VI of the overlying cortex were visible. None of our injections, whether or not callosal and cortical areas had been stained, resulted in supragranular cortical neurons in the SI accumulating enough toxin to be visible.

Anatomical results

Corticostriatal neurons on both sides of the brain were retrogradely labelled from injections limited to the appropriate area of somatosensory striatum. In the ipsilateral cortex, neurons throughout layer V in the SI and including some of the secondary somatosensory cortex were retrogradely labelled with cholera toxin (Figs 2B, 3). Labelled cells were also visible in anterior areas of the cortex (Fig. 2A). In the ipsilateral cortex, the cells were concentrated in the upper parts of layer V (Fig. 2C), but with occasional pyramidally shaped cells in the deeper part of the layer. It is tempting to suggest that the deeper cells were part of the barrel columns in the SI, but we have no direct proof of this because coronal sections, which were anyway not stained for cytochrome oxidase, were taken in only two animals.

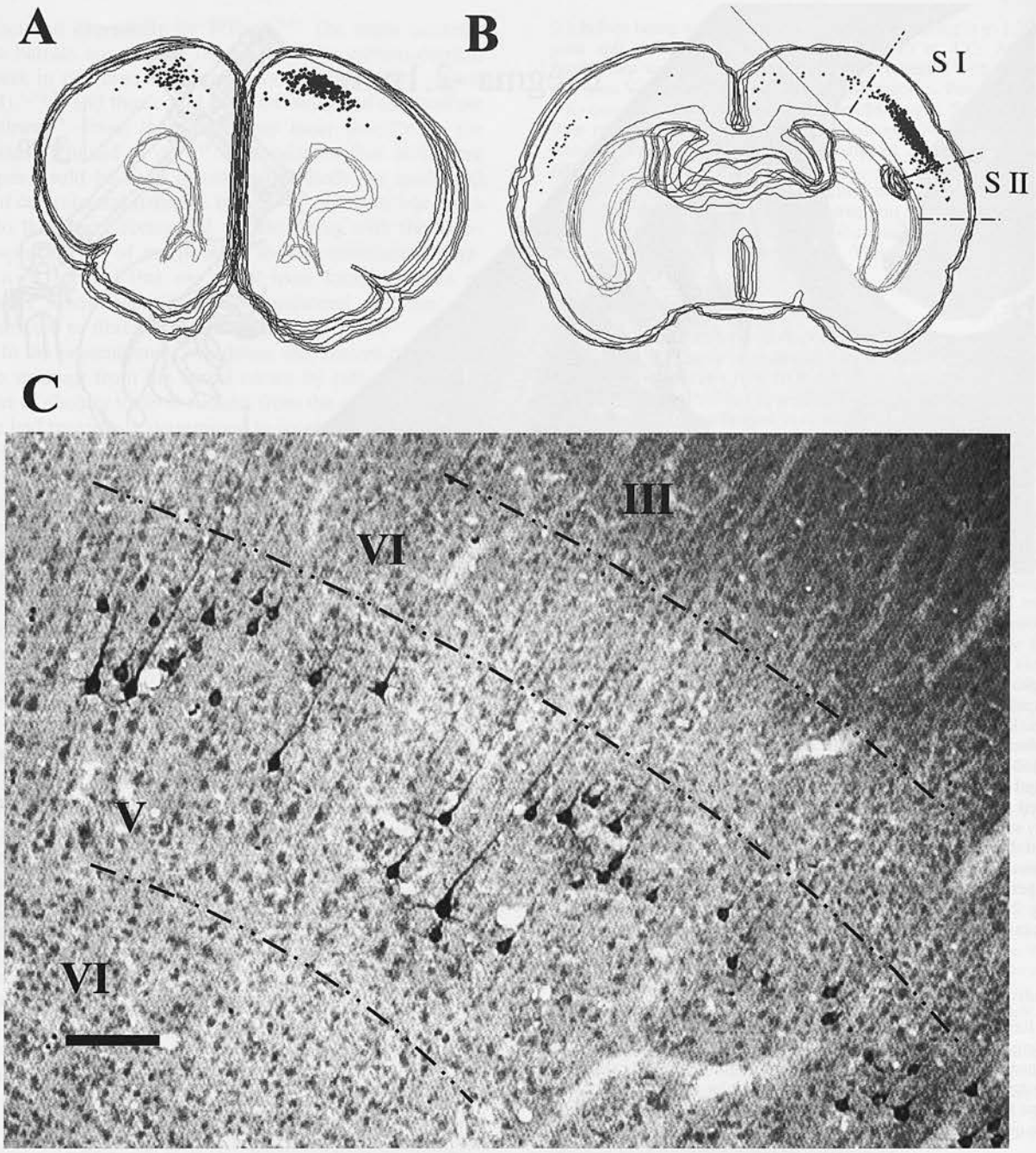

Fig. 2. The distribution of cholera toxin-labelled cells in the cortex. Ten sections anterior to the anterior commissure are shown in A, while six in the region of the injection site are superimposed in B. The approximate extent of the SI and secondary somatosensory cortex (SII) is marked in the top section. A photomicrograph (C) of a coronal section through the cerebral cortex in the barrel field shows cells in layer V below the barrels. Although the majority of the cells are in the upper part of the layer, there are also some deeper layer V cells. The cells may be clumped together below individual barrels in this particular section. Scale bar in C = 100 μm. The dashed lines mark border areas between layers III, IV, V and VI.

Sections parallel to the pia (Fig. 3) gave a clear picture of the distribution of cells with respect to barrels (Fig. 3A, C), but it was harder to delineate the layers in sections of this kind; it was clear in coronal sections that here too the cells were in layer V. The differences in the numbers of cells on the two sides are dramatically illustrated in anterior areas (Fig. 2A) and in Fig. 3A, where all the labelled cells in the two barrel cortices are superimposed in alignment with the barrels. On the ipsilateral side, the barrel outlines are completely obscured by cells (Fig. 3A), while in the contralateral cortex most of the cells were between the barrels or on the barrel boundaries. The groups of cells are at equivalent depths within the cortices (Fig. 3B), and there is no obvious reason to suggest that the deeper cells seen in Fig. 2C would be absent on the contralateral side. On

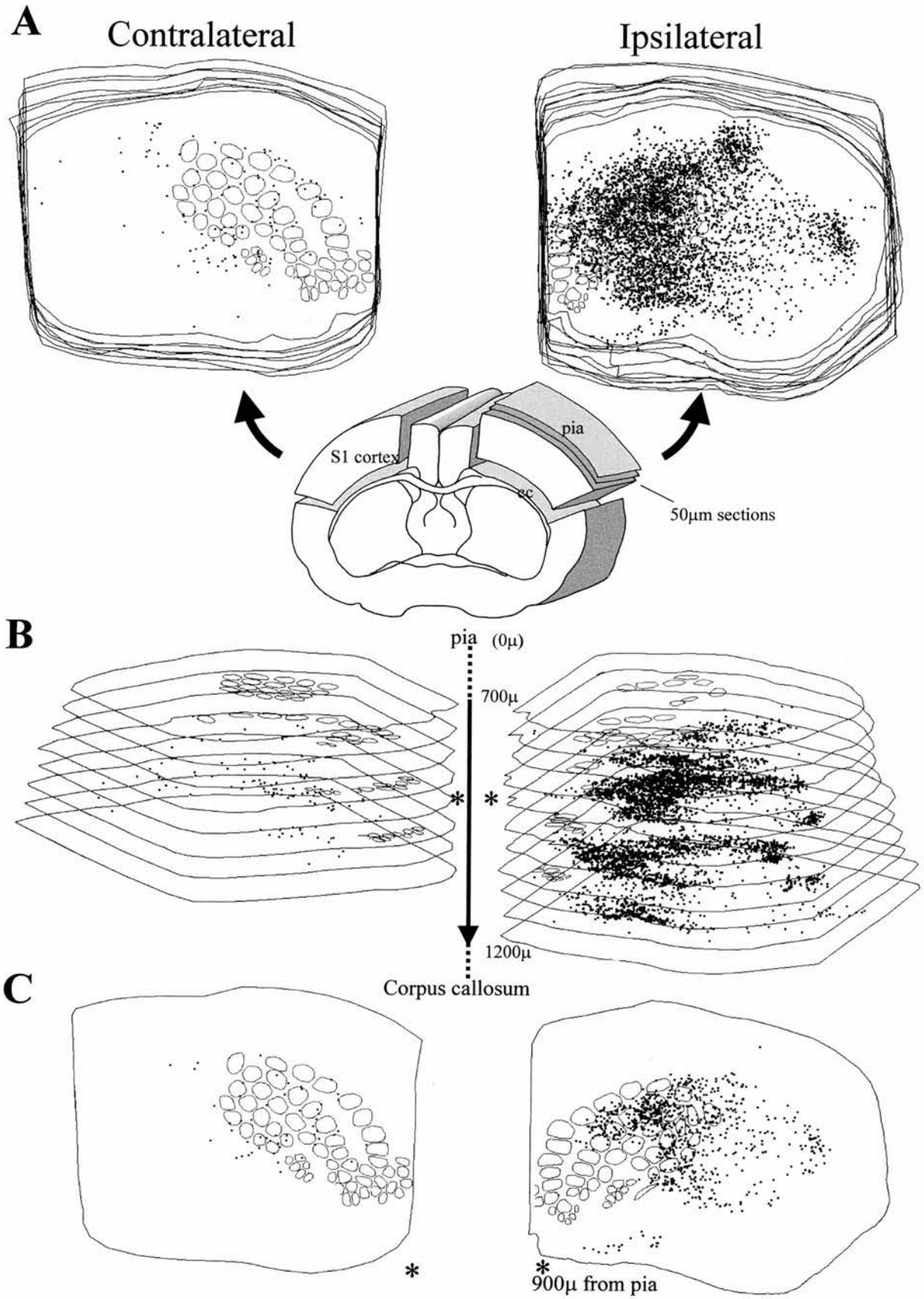

Fig. 3. Neurolucida-generated distributions of cholera toxin-labelled cells in the cortices after a striatal injection. All the sections in which cells and barrels are detected are superimposed in A. The individual stacks of sections from 700 μm below the pia to 1200 μm are illustrated in three dimensions in B. Representative single sections (900 μm below the surface; marked with asterisks in the stack) are displayed in C, with the map of the barrel field derived from all the relevant sections superimposed for reference. In this example, 83% of the cells were completely outside the outlines of the barrels contralaterally and 57% of those labelled ipsilateraly were outside the boundaries of the barrels. In other animals, the contrast was at least as marked.

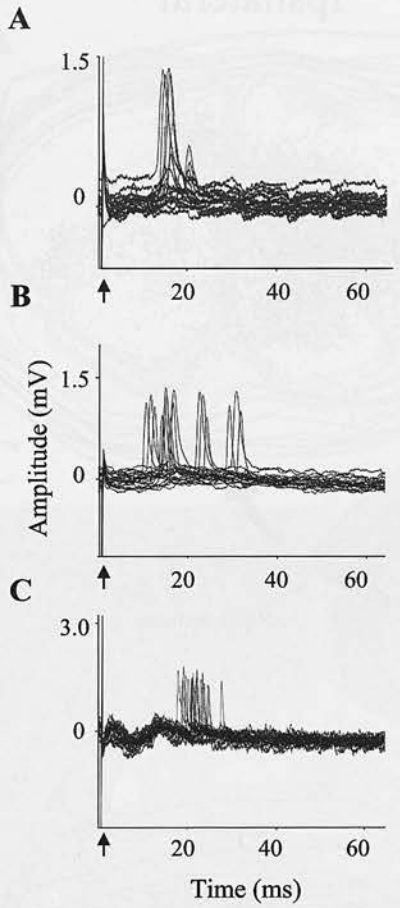

Fig. 4. Representative extracellular records with different latencies of response to stimulation of the contralateral whisker pad. The stimuli were applied at the arrows and the three cells were recorded at depths below the cortical surface of 3774 μm (A), 3250 μm (B) and 4572 μm (C). The average latencies to the first spike (±S.D.) for each record were: (A) 14.5 ± 2.01 ms; (B) 14.3 ± 2.1 ms; (C) 21.13 ± 4.5 ms. In this extracellular study, multiple action potentials were often initiated by the stimulus.

both sides, no cells were observed in the superficial (I–IV) or in deep (VI) layers of the SI.

Physiological results

Extracellular electrophysiology. A total of 59 striatal cells was recorded extracellularly and, of these, 50 responded to the whisker pad stimulus. Neurons that responded were found in the striatum 0.9–2.12 mm posterior to bregma, whilst more anterior striatal neurons did not respond. Representative traces of three cells with different latencies are shown in Fig. 4. The mean latencies for the two forms of stimulation were not significantly different (whisker pad 14.87 ± 5.87 ms, contralateral cortex 15.86 ± 6.52 ms; paired *t*-test, $P > 0.05$). The spontaneous firing rates ranged from 0.50 to 4.54 Hz.

Intracellular electrophysiology. A total of 47 striatal cells was recorded intracellularly. A neuron was considered to be successfully impaled if the membrane potential was lower than −50 mV. Of these, 37 cells responded to both electrical whisker pad stimulation and contralateral cortical stimulation. Cells that responded were in the striatum (0.92–2.12 mm posterior to bregma), while the six non-responding cells were in the anterior striatum (0.4 mm posterior to bregma). In one experimental animal, four cells responded to whisker pad stimulation only, but histological examination showed that the stimulating electrode had been misplaced in this animal. The mean latencies for the two forms of stimulation were again not significantly different (whisker pad 13.23 ± 4.25 ms, contralateral cortex 16.58 ± 7.56 ms; paired *t*-test, $P > 0.05$).

Striatal neurons had spontaneous shifts in membrane potential which are typical of medium-sized densely spiny cells. The depolarised state or the "up" state had a potential of −50 to −60 mV, while the membrane potential of the hyperpolarised state ranged from −75 to −80 mV. Neurons sometimes fired during an "up" state with an action potential height of 50–70 mV. The spontaneous firing rates of the cells ranged from 0.5 to 10.2 Hz. Of the 37 cells that responded to both routes of stimulation, three cells did not fire any action potentials. These three cells, however, responded with an EPSP to the whisker pad and to cortical stimulation. The non-firing cells had an average resting membrane potential of −90 mV.[40] Cells that responded had an EPSP that usually lasted for 50 ms, including a slow return of the membrane potential to baseline values. This was sometimes followed by a period of prolonged silence that lasted for longer than 150 ms.

Relationships between cortical and striatal cell responses to whisker pad stimulation. In some animals, we recorded cortical neurons that responded to stimulation of the whisker pad. Latencies were short (7.5 ms on average), the response was very reliable (Fig. 5A) and the EPSP was followed by a prolonged hyperpolarisation which lasted for more than 100 ms. Latencies to whisker pad stimulation in striatal cells were sometimes only slightly longer (8 ms in the example from the same animal in Fig. 5B, but mean 13 ± 4 ms for all cells). Striatal cells were silent after the EPSP for at least 100 ms, usually 150 ms.

Ipsilateral versus contralateral cortical stimulation. Contralateral cortical stimuli gave rise to EPSPs with rise times significantly slower than in the case of the ipsilateral cortex stimulated via the whisker pad (6.14 ± 4.15 vs 2.7 ± 0.86 ms; paired *t*-test, $P < 0.001$). The rise times of EPSPs brought about by contralateral cortical stimulation were also much more variable. The EPSP in response to the stimulation of the whisker pad (Fig. 6A) has a rise time of 2.3 ms and the contralateral cortical EPSP in the same cell (Fig. 6B) has a rise time of 5.7 ms. Action potentials arose from contralateral cortex-derived EPSPs with more variable latencies.

Morphology of filled cells. A total of 20 cells was successfully filled and visualised. All the filled cells were of the medium-sized densely spiny projection neuron type. A cell that was filled with biocytin for

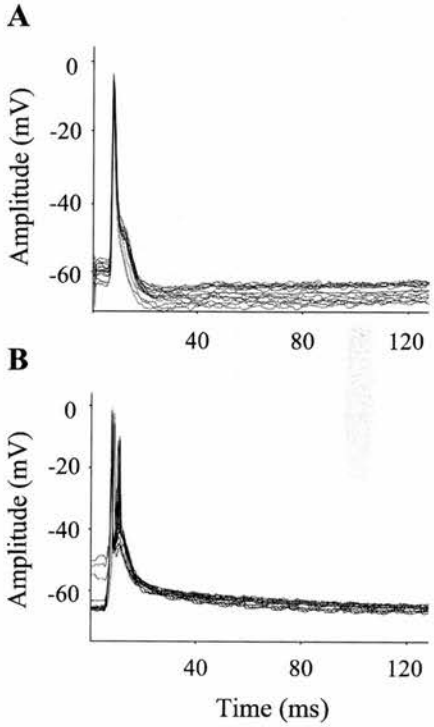

Fig. 5. The contrast between cortical and striatal cell responses to stimulation of the whisker pad. The cortical cell in A was recorded at a depth of 2293 μm. The cell had a membrane potential of −57 mV and a mean latency of 7.41 ± 0.89 ms. The EPSP is followed by a prolonged hyperpolarisation, which lasted for longer than the record. B shows the responses of a striatal cell from the same animal with a membrane potential of −60 mV. This cell lay just under the corpus callosum. The average latency of response was 8.0 ± 1.2 ms, the EPSP was complete 53 ms later and the cell was then silent until the end of the record.

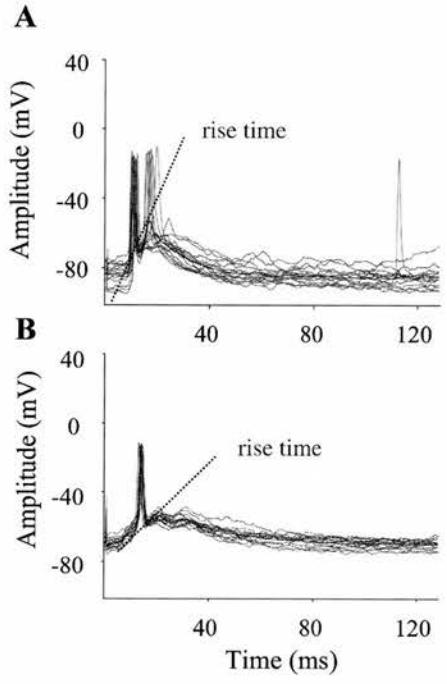

Fig. 6. Contrasting responses in the same striatal neuron to whisker pad and to contralateral cortical stimulation. The whisker pad EPSP (A) has a rise time of 2.3 ms and the contralateral cortical EPSP (B) has a rise time of 5.7 ms. The variability in initial latency of action potentials was much greater in the responses to contralateral cortex stimulation, in the majority of cells. This case is less representative of that, but has a rise time of the EPSP close to the average for the population (6.14 ± 4.15 ms). The dotted lines in each figure represent the rise time estimated from each of the average traces.

20 min is shown in Fig. 7. At higher magnification (inset), the spines on the dendrites are easily visible.

DISCUSSION

The results of the retrograde tracing experiments demonstrate very clearly that cortical cells projecting to the contralateral striatum (the diffuse pathway of our previous study[44]) inhabit layer V below the septa between the barrels of the SI. Ipsilaterally to the injections, cortical cells in layer V were labelled in all of the SI and in several related areas of cortex. This retrograde identification of cells below the septa in both cortices suggests, in agreement with earlier studies, that the projections of the diffuse corticostriatal system are bilateral rather than only contralateral. In marked contrast, the source of the topographic system is ipsilateral and derives from layer V neurons below the barrels themselves. Physiological investigations suggest that both of the pathways are able to drive the output cells of the relevant area of the striatum to fire action potentials.

Anatomical considerations

Other reports[12,13,22,23] show that the corticostriatal system includes neurons of the supragranular layers, and these could be the source of the diffuse bilateral fibres. We were unable to provide positive evidence that this was so in the SI by injecting the same barrel at supragranular and infragranular depths (Wright A. K. and Arbuthnott G. W., unpublished results). In their detailed investigation of the corticostriatal system of the rat using horseradish peroxidase injections into the striatum, McGeorge and Faull[22,23] showed that input to the striatum arose from cortical cells in layer V and also from supragranular layers in some cortical areas. Some of the injections in these earlier studies did fill cells in the parietal cortex but, in agreement with our more focused study, this area of cortex had few supragranular cells. In the present study, all the cortical cells in the SI were in layer V, except when the injection site included the corpus callosum or overlying cortex, in which case some cells in layer VI were also filled with cholera toxin. The vast majority of the cells were within the upper part of layer V, a result in agreement with a previous study of the source of corticofugal cells. Mercier *et al.*[24] filled the somatosensory area of the striatum with large injections of horseradish peroxidase and observed cells limited to the upper part of layer V (their Va). Injections in the pontine nuclei, in contrast, labelled cortical neurons that were restricted to the lower parts of layer V (their Vb).

The SI is known to have relatively few neurons that project to the contralateral cortex via the corpus callosum. Recent work has identified the cells in the septa

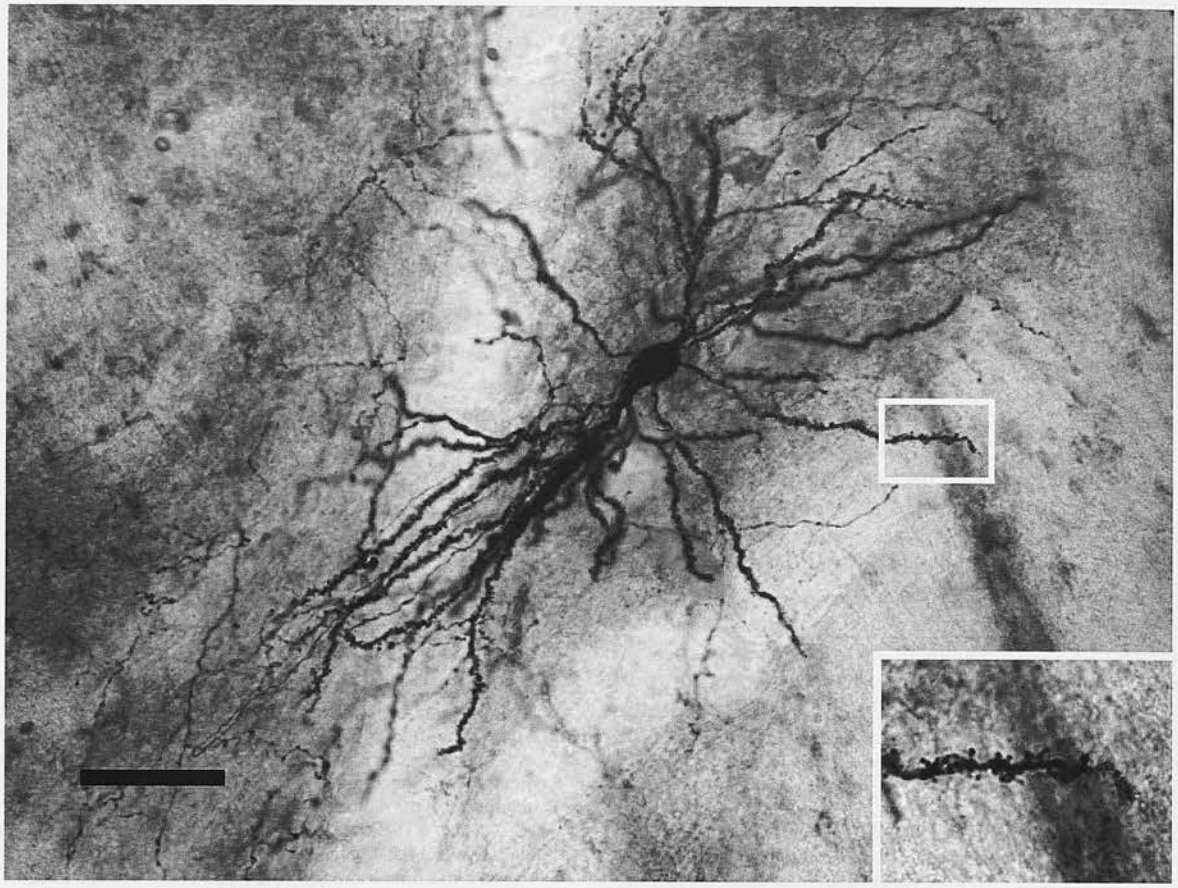

Fig. 7. The representative morphology of the striatal cells recorded intracellularly. The photomontage shows a cell that was filled with biocytin for 20 min. At higher magnification (inset), one is able to see the spines on the dendrites. Scale bar = 50 μm in the main picture.

surrounding the barrels as the source of the majority of both ipsilateral and contralateral cortico-cortical connections in this area of cortex.[6,25] This suggests that, in this area, just as in the agranular areas studied by Wilson,[41] bilaterally projecting corticostriatal cells also project to the cortex bilaterally.

Physiological considerations

The success of the present experiments was due in part to the previous detailed mapping of whisker-related input to the striatum. Electrodes placed only 500 μm anterior to the target area resulted in no sign of an excitatory response to the periphery in both intracellular and extracellular recordings. There have been a few attempts to map peripheral inputs to the striatum physiologically,[31–33] but in general they are less common than anatomical studies. There may be several reasons for this, but it is clear from our own work that both the anaesthetic and the electrode placement are important.

In a previous study some years ago, we looked hard for responses to forepaw stimulation under halothane anaesthesia without success and resorted to cortical stimulation.[4] The chloralose-based anaesthetic used in the present study is known to preserve peripheral inputs to the spinal cord and to make cortical cells with wide peripheral receptive fields more commonly detected.[3] An earlier study published only as an abstract found that peripheral stimulation of the forepaws could reliably evoke extracellularly recorded responses in the striatum of rats anaesthetised with chloralose and halothane.[38] This abstract also mentions that such responses were not detected after destruction of dopamine fibres in the striatum by 6-hydroxydopamine injection. Future experiments are planned to study the effects of the loss of dopamine upon the responses of striatal cells to stimulation of the kinds used in our present experiments.

It is tempting to think of the contralateral cortical stimulation as inducing input only from the contralaterally projecting cells, but earlier work suggests that as much as 50% of the EPSP derived from the contralateral cortex is dependent upon an axon reflex from projections of ipsilateral corticostriatal terminals arising from cells that project to both striata and to the contralateral cortex.[41] The same study, however, provides evidence that contralateral stimulation of descending corticofugal fibres does not result in EPSPs in striatal cells. Thus, it seems likely that the two fibre systems are stimulated differently by our choice of stimulation sites. Whisker pad stimulation had the advantage of stimulating many whisker nerves simultaneously, so that the input was relatively massive, synchronous and likely to be directed,

at least initially, to the barrels. Activation will eventually spread to the diffuse system derived from the neurons below the septa, but it seems clear that the first activity in the barrel cortex in response to stimulation of the whisker pad will be in the barrels themselves. The situation is obviously different in the many studies of the corticostriatal system *in vitro.*

Relevance to in vitro *studies of the corticostriatal system*

In several different laboratories, including our own, the corticostriatal system is studied *in vitro.* Slices are made either angled in the plane of the corticostriatal fibres from the frontal cortex,[2,15,16] or in a coronal plane when most of the fibres will have been severed. Stimulation of the callosum in either preparation leads to robust EPSPs in striatal neurons, but only in the angled slice are responses obtained by stimulation restricted to the cortex itself. Responses are not usually obtained from medial cortical areas, even in the angled slice.[16] In contrast, it is always possible to obtain robust EPSPs from the subcortical white matter in either preparation. One likely explanation for this is that stimulation in the white matter activates cut fibres from both ipsilateral and contralateral cortex, and the summation of the EPSPs from both sources increases the chances of clear-cut responses from the cells. Thus, the long-term depression and long-term potentiation (LTP) that have been recorded in those slices where subcortical white matter was stimulated may well reflect the result of activation of both corticostriatal pathways.

Long-term potentiation in vivo

When LTP in a corticostriatal system has been reported *in vivo*, it has been with stimulation of the ipsilateral cortex.[7,8] In an attempt to produce the same phenomena from the contralateral cortex, Reynolds and Wickens[30] were less successful and, indeed, earlier studies of the corticostriatal system, although showing some short-term potentiation, could not demonstrate LTP.[4,35] These earlier studies used the ipsilateral cortex as the stimulation site, but applied the stimulation to prefrontal regions and recorded in the head of the caudate. Although it is tempting to relate the LTP to the ipsilateral "topographic" fibre system, some caution is required in view of the demonstration that both systems are present in contralateral corticostriatal projections in the studies by Kincaid *et al.*[17,18] However, it is possible that the results of this tracing study were confused by their larger injections of biotinylated dextran amine, having filled some cells which are part of yet another corticostriatal system, which is either not present in the somatosensory cortex or never filled in our sample.

CONCLUSIONS

In the part of the striatum that receives input from the barrel area of the somatosensory cortex, the input from the contralateral cortex arises in the neurons of layer V below the septa between the barrels. The same population of cells is also retrogradely labelled in the ipsilateral cortex, suggesting that the diffuse cortiostriatal system is bilaterally projecting, whereas the topographical projection from the barrels arises only in the ipsilateral cortex.

The bilateral system, although slower in conduction velocity, seems just as able to initiate EPSPs in striatal neurons as the topographical system after activation of the barrels from the periphery. EPSPs following electrical stimulation of the contralateral whisker pad have short latencies and fast rise times, while contralateral cortex stimulation resulted in more slowly rising EPSPs and more variable latencies of action potential initiation in the same striatal neurons.

Acknowledgements—This work was supported by Wellcome Trust Grant No. 054303. We are grateful to Dr C. A. Ingham for critical reading of the manuscript.

REFERENCES

1. Ackers R. M. and Killackey H. P. (1978) Organisation of the corticocortical connections in the parietal cortex of the rat. *J. comp. Neurol.* **181,** 513–538.
2. Arbuthnott G. W., MacLeod N. and Rutherford A. (1985) The rat cortico-striatal pathway *in vitro. J. Physiol., Lond.* **367,** 102–102P.
3. Baker M. A., Tyner C. F. and Towe A. L. (1971) Observations on single neurones in the sigmoid gyri of awake unparalysed cats. *Expl Neurol.* **32,** 388–403.
4. Brown J. R. and Arbuthnott G. W. (1983) The electrophysiology of dopamine (D2) receptors: a study of the actions of dopamine on corticostriatal transmission. *Neuroscience* **10,** 349–355.
5. Carvell G. E. and Simons D. J. (1987) Thalamic and corticocortical connections of the second somatic sensory area of the mouse. *J. comp. Neurol.* **265,** 409–427.
6. Chapin J. K., Sadeq M. and Guise L. U. (1987) Corticocortical connections within the primary somatosensory cortex of the rat. *J. comp. Neurol.* **263,** 326–346.
7. Charpier S. and Deniau J. M. (1997) *In vivo* activity-dependent plasticity at cortico-striatal connections: evidence for physiological long-term potentiation. *Proc. natn. Acad. Sci. USA* **94,** 7036–7040.
8. Charpier S., Mahon S. and Deniau J. M. (1999) *In vivo* induction of striatal long-term potentiation by low frequency stimulation of the cerebral cortex. *Neuroscience* **91,** 1209–1222.
9. Cowan R. L. and Wilson C. J. (1994) Spontaneous firing patterns and axonal projections of single corticostriatal neurons in the rat medial agranular cortex. *J. Neurophysiol.* **71,** 17–32.
10. Donoghue J. P. and Herkenham M. (1986) Neostriatal projections from individual cortical fields conform to histochemically distinct striatal compartments in the rat. *Brain Res.* **365,** 397–403.
11. Flaherty A. W. and Graybiel A. M. (1995) Motor and somatosensory corticostriatal projection magnifications in the squirrel monkey. *J. Neurophysiol.* **74,** 2638–2648.
12. Gerfen C. R. (1989) The neostriatal mosaic: striatal patch matrix is related to cortical lamination. *Science* **246,** 385–388.

13. Gerfen C. R. and Rutherford A. (1988) Laminar origin of patch- and matrix-directed corticostriatal projections in the rat. *Soc. Neurosci. Abstr.* **10,** 76.
14. Hattori T., McGeer E. G. and McGeer P. L. (1979) Fine structural analysis of the cortico-striatal pathway. *J. comp. Neurol.* **185,** 347–354.
15. Jiang Z. G. and North R. A. (1991) Membrane properties and synaptic responses of rat striatal neurones *in vitro*. *J. Physiol., Lond.* **443,** 533–553.
16. Kawaguchi Y., Wilson C. J. and Emson P. C. (1989) Intracellular recording of identified neostriatal patch and matrix spiny cells in a slice preparation preserving cortical inputs. *J. Neurophysiol.* **62,** 1052–1068.
17. Kincaid A. E. and Wilson C. J. (1996) Corticostriatal innervation of the patch and matrix in the rat neostriatum. *J. comp. Neurol.* **374,** 578–592.
18. Kincaid A. E., Zheng T. and Wilson C. J. (1998) Connectivity and convergence of single corticostriatal axons. *J. Neurosci.* **18,** 4722–4731.
19. Kunzle H. (1975) Bilateral projections from precentral motor cortex to the putamen and other parts of the basal ganglia. An autoradiographic study in *Macaca fascicularis*. *Brain Res.* **88,** 195–209.
20. Kunzle H. (1977) Projections from the primary somatosensory cortex to the basal ganglia and thalamus in the monkey. *Expl Brain Res.* **30,** 481–492.
21. Malach R. and Graybiel A. M. (1987) The somatic sensory corticostriatal projection: patchwork of somatic sensory zones. *Basal Ganglia and Behavior: Sensory Aspects of Motor Functioning*. Hans Huber, Toronto.
22. McGeorge A. J. and Faull R. L. M. (1987) The organization and collateralization of corticostriate neurones in the motor and sensory cortex of the rat brain. *Brain Res.* **423,** 318–324.
23. McGeorge A. J. and Faull R. L. M. (1989) The organization of the projection from the cerebral cortex to the striatum in the rat. *Neuroscience* **29,** 503–537.
24. Mercier B. E., Legg C. R. and Glickstein M. (1990) Basal ganglia and cerebellum receive different somatosensory information in rats. *Proc. natn. Acad. Sci. USA* **87,** 4388–4392.
25. Olavarria J., Van Sluyters R. C. and Killackey H. P. (1984) Evidence for the complementary organization of callosal and thalamic connections within rat somatosensory cortex. *Brain Res.* **291,** 364–368.
26. Parthasarathy H. B., Schall J. D. and Graybiel A. M. (1992) Distributed but convergent ordering of corticostriatal projections: analysis of the frontal eye field and the supplementary eye field in the macaque monkey. *J. Neurosci.* **12,** 4468–4488.
27. Paxinos G. and Watson C. (1986) *The Rat Brain in Stereotaxic Coordinates*. Academic, New York.
28. Ragsdale C. W. Jr and Graybiel A. M. (1981) The fronto-striatal projection in the cat and monkey and its relationship to inhomogeneities established by acetylcholinesterase histochemistry. *Brain Res.* **208,** 259–266.
29. Redgrave P., Prescott T. J. and Gurney K. (1999) The basal ganglia: a vertebrate solution to the selection problem? *Neuroscience* **89,** 1009–1023.
30. Reynolds J. N. J. and Wickens J. R. (2000) Substantia nigra dopamine regulates synaptic plasticity and membrane potential fluctuations in the rat neustriatum, *in vivo*. *Neuroscience* **99,** 199–203.
31. Richards C. D. and Taylor D. C. M. (1982) Electrophysiological evidence for a somatotopic sensory projection to the striatum of the rat. *Neurosci. Lett.* **30,** 235–240.
32. Schneider J. S. and Lidsky T. I. (1981) Processing of somatosensory information in the striatum of behaving cats. *J. Neurophysiol.* **45,** 841–851.
33. Sedgwick E. M. and Williams T. D. (1967) The response of single units in the caudate nucleus to peripheral stimulation. *J. Physiol., Lond.* **189,** 281–298.
34. Selemon L. D. and Goldman-Rakic P. S. (1985) Longitudinal topography and interdigitation of corticostriatal projections in the rhesus monkey. *J. Neurosci.* **5,** 776–794.
35. Spencer H. J. (1999) Antagonism of cortical excitation of striatal neurones by glutamic acid diethyl ester: evidence for glutamic acid as an excitatory transmitter in the rat striatum. *Brain Res.* **102,** 91–101.
36. Suri R. E. and Schultz W. (1999) A neural network model with dopamine-like reinforcement signal that learns a spatial delayed response task. *Neuroscience* **91,** 871–890.
37. Tanaka D., Gorska T. and Dutkiewicz K. (1980) Corticostriate projection patterns and synaptic morphology in the puppy caudate nucleus. *Expl Neurol.* **70,** 98–108.
38. Ungersted U., Ljungberg T., Ranje C., Schultz W. and Tulloch I. F. (1977) Neuronal transmission and animal behaviour—a search for correlations in the central dopamine pathways. *Proc. Int. Union physiol. Sci.* **12,** 709.
39. Van Hoesen G. W., Yeterian E. H. and Lavisso-Mourey R. (1981) Widespread corticostriate projections from temporal cortex of the rhesus monkey. *J. comp. Neurol.* **199,** 205–219.
40. Wickens J. R. and Wilson C. J. (1998) Regulation of action-potential firing in spiny neurons of the rat neostriatum *in vivo*. *J. Neurophysiol.* **79,** 2358–2364.
41. Wilson C. J. (1987) Morphology and synaptic connections of crossed corticostriatal neurons in the rat. *J. comp. Neurol.* **263,** 567–580.
42. Wong-Riley M. T. T. and Welt C. (1980) Histochemical changes in cytochrome oxidase of cortical barrels after vibrissal removal in neocortical and adult mice. *Proc. natn. Acad. Sci. USA* **77,** 2333–2337.
43. Wright A. K., Norrie L. and Arbuthnott G. W. (2000) Corticofugal axons from adjacent "barrel" columns of rat somatosensory cortex: cortical and thalamic terminal patterns. *J. Anat.* **196,** 379–390.
44. Wright A. K., Norrie L., Ingham C. A., Hutton E. A. M. and Arbuthnott G. W. (1999) Double anterograde tracing of outputs from adjacent "barrel columns" of rat somatosensory cortex. Neostriatal projection patterns and terminal ultrastructure. *Neuroscience* **88,** 119–133.
45. Yeterian E. H. and Van Hoesen G. W. (1978) Cortico-striate projections in the rhesus monkey: the organization of certain cortico-caudate connections. *Brain Res.* **139,** 43–63.

(*Accepted* 1 *December* 2000)

A PHYSIOLOGICAL INVESTIGATION OF THE TWO CORTICOSTRIATAL SYSTEMS IN RAT SOMATSENSORY STRIATUM

S. Ramanathan, A. K. Wright, and G. W. Arbuthnott*

1. ABSTRACT

In Chloralose and Urethane (1% & 10%; 1.0 ml/Kg, i.p.) anaesthetised rats we have studied the responses of single striatal neurones to stimulation of the contralateral barrel cortex and of the contralateral whisker pad. The effects of cortical stimulation are likely to be transmitted along the 'diffuse' pathway that projects bilaterally to the striatum. Stimulation of the whisker pad would probably activate the other corticostriatal system, which arises as collaterals from corticofugal fibres. The synchronous volley arising from the electrical stimulus to the whisker pad would have travelled via brain stem and thalamus to the barrel centres in the somatosensory cortex. It is from the barrels that the ipsilateral, topographic system arises and so the peripheral stimulus would be able to activate this system first. Later phases of the response might include activation of the septa surrounding the barrels and hence of the diffuse system.

Both stimuli are able to depolarise the spiny neurones to their firing threshold. The excitatory postsynaptic potentials (EPSPs) from the two stimulus sites had similar latencies (in spite of very different path lengths and numbers of synapses *en route*). However, the responses to whisker pad stimulation were rapidly rising and showed very little variation in latency to action potential generation, while the contralateral cortically derived EPSPs were slower to rise and the spike initiation latency was more variable. These characteristics might be predicted from the morphology of the two systems.

* S. Ramanathan, A. K. Wright, G. W. Arbuthnott, University of Edinburgh, Dept. of Pre-Clinical Vet. Sciences, R. D. S. V. S., Summerhall, EH9 1QH, United Kingdom.

The Basal Ganglia VII
Edited by Nicholson and Faull, Kluwer Academic/Plenum Publishers, 2002

2. INTRODUCTION

The striatum is the main input nucleus of the basal ganglia. There is representation of each area of the cortex in the striatum and it is considered to be the major integrative component of the basal ganglia (Selemon, Goldman-Rakic, 1985) (McGeorge, Faull, 1989). The main neuronal type in the striatum is the GABAergic medium spiny projection neurone, which in rodents make up 90-95% of the neuronal population (Bolam, Bennet, 1995; Gerfen, Wilson, 1996). These spiny neurones receive a direct cortical input onto their dendritic spines (Somogyi et al., 1981) which shapes the activity of the cells (Wilson et al., 1983; Wilson, Kawaguchi, 1996).

In rodents, the mystacial vibrissae (whiskers) are the principle tactile receptors. The sensory information obtained from the whiskers provides an important input for locomotion. The information from the whiskers is processed in Layer IV of the neocortex by groups of neurones arranged in discrete functional units known as barrels (Woolsey, van der Loos, 1970).

Recent anterograde tracing studies have shown that there are at least two morphologically distinct corticostriatal pathways that arise from the barrel cortex (Wright et al., 1999). One of these, referred to as the 'discrete pathway', is topographic in nature giving rise to a somatotopic representation of the barrel cortex in the striatum. The projection is composed of thick fibres arising from collaterals of the descending somatosensory fibres leaving the corticofugal bundles at right angles. The axons give rise to several large 'boutons en passant' and the terminal areas of these run parallel to the internal border of the callosum. The second projection, referred to as the 'diffuse pathway', is composed of fine fibres, does not posses the clear topography of the discrete pathway and is bilateral. In agreement with previous work (Cowan, Wilson, 1994; Wilson, 1986; Wilson, 1987), these fine fibres are thought to be part of a diffuse system of corticostriatal axons that innervate both cortices and striata (Wright et al., 2001). They arise from the septa between the barrels and leave the corpus callosum at an acute angle (Wright et al., 2001). Electron microscopy has revealed that both types of fibres make contact with the dendritic spines of the medium spiny striatal projection neurones and form asymmetric synapses (Wright et al., 1999).

There have been few reports of responses in the striatum of rats to stimulation of the periphery. Stimulation of various parts of the body and concurrent recordings in cats and rats seems to suggest that there is a sensory map of the body in the striatum (Cho, West, 1997; Richards, Taylor, 1982; Sedgwick, Williams, 1967; West et al., 1990). Preliminary experiments have shown that it is possible to record excitatory postsynaptic potentials (EPSPs) in spiny neurones of the striatum in response to stimulation of the contralateral cortex (via activation of the diffuse pathway) and the contralateral whisker pad (via activation of the ipsilateral barrel cortex) (Wright et al., 2001). Stimulation of the whisker pad resulted in EPSPs that had a rapid rise time with little variation in latency. Contralateral cortical stimulation gave rise to EPSPs, which were much slower and more variable. The latency of the responses was similar for both stimulation parameters even though the pathway from the whisker pad to the striatum is polysynaptic, containing at least four synapses whereas the contralateral pathway is monosynaptic. *In vivo* experiments by Wickens and Wilson (Wickens, Wilson, 1998) showed that some cortical inputs were unable to raise striatal cells to threshold. This suggests that while some cortical inputs are capable of firing striatal cells others might be involved in priming them by depolarising the cells. Early electrophysiological data from

stimulation of the diffuse and topographic pathways suggests that the diffuse pathway might prime the striatal cells while the excitation of the topographic pathway might cause the striatal cells to fire action potentials. However, the interaction of these two pathways has not yet been studied. The aim of the current experiments was to investigate the interaction of the two systems at the level of a single striatal cell.

3. METHODS

Seventeen male Sprague Dawley rats (300-350g) were anaesthetised intra-peritoneally with 1ml/100g body weight of a 1% α-chloralose 10% urethane mix in distilled water. Stable levels of anaesthesia were maintained throughout with additional anaesthetic (10% of original dose, approximately once every six hours), to ensure the absence of a foot withdrawal reflex.

The animal was transferred to a stereotaxic apparatus and its head secured in a frame via ear and tooth bars. Body temperature was maintained at 37^0C throughout using a homeothermic blanket and a rectal probe. A slit was made in the atlanto-occipital membrane and a cerebrospinal fluid drain created in order to reduce intracerebral pressure. Holes were drilled in the skull 2.1mm posterior and 5.0mm lateral to the bregma on both sides. A contralateral stimulating electrode (Harvard Apparatus) was then lowered to a depth of 2.5mm so that it straddled Layer V of the somatosensory cortex. A dental cement wall about 1cm tall was built around the site of the recording electrode placement. The dura was slit to expose the cortical surface at the recording site to facilitate the passage of the recording electrode. Stimulation of the left whisker pad was carried out between a pair of insect pins connected to a constant voltage stimulator.

Intracellular recordings were made from glass electrodes containing 2M potassium acetate or 1M potassium acetate and 5% biocytin with resistances of 40-100MΩ. The electrode was advanced into the cortex at an angle of 90^0 to the cortical surface and then advanced to a depth of 2,500μm when the dental cement well was filled with molten paraffin wax to stabilise the electrode. From a depth of 2,500μm the electrode was advanced in 2μm steps until a neurone was impaled. A neurone was considered to be successfully impaled if the membrane potential was stable and below –60mV.

Once inside the cell, the response of the cell to whisker pad and contralateral cortical stimulation was determined. The cells were stimulated below the threshold for the firing of action potentials. The interaction of the two systems was then studied using a paired protocol. After an initial stimulus, a second stimulus was delivered at fixed time intervals. This protocol was carried out to study the interaction of the two different pathways (topographic-diffuse, diffuse-topographic) compared to the effects of a pathway on itself (topographic-topographic, diffuse-diffuse).

Records obtained were acquired using a Macintosh based data acquisition system – MacLab Scope. Eight consecutive sweeps were taken per time interval. The latency, rise-time and peak amplitude of the response of the neurone to each stimuli was measured. The peak amplitude at the different time intervals was compared using a one-way ANOVA and Tukey's multiple comparison test.

4. RESULTS

Records were obtained from 10 striatal cells. Neurones that responded were found in the striatum 0.9mm to 2.12mm posterior to the bregma, whilst more anterior or posterior striatal neurones did not respond. All 10 cells responded to both the whisker and contralateral cortical stimuli. A cell was included in the analysis only if all four paired interaction protocols were carried out.

The mean latencies and the peak amplitude for the two forms of stimulation were not significantly different (Paired T-Test, $P > 0.05$). A two-tailed paired t-test was done on the rise time of the excitatory post-synaptic potentials (EPSPs) and they were found to be significantly different ($P < 0.05$). The EPSPs to whisker pad stimulation had a rapid rise time, which were relatively consistent while stimulation of the contralateral cortex, gave rise to responses that rose to a peak more slowly and were more variable.

Table 1. Summary of response of striatal cells to barrel cortex stimulation.

Stimulus	Latency (ms)	Rise time (ms)	Peak amplitude (mV)
Whisker pad	8.496 (1.796)	4.141 (1.896)	11.995 (6.341)
C. Cortex	7.818 (2.252)	11.019 (5.550)	11.877 (9.704)

Mean values (± standard deviation) of responding striatal cells to electrical whisker pad stimulation and contralateral cortical (C. Cortex) stimulation.

4.1. Whisker – Cortex Interaction

Electrical stimulation of the whisker pad did not inhibit the response of striatal cells to contralateral cortical stimulation when the cortical stimulus was delivered 10ms after whisker stimulation. The EPSP of the neurones to contralateral cortical stimulation {mean ± standard error (11.877 ± 2.01)} was significantly decreased at time intervals of 20ms (0.267 ± 0.999) and 40ms (6.446 ± 1.743) (ANOVA, $P<0.001$, Tukey's test).

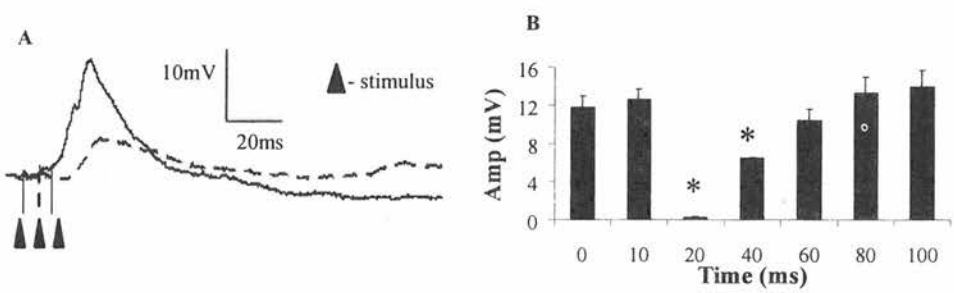

Figure 1. Response of striatal cells to a contralateral cortical stimulation, fixed time intervals after a whisker pad stimulus. (A) The representative cell has a membrane potential of –64mV. The traces are the average of 8 sweeps and they illustrate the response of the cell to contralateral cortical stimulation 10ms after whisker pad stimulation. The dashed trace is the response of the cell to contralateral cortical stimulation alone. With a time interval of 10ms between the two stimuli the cell is able to respond to the second stimulus. (B) The graph summarises the response (mean peak amplitude ± S.E) of 10 cells to cortical stimulation at fixed time intervals after a whisker stimulus. (*) denotes a significant difference from the control value at time 0 (ANOVA, $P<0.001$, Tukey's test).

4.2. Whisker – Whisker Interaction

Stimulation of the whisker pad leads to a prolonged inhibition, lasting 140ms during which the response of the striatal cells to the second whisker stimulus was significantly decreased. As the cells recovered from the inhibition the rise time of the EPSPs was significantly slower till the time interval of 120ms (8.026 ± 0.429) after which the rise time was similar to control values (4.141 ± 0.600).

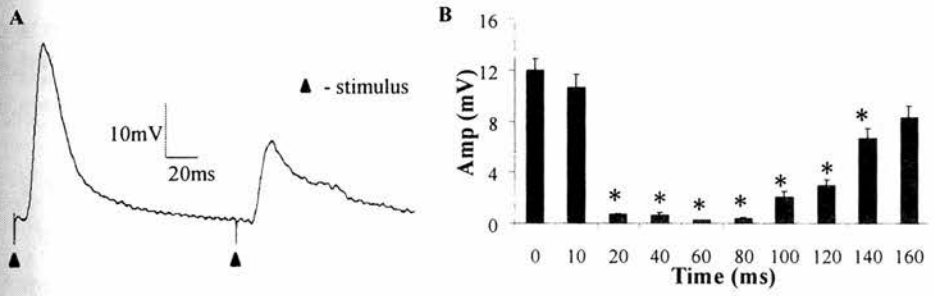

Figure 2. Response of striatal cells to 2 whisker pad stimuli delivered fixed time intervals apart. (A) The trace illustrates the response of a cell to 2 whisker pad stimuli 120ms apart. The cell has a membrane potential of –85mV. The EPSP to the initial whisker pad stimulation has a rise time of 3.195ms while the response to the second whisker pad stimulation has a rise time of 7.500ms. (B) The graph summarises the response of 10 cells to 2 whisker pad stimuli delivered fixed time intervals apart. (*) denotes a significant difference from the control value at time 0 (ANOVA, $P<0.001$, Tukey's test).

4.3. Cortex – Whisker Interaction

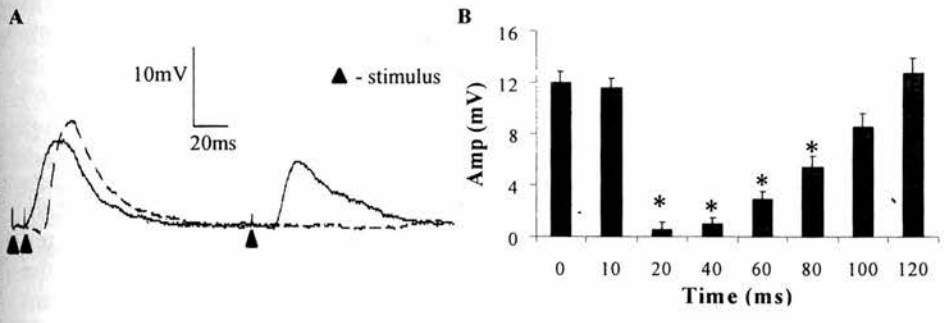

Figure 3. Response of striatal cells to whisker pad stimulus, fixed time intervals after a contralateral cortical stimulation. (A) The cell has a membrane potential of –65mV. The averaged traces of 8 sweeps illustrate the response of the cell to whisker pad stimulation 120ms after contralateral cortical stimulation. The dashed trace is the response of the cell to whisker pad stimulation only. (B) The graph summarises the response of 10 cells to whisker pad stimulation delivered at fixed time intervals after an initial contralateral cortical stimulation. (*) denotes a significant difference from the control value at time 0 (ANOVA, $P<0.001$, Tukey's test).

Contralateral cortical stimulation did not inhibit the response of striatal cells to whisker pad stimulation when the 2 stimuli were 10ms apart. The EPSP of the neurones to the whisker pad stimulation (11.995 ± 2.005) was significantly decreased at time intervals of 20ms (0.575 ± 1.771), 40ms (1.007 ± 0.993), 60ms (2.904 ± 1.529) and 80ms (5.425 ± 2.356) (ANOVA, $P<0.001$, Tukey's test). The rise time of the whisker stimulus was also significantly slower from 20ms to 60ms when compared to control values.

4.4. Cortex - Cortex Interaction

Stimulation of the contralateral cortex inhibited the response of striatal cells to a second contralateral cortical stimulation. The cells were able to respond to the second contralateral stimuli when it was delivered 80ms after the initial stimulus.

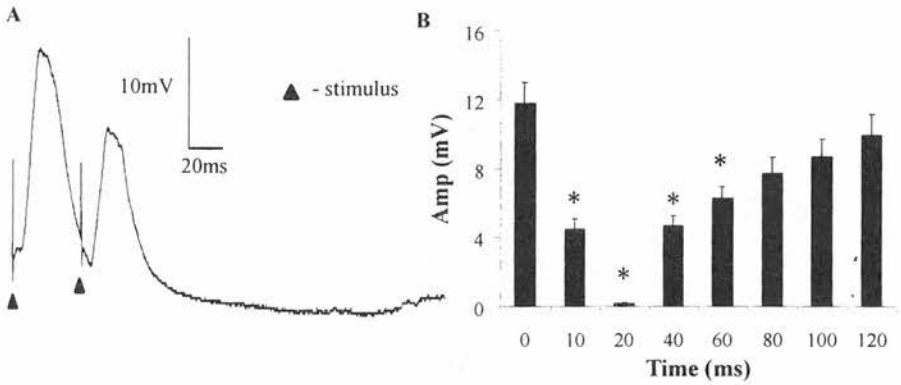

Figure 4. Response of striatal cells to 2 contralateral cortical stimuli, delivered fixed time intervals apart. (A) The trace illustrates the response of a cell to 2 contralateral barrel cortical stimuli 40ms apart. The cell has a membrane potential of –87mV. The EPSP to the second cortical stimuli has a peak amplitude of 15mV. (B) The graph summarises the response of 10 cells to 2 contralateral cortical stimuli delivered fixed time intervals apart. (*) denotes a significant difference from the control value at time 0 (ANOVA, $P<0.001$, Tukey's test).

4.5. Amplitude of Response versus Membrane Potential

The membrane potential of the cell affected the amplitude of the response of the cell. From each cell the membrane potential and corresponding peak amplitude was measured when either the whisker pad or the contralateral cortex was stimulated. The size of the EPSP of a striatal neurone to either form of stimulation was found to be partly dependent on its membrane potential. Cells in the 'up' state with membrane potentials of around – 60mV responded to sub-threshold stimulation with EPSPs of smaller peak amplitudes compared to cells in the 'down' state with membrane potentials of around – 85mV. The correlation coefficient of the size of EPSP and membrane potential is 0.870.

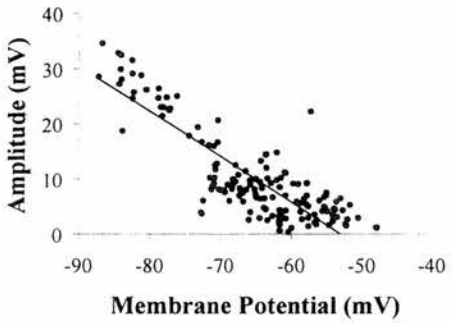

Figure 5. The graph shows the relationship between the size of the response of 10 striatal cells and their membrane potential. The slope of the line of best fit is 0.757.

5. DISCUSSION

Postsynaptic potentials were evoked in striatal neurones by stimulation of the ipsilateral and contralateral barrel cortex, which is known to project to the striatum (Wright et al., 1999). Electrical stimulation of the whisker pad ensures a synchronous, massive input directed initially to the barrel cortex, and leads to the activation of the collateral branches from the corticofugal fibres in the rat, including the corticothalamic systems (Wright et al., 2000). Stimulation of the contralateral cortex however evokes synaptic potentials from a more restricted subpopulation of crossed corticostriatal neurones, similar to the bilaterally projecting corticostriatal/cortico-cortical cells from the agranular cortex (Wilson, 1987). These septal cells have been identified as the main source of cortico-cortical connections in the somatosensory cortex (Chapin et al., 1987; Olavarria et al., 1984). The diffuse, corticostriatal pathway and the topographic pathway interact at the level of a single striatal cell.

The response of a striatal cell to a single stimulus was an EPSP followed by a period of silence which lasted 100-300ms. The latency of the response to both forms of stimulation was not significantly different whereas the rise time for contralateral cortical stimulation was significantly slower and more variable. This agrees with previous results (Wright et al., 2001). Results from the interaction paradigm indicate that the post-synaptic responses to the second stimulus are related to the order and source as well as the interval between the two stimuli. In 3 of the 4 pairing protocols, when the onset of the EPSP evoked by the second stimulus coincided with part of the EPSP evoked by the first stimulus the two EPSPs were additive. This has been previously reported by Hull and associates (Hull et al., 1973). This additive effect, however, was not observed when both stimuli were from the contralateral barrel cortex.

When the second stimulus was delivered during the inhibitory phase of the cell, the cell was unable to respond. However the recovery time of the cell from inhibition was different in all 4 conditions. The inhibition observed has been proposed to be due to disfacilitation as seen by the destructive effects of cortical and thalamic lesions (Wilson et al., 1983). Thus during a period of active inhibition of cortical and thalamic neurones the excitability of polysynaptic pathways to the striatum is reduced, depriving striatal neurones of a steady subthreshold depolarisation. This theory of disfacilitation while

explaining the prolonged period of inhibition observed in the whisker-whisker interaction protocol, does not hold true for the relatively rapid recovery of the striatal cells to the second stimulus in the other 3 conditions.

Another possible explanation for the different responses of the striatal cells could be the different effects of whisker deflection on the barrel cortex itself. Intracellular recordings *in vivo* from anaesthetised rats indicate that the initial response of barrel neurones to whisker deflection is typically an EPSP followed by an IPSP (inhibitory potential) and these EPSP-IPSP sequences have been well documented in the rat barrel cortex (Carvell, Simons, 1988; Zhu, Connors, 1999). However, some cells respond with only IPSPs (Agmon, Connors, 1992; Moore, Nelson, 1998) and it has been shown recently that these cells are found in or at the border of septa (Sachdev et al., 2000b). While, in these experiments, stimulation of the diffuse corticostriatal pathway was able to raise the spiny cells to firing threshold, the effect of inhibition of septal cells and the effect on the ipsilateral barrel cortex has not been investigated. The inhibitory response seen in cortical cells after whisker stimulation is mediated by intracortical inhibitory interneurones. These interneurones are excited by thalamocortical afferents and in turn inhibit cortical neurones (Agmon, Connors, 1992; Simons, Carvell, 1989). These interneurones play a role in feed-forward inhibition in the barrel cortex (Porter et al., 2001). The connectivity of the crossed cortico-cortical fibres to these interneurones is still unknown.

The size of the response of a striatal cell to stimulation was found to be partly dependent on the membrane potential of the cell. Cells in the down state have a higher input resistance and thus have larger amplitude EPSPs when compared to cells in the up state. A similar finding was observed in the primary somatosensory cortical neurones, where a whisker deflection in spite of producing a larger EPSP, was less effective in producing a spike when the cell was hyperpolarised, compared to its depolarised state (Sachdev et al., 2000a).

The two corticostriatal pathways arising from the barrel cortex can be distinguished both morphologically as well as electrophysiologically. It thus provides a good model to study the possible effects of the two systems on the striatum.

6. ACKNOWLEDGEMENTS

The work was supported by Wellcome Trust Grant Number 060848. The authors would like to thank Ms Karen Wahl for her critical reading of the manuscript.

7. REFERENCES

Agmon, A., Connors, B.W., 1992, Correlation between firing pattern and thalamocortical synaptic responses of neurons in the mouse barrel cortex, *J.Neurosci.* **12**:319-329.

Bolam, J.P., Bennet, B., 1995, The microcircuitry of the neostriatum, In: Anonymouspp 1-19. Austin: R.G. Landes Company.

Carvell, G.E., Simons, D.J., 1988, Membrane Potential changes in Rat Sm1 Cortical Neurons evoked by Controlled Stimulation of Mystacial Vibrissae, *Brain Res.* **448**:186-191.

Chapin, J.K., Sadeq, M., Guise, L.U., 1987, Corticocortical connections within the primary somatosensory cortex of the rat, *J.Comp.Neurol.* **263**:326-346.

Cho, J., West, M.O., 1997, Distributions of single neurones realted to body parts in the lateral striatum of the rat, *Br.Res.* **756**:241-246.

Cowan, R.L., Wilson C.J., 1994, Spontaneous firing patterns and axonal projections of single corticostriatal neurons in the rat medial agranular cortex, *J.Neurophysiol.* **71**:17-32.

Dube, L., Smith, A.D., Bolam, J.P., 1988, Identification of synaptic terminals of thalamic or cortical origin in contact with distinct medium-size spiny neurons in the rat neostriatum, *J.Comp.Neurol.* **267**:455-471.

Gerfen, C.R., Wilson, C.J., 1996, The basal ganglia, In: Integrated systems of the CNS, part III. Cerebellum, basal ganglia and olfactory system (Swanson LW, Bjorkland A, Hokfelt T eds), Amsterdam: Elsevier Press.

Hull, C.D., Bernardi, G., Price, D.D., Buchwald, N.A., 1973, Intracelluar responses of caudate neurons to temporally and spatially combined stimuli, *Exp.Neuro.* **38**:324-336.

McGeorge, A.J., Faull, R.L.M., 1989, The organization of the projection from the cerebral cortex to the striatum in the rat, *Neurosci.* **29**:503-537.

Moore, C.I., Nelson, S.B., 1998, Spatio-temporal subthreshold receptive fields in the vibrissa representation of rat primary somatosensory cortex, *J.Neurophysiol.* **80**:2882-2892.

Olavarria, J., Van Sluyters, R.C., Killackey H. P., 1984, Evidence for the comlementary organization of callosal and thalamic connections within rat somatosensory cortex, *Brain Res.* **291**:364-368.

Porter, J.T., Johnson, C.K., Agmon, A., 2001, Diverse types of interneurons generate thalamus-evoked feedforward inhibition in the mouse barrel cortex, *J.Neurosci.* **21**:2699-2710.

Richards, C.D., Taylor, D.C.M., 1982, Electrophysiological evidence for a somatotopic sensory projection to the striatum of the rat, *Neurosci.Letts.* **30**:235-240.

Sachdev, R.N.S., Ebner, F.F., Wilson, C.J., 2000a, Spontaneous subthreshold potential fluctuations of s1 cortical neurons influence action potential occurence following whisker deflection, *Society for Neuroscience Abstracts* **26**:133(Abstract)

Sachdev, R.N.S., Sellien, H., Ebner, F.F., 2000b, Direct inhibition evoked by whisker stimulation in somatic sensory (SI) barrel field cortex of the awake rat, *J.Neurophysiol.* **84**:1497-1504.

Sedgwick, E.M., Williams, T.D., 1967, The response of single units in the caudate nucleus to peripheral stimulation, *J.Physiol.* **189**:281-298.

Selemon, L.D., Goldman-Rakic, P.S., 1985, Longitudinal topography and interdigitation of corticostriatal projections in the rhesus monkey, *J.Neurosci.* **5**:776-794.

Simons, D.J., Carvell, G.E., 1989, Thalamocortical response transformation in the rat vibrissa/barrel system, *J.Neurophysiol.* **61**:311-330.

Somogyi, P., Bolam, J.P., Smith, A.D., 1981, Monosynaptic cortical input and local axon collaterals of identified striatonigral neurons. A light and electron microscopic study using the golgi-peroxidase transport degeneration procedure, *J.Comp.Neurol.* **195**:567-584.

West, M.O., Carelli, R.M., Pomerantz, M., Cohen, S.M., Gardner, J.P., Chapin, J.K., Woodward, D.J., 1990, A region in the dorsolateral striatum of the rat exhibiting single-unit correlations with specific locomotor limb movements, *J.Neurophysiol.* **64**:1233-1246.

Wickens, J.R., Wilson, C.J., 1998, Regulation of action potential firing in spiny neurons of the rat neostriatum in vivo, *J.Neurophysiol.* **79**:2358-2364.

Wilson, C.J., 1986, Postsynaptic potentials evoked in spiny neostriatal projection neurons by stimulation of ipsilateral and contralateral neocortex, *Br.Res.* **367**:201-213.

Wilson, C.J., 1987, Morphology and synaptic connections of crossed corticostriatal neurons in the rat, *J.Comp.Neurol.* **263**:567-580.

Wilson, C.J., Chang, H.T., Kitai, S.T., 1983, Disfacilitation and long-lasting inhibition of neostriatal neurons in the rat, *Exp.Br.Res.* **51**:227-235.

Wilson, C.J., Kawaguchi, Y., 1996, The origins of two-state spontaneous membrane potential fluctuations of neostriatal spiny neurones, *J.Neurosci.* **16**:2397-2410.

Woolsey, T.A., van der Loos, H., 1970, The structural organisation of layer IV in the somatosensory region (SI) of mouse cerebral cortex, *Brain Res.* **17**:205-242.

Wright, A.K., Norrie, L., Arbuthnott, G.W., 2000, Corticofugal axons from adjacent 'barrel' columns of rat somatosensory cortex: Cortical and thalamic terminal patterns, *J.Anat.* **196**:379-390.

Wright, A.K., Norrie, L., Ingham, C.A., Hutton, E.A.M., Arbuthnott, G.W., 1999, Double anterograde tracing of outputs from adjacent "barrel columns" of rat somatosensory cortex. Neostriatal projection patterns and terminal ultrastructure, *Neurosci.* **88**:119-133.

Wright, A.K., Ramanathan, S., Arbuthnott, G.W., 2001, Identification of the source of the bilateral projection system from cortex to somatosensory neostriatum and an exploration of its physiological actions, *Neurosci.* **103**:87-96.

Zhu, J.J., Connors, B.W., 1999, Intrinsic firing patterns and whisker-evoked synaptic responses of neurons in the rat barrel cortex, *J.Neurophysiol.* **81**:1171-1183.

explaining the prolonged period of inhibition observed in the whisker-whisker interaction protocol, does not hold true for the relatively rapid recovery of the striatal cells to the second stimulus in the other 3 conditions.

Another possible explanation for the different responses of the striatal cells could be the different effects of whisker deflection on the barrel cortex itself. Intracellular recordings *in vivo* from anaesthetised rats indicate that the initial response of barrel neurones to whisker deflection is typically an EPSP followed by an IPSP (inhibitory potential) and these EPSP-IPSP sequences have been well documented in the rat barrel cortex (Carvell, Simons, 1988; Zhu, Connors, 1999). However, some cells respond with only IPSPs (Agmon, Connors, 1992; Moore, Nelson, 1998) and it has been shown recently that these cells are found in or at the border of septa (Sachdev et al., 2000b). While, in these experiments, stimulation of the diffuse corticostriatal pathway was able to raise the spiny cells to firing threshold, the effect of inhibition of septal cells and the effect on the ipsilateral barrel cortex has not been investigated. The inhibitory response seen in cortical cells after whisker stimulation is mediated by intracortical inhibitory interneurones. These interneurones are excited by thalamocortical afferents and in turn inhibit cortical neurones (Agmon, Connors, 1992; Simons, Carvell, 1989). These interneurones play a role in feed-forward inhibition in the barrel cortex (Porter et al., 2001). The connectivity of the crossed cortico-cortical fibres to these interneurones is still unknown.

The size of the response of a striatal cell to stimulation was found to be partly dependent on the membrane potential of the cell. Cells in the down state have a higher input resistance and thus have larger amplitude EPSPs when compared to cells in the up state. A similar finding was observed in the primary somatosensory cortical neurones, where a whisker deflection in spite of producing a larger EPSP, was less effective in producing a spike when the cell was hyperpolarised, compared to its depolarised state (Sachdev et al., 2000a).

The two corticostriatal pathways arising from the barrel cortex can be distinguished both morphologically as well as electrophysiologically. It thus provides a good model to study the possible effects of the two systems on the striatum.

6. ACKNOWLEDGEMENTS

The work was supported by Wellcome Trust Grant Number 060848. The authors would like to thank Ms Karen Wahl for her critical reading of the manuscript.

7. REFERENCES

Agmon, A., Connors, B.W., 1992, Correlation between firing pattern and thalamocortical synaptic responses of neurons in the mouse barrel cortex, *J.Neurosci.* **12**:319-329.

Bolam, J.P., Bennet, B., 1995, The microcircuitry of the neostriatum, In: Anonymouspp 1-19. Austin: R.G. Landes Company.

Carvell, G.E., Simons, D.J., 1988, Membrane Potential changes in Rat Sm1 Cortical Neurons evoked by Controlled Stimulation of Mystacial Vibrissae, *Brain Res.* **448**:186-191.

Chapin, J.K., Sadeq, M., Guise, L.U., 1987, Corticocortical connections within the primary somatosensory cortex of the rat, *J.Comp.Neurol.* **263**:326-346.

EFFECTS OF DOPAMINE ON INTERACTION OF THE TWO CORTICOSTRIATAL SYSTEMS IN RAT SOMATOSENSORY STRIATUM.

S. Ramanathan, A. K. Wright, G. W. Arbuthnott

University of Edinburgh, Center for Neuroscience
Department of Preclinical Veterinary Sciences, Summerhall
Edinburgh, EH9 1NA, Scotland, United Kingdom

ABSTRACT

The intracellular responses of single striatal neurones under Chloralose and Urethane (1% & 10%; 10ml/Kg, i.p.) anaesthesia to stimulation of the contralateral barrel cortex and whisker pad were studied in normal rats and in rats with unilateral 6-hydroxydopamine lesion of midbrain dopaminergic neurones. In normal rats both stimuli depolarise striatal cells and EPSPs in response to whisker pad stimulation have a rapid rise time, while the contralateral cortically derived EPSPs are slower to rise and the spike initiation latency more variable. The two pathways also interact at the level of a single striatal cell. In dopamine depleted animals both stimuli were also able to depolarise the spiny neurones to their firing threshold. However the EPSPs to whisker pad stimulation were significantly slower to rise compared to control animals and were similar to cortically derived EPSPs. The interaction of the two pathways was also affected by the loss of dopamine.

1. INTRODUCTION

The striatum is the main input nucleus of the basal ganglia. There is representation of each area of the cortex in the striatum, which is considered to be the major integrative component of the basal ganglia [1, 2]. The main neuronal type in the striatum is the GABAergic medium sized densely spiny projection neurone, which in rodents makes up 90-95% of the neuronal population [3, 4]. These spiny neurones receive a direct cortical input onto their dendritic spines [5] which shapes the activity of the cells [6, 7].

In rodents, the mystacial vibrissae (whiskers) are the principle tactile receptors. The sensory information obtained from the whiskers provides an important input for locomotion. The information from the whiskers is processed in Layer IV of the neocortex by groups of neurones arranged in discrete functional units known as barrels [8].

Recent anterograde tracing studies have shown that there are at least two morphologically distinct corticostriatal pathways that arise from the barrel cortex [9]. One of these, referred to as the 'discrete pathway', is topographic in nature giving rise to a somatotopic representation of the barrel cortex in the striatum. The projection is composed of thick fibres arising from collaterals of the descending somatosensory fibres leaving the corticofugal bundles at right angles. The axons give rise to several large 'boutons en passant' and the terminal areas of these run parallel to the internal border of the callosum. The second projection, referred to as the 'diffuse pathway', is composed of fine fibres, does not posses the clear topography of the discrete pathway and is bilateral. In agreement with previous work [10-12], these fine fibres are thought to be part of a diffuse system of corticostriatal axons that innervate both cortices and striata [13]. They arise from the septa between the barrels and leave the corpus callosum at an acute angle [13]. Electron microscopy has revealed that both types of fibres make contact with the dendritic spines of the medium spiny striatal projection neurones and form asymmetric synapses [9].

There have been some reports of responses in the striatum of rats to stimulation of the periphery. Stimulation of various parts of the body and concurrent recordings in cats and rats seems to suggest that there is a sensory map of the body in the striatum [14-17]. Preliminary experiments have shown that it is possible to record excitatory postsynaptic potentials (EPSPs) in spiny neurones of the striatum in response to stimulation of the contralateral cortex (via activation of the diffuse pathway) and the contralateral whisker pad (via activation of the ipsilateral barrel cortex) [13]. The response of a striatal cell to a single stimulus was an EPSP followed by a period of silence, which lasted 100-300ms. Stimulation of the whisker pad resulted in EPSPs that had a rapid rise time with little variation in latency. Contralateral cortical

stimulation gave rise to EPSPs, which were much slower and more variable. The latency of the responses was similar for both stimulation sites even though the pathway from the whisker pad to the striatum is polysynaptic, containing at least four synapses whereas the contralateral pathway is monosynaptic.

The substantia nigra provides a major dopaminergic input to the striatum [20]. The medium spiny projection neurones receive a dopaminergic input onto the neck of the spines [21, 22].

There is evidence for actions of dopamine on the corticostriatal pathway [23, 24]. Studies that examined the effect of dopamine on the single unit activity of striatal cells showed that dopamine decreased evoked spike activity [25, 26]. However this was found to be a dose dependent effect with lower doses of dopamine facilitating glutamate-evoked spiking whereas higher doses inhibit it [27, 28]. *In vivo* experiments in which the median forebrain bundle was stimulated to evoke dopamine release found an enhancement of spontaneous discharge in a subset of medium spiny neurones [29]. Both long term potentiation (LTP) and depression (LTD), have been described at corticostriatal synapses. It has been hypothesised that these two forms of synaptic plasticity might represent the cellular mechanisms for the long term regulation exerted by the striatum on the basal ganglia activity as a means of storage of motor skills. The effects of dopamine may involve synaptic plasticity in the striatum and this suggestion is the topic of recent reviews [30-32].

The destruction of dopamine neurones by 6-hydroxydopamine (6-OHDA) treatment, causes rats to lose their ability to orientate towards tactile stimuli [33]. Ungerstedt and associates [34] reported that the responses of striatal cells to peripheral stimulation was not detected after the removal of dopamine. Spine density of striatal neurones has been shown to decrease after the loss of dopamine [35, 36]. More recently the same group [37] have also shown that after a lesion of the dopamine system the total number of asymmetric boutons in the striatum decreases, with an increase in the density of a sub-population of asymmetric boutons which have complex synaptic specialisations. The loss of dopamine has also been shown to affect the electrophysiological behaviour of striatal cells [38-41].

The aim of the current experiments was to study the responses of striatal cells to the two forms of stimuli and the interaction of the stimuli and to determine if the loss of dopamine affects the response of the cells.

2. MATERIALS AND METHODS

Seven male Sprague Dawley rats (200-250g) were anaesthetised with halothane in O_2 and injected with 2μl of saline containing 6μg of 6-OHDA and 0.4μl of ascorbic acid into the right medial forebrain bundle (AP-3.8mm, L-1.5, DV-8.0). The success of the lesion was tested [42] 9 or 10 days after the operation by determining the number of turns the animals make in response to the administration of apomorphine (0.25mg/Kg, in H_2O, i.p.). Those animals that turned >200 complete circles away from the injected side in 45min were considered to have at least 90% loss of dopamine from the lesioned side and were used for electrophysiological experiments 30 days post-lesion.

Lesioned and control rats (N=25) were anaesthetised intra-peritoneally with 1ml/100g body weight of a 1% α-chloralose 10% urethane mix in distilled water. Stable levels of anaesthesia were maintained throughout with additional anaesthetic (10% of original dose), to ensure the absence of a foot withdrawal reflex. The animal was transferred to a stereotaxic apparatus and its head secured in a frame via ear and tooth bars. Body temperature was maintained at 37^0C throughout using a homeothermic blanket and a rectal probe. A slit was made in the atlanto-occipital membrane and a cerebrospinal fluid drain created in order to reduce intracerebral pressure. Holes were drilled in the skull (AP-2.1mm, L-5.0mm) on both sides. A contralateral stimulating electrode (Harvard Apparatus) was then lowered to a depth of 2.5mm so that it straddled Layer V of the somatosensory cortex. Stimulation of the left whisker pad was carried out between a pair of insect pins connected to a constant voltage stimulator.

Intracellular recordings were made from glass electrodes containing 3M potassium acetate with resistances of 50-110MΩ. The electrode was advanced into the cortex at an angle of 90^0 to the cortical surface and then advanced to a depth of 2,500μm after which the electrode was advanced in 2μm steps until a neurone was impaled. A neurone was considered to be successfully impaled if the membrane potential was stable and below –60mV.

Once inside the cell, the response of the cell to whisker pad and contralateral cortical stimulation was determined. The cells were stimulated below the threshold for the firing of action potentials. The interaction of the two systems was then studied using a paired protocol. After an initial stimulus, a second stimulus was delivered at fixed time intervals. This protocol was carried out to study the interaction of the two different pathways (barrel cortex-septa, septa-barrel cortex) compared to the effects of a pathway on itself (barrel cortex-barrel cortex, septa-septa).

Records obtained were acquired using a PC based data acquisition system (Signal 2.04). Eight consecutive sweeps were taken per time interval. The latency, rise-time and peak amplitude of the response of the neurone to each stimulus was measured. The peak amplitude at the different time intervals was compared using a one-way ANOVA and Tukey's multiple comparison test.

3. RESULTS

Neurones that responded (N=25) were found in the striatum 0.9mm to 2.12mm posterior to the Bregma, whilst more anterior or posterior striatal neurones did not respond. All cells responded to both the whisker and contralateral cortical stimuli. A cell was included in the analysis only if all four paired interaction protocols were carried out.

In control animals both forms of stimuli were able to raise the striatal cells to firing threshold. The response of a striatal cell to a single stimulus was an EPSP followed by a period of silence, which lasted 100-300ms. The latency and rise time of the EPSP from stimulating the whisker pad (barrel centre) were 8.49±1.79 ms and 4.14±1.89 ms respectively while responses to the contralateral cortical (septal cell) stimulation had a latency not significantly different at 7.82±2.25 ms but the rise time was significantly slower at 11.02±5.56 ms.

The interaction of these two pathways with each other (barrel cortex-septa, septa-barrel cortex) and effects of a pathway on itself (barrel cortex-barrel cortex, septa-septa) were studied [18]. Results from these interaction studies indicate that the post-synaptic responses to the second stimulus were related to the order and source of the stimulation as well as to the interval between the two stimuli (Fig. 1). In 3 of the 4 pairing protocols, when the onset of the EPSP evoked by the second stimulus coincided with part of the EPSP evoked by the first stimulus the two EPSPs were additive. This has been previously reported by Hull and associates [19]. This additive effect, however, was not observed when both stimuli were from the contralateral barrel cortex (septal stimulation). When the second stimulus was delivered after 20 ms, the cell was unable to respond. However the recovery of the cell from inhibition was different in all 4 conditions e.g. stimulation of the barrel centres inhibited responses to septal cell stimulation for approximately 40ms whereas a second barrel centre derived EPSP was inhibited for 140ms.

Records were obtained from 8 striatal cells in the lesioned animals. Neurones that responded were found in the striatum 0.9mm to 2.12mm posterior to the Bregma, whilst more anterior or posterior striatal neurones did not respond. All 8 cells responded to both the whisker and contralateral cortical stimuli. A cell was included in the analysis only if all four paired interaction protocols were carried out.

The mean latencies and the peak amplitude for the two forms of stimulation were not significantly different (Paired T-Test, $P > 0.05$). The latency of response to barrel centre stimulation was significantly increased compared to control (10.13±0.38ms ANOVA, Tukey's multiple comparison, $P < 0.05$) [18]. A two-tailed paired t-test was done on the rise time of the EPSPs (11.34±1.0ms, barrel centre and 15.03 ± 1.0ms septa) and they were not significantly different (Paired T-Test, $P > 0.05$). The rise time of the EPSP for barrel centre stimulation was significantly different from control animals (ANOVA, Tukey's multiple comparison, $P < 0.05$).

Dopamine has an effect on the interaction of the two corticostriatal pathways. The summation of EPSP amplitude observed when the stimuli were delivered 10ms apart in control animals [18] was no longer present (Fig. 1). The inhibitory phase, in which the striatal cell was unable to respond to a second stimulus, was also increased when the second stimulus arose from the barrel centres in dopamine depleted animals (Fig.1).

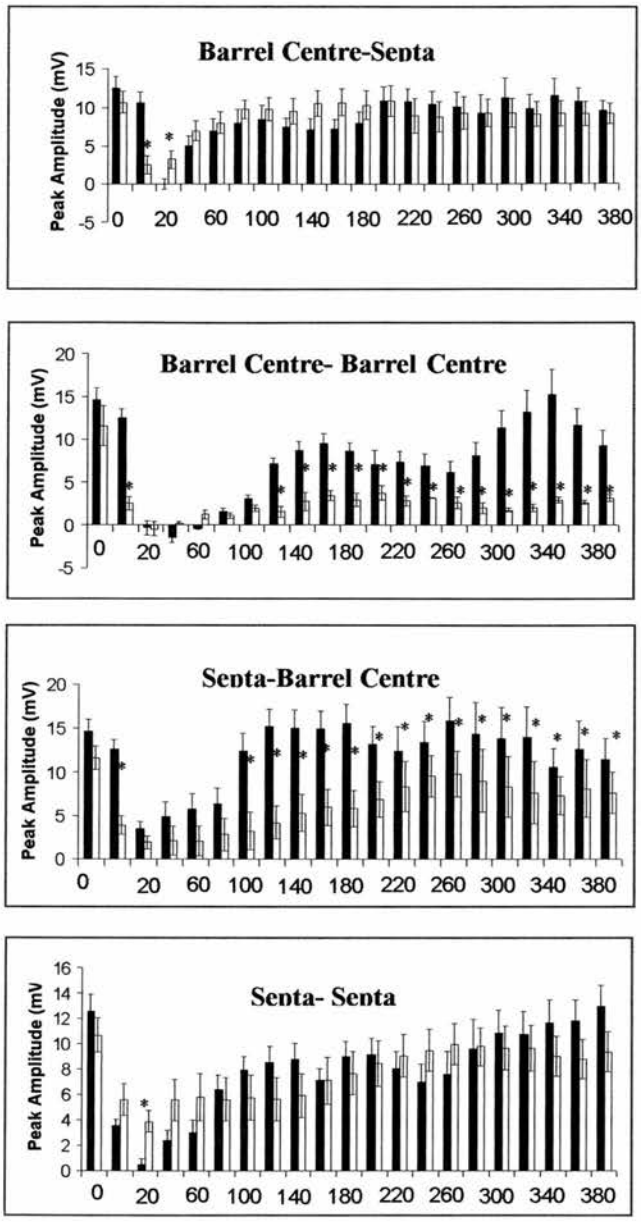

Figure. 1: Interaction of the two corticostriatal pathways at different time intervals.

The graphs illustrate the response and recovery of the cells to the paired protocol. The response at time 0 is the peak amplitude of the cell to the stimulus alone. An asterisk (*) denotes significant difference in peak amplitude between the control and lesion animals (ANOVA, Turkey's multiple comparison, $P < 0.05$)

4. DISCUSSION

The loss of dopamine affects the corticostriatal pathways arising from the barrel cortex. The response of striatal cells to stimulation of barrel centres is altered with an increase in both latency and rise time. Thus stimulation of the barrel centre elicits a response which is similar to when the septal cells are stimulated. Thus one possible effect of the loss of dopamine could be the alteration of responses to barrel centre stimulation to that of septal cells stimulation. This hypothesis is further supported by interaction of the two pathways at short time intervals. In control animals when both stimuli were from the contralateral barrel cortex (septal stimulation) there was no summation of EPSPs at a time interval of 10ms[18]. However the EPSPs were summated at the same time interval for the other 3 pairing protocols. In lesioned animals no summation of EPSPs were observed i.e. the cells behaved as they would under dual stimulation of the septal cells. This would be the expected observation if stimulation of the barrel centre elicits a response, which is similar to when the septal cells are stimulated.

This however cannot be the only effect of the loss of dopamine. The period of inhibition seen in striatal cells after 6-OHDA treatment is significantly increased. Thus the loss of dopamine may have other effects. It could affect thalamaocortical and/or thalamostriatal circuits as well the circuits within the barrel centres themselves. Thus the role of dopamine in processing corticostriatal information arising from the barrel cortex is complex.

5. BIBLIOGRAPHY

[1] Selemon, L.D. and P.S. Goldman-Rakic, *Longitudinal topography and interdigitation of corticostriatal projections in the rhesus monkey.* J. Neurosci., 1985. **5**: p. 776-794.

[2] McGeorge, A.J. and R.L. Faull, *The organization of the projection from the cerebral cortex to the striatum in the rat.* Neuroscience, 1989. **29**(3): p. 503-37.

[3] Bolam, J.P. and B. Bennett, *The microcircuitry of the neostriatum.* 1995, Austin: R.G. Landes Company. 1-19.

[4] Gerfen, C.R. and C.J. Wilson, *The Basal Ganglia.* Handbook of Chemical Neuroanatomy, Integrated systems of the CNS, Part III., ed. T.H.a.L.S. A. Bjorklund. Vol. 12. 1996: Elsevier Science. 369-466.

[5] Somogyi, P., J.P. Bolam, and A.D. Smith, *Monosynaptic cortical input and local axon collaterals of identified striatonigral neurons. A light and electron microscopic study using the Golgi-peroxidase transport-degeneration procedure.* J. Comp. Neurol., 1981. **195**: p. 567-584.

[6] Wilson, C.J., H.T. Chang, and S.T. Kitai, *Disfacilitation and long-lasting inhibition of neostriatal neurons in the rat.* Exp Brain Res, 1983. **51**: p. 227-235.

[7] Wilson, C.J. and Y. Kawaguchi, *The origins of two state spontaneous membrane potential fluctuations of neostriatal spiny neurons.* J Neurosci, 1996. **16**(7): p. 2397-2410.

[8] Woolsey, T.A. and H. Van der Loos, *The structural organization of layer IV in the somatosensory region (SI) of mouse cerebral cortex. The description of a cortical field composed of discrete cytoarchitectonic units.* Brain Res, 1970. **17**(2): p. 205-42.

[9] Wright, A.K., et al., *Double anterograde tracing of outputs from adjacent "barrel columns" of rat somatosensory cortex. Neostriatal projection patterns and terminal ultrastructure.* Neuroscience, 1999. **88**(1): p. 119-113.

[10] Cowan, R.L. and C.J. Wilson, *Spontaneous firing patterns and axonal projections of single corticostriatal neurons in the rat medial agranular cortex.* J. Neurophysiol., 1994. **71**(1): p. 17-32.

[11] Wilson, C.J., *Postsynaptic potentials evoked in spiny neostriatal projection neurons by stimulation of ipsilateral and contralateral neocortex.* Brain Res, 1986. **367**: p. 201-213.

[12] Wilson, C.J., *Morphology and synaptic connections of crossed corticostriatal neurons in the rat.* J Comp Neurol, 1987. **263**: p. 567-580.

[13] Wright, A.K., S. Ramanathan, and G.W. Arbuthnott, *Identification of the source of the bilateral projection system from cortex to somatosensory neostriatum and an exploration of its physiological actions.* Neuroscience, 2001. **103**(1): p. 87-96.

[14] Cho, J. and M.O. West, *Distributions of single neurones related to body parts in the lateral striatum of the rat.* Brain research, 1997. **756**: p. 241-246.

[15] Richards, C.D. and D.C.M. Taylor, *Electrophysiological evidence for a somatotopic sensory projection to the striatum of the rat.* Neurosci. Lett., 1982. **30**: p. 235-240.

[16] Sedgwick, E.M. and T.D. Williams, *The response of single units in the caudate nucleus to peripheral stimulation.* J. Physiol., Lond., 1967. **189**: p. 281-298.

[17] West, M.O., et al., *A region in the dorsolateral striatum of the rat exhibiting single-unit correlations with specific locomotor limb movements.* J Neurophysiol, 1990. **64**: p. 1233-1246.

[18] Ramanathan, S., A.K. Wright, and G.W. Arbuthnott, *A physiological investigation of the two corticostriatal systems in rat somatosensory striatum.* The Basal Ganglia VII. Vol. VII. 2001, New York: Plenum Press *(in press)*.

[19] Hull, C.D., et al., *Intracellular responses of caudate neurons to temporally and spatially combined stimuli.* Exp Neurol, 1973. **38**(2): p. 324-36.

[20] Anden, N.E., et al., *Demonstration and mapping out of nigro-neostriatal dopamine neurons.* Life Sci., 1964. **3**: p. 523-530.

[21] Freund, T.F., J. Powell, and A.D. Smith, *Tyrosine hydroxylase-immunoreactive boutons in synaptic contact with identified striatonigral neurons, with particular reference to dendritic spines.* Neuroscience, 1984. **13**: p. 1189-1215.

[22] Smith, A.D. and J.P. Bolam, *The neural network of the basal ganglia as revealed by the study of synaptic connections of identified neurones.* Trends Neurosci., 1990. **13**: p. 259-265.

[23] Arbuthnott, G.W., et al., *Presynaptic actions of dopamine in the neostriatum.* The Basal Ganglia- Structure and Function, ed. J.S. McKenzie, R.E. Kemm, and L.N. Wilcock. 1984, New York: Plenum Press. 173-203.

[24] Wickens, J.R., A.J. Begg, and G.W. Arbuthnott, *Dopamine reverses the depression of rat corticostriatal synapses which normally follows high-frequency stimulation of cortex in vitro.* Neuroscience, 1996. **70**(1): p. 1-5.

[25] Brown, J.R. and G.W. Arbuthnott, *The electrophysiology of dopamine (D2) receptors: a study of the actions of dopamine on corticostriatal transmission.* Neuroscience, 1983. **10**: p. 349-355.

[26] Johnson, S.W., M.R. Palmer, and R. Freedman, *Effects of dopamine on spontaneous and evoked activity of caudate neurons.* Neuropharmacology, 1983. **22**: p. 843-851.

[27] Hu, X.-T. and R.Y. Wang, *Comparison of effects of D-1 and D-2 dopamine receptor agonists on neurons in the rat caudate putamen: An electrophysiological study.* J Neurosci, 1989. **8**: p. 4340-4348.

[28] Hu, X.-T. and F.J. White, *Dopamine enhances glutamate-induced excitation of rat striatal neurons by cooperative activation of D1 and D2 class receptors.* Neurosci Lett, 1997. **224**(1): p. 61-65.

[29] Gonon, F., *Prolonged and extrasynaptic excitatory action of dopamine mediated by D1 receptors in the rat striatum in vivo.* J Neurosci, 1997. **17**(15): p. 5972-5978.

[30] Calabresi, P., et al., *Synaptic plasticity and physiological interactions between dopamine and glutamate in the striatum.* Neurosci Biobehav Rev, 1997. **21**: p. 519-523.

[31] Calabresi, P., et al., *Synaptic transmission: from plasticity to neurodegeneration.* Progress in neurobiology, 2000. **61**: p. 231-265.

[32] Nicola, S.M., D.J. Surmeier, and R.C. Malenka, *Dopaminergic modulation of neuronal excitability in the striatum and nucelus accumbens.* Annual Review of Neuroscience, 2000. **23**: p. 185-215.

[33] Ljungberg, T. and U. Ungerstedt, *Sensory inattention produced by 6-hydorxy-dopamine-induced degeneration of ascending dopamine neurones in the brain.* Exp. Neurol., 1976. **53**: p. 585-600.

[34] Ungersted, U., et al. in *Proc. Int. Union Physiol. Sciences.* 1977.

[35] Ingham, C.A., S.H. Hood, and G.W. Arbuthnott, *Spine density on neostriatal neurones changes with 6-hydroxydopamine lesions and with age.* Brain Res, 1989. **503**: p. 334-338.

[36] Ingham, C.A., et al., *Morphological changes in the rat neostriatum after unilateral 6-hydroxydopamine injections into the nigrostriatal pathway.* Exp Brain Res, 1993. **93**: p. 17-27.

[37] Ingham, C.A., et al., *Plasticity of synapses in the rat neostriatum after unilateral lesion of the nigrostriatal dopaminergic pathway.* J Neurosci, 1998. **18**: p. 4732-4743.

[38] Tseng, K.Y., et al., *Cortical slow oscillatory activity is reflected in the membrane potential and spike trains of striatal neurons in rats with chronic nigrostriatal lesions.* J Neurosci, 2001. **21**(16): p. 6430-9.

[39] Calabresi, P., et al., *Electrophysiology of dopamine-denervated striatal neurons. Implications for Parkinson's disease.* Brain, 1993. **116 (Pt 2)**: p. 433-52.

[40] Galarraga, E., et al., *Spontaneous synaptic potentials in dopamine-denervated neostriatal neurons.* Neurosci Lett, 1987. **81**: p. 351-355.

[41] Onn, S.P. and A.A. Grace, *Alterations in electrophysiological activity and dye coupling of striatal spiny and aspiny neurons in dopamine-denervated rat striatum recorded in vivo.* Synapse, 1999. **33**(1): p. 1-15.

[42] Ungerstedt, U. and G.W. Arbuthnott, *Quantitative recordings of rotational behaviour in rats after 6-hydroxy-dopamine lesions of the nigrostriatal dopamine system.* Brain Res, 1970. **24**: p. 485-493.

Synaptic Convergence of Motor and Somatosensory Cortical Afferents onto GABAergic Interneurons in the Rat Striatum

Sankari Ramanathan,[1] Jason J. Hanley,[1] Jean-Michel Deniau,[2] and J. Paul Bolam[1]

[1]Medical Research Council Anatomical Neuropharmacology Unit, Department of Pharmacology, Oxford, OX1 3TH, United Kingdom, and [2]Institut National de la Santé et de la Recherche Médicale U114, Collège de France, 75321 Paris Cedex 05, France

Cortical afferents to the basal ganglia, and in particular the corticostriatal projections, are critical in the expression of basal ganglia function in health and disease. The corticostriatal projections are topographically organized but also partially overlap and interdigitate. To determine whether projections from distinct cortical areas converge at the level of single interneurons in the striatum, double anterograde labeling from the primary motor (M1) and primary somatosensory (S1) cortices in the rat, was combined with immunolabeling for parvalbumin (PV), to identify one population of striatal GABAergic interneurons.

Cortical afferents from M1 and S1 gave rise to distinct, but partially overlapping, arbors of varicose axons in the striatum. PV-positive neurons were often apposed by cortical terminals and, in many instances, apposed by terminals from both cortical areas. Frequently, individual cortical axons formed multiple varicosities apposed to the same PV-positive neuron. Electron microscopy confirmed that the cortical terminals formed asymmetric synapses with the dendrites and perikarya of PV-positive neurons as well as unlabelled dendritic spines. Correlated light and electron microscopy revealed that individual PV-positive neurons received synaptic input from axon terminals derived from both motor and somatosensory cortices.

These results demonstrate that, within areas of overlap of functionally distinct projections, there is synaptic convergence at the single cell level. Sensorimotor integration in the basal ganglia is thus likely to be mediated, at least in part, by striatal GABAergic interneurons. Furthermore, our findings suggest that the pattern of innervation of GABAergic interneurons by cortical afferents is different from the cortical innervation of spiny projection neurons.

Key words: GABA; striatum; corticostriatal; parvalbumin; cortex; basal ganglia

The basal ganglia are a group of subcortical nuclei that are intimately involved in the control of movement. One of their major roles is to integrate sensory, motor, associative, and limbic information in the production of context-dependent behaviors (Graybiel, 1990, 1995). Anatomical and physiological data suggest that cortical information transmitted to the basal ganglia via the corticostriatal projection is channeled into parallel functional circuits that remain segregated at each level of the corticobasal ganglia-thalamo-cortical loops (Alexander et al., 1986, 1990; Alexander and Crutcher, 1990; DeLong, 1990; Hoover and Strick, 1993; Parent and Hazrati, 1995; Middleton and Strick, 2000). In addition to this organization underlying "parallel processing", the possibility for integration of diverse information within, and between, these loops also exists (Nauta and Domesick, 1984; Francois et al., 1987; Flaherty and Graybiel, 1991, 1993, 1995; Parthasarathy et al., 1992; Graybiel, 1995; Beiser et al., 1997; Maurin et al., 1999; Haber et al., 2000; Hoffer and Alloway, 2001; Kolomiets et al., 2001). Indeed, anatomical substrates that may underlie the integration of diverse information within the basal ganglia at the synaptic level have been identified (Somogyi et al., 1981b; Bevan et al., 1996, 1997). For instance, neurons of the substantia nigra pars compacta that project to the dorsal (motor and associative) striatum receive synaptic input from neurons located in the ventral (limbic) striatum (Somogyi et al., 1981b). Similarly, although there is a clear topography of the caudal projections of the ventral pallidum (limbic) and the globus pallidus (motor and associative), there are regions of overlap in the substantia nigra, subthalamic nucleus, and entopeduncular nucleus where synaptic convergence of the two divisions of the pallidal complex occurs at the single cell level (Bevan et al., 1996, 1997).

The striatum is also a site of functional convergence. Although the corticostriatal projections are highly topographically organized, they partially overlap and interdigitate (Malach and Graybiel, 1986; Gerfen, 1989; Flaherty and Graybiel, 1991, 1993, 1995; Parthasarathy et al., 1992; Brown et al., 1998; Takada et al., 1998; Hoffer and Alloway, 2001). Anatomical data suggests that corticostriatal projections from reciprocally connected cortical regions are more likely to have overlapping arborizations within the striatum (Yeterian and Van Hoesen, 1978; Pearson et al., 1983; Flaherty and Graybiel, 1993). Furthermore, projections from functionally related, but distinct, cortical regions (primary motor and primary somatosensory cortices) have been shown to converge in the striatum (Flaherty and Graybiel, 1993; Hoffer and Alloway, 2001). Electrophysiological analyses have shown striatal neurons to respond to both somatosensory and auditory stimuli in rats (Chudler et al., 1995) and to tactile, auditory, and visual stimuli in cats (Wilson et al., 1983b; Schneider, 1991).

Received May 20, 2002; revised June 21, 2002; accepted June 25, 2002.

This work was supported by the Medical Research Council (UK) and the European Community (BIOMED 2 Project: BMH4-CT-97-2215). We thank Caroline Francis and Paul Jays for technical support. We also thank Justin Boyes, Peter Magill, and Ahmed Sadek for their comments on this manuscript.

Correspondence should be addressed to J. P. Bolam, Medical Research Council Anatomical Neuropharmacology Unit, Department of Pharmacology, Mansfield Road, Oxford, OX1 3TH, UK. E-mail: paul.bolam@pharm.ox.ac.uk.

S. Ramanathan's present address: Department of Preclinical Veterinary Sciences, Royal (Dick) School of Veterinary Sciences, University of Edinburgh, Edinburgh, EH9 1QH, UK.

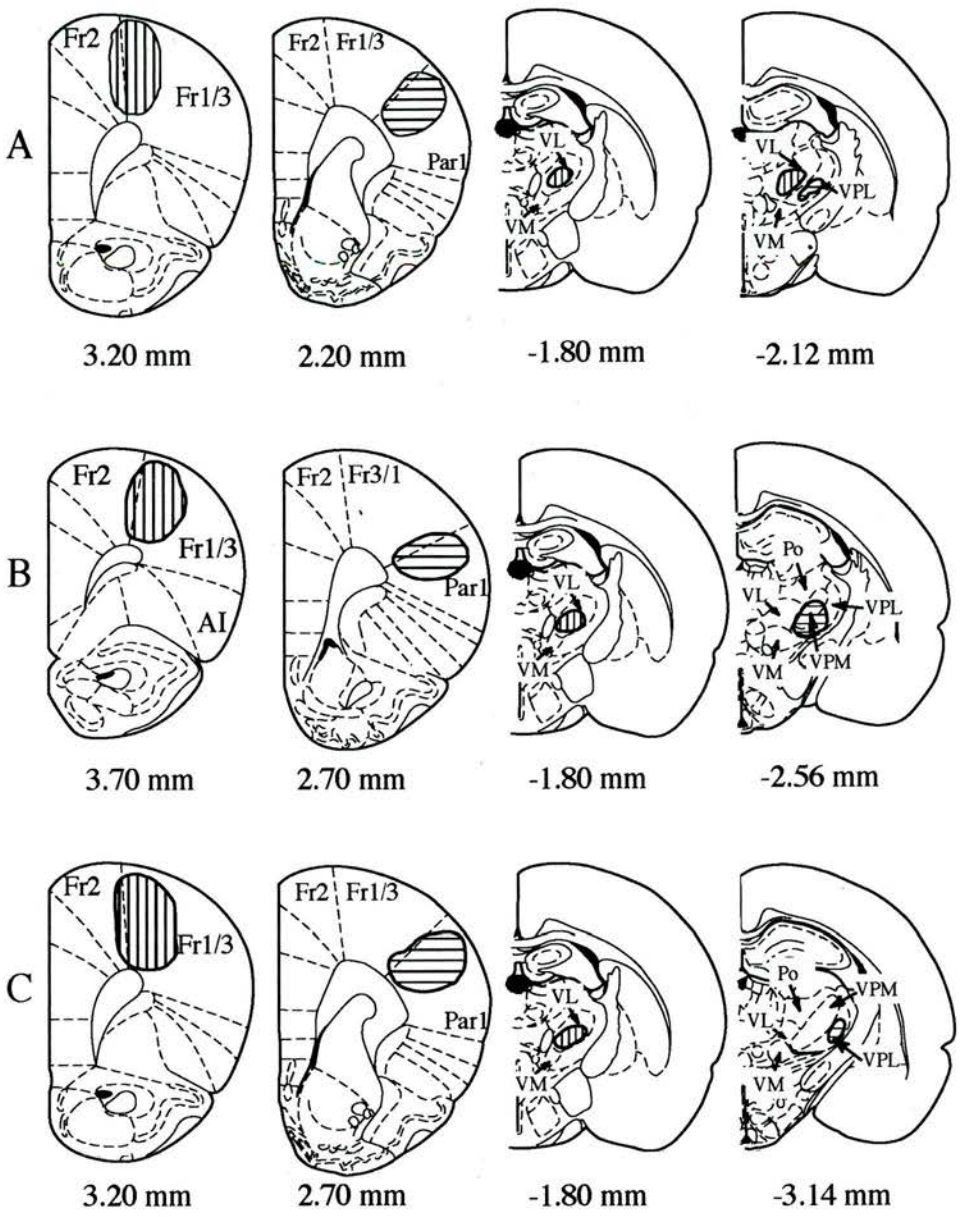

Figure 1. Schematic representations (modified from Paxinos and Watson, 1997) of the sites of injection of PHAL in M1 (*vertical hatching*) and BDA in S1 (*horizontal hatching*) and the corresponding labeling in the thalamus in the three animals used in the electron microscopic analysis. The deposits of PHAL were confined to frontal cortex areas 1 and 3 with a slight encroachment in area 2. In each animal the thalamic labeling was confined to the ventrolateral nucleus of the thalamus. The BDA deposits were confined to parietal cortex, area 1, and labeling in the thalamus was confined to the lateral and medial aspects of the posterior nucleus. The figures denote the position in millimeters with respect to bregma (Paxinos and Watson, 1997). *VL*, Ventrolateral nucleus of thalamus; *VM*, ventromedial nucleus of thalamus; *VPL*, lateral aspect of ventroposterior nucleus of thalamus; *VPM*, medial aspect of ventroposterior nucleus of thalamus.

The main target of corticostriatal terminals are the spines of the GABAergic medium spiny projection neurons (Kemp and Powell, 1971b; Frotscher et al., 1981; Somogyi et al., 1981a; Dubé et al., 1988; Smith et al., 1994) and the cortical input shapes the activity of these neurons (Wilson et al., 1983a; Wilson, 1995; Wilson and Kawaguchi, 1996; Mahon et al., 2001). The second major target of the cortical input to the striatum is the class of GABAergic interneuron (Lapper et al., 1992; Bennett and Bolam, 1994) that expresses the calcium-binding protein parvalbumin (PV) (Cowan et al., 1990; Kita et al., 1990). The major target of these interneurons are the proximal regions of spiny projection neurons, and an individual interneuron may contact many hundreds of spiny neurons (Cowan et al., 1990; Kita et al., 1990; Kita, 1993; Bennett and Bolam, 1994). It has been proposed that they provide a feedforward inhibitory control of spiny neurons (Pennartz and Kitai, 1991; Jaeger et al., 1994; Kita, 1996; Plenz and Kitai, 1998) and indeed, they generate inhibitory synaptic potentials that are able to delay, curb, or possibly synchronize, the generation of action potentials in spiny projection neurons (Koos and Tepper, 1999).

In view of the critical position of PV-positive, GABAergic interneurons in the circuitry of the striatum and the fact that they are activated more easily and over a larger volume of striatum after cortical stimulation than are spiny neurons (Parthasarathy and Graybiel, 1997), we chose to analyze the cortical input to these neurons. Thus, the aims were to determine whether cortical afferents from the primary motor cortex (M1) and primary somatosensory cortex (S1) converge on individual PV-positive interneurons and to provide insight into the pattern of innervation of these neurons by individual cortical axons.

MATERIALS AND METHODS

Surgery. The experiments were performed on adult female Wistar rats (200–350 gm; Charles River, Margate, Kent, UK). Environmental conditions for housing of the rats and all procedures that were performed on them were in accordance with the Animals (Scientific Procedures) Act of 1986 and the policy on the use of animals issued by the Society for

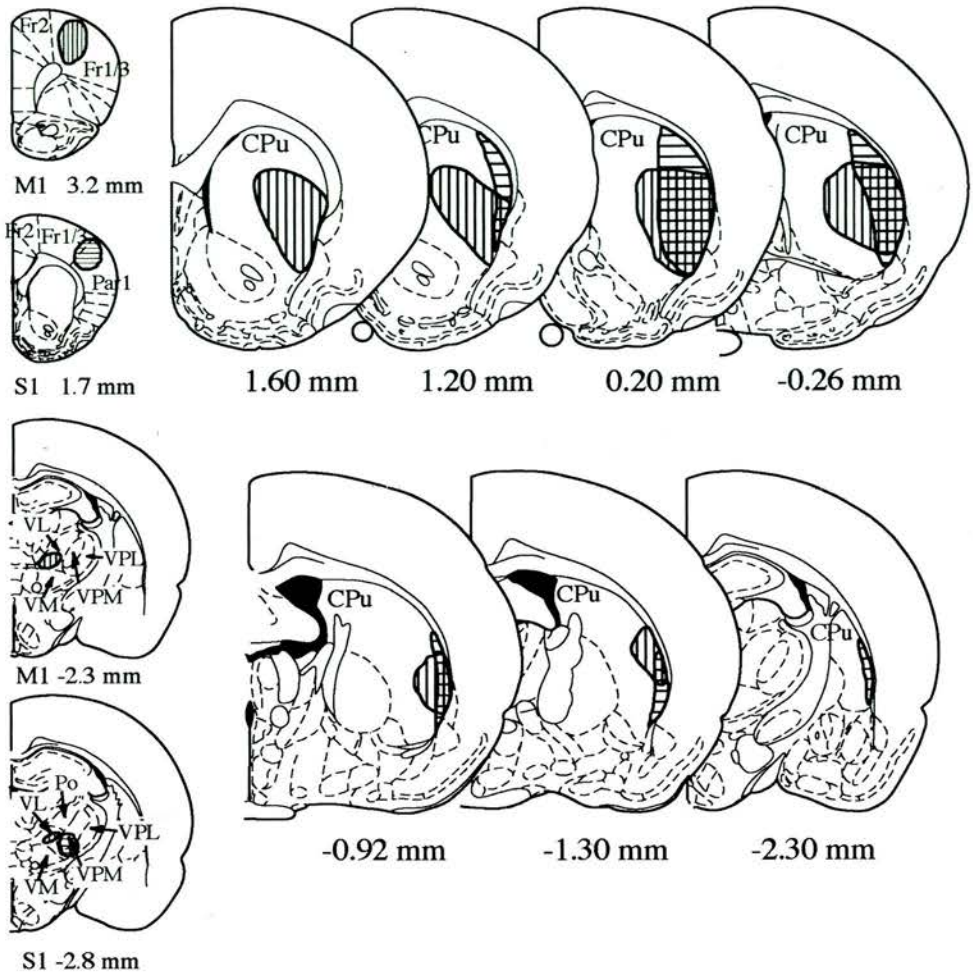

Figure 2. Schematic representations (modified from Paxinos and Watson, 1997) of the sites of injection of PHAL in primary motor cortex (*M1*) and BDA in the primary somatosensory cortex (*S1*), the corresponding labeling in the thalamus and the anterograde labeling in the striatum (caudate–putamen; *CPu*). In each diagram the PHAL injection and the corresponding transport sites are indicated by *vertical hatching*, and the BDA injection and transport sites are indicated by *horizontal hatching*. The figures denote the position in millimeters with respect to bregma (Paxinos and Watson, 1997).

Neuroscience. Twelve rats were anesthetized by intraperitoneal injections of a mixture of fentanyl and fluanisone (0.135 mg/ml and 10 mg/ml, respectively; Hypnorm; Janssen-Cilag Ltd., High Wycombe, UK) and midazolam (5 mg/ml; Hypnovel; Roche Products Ltd., Welwyn Garden City, UK) (1:1:2 with sterile water: 2.7 ml/kg) and the head secured in a stereotaxic frame. The animals received unilateral deposits of *Phaseolus vulgaris* leucoagglutinin [PHAL; 2.5% in 0.1 M phosphate buffer (PB), pH 8.0; Vector Laboratories, Peterborough, UK] in the primary motor cortex and biotinylated dextran amine (BDA; 10% in 0.9% NaCl; Molecular Probes, Eugene, OR) in the primary somatosensory cortex. The anterograde tracers were delivered by iontophoresis via glass micropipettes of 7–50 μm internal tip diameter using a pulsed (7 sec on/7 sec off) positive cathodal current (7–10 μA) over 10–15 min. Three deposits were made in each region. After a survival time of 5–8 d, the rats were deeply anesthetized with sodium pentobarbital (Sagatal, 200 mg/kg; Rhône Mérieux, Tallaght, Dublin) and perfused transcardially with 50–100 ml of PBS (0.01 M, pH 7.4) followed by 300 ml of 0.1–0.2% glutaraldehyde and 3% paraformaldehyde in 0.1 M PB. Some animals were post-perfused with ~100 ml of PBS.

Preparation of tissue for light microscopy. Coronal sections of the tracer injection sites, thalamus, and striatum were cut on a vibrating microtome at 70 μm. Sections were incubated for 30 min in 0.3% Triton X-100 in PBS (PBST), washed in PBS, and then treated with 1% bovine serum albumin and 1% normal goat serum in PBS (PBS–BSA) for 2 hr at room temperature. The injected and transported BDA was revealed using the avidin–biotin–peroxidase complex method (ABC; 1:100 in PBST–BSA; Vector Laboratories) with 3,3′-diaminobenzidine (DAB; 25 mg/100 ml Tris buffer; Sigma, Dorset, UK; 0.006% H_2O_2) as the chromogen for the peroxidase reaction. To reveal the injected and transported PHAL, sections were incubated overnight in rabbit anti-PHAL (1:1000 in PBST–BSA; Vector Laboratories), treated with goat anti-rabbit IgG (1:200 in PBST–BSA; Dako, High Wycombe, UK) for 2 hr, followed by a 1 hr incubation in rabbit peroxidase–antiperoxidase (PAP) (1:100 in PBST–BSA; Dako), all at room temperature. The bound peroxidase was then revealed with DAB in the presence of nickel ions (nDAB). In some animals the BDA was revealed with nDAB and the PHAL with DAB. Parvalbumin-immunoreactive structures were revealed by incubation in mouse anti-PV (1:1000 in PBST-BSA; Swant, Bellinzona, Switzerland) for 24–36 hr at 4°C followed by goat anti-mouse IgG (1:200 in PBST–BSA; Jackson ImmunoResearch, West Grove, PA) for 2 hr at room temperature and mouse PAP (1:100; Dako) with Vector SG as chromogen for the peroxidase reaction.

Preparation of tissue for electron microscopy. The striata of six animals were processed for electron microscopy. To increase the penetration of reagents, the sections were freeze-thawed in isopentane (BDH Chemicals, Poole, UK) cooled in liquid nitrogen up to three times. The sections were washed several times in PBS before the tracers and parvalbumin-immunoreactive structures were revealed. The method was as described

→

Figure 3. Light microscopy of convergence of motor and somatosensory afferents in the striatum: parvalbumin-immunostained perikarya (*PV*) and axons anterogradely labeled with PHAL from M1 and axons anterogradely labeled with BDA from S1. In these cases the PHAL-containing motor cortical fibers were revealed using DAB as the chromogen for the peroxidase reaction giving a brown reaction product. The BDA-containing axons were labeled with nickel DAB as the chromogen giving the blue reaction product. These digital images and those in Figures 5, *A* and *D*, and 6, *A* and *D*, were prepared from scanned images of color photomicrographs and have been color balanced in Adobe Photoshop 6.0. They are derived from sections that were prepared for light microscopic analysis only. *A*, This parvalbumin-immunolabeled neuron (*PV*)is in a region containing (*Figure legend continues.*)

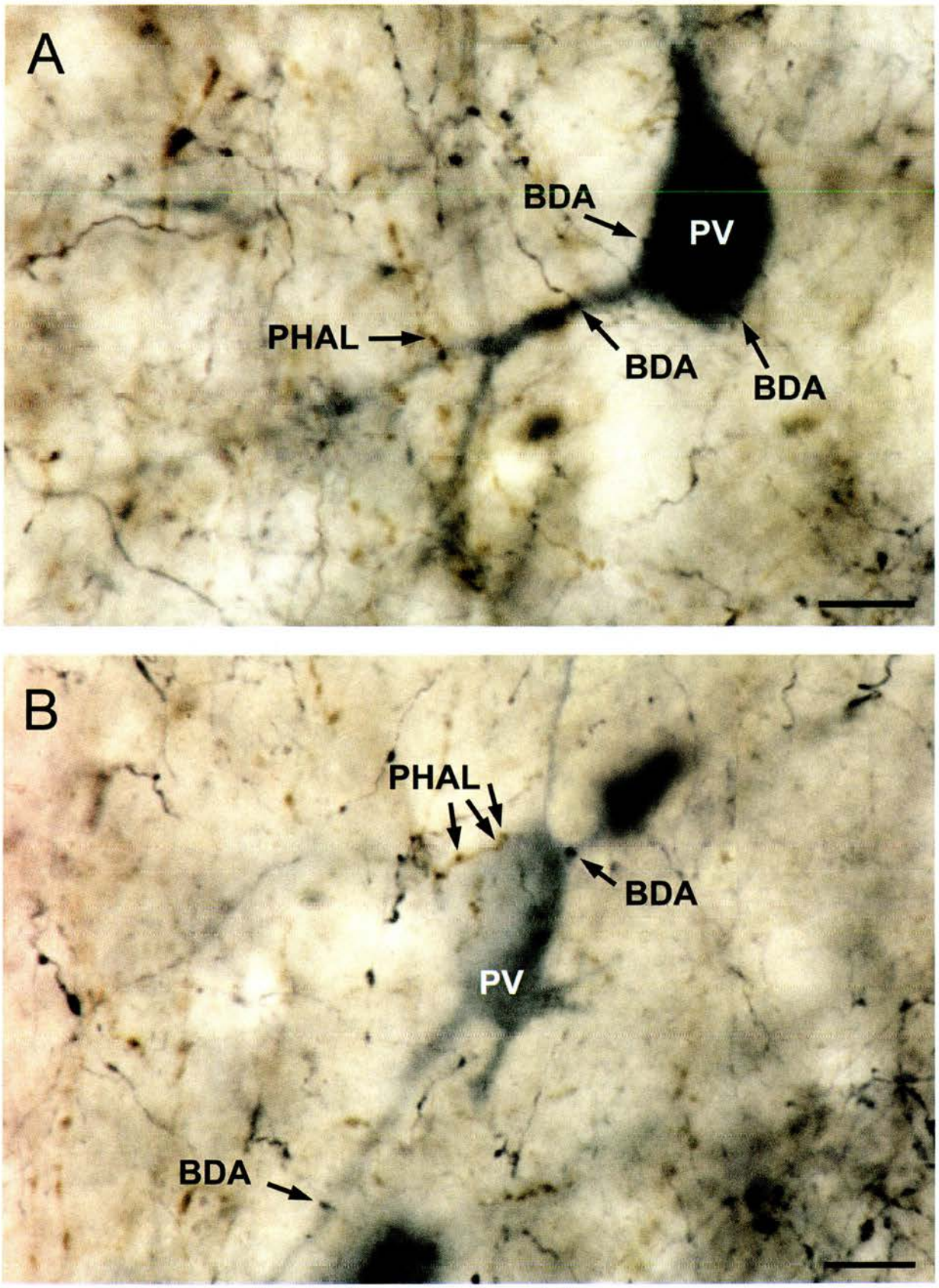

(*Figure legend continued.*) many PHAL- and BDA-labeled axons, many of which are closely apposed to the labeled neuron. At this focal depth there are several BDA-labeled boutons apposed to the perikaryon and proximal dendrite, and a PHAL-labeled bouton also closely apposes the dendrite. *B*, Montage of a second parvalbumin-immunolabeled neuron (*PV*) that is apposed by boutons derived from the motor cortex (*PHAL*) and somatosensory cortex (*BDA*). Note that the PHAL-labeled axon gives rise to several boutons that are apposed to the PV-positive perikaryon. Scale bars, 10 μm.

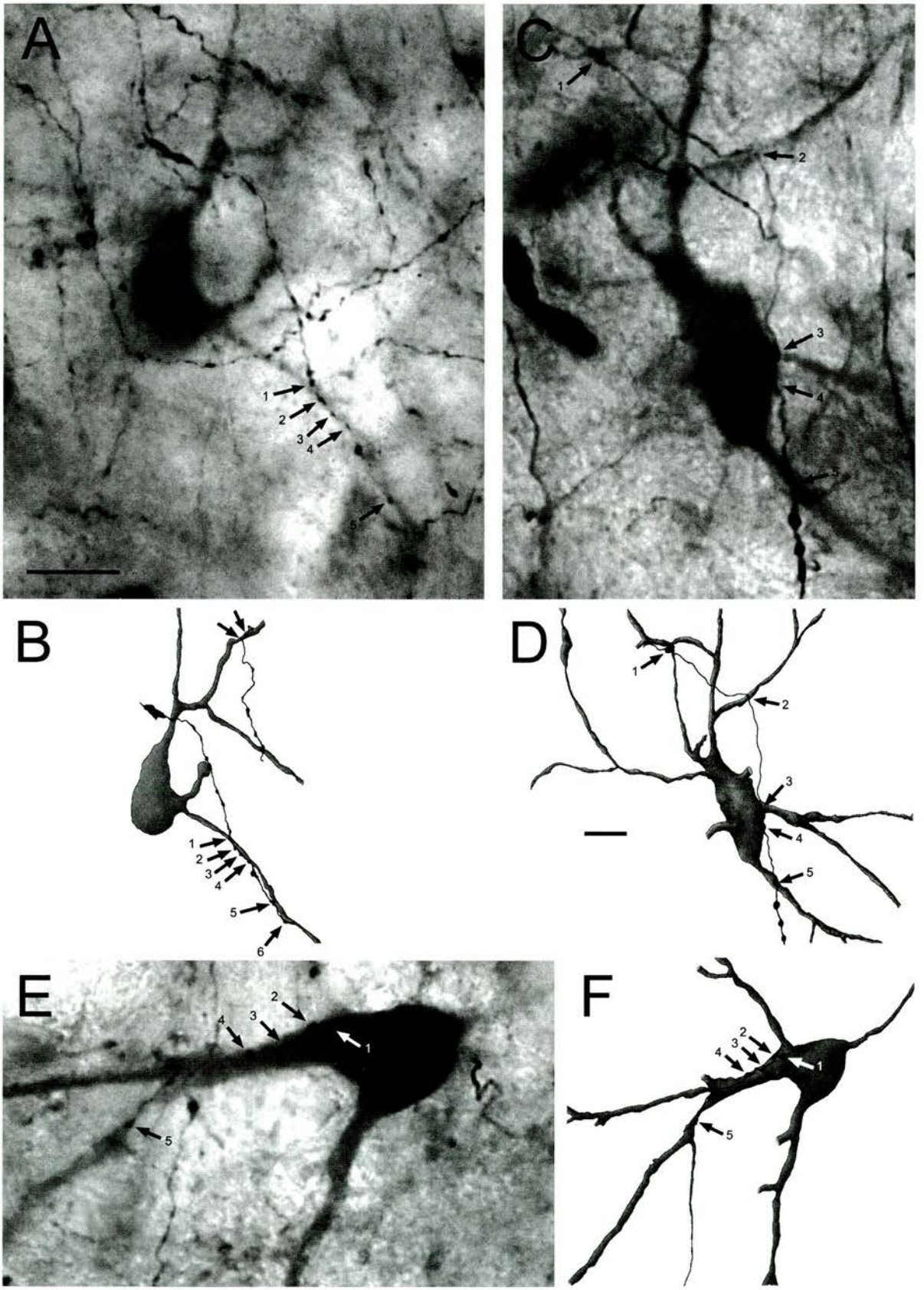

Figure 4. Light microscopic digital images and corresponding camera lucida drawings of striatal parvalbumin-positive neurons and individual cortical axons forming multiple appositions. *A*, *B*, Digital montage (*A*) and drawing (*B*) of a parvalbumin-positive interneuron and anterogradely labeled cortical fibers in the striatum. The PV-positive neuron gave rise to several immunolabeled dendrites, one of which was closely apposed by an axon anterogradely labeled with BDA from the somatosensory cortex. The axon gave rise to six varicosities that closely apposed the dendrite (*Figure legend continues.*)

above with the omission of Triton X-100 from all solutions. The labeled sections of the striatum were postfixed in 1% osmium tetroxide (Oxkem), 5% β-D-glucose (BDH Chemicals) in 0.1 M PB at pH 7.4 for 60–70 min. (Acsady et al., 1996). The sections were dehydrated through a graded series of dilutions of acetone (with 1% uranyl acetate in the 70% solution) and infiltrated with resin overnight (Durcupan; Fluka Chemicals). They were then mounted in resin on glass microscope slides and polymerized at 60°C for 48 hr.

Analysis of material. All sections containing the sites of injection of the tracers were examined to ensure that they were correctly placed. The locations of the injection sites were also confirmed by analysis of sections of the thalamus for anterogradely and retrogradely labeled structures. Sections of the striatum from those animals in which the injections were correctly located were examined in the light microscope for the anterograde tracers and PV immunoreactivity. In some animals the anterograde labeling was plotted and recorded schematically. Particular attention was paid to regions of overlap of the two tracers. In these areas, PV-immunoreactive neuronal perikarya and emerging dendrites were examined at high magnification, and the positions of anterogradely labeled terminals closely apposed to them was noted. In some cases PV-positive neurons and individual cortical axons were drawn with the aid of a drawing tube and photographed digitally.

In a semiquantitative analysis, a single section of the striatum from three rats that were prepared for light microscopy (i.e., Triton X-100 included in the incubations) were analyzed at high magnification. The selected sections were those in which the region of overlap of the anterograde labeling from the two regions of the cortex was the most extensive. The location of each PV-positive perikaryon and emerging dendrites was noted. The proportion apposed by anterogradely labeled terminals derived from either region of the cortex was noted.

From the tissue that was processed for electron microscopy, eight PV-immunoreactive neurons (from four animals) whose cell bodies and/or dendrites were identified as being apposed by anterogradely labeled terminals from both regions of the cortex in the light microscope, were selected for further study. The cells were drawn and photographed at high magnification and examined by correlated light and electron microscopy. The coverslip overlying the tissue was removed using a razor blade. The area of interest was cut from the microscope slide and glued to the top of a blank cylinder of resin using cyanoacrylate glue. Serial ultrathin sections of 40–60 nm thickness were cut on a Reichert-Jung Ultracut E ultramicrotome (Leica, Nussloch, Germany) and collected on Pioloform-coated single slot copper grids. The ultrathin sections were then contrasted with lead citrate for 2–3 min and examined in a Philips CM 10 electron microscope.

RESULTS

Light microscopic observations

Appearance of the reaction products

The anterogradely labeled and immunolabeled structures were visualized with different chromogens for the peroxidase reactions that were distinguishable at the light microscopic level. Structures visualized with DAB as the chromogen for the peroxidase reaction were characterized by the presence of the typical reddish brown amorphous reaction product (see Fig. 3), and those visualized with nDAB contained the typical blue–black reaction product (see Fig. 3). Parvalbumin-immunoreactive structures were visualized using Vector SG as the chromogen and were characterized by the presence of a grayish blue reaction product that was less homogeneous that the DAB reaction products (see Fig. 3). The use of osmium tetroxide solution supplemented with glucose maintained color separation, at the light microscopic level, between different reaction products in the sections that were prepared for examination by both light and electron microscopy (Acsady et al., 1996) (see Figs. 5*D*, 6*A,D*).

Injection sites

The location of the injection sites of the two anterograde tracers (PHAL and BDA) was confirmed by visualization of the tracers in the M1 and S1 cortices (Figs. 1, 2). In the majority of cases the deposits of the two tracers were clearly separated. They spanned most of the cortical laminas without inclusion of the underlying corpus callosum. In some cases there were retrogradely labeled neurons of S1 close to the M1 injection site. However, these retrogradely labeled neurons were clearly separate from the filled neurons at the injection site; they constituted only very few neurons and were thus unlikely to influence the findings.

The location of the injections was confirmed by the analysis of the coincidental anterograde and retrograde labeling of thalamic nuclei. The motor cortex is innervated by thalamocortical projections mainly from the ventromedial and ventrolateral thalamic nuclei and in turn sends projections back to these motor nuclei (Cicirata et al., 1986, 1990). The somatosensory cortex is reciprocally connected to the ventrobasal nuclei, the intralaminal nucleus centralis lateralis, and the medial portion of the posterior thalamic group (Price and Webster, 1972; Nothias et al., 1988; Bourassa and Deschenes, 1995). In four of the six animals prepared for electron microscopy the labeling of thalamic nuclei was distinct for both the injection sites, and cells from these animals were studied at the ultrastructural level. In the remaining two animals there was clearly an overlap of the two injection sites in the different cortical territories as indicated by the thalamic labeling, these animals, and those prepared for light microscopy in which overlap of injections occurred, were excluded from the analysis.

Distribution of anterograde labeling

The deposits of PHAL and BDA in the M1 and S1 cortices, respectively, led to intense labeling of corticostriatal projections that were topographically organized and largely consistent with previous observations. The corticostriatal axons were collected in the fascicles of axon bundles traversing the striatum, and axonal arbors were primarily located around the fiber fascicles. The typical pattern of innervation of the striatum from M1 is illustrated in Figure 2. Anterogradely labeled fibers occurred in a band of striatum extending from ~1.6 mm rostral of bregma to ~1.3 mm caudal of it. Anterograde labeling from S1 occurred in a band in the lateral aspects of the striatum extending from ~1.2 mm rostral of bregma to ~2.3 mm caudal. The band extended over a large part of the striatum in the dorsoventral plane and, at its maximum extent, occupied approximately one-third of the striatum in the mediolateral plane (Fig. 2).

A large part of the more lateral and caudal aspects of the projection from M1 overlapped with the projection from S1. In these regions the two sets of anterogradely labeled terminals were intermixed to such an extent that axonal varicosities derived from

←

(*Figure legend continued.*) (*small arrows, 1–6*), five of which are visible in the light micrograph (*1–5*). The neuron was also apposed by two varicosities of an axon anterogradely labeled from the motor cortex that is not visible at the focal depth of the micrograph but is shown in the drawing (*two arrows, top right*). *C, D,* A parvalbumin-positive neuron apposed by an axon anterogradely labeled with PHAL from the motor cortex. The axon give rise to five boutons that closely appose the dendrites and perikaryon of the labeled neuron. *E, F,* A parvalbumin-positive neuron apposed by an axon anterogradely labeled with BDA from the somatosensory cortex. The axon gave rise to five boutons that closely apposed the perikaryon and dendrites of the labeled neuron. Scale bars: *A, C, E,* 10 μm; *B, D, F,* 10 μm.

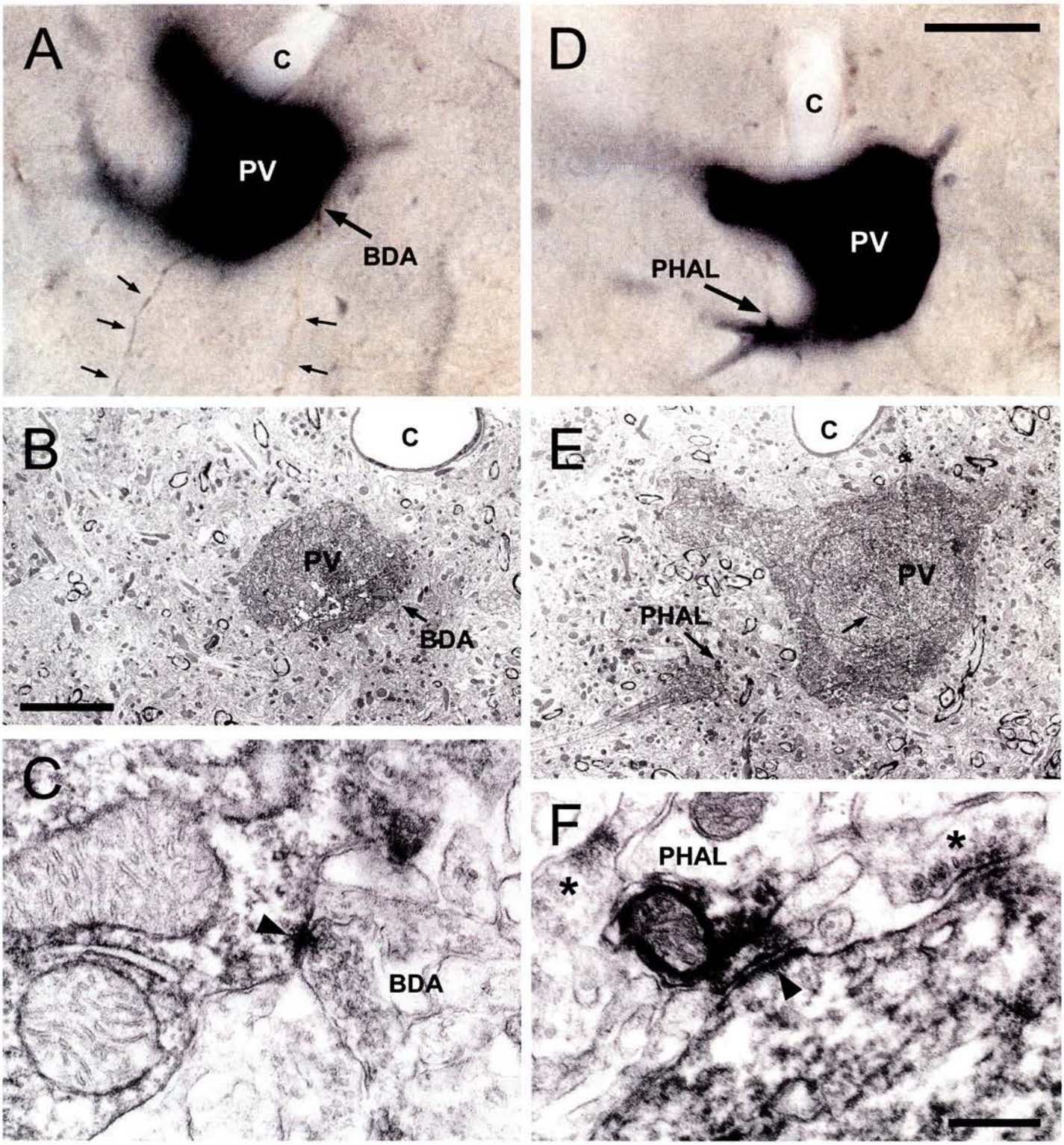

Figure 5. Synaptic convergence of motor and somatosensory cortical afferents onto a parvalbumin-positive, GABAergic interneuron in the striatum: correlated light and electron microscopy. *A*, Light micrograph of a parvalbumin-immunostained neuron (*PV*) labeled using Vector SG as the substrate for the peroxidase reaction. The neuron was located in a region containing fibers anterogradely labeled with PHAL from the motor cortex (PHAL, nDAB as chromogen; *blue fiber* indicated by *small arrows* on the *left*) and with BDA from the somatosensory cortex (BDA, DAB as chromogen; *brown fiber* indicated by *small arrows* on the *right*). The axon from the somatosensory cortex gives rise to several varicosities, one of which closely apposes the perikaryon (*BDA, large arrow*). The capillary (*c*) is labeled as a landmark between the light and electron microscopic levels. *B*, Low-power electron micrograph of part of the same perikaryon and the BDA-labeled, somatosensory cortical bouton closely apposed to it (*BDA, arrow*). *C*, High-power electron micrograph of the BDA-labeled bouton from the somatosensory cortex. The labeled terminal forms an asymmetrical synaptic contact (*arrowhead*) with the parvalbumin-immunolabeled neuron. *D*, Digital light micrograph of the same parvalbumin-immunolabeled neuron (*PV*) at a deeper focal depth. At this level the neuron is apposed by a PHAL-positive bouton (*PHAL, arrow*) derived from the motor cortex. *E*, Low-power electron micrograph at about the same level as in *D*. The perikaryon, part of a dendrite, and the PHAL-labeled bouton (*Figure legend continues.*)

the different cortical territories were often observed in close proximity (Figs. 3, 4*B*, 5*A,D,* 6*A,D*).

Parvalbumin-positive GABAergic interneurons

Parvalbumin-positive interneurons were identified by the gray reaction product formed by the Vector SG. Perikarya and proximal dendrites, as well as isolated dendrites, were labeled. Their morphology and distribution were consistent with previous studies (Cowan et al., 1990; Kita et al., 1990; Bennett and Bolam, 1994). The labeled neurons had medium-sized cell bodies, which were oval, or fusiform in shape. In some cases, indentations of the nuclear membrane were visible. Labeled primary dendrites branched close to the cell body and the secondary dendrites were generally smooth but sometimes gave rise to varicosities (Figs. 3, 4). Higher order dendrites were usually not labeled. The heaviest labeling of PV-positive structures was in the dorsolateral aspect of the striatum. Although the striatum is known to possess a dense network of PV-positive local axons and axonal boutons, PV-positive axonal fields were usually not labeled in the present study. This may reflect the sensitivity of the chromogen used and the fact that the immunostaining for PV was performed last.

Light microscopic analysis of convergence of cortical terminals on PV-positive neurons

Parvalbumin-positive neuronal perikarya and dendrites were intermingled among axons and axonal boutons anterogradely labeled from both M1 and S1 cortices (Fig. 3). The PV-positive structures were often closely apposed by the anterogradely labeled boutons, consistent with previous observations of cortical input to this class of neuron (Lapper et al., 1992; Bennett and Bolam, 1994). In many cases, an individual PV-positive neuronal perikaryon or isolated dendrite was closely apposed by terminals anterogradely labeled from M1 and terminals anterogradely labeled from S1 (Fig. 3). Examination of all PV-positive perikarya and emerging dendrites (but not isolated dendrites) in single sections at the level of the greatest extent of overlap of the two projections, revealed that up to 51% (range, 35.4–50.9) of PV-positive neurons were apposed by terminals derived from the cortex. Up to 46% (range, 24.7–46.2) of those that were apposed by cortical terminals were apposed by terminals derived from both cortical regions, which represents up to 23% (range, 8.8–23.5) of all PV-positive neurons in the single sections. In addition, single axons anterogradely labeled from either M1 or S1 were frequently found to form multiple appositions with individual PV-positive interneurons within a few microns (Fig. 4). They commonly gave rise to two or three boutons apposed to an individual PV-positive neuron, although as many as six were observed (Fig. 4).

Electron microscopic observations

To confirm that the appositions observed in the light microscopic analysis were indeed synapses, PV-positive neurons were examined by electron microscopy. Correlated light and electron microscopy was performed because the extent and quality of immunohistochemical and histochemical staining is reduced in material prepared for electron microscopy. A total of eight PV-positive neurons (two from each of the four rats) that were apposed by terminals from both M1 and S1 were selected at the light microscopic level for study in the electron microscope.

In the electron microscope the cell bodies and dendrites of the labeled PV-positive structures contained an amorphous, electron-dense reaction product similar to that previously reported for Vector SG (Hussain et al., 1996; Hanley and Bolam, 1997). Ultrastructural features of the PV-immunoreactive structures were consistent with previous descriptions (Kita et al., 1990; Lapper et al., 1992; Bennett and Bolam, 1994). They possessed a relatively large volume of cytoplasm that was rich in organelles such as mitochondria, ribosomes, and Golgi apparatus (Figs. 5*B,C,E,F,* 6*B,C,E,F*). The nuclear membrane possessed indentations (Figs. 5*E,* 6*E*), and intranuclear inclusions were often observed (Fig. 5*E*). Anterogradely labeled axon terminals were identified by the presence of reaction product as well as by their position in relation to landmarks such as blood vessels, unstained neurons, and glial cells (Figs. 5*B,C,E,F,* 6*B,C,E,F*). Axons and terminals that were visualized using nDAB were more intensely stained than DAB-labeled structures (compare Figs. 5*C,F,* 6*C,F*). Consistent with previous studies (Kemp and Powell, 1971a; Somogyi et al., 1981a; Dubé et al., 1988; Smith et al., 1994; Hersch et al., 1995) the anterogradely labeled corticostriatal boutons were packed with round vesicles and usually contained one or more mitochondria (Figs. 5*C,F,* 6*C,F*). They formed asymmetric synapses with dendritic spines and with dendritic shafts. The terminals were variable in size, and some of the larger boutons were similar in morphology to the boutons of the "discrete" corticostriatal projection from the barrel cortex (Wright et al., 1999). The correlated light and electron microscopy revealed that they also formed asymmetric synapses on the cell body and proximal dendrites of PV-positive interneurons (Figs. 5, 6). Of the eight cells studied, five of them (from three rats) were found to receive convergent synaptic input from both the M1 and S1 cortices (Figs. 5, 6). In one of the neurons that received the convergent input, three synapses from the motor cortex arose from a single axon.

Of the three neurons that were examined by correlated light and electron microscopy and failed to reveal convergent input from the cortex, two were abandoned because of poor ultrastructural preservation. In only one case was a labeled bouton identified at the light microscopic level found not to make contact with the PV-positive neuron; the bouton, anterogradely labeled from S1, made synaptic contact with an adjacent, unstained dendritic spine (data not shown).

In addition to the labeled boutons identified at both the light and electron microscopic levels, additional labeled boutons were observed in contact with the PV-positive neurons. These boutons ($n = 6$) had the morphology of corticostriatal boutons and formed asymmetric synapses, and they were usually found below the PV-labeled cell bodies. In addition to these, many unlabelled boutons formed asymmetric synaptic contacts with PV-immunolabeled cell bodies and dendrites.

←

(*Figure legend continued.*) derived from the motor cortex are present. Note the position of the capillary (*c*) for correlation between light and electron microscopic levels. The immunostained neuron possesses an intranuclear inclusion (*small arrow*), a feature typical of GABAergic interneurons in the striatum. *F*, High-power electron micrograph of the PHAL-positive bouton forming an asymmetrical synaptic contact (*arrowhead*) with the parvalbumin-positive dendritic shaft. Note that the reaction product formed by the nDAB is more intense than that formed by the DAB as seen in *C*. Two unlabelled axonal boutons are indicated by *asterisks*. Scale bars: *A, D,* 12.5 μm; *B, E,* 5 μm; *C, F,* 0.25 μm.

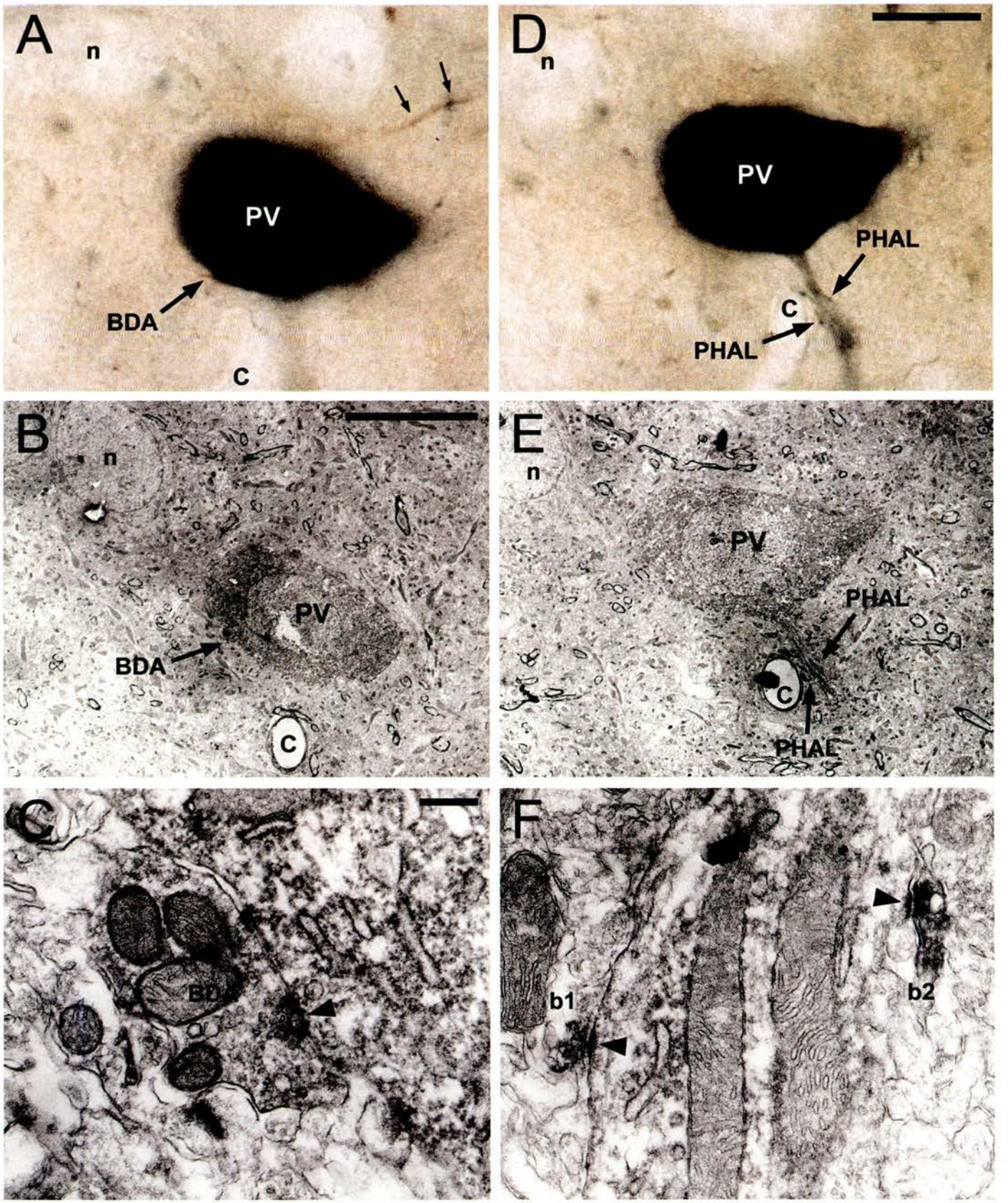

Figure 6. Synaptic convergence of motor and somatosensory cortical afferents onto a parvalbumin-immunolabeled, GABAergic interneuron in the striatum: correlated light and electron microscopy. *A*, Light micrograph of a parvalbumin-positive neuron (*PV*; Vector SG as chromogen for the peroxidase reaction) that is closely apposed by a BDA-positive bouton (*BDA, arrow*) that was anterogradely labeled from the somatosensory cortex (DAB as chromogen for the peroxidase reaction, brown reaction product). Note the additional axon anterogradely labeled from the somatosensory cortex in the *top right* of the micrograph (*small arrows*). An unstained neuron (*n*) and a capillary (*c*) are labeled for correlation (*Figure legend continues.*)

DISCUSSION

Synaptic convergence in the striatum

The primary objective of the present study was to determine whether synaptic convergence of somatosensory and motor corticostriatal projections occurs at the level of single interneurons in the areas of overlap of these projections. The main finding is that somatosensory and motor corticostriatal afferents do indeed form convergent synapses with individual PV-positive striatal interneurons, indicating that one aspect of sensory-motor integration performed by the basal ganglia occurs at the level of single cells in the striatum.

The major targets of corticostriatal axons are the dendritic spines of spiny projection neurons and the dendritic shafts of PV-positive, GABAergic interneurons (Kemp and Powell, 1971a; Somogyi et al., 1981a; Lapper et al., 1992; Bennett and Bolam, 1994). Our analysis was confined to the latter class of neuron and light microscopy revealed that the dendrites and perikarya of PV-positive, GABAergic interneurons were apposed by terminals derived from both the primary motor and somatosensory cortices. The analysis of sections at the level of the densest overlap of the two projections revealed that this was a common phenomenon, because up to a half of PV-positive neurons that were apposed by terminals derived from the cortex had convergent appositions from both regions of the cortex. This value is likely to be an underestimate of the true incidence of convergence as numerous isolated PV-positive dendrites were apposed by both sets of terminals and at least some of these may have arisen from the PV-positive perikarya and proximal dendrites that were not found to be apposed by both sets of cortical terminals. Furthermore, the entire projection from the areas of cortex that received the deposits of the tracers is unlikely to have been labeled, nor is the entire dendritic arbor of a PV-positive neuron likely to be immunolabeled.

To confirm that the convergent appositions that we observed at the light microscopic level were indeed synaptic connections, analysis was performed at the electron microscopic level. Because of the lower frequency of convergent appositions observed at the light microscopic level in material prepared for electron microscopy and because of the difficulty in distinguishing DAB and nickel DAB reaction products at the electron microscopic level, we performed the analysis by correlated light and electron microscopy. This analysis revealed that indeed, the PV-positive interneurons receive convergent synaptic input from both the primary motor and sensory cortices. The cortical terminals formed asymmetric synapses with the dendritic shafts and perikarya of the PV-positive neurons. Of the six neurons analyzed in detail at the electron microscopic level, in only one case did the apposing bouton identified at the light microscopic level not form synaptic contact with the PV-positive neuron. The identification of synaptic convergence in five of the six cases implies that the light microscopic analysis closely reflects the incidence of synaptic connections and that the phenomenon of convergence of motor and somatosensory inputs to PV-positive, GABAergic interneurons is a common event.

These findings imply that PV-positive, GABAergic interneurons play a role in sensorimotor integration in the striatum. Although their precise role remains undetermined, it is likely that the sensory and motor information integrated by PV-positive, GABAergic interneurons is transmitted to spiny projection neurons in such a form as to control the output of a selected group of spiny neurons by shunting cortical excitation and/or by synchronization of their activity (Plenz and Kitai, 1998; Koos and Tepper, 1999).

Because spiny projection neurons are the major target of the corticostriatal projection, there are additional possibilities for the synaptic convergence of corticostriatal afferents. It remains to be established whether the input from the two regions of the cortex is targeted at distinct populations of spiny neurons projecting to the same or different regions or whether they converge on the same spiny projection neurons. Similarly, synaptic convergence may occur on other classes of interneurons.

Pattern of cortical innervation of PV-positive interneurons

An additional observation that was made in the present study has a bearing on the principles of organization of the corticostriatal projections. At the light microscopic level, single axons from M1 or S1 were often seen to form multiple appositions (up to six were observed) within a small distance on a single PV-positive interneuron. In one case it was confirmed by electron microscopy that the closely spaced multiple appositions do form synaptic contacts. It has been calculated that a single cortical axon will form ~40 synapses within the volume of striatum occupied by a single spiny neuron. Because that same volume of striatum will contain 2845 spiny neurons (each of which receive ~5000 cortical synapses), the probability of an individual cortical axon contacting a spiny neuron is low (Kincaid et al., 1998). The same volume of striatum will contain ~18 PV-positive neurons, based on the estimate of 16,875 PV-positive neurons (Luk and Sadikot, 2001) and 2.72 million spiny neurons (Oorschot, 1996) in the striatum and assuming an even distribution (which may in fact not be the case: see Cowan et al., 1990; Kita et al., 1990). If cortical axons innervate striatal neurons in a nonselective way, then the probability of a cortical axon contacting a PV-positive neuron is very low, and the probability of it forming more than one contact is even lower (Kincaid et al., 1998; Zheng and Wilson, 2002). However, we commonly observed multiple appositions in contact with an individual PV-positive neuron and thus, cortical axons must, in some way, show selectivity for the PV-positive neurons. Given that the same volume of striatum contains 381,180 cortical axons (Kincaid et al., 1998; Zheng and Wilson, 2002), those axons that form multiple contacts with the 18 PV-positive neurons must, therefore, be a subpopulation. It remains to be established which of the several classes of cortical neurons that innervate the stria-

←

(*Figure legend continued.*) between the light and electron microscopic levels. *B*, Low-power electron micrograph of the same neuron and the bouton anterogradely labeled with BDA from the somatosensory cortex. *C*, High-power electron micrograph of the PHAL-labeled bouton forming an asymmetric synapse (*arrowhead*) with the parvalbumin-positive neuron. *D*, The same neuron at a deeper focal depth. The proximal dendrite of the neuron is apposed by two boutons (*b1* and *b2*), derived from two axons that were anterogradely labeled with PHAL from the motor cortex. *E*, Low-power electron micrograph at about the same level, of the perikaryon and dendrite and the two PHAL-labeled boutons from the motor cortex. The unstained neuron (*n*) and capillary (*c*) are labeled for correlation between the light and electron microscopic levels. *F*, High-power electron micrograph of the two PHAL-positive boutons derived from the motor cortex, forming asymmetric synapses (*arrowheads*) with the proximal dendrite of the parvalbumin-positive, GABAergic interneuron. Scale bars: *A, D,* 12.5 μm; *B, E,* 5 μm; *E, F,* 0.5 μm.

tum provides this selective innervation (Gerfen and Wilson, 1996; Kincaid and Wilson, 1996).

From the light microscopic analysis it was apparent that an individual cortical axon that was apposed to a PV-positive structure also gave rise to boutons not apposed to PV-positive structures. This implies that individual cortical axons contact both PV-positive interneurons and spiny neurons and/or other classes of interneurons. An intriguing possibility is that the PV-positive, GABAergic interneurons and the population of spiny neurons contacted by the same cortical axons are bound together by the axon collaterals of the interneuron, thereby forming some type of modular arrangement. It should be noted, however, that the influence of GABAergic interneurons is likely to extend beyond their axonal field because they are interconnected by dendritic gap junctions (Kita et al., 1990; Kita, 1993; Koos and Tepper, 1999).

Together with differences in intrinsic membrane properties (Kawaguchi, 1993; Plenz and Kitai, 1998; Koos and Tepper, 1999), the finding that PV-positive interneurons receive multiple contacts from a single axon also suggests that they may be activated by a weaker and/or less synchronized cortical input than is required to activate a striatal projection neuron (Wilson, 1995; Stern et al., 1997; Charpier et al., 1999). Thus, GABAergic interneurons are likely to be more responsive to cortical inputs than spiny neurons. This suggestion is consistent with the studies of Parthasarathy and Graybiel (1997), who showed that weak cortical stimulation was unable to activate a large number of projection neurons but was able to induce immediate early gene expression in PV-positive interneurons. It may be that although many corticostriatal neurons need to fire synchronously to evoke activity in spiny projection neurons (Wilson, 1995; Stern et al., 1997; Charpier et al., 1999), input from fewer corticostriatal neurons, albeit from different cortical regions, is needed to activate PV-positive interneurons. Thus, PV interneurons may shunt coincident cortical activity in suboptimally excited striatal spiny cells (Parthasarathy and Graybiel, 1997; Plenz and Kitai, 1998; Koos and Tepper, 1999). Only when cortical input to the spiny neurons is sufficiently large will the shunting be overcome and the selected population of spiny neurons be allowed to reach firing threshold.

The overlapping corticostriatal projections from primary motor and somatosensory cortices do not remain segregated at the single cell level of the striatum, but rather, give rise to convergent synapses on individual PV-positive GABAergic interneurons. Thus, one mechanism by which the basal ganglia integrates sensory and motor information is through convergent cortical inputs to GABAergic interneurons which, in turn, transmit this integrated information to spiny projection neurons to shunt excitatory inputs to these cells or synchronizes their activity.

REFERENCES

Acsady L, Gorcs TJ, Freund TF (1996) Different populations of vasoactive intestinal polypeptide-immunoreactive interneurons are specialized to control pyramidal cells or interneurons in the hippocampus. Neuroscience 73:317–334.

Alexander GE, Crutcher ME (1990) Functional architecture of basal ganglia circuits: neural substrates of parallel processing. Trends Neurosci 13:266–271.

Alexander GE, DeLong MR, Strick PL (1986) Parallel organization of functionally segregated circuits linking basal ganglia and cortex. Annu Rev Neurosci 9:357–381.

Alexander GE, Crutcher MD, DeLong MR (1990) Basal ganglia-thalamocortical circuits: parallel substrates for motor, oculomotor, "prefrontal" and "limbic" functions. In: Prefrontal cortex: its structure, function and pathology (Uylings HBM, Vaneden CG, Debruin JPC, Corner MA, Feenstra MGP, eds), pp 119–146. Amsterdam: Elsevier.

Beiser DG, Hua SE, Houk JC (1997) Network models of the basal ganglia. Curr Opin Neurobiol 7:185–190.

Bennett BD, Bolam JP (1994) Synaptic input and output of parvalbumin-immunoreactive neurones in the neostriatum of the rat. Neuroscience 62:707–719.

Bevan MD, Smith AD, Bolam JP (1996) The substantia nigra as a site of synaptic integration of functionally diverse information arising from the ventral pallidum and the globus pallidus in the rat. Neuroscience 75:5–12.

Bevan MD, Clarke NP, Bolam JP (1997) Synaptic integration of functionally diverse pallidal information in the entopeduncular nucleus and subthalamic nucleus in the rat. J Neurosci 17:308–324.

Bourassa J, Deschenes M (1995) Corticothalamic projections from the primary visual cortex in rats: a single fiber study using biocytin as an anterograde tracer. Neuroscience 66:253–263.

Brown LL, Smith DM, Goldbloom LM (1998) Organizing principles of cortical integration in the rat neostriatum: corticostriate map of the body surface is an ordered lattice of curved laminae and radial points. J Comp Neurol 392:468–488.

Charpier S, Mahon S, Deniau JM (1999) In vivo induction of striatal long-term potentiation by low-frequency stimulation of the cerebral cortex. Neuroscience 91:1209–1222.

Chudler EH, Sugiyama K, Dong WK (1995) Multisensory convergence and integration in the neostriatum and globus pallidus of the rat. Brain Res 674:33–45.

Cicirata F, Angaut P, Cioni M, Serapide MF, Papale A (1986) Functional organization of thalamic projections to the motor cortex. An anatomical and electrophysiological study in the rat. Neuroscience 19:81–99.

Cicirata F, Angaut P, Serapide MF, Panto MR (1990) Functional organization of the direct and indirect projection via the reticularis thalami nuclear complex from the motor cortex to the thalamic nucleus ventralis lateralis. Exp Brain Res 79:325–337.

Cowan RL, Wilson CJ, Emson PC, Heizmann CW (1990) Parvalbumin-containing GABAergic interneurons in the rat neostriatum. J Comp Neurol 302:197–205.

DeLong MR (1990) Primate models of movement disorders of basal ganglia origin. Trends Neurosci 13:281–285.

Dubé L, Smith AD, Bolam JP (1988) Identification of synaptic terminals of thalamic or cortical origin in contact with distinct medium size spiny neurons in the rat neostriatum. J Comp Neurol 267:455–471.

Flaherty AW, Graybiel AM (1991) Corticostriatal transformations in the primate somatosensory system. Projections from physiologically mapped body-part representations. J Neurophysiol 66:1249–1263.

Flaherty AW, Graybiel AM (1993) Two input systems for body representations in the primate striatal matrix: experimental evidence in the squirrel monkey. J Neurosci 13:1120–1137.

Flaherty AW, Graybiel AM (1995) Motor and somatosensory corticostriatal projection magnifications in the squirrel monkey. J Neurophysiol 74:2638–2648.

Francois C, Yelnik J, Percheron G (1987) Golgi study of the primate substantia nigra II. Spatial organization of dendritic arborizations in relation to the cytoarchitectonic boundaries and to the striatonigral bundle. J Comp Neurol 265:473–493.

Frotscher M, Rinne U, Hassler R, Wagner A (1981) Termination of cortical afferents on identified neurons in the caudate nucleus of the cat. A combined Golgi-EM degeneration study. Exp Brain Res 41:329–337.

Gerfen CR (1989) The neostriatal mosaic: striatal patch-matrix organization is related to cortical lamination. Science 246:385–388.

Gerfen CR, Wilson CJ (1996) The Basal Ganglia. In: Integrated systems of the CNS, Part III, Handbook of chemical neuroanatomy (Björklund A, Hökfelt T, and Swanson L, eds), pp 369–466. Amsterdam: Elsevier.

Graybiel AM (1990) Neurotransmitters and neuromodulators in the basal ganglia. Trends Neurosci 13:244–254.

Graybiel AM (1995) Building action repertoires: memory and learning functions of the basal ganglia. Curr Opin Neurobiol 5:733–741.

Haber SN, Fudge JL, McFarland NR (2000) Striatonigrostriatal pathways in primates form an ascending spiral from the shell to the dorsolateral striatum. J Neurosci 20:2369–2382.

Hanley JJ, Bolam JP (1997) Synaptology of the nigrostriatal projection in relation to the compartmental organization of the neostriatum in the rat. Neuroscience 81:353–370.

Hersch SM, Ciliax BJ, Gutekunst CA, Rees HD, Heilman CJ, Yung KKL, Bolam JP, Ince E, Yi H, Levey AI (1995) Electron microscopic analysis of D1 and D2 dopamine receptor proteins in the dorsal striatum and their synaptic relationships with motor corticostriatal afferents. J Neurosci 15:5222–5237.

Hoffer ZS, Alloway KD (2001) Organization of the corticostriatal projections from the vibrissal representations in the primary motor and somatosensory cortical areas of rodents. J Comp Neurol 439:87–103.

Hoover JE, Strick PL (1993) Multiple output channels in the basal ganglia. Science 259:819–821.

Hussain Z, Johnson LR, Totterdell S (1996) A light and electron microscopic study of NADPH-diaphorase-, calretinin- and parvalbumin-

containing neurons in the rat nucleus accumbens. J Chem Neuroanat 10:19–39.
Jaeger D, Kita H, Wilson CJ (1994) Surround inhibition among projection neurons is weak or nonexistent in the rat neostriatum. J Neurophysiol 72:2555–2558.
Kawaguchi Y (1993) Physiological, morphological, and histochemical characterization of three classes of interneurons in rat neostriatum. J Neurosci 13:4908–4923.
Kemp JM, Powell TPS (1971a) The site of termination of afferent fibres in the caudate nucleus. Philos Trans R Soc Lond B Biol Sci 262:413–427.
Kemp JM, Powell TPS (1971b) The termination of fibres from the cerebral cortex and thalamus upon dendritic spines in the caudate nucleus: a study with the Golgi method. Philos Trans R Soc Lond B Biol Sci 262:429–439.
Kincaid AE, Wilson CJ (1996) Corticostriatal innervation of the patch and matrix in the rat neostriatum. J Comp Neurol 374:578–592.
Kincaid AE, Zheng T, Wilson CJ (1998) Connectivity and convergence of single corticostriatal axons. J Neurosci 18:4722–4731.
Kita H (1993) GABAergic circuits of the striatum. In: Chemical signalling in the basal ganglia (Arbuthnott GW, Emson PC, eds), pp 51–72. Amsterdam: Elsevier.
Kita H (1996) Glutamatergic and GABAergic postsynaptic responses of striatal spiny neurons to intrastriatal and cortical stimulation recorded in slice preparations. Neuroscience 70:925–940.
Kita H, Kosaka T, Heizmann CW (1990) Parvalbumin-immunoreactive neurons in the rat neostriatum: a light and electron microscopic study. Brain Res 536:1–15.
Kolomiets BP, Deniau JM, Mailly P, Menetrey A, Glowinski J, Thierry AM (2001) Segregation and convergence of information flow through the cortico-subthalamic pathways. J Neurosci 21:5764–5772.
Koos T, Tepper JM (1999) Inhibitory control of neostriatal projection neurons by GABAergic interneurons. Nat Neurosci 2:467–472.
Lapper SR, Smith Y, Sadikot AF, Parent A, Bolam JP (1992) Cortical input to parvalbumin-immunoreactive neurones in the putamen of the squirrel monkey. Brain Res 580:215–224.
Luk KC, Sadikot AF (2001) GABA promotes survival but not proliferation of parvalbumin-immunoreactive interneurons in rodent neostriatum: an in vivo study with stereology. Neuroscience 104:93–103.
Mahon S, Deniau JM, Charpier S (2001) Relationship between EEG potentials and intracellular activity of striatal and cortico-striatal neurons: an in vivo study under different anesthetics. Cereb Cortex 11:360–373.
Malach R, Graybiel AM (1986) Mosaic architecture of the somatic sensory-recipient sector of the cat's striatum. J Neurosci 6:3436–3458.
Maurin Y, Banrezes B, Menetrey A, Mailly P, Deniau JM (1999) Three-dimensional distribution of nigrostriatal neurons in the rat: Relation to the topography of striatonigral projections. Neuroscience 91:891–909.
Middleton FA, Strick PL (2000) Basal ganglia and cerebellar loops: motor and cognitive circuits. Brain Res Rev 31:236–250.
Nauta WJH, Domesick VB (1984) Afferent and efferent relationships of the basal ganglia. In: Functions of the basal ganglia (Evered D, O'Connor M, eds), pp 3–23. London: Pitman.
Nothias F, Wictorin K, Isacson O, Bjorklund A, Peschanski M (1988) Morphological alteration of thalamic afferents in the excitotoxically lesioned striatum. Brain Res 461:349–354.
Oorschot DE (1996) Total number of neurons in the neostriatal, pallidal, subthalamic, and substantia nigral nuclei of the rat basal ganglia: a stereological study using the cavalieri and optical disector methods. J Comp Neurol 366:580–599.
Parent A, Hazrati L-N (1995) Functional anatomy of the basal ganglia. 1. The cortico-basal ganglia-thalamo-cortical loop. Brain Res Rev 20:91–127.
Parthasarathy HB, Graybiel AM (1997) Cortically driven immediate-early gene expression reflects modular influence of sensorimotor cortex on identified striatal neurons in the squirrel monkey. J Neurosci 17:2477–491.
Parthasarathy HB, Schall JD, Graybiel AM (1992) Distributed but convergent ordering of corticostriatal projections: analysis of the frontal eye field and the supplementary eye field in the macaque monkey. J Neurosci 12:4468–4488.
Paxinos G, Watson C (1997) The rat brain in stereotaxic coordinates, Ed 3. Sydney: Academic.
Pearson RCA, Gatter KC, Powell TPS (1983) The cortical relationships of certain basal ganglia and the cholinergic basal forebrain nuclei. Brain Res 261:327–330.
Pennartz CM, Kitai ST (1991) Hippocampal inputs to identified neurons in an in vitro slice preparation of the rat nucleus accumbens: evidence for feed-forward inhibition. J Neurosci 11:2838–2847.
Plenz D, Kitai ST (1998) Up and down states in striatal medium spiny neurons simultaneously recorded with spontaneous activity in fast-spiking interneurons studied in cortex-striatum-substantia nigra organotypic cultures. J Neurosci 18:266–283.
Price TR, Webster KE (1972) The cortico-thalamic projection from the primary somatosensory cortex of the rat. Brain Res 44:636–640.
Schneider JS (1991) Responses of striatal neurons to peripheral sensory stimulation in symptomatic MPTP-exposed cats. Brain Res 544:297–302.
Smith Y, Bennett BD, Bolam JP, Parent A, Sadikot AF (1994) Synaptic relationships between dopaminergic afferents and cortical or thalamic input in the sensorimotor territory of the striatum in monkey. J Comp Neurol 344:1–19.
Somogyi P, Bolam JP, Smith AD (1981a) Monosynaptic cortical input and local axon collaterals of identified striatonigral neurons. A light and electron microscopic study using the Golgi-peroxidase transport-degeneration procedure. J Comp Neurol 195:567–584.
Somogyi P, Bolam JP, Totterdell S, Smith AD (1981b) Monosynaptic input from the nucleus accumbens-ventral striatum region to retrogradely labelled nigrostriatal neurones. Brain Res 217:245–263.
Stern EA, Kincaid AE, Wilson CJ (1997) Spontaneous subthreshold membrane potential fluctuations and action potential variability of rat corticostriatal and striatal neurons in vivo. J Neurophysiol 77:1697–1715.
Takada M, Tokuno H, Nambu A, Inase M (1998) Corticostriatal projections from the somatic motor areas of the frontal cortex in the macaque monkey: segregation versus overlap of input zones from the primary motor cortex, the supplementary motor area, and the premotor cortex. Exp Brain Res 120:114–128.
Wilson CJ (1995) The contribution of cortical neurons to the firing pattern of striatal spiny neurons. In: Models of information processing in the basal ganglia (Houk JC, Davis JD, Beiser DG, eds), pp 29–50. Cambridge, MA: MIT.
Wilson CJ, Kawaguchi Y (1996) The origins of two-state spontaneous membrane potential fluctuations of neostriatal spiny neurons. J Neurosci 16:2397–2410.
Wilson CJ, Chang HT, Kitai ST (1983a) Disfacilitation and long-lasting inhibition of neostriatal neurons in the rat. Exp Brain Res 51:227–235.
Wilson JS, Hull CD, Buchwald NA (1983b) Intracellular studies of the convergence of sensory input on caudate neurons of cat. Brain Res 270:197.
Wright AK, Norrie L, Ingham CA, Hutton EA, Arbuthnott GW (1999) Double anterograde tracing of outputs from adjacent "barrel columns" of rat somatosensory cortex. Neostriatal projection patterns and terminal ultrastructure. Neuroscience 88:119–133.
Yeterian EH, Van Hoesen GW (1978) Cortico-striate projections in the rhesus monkey: the organization of certain cortico-caudate connections. Brain Res 139:43–63.
Zheng T, Wilson CJ (2002) Corticostriatal combinatorics: the implications of corticostriatal axonal arborizations. J Neurophysiol 87:1007–1017.